UNIWERSYTET IM. ADAMA MICKIEWICZA W POZNANIU
WYDZIAŁ CHEMII

Rozprawa doktorska

Synteza, struktura i właściwości fotofizyczne nowych cyklometalowanych kompleksów irydu(III) jako potencjalnych emiterów fosforescencyjnych dla organicznych diod elektroluminescencyjnych (OLED)

Synthesis, structure, and photophysical properties of new cyclometalated iridium(III) complexes as potential phosphorescent emitters for organic light-emitting diodes (OLED)

mgr Bartosz Orwat

Promotor pracy doktorskiej: Prof. UAM dr hab. Ireneusz Kownacki

Praca została wykonana w Zakładzie Chemii i Technologii Związków Krzemu
Wydziału Chemii Uniwersytetu im. Adama Mickiewicza w Poznaniu

UNIWERSYTET
IM. ADAMA MICKIEWICZA
W POZNANIU

Poznań 2020

Z całego serca dziękuję

Panu Prof. UAM dr hab. Ireneuszowi Kownackiemu

za opiekę merytoryczną przez cały okres studiów,
owocne dyskusje na różnorakie tematy, ogrom przekazanej wiedzy
oraz nieocenione wsparcie w każdym działaniu

Narzeczonej Julii

za nieskończone pokłady cierpliwości, wyrozumiałość i wsparcie,
szczególnie w najtrudniejszych chwilach

Rodzicom i Siostrze

za uczynienie mnie tym, kim jestem i niegasnącą wiarę we mnie

Kolegom i Koleżankom z Centrum Zaawansowanych Technologii

za wsparcie, wspaniałą atmosferę w pracy i wspólnie spędzony czas

Spis treści

1. Wykaz stosowanych skrótów ... 7
2. Streszczenie w języku polskim ... 9
3. Streszczenie w języku angielskim ... 10
4. Ankieta dorobku naukowego ... 11
4.1. Publikacje wchodzące w skład rozprawy ... 11
4.2. Pozostałe publikacje ... 11
4.3. Patenty i zgłoszenia patentowe ... 12
4.4. Staże naukowe ... 12
4.5. Udział w konferencjach naukowych ... 12
4.6. Udział w grantach badawczych ... 13
4.7. Stypendia i nagrody ... 14
5. Wstęp ... 15
6. Cel pracy i uzasadnienie podjęcia tematyki badawczej ... 25
7. Omówienie publikacji będących podstawą rozprawy ... 26
7.1. Jonowe związki kompleksowe o strukturze $[Ir(bzq)_2(N\hat{}N)]^+A^-$ ... 26
7.2. Kompleksy Ir(III) zawierające fluorowane *β*-ketoiminianowe ligandy pomocnicze ... 33
7.3. Kompleksy Ir(III) zawierające *N*-arylopodstawione ligandy β-ketoiminianowe ... 39
7.4. Funkcjonalizacja benzo[*h*]chinoliny w pozycji 5 ... 45
7.5. Dwurdzeniowe kompleksy irydu(III) o strukturze $[Ir(C\hat{}N)_2(\mu\text{-}Cl)]_2$ ... 53
7.6. Związki kompleksowe irydu(III) zawierające 5-funkcjonalizowane pochodne bzq ... 62
8. Podsumowanie i wnioski ... 67
9. Literatura ... 70
10. Oświadczenia współautorów ... 76
11. Kopie publikacji wchodzących w skład rozprawy ... 81

1. Wykaz stosowanych skrótów

W przedstawionej rozprawie zachowano symbolikę związków stosowaną w publikacjach źródłowych, dodając do nich po myślniku końcówkę wskazującą źródło odniesienia, np. **1-P1** oznacza związek o symbolu **1**, opisywany w pracy [**P1**].

[**Pd**] – związek kompleksowy palladu, ogólnie

acac – acetyloacetonian

ACN – acetonitryl

Ar – aryl

BINAP – 2,2'-bis(difenylofosfino)-1,1'-binaftyl

bpy – 2,2'-bipirydyna

bzq/bzqH – ligand powstały w skutek usunięcia protonu z pozycji 10 benzo[*h*]chinoliny / benzo[*h*]chinolina

CD_2Cl_2 – dichlorometan deuterowany

$CDCl_3$ – chloroform deuterowany

CID – kolizyjnie indukowana dysocjacja (ang. *collision-induced dissociation*)

COD – *cis*,*cis*-1,5-cyklooktadien

dba – dibenzylidenoaceton (1,5-difenylo-1,4-pentadien-3-on)

DCE – 1,2-dichloroetan

Dimer – skrótowe określenie dwurdzeniowych μ-chlorkowych związków kompleksowych irydu(III) o strukturze $[Ir(C\hat{}N)_2(\mu\text{-}Cl)]_2$

DMF – *N*,*N*-dimetyloformamid

DMSO/DMSO-d_6 – dimetylosulfotlenek/dimetylosulfotlenek deuterowany

DP – potencjał deklasteryzacyjny (ang. *declustering potential*)

dtbbpy – 4,4'-di-tert-butylo-2,2'-bipirydyna

EA – powinowactwo elektronowe (ang. *electron affinity*)

E_g – przerwa energetyczna HOMO-LUMO (ang. *energy gap*)

eq - ekwiwalent

ESI-MS – spektrometria mas sprzężona z jonizacją typu electrospray

fac – izomer facjalny

HCl – kwas chlorowodorowy

IP – potencjał jonizacji (ang. *ionization potential*)

ITO – mieszany tlenek indu i cyny

IQE – wewnętrzna wydajność kwantowa (ang. *internal quantum efficiency*)

Kompleks – synonim określenia „związek kompleksowy" przez część chemików uważany za żargonowy, jednakże bardzo powszechnie stosowany w chemii koordynacyjnej, szczególnie w języku angielskim

LC – przejście elektronowe w obrębie liganda (ang. *ligand-centered*)

LEEC – elektroluminescencyjne ogniwo chemiczne (ang. *Light-Emitting Electrochemical Cell*)

LLCT – przejście ligand-ligand z przeniesieniem ładunku (ang. *ligand-to-ligand charge transfer*)

mer – izomer meridionalny

MLCT – przejście metal-ligand z przeniesieniem ładunku (ang. *metal-to-ligand charge transfer*)

MW – promieniowanie mikrofalowe (ang. *microwaves*)

NaOtBu – *tert*-butanolan sodu

NBS – *N*-bromosukcynoimid

NMP – *N*-metylopirolidon

NMR –magnetyczny rezonans jądrowy (ang. *Nuclear Magnetic Resonance*)

OB – łaźnia olejowa (ang. *oil bath*)

OLED – dioda elektroluminescencyjna (ang. *Organic Light-Emitting Diode*)

One-pot – określenie stosowane do opisu procesu, na który składa się więcej niż jedna reakcja chemiczna, zachodzące jednocześnie w tym samym naczyniu reakcyjnym

PBD – 2-*tert*-butylofenylo-5-bifenyl-1,3,4-oksadiazol

PEDOT:PSS – mieszanina poli(3,4-etyleno-1,4-dioksytiofen) oraz sulfonowanego polistyrenu

Ph – fenyl

phen – 1,10-fenantrolina

POSS – oligomeryczny poliedryczny silsekwioksan (ang. *Polyhedral Oligomeric Silsesquioxane*)

PVK – poli(winylokarbazol)

ppm – części na milion

ppy/ppyH – ligand powstały w skutek usunięcia protonu z pozycji 1 2-fenylopirydyny / 2-fenylopirydyna

t – temperatura

TADF – termicznie aktywowana opóźniona fluorescencja (ang. *thermally activated delayed fluorescence*)

THF – tetrahydrofuran

TsO – grupa 4-toluenosulfonylowa

TfO – grupa trifluorometanosulfonylowa

QY – wydajność kwantowa (ang. *quantum yield*)

UV-Vis – spektroskopia absorpcyjna w zakresie widzialnym i ultrafioletowym

XRD – dyfrakcja rentgenowska (ang. *X-Ray Diffraction)*

2. Streszczenie w języku polskim

Przedstawiona rozprawa podejmuje bardzo istotne zagadnienie z obszaru chemii i inżynierii materiałów, jakim jest technologia OLED. Organiczne panele elektroluminescencyjne od kilku lat są powszechnie dostępne na rynku komercyjnym w postaci ekranów stosowanych w telefonach komórkowych, tabletach oraz odbiornikach telewizyjnych. Panele wyświetlające obraz są wykonane w technologii RGB, w których związki koordynacyjne irydu(III) pełnią rolę fosforescencyjnych emiterów światła czerwonego oraz zielonego. Z uwagi na wydajność kwantową emisji oraz stabilność, szczególnie użyteczne okazały się emitery zawierające w swojej strukturze *C,N*-cyklometalujące ligandy 2-fenylopirydynianowe oraz ich pochodne. Zainteresowanie wzbudził kontrast pomiędzy rozległością wiedzy na temat wspomnianej klasy związków, a ubogim stanem wiedzy na temat analogicznych kompleksów irydu(III) wyposażonych w ligandy benzo[*h*]chinolinianowe. Wykorzystanie tego typu pochodnych wydało się bardzo atrakcyjne z powodu zbliżonego rozmiaru kieszeni koordynacyjnej benzo[*h*]chinoliny i 2-fenylopirydyny, ale znacznie sztywniejszej struktury i większego stopnia koniugacji tej pierwszej, co mogło mieć istotny wpływ na właściwości kompleksów wyposażonych w tego typu ligand. Wobec powyższego, niniejsza rozprawa podejmuje tematykę projektowania i otrzymywania nowych związków koordynacyjnych irydu(III) zawierających motyw benzo[*h*]chinoliny oraz analizę wpływu zmian strukturalnych na właściwości fotofizyczne, elektroluminescencyjne, termiczne, elektrochemiczne i spektroskopowe wybranych klas związków ukierunkowanych na zastosowanie w technologii OLED. W szczególności skupiono się na następujących zagadnieniach:

- Kompleksach jonowych o ogólnym wzorze $[Ir(bzq)_2(N\hat{}N)]^+A^-$, wyposażonych w strukturalnie zróżnicowane ligandy *N,N*-donorowe [**P1**]
- Kompleksach obojętnych typu $[Ir(bzq)_2(N\hat{}O)]$, stabilizowanych β-ketoiminianowymi ligandami funkcjonalizowanymi atomami fluoru [**P2**]
- Kompleksach obojętnych o wzorze ogólnym $[Ir(bzq)_2(N\hat{}O)]$, stabilizowanych β-ketoiminianowymi ligandami podstawionymi różnorodnymi ugrupowaniami arylowymi [**P3**]
- Opracowaniu efektywnych metod otrzymywania nowych pochodnych benzo[*h*]chinoliny, jako potencjalnych prekursorów ligandów dla emiterów fosforescencyjnych [**P4**]
- Opracowaniu efektywnej metody syntezy dwurdzeniowych kompleksów irydu(III) o strukturze $[Ir(C\hat{}N)_2(\mu\text{-}Cl)]_2$, z użyciem nowych ligandów będących pochodnymi bzq oraz badania ich zachowania w rozpuszczalnikach koordynujących [**P5**]
- Syntezie nowych kompleksów irydu(III) o strukturach $[Ir(C\hat{}N)_2(N\hat{}N)]^+A^-$ oraz $[Ir(C\hat{}N)_3]$, wyposażonych w nowe ligandy będące pochodnymi bzq [**materiał nieopublikowany**]

Badania opisane w rozprawie były realizowane w ramach projektu OPUS 6 pt. *Nowe emitery fosforescencyjne dla organicznych diod elektroluminescencyjnych*, w grupie Prof. UAM dr hab. Ireneusza Kownackiego z Zakładu Chemii i Technologii Związków Krzemu Uniwersytetu im. Adama Mickiewicza (kierownika projektu). Realizacja projektu była prowadzona w ścisłej współpracy z grupami badawczymi: Prof. dr hab. inż. Jacka Ulańskiego z Katedry Fizyki Molekularnej Politechniki Łódzkiej, Prof. dr hab. Mieczysława Łapkowskiego z Katedry Fizykochemii i Technologii Polimerów Politechniki Śląskiej, Prof. dr hab. Marcina Hoffmanna z Zakładu Chemii Kwantowej Uniwersytetu im. Adama Mickiewicza oraz Prof. dr hab. Macieja Kubickiego z Zakładu Krystalografii Uniwersytetu im. Adama Mickiewicza.

3. Streszczenie w języku angielskim

Presented dissertation deals with a very important subject in the field of chemistry and material engineering, that is the OLED technology. Organic electroluminescent panels have been widely available on the commercial market for several years, in the form of screens used in mobile phones, tablets and TV sets. The display panels are produced in RGB technology, in which iridium(III) coordination compounds act as phosphorescent emitters of red and green light. Because of their high emission quantum efficiency and stability, the emitters containing 2-phenylpyridinato ligands and their derivatives have proved to be particularly useful. An interesting issue was the contrast between an extensive state of knowledge on the abovementioned compounds and a poor state of knowledge on analogous iridium(III) complexes equipped with benzo[*h*]quinolinato ligands. Application of the latter seemed interesting because of the similar size of benzo[*h*]quinoline and 2-phenylpyridine coordination pockets, but much more rigid structure and a greater degree of conjugation of the former, which could have a significant impact on the properties of complexes equipped with this type of ligand. With regard to the above, this dissertation concerns the subject of the design and synthesis of new iridium(III) coordination compounds equipped with benzo[*h*]quinoline motif, as well as the analysis of the structural changes impact on photophysical, electroluminescent, thermal, electrochemical and spectroscopic properties of selected classes of compounds targeted at the application in OLED technology. To be more exact, the dissertation covers the following issues:

- Ionic complexes of general formula $[Ir(bzq)_2(N\hat{}N)]^+A^-$, equipped with various *N,N*-donating ligands [**P1**]
- Neutral complexes of general formula $[Ir(bzq)_2(N\hat{}O)]$, stabilized with fluorinated β-ketoiminato ligands [**P2**]
- Neutral complexes of general formula $[Ir(bzq)_2(N\hat{}O)]$, stabilized with aryl-substituted β-ketoiminato ligands [**P3**]
- Development of efficient methods for the synthesis of new benzo[*h*]quinoline derivatives as potential ligand precursors for phosphorescent emitters [**P4**]
- Development of efficient method for the synthesis of iridium(III) binuclear complexes of general formula $[Ir(C\hat{}N)_2(\mu\text{-}Cl)]_2$ equipped with new bzq-based ligands and studies of their behavior in the coordinating solvents environment [**P5**]
- Synthesis of new functionalized bzq-based iridium(III) complexes of general formula $[Ir(C\hat{}N)_2(N\hat{}N)]^+A^-$ and $[Ir(C\hat{}N)_3]$ [**results unpublished**]

The research work described in the dissertation was carried out as a part of the OPUS 6 project entitled *New phosphorescent emitters for organic electroluminescent diodes*, in the group of Prof. UAM dr hab. Ireneusz Kownacki from the Department of Chemistry and Technology of Silicon Compounds of Adam Mickiewicz University (project manager). The project was carried out in close cooperation with the following research groups: Prof. dr hab. eng. Jacek Ulański from the Department of Molecular Physics of Łódź University of Technology, Prof. dr hab. Mieczysław Łapkowski from the Department of Physical Chemistry and Technology of Polymers of Silesian University of Technology, Prof. dr hab. Marcin Hoffmann from the Quantum Chemistry Department of Adam Mickiewicz University, and Prof. dr hab. Maciej Kubicki from the Department of Crystallography of Adam Mickiewicz University.

4. Ankieta dorobku naukowego

4.1. Publikacje wchodzące w skład rozprawy

[**P1**] **B. Orwat**, E. Witkowska, I. Kownacki*, M.-J. Oh, M. Hoffmann, M. Kubicki, I. Grzelak, B. Marciniec, I. Głowacki, B. Łuszczyńska, G. Wiosna-Sałyga, J. Ulański, P. Ledwoń, M. Łapkowski; *Microwave-assisted one-pot synthesis of new ionic cyclometalated iridium complexes of $[Ir(bzq)_2(N^N)]^+A^-$ type and their selected electroluminescent properties*; *Dalton Transactions* **2017**, vol. 426, p. 9210, **IF_{2017} = 3.93**

[**P2**] E. Witkowska, G. Wiosna-Sałyga*, I. Głowacki, **B. Orwat**, M.-J. Oh, I. Kownacki*, M. Kubicki, B. Gierczyk, M. Dutkiewicz, P. Cieszko, B. Łuszczyńska, J. Ulański, I. Grzelak, M. Hoffmann, P. Ledwoń, M. Łapkowski; *Effect of fluorine substitution of the b-ketoiminate ancillary ligand on photophysical properties and electroluminescence ability of new iridium(III) complexes*; *Journal of Materials Chemistry C* **2018**, vol. 6, p. 8688, **IF_{2018} = 6.28**

[**P3**] E. Witkowska, **B. Orwat**, M.-J. Oh, G. Wiosna-Sałyga*, I. Głowacki, I. Kownacki*, K. Jankowska, M. Kubicki, B. Gierczyk, M. Dutkiewicz, I. Grzelak, M. Hoffmann, J. Nawrocik, G. Krajewski, J. Ulański, P. Ledwoń, M. Łapkowski; *Effect of β-Ketoiminato Ancillary Ligand Modification on Emissive Properties of New Iridium Complexes*; *Inorganic Chemistry* **2019**, vol. 58, p. 15671, **IF_{2018} = 4.76**

[**P4**] **B. Orwat**, M.-J. Oh, M. Kubicki, I. Kownacki*; *Synthesis of 5-Substituted Benzo[h]quinoline Derivatives via Reactions Involving C(sp^2)-Br Bond Activation; Advanced Synthesis & Catalysis* **2018**, vol. 360, p. 3331, **IF_{2018} = 5.20**

[**P5**] **B. Orwat***, M.-J. Oh, M. Zaranek, M. Kubicki, R. Januszewski, I. Kownacki*; *Microwave-accelerated C,N-cyclometalation as a route to chloro-bridged iridium(III) binuclear precursors of phosphorescent materials: optimization, synthesis, and studies of the Ir(III) dimers behavior in coordinating solvents; Inorganic Chemistry* **2020**, vol. 59, p. 9163, **IF_{2018} = 4.76**

Sumaryczny IF = 24.93

4.2. Pozostałe publikacje

1. A. Bartkowiak, **B. Orwat***, M. Zalas, P. Ledwoń, I. Kownacki, W. Tejchman; *2-Thiohydantoin Moiety as a Novel Acceptor/Anchoring Group of Photosensitizers for Dye-Sensitized Solar Cells*; *Materials* **2020**, vol. 13, p. 2065, **IF_{2018} = 3.26 (publikacja wyróżniona na okładce numeru czasopisma)**
2. W. Tejchman, **B. Orwat***, I. Korona-Głowniak, A. Barbasz, I. Kownacki, G. Latacz, J. Handzlik, E. Żesławska, A. Malm; *Highly efficient microwave synthesis of rhodanine and 2-thiohydantoin derivatives and determination of relationships between their chemical structures and antibacterial activity*; *RSC Advances* **2019**, vol. 9, p. 39367, **IF_{2018} = 3.16**
3. I. Grzelak*, **B. Orwat**, I. Kownacki, M. Hoffmann; *Quantum-chemical studies of homoleptic iridium(III) complexes in OLEDs: fac versus mer isomers*; *Journal of Molecular Modeling* **2019**, vol. 25, p. 154, **IF_{2018} = 1.33**
4. R. Januszewski, M. Dutkiewicz*, **B. Orwat**, H. Maciejewski, B. Marciniec; *A library of multisubstituted cyclotriphosphazenes – molecular scaffolds for hybrid materials*; *New Journal of Chemistry* **2018**, vol. 42, p. 15552, **IF_{2018} = 3.09**

5. M. Zaranek, M. Skrodzki, J. Szudkowska-Frątczak, M. Dodot, I. Kownacki, **B. Orwat**, P. Pawluć*; *Iridium-catalysed desilylative acylation of 1-alkenylsilanes*; *Journal of Molecular Catalysis A: Chemical* **2017**, vol. 426, p. 75, **IF_{2017} = 4.36**
6. I. Kownacki*, **B. Orwat**, B. Marciniec*; *Iridium-promoted conversion of chlorosilanes to alkynyl derivatives in one-pot reaction sequence; Organometallics* **2014**, vol. 33, p. 3051, **IF_{2014} = 4.05**
7. I. Kownacki*, **B. Orwat**, B. Marciniec*, A. Kownacka; *A new and efficient route for the synthesis of alkynyl functionalized silicon derivatives; Tetrahedron Letters* **2014**, vol. 55, p. 548, **IF_{2014} = 2.41**

4.3. Patenty i zgłoszenia patentowe

1. I. Kownacki, **B. Orwat**, B. Marciniec, G. Wiosna-Sałyga, B. Łuszczyńska, I. Głowacki, J. Ulański; *Nowe jonowe kompleksy irydu(III) oraz sposób ich syntezy i ich zastosowanie, jako emitery fosforescencyjne*; nr zgłoszenia PL418615, **2016**
2. I. Kownacki, **B. Orwat**, B. Marciniec; *Sposób syntezy jonowych kompleksów irydu(III)*; nr zgłoszenia PL418616, **2016**
3. G. Wiosna-Sałyga, B. Łuszczyńska, I. Głowacki, J. Ulański, I. Kownacki, **B. Orwat**, B. Marciniec; *Organiczne diody elektroluminescencyjne z nowymi warstwami emisyjnymi*; nr zgłoszenia PL418617, **2016**
4. I. Kownacki, B. Marciniec, B. Dudziec, A. Kownacka, M. Majchrzak, M. Szulc, **B. Orwat**; *Catalytic method for obtaining substituted (triorganosilyl)alkynes and their derivatives*; nr patentu: US9518069 B2, **2016**
5. I. Kownacki, B. Marciniec, B. Dudziec, A. Kownacka, M. Majchrzak, **B. Orwat**; *(Triorganosilyl)alkynes and a new catalytic method for obtaining new and conventional substituted (triorganosilyl)alkynes and their derivatives*; nr patentu: EP 2658861 B1, CN103328489 B, KR101631132 B1, JP5886876 B2, US9108994 B2, **2015-2016**

4.4. Staże naukowe

1. Katedra Fizyki Molekularnej, Wydział Chemiczny Politechniki Łódzkiej, **2017** (1 miesiąc)
   Opiekunowie: Prof. dr hab. Jacek Ulański, Prof. PŁ dr hab. inż. Ireneusz Głowacki

4.5. Udział w konferencjach naukowych

1. *Wspomagana mikrofalowo synteza nowych pochodnych pirydoimidazolu w układzie one-pot*; III Ogólnopolskie Sympozjum Chemii Bioorganicznej, Organicznej i Biomateriałów BioOrg, 07 XII **2019**, Poznań, Polska **(wystąpienie ustne - nagroda za najlepszą prezentację)**
2. *New phosphine oxide and carbazole-based hosts for blue OLEDs*; 24th International Krutyń Summer School, 01-07 IX **2019**, Krutyń, Polska **(poster)**
3. *Synthesis and characterization of new hosts for deep blue OLEDs*; Workshop on Progress in Nanotechnology and Optoelectronics, 25-27 IV **2019**, Łódź, Polska **(poster)**
4. *Synteza i charakterystyka nowych C,N-cyklometalowanych kompleksów irydu(III)*; 61 Zjazd Naukowy Polskiego Towarzystwa Chemicznego, 17-21 IX **2018**, Kraków, Polska **(wystąpienie ustne)**
5. *Synthesis and investigation on new iridium(III) complexes as phosphorescent dopants for organic light-emitting diodes; Synthesis of new benzo[h]quinoline derivatives and their application in preparation of new iridium(III) complexes*; 28th International Conference on Organometallic Chemistry, 15-20 VII **2018**, Florencja, Włochy **(poster; poster)**

6. *Synteza i charakterystyka właściwości nowych kompleksów irydu(III) jako emiterów dla diod OLED*; IV Poznańskie Sympozjum Młodych Naukowców, 18 XI **2017**, Poznań, Polska **(wystąpienie ustne)**
7. *Synteza i charakterystyka właściwości fotofizycznych nowych C,N-cyklometalowanych kompleksów irydu(III) jako fosforescencyjnych emiterów dla organicznych diod elektroluminescencyjnych*; 60 Zjazd Naukowy Polskiego Towarzystwa Chemicznego, 17-21 IX **2017**, Wrocław, Polska **(poster)**
8. *Synthesis and investigation of photophysical properties of the new C,N-cyclometalated iridium(III) complexes as a phosphorescent dopants for organic light-emitting diodes*; *Iridium-promoted silylation of terminal alkynes with halosilanes*; XI Copernican International Young Scientists Conference, 28-30 VI **2017**, Toruń, Polska **(wystąpienie ustne - nagroda za najlepszą prezentację; poster)**
9. *Synthesis and investigation of photophysical properties of the new C,N-cyclometalated iridium(III) complexes as a phosphorescent dopants for organic light-emitting diodes*; 17th International Seminar of PhD Students on Organometallic and Coordination Chemistry, 02-06 IV **2017**, Kraskov, Czechy **(wystąpienie ustne)**
10. *Synteza nowych pochodnych benzo[h]chinoliny oraz ich zastosowanie w otrzymywaniu nowych kompleksów irydu(III), jako potencjalnych emiterów diod OLED*; III Poznańskie Sympozjum Młodych Naukowców, 05 XI **2016**, Poznań, Polska **(poster)**
11. *Synteza nowych ketoiminowych kompleksów irydu(III) o potencjalnym zastosowaniu w technice OLED*; *Synteza nowych pochodnych benzo[h]chinoliny oraz ich zastosowanie w otrzymywaniu nowych kompleksów irydu(III), jako potencjalnych emiterów diod OLED;* 59 Zjazd Naukowy Polskiego Towarzystwa Chemicznego, 19-23 IX **2016**, Poznań, Polska **(poster; poster)**
12. *Iridium-promoted silylation of terminal alkynes with halosilanes*; 8th European Silicon Days, 28-31 VIII **2016**, Poznań, Polska **(poster)**
13. *Nowa katalityczna metoda synteza alkinylosilanów i ich zastosowanie do otrzymywania pi-sprzężonych związków krzemoorganicznych*; II Poznańskie Sympozjum Młodych Naukowców Nowe Oblicze Nauk Przyrodniczych, 14 XI **2015**, Poznań, Polska **(poster)**
14. *Synteza nowych monomerów krzemoorganicznych jako potencjalnych prekursorów polimerowych matryc diod OLED*; 58 Zjazd Naukowy Polskiego Towarzystwa Chemicznego, 21-25 IX **2015**, Gdańsk, Polska **(poster)**

4.6. Udział w grantach badawczych

1. **PRELUDIUM 2018/29/N/ST5/02926 – <u>kierownik</u>**
   Synteza i charakterystyka nowych emiterów dla niebieskich OLEDów (Organicznych Diod Elektroluminescencyjnych)
2. **OPUS 2013/11/B/ST5/01334 – wykonawca**
   Nowe emitery fosforescencyjne dla organicznych diod elektroluminescencyjnych
3. **SONATINA 2019/32/C/ST4/00178 – wykonawca**
   Synteza nowych funkcjonalizowanych poliolefin
4. **Program Operacyjny Inteligentny Rozwój 2014-2020 POIR.04.01.02-00-0045/17-00 – wykonawca**
   Mobilny system suszenia izolacji transformatorów rozdzielczych z wykorzystaniem medium ciekłego
5. **MAESTRO 2011/02/A/ST5/00472 – wykonawca**
   Kataliza metalonieorganiczna - nowa strategia syntezy metaloorganicznych reagentów, polimerów i nanomateriałów

4.7. Stypendia i nagrody

1. Nagroda zespołowa Rektora UAM za osiągnięcia naukowe; **2019**
2. Stypendium naukowe Rektora UAM; **2018**
3. Stypendium Doktoranckie; **2014-2018**
4. Nagroda Polskiego Towarzystwa Chemicznego za najlepszą pracę magisterską; **2015**
5. Zwiększenie stypendium doktoranckiego z dotacji podmiotowej na dofinansowanie zadań projakościowych; **2014-2015**
6. Stypendium Rektora UAM dla najlepszych doktorantów; **2014-2015**
7. Jednorazowe stypendium naukowe Marszałka Województwa Wielkopolskiego; **2014**
8. Medal dla najlepszych absolwentów za wybitne osiągnięcia w nauce i wyróżniający udział w życiu Uniwersytetu im. Adama Mickiewicza w Poznaniu; **2014**
9. Stypendium Ministra Nauki i Szkolnictwa Wyższego za wybitne osiągnięcia; **2012-2013**
10. Finalista konkursu *Złoty medal chemii* Instytutu Chemii Fizycznej PAN; **2012**
11. Stypendium motywacyjne współfinansowane ze środków Unii Europejskiej w ramach Europejskiego Funduszu Społecznego Program Operacyjny Kapitał Ludzki *Chemia Warta Poznania;* **2012-2014**
12. Stypendium Rektora UAM dla najlepszych studentów; **2011-2014**
13. Stypendium motywacyjne współfinansowane ze środków Unii Europejskiej w ramach Europejskiego Funduszu Społecznego Program Operacyjny Kapitał Ludzki *Poczuj Chemię do Chemii;* **2009-2012**

5. Wstęp

Pomimo, że wyświetlacze OLED na dobre zagościły na rynku konsumenckim jako elementy urządzeń mobilnych oraz odbiorników telewizyjnych, tematyka diod organicznych nadal cieszy się bardzo dużym zainteresowaniem środowiska naukowego, jako alternatywa mogąca w przyszłości całkowicie zastąpić pozostałe technologie oświetleniowe i wyświetlania obrazu. W porównaniu do najpowszechniej stosowanych paneli LCD, ekrany OLED cechują się lepszym poziomem czerni, większym kontrastem, szerszym kątem widzenia, bogatszą paletą wyświetlanych barw, większą jednorodnością obrazu, mniejszą grubością paneli, a także porównywalnym lub nawet niższym zużyciem energii. Wymienione cechy w połączeniu z możliwością produkcji paneli tanimi technikami drukarskimi są powodem szczególnie intensywnego rozwoju tej dziedziny.

Początki technologii OLED sięgają połowy XX wieku i obejmują dwa istotne wydarzenia, a mianowicie odkrycie przez Bernanose'a zjawiska elektroluminescencji oranżu akrydyny w postaci cienkiego filmu lub rozproszonego w celulozie,[1-3] a także zaobserwowanie przez Pope'a elektroluminescencji kryształów związków organicznych, np. antracenu (Rys. 1).[4,5] Jednakże, przełom nastąpił w 1987 roku, kiedy to Tang i VanSlyke skonstruowali pierwszą diodę fluorescencyjną na bazie hydroksychinolinianu glinu(III), która emitowała światło barwy zielonej (Rys. 1).[6] Powyższe odkrycie stało się impulsem do intensywnego rozwoju tej technologii, szczególnie w kontekście poszukiwania nowych materiałów charakteryzujących się emisją w szerokim zakresie pasma widzialnego. Dogodnymi do tego celu substancjami okazały się różnorodne małocząsteczkowe związki organiczne, takie jak perylen, rubren, chinakrydon oraz ich pochodne[7] lub polimery, takie jak poli(winylokarbazol)[8] poli(fluoren)[9], poli(*para*-fenylen)[10], a także pochodne poli(*para*-fenyleno-winylenu).[11,12]

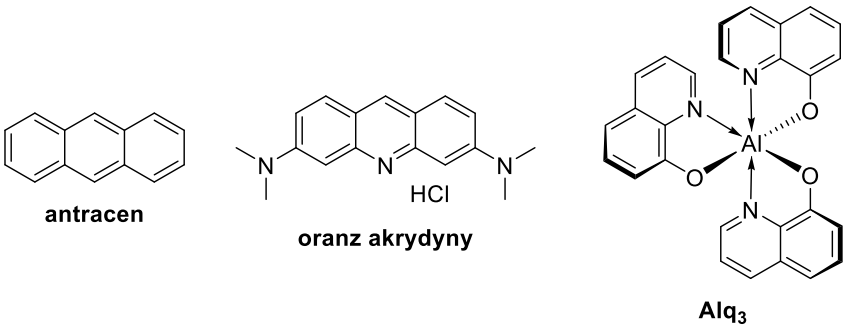

Rys. 1. *Struktury chemiczne pierwszych związków o właściwościach elektroluminescencyjnych.*

W przypadku powyższych substancji możliwe jest wykorzystanie jedynie stanów singletowych, które stanowią zaledwie 25 % populacji wszystkich stanów wzbudzonych. Z kolei diody oparte na emiterach fosforescencyjnych i TADF są zdolne do osiągania 100 % wewnętrznej wydajności kwantowej. Z tego względu, w komercyjnych panelach czerwone oraz zielone emitery fluorescencyjne zostały wyparte przez te fosforescencyjne, co niestety nie objęło także emiterów niebieskich. Problemem okazała się ich krótka żywotność spowodowana relatywnie długim czasem życia stanów wzbudzonych oraz wysoką energia tych stanów, prowadząc do degradacji urządzeń w następstwie zachodzących w warstwie emisyjnej procesów relaksacji bezpromienistej. Ten impas jest przyczyną, dla której liczne grupy badawcze są zaangażowane w prowadzenie badań nad poszukiwaniem nowych organicznych lub metaloorganicznych układów elektroluminescencyjnych, których efektem ma być poprawa właściwości użytkowych OLEDów.[13,14]

Diody OLED są urządzeniami o konstrukcji warstwowej, grubości rzędu kilkuset nanometrów, emitującymi promieniowanie świetlne w skutek przepływu prądu elektrycznego.[15]

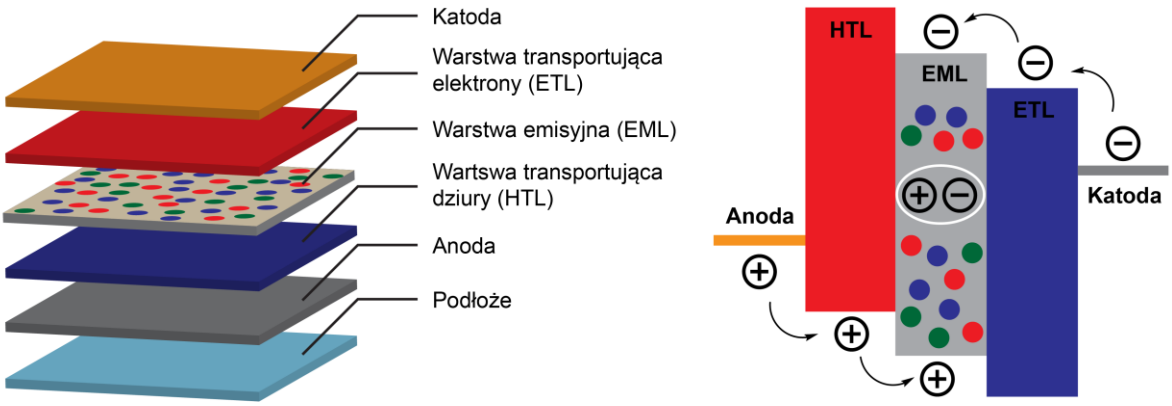

Rys. 2. *Ogólny schemat urządzenia OLED oraz ilustracja zasady działania.*

Takie diody muszą się składać przynajmniej z anody i katody oraz umieszczonej pomiędzy nimi warstwy emisyjnej, aczkolwiek mogą zawierać także dodatkowe warstwy (Rys. 2). Każda warstwa składowa spełnia ściśle określoną funkcję. Katoda służy do wstrzykiwania elektronów, z kolei na anodzie generowane są dziury elektronowe. Wygenerowane nośniki ładunków są przenoszone przez warstwy wspomagające ich transport, trafiając do warstwy emisyjnej. W niej dziury elektronowe i elektrony spotykają się i tworzą pary związane oddziaływaniem elektrostatycznym, nazywane ekscytonami. Rekombinacja promienista ekscytonów z udziałem emitera znajdującego się w warstwie emisyjnej powoduje emisję promieniowania o charakterystycznej długości fali. Struktura chemiczna determinuje nie tylko na barwę emitowanego światła, ale także znacząco wpływa na efektywność pracy całego urządzenia.

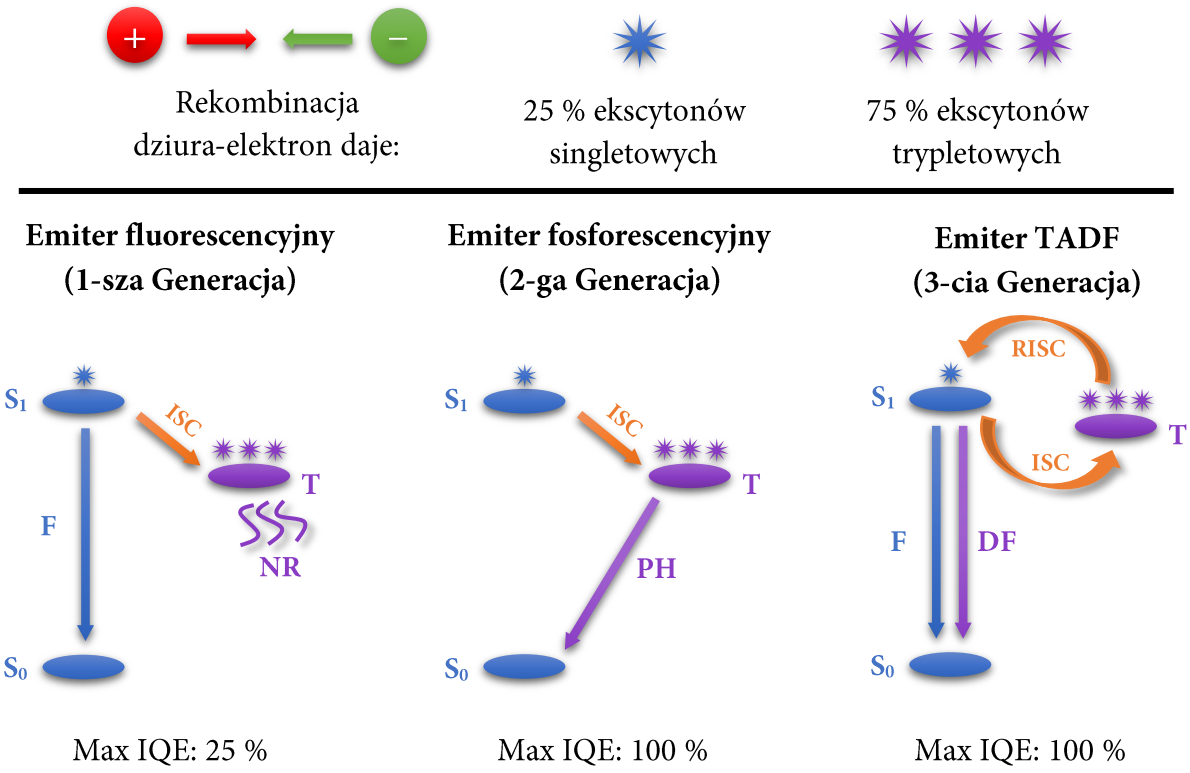

Rys. 3. *Porównanie mechanizmów emisji promieniowania w trzech klasach emiterów (S – stan singletowy, T – stan trypletowy, NR – bezpromieniste rozproszenie energii, F – fluorescencja, PH – fosforescencja, DF – opóźniona fluorescencja, ISC – przejście międzysystemowe, RISC – odwrócone przejście międzysystemowe).*

W zależności od mechanizmu emisji promieniowania, można wyróżnić trzy główne klasy emiterów stosowanych w organicznych diodach (Rys. 3). Historycznie pierwszą poznaną klasą były emitery fluorescencyjne, będące najczęściej czysto organicznymi związkami, efektywnie wykorzystującymi jedynie stany singletowe. Zgodnie z regułami statystyki spinowej, w skutek parowania elektronów i dziur elektronowych powstaje 25 % ekscytonów singletowych oraz 75 % ekscytonów trypletowych.[16] Emitery fluorescencyjne teoretycznie są w stanie wykorzystać do emisji jedynie stany singletowe, gdyż przejścia ze stanów trypletowych są dla nich wzbronione i ulegają one dezaktywacji w sposób bezpromienisty. Z kolei ich zaletą jest bardzo krótki czas życia stanów wzbudzonych (rzędu nanosekund), odpowiadający za spożytkowanie energii stanów singletowych na oczekiwaną emisję promieniowania, a nie na przykład degradację wiązań chemicznych emitera i jego otoczenia. Drugą generację stanowią emitery fosforescencyjne, w których emisja zachodzi ze stanów trypletowych.[17] Są to najczęściej związki koordynacyjne metali ciężkich, które wykazują zdolność do promienistej rekombinacji stanów trypletowych dzięki sprzężeniu spinowo-orbitalnemu, którego występowanie jest charakterystyczne dla pierwiastków o dużej liczbie atomowej. Dzięki temu są one w stanie osiągać teoretyczną wydajność kwantową na poziomie 100 %.[18] Z kolei do wad tej klasy emiterów należy zaliczyć dłuższe czasy życia stanów wzbudzonych względem emiterów fluorescencyjnych (rzędu mikrosekund) oraz przede wszystkim, wysokie koszty wytwarzania tego typu emiterów wynikające z cen metali ciężkich w nich zawartych. Najnowszą, trzecią generację stanowią emitery TADF, bazujące na zjawisku termicznie aktywowanej opóźnionej fluorescencji. Jest to rodzina emiterów czysto organicznych lub kompleksów metali przejściowych, w których emisja zachodzi wyłącznie ze stanów singletowych, a stany trypletowe mogą zostać do nich przekonwertowane.[19] Efekt taki osiąga się poprzez specjalnie zaprojektowaną strukturę chemiczną, mającą na celu zminimalizowanie nakładania poziomów HOMO i LUMO. Skutkuje to niewielką różnicą energii stanów singletowych i trypletowych tak, że możliwe jest odwrócone przejście międzysystemowe aktywowane energią termiczną (RISC). Zaletą emiterów TADF jest możliwość uzyskania wewnętrznej wydajności kwantowej na poziomie 100 % oraz wyeliminowanie kosztownych metali szlachetnych w przypadku struktur czysto organicznych, aczkolwiek w ostatnich latach na popularności zyskały m.in. emitery TADF na bazie złota.[20-22] Funkcja stanu trypletowego jako magazynu energii stanowi jednocześnie największy mankament tego typu emiterów, gdyż skutkuje to bardzo długimi czasami życia stanów wzbudzonych (rzędu kilku do nawet kilkuset mikrosekund), co w konsekwencji może prowadzić do szybko postępującej degradacji cząsteczek emitera. Nadzieje pokładane w emiterach TADF na przełamanie impasu w konstrukcji jednocześnie wydajnych oraz stabilnych niebieskich diod jak dotąd nie zostały zrealizowane, właśnie ze względu na niestabilność tych emiterów spowodowaną relatywnie długimi czasami życia ich stanów wzbudzonych.[23] Bilans powyższych wad i zalet poszczególnych klas emiterów powoduje, że wszystkie z nich są nadal intensywnie badane i rozwijane.

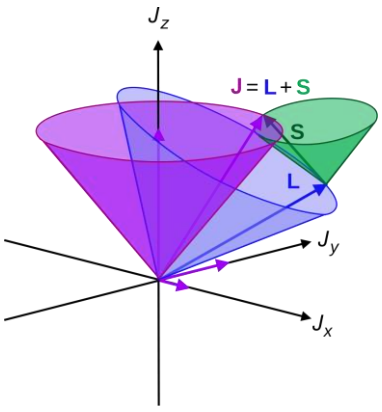

Rys. 4. *Ilustracja sprzężenia spinowo-orbitalnego (J – całkowity moment pędu, L – orbitalny moment pędu, S – spinowy moment pędu).*

Jak wspomniano wcześniej, jako emitery fosforescencyjne najczęściej służą związki zawierające metale ciężkie, między innymi pallad, ruten, iryd, platynę, osm.[24] Jest to podyktowane występowaniem silnego sprzężenia spinowo-orbitalnego umożliwiającego promieniste wykorzystanie energii zarówno stanów singletowych, jak i trypletowych (Rys. 4).[25] Spośród znanych emiterów fosforescencyjnych, na szczególną uwagę zasługują cyklometalowane związki koordynacyjne irydu(III), ponieważ charakteryzują się one szeregiem cech, które uczyniły je najczęściej badanymi materiałami pod kątem zastosowań optoelektronicznych wśród kompleksów wszystkich ciężkich metali przejściowych.[26] Do ich zalet można zaliczyć: bardzo dużą różnorodność w projektowaniu ich struktur, przestrajalność barwy emisji w szerokim zakresie, przynależność do szóstego szeregu układu okresowego faworyzująca zniesienie degeneracji orbitali 5d, wysokie wydajności kwantowe emisji, możliwość wpływania na czas życia stanów trypletowych, odporność na foto-, termo- oraz chemodegradację. Większość tych cech jest determinowana jedną z najwyższych liczb atomowych irydu wśród stabilnych pierwiastków, która odpowiada za relatywnie krótkie czasy życia stanów wzbudzonych oraz wysokie wydajności kwantowe, poprzez silne sprzężenie spinowo-orbitalne. Ponadto, typowa liczba koordynacyjna wynosząca 6 na III stopniu utlenienia stwarza możliwość przyłączania wielu różnych ligandów, które pozwalają modyfikować barwę emitowanego światła (Rys. 5).[26]

Rys. 5. *Ilustracja możliwości przestrajania emisji kompleksów irydu(III) w zależności od ich budowy.*[27]

Jednym z pierwszych kompleksów irydu(III), który zainicjował tak duże zainteresowanie związkami tego metalu w kontekście ich zastosowań jako emiterów fosforescencyjnych, był *fac*-[Ir(ppy)$_3$].[28] Wynikało to właśnie z bardzo dużej wydajności kwantowej emisji, sięgającej aż 97 %, w powiązaniu z relatywnie krótkim czasem życia stanu wzbudzonego.[29] Od tego czasu otrzymanych i przebadanych zostało wiele kompleksów wyposażonych w ligandy ppy oraz jego pochodne, z uwzględnieniem kompleksów homoleptycznych oraz heteroleptycznych, zarówno neutralnych, jak i jonowych.[30] Oprócz tego, opracowano także wiele innych ligandów cyklometalujących, między innymi pochodnych fenylopirydyny, 2-tiofen-2-ylopirydyny, 1-fenyloizochinoliny, regioizomerów fenylotriazoli, *N*-fenyloimidazolu, *N*-fenylobenzimidazolu i wiele, wiele innych.[31-35] Badania kompleksów w nie wyposażone udowodniły bardzo szeroką przestrajalność właściwości emiterów w zależności od struktury chemicznej liganda. Struktury przykładowych irydowych emiterów przedstawiono na Rys. 6, a zainteresowanemu czytelnikowi należy polecić książkę zatytułowaną *Iridium(III) in Optoelectronic and Photonics Applications* pod redakcją E. Zysmana-Colmana, która stanowi niezwykle obszerne i wyczerpujące kompendium wiedzy na temat związków koordynacyjnych irydu stosowanych w optoelektronice.[26]

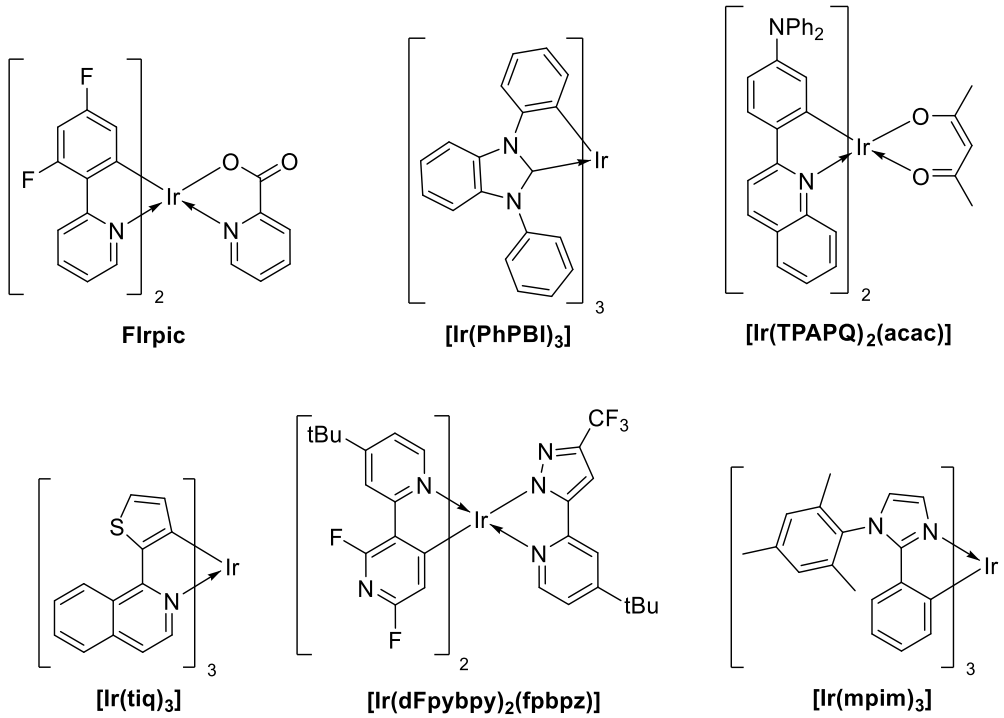

Rys. 6. *Przykłady znanych kompleksów irydu(III) o właściwościach elektroluminescencyjnych.*[26]

Analizując zebraną literaturę dostrzeżono pewną lukę, którą był bardzo ubogi stan wiedzy (na dzień rozpoczęcia badań) na temat kompleksów irydu(III) wyposażonych w analogiczne do 2-fenylopirydynianowych, ligandy benzo[*h*]chinolinianowe. Było to tym bardziej zastanawiające, że kompleksy irydu(III) zawierające skoordynowany ligand bzq były jednymi z pierwszych dwurdzeniowych otrzymanych przez Nonoyamę już w 1974 roku.[36] Jeśli chodzi o kompleksy monordzeniowe, to znane były wyłącznie [Ir(bzq)$_2$(acac)] oraz [Ir(bzq)$_3$] (Rys. 7).[37,38] Temat ten wydawał się interesujący z powodu podobnego rozmiaru kieszeni koordynacyjnej benzo[*h*]chinoliny i 2-fenylopirydyny, ale także znacznie sztywniejszej struktury i większego stopnia koniugacji tej pierwszej, co mogło mieć istotny wpływ na właściwości kompleksów wyposażonych w tego typu ligand.

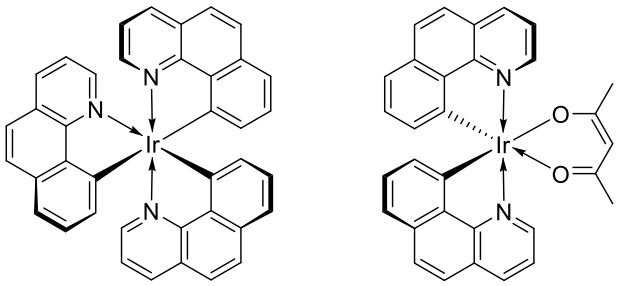

Rys. 7. *Struktury kompleksów irydu(III) z ligandem bzq znanych na dzień rozpoczęcia badań.*

Pierwotnie w roli emiterów OLED badane były głównie związki neutralne, jednak z czasem obiektem zainteresowania naukowców zaczęły się stawać także kompleksy jonowe wyposażone w ligandy *C,N*-cyklometalujące oraz *N,N*-donorowe ligandy pomocnicze. Badania te w dużej mierze obejmowały związki osmu,[39,40] rutenu[37,41-46] oraz renu.[47,48] Jeśli chodzi o jonowe związki irydu(III), to były one głównie badane w kontekście ich zastosowania w roli markerów fluorescencyjnych[49-53] oraz emiterów w urządzeniach LEEC.[54-56]

Jednym z pierwszych kompleksów irydu przebadanym w roli emitera OLED był $[Ir(ppy)_2(dtbbpy)]PF_6$, przedstawiony na Rys. 8.[57] Rozwój tematyki miękkich soli irydu(III) był sukcesywnie kontynuowany przez innych badaczy, prowadząc do poszerzenia wiedzy na ich temat i raportowania urządzeń OLED o coraz lepszych parametrach.[58-60] W tym miejscu należy podkreślić, że postęp w tej dziedzinie nie obejmował związków zawierających skoordynowany ligand bzq.

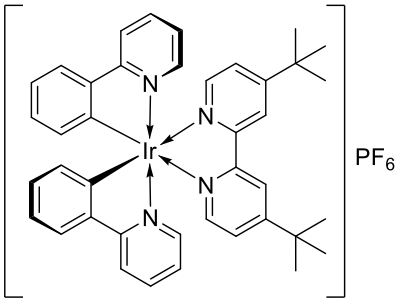

$[Ir(ppy)_2(dtbbpy)]PF_6$

Rys. 8. *Jeden z pierwszych cyklometalowanych kationowych irydowych emiterów OLED.*

Także neutralne kompleksy heteroleptyczne wyposażone w różnorodne ligandy pomocnicze, przykładowo *O,O*- oraz *N,O*-donorowe (Rys. 9), stanowią ciekawą grupę związków koordynacyjnych, zwłaszcza w kontekście ich wykorzystania jako emiterów fosforescencyjnych. Szczególnie intensywnie eksploatowana była tematyka kompleksów acetyloacetonianowych, z uwagi na łatwość ich syntezy względem kompleksów homoleptycznych.[37,61-63] Na uwagę zasługują także kompleksy wyposażone w ligand 8-hydroksychinolinianowy[6,64,65] oraz pikolinianowy, obecny na przykład w strukturze najbardziej popularnego jasnoniebieskiego emitera, czyli FIrpic.[66] Ewolucję ligandów acetyloacetonianowych w kierunku układów *N,O*-chelatowych mogły stanowić *β*-ketoiminiany (Rys. 9d). Wykorzystanie *N,O*-donorowego liganda *β*-ketoiminianowego ma zaletę, którą jest możliwość wpływania na gęstość elektronową bezpośrednio na atomie *N*-donorowym poprzez syntetycznie łatwą zmianę podstawnika R. W momencie rozpoczęcia realizacji projektu kompleksy irydu(III) zawierające tego typu ligandy nie były w ogóle znane, a prace Teetsa dotyczące tego zagadnienia pojawiły się kilka lat później,[67,68] potwierdzając słuszność obranego przez nas kierunku badań, gdyż w opublikowanych artykułach szczegółowo omówiono szereg bardzo ciekawych zależności pomiędzy strukturą liganda pomocniczego a właściwościami badanych kompleksów. Jednakże, w literaturze nie były dostępne żadne doniesienia na temat *β*-ketoiminianowych kompleksów irydu(III) zawierających w swojej strukturze ligand bzq.

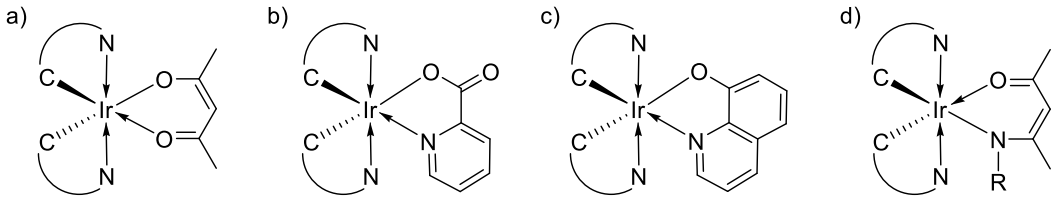

Rys. 9. *Schematyczne przedstawienie związków koordynacyjnych irydu(III) wyposażonych w acetyloacetonianowy (a), pikolinianowy (b), 8-hydroksychinolinianowy (c) oraz β-ketoiminianowy ligand pomocniczy (d).*

Na uwagę zasługuje także aspekt chemicznej modyfikacji cyklometalującego liganda, mający na celu przestrajanie emisji poprzez zmianę poziomów energetycznych HOMO i LUMO. Fundamentem do tych rozważań jest nierównomierne rozmieszczenie orbitali HOMO i LUMO w cząsteczce emitera irydowego, ukazane na przykładzie kompleksu *fac*-$[Ir(ppy)_3]$ na Rys. 10. W przypadku *C,N*-cyklometalowanych emiterów

irydowych poziomy HOMO zwyczajowo są zlokalizowane głównie na atomie centralnym oraz ligandzie cyklometalującym (z przesuniętym środkiem ciężkości w kierunku części *C*-donorowej), z kolei poziomy LUMO są zlokalizowane na ligandzie cyklometalującym lub ligandzie pomocniczym. Dzięki takiemu stanowi rzeczy, istnieje możliwość selektywnego wpływania na poziomy energetyczne orbitali granicznych poprzez umieszczanie podstawników o różnych właściwościach elektronowych w odpowiednich pozycjach szkieletu liganda. Za najlepszy przykład może tu posłużyć zdecydowanie najbardziej rozpoznawany jasnoniebieski emiter FIrpic, zawierający dwa *C,N*-cyklometalujące ligandy 2-(4,6-difluorofenylo)pirydynianowe oraz jeden pikolinianowy ligand pomocniczy.[69,70] Przyczyną jasnoniebieskiej emisji tego kompleksu jest właśnie obecność atomów fluoru przy pierścieniach fenylowych, która powoduje stabilizację w dużej mierze zlokalizowanego w ich regionie poziomu HOMO, przy znacznie mniejszym wpływie na poziom LUMO. W efekcie, przerwa energetyczna HOMO-LUMO ulega zwiększeniu względem kompleksu pozbawionego atomów fluoru.

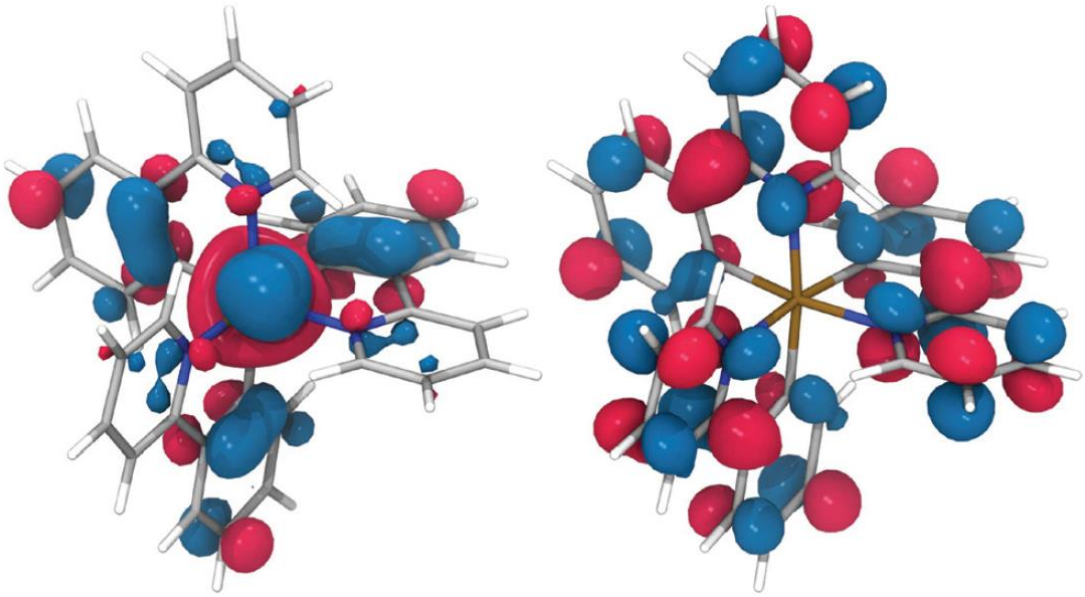

Rys. 10. *Wizualizacje poziomów HOMO (lewo) oraz LUMO (prawo) dla kompleksu fac-[Ir(ppy)$_3$].*[71]

Wpływ ten został wyjaśniony efektami elektronowymi wywieranymi przez podstawniki przy pierścieniu aromatycznym, który można mierzyć przy pomocy parametrów Hammetta. Na bazie tej koncepcji został opracowany model pozwalający przewidywać przesunięcie emisji kompleksów w zależności od typu i miejsca przyłączenia do liganda różnych podstawników.[71] Intrygujące byłoby przeprowadzenie podobnych rozważań dla kompleksów wyposażonych w ligand bzq.

Próby przewidywania wpływu modyfikacji chemicznej liganda bzq skoordynowanego do atomu irydu, przy pomocy obliczeń kwantowo-chemicznych, zostały już przeprowadzone i opublikowane.[72] Przedmiotem rozważań zawartych w cytowanym artykule były rezultaty badań teoretycznych nad izomerami *mer* oraz *fac* homoleptycznych kompleksów irydu(III), w których ligand cyklometalujący wyposażono w podstawniki o charakterze elektronodonorowym (metoksy, fenoksy, dimetyloamino), elektronoakceptorowym (fluoro, pentafluorofenylo) oraz wspomagających transport dziur elektronowych (4-(*N*-difenyloamino)fenylo)), zaprezentowanych na Rys. 11. Najbardziej istotnym parametrem poruszanym w omawianej publikacji, z perspektywy zastosowań optoelektronicznych tego typu materiałów, było rozmieszczenie HOMO i LUMO oraz położenie ich poziomów energetycznych. Parametry te determinują wartość przerwy energetycznej i są bardzo pomocne przy formułowaniu strategii mającej na celu zmianę E_g poprzez modyfikacje struktury chemicznej liganda, a tym samym również docelowego kompleksu.

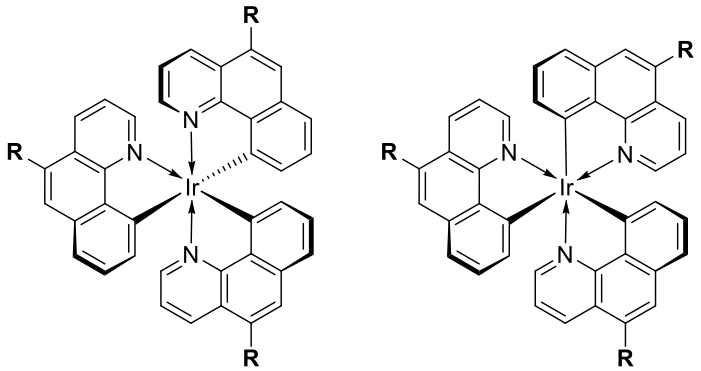

R = H (**1**), F (**2**), OMe (**3**), OPh (**4**), NMe_2 (**5**), C_6F_5 (**6**), *p*-C_6H_4-NPh_2 (**7**)

Rys. 11. *Struktury chemiczne badanych kompleksów bazujących na rdzeniu [Ir(bzq)$_3$].*

Najprostszym modelem do zilustrowania tego przykładu był niemodyfikowany kompleks [Ir(bzq)$_3$] (**1**), a konkretnie jego izomer facjalny, w którym wszystkie ligandy są równoważne chemicznie. Rzut na płaszczyznę jednego z ligandów w takim kompleksie z nałożonymi wizualizacjami orbitali granicznych przedstawiono na Rys. 12. Przyglądając się temu rysunkowi zauważyć można, że rozmieszczenie HOMO i LUMO jest nierównomierne. HOMO w głównej mierze jest zlokalizowany na pierścieniu *C*-donorowym liganda oraz atomie centralnym, z kolei LUMO głównie obejmuje fragment *N*-donorowy liganda oraz środkowy pierścień łączący. Takie rozmieszczenie orbitali w obrębie cząsteczki stwarza możliwość relatywnie selektywnego oddziaływania na nie poprzez dokonywanie chemicznej modyfikacji liganda w określonych pozycjach. Biorąc pod uwagę aspekt syntetyczny, czyli możliwość funkcjonalizacji benzo[*h*]chinoliny w pozycji 5, do dalszych rozważań teoretycznych wybrano właśnie pochodne funkcjonalizowane w tej pozycji. Było to jak najbardziej uzasadnione w oparciu o przedstawiony na Rys. 12 model, który wskazywał na możliwość silniejszego oddziaływania podstawników wprowadzonych w tej pozycji na wartość energii LUMO, aniżeli HOMO.

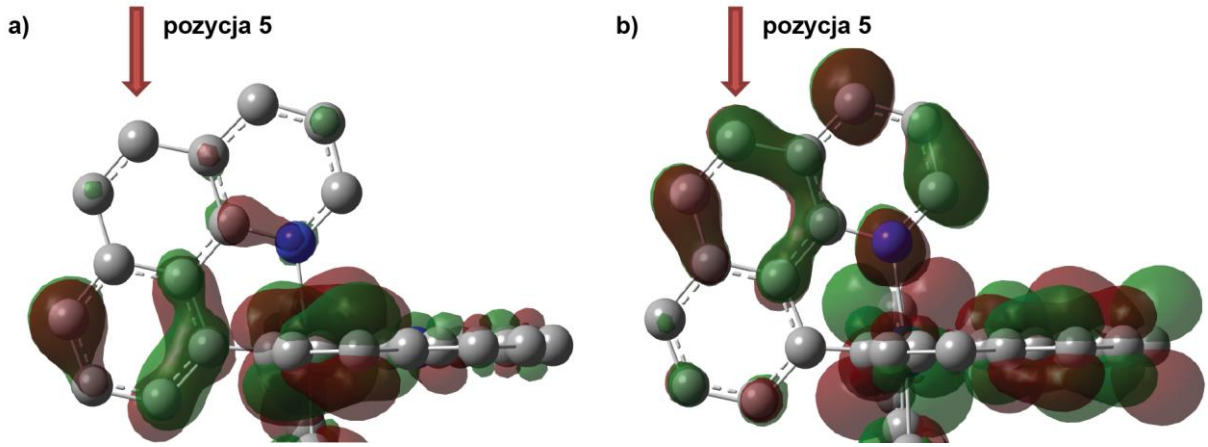

Rys. 12. *Rzut na płaszczyznę jednego z ligandów w fac-[Ir(bzq)$_3$] z nałożoną wizualizacją HOMO (a) i LUMO (b). Strzałką oznaczono lokalizację pozycji 5 liganda.*

Analizując otrzymane dane stwierdzono, że obliczone poziomy energetyczne są zależne od struktury chemicznej liganda. Oczywiście, wyników tych obliczeń nie należy interpretować w sposób bezwzględny, lecz w sposób porównawczy, najlepiej w odniesieniu do związku modelowego dla całej serii (**1**). Przyłączenie grup zawierających atomy fluoru (kompleksy **2** oraz **6**) powodowało zauważalne obniżenie poziomów energetycznych HOMO i LUMO. Był to efekt jak najbardziej spodziewany, gdyż podstawniki

elektronowyciągające powinny przesuwać gęstość elektronową w swoim kierunku, prowadząc do stabilizacji pobliskiego orbitalu. Stabilizacja ta była bardziej widoczna w przypadku LUMO niż HOMO, co potwierdza zróżnicowany wpływ podstawników elektronowyciągających w pozycji 5 na poziomy energetyczne obydwu typów orbitali granicznych badanych kompleksów. W przypadku podstawników elektronodonorowych (kompleksy **3**, **4**, **5** oraz **7**) stwierdzono odwrotny efekt. Mianowicie, powodowały one podwyższenie poziomów energetycznych względem referencyjnego kompleksu **1**. Jest to zgodne z oczekiwaniami, gdyż tego typu podstawniki powinny przesuwać gęstość elektronową w kierunku liganda, skutkując destabilizacją orbitali zlokalizowanych w jego obrębie. Obliczenia teoretyczne wykazały także, że każda proponowana zmiana struktury chemicznej liganda, niezależnie od charakteru elektronowego przyłączanego podstawnika, powinna przynajmniej w minimalnym stopniu obniżać przerwę energetyczną, tym samym powodując batochromowe przesunięcie maksimów absorpcji i emisji kompleksów wyposażonych w proponowane podstawniki. Przypuszcza się, że jest to związane ze zwiększeniem koniugacji, co w przypadku związków organicznych zwykle prowadzi do obniżenia wartości przerwy HOMO-LUMO. Ponadto, stwierdzono ogólną zależność polegającą na wyróżnianiu się izomerów *fac* większą wartością przerwy energetycznej od ich odpowiedników *mer*, co jest zgodne z danymi literaturowymi dla kompleksów zawierających pochodne ppy.[62] Konkluzją pracy było stwierdzenie zasadności funkcjonalizacji liganda benzo[*h*]chinolinianowego, gdyż strategia ta mogłaby się okazać przydatna w otrzymywaniu kompleksów irydu(III) o ciekawych właściwościach fosforescencyjnych.

Monordzeniowe kompleksy irydu(III) są często obiektem badań pod względem możliwości ich zastosowań jako biosensory, fotokatalizatory oraz emitery fosforescencyjne.[26,73,74] Wśród ostatnich najciekawszych doniesień na ten temat można wyróżnić artykuły opisujące panele OLED zbudowane z oligomerycznych łańcuchów zawierających kompleksy irydu(III) w roli emiterów oraz mediatorów polimeryzacji;[75] kompleksy irydu(III) o właściwościach mechanochromowych, mogących służyć jako mechaniczne lub chemiczne sensory;[76,77] oraz nietoksycznych związków służących do barwienia komórek rakowych szyjki macicy.[78] Zdecydowanie najpopularniejszą drogą syntezy tego typu materiałów jest rozszczepienie μ-chlorkowych dwurdzeniowych cyklometalowanych kompleksów irydu(III) o ogólnym wzorze $[Ir(C\hat{}N)_2(\mu\text{-}Cl)]_2$ z użyciem prekursora dodatkowego liganda, w obecności odpowiedniej zasady. Analizując literaturę na ten temat zauważono, jak nieproporcjonalnie mało uwagi jest poświęcane tym ważnym związkom pośrednim, biorąc pod uwagę ich kluczową rolę w wielu szlakach syntetycznych. Fakt ten wynika głównie z małego zainteresowania dimerami samymi w sobie, a traktowaniem ich jako związki pośrednie w syntezie bardziej złożonych układów koordynacyjnych. W wielu przypadkach było to przyczyną pomijania wydajności syntez dimerów, a nawet brakiem ich charakterystyki spektroskopowej, co z czasem stało się dość powszechną praktyką.[37,62,79-81] Jednakże, utrudnia to ocenę skuteczności metod ich otrzymywania, a także rzutuje na wydajności końcowych produktów dłuższych szlaków syntetycznych, co ma niebagatelne znaczenie z powodu ceny irydu i jego związków. Syntezy tego typu dimerów zwyczajowo prowadzi się ogrzewając chlorek irydu oraz prekursor liganda w mieszaninie alkoholu z wodą (Rys. 13). Wadą wielu opisanych preparatyk jest umiarkowana wydajność otrzymywanych produktów, długi czas reakcji (do 48 godzin), relatywnie duże ilości stosowanych rozpuszczalników, a w nielicznych przypadkach konieczność oczyszczania produktu przy pomocy chromatografii flash.[82-89] Wszystko to sprawia, że opracowanie uniwersalnej i skutecznej metody syntezy tego typu związków jest nadal pożądane. Możliwość zniwelowania wyżej wymienionych mankamentów oferuje wykorzystanie pozytywnego wpływu promieniowania mikrofalowego na przebieg reakcji cyklometalacji, co zostało potwierdzone we wcześniejszych doniesieniach literaturowych na ten temat.[90-92] Niestety, opisane w nich warunki rekcji nie tworzą spójnego obrazu i brak w nich wyraźnego porównania wpływu mikrofal na przebieg reakcji względem innych klasycznych źródeł ciepła.

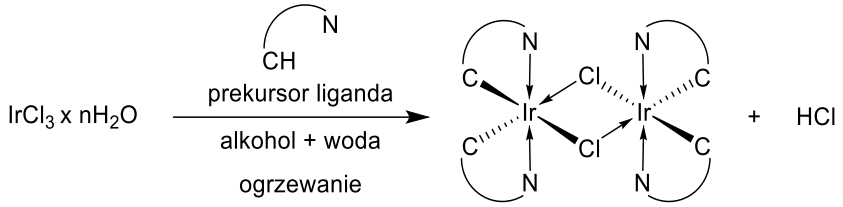

Rys. 13. *Ogólny schemat najpopularniejszej reakcji tworzenia μ-chlorkowych dwurdzeniowych kompleksów irydu(III).*

Ponadto, jak dotąd nie został wyjaśniony wpływ wody na przebieg reakcji cyklometalacji, a jedynie odnotowano konieczność jej stosowania w praktycznie każdej opisanej metodologii.[93] Wobec powyższego, szczególnie interesujące byłoby zgłębienie problematyki syntezy dimerów w warunkach wspomagania promieniowaniem mikrofalowym, opracowanie efektywnej metodologii otrzymywania μ-chlorkowych dimerów, określenie wpływu dodatku wody na przebieg reakcji oraz przy okazji otrzymanie nowych związków wyposażonych w ligandy zawierające różne grupy funkcyjne, które stanowiłyby atrakcyjne prekursory do dalszych przekształceń.

Konkludując wstęp literaturowy, wykazano w nim spory potencjał do zgłębienia tematyki kompleksów irydu(III) zawierających w swojej strukturze ligandy benzo[*h*]chinolinianowe. Ponadto, szeroki wachlarz możliwości stwarza funkcjonalizacja benzo[*h*]chinoliny i wykorzystanie jej pochodnych w syntezie nowych cyklometalowanych związków irydu(III), których właściwości mogą uczynić je przydatnymi w optoelektronice oraz bioobrazowaniu.

6. Cel pracy i uzasadnienie podjęcia tematyki badawczej

W przedstawionym przeglądzie literaturowym wykazano, że związki koordynacyjne irydu(III) zawierające w swojej strukturze ligandy bzq mogą cechować się ciekawymi właściwościami elektroluminescencyjnymi, które można modyfikować poprzez zmianę otoczenia koordynacyjnego jonu irydu. W związku z powyższym, za cel pracy obrano zaprojektowanie struktur i opracowanie metod otrzymywania nowych irydowych emiterów zawierających bzq jako główny ligand *C,N*-cyklometalujący oraz określenie relacji pomiędzy strukturą chemiczną, a właściwościami fotofizycznymi, elektroluminescencyjnymi, elektrochemicznymi i spektroskopowymi otrzymanych związków koordynacyjnych. Badania podjęte w ramach niniejszej pracy obejmowały syntezę i interpretację wyników badań następujących klas związków:

- Kompleksów jonowych o ogólnym wzorze $[Ir(bzq)_2(N\hat{}N)]^+A^-$, wyposażonych w strukturalnie zróżnicowane ligandy *N,N*-donorowe [**P1**]
- Kompleksów obojętnych typu $[Ir(bzq)_2(N\hat{}O)]$, stabilizowanych β-ketoiminianowymi ligandami funkcjonalizowanymi atomami fluoru [**P2**]
- Kompleksów obojętnych o wzorze ogólnym $[Ir(bzq)_2(N\hat{}O)]$, stabilizowanych β-ketoiminianowymi ligandami podstawionymi różnorodnymi ugrupowaniami arylowymi [**P3**]

Ponadto, prace badawcze podjęte w ramach niniejszej dysertacji objęły swoim zakresem także syntezę nowych pochodnych benzo[*h*]chinoliny oraz zademonstrowanie ich potencjału aplikacyjnego w syntezie *C,N*-cyklometalowanych kompleksów irydu(III). Wyniki tych prac otwierają możliwość oceny wpływu modyfikacji struktury chemicznej *C,N*-donorowych ligandów w przyszłych badaniach właściwości elektroluminescencyjnych. Prace te obejmowały następujące zagadnienia:

- Opracowanie efektywnych metod otrzymywania nowych pochodnych benzo[*h*]chinoliny, jako potencjalnych prekursorów ligandów dla emiterów fosforescencyjnych [**P4**]
- Opracowanie efektywnej metody syntezy dwurdzeniowych kompleksów irydu(III) o strukturze $[Ir(C\hat{}N)_2(\mu\text{-}Cl)]_2$ z użyciem nowych ligandów będących pochodnymi bzq oraz badania ich zachowania w rozpuszczalnikach koordynujących [**P5**]
- Syntezę nowych kompleksów irydu(III) o strukturach $[Ir(C\hat{}N)_2(N\hat{}N)]^+A^-$ oraz $[Ir(C\hat{}N)_3]$, wyposażonych w nowe ligandy będące pochodnymi bzq [**materiał nieopublikowany**]

Sformułowane cele były realizowane w ramach projektu OPUS 6 pt. *Nowe emitery fosforescencyjne dla organicznych diod elektroluminescencyjnych*, w grupie Prof. UAM dr hab. Ireneusza Kownackiego (kierownika projektu). Realizacja projektu była prowadzona we współpracy z grupami badawczymi: Prof. dr hab. inż. Jacka Ulańskiego z Katedry Fizyki Molekularnej Politechniki Łódzkiej, odpowiedzialną za badania fotofizyczne, wytwarzanie i charakterystykę diod (Dr inż. Ewelina Witkowska, Dr inż. Gabriela Wiosna-Sałyga, Dr hab. inż. Ireneusz Głowacki, Dr hab. inż. Beata Łuszczyńska); Prof. dr hab. Mieczysława Łapkowskiego z Katedry Fizykochemii i Technologii Polimerów Politechniki Śląskiej, odpowiedzialną za badania elektrochemiczne (Dr inż. Przemysław Ledwoń); Prof. dr hab. Marcina Hoffmanna z Zakładu Chemii Kwantowej Uniwersytetu im. Adama Mickiewicza, odpowiedzialną za obliczenia kwantowo-chemiczne (Dr inż. Izabela Grzelak) oraz Prof. dr hab. Macieja Kubickiego z Zakładu Krystalografii Uniwersytetu im. Adama Mickiewicza, odpowiedzialną za analizę rentgenostrukturalną. Analiza wyników uzyskanych przez współpracowników stanowi nieodłączne dopełnienie założonych celów syntetycznych niniejszej pracy. Udział w projekcie wymagał nadawania kierunku prowadzonym badaniom oraz koordynowania wyników pracy wszystkich zespołów, z uwagi na nadrzędną rolę grupy Prof. UAM dr hab. Ireneusza Kownackiego oraz fakt, iż analiza jakichkolwiek materiałów wymagała w pierwszej kolejności ich otrzymania. Opis realizacji zadań leżących u podstaw przedstawionej dysertacji został zawarty w kolejnych paragrafach.

7. Omówienie publikacji będących podstawą rozprawy

7.1. Jonowe związki kompleksowe o strukturze $[Ir(bzq)_2(N^N)]^+A^-$

Pierwszy artykuł przedstawionego cyklu [**P1**] porusza zagadnienie jonowych kompleksów irydu(III) stabilizowanych dwoma ligandami bzq i jednym ligandem *N,N*-donorowym. Ideą pracy było przeprowadzenie syntez związków koordynacyjnych irydu(III) oraz skorelowanie ich właściwości fotofizycznych, elektrochemicznych oraz elektroluminescencyjnych ze strukturą oraz właściwościami elektronowymi liganda pomocniczego. Związki zawierające komercyjnie dostępne pochodne 2,2'-bipirydyny oraz 1,10-fenantroliny zostały otrzymane w układzie *one-pot* z wykorzystaniem wspomagającego wpływu promieniowania mikrofalowego (Rys. 14).

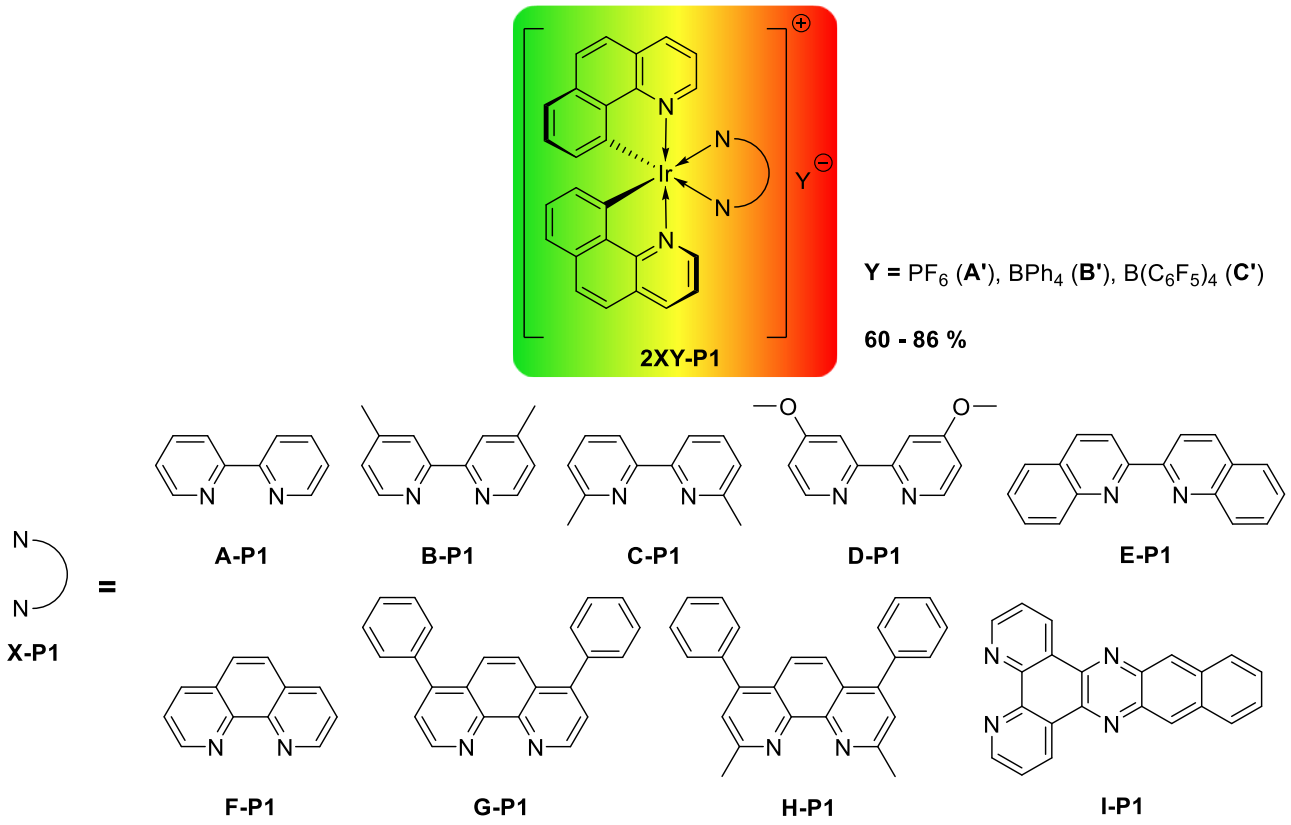

Rys. 14. *Schematyczne przedstawienie związków analizowanych w pracy [**P1**].*

Związki koordynacyjne irydu(III) o podobnej budowie były jak dotąd badane głównie pod kątem zastosowania jako markery fluorescencyjne w układach biologicznych[49,50,52,53,94] oraz jako emitery w urządzeniach typu LEEC.[54,55] Potencjał aplikacyjny w tych dziedzinach opierał się na jonowym charakterze tych związków, który czynił je rozpuszczalnymi w polarnych rozpuszczalnikach (takich jak woda) oraz przewodzącymi prąd elektryczny ich roztworów w skutek dysocjacji. Niemniej jednak, w literaturze można było napotkać także nieliczne doniesienia opisujące zastosowanie tego typu jonowych układów fosforescencyjnych w konstrukcji OLEDów, jak miało to miejsce w przypadku $[Ir(ppy)_2(dtbbpy)]PF_6$.[57] Większość związków irydu(III) o właściwościach elektroluminescencyjnych opisanych w przytoczonych powyżej źródłach stabilizowana była ppy lub jej pochodnymi jako ligandami *C,N*-cyklometalującymi, podczas gdy w przypadku markerów biologicznych, przebadane zostało szersze spektrum ligandów obejmujące także bzq. W związku z tym, postanowiono otrzymać oraz gruntownie zbadać kompleksy irydu(III) stabilizowane

dwoma ligandami bzq oraz jednym *N,N*-donorowym ligandem pomocniczym, ukierunkowując pracę na ich zastosowanie w konstrukcji OLEDów. Skorelowano przy tym wpływ budowy chemicznej emiterów na ich właściwości fotofizyczne, elektrochemiczne, termiczne oraz elektroluminescencyjne.

Badania rozpoczęto od przeprowadzenia syntez docelowych związków koordynacyjnych. W początkowej fazie prac odwołano się do literaturowych metod, według których kompleksy o podobnej strukturze były zazwyczaj otrzymywane dwuetapowo.[50,95-105] Pierwszy z nich obejmował reakcję dwurdzeniowego μ-chlorkowego kompleksu irydu(III) o strukturze $[Ir(C^N)_2(\mu\text{-}Cl)]_2$ z ligandem *N,N*-donorowym, dając kompleks o strukturze $[Ir(C^N)_2(N^N)]Cl$. Drugim etapem była wymiana anionu chlorkowego z zewnętrznej sfery koordynacyjnej na inny docelowy anion. Zasadniczą wadą tego szlaku syntetycznego była jego czaso- i pracochłonność, wynikająca z konieczności izolacji oraz oczyszczania produktu pośredniego. Ponadto, wydajności otrzymywanych w ten sposób związków z użyciem zatłoczonych sterycznie ligandów pomocniczych bywały relatywnie niskie. W tych niedogodnościach dostrzeżono możliwość zmniejszenia nakładu pracy na syntezę docelowych materiałów poprzez przeprowadzenie reakcji zgodnie z ideą *one-pot*, polegającą na skondensowaniu dwóch reakcji chemicznych do jednej operacji, poprzez umieszczenie wszystkich wymaganych komponentów w tym samym naczyniu reakcyjnym, w tym samym czasie (Rys. 15).

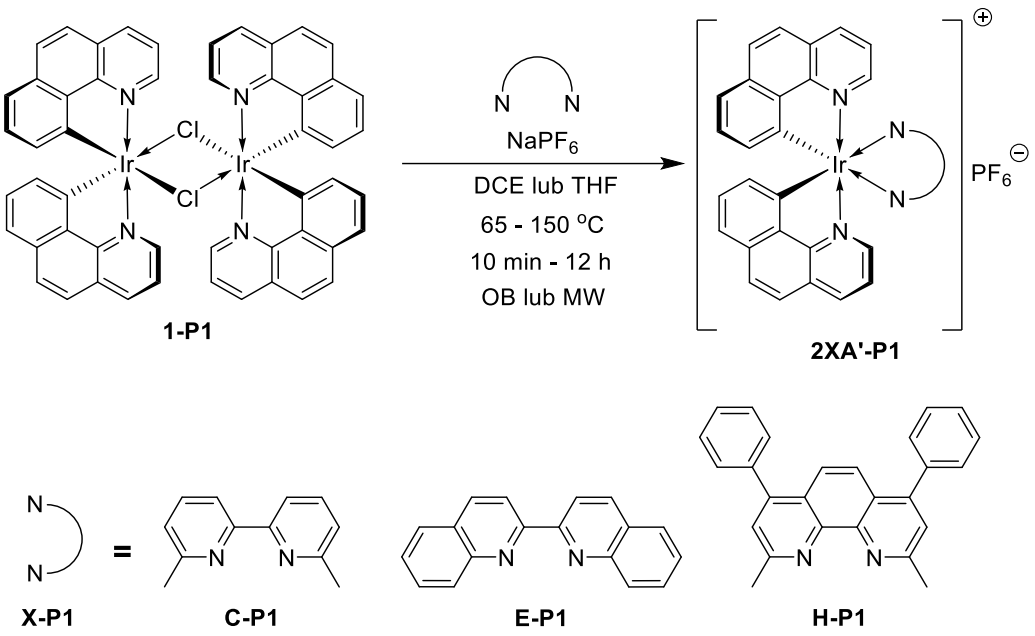

Rys. 15. *Schemat procesu one-pot prowadzącego do otrzymania docelowych kompleksów irydu(III).*

Do testów wyselekcjonowano dwa rozpuszczalniki (DCE i THF) oraz ligandy o relatywnie dużej zawadzie sterycznej, czyli 6,6-dimetylo-2,2-bipirydynę (**C-P1**), 2,2-bischinolinę (**E-P1**) i 2,9-dimetylo-4,7-difenylo-1,10-fenantrolinę (**H-P1**). Pierwsze rezultaty nie były obiecujące, gdyż uzyskano jedynie zanieczyszczone produkty (stwierdzone przy pomocy analizy ^{1}H NMR), w dodatku z niewielkimi wydajnościami (Tabela 1). W obliczu tego niepowodzenia postanowiono spróbować przeprowadzenia reakcji testowej w reaktorze mikrofalowym, w oparciu o potwierdzone pozytywne efekty zastosowania promieniowania mikrofalowego w syntezie organicznej.[106-113] Reakcje przeprowadzono w temperaturze 150 °C wyłącznie w THF, gdyż jest to rozpuszczalnik lepiej absorbujący mikrofale aniżeli DCE oraz cechujący się właściwościami koordynującymi, co mogło mieć pozytywny efekt na aktywację prekursora **1-P1**. W rezultacie uzyskano znaczącą poprawę efektywności otrzymywania związku **2CA'-P1** w stosunku do reakcji prowadzonej w łaźni olejowej (Tabela 1).

Ponadto, udało się obniżyć molowy nadmiar stosowanego liganda pomocniczego oraz $NaPF_6$ do wartości wynoszącej zaledwie 2,5 %. Opracowane warunki okazały się także skuteczne w syntezie kompleksów **2EA'-P1** oraz **2HA'-P1** względem wcześniejszych prób przeprowadzonych w łaźni olejowej.

Tabela 1. *Parametry reakcji testowych i wydajności uzyskanych produktów.*

Kompleks	Rozpuszczalnik	Stosunek molowy reagentów 1-P1 : Ligand : $NaPF_6$	Temperatura [°C]	Czas [h]	Wydajność [%]
2CA'-P1	DCE	1 : 2.2 : 2.2	65	12	26
	THF	1 : 2.2 : 2.2	65	12	36
		1 : 2.05 : 2.05	150	0.167	12
		1 : 2.05 : 2.05	150	0.167	64*
2EA'-P1	DCE	1 : 2.2 : 2.2	65	12	19
	THF	1 : 2.2 : 2.2	65	12	28
		1 : 2.05 : 2.05	150	0.167	78*
2HA'-P1	DCE	1 : 2.2 : 2.2	65	12	24
	THF	1 : 2.2 : 2.2	65	12	33
		1 : 2.05 : 2.05	150	0.167	77*

* oznacza reakcję przeprowadzoną w reaktorze mikrofalowym

Syntezy pozostałych kompleksów przedstawionych na Rys. 14 przeprowadzono według zoptymalizowanej metodologii, uzyskując docelowe kompleksy z wydajnościami w zakresie 60 – 86 %. Identyfikacji oraz potwierdzenia czystości wszystkich związków dokonano przy użyciu techniki ^{1}H NMR, a struktury dwóch z nich dodatkowo potwierdzono analizą rentgenostrukturalną (Rys. 16).

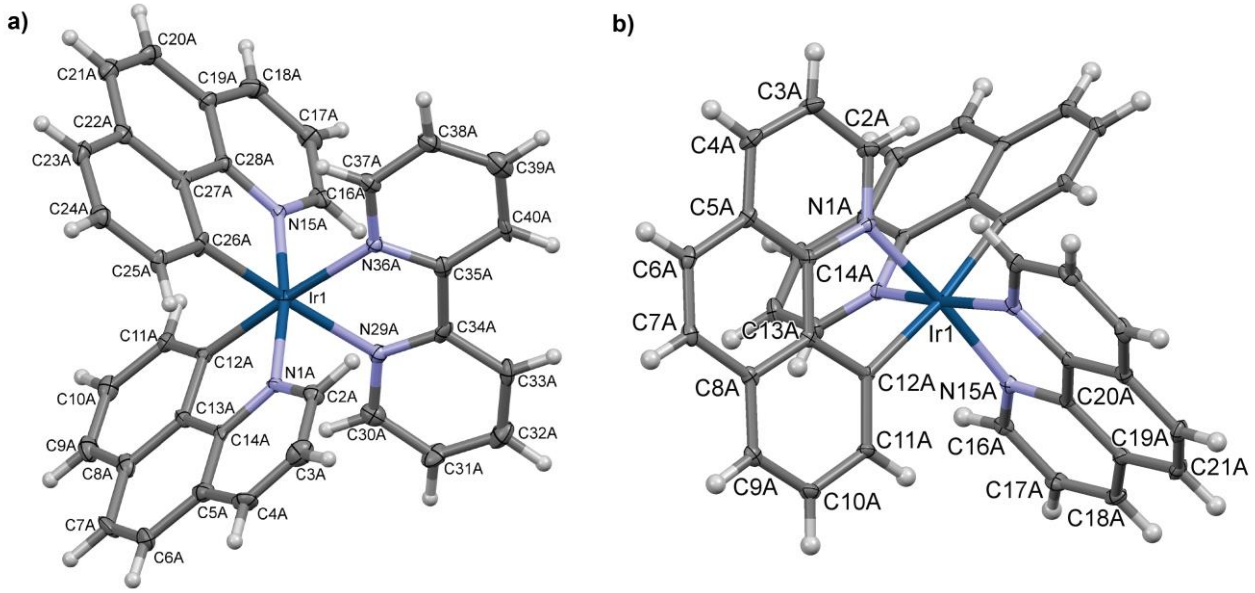

Rys. 16. *Struktury krystaliczne związków* ***2AA'-P1*** *(a) oraz* ***2FA'-P1*** *(b).*

W artykule zamieszczono również rezultaty badań właściwości termicznych otrzymanych kompleksów. Najważniejszym wnioskiem płynącym z analizy termograwimetrycznej było stwierdzenie stabilności badanych związków kwalifikującej je do zastosowania jako emitery dla diod OLED (temperatura ubytku 5 % masy dla wszystkich związków wynosiła powyżej 120 °C, temperatury raczej nieosiągalnej w warunkach pracy diod).

Następnym etapem charakterystyki związków zamieszczonym w publikacji były pomiary woltamperometryczne, mające na celu określenie potencjałów utleniania i redukcji, a tym samym wyznaczenia

IP oraz EA. Wartości te powinny korelować z poziomami energetycznymi HOMO i LUMO. Z badań wykluczono kompleksy **2IA'-P1** oraz wszystkie wyposażone w anion $[BPh_4]^-$, z uwagi na niestabilność związku wyposażonego w ligand **I-P1** oraz obserwację utleniania anionu $[BPh_4]^-$, która zaburzała określenie IP związków kompleksowych z tym przeciwjonem. Wyniki przedstawiono w Tabeli 2.

Tabela 2. *Wyniki charakterystyki elektrochemicznej związków kompleksowych.*

Związek	$E_{ox\ onset}$ [V]	$E_{red\ onset}$ [V]	E_g [eV]	IP [eV]	EA [eV]
2AA'-P1	0.69	-1.71	2.40	5.8	3.4
2BA'-P1	0.47	-1.74	2.21	5.6	3.4
2CA'-P1	0.47	-1.73	2.20	5.6	3.4
2DA'-P1	0.49	-1.75	2.24	5.6	3.4
2EA'-P1	0.47	-1.26	1.73	5.6	3.8
2FA'-P1	0.73	-1.67	2.40	5.8	3.4
2GA'-P1	0.51	-1.66	2.17	5.6	3.4
2HA'-P1	0.41	-1.68	2.09	5.5	3.4

Wyniki badań elektrochemicznych wykazały, że kompleksy wyposażone w 2,2'-bipirydynę (**2AA'-P1**) oraz 1,10-fenantrolinę (**2FA'-P1**) powinny cechować się największą, a kompleks **2EA'-P1** zawierający 2,2-bischinolinę najmniejszą elektrochemiczną przerwą energetyczną (E_g). Z kolei kompleksy wyposażone w pozostałe ligandy wykazywały wartości pośrednie, oscylujące wokół 2.2 eV. Był to dość niespodziewany wynik, gdyż oczekiwano większego zróżnicowania wpływu zmiany liganda pomocniczego na przerwę energetyczną. Z literatury wynikało, że zmiana *N,N*-donorowego liganda powinna głównie modyfikować energię poziomu LUMO kompleksu, gdyż to właśnie w obrębie liganda pomocniczego powinien być zlokalizowany ten orbital. W przeciwieństwie, prawie wszystkie związki charakteryzowały się tym samym EA na poziomie 3.4 eV. Sugerowało to, że w obserwowany proces redukcji najprawdopodobniej nie jest zaangażowany orbital LUMO odpowiedzialny za przejście elektronowe w trakcie emisji promieniowania, a zachodzi inny proces elektrochemiczny, wspólny dla większości struktur. Jedynym wyraźnie wyróżniającym się związkiem był **2EA'-P1**, co można powiązać z największym stopniem koniugacji liganda *N,N*-donorowego, która powodowała znaczne obniżenie energii poziomu LUMO tego kompleksu. Jeśli chodzi o energię poziomu HOMO, to ulegała ona zmianie w zakresie około 0.3 eV, co wynika ze zmiany gęstości elektronowej na atomie centralnym w zależności od charakteru donorowego liganda pomocniczego.

W artykule zamieszczono także rezultaty badań teoretycznych, zmierzających do określenia rozmieszczenia orbitali granicznych oraz przewidywania przerw energetycznych badanych związków kompleksowych. Opracowane wyniki zamieszczono na Rys. 17. Wyników tych nie należy traktować w sposób dosłowny, lecz interpretować w sposób porównawczy, bardziej celem określenia trendu wpływu modyfikacji struktury, niż ustalenia bezwzględnej wartości parametrów. Zgodnie z oczekiwaniami, poziomy HOMO były zlokalizowane na atomie centralnym oraz ligandzie *C,N*-donorowym, z kolei poziomy LUMO na *N,N*-donorowym ligandzie pomocniczym. Ponadto, obliczenia wykonane dla kompleksów będących pochodnymi bpy wskazywały, że obecność podstawników elektronodonorowych (metylo, metoksy; **2BA'-P1**, **2CA'-P1**, **2DA'-P1**) powinna powodować zwiększenie przerwy energetycznej względem **2AA'-P1**. Z kolei kompleks **2EA'-P1** zawierający ligand pomocniczy o największym stopniu koniugacji cechował się najmniejszą przerwą energetyczną, co sugerowało wyraźne batochromowe przesunięcie jego maksimum emisji względem **2AA'-P1**. W przypadku kompleksów będących pochodnymi phen otrzymano dość niespójne wyniki, gdyż wprowadzenie podstawników fenylowych powinno powodować zwiększenie koniugacji i obniżenie przerwy

energetycznej. W opozycji do tego, kompleks **2GA'-P1** wykazywał się większą przerwą w odniesieniu do związku **2FA'-P1**. Z kolei kompleks wyposażony w dodatkowe elektronodonorowe podstawniki metylowe na ligandzie pomocniczym (**2HA'-P1**) wykazywał się najmniejszą przerwą energetyczną z całej serii pochodnych phen. Przy współczynniku korelacji równym 0.79 należy interpretować wyniki obliczeń z dużą ostrożnością.

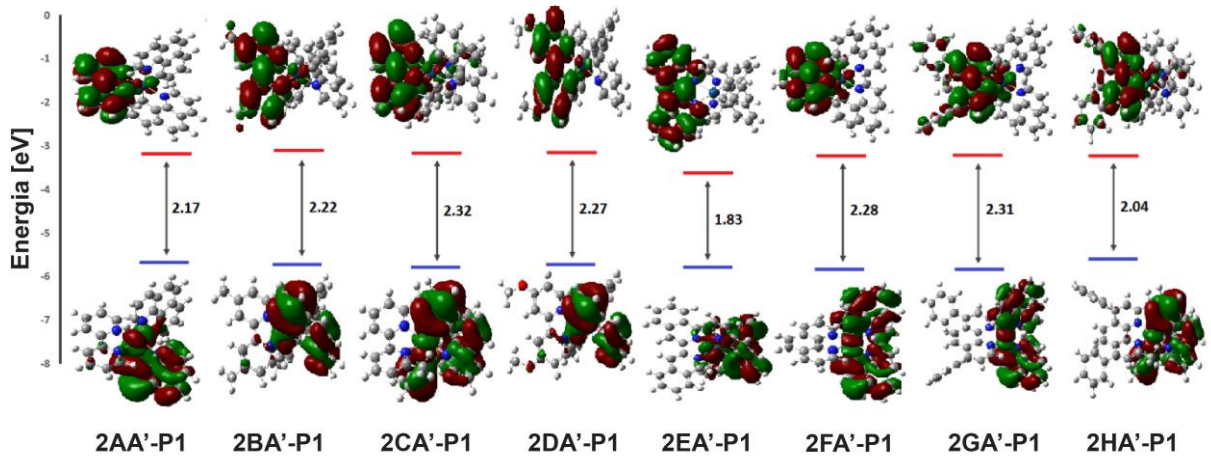

Rys. 17. *Wizualizacje obliczonych HOMO (dolny rząd) i LUMO (górny rząd) oraz przerwy energetyczne kompleksów* ***P1****.*

Kolejnym aspektem analizy badanych związków były ich właściwości fotofizyczne, poczynając od pomiarów widm absorpcji i fotoluminescencji w roztworze chlorobenzenowym. Wszystkie związki cechowała obecność pasma absorpcji typu MLCT w okolicach 420 nm, które były relatywnie słabe z uwagi na ich spinowo wzbroniony charakter. Oprócz tego, obserwowano znacznie bardziej intensywne pasma poniżej 400 nm, które przypisano dozwolonym przejściom typu LC. Dopiero badania fotoluminescencji objawiły wyraźny, oczekiwany wpływ zmiany liganda *N,N*-donorowego (Rys. 18). Kompleks zawierający ppy (**2AA'-P1**) wykazywał maksimum emisji przy 610 nm, a te wyposażone w podstawniki elektronodonorowe (**2BA'-P1**, **2CA'-P1** oraz **2DA'-P1**) wykazywały przesunięcie hipsochromowe o wartości maksymalnej 58 nm. Z kolei kompleks **2EA'-P1** zawierający ligand o zwiększonym stopniu aromatyczności wykazał przesunięcie batochromowe o wartości 45 nm. W przypadku serii kompleksów z ligandami na bazie rdzenia 1,10-fenantrolinowego również zaobserwowano przesunięcie batochromowe związane z wprowadzeniem podstawników fenylowych (zwiększających koniugację), jednak efekt ten był zdecydowanie mniej wyraźny. W ten sposób potwierdzono oczekiwany trend zmian przerwy energetycznej.

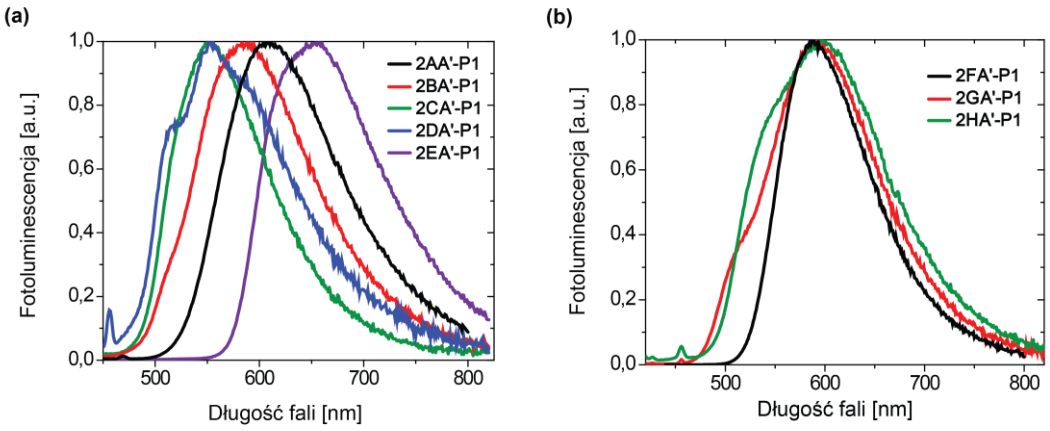

Rys. 18. *Znormalizowane widma emisji kompleksów* ***2(A-F)A'-P1*** *(a) oraz* ***2(F-H)A'-P1*** *(b) w roztworze.*

Zmierzona została także wydajność kwantowa fotoluminescencji, która osiągała 9 % w przypadku kompleksu **2EA'-P1** w atmosferze powietrza. Wydajności te były zauważalnie większe podczas pomiarów w odtlenionych roztworach, co dodatkowo potwierdza fosforescencyjny charakter emiterów, gdyż tlen jest znanym wygaszaczem wzbudzonych stanów trypletowych. W tego typu pomiarach, najwyższe wartości zostały zarejestrowane dla kompleksów fenantrolinowych. Na uwagę zasługuje największa różnica wydajności kwantowej pomiędzy roztworem odtlenionym i nieodtlenionym w przypadku kompleksu **2FA'-P1**.

Ostatnim aspektem badań przedstawionym w pracy [**P1**] była analiza parametrów pracy prostych diod, wykonanych w konfiguracji ITO/PEDOT:PSS/PVK:PBD + kompleks/Ca/Ag. Do wykonania testowych urządzeń OLED zostały wyselekcjonowane **2AA'-P1**, **2EA'-P1**, **2FA'-P1** oraz **2GA'-P1**, związki cechujące się najwyższymi wydajnościami kwantowymi emisji w roztworze. Przede wszystkim zaobserwowano, że podczas badań elektroluminescencji zanika pasmo od matrycy, co sugeruje znacznie bardziej efektywny transfer energii z matrycy do emitera, niż w przypadku fotoluminescencji w warstwie. Dla wszystkich czterech kompleksów zaobserwowano hipsochromowe przesunięcie emisji względem fotoluminescencji w warstwie, co zostało powiązane ze zwiększeniem sztywności ośrodka, powodując przyjmowanie odmiennych konformacji molekuł emiterów. Najwyższą luminancją oraz wydajnością prądową cechowała się dioda oparta o emiter **2FA'-P1**, co korelowało z zarejestrowaniem najwyższej wydajności kwantowej fotoluminescencji tego kompleksu wśród wszystkich badanych związków (Rys. 19).

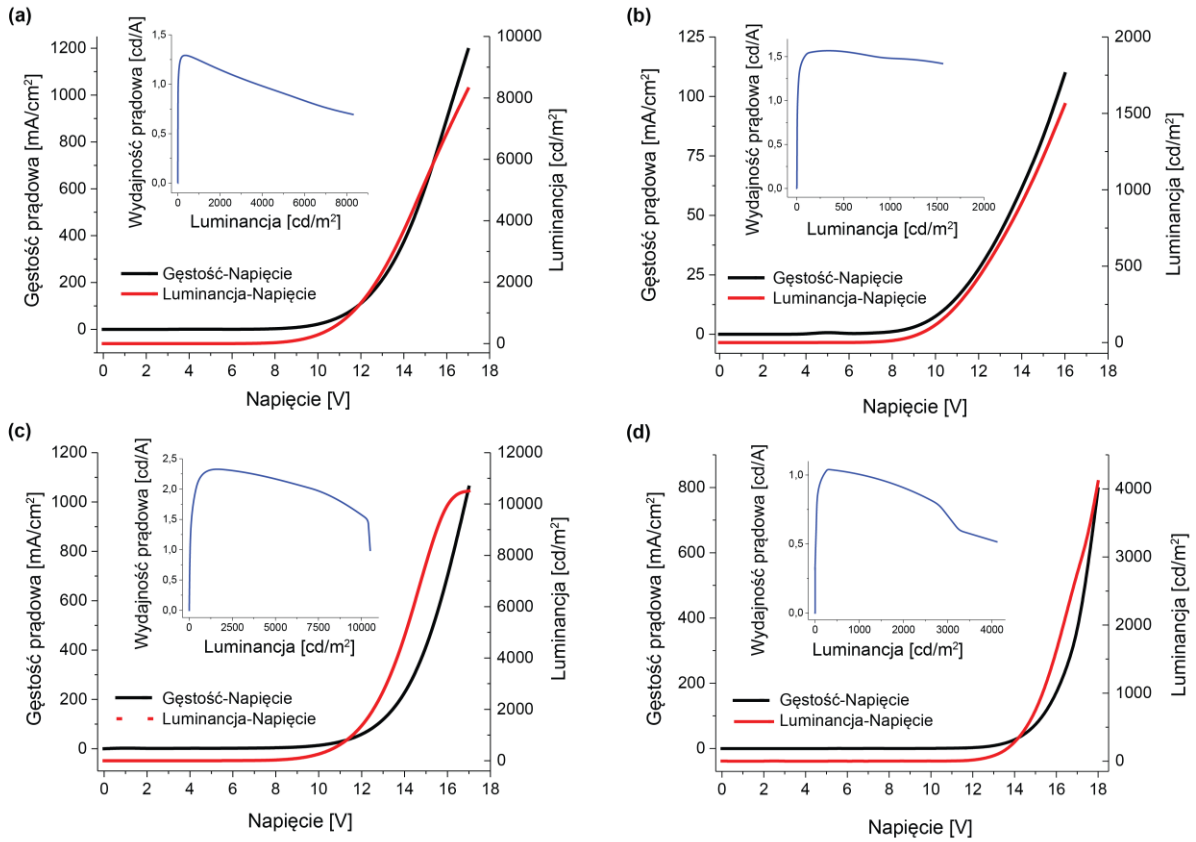

Rys. 19. *Charakterystyka prądowo-napięciowa diod wykonanych z użyciem emiterów* ***2AA'-P1*** *(a),* ***2EA'-P1*** *(b),* ***2FA'-P1*** *(c) oraz* ***2GA'-P1*** *(d).*

Podsumowując, w ramach pracy [**P1**] dokonano syntezy szeregu związków kompleksowych o wzorze ogólnym $[Ir(bzq)_2(N\hat{}N)]^+A^-$, zawierających różne ligandy pomocnicze bazujące na strukturze 2,2'-

bipyrydyny oraz 1,10-fenantroliny. Związki te otrzymano w asyście promieniowania mikrofalowego, która umożliwiła syntezę docelowych związków w czasie zaledwie 10 minut. Otrzymane materiały zostały scharakteryzowane przez współpracujące grupy badawcze pod kątem właściwości termicznych, elektrochemicznych i fotofizycznych oraz skorelowane z wynikami modelowania kwantowo-chemicznego. Analiza uzyskanych danych pozwoliła stwierdzić efekt przestrajania pasma emisji w zależności od struktury liganda pomocniczego. Wyposażanie ligandów *N,N*-donorowych w podstawniki elektronodonorowe powodowało przesunięcie emisji w kierunku niebieskim, z kolei zwiększanie stopnia koniugacji powodowało przesunięcie w kierunku czerwonym. Wybrane kompleksy posłużyły jako emitery do wytworzenia prostych OLEDów. Najbardziej efektywne diody cechowały się dobrymi parametrami pracy biorąc pod uwagę wykonanie ich technikami roztworowymi oraz brak optymalizacji struktury urządzeń.

7.2. Kompleksy Ir(III) zawierające fluorowane β-ketoiminianowe ligandy pomocnicze

W kolejnym artykule [**P2**] przedstawiono rezultaty badań dotyczących heteroleptycznych neutralnych kompleksów irydu(III) o ogólnym wzorze [Ir(bzq)$_2$(N^O)], stabilizowanych *N,O*-donorowymi ligandami β-ketoiminianowymi wyposażonymi w fluorowane ugrupowania aromatyczne. Ideą pracy było otrzymanie serii związków koordynacyjnych oraz skorelowanie ich właściwości fotofizycznych, termicznych, elektrochemicznych i teoretycznych w odniesieniu do stopnia oraz miejsca podstawienia atomami fluoru liganda pomocniczego. Zwieńczeniem pracy była dyskusja parametrów OLEDów wykonanych techniką roztworową z użyciem nowych kompleksów w roli emiterów fosforescencyjnych (Rys. 20).

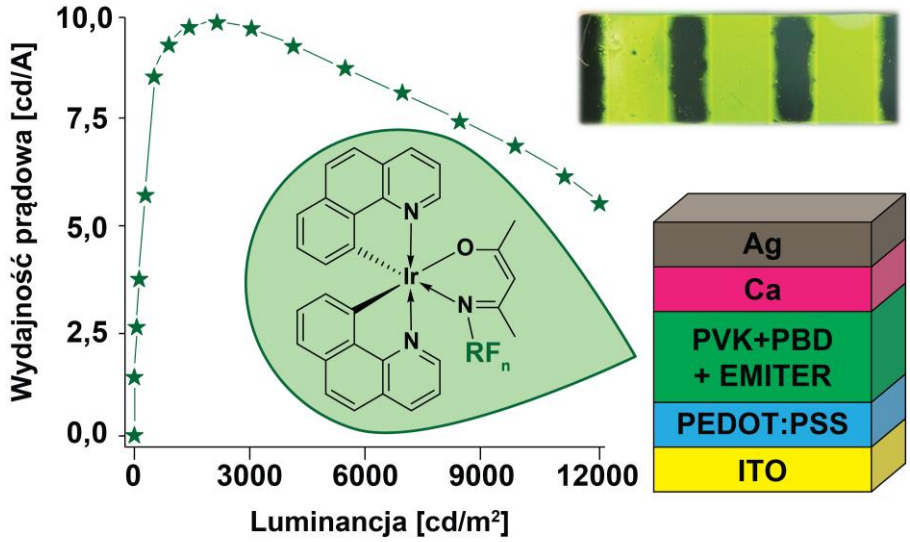

Rys. 20. *Graficzne przedstawienie zagadnień poruszanych w pracy [**P2**].*

Na podstawie przeglądu literaturowego wyselekcjonowano do badań kompleksy irydu(III) wyposażone w dwa ligandy bzq oraz jeden pomocniczy ligand *β*-ketoiminianowy o zmiennym stopniu podstawienia atomami fluoru podstawnika *N*-arylowego. Punktem wyjścia do realizacji tego pomysłu była synteza prekursorów ligandów zawierających w swojej strukturze pierścień fenylowy podstawiony atomami

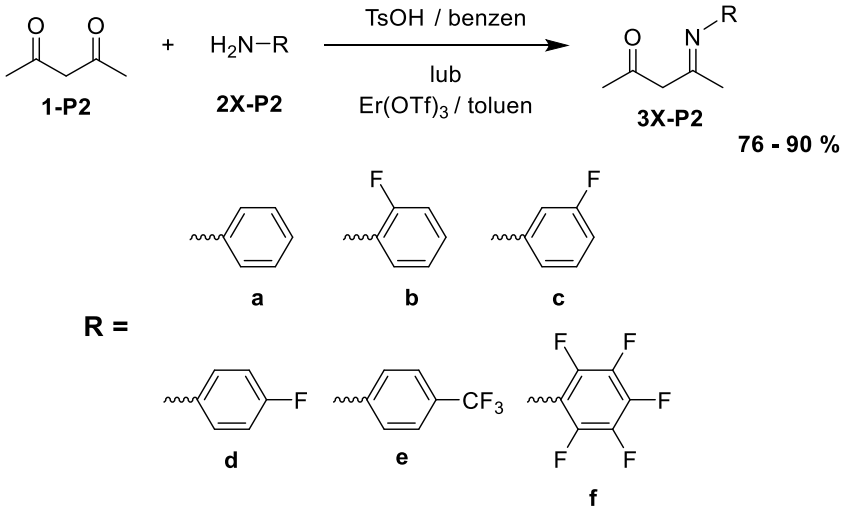

Rys. 21. *Schemat otrzymywania β-ketoimin w pracy [**P2**].*

fluoru w pozycjach *orto*, *meta* i *para*, grupą trifluorometylową w pozycji *para* oraz perfluorowany pierścień fenylowy. Związki te zostały otrzymane w reakcji kondensacji pomiędzy acetyloacetonem, a odpowiednimi pochodnymi aniliny, z wykorzystaniem kwasu *para*-toluenosulfonowego lub soli erbu(III) w roli katalizatorów (Rys. 21).[114,115] Otrzymane *β*-ketoiminy posłużyły do syntezy docelowych związków kompleksowych, na drodze rozszczepienia *μ*-chlorkowego kompleksu **4-P2** w środowisku zasadowym (Rys. 22a). Tym razem również skorzystano z wspomagającego efektu promieniowania mikrofalowego, co pozwoliło uzyskać oczekiwane produkty w czasie jedynie 10 minut. Ostatni kompleks **5g-P2** został otrzymany przypadkowo podczas syntezy związku **5f-P2**, gdy w układzie znalazła się niewielka ilość 2-metoksyetanolu (musiała to być pozostałość po otrzymaniu dimeru **4-P2**) i doszło do substytucji atomu fluoru w pozycji *para*. Postanowiono ten kompleks także włączyć do badań, a jego synteza została powtórzona intencjonalnie z użyciem ściśle określonej ilości 2-metoksyetanolanu sodu (Rys. 22b).

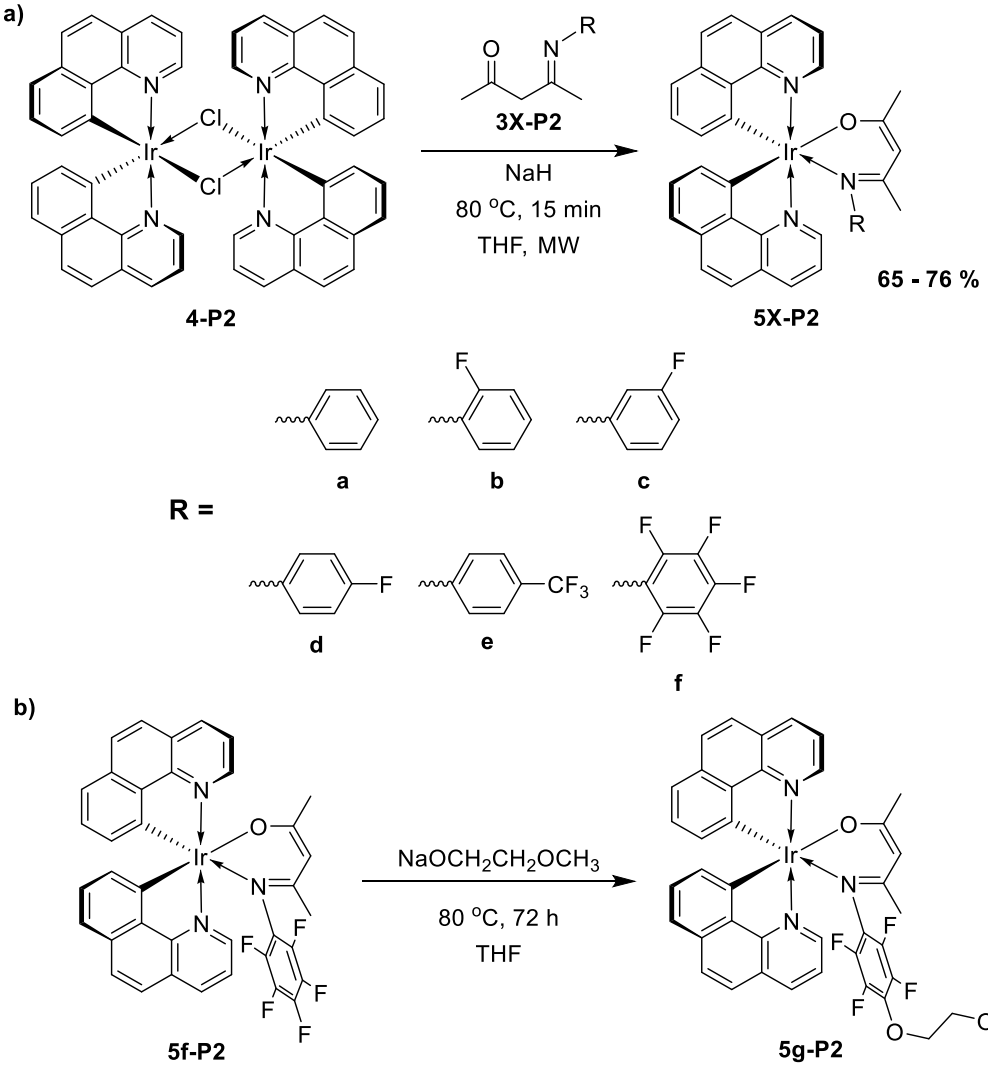

Rys. 22. *Schemat otrzymywania kompleksów β-ketoiminianowych.*

Struktury otrzymanych kompleksów potwierdzono analizą ^{1}H NMR oraz dyfrakcji promieniowania rentgenowskiego na wyhodowanych monokryształach. Analiza XRD wykazała, że geometria wielościanu koordynacyjnego utworzonego przez atomy donorowe zbliżona jest do regularnego oktaedru (Rys. 23).

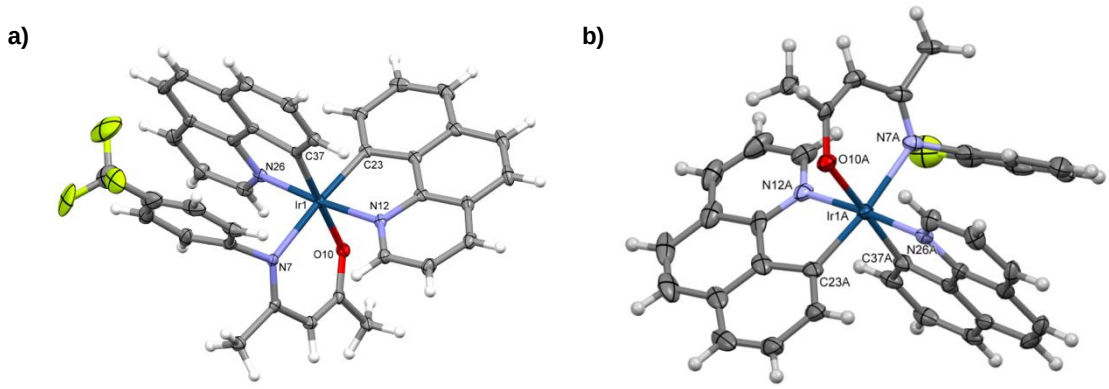

Rys. 23. *Struktury krystaliczne związków* ***5b-P2*** *(a) oraz* ***5e-P2*** *(b).*

Analiza termograwimetryczna otrzymanych kompleksów wykazała ich zaskakująco dużą stabilność termiczną, gdyż 5-procentowy ubytek masy każdej próbki przypadał dopiero w okolicach 270 °C. Tym samym potwierdzono wystarczającą stabilność termiczną tych związków do zastosowania w roli emiterów OLED.

W dalszej kolejności przystąpiono do analizy właściwości elektrochemicznych. Woltamperometria cykliczna potwierdziła niewielki wpływ zmian struktury chemicznej na potencjał jonizacji badanych związków, pozostając bez wpływu na wartość powinowactwa elektronowego (Tabela 3). Poczynione obserwacje wyraźnie sugerowały, że na ligandzie ketoiminianowym powinien być zlokalizowany przede wszystkim poziom HOMO, a w znacznie mniejszym stopniu LUMO. Stopień wpływu na IP był zależny od ilości podstawników fluorowych znajdujących się przy pierścieniu fenylowym i osiągał szczyt w przypadku kompleksów **5f-P2** oraz **5g-P2**, co wskazuje na stabilizację poziomu HOMO poprzez elektronowyciągający charakter atomów fluoru. Jednakże, wpływ ten nie był tak zauważalny jak w przypadku modyfikacji szkieletu ketoiminianu.[68]

Tabela 3. *Wyniki pomiarów woltamperometrycznych kompleksów z serii* ***P2****.*

Związek	$E_{ox\ onset}$ [V]	$E_{red\ onset}$ [V]	E_g [eV]	IP [eV]	EA [eV]
5a-P2	0.14	-2.44	2.58	5.2	2.7
5b-P2	0.21	-2.42	2.63	5.3	2.7
5c-P2	0.18	-2.39	2.57	5.3	2.7
5d-P2	0.18	-2.43	2.62	5.3	2.7
5e-P2	0.12	-2.36	2.48	5.2	2.7
5f-P2	0.32	-2.41	2.73	5.4	2.7
5g-P2	0.30	-2.39	2.69	5.4	2.7

Kolejnym analizowanym aspektem były wyniki obliczeń kwantowo-chemicznych, które również potwierdziły przyjmowanie geometrii lekko zniekształconego oktaedru przez badane związki. Jednakże, najbardziej istotne z punktu widzenia analizy ich właściwości było rozmieszczenie orbitali granicznych oraz wartości przewidywanych przerw energetycznych, które zostały przedstawione na Rys. 24. Jak można zauważyć, poziomy HOMO są zlokalizowane we wszystkich przypadkach na atomie centralnym, ligandach *C,N*-cyklometalujących oraz ligandzie pomocniczym, ale jedynie w niewielkim stopniu na podstawniku *N*-fenylowym. Prawdopodobnie to jest przyczyną niewielkiego wpływu stopnia fluorowania na IP badanych związków. Z kolei poziomy LUMO znajdowały się głównie na ligandach *C,N*-cyklometalujących, co odpowiada za brak efektu zmiany struktury chemicznej na obserwowaną wartość EA.

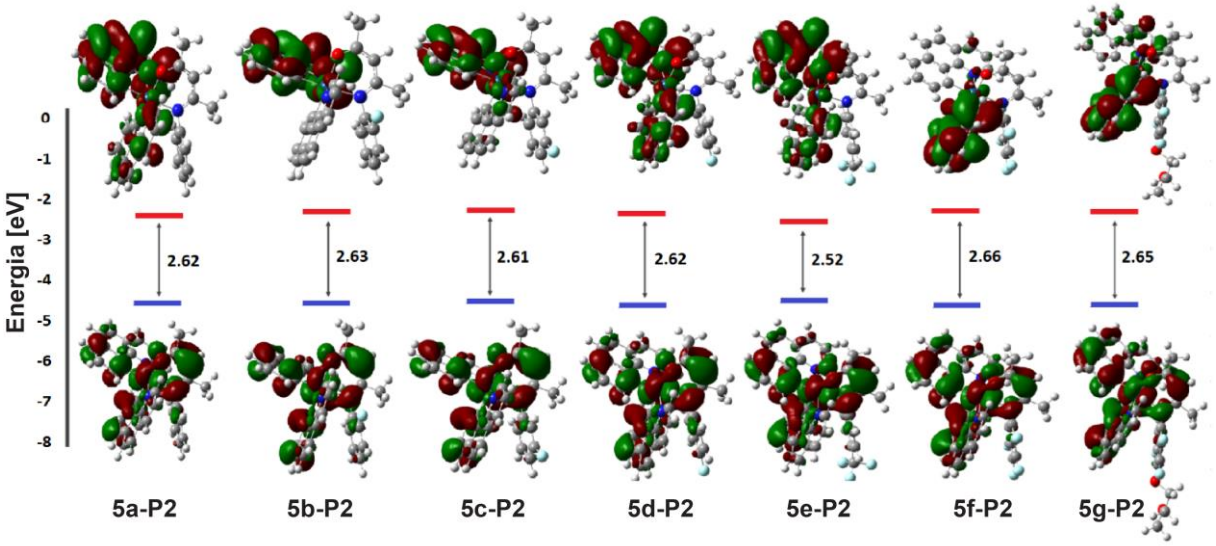

Rys. 24. *Wymodelowane orbitale HOMO (dolny rząd) oraz LUMO (górny rząd) wraz wartościami przerw energetycznych kompleksów omawianych w pracy [**P2**].*

Przewidywane przerwy energetyczne zawierały się w bardzo wąskich granicach, z największymi wartościami dla kompleksów zawierających największą ilość atomów fluoru przyłączonych bezpośrednio do pierścienia fenylowego (**5f-P2** i **5g-P2**) oraz najmniejszą wartością dla kompleksu **5e-P2**, zawierającego trzy atomy fluoru przyłączone do pierścienia poprzez dodatkowy atom węgla, w postaci grupy trifluorometylowej. Rezultaty te pokrywały się z wynikami badań elektrochemicznych, jednakże należy podkreślić, że obie gałęzie badań sugerowały niewielkie przestrajanie położenia pasma emisji (zmianę E_g).

Powyższy wniosek mogła zweryfikować jedynie analiza właściwości fotofizycznych badanych związków koordynacyjnych. Wszystkie one wykazywały się bardzo podobnymi widmami absorpcji, na których można było zaobserwować szerokie pasma w zakresie 420-550 nm, które przypisano przejściom MLCT. Wzbudzanie w tym zakresie pozwoliło zarejestrować widma fotoluminescencji, przedstawione na Rys. 25.

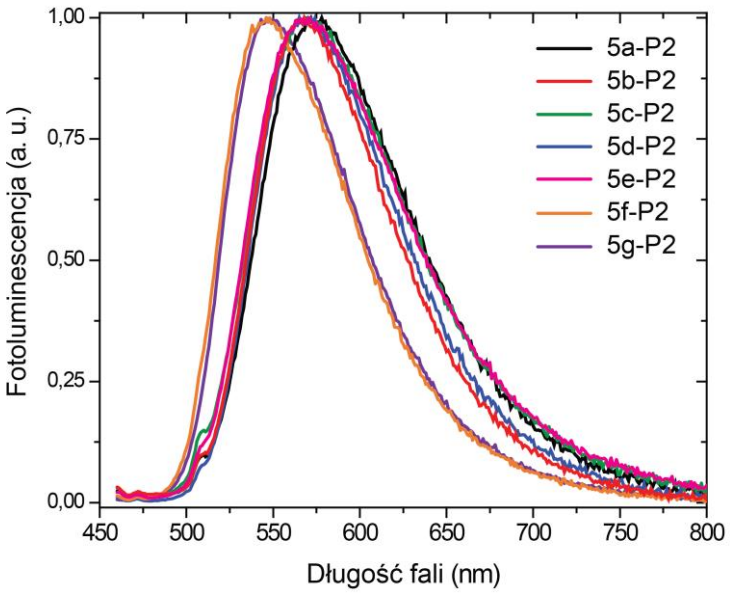

Rys. 25. *Znormalizowane widma fotoluminescencji kompleksów serii **P2** w chlorobenzenie.*

Jak można zauważyć, zostały zarejestrowane bardzo szerokie pasma, typowe dla przejść ze stanów trypletowych. Co ciekawe, z całej grupy zauważalnie wyróżniały się kompleksy **5f-P2** oraz **5g-P2**, których maksima emisji były przesunięte hipsochromowo. Tak jak przypuszczano, zaobserwowano niewielki wpływ podstawienia fluorem na położenie maksimum emisji. Związki zawierające przynajmniej 4 atomy fluoru (**5f-P2** oraz **5g-P2**) emitowały przy 546–547 nm, związki zawierające jeden atom fluoru (**5b-P2, 5c-P2** oraz **5d-P2**) w zakresie 567–568 nm, a związek referencyjny **5a-P2** nie zawierający żadnego atomu fluoru, emitował przy 577 nm. Trend ten potwierdza indukcyjny efekt podstawienia pierścienia *N*-fenylowego na stabilizację poziomu HOMO i zwiększanie przerwy energetycznej (zmniejszanie λ_{max}). Jedynym wyjątkiem był związek **5e-P2** zawierający trzy atomy fluoru (λ_{max} = 569 nm), których efekt był wyraźnie osłabiony z uwagi na niebezpośrednie przyłączenie do pierścienia fenylowego. Intrygujące było jednak to, że nie stwierdzono wpływu regiopodstawienia na przestrajanie w serii **5b-P2, 5c-P2** oraz **5d-P2**. Zmierzone wydajności kwantowe fotoluminescencji były bardzo niskie w atmosferze powietrza i wyraźnie rosły w odtlenionych roztworach, aż do wartości 44 % dla kompleksu **5d-P2**, potwierdzając fosforescencyjny charakter emisji.

Bardzo podobne widma emisji zaobserwowano w przypadku pomiaru fotoluminescencji 1 % emitera w filmie PVK/PBD, z wyjątkiem przesunięcia hipsochromowego wszystkich pasm, związanego z efektem usztywnienia matrycy. Na widmach zauważalne było także pasmo pochodzące od ekscipleksów pomiędzy komponentami matrycy,[116] świadczące o niecałkowitym transferze energii do emitera. Najbardziej efektywne w tym aspekcie okazały się kompleksy zawierające przynajmniej cztery atomy fluoru, gdyż pasmo ekscipleksowe było w ich przypadku najmniej intensywne, a wydajności kwantowe fotoluminescencji w filmie największe (Rys. 26).

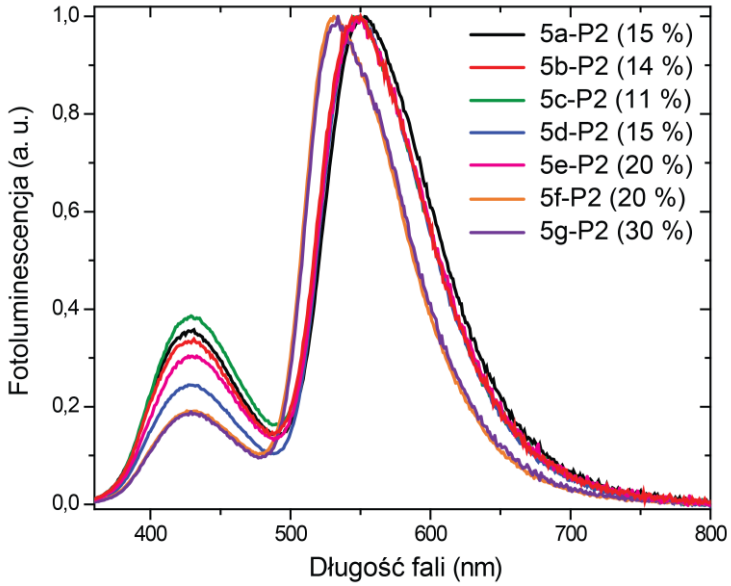

Rys. 26. *Znormalizowane widma fotoluminescencji badanych kompleksów w warstwie PVK/PBD. W nawiasach podano wydajności kwantowe fotoluminescencji.*

Ostatnim analizowanym aspektem były parametry pracy prostych diod przygotowanych w oparciu o badane związki kompleksowe. Jak się okazało, wcześniej opisane trendy dotyczące wpływu ilości atomów fluoru na przesunięcie maksimum emisji zostały zachowane, gdyż najkrótsze długości fali emitowały diody oparte o **5f-P2** oraz **5g-P2**, a najdłuższą dioda oparta o **5a-P2**. Jednakże należy podkreślić, że różnice były na niewielkim poziomie, gdyż maksima emitowanych pasm dla wszystkich kompleksów zawierały się w przedziale 17 nm. Jeśli chodzi o wydajność pracy, to zaobserwowano zupełnie odwrotny trend względem

fotoluminescencji w warstwie, w której najwyższe wydajności kwantowe uzyskały kompleksy **5(e-g)-P2**. W przypadku elektroluminescencji, diody zawierające te emitery uzyskiwały najgorsze parametry w serii (Tabela 4). Najlepszymi parametrami pracy cechowały się diody zawierające emitery **5a-P2**, **5b-P2** oraz **5d-P2**, przy czym dominowały te wyposażone w jeden atom fluoru w pozycji *orto* oraz *para* pierścienia *N*-fenylowego. W ten sposób został potwierdzony pozytywny efekt wprowadzenia atomów fluoru do referencyjnej struktury **5a-P2** na właściwości elektroluminescencyjne badanych związków.

Tabela 4. *Parametry pracy urządzeń opartych o emitery z serii* ***P2.***

Związek	Maksymalna luminancja [cd/m^2]	Maksymalna wydajność prądowa [cd/A]	Zewnętrzna wydajność kwantowa [%]	Maksimum elektroluminescencji [nm]
5a-P2	9 500	9.1	2.71	560
5b-P2	10 000	9.7	2.75	553
5c-P2	6 200	7.0	1.80	556
5d-P2	13 000	9.8	2.68	554
5e-P2	4 800	6.7	1.99	559
5f-P2	5 000	4.1	1.13	543
5g-P2	5 000	5.8	1.65	550

Podsumowując, w ramach pracy [**P2**] zostały zaprojektowane i otrzymane związki kompleksowe o wzorze ogólnym [Ir(bzq)$_2$(N^O)], zawierające pomocniczy ligand *β*-ketoiminianowy o zróżnicowanym stopniu podstawienia atomami fluoru. Po raz kolejny potwierdzono skuteczność promieniowania mikrofalowego w syntezie związków kompleksowych irydu(III), gdyż docelowe związki zostały otrzymane w czasie zaledwie 10 minut. Materiały te zostały scharakteryzowane przez współpracujące grupy badawcze pod kątem właściwości termicznych, elektrochemicznych i fotofizycznych oraz skorelowane z wynikami modelowania kwantowo-chemicznego. Analiza uzyskanych danych pozwoliła stwierdzić niewielki efekt przestrajania pasma emisji poprzez stabilizację poziomu HOMO dzięki indukcyjnemu efektowi atomów fluoru, w zależności od ich ilości w strukturze chemicznej liganda *N,O*-donorowego. Zamiast tego, stwierdzono bardzo duży wpływ na wydajności kwantowe fotoluminescencji oraz parametry pracy diod skonstruowanych z udziałem badanych związków. W fotoluminescencji najefektywniej sprawowały się kompleksy zawierające cztery lub pięć atomów fluoru w strukturze, z kolei w elektroluminescencji najefektywniejsze okazały się kompleksy zawierające podstawnik *para*- oraz *orto*-fluorofenylowy. Najbardziej efektywne diody cechowały się bardzo dobrymi parametrami pracy (maksymalna luminancja na poziomie 13 000 cd/m^2, maksymalna wydajność prądowa rzędu 10 cd/A) biorąc pod uwagę wykonanie ich technikami roztworowymi oraz brak optymalizacji struktury urządzeń.

7.3. Kompleksy Ir(III) zawierające *N*-arylopodstawione ligandy β-ketoiminianowe

Praca [**P3**] jest kontynuacją tematyki heteroleptycznych związków koordynacyjnych irydu(III) o ogólnym wzorze [Ir(bzq)$_2$(N^O)], tym razem wyposażonych w *N,O*-donorowe ligandy *β*-ketoiminianowe zawierające różnorodne ugrupowania aromatyczne oparte o rdzeń benzenu, naftalenu i antracenu. Koncepcja pracy była bliźniaczo podobna do poprzedniej i również obejmowała syntezę zaprojektowanych kompleksów oraz analizę ich właściwości w relacji do struktury chemicznej ugrupowania arylowego połączonego z ketoiminianowym atomem azotu. Abstrakt graficzny publikacji przedstawiono na Rys. 27.

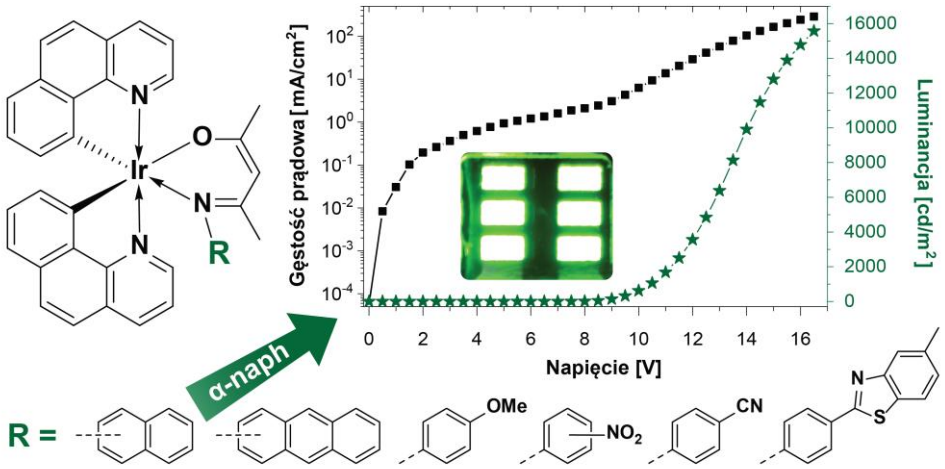

Rys. 27. *Przedstawienie struktur analizowanych związków wraz z parametrami pracy najwydajniejszego emitera.*

Kontynuując tematykę kompleksów *β*-ketoiminianowych rozpoczętą we wcześniejszej pracy [**P2**], w ramach której potwierdzono wpływ struktury podstawnika przyłączonego do atomu azotu liganda pomocniczego na właściwości emisyjne oraz wykazano, że najlepszymi parametrami pracy cechowała się dioda oparta o emiter wyposażony w podstawnik *N*-(*para*-fluorofenylowy), w kolejnej pracy postanowiono bardziej szczegółowo zbadać efekt zmiany podstawnika *para* pierścienia *N*-fenylowego. Dodatkowe kompleksy zawierające grupę nitrową w pozycji *meta* oraz *orto* zostały otrzymane celem zgłębienia wyróżniających się właściwości elektrochemicznych tej klasy związków. Ponadto, intencją było zbadanie efektu obecności oraz regiopodstawienia grup poliaromatycznych, takich jak naftyl oraz antracenyl, gdyż dotychczasowe prace w tym zakresie były ograniczone jedynie do kompleksów *N*-fenylowych.[67,68,117]

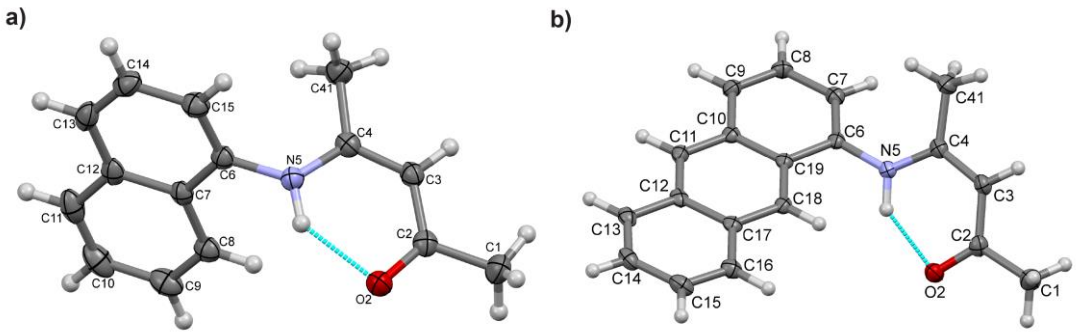

Rys. 28. *Przykładowe struktury krystaliczne ketoimin* ***3h-P3*** *(a) oraz* ***3j-P3*** *(b).*

Prace syntetyczne rozpoczęto od otrzymania odpowiednich *β*-ketoimin zgodnie z procedurami opisanymi w poprzedniej pracy [**P2**]. Jedynie *β*-ketoimin zawierających podstawniki *N*-antracenylowe (**3(j-k)**-

P3) nie udało się uzyskać wcześniej opracowanymi sposobami. W związku z powyższym, dla tej grupy pochodnych opracowano alternatywne warunki ich syntezy z użyciem reaktora mikrofalowego. Wszystkie potrzebne prekursory ligandów zostały uzyskane z wydajnościami sięgającymi 90 % (Rys. 29a). Analiza rentgenostrukturalna potwierdziła otrzymanie zakładanych związków, które występowały w fazie krystalicznej w formie enolowej, stabilizowanej wiązaniem wodorowym N–H···O (Rys. 28).

Kolejnym krokiem była synteza docelowych związków koordynacyjnych z wykorzystaniem prekursorów ligandów *β*-ketoiminianowych poprzez rozszczepienie dimeru **4-P3** w warunkach zasadowych (Rys. 29b). Tym razem syntezy przeprowadzono w łaźni olejowej zamiast w reaktorze mikrofalowym. Przyczyna tego była prozaiczna, a mianowicie tymczasowa awaria reaktora wymuszająca skorzystanie z klasycznego źródła ciepła. W trakcie analizy ^{1}H NMR zaobserwowano, że niektóre z otrzymanych związków (**5(c,f,i,k,l)-P3**) stanowiły mieszaniny izomerów, których rozdzielenie na kolumnie chromatograficznej okazało się niemożliwe.

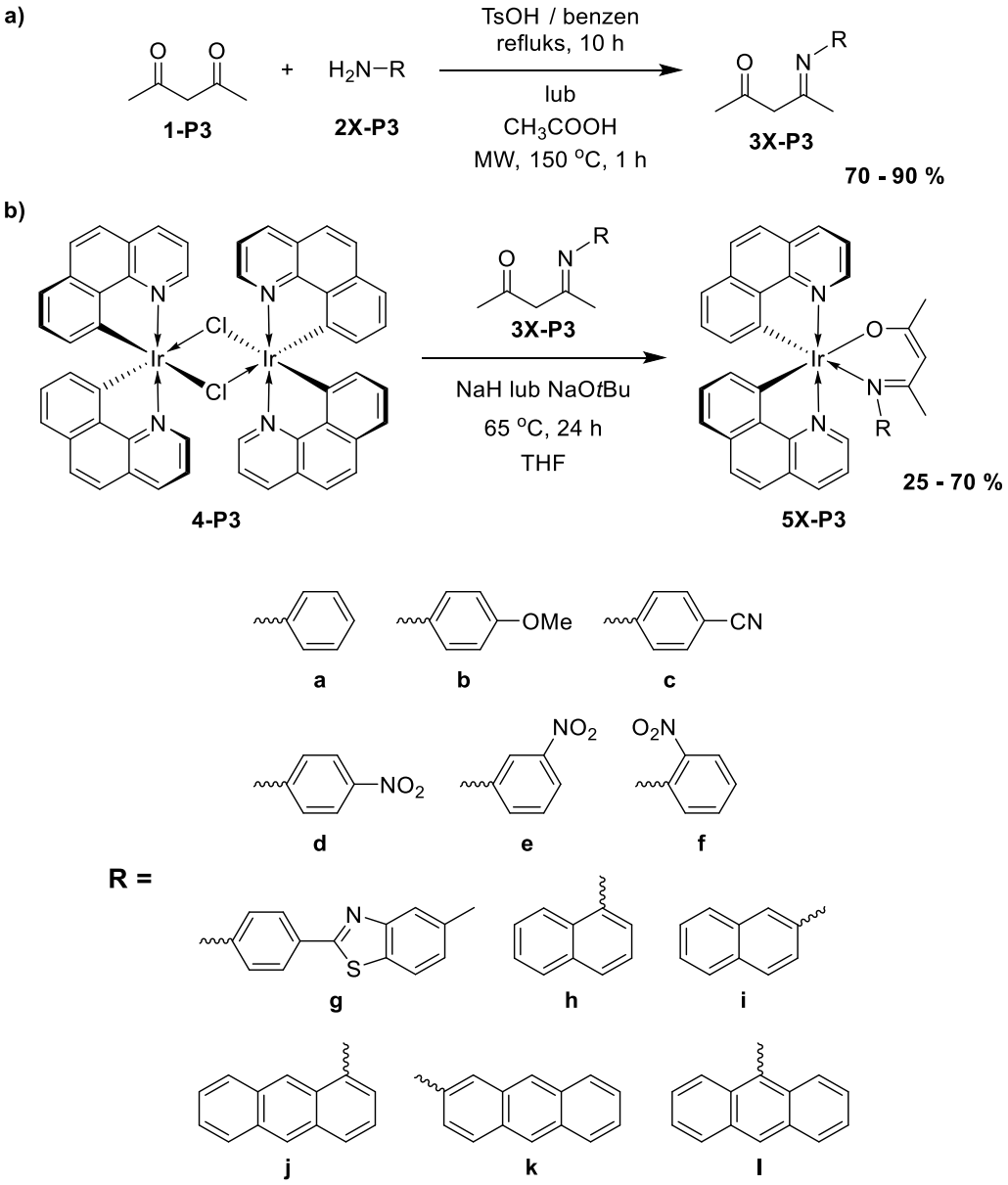

Rys. 29. *Schemat otrzymywania β-ketoimin oraz związków kompleksowych badanych w pracy [**P3**].*

Analiza XRD monokryształów wykazała, że przyczyną izomerii jest odmienne skoordynowanie *N,O*-donorowego liganda pomocniczego, prawdopodobnie spowodowane właściwościami stereoelektronowymi podstawników *N*-arylowych oraz ich oddziaływaniem π-π stackingowym z ligandem bzq. Przykładowe struktury kompleksów zaprezentowano na Rys. 30. W ramach badań nieopisanych w artykule [**P3**] udało się wyizolować czysty izomer związku **5j-P3** oraz porównać jego właściwości fotofizyczne i elektroluminescencyjne z tymi uzyskanymi dla nierozdzielonej mieszaniny izomerów. Charakterystyki obu próbek były praktycznie identyczne, co wpłynęło na decyzję o kontynuowaniu badań pozostałych mieszanin izomerów.

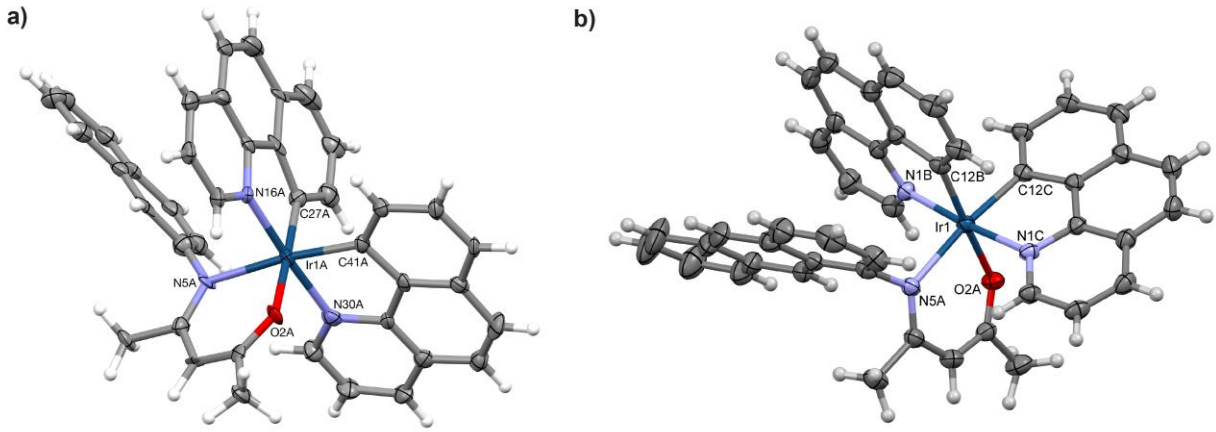

Rys. 30. *Przykładowe struktury krystaliczne kompleksów* ***5i-P3*** *(a) oraz* ***5j-P3*** *(b).*

Analiza termograwimetryczna kompleksów będących przedmiotem dyskusji wykazała ich stabilność termiczną do temperatury przynajmniej 230 °C (ubytek 5% masy), co potwierdzało brak przeciwskazań w aspekcie stabilności termicznej do kontynuowania ich badań.

Tabela 5. Wyniki badań elektrochemicznych związków omawianych w pracy [**P3**].

Związek	$E_{ox\ onset}$ [V]	$E_{red\ onset}$ [V]	E_g [eV]	IP [eV]	EA [eV]
5a-P3	0.17	-2.32	2.49	5.3	2.8
5b-P3	0.12	-2.20	2.32	5.2	2.9
5c-P3	0.21	-2.15	2.36	5.3	3.0
5d-P3	0.26	-1.73	1.99	5.4	3.4
5e-P3	0.26	-1.70	1.96	5.4	3.4
5f-P3	0.17	-1.72	1.89	5.3	3.4
5g-P3	0.29	-2.35	2.64	5.4	2.8
5h-P3	0.23	-2.28	2.51	5.3	2.8
5i-P3	0.16	-2.31	2.47	5.3	2.8
5j-P3	0.20	-2.29	2.49	5.3	2.8
5k-P3	0.18	-2.26	2.44	5.3	2.8
5l-P3	0.15	-2.31	2.46	5.3	2.8

Kolejnym aspektem poruszanym w pracy była analiza wyników woltamperometrii cyklicznej (Tabela 5). Jak można zauważyć, zmiana struktury chemicznej miała niewielki wpływ na wartości IP analizowanych związków, czego oczekiwano w oparciu o wyniki pracy [**P2**]. Poziom HOMO zlokalizowany w niewielkim stopniu na podstawniku *N*-arylowym powinien być destabilizowany obecnością elektronodonorowej grupy metoksylowej (**5b-P3**) oraz stabilizowany obecnością elektronowyciągających grup nitrowej i 5-metylo-2-

benzotiazylowej (**5d-P3**, **5e-P3**, **5g-P3**), czego odzwierciedleniem było odpowiednio obniżenie oraz podwyższenie wartości IP względem kompleksu referencyjnego **5a-P3**. O ile zmiana struktury mogła mieć wpływ na wartość IP, o tyle nie spodziewano się jej wpływu na EA. Ku zaskoczeniu, zaobserwowano bardzo duże odchylenie od referencyjnej wartości 2.8 eV w przypadku kompleksów wyposażonych w grupę nitrową (**5(d-f)-P3**) oraz mniejsze odchylenie w przypadku grupy nitrylowej (**5c-P3**), co przekładało się na odpowiednio niższą wartość E_g tych kompleksów. Wyniki te wydawały się nielogiczne, gdyż ewentualnie można było oczekiwać niewielkiej stabilizacji poziomu HOMO, która powinna prowadzić do zwiększenia E_g. Z kolei wszystkie kompleksy zawierające podstawniki czysto węglowodorowe cechowały się podobnymi przerwami energetycznymi w okolicach 2.5 eV. Przyczyny tych rozbieżności postanowiono wyjaśnić przy pomocy obliczeń kwantowo-chemicznych.

Obliczenia bardzo dobrze odzwierciedlały wyniki pomiarów elektrochemicznych, wskazując znaczące obniżenie przerwy energetycznej kompleksów zawierających grupę nitrową oraz zbliżone wartości dla pozostałych związków. Podobnie jak w poprzedniej pracy, obliczenia wykazały umiejscowienie HOMO głównie na atomie metalu, części *C*-donorowej liganda cyklometalującego oraz szkielecie ketoiminianu. Z kolei poziomy LUMO znajdowały się głównie na ligandach cyklometalujących, z wyjątkiem kompleksów wyposażonych w grupę nitrową, w przypadku których znajdował się on głównie na pierścieniu nitrofenylowym. Porównanie wizualizacji orbitali granicznych reprezentatywnych kompleksów **5a-P3** oraz **5f-P3** przedstawiono na Rys. 31.

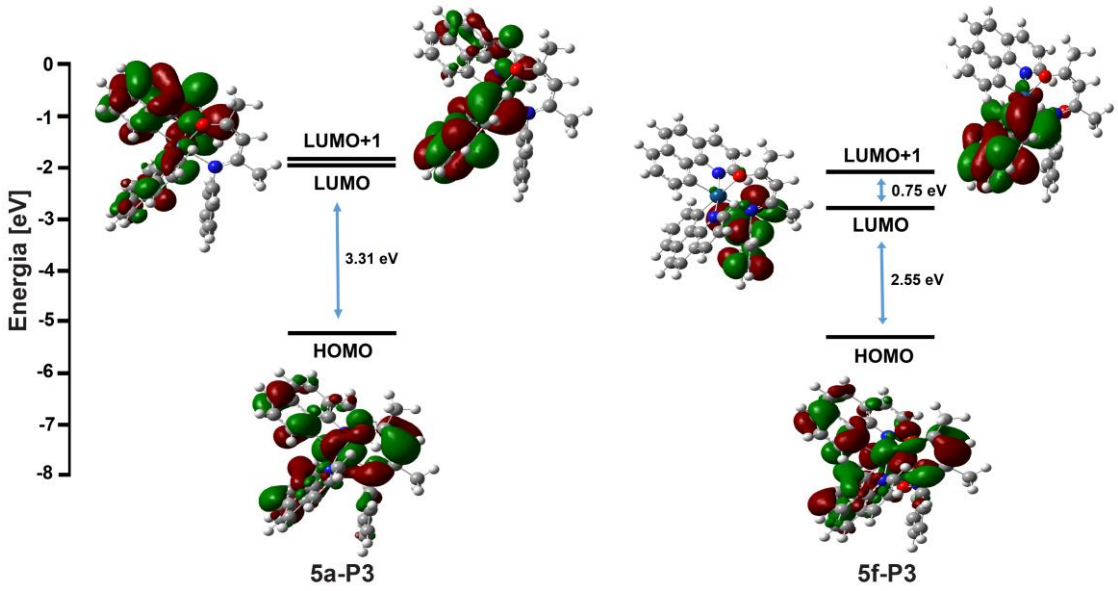

Rys. 31. *Wizualizacje obliczonych orbitali granicznych związków **5a-P3** oraz **5f-P3**.*

Jak można zauważyć, przerwa energetyczna HOMO – LUMO+1 kompleksu **5f-P3** była praktycznie identyczna z przerwą HOMO – LUMO kompleksu **5a-P3**. Podobnie wyglądał także kontur orbitalu LUMO+1 kompleksu **5f-P3** oraz orbitali LUMO i LUMO+1 kompleksu **5a-P3**. Jedyną wyraźną różnicę stanowiła obecność dodatkowego nieobsadzonego poziomu związanego z obecnością grupy nitrowej, który zmieniał notację wyżej położonych poziomów. Tym samym obliczenia pozwoliły stwierdzić, że obniżenie EA dla kompleksów **5(d-f)-P3** w pomiarach elektrochemicznych jest spowodowane wprowadzeniem dodatkowego nieobsadzonego orbitalu grupy nitrowej, a wyznaczony potencjał redukcji tak naprawdę odpowiada procesowi redukcji tej grupy. Niewielki stopień pokrywania się poziomów HOMO i LUMO kompleksu **5f-P3** stanowił dowód, że oznaczona elektrochemicznie przerwa energetyczna nie musi odpowiadać przerwie optycznej, gdyż przejście

elektronowe odpowiedzialne za emisję w kompleksach **5(d-f)-P3** nie będzie zachodziło pomiędzy orbitalami HOMO i LUMO, ale raczej HOMO i LUMO+1. Wobec tego należało oczekiwać, że wszystkie badane kompleksy będą cechowały się zbliżonymi długościami emitowanych fal.

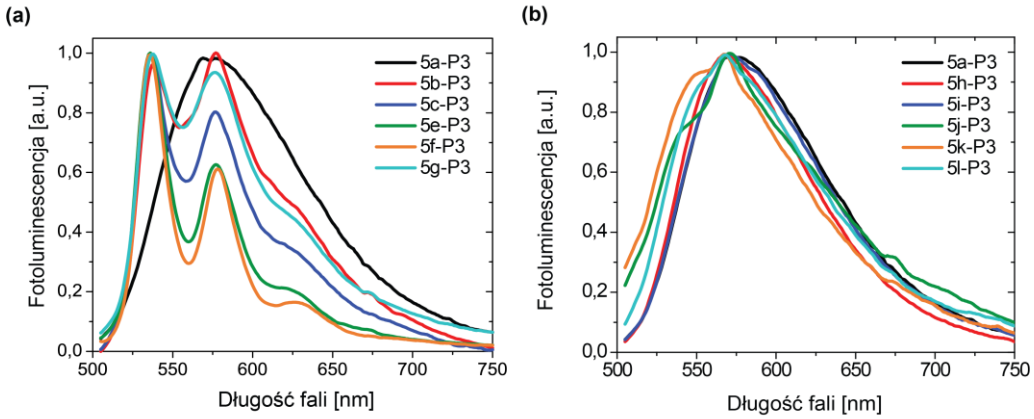

Rys. 32. *Znormalizowane widma fotoluminescencji kompleksów z funkcjonalizowanym podstawnikiem N-fenylowym (a) oraz czysto węglowodorowymi podstawnikami N-arylowymi (b) w chlorobenzenie.*

Pierwsze potwierdzenie powyższej tezy stanowiły pomiary widm absorpcji badanych związków w roztworze, które były bardzo zbliżone w zakresie powyżej 400 nm, w którym oczekiwano pasm MLCT. Zaobserwowano jedynie różnice w zakresie krótkofalowym, w którym należało się spodziewać odmiennych pasm od przejść $\pi-\pi^*$. Na tym etapie zaprzestano dalszych badań kompleksu **5d-P3**, gdyż okazał się on nietrwały w warunkach pomiaru. Znacznie ciekawsze rezultaty zostały uzyskane podczas badania fotoluminescencji w roztworze (Rys. 32). Okazało się, że związki zawierające podstawnik *N*-fenylowy z grupą funkcyjną wykazywały ustrukturyzowaną emisję, a związki wyposażone w czysto węglowodorowe podstawniki *N*-arylowe cechowały się szerokim pasmem emisji charakterystycznym dla przejść MLCT. Co ciekawe, fenomen ten nie był obserwowany podczas badań fotoluminescencji w filmie PVK/PBD, a kompleksy go wykazujące charakteryzowały się pogorszonym transferem energii, co objawiało się stosunkiem intensywności pomiędzy pasmami pochodzącymi od emitera i matrycy (Rys. 33). Zamiast tego, kompleksy zawierające podstawniki antracenylowe wykazywały dodatkowe pasma długofalowe świadczące o degradacji podstawnika *N*-arylowego, co zostało także potwierdzone w późniejszych badaniach elektroluminescencyjnych. Najwyższa wydajność kwantowa fotoluminescencji w filmie została zarejestrowana dla kompleksu **5h-P3** (18 %).

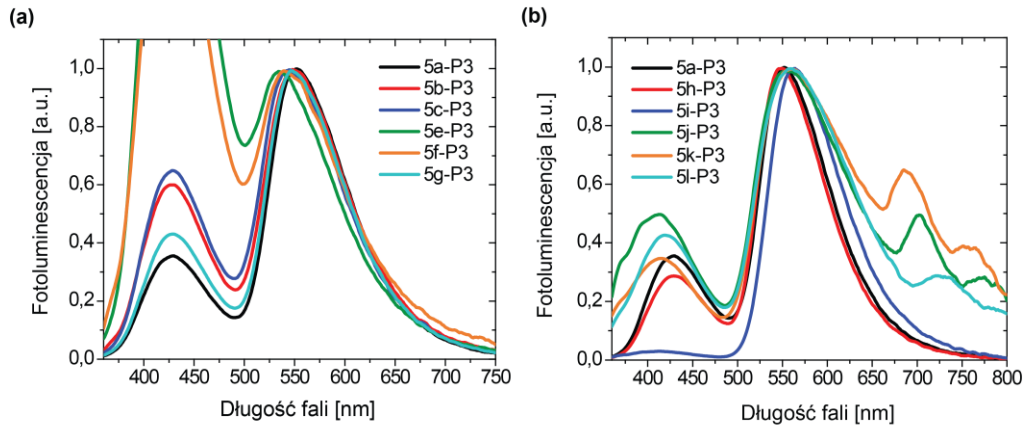

Rys. 33. *Znormalizowane widma fotoluminescencji kompleksów z funkcjonalizowanym podstawnikiem N-fenylowym (a) oraz czysto węglowodorowymi podstawnikami N-arylowymi (b) w filmie PVK/PBD.*

W oparciu o kompleksy serii **P3** zostały przygotowane proste diody elektroluminescencyjne o konfiguracji ITO/PEDOT:PSS/PVK:PBD + emiter/Ca/Ag. Parametry pracy tych diod zostały zebrane w Tabeli 6. Na widmach elektroluminescencji nie obserwowano pasm od matrycy widocznych w badaniach fotoluminescencji, co świadczyło o całkowitym transferze energii do cząsteczek emiterów. Zgodnie z oczekiwaniami, maksima emitowanych pasm ulegały jedynie niewielkiemu przestrajaniu pod wpływem zmian struktury ligandów pomocniczych. Zamiast tego, stwierdzono bardzo duży wpływ budowy tego liganda na wydajność foto- i elektroluminescencji. Najlepsze parametry uzyskały diody zawierające emitery **5(a,b,g,h,i)-P3**, czyli takie wyposażone w podstawniki bogate w elektrony (metoksy oraz węglowodorowe ugrupowania aromatyczne). Pochodne antracenylowe nie wpasowywały się w ten trend z uwagi na ich niewielką stabilność w warunkach przepływu prądu. Najlepszym emiterem okazał się kompleks **5h-P3**, na którego bazie dioda wykazywała maksymalną luminancję bliską 16 000 cd/m^2, maksymalną wydajność prądową w okolicach 12 cd/A oraz zewnętrzną wydajnością kwantową wynoszącą 3.2 %. Były to wartości zauważalnie lepsze niż zarejestrowane dla referencyjnego związku **5a-P3** i bardzo dobre jak na tak proste urządzenia o niezoptymalizowanej strukturze.

Tabela 6. *Parametry pracy diod opisanych w artykule [**P3**].*

Związek	Maksymalna luminancja [cd/m^2]	Maksymalna wydajność prądowa [cd/A]	Zewnętrzna wydajność kwantowa [%]	Maksimum elektroluminescencji [nm]
5a-P3	9 500	9.1	2.71	559
5b-P3	1 400	2.6	0.83	565
5c-P3	600	1.5	0.48	559
5e-P3	180	0.2	0.07	567
5f-P3	580	0.3	0.10	563
5g-P3	4 200	3.8	1.13	559
5h-P3	15 700	12.3	3.20	556
5i-P3	5 500	4.2	1.45	569
5j-P3	50	0.02	0.01	587, 715
5k-P3	100	0.06	0.03	625, 697, 765
5l-P3	70	0.02	0.02	575, 740

Podsumowując, w artykule [**P3**] podjęto tematykę kompleksów o ogólnym wzorze [Ir(bzq)$_2$(N^O)], zawierających *β*-ketoiminianowe ligandy pomocnicze wyposażone w podstawniki *N*-fenylowe funkcjonalizowane w pozycji *para* oraz podstawniki *N*-naftylowe i *N*-antracenylowe. Związki te zostały zaprojektowane i otrzymane w celu zobrazowania wpływu podstawnika *N*-arylowego na ich właściwości elektrochemiczne oraz foto- i elektroluminescencyjne. Analiza wyników charakterystyki otrzymanych materiałów i modelowania kwantowo-chemicznego pozwoliła wyjaśnić przyczyny odmiennego zachowania kompleksów wyposażonych w grupę nitrową. Zgodnie z oczekiwaniami, efekt przestrajania pasma emisji kompleksów był relatywnie niewielki, a wszystkie związki były emiterami barwy zielonej. Zamiast tego, stwierdzony został bardzo duży wpływ budowy chemicznej emiterów na efektywność foto- i elektroluminescencji. Najbardziej efektywny okazał się emiter zawierający podstawnik 1-naftylowy, na którego bazie dioda wykazywała maksymalną luminancję sięgającą 16 000 cd/m^2. Z kolei związki wyposażone w grupy *N*-antracenylowe okazały się wyjątkowo niestabilne, co zdecydowanie wyklucza ich zastosowanie w optoelektronice.

7.4. Funkcjonalizacja benzo[*h*]chinoliny w pozycji 5

Artykuł [**P4**] zaprezentowanego cyklu prac dotyczy otrzymywania nowych pochodnych benzo[*h*]chinoliny podstawionych w pozycji 5 zróżnicowanymi grupami funkcyjnymi, stanowiących potencjalne prekursory ligandów *C,N*-cyklometalujących. Celem tej pracy było opracowanie szlaków syntetycznych i warunków reakcji umożliwiających przyłączenie ugrupowań o właściwościach elektronodonorowych, elektronoakceptorowych, wspomagających transport dziur elektronowych, a także o dużej zawadzie sterycznej, na drodze aktywacji wiązania C-Br (Rys. 34). Prace zostały zainspirowane wnioskami sformułowanymi w artykule, w którym na podstawie obliczeń DFT wykazano możliwość oddziaływania na poziomy energetyczne kompleksów typu [Ir(bzq)$_3$] poprzez modyfikację struktury liganda bzq.[72] W pracy zaimplementowano ogrzewanie układu reakcyjnego promieniowaniem mikrofalowym, co pozwoliło otrzymać część oczekiwanych produktów z wysoką wydajnością i w bardzo krótkim czasie.

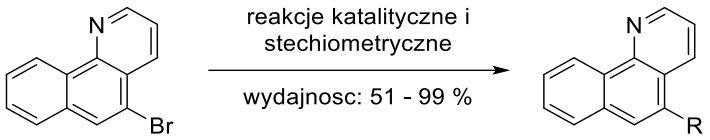

R = OMe, OPh, NH2, NMe_2, NPh_2, *p*-C_6H_4-NPh_2, N-karbazolil,
N-fenotiazyl, F, C_6F_5, $SiMe_2H$, $SiMe_2$-CH_2CH_2-$SiMe_2$O-POSSiBu

Rys. 34. *Ogólny schemat otrzymywania pochodnych benzo[h]chinoliny.*

W oparciu o szczegółowy przegląd literaturowy ustalono, że otrzymanie docelowych pochodnych bzqH na drodze formacji pierścienia heterocyklicznego (reakcja Skraupa) byłoby bardzo nieefektywne, ze względu na zwyczajowo umiarkowaną wydajność tego procesu, konieczność stosowania kosztownych katalizatorów oraz drastyczne warunki prowadzenia procesu indukujące degradacje wielu grup funkcyjnych.[118-127] Ponadto, znacznej komplikacji uległby szlak syntetyczny, gdyż wymagałoby to otrzymanie komercyjnie niedostępnych substratów już wyposażonych w pożądane grupy funkcyjne. Odrzucono również opcję bezpośredniej funkcjonalizacji benzo[*h*]chinoliny poprzez aktywację wiązania C-H, gdyż zgodnie z wieloma źródłami przebiega ona głównie w pozycji 10, tym samym uniemożliwiając zastosowanie otrzymanego produktu w roli liganda cyklometalującego. Wobec tego, strategię syntetyczną postanowiono oprzeć o reakcje tworzenia wiązań pojedynczych, prowadzone w warunkach zapewniających kompatybilność z grupami funkcyjnymi o zróżnicowanym charakterze chemicznym. Spełnienie tych kryteriów było możliwe dzięki wykorzystaniu wszechstronnej reaktywności wiązania C-Br w stechiometrycznych reakcjach metaloorganicznych oraz reakcjach katalitycznych prowadzonych w obecności związków metali przejściowych.

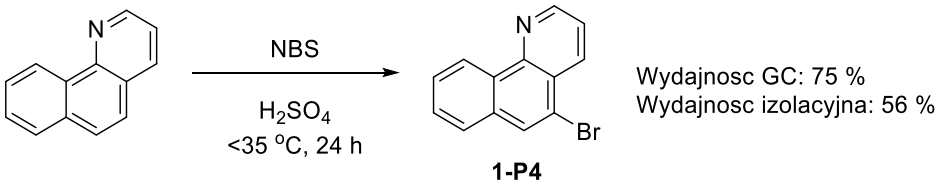

Rys. 35. *Bromowanie benzo[h]chinoliny.*

Związkiem wyjściowym dla wszystkich opisanych przemian była 5-bromobenzo[*h*]chinolina (**1-P4**), która okazała się być głównym produktem bromowania benzo[*h*]chinoliny z użyciem NBS w kwasie siarkowym (Rys. 35), opartego na procedurze bromowania chinoliny.[128] Ponadto, koncept funkcjonalizacji benzo[*h*]chinoliny w pozycji 5 był zgodny z wynikami pracy, w której wykazano różnice w lokalizacji orbitali

HOMO i LUMO w obu izomerach [Ir(bzq)$_3$], szczególnie w obszarze liganda cyklometalującego.[72] Dzięki temu, obecność grupy funkcyjnej w pozycji 5 skoordynowanej bzq powinna mieć większy wpływ na LUMO niż na HOMO odpowiedniego kompleksu, umożliwiając zmianę właściwości związków kompleksowych irydu(III) ją zawierających, co stanowi dodatkową zaletę z perspektywy chemii materiałowej.

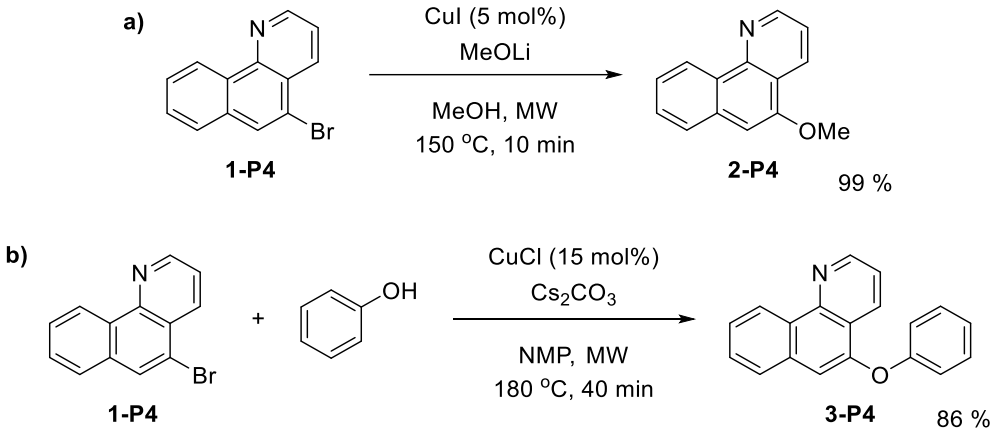

Rys. 36. *Katalizowane związkami miedzi tworzenie wiązań C-O.*

W początkowej fazie prac podjęto próby przyłączenia do rdzenia benzo[*h*]chinolinowego grup metoksylowej i fenoksylowej, w wyniku utworzenia wiązania C-O. Adaptacja znanych z literatury procedur alkoksylowania bromoarenów przy użyciu metanolanu sodu w obecności jodku miedzi(I) oraz metanolu w obecności węglanu cezu i katalizatora palladowego zakończyła się niepowodzeniem,[129,130] gdyż w tych warunkach zachodziła jedynie debrominacja wyjściowego substratu. Nieoczekiwanie prosta zmiana w doborze reagentów, polegająca na zamianie metanolanu sodu na metanolan litu, doprowadziła do zahamowania niepożądanego procesu i selektywnego otrzymania oczekiwanej 5-metoksybenzo[*h*]chinoliny (**2-P4**).[131] Dzięki zastosowaniu mikrofalowego reaktora ciśnieniowego uzyskano pełną konwersję halogenkowego substratu w bardzo krótkim czasie (10 min), a produkt wyizolowano z praktycznie ilościową wydajnością (Rys. 36a). Synteza 5-fenoksybenzo[*h*]chinoliny (**3-P4**) wymagała odmiennego podejścia z uwagi na zdecydowanie bardziej kwasowy charakter fenolu względem metanolu, a tym samym niższą nukleofilowość anionu fenolanowego względem anionu metanolanowego. Badania rozpoczęto od zaadoptowania układu katalitycznego umożliwiającego efektywne O-arylowanie fenoli, opartego o jodek miedzi(I) i acetyloacetonian żelaza(III).[132] Krótka optymalizacja warunków reakcji sprowadzająca się do zwiększenia ilości użytych katalizatorów, wydłużenia czasu i zwiększenia temperatury reakcji, umożliwiła uzyskanie pełnej konsumpcji halogenkowego substratu. Jednakże, wydajność wyizolowanego produktu wyniosła zaledwie 20 %, co świadczyło o degradacji produktu lub substratu. Zamiast dalszej optymalizacji nieefektywnego procesu, postanowiono poszukać procedury O-arylowania z wykorzystaniem innych reagentów. W ten sposób natrafiono na pracę opisującą arylowanie w środowisku NMP, w obecności węglanu cezu i katalitycznych ilości halogenków miedzi(I).[133] Przeprowadzenie reakcji z użyciem **1-P4** według opisanych w cytowanym źródle warunków doprowadziło do uzyskania konwersji na poziomie 54 %, bez śladów debrominacji tego reagenta. Uzyskanie pozytywnego rezultatu zachęciło do dalszej optymalizacji warunków. W rezultacie przeprowadzenia reakcji w reaktorze mikrofalowym i zwiększenia ilości katalizatora oraz temperatury reakcji, osiągnięto prawie całkowitą konwersję pochodnej **1-P4**. Ponadto, wprowadzone modyfikacje literaturowej procedury umożliwiły także skrócenie czasu reakcji, podnosząc efektywność całego procesu. Finalnie, oczekiwany produkt **3-P4** uzyskano z 86-procentową wydajnością izolacyjną (Rys. 36b).

Oprócz przyłączania grup elektronodonorowych w oparciu o tworzenie wiązania C-O, postanowiono także przeprowadzić syntezę aminowych pochodnych benzo[*h*]chinoliny na drodze formacji wiązania C-N. Biorąc pod uwagę bardziej zasadowy charakter atomu azotu w odróżnieniu od atomu tlenu grup alkoksylowych i aryloksylowych, można było oczekiwać, że aminowe grupy będą wykazywały silniejszy efekt przesuwania gęstości elektronowej w kierunku bzqH. Ponadto, w dalszym toku badań 5-aminobenzo[*h*]chinolina (**4-P4**) okazała się bardzo przydatnym prekursorem do otrzymywania innych 5-*N*-funkcyjnych pochodnych benzo[*h*]chinoliny.

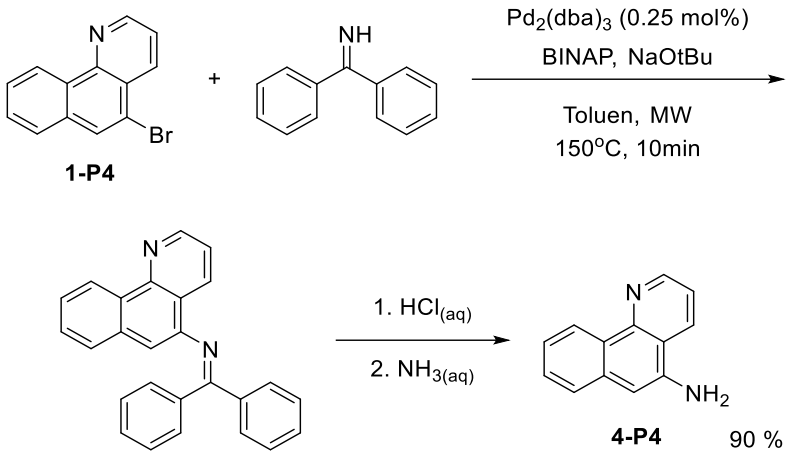

Rys. 37. *Synteza 5-aminobenzo[h]chinoliny z wykorzystaniem ketoiminy w roli syntonu grupy aminowej.*

Mając na uwadze strukturę produktu, najprostszym szlakiem syntetycznym umożliwiającym otrzymanie takiego związku wydawało się bezpośrednie aminowanie **1-P4** z użyciem amoniaku w obecności katalitycznych ilości związków miedzi. W oparciu o literaturę źródłową przetestowano wiele procedur prowadzących do aminofunkcyjnych związków arylowych, wykorzystujących w roli katalizatorów tlenek, chlorek oraz jodek miedzi(I).[134-137] Niestety, żaden z opisanych sposobów nie dawał satysfakcjonujących rezultatów, ze względu na znikomą konwersję substratu lub niewielką selektywność procesu. W najlepszym przypadku uzyskano 30 % konwersji **1-P4** do oczekiwanego produktu przy zastosowaniu 10 mol% jodku miedzi(I), 40 mol% acetyloacetonu oraz węglanu cezu w roli zasady.[137] Jednakże, wiązało się to ze znaczącym udziałem produktu debrominacji w mieszaninie poreakcyjnej (11 %). Przeprowadzenie tej reakcji w reaktorze mikrofalowym w temperaturze 150°C w czasie 10 min umożliwiło podwyższenie konwersji do 43 %, jednak nie zniwelowało ubocznego procesu debrominacji, gdyż zawartość benzo[*h*]chinoliny w mieszaninie poreakcyjnej osiągała wartość 12 %. Przebieg niepożądanego procesu ubocznego powodował nie tylko obniżenie dostępności substratu dla właściwej reakcji, ale także utrudniał izolację czystego produktu. W obliczu nieskuteczności protokołów syntetycznych opierających się na katalizie związkami miedzi, podjęto poszukiwania alternatywnych sposobów umożliwiających efektywne otrzymanie związku **4-P4**. W literaturze natrafiono na koncepcję tzw. „surogatów" amoniaku, czyli związków chemicznych będących jego pochodnymi, których reaktywność umożliwia łatwiejsze przeprowadzenie pożądanej transformacji chemicznej i odzyskanie funkcji aminowej po usunięciu grupy ochronnej.[138-143] Szczególnie interesujące wydało się zastosowanie iminy benzofenonu w roli takiego surogatu, ze względu na łatwość usunięcia grupy blokującej oraz potwierdzoną skuteczność w aminowaniu bromoarenów na drodze reakcji Buchwalda-Hartwiga.[144] Reakcja sprzęgania **1-P4** i wspomnianej wyżej ketiminy w obecności katalizatora palladowego przebiegała bardzo selektywnie w warunkach zaczerpniętych z literatury, dlatego postanowiono przetestować jej przebieg również w reaktorze mikrofalowym. W efekcie uzyskano ilościową konwersję bromopochodnej **4-P4** do produktu zaledwie w ciągu 10 minut (Rys. 37). Hydroliza produktu pośredniego w warunkach kwasowych przebiegała bardzo szybko, co

objawiało się wytrąceniem osadu wolnego benzofenonu. Zasadowy charakter produktu **4-P4** odpowiadał za jego przejście do fazy wodnej, dzięki czemu można było łatwo usunąć wydzielony keton poprzez ekstrakcję rozpuszczalnikiem organicznym. Po zneutralizowaniu ekstraktu uzyskano docelowy produkt **4-P4** ze skumulowaną wydajnością 90 %.

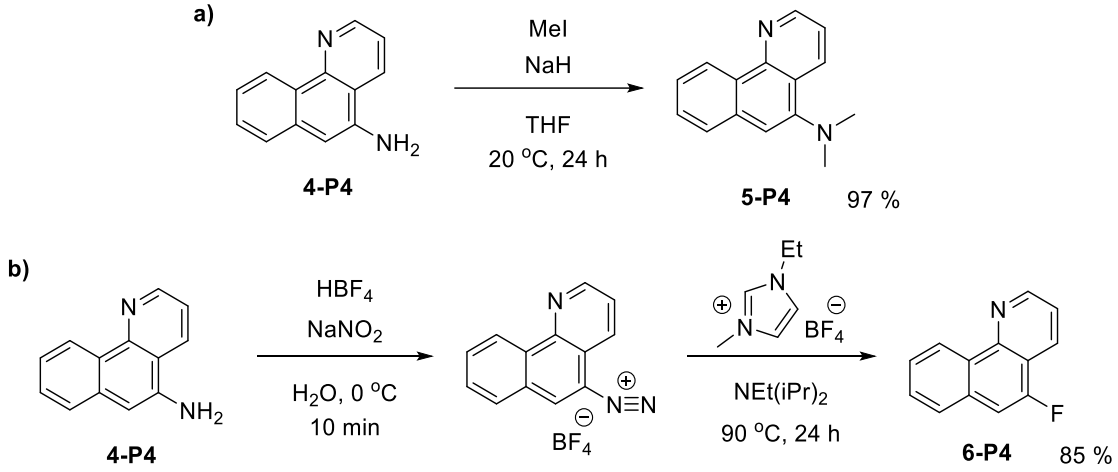

Rys. 38. *Przekształcenia 5-aminobenzo[h]chinoliny.*

Pierwszorzędowe grupy aminowe przyłączone do układów aromatycznych są relatywnie wrażliwe na utlenianie, dlatego wartym rozważenia było zabezpieczenie tej grupy w **4-P4** poprzez podstawienie atomów wodoru. Alkilowanie grupy aminowej przeprowadzono w łagodnych warunkach z użyciem wodorku sodu i jodku metylu, tak aby uniknąć czwartorzędowania. W rezultacie otrzymano 5-dimetyloaminobenzo[*h*]chinolinę (**5-P4**) z wydajnością bliską ilościowej (Rys. 38a).

Aminowa pochodna **4-P4** okazała się być także dogodnym reagentem w otrzymywaniu 5-fluorobenzo[*h*]chinoliny (**6-P4**), potencjalnego liganda *C,N*-cyklometalującego wyposażonego w podstawnik o właściwościach silnie elektronowyciągających. Pierwsze próby fluorowania benzo[*h*]chinoliny z użyciem

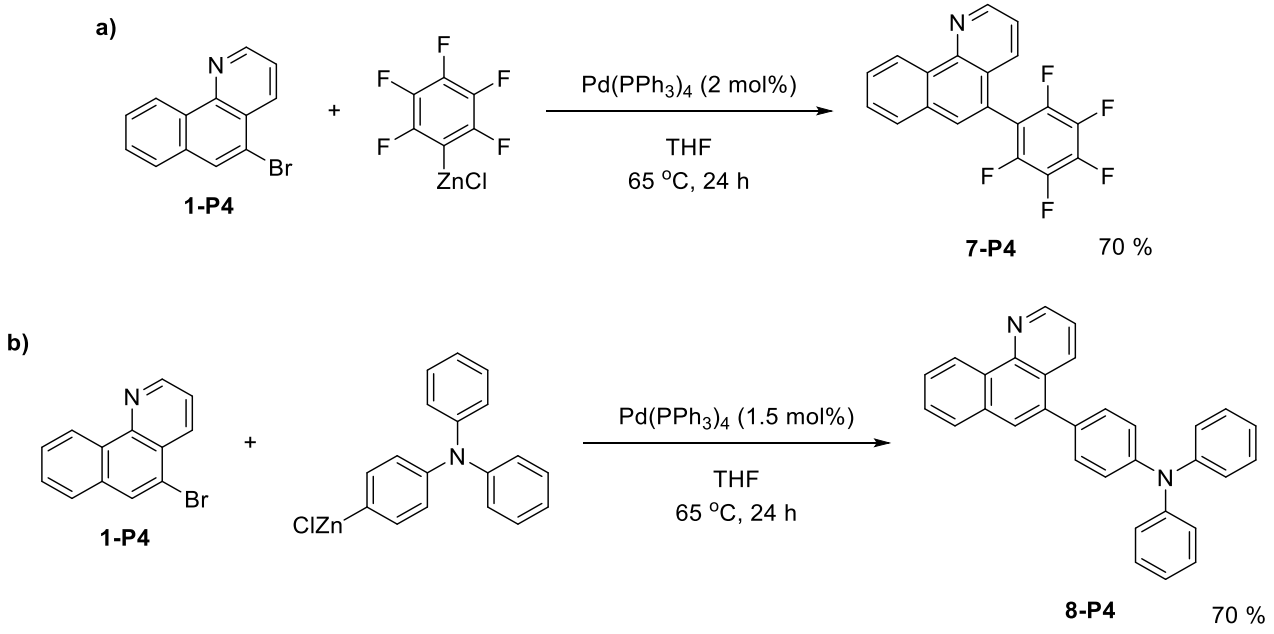

Rys. 39. *Otrzymywanie pochodnych benzo[h]chinoliny na drodze sprzęgania Negishi.*

komercyjnie dostępnego środka Selectfluor® przebiegały z bardzo niską selektywnością, prowadząc do skomplikowanej mieszaniny wielu regioizomerów. Rozdzielenie takiej mieszaniny było praktycznie niemożliwe w skali preparatywnej. Dlatego, syntezy **6-P4** postanowiono dokonać poprzez przekształcenie grupy funkcyjnej w uprzednio selektywnie sfunkcjonalizowanej pochodnej benzo[*h*]chinoliny. Analiza retrosyntetyczna pozwoliła wytypować reakcję Balza-Schiemanna jako potencjalny szlak syntetyczny. Reakcja ta polega na konwersji aminoarenów do soli diazoniowych z anionem tetrafluoroboranowym, których rozkład daje fluoroareny z zachowaniem regioselektywności.[145] Dzięki zastosowaniu opisanej metodologii udało się otrzymać odpowiednią sól diazoniową ze związku **4-P4**, którą następnie przekształcono do docelowego związku **6-P4** poprzez ogrzewanie utworzonego tetrafluoroboranu diazoniowego w cieczy jonowej. Właściwy produkt otrzymano z sumaryczną wydajnością 85 % (Rys. 38b).

Kolejnym podjętym wyzwaniem było przyłączenie ugrupowań aromatycznych o charakterze elektronowyciągającym (podstawnika pentafluorofenylowego) oraz wspomagającym przewodnictwo dziurowe (ugrupowanie 4-(*N,N*-difenyloamino)fenylowe) w wyniku utworzenia wiązania C-C. Syntezę docelowych związków rozważano na drodze trzech reakcji sprzęgania: Kumady, Suzuki-Miyaura oraz Negishi. Z uwagi na relatywnie wysoką nukleofilowość związków Grignarda (wykorzystywanych w reakcji Kumady) mogącą powodować reakcje uboczne związane z aktywacją wiązania C-F, a także konieczność uprzedniego otrzymania i wyizolowania odpowiednich kwasów boronowych (stosowanych w sprzęganiu Suzuki-Miyaura), to reakcję Negishi wytypowano jako najbardziej dogodną. Łatwe do otrzymania reagenty cynkoorganiczne poddano sprzęganiu z **1-P4** we wrzącym THF, w obecności katalitycznych ilości [$Pd(PPh_3)_4$] (Rys. 39). Obie reakcje przebiegły selektywnie, w rezultacie umożliwiając uzyskanie czystych produktów **7-P4** oraz **8-P4** z wydajnościami 70 %.

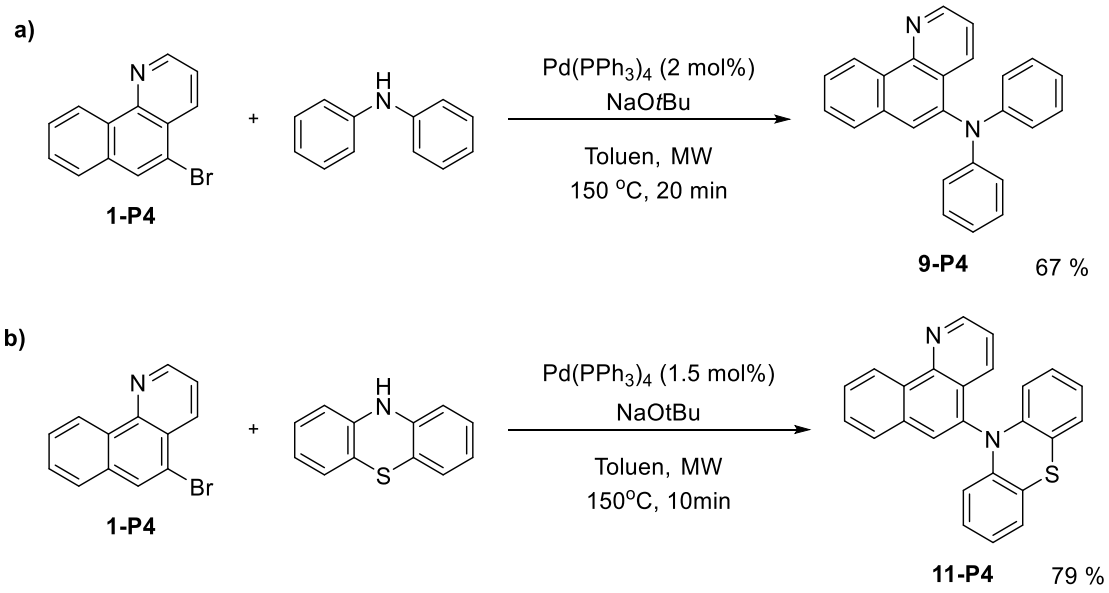

Rys. 40. *Otrzymywanie pochodnych benzo[h]chinoliny na drodze N-aminowania Buchwalda-Hartwiga.*

Pozostając w temacie wyposażania benzo[*h*]chinoliny w ugrupowania wspomagające transport dziur elektronowych, grupę tych związków rozszerzono o kolejne przykłady wykorzystując tworzenie wiązań C-N w reakcji aminowania Buchwalda-Hartwiga. W roli reagentów do sprzęgania z **1-P4** wytypowano difenyloaminę oraz fenotiazynę, ugrupowania znane z przewodnictwa dziurowego indukowanego obecnością heteroatomów i wiązań wielokrotnych. W oparciu o bardzo pozytywny przebieg sprzęgania **1-P4** z iminą benzofenonu w obecności związków palladu, postanowiono w pierwszej kolejności przetestować opracowane wcześniej

warunki reakcji dla otrzymywania **4-P4**, zastępując jedynie katalizator bardziej przystępnym kompleksem [$Pd(PPh_3)_4$] (Rys. 40). Zaskakująco, w obu przypadkach uzyskano całkowitą konwersję **1-P4** w bardzo krótkim czasie już podczas pierwszej próby. Przebieg reakcji można było obserwować wizualnie poprzez wytrącający się osad bromku sodu, który zaczął się pojawiać bardzo szybko już przed osiągnięciem zadanej temperatury reakcji. Po szybkiej procedurze oczyszczania metodą chromatografii flash, uzyskano 5-(difenyloamino)benzo[*h*]chinolinę (**9-P4**) oraz 5-(*N*-fenotiazylo)benzo[*h*]chinolinę (**11-P4**) z wydajnościami odpowiednio 67 % i 79 %.

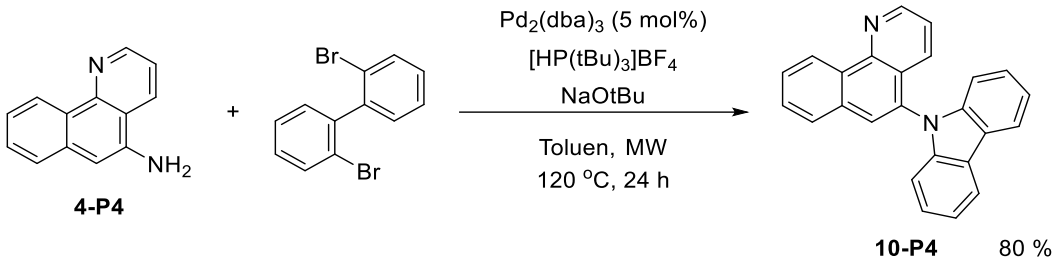

Rys. 41. *Skuteczna synteza 5-karbazolilobenzo[h]chinoliny na drodze podwójnego sprzęgania Buchwalda-Hartwiga.*

Ostatnim otrzymanym przykładem pochodnej benzo[*h*]chinoliny wyposażonym w ugrupowanie wspomagające przewodnictwo dziurowe była 5-(*N*-karbazolilo)benzo[*h*]chinolina (**10-P4**). Opierając się na zakończonych powodzeniem syntezach pochodnych **9-P4** oraz **11-P4**, związek **10-P4** postanowiono otrzymać w podobnych warunkach, czyli na drodze utworzenia wiązania C-N wykorzystując **1-P4** oraz karbazol. Niestety, w przypadku tego typu substratów wygenerowanie wiązania C-N w oparciu o literaturowe metody okazało się nie być trywialne jak przypuszczano.[146-148] Zastosowanie kombinacji różnych prekatalizatorów (octan palladu(II), [$Pd_2(dba)_3$], [$PdCl_2(fosfina)_2$]), fosfin (tris-*tert*-butylofosfina, tricykloheksylofosfina, trifenylofosfina, *rac*-BINAP) oraz zasad (*tert*-butanolan sodu i potasu) w toluenie nie doprowadziło do otrzymania choćby śladowych ilości oczekiwanego produktu. Wszystkie układy reakcyjne okazały się nieefektywne zarówno w łaźni olejowej (110 °C, 24h) , jak i w reaktorze mikrofalowym (150 °C, 60 min). Problem ten rozwiązano poprzez zmianę strategii syntetycznej, która polegała na zamianie stosowanych substratów (Rys. 41). W odróżnieniu od wcześniejszego podejścia, tym razem otrzymanie docelowego związku wymagało utworzenia pierścienia heterocyklicznego poprzez formację dwóch wiązań C-N.[149] W celu uniknięcia przebiegu niepożądanego procesu oligomeryzacji substratów, podwójne aminowanie Buchwalda-Hartwiga pomiędzy aminofunkcyjną **4-P4** oraz 2,2'-dibromobifenylem przeprowadzono w obniżonej temperaturze (120 °C) oraz wydłużonym czasie (24 h) względem transformacji przedstawionych na Rys. 40. W rezultacie pochodną **10-P4** otrzymano z wydajnością 80 %. Zaskakująco, układ katalityczny skuteczny w utworzeniu dwóch wiązań C-N okazał się wcześniej być nieefektywny w reakcji tworzenia pojedynczego wiązania C-N pomiędzy **1-P4** oraz karbazolem.

Ostatnim celem syntetycznym opisanym w pracy [**P4**] było otrzymanie pochodnej benzo[*h*]chinoliny wyposażonej w ugrupowanie o dużej zawadzie sterycznej, mogącej pełnić rolę liganda inhibitującego agregację irydowych emiterów fosforescencyjnych, tym samym ograniczając możliwość przebiegu niekorzystnego procesu stężeniowego wygaszania stanów trypletowych. W oparciu o doświadczenie członków zespołu Zakładu Chemii i Technologii Związków Krzemu, postanowiono wykorzystać steryczne właściwości POSS. Jako obiekt do badań wybrano silseskwioksan zwierający siedem grup izobutylowych oraz grupę dimetylowinylosiloksylową (przedstawioną na Rys. 42), chcąc wykorzystać reaktywność wiązania C=C grupy winylowej. Pierwsza próba połączenia benzo[*h*]chinoliny oraz ugrupowania POSS polegała na reakcji Hecka pomiędzy **1-P4** oraz winylową pochodną POSS w oparciu o cytowaną literaturę.[150]

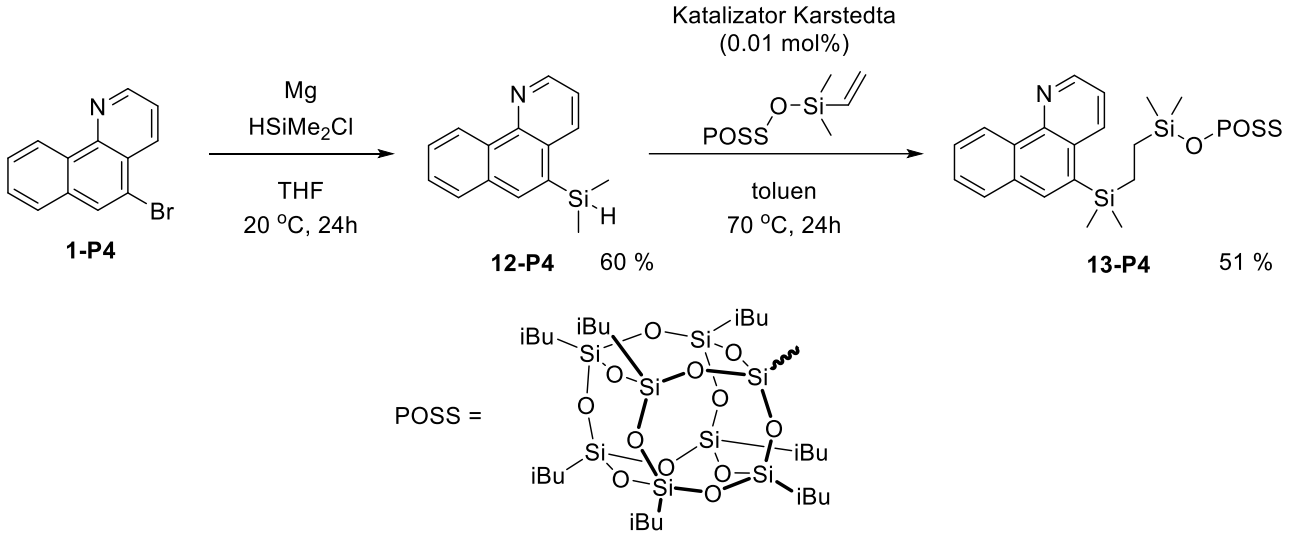

Rys. 42. *Synteza pochodnych krzemowych benzo[h]chinoliny.*

Niestety, w mieszaninie poreakcyjnej nie udało się zaobserwować nawet śladowych ilości oczekiwanego produktu, co świadczyło o wyjątkowej inertności tego układu reagentów. Zatem, w celu podstawienia benzo[*h*]chinoliny ugrupowaniem POSS postanowiono zaimplementować reakcję hydrosililowania, najpowszechniej stosowane narzędzie syntetyczne w chemii związków krzemoorganicznych.[151] Jednakże, wymagało to rozszerzenia szlaku syntetycznego o dodatkową pochodną benzo[*h*]chinoliny, zawierającą w swojej strukturze reaktywne wiązanie Si-H. 5-dimetylosililobenzo[*h*]chinolinę (**12-P4**) otrzymano w reakcji substytucji nukleofilowej atomu chloru w $HSiClMe_2$ z użyciem związku Grignarda wytworzonego z **1-P4** (Rys. 42). Kluczem do sukcesu było przeprowadzenie reakcji tworzenia związku magnezoorganicznego i substytucji metodą *in-situ*. Polegała ona na wkraplaniu roztworu **1-P4** do układu zawierającego aktywowany magnez oraz $HSiClMe_2$. Wcześniej wybraną winylofunkcyjną pochodną POSS udało się poddać reakcji hydrosililowania z użyciem związku **12-P4** w obecności katalizatora Karstedta, otrzymując oczekiwaną pochodną benzo[*h*]chinoliny wyposażoną w ugrupowanie o dużej zawadzie sterycznej (**13-P4**). Niezależnie wygenerowana magnezoorganiczna pochodna związku **1-P4** tworzyła czarny roztwór w THF oraz nie reagowała z chlorosilanem w oczekiwany sposób, co może świadczyć o jej degradacji lub dezaktywacji na skutek koordynacji N→Mg.

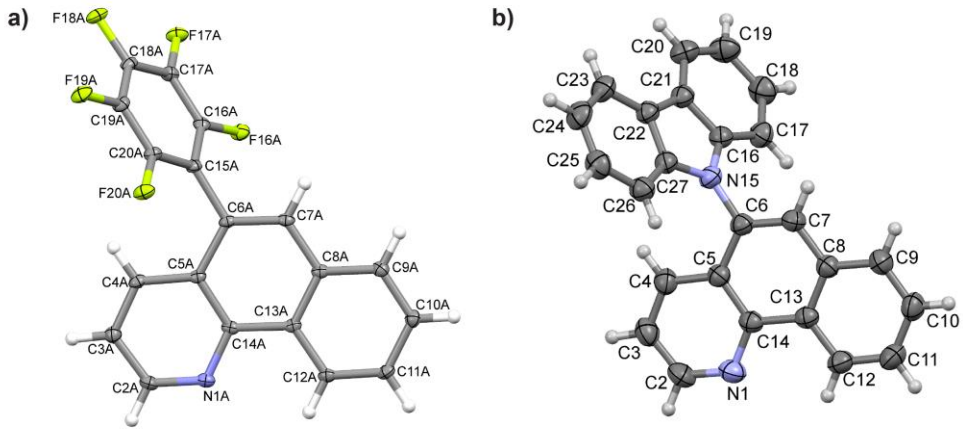

Rys. 43. *Przykładowe struktury krystaliczne związków **7-P4** (a) oraz **10-P4** (b).*

Podsumowując, w omawianej publikacji przedstawiono szereg metod umożliwiających otrzymanie dotąd nie opisanych w literaturze pochodnych benzo[*h*]chinoliny zawierających różne grupy funkcyjne w pozycji 5. Otrzymane związki scharakteryzowano przy pomocy analizy NMR, a strukturę kilku z nich potwierdzono analizą XRD (Rys. 43). Ideą, która przeświecała wprowadzeniu tego typu grup była zmiana gęstości elektronowej na rdzeniu liganda, wspomaganie półprzewodnictwa dziurowego oraz zwiększenie zawady sterycznej utrudniającej agregację. Wszystkie otrzymane związki posiadały kieszeń koordynacyjną zdolną do *C,N*-cyklometalacji, co czyni je potencjalnymi ligandami dla atomów metali przejściowych, szczególnie fosforescencyjnych emiterów użytecznych w technologii OLED.

7.5. Dwurdzeniowe kompleksy irydu(III) o strukturze $[Ir(C\hat{}N)_2(\mu\text{-}Cl)]_2$

Ostatni artykuł z przedstawionego cyklu [**P5**] podejmuje tematykę otrzymywania μ-chlorkowych dwurdzeniowych kompleksów irydu(III) oraz charakterystykę ich właściwości spektroskopowych. Kompleksy te mają szczególne znaczenie dla technologii OLED, gdyż bardzo często pełnią rolę związków pośrednich w szlakach syntetycznych irydowych emiterów fosforescencyjnych. Do największymi atutów tej pracy należy zaliczyć: usprawnienie metodologii otrzymywania dwurdzeniowych kompleksów dzięki wykorzystaniu promieniowania mikrofalowego; syntezę nowych przykładów związków wyposażonych w grupy elektronodonorowe, elektronowyciągające oraz wspomagające przewodnictwo dziurowe; a także szczegółowe wyjaśnienie wątpliwości wokół zachowania tej klasy związków w obecności rozpuszczalników koordynujących. Wszystkie te aspekty ujęto schematycznie na abstrakcie graficznym (Rys. 44).

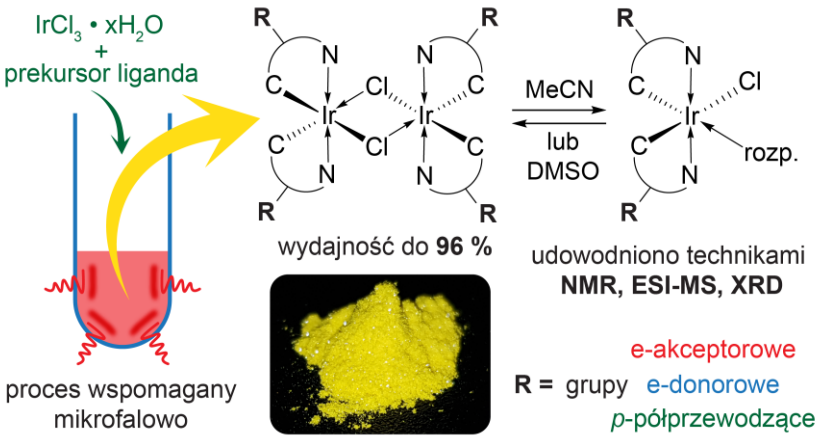

Rys. 44. *Graficzne przedstawienie zagadnień poruszanych w publikacji [**P5**].*

Inspirację do podjętych badań stanowił kontrast pomiędzy mnogością doniesień literaturowych opisujących syntezę dimerów w klasycznych, dla tego typu reakcji, warunkach (ogrzewanie w łaźni olejowej przez około 24 godziny)[82-89] oraz niewielką liczbą doniesień na temat syntez prowadzonych z użyciem niekonwencjonalnych źródeł energii (takich jak promieniowanie mikrofalowe).[90-93] Tym bardziej, że w literaturze jak dotąd nie odnotowano spójnego porównania wpływu medium grzewczego na efektywność reakcji tworzenia dimerów. Ponadto, dodatkowy impuls stanowiły pozytywne efekty zastosowania promieniowania mikrofalowego w syntezie organicznej, zaobserwowane w trakcie innych badań własnych.[152-154] Jako reakcję modelową wybrano syntezę związku **$[Ir(\mu\text{-}Cl)(ppy)_2]_2$-P5** z użyciem uwodnionego chlorku irydu(III) oraz 2-fenylopirydyny w środowisku 2-metoksyetanolu oraz wody (Rys. 45).

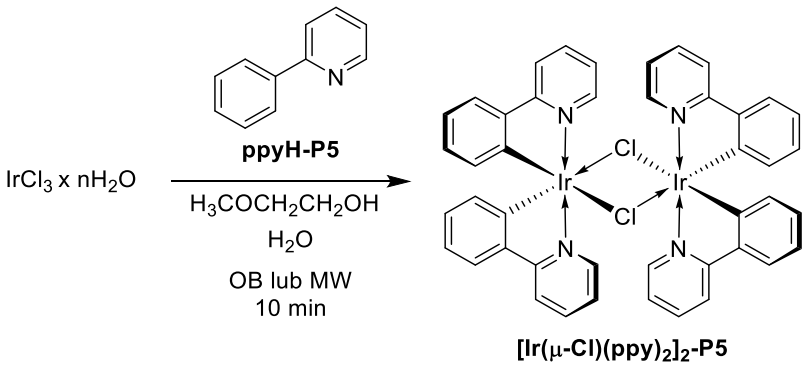

Rys. 45. *Schemat reakcji modelowej.*

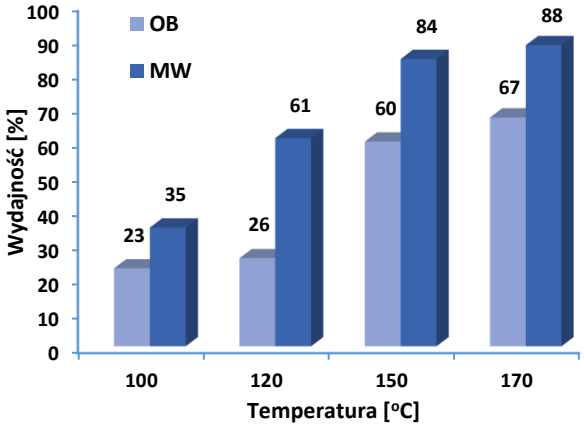

Rys. 46. *Wydajność reakcji modelowej w zależności od temperatury i medium grzewczego.*

Wyniki wstępnych prób cyklometalacji w reaktorze mikrofalowym wypadły bardzo pozytywnie, dlatego zdecydowano o przeprowadzeniu szeregu systematycznych badań, mających na celu zobrazowanie efektu medium grzewczego oraz temperatury na przebieg reakcji (Rys. 46). W oparciu o uzyskane dane stwierdzono wyraźny wpływ obu zmiennych na wydajność otrzymywanego produktu **[Ir(*μ*-Cl)(ppy)$_2$]$_2$-P5**. Podsumowując rezultaty uzyskane podczas tych badań stwierdzono, że wydajność rosła wraz ze wzrostem temperatury reakcji, a proces wspomagany promieniowaniem mikrofalowym przebiegał bardziej efektywnie, aniżeli z użyciem klasycznego medium grzewczego. Okazało się, że najwydajniej reakcja przebiegała w reaktorze mikrofalowym, w temperaturze 170 °C, w czasie 10 minut. Niemniej jednak, niektóre ligandy mogą okazać się niestabilne w tak drastycznych warunkach (należy mieć na uwadze wydzielający się podczas cyklometalacji HCl), co zostało odnotowane w literaturze,[93] a także dostrzeżone w trakcie otrzymywania niektórych dimerów prezentowanych w pracy [**P5**]. Mając powyższe na uwadze, zadecydowano o wyborze niższej temperatury (150 °C) jako optymalnej dla tego procesu, gdyż skutkowało to jedynie minimalnym obniżeniem wydajności, pozwalając w zamian uniknąć pracochłonnego oczyszczania końcowych produktów od zanieczyszczeń powstałych w skutek degradacji.

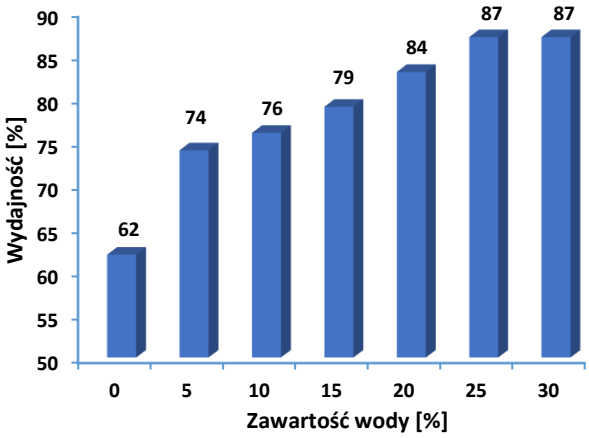

Rys. 47. *Wpływ zawartości wody w środowisku reakcji modelowej na wydajność.*

Kolejnym parametrem, który został przeanalizowany w ramach prezentowanej pracy była zawartość wody w układzie reakcyjnym. W oparciu o dane literaturowe stwierdzono, że woda jest niezbędna do właściwego przebiegu reakcji tworzenia oczekiwanych dimerów.[82-89,93] Jednakże, kwestia ta nie była w żaden

sposób systematycznie przebadana w dostępnych źródłach literaturowych, a opisane metodologie cechowały się relatywnie dużą zmiennością tego parametru. W odpowiedzi na napotkaną lukę przeprowadzono serię testów, w których jedyną zmienną była procentowa zawartość wody w środowisku reakcji. Otrzymane rezultaty przedstawiono w formie wykresu na Rys. 47. Jak można zauważyć, dodatek wody ma bardzo duże znaczenie dla efektywności zachodzącego procesu. Maksymalną wydajność uzyskano przy 25-procentowej zawartości wody w układzie, a dalsze jej zwiększanie nie przynosiło korzyści. Wręcz przeciwnie, zbyt duży dodatek wody może negatywnie wpływać na rozpuszczalność organicznych prekursorów ligandów, tym samym zmniejszając ich stężenie w roztworze, co może mieć przełożenie na znacznie niższą wydajność oczekiwanego produktu. Warto przy tym wspomnieć, że w przypadku braku dodatku wody obserwowano wyraźne cząstki nieprzereagowanego chlorku irydu(III) w mieszaninie poreakcyjnej. Mając na uwadze poczynione obserwacje należy przyjąć, że woda jako polarny rozpuszczalnik pełni dwojaką rolę w badanym procesie: podnosi stężenie jonów metalu w roztworze wspomagając rozpuszczalność chlorku irydu, oraz poprawia efektywność transferu energii poprzez wspomaganie absorpcji promieniowania mikrofalowego. W efekcie potwierdzono, że najlepsze rezultaty daje prowadzenie wspomaganej mikrofalowo reakcji w mieszaninie woda : 2-metoksyetanol w stosunku 1 : 3. Wielką zaletą zoptymalizowanej metodologii było otrzymywanie produktu w formie krystalicznej, która ułatwiała jego izolację.

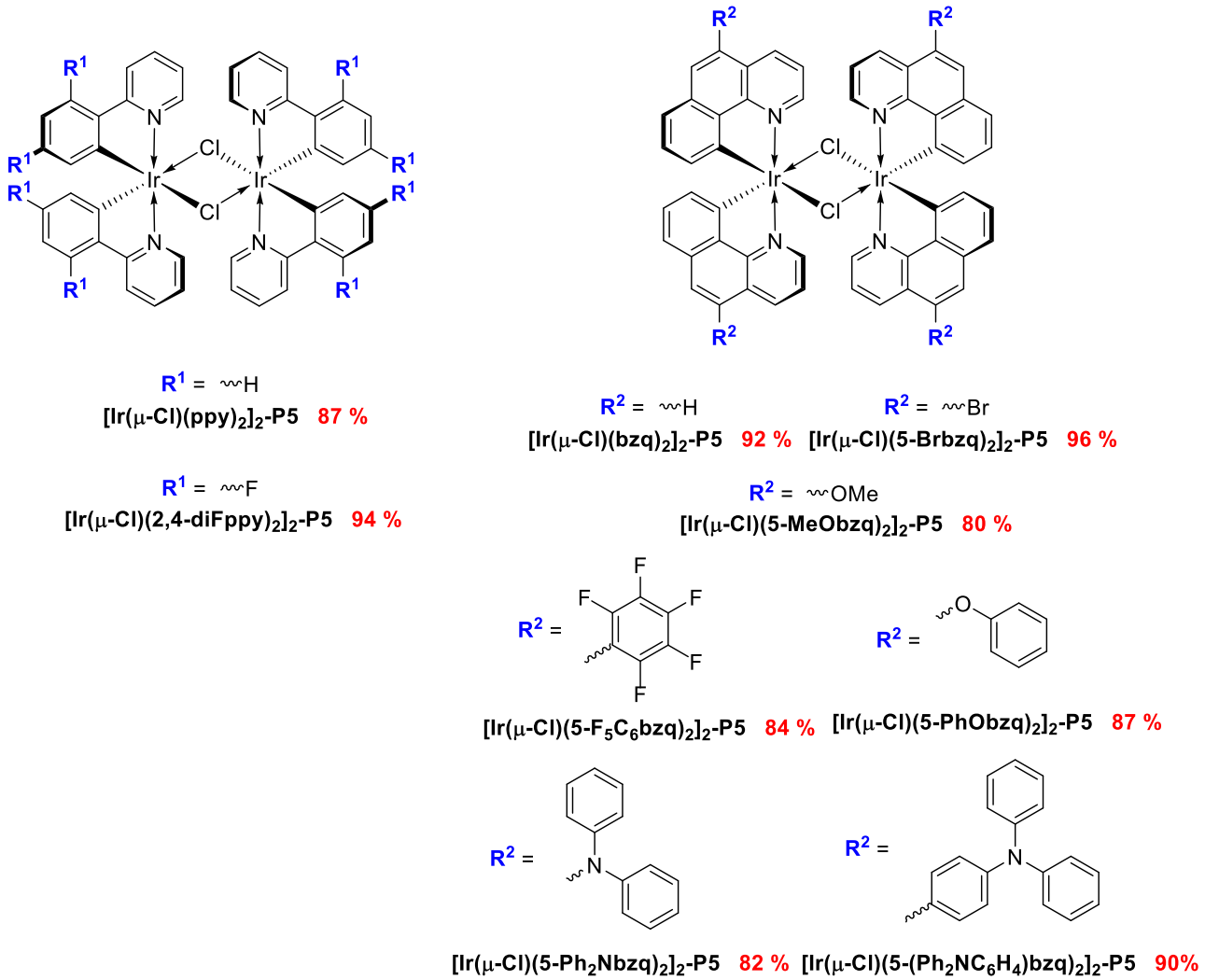

Rys. 48. *Wzory strukturalne otrzymanych dwurdzeniowych kompleksów μ-chlorkowych wraz z wydajnościami reakcji.*

W oparciu o warunki reakcji zoptymalizowane dla modelowego układu reagentów, przeprowadzono syntezy rodziny dwurdzeniowych kompleksów wykorzystując także prekursory ligandów opisane w artykule **P4** (**1-P4**, **2-P4**, **3-P4**, **7-P4**, **8-P4**, **9-P4**). Oprócz nowych, otrzymano także znane z literatury związki **[Ir(μ-Cl)(2,4-diFppy)$_2$]$_2$-P5** oraz **[Ir(μ-Cl)(bzq)$_2$]$_2$-P5**, oba z bardzo wysokimi wydajnościami. Wzory otrzymanych związków zawierających motyw strukturalny ppy oraz bzq przedstawiono na Rys. 48. W grupie otrzymanych kompleksów znalazły się przykłady dimerów wyposażonych w grupy elektronodonorowe (metoksy, fenoksy), elektronowyciągające (bromo, pentafluorofenylo) oraz wspomagające przewodnictwo dziurowe (*N*-difenyloamino, 4-(*N*-difenyloamino)fenylo). Relatywnie agresywne środowisko reakcji nie miało negatywnego wpływu na selektywność procesu, w tym stabilność wiązań C-F oraz C-Br, a także regioselektywność cyklometalacji w przypadku **5-Ph$_2$NbzqH-P5**. Otrzymane związki stanowią pierwsze przykłady cyklometalowanych kompleksów irydu(III) stabilizowanych ligandami będącymi pochodnymi bzq, co może mieć duże znaczenie dla technologii OLED biorąc pod uwagę szeroką użyteczność emiterów bazujących na ligandach będących pochodnymi ppy. W dodatku, **[Ir(μ-Cl)(5-Brbzq)$_2$]$_2$-P5** stanowi bardzo użyteczny substrat do dalszych przekształceń na drodze aktywacji wiązania C-Br. Wszystkie wymienione dimery zostały otrzymane z bardzo wysokimi wydajnościami, co stanowi niewątpliwą zaletę tej metodologii z uwagi na wysoką cenę irydu i jego związków.

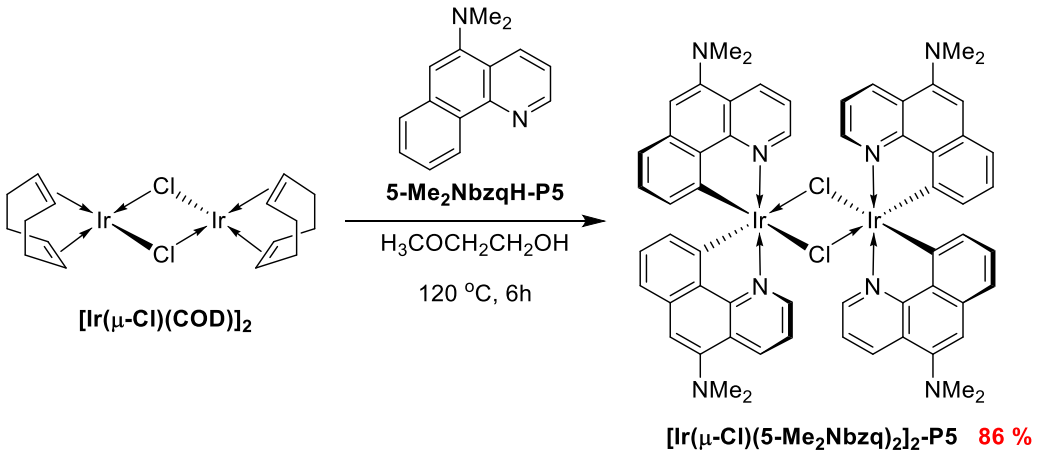

Rys. 49. *Alternatywna metoda otrzymywania* ***[Ir(μ-Cl)(5-Me$_2$Nbzq)$_2$]$_2$-P5***.

Niestety, opracowana metodologia zawiodła w przypadku syntezy związku **[Ir(μ-Cl)(5-Me$_2$Nbzq)$_2$]$_2$-P5**. Jak się później okazało, nie było to spowodowane wpływem promieniowania mikrofalowego, gdyż rezultat próby przeprowadzonej w łaźni olejowej był równie niesatysfakcjonujący. Przypuszczalnie był to efekt obecności grupy dimetyloaminowej w ligandzie, poprzez jej silne oddziaływanie z HCl wydzielającym się w trakcie cyklometalacji, co jest niezależne od medium grzewczego. Problem udało się rozwiązać poprzez zaimplementowanie innej metodologii, w trakcie której pH nie ulega zmianie.[155] W tym wariancie rolę prekursora metalu pełnił kompleks **[Ir(μ-Cl)(COD)]$_2$**, a obecność wody w środowisku reakcji nie była konieczna (Rys. 49). Finalnie udało się otrzymać docelowy związek z wydajnością 86 %.

Oprócz wcześniej wymienionych kompleksów dwurdzeniowych zawierających 5-członowe pierścienie cyklometalowane, w publikacji [**P5**] opisano także syntezę dimerów charakteryzujących się 6-członowym pierścieniem cyklometalowanym. Związki tego typu okazały się przydatne w konstrukcji emiterów fosforescencyjnych z uwagi na brak sprzężenia pomiędzy częściami *C*- oraz *N*- donorowymi, umożliwiający w miarę niezależne wpływanie na gęstość elektronową w tych dwóch obszarach liganda.[156-159] Cecha ta ma szczególne znaczenie w konstrukcji emiterów fosforescencyjnych z zakresu światła niebieskiego. W omawianej pracy [**P5**] została opisana synteza dimerów z wykorzystaniem dwóch pochodnych 2-fenoksypirydyny:

PhOPyMeH-P5 oraz **F$_3$CPhOPyH-P5** (Rys. 50). Otrzymane związki stanowią atrakcyjny substrat do dalszych przekształceń.

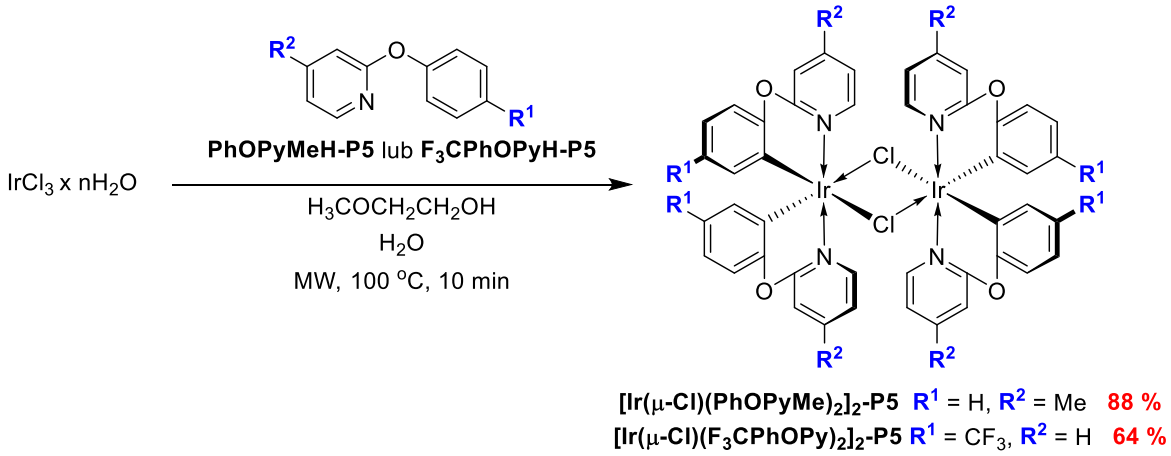

Rys. 50. *Schemat otrzymywania dimerów z wykorzystaniem pochodnych 2-fenoksypirydyny.*

Podsumowując część syntetyczną, wszystkie opisane dimery zostały otrzymane z dobrymi lub bardzo dobrymi wydajnościami. Największą zaletę opisanej metodologii stanowił niezwykle krótki czas reakcji (10 minut), mocno kontrastujący z metodologiami opisywanymi w głównym nurcie tej tematyki. Ponadto, w większości doniesień literaturowych dimery były syntezowane w formie surowej i wykorzystywane do dalszych przekształceń bez oczyszczania, a w niektórych źródłach ich czystość nawet nie była weryfikowana.[37,62,79-81] W opozycji do tego, w omawianej publikacji [**P5**] potwierdzono wysoką czystość otrzymanych materiałów za pomocą technik spektroskopowych. Opublikowane zostały także dwie struktury krystaliczne potwierdzające otrzymanie docelowych związków chemicznych.

Analiza ^{1}H NMR otrzymanych dimerów rozpuszczonych w DMSO-d$_6$ ujawniła dość niespodziewany rezultat, jakim było zaobserwowanie podwojonej ilości sygnałów pochodzących od ligandów cyklometalujących. Przykładowe widmo zarejestrowane dla związku **[Ir(*μ*-Cl)(ppy)$_2$]$_2$-P5** przedstawiono na Rys. 51. Było to o tyle niespodziewane, że ligandy w tego typu związkach kompleksowych powinny się charakteryzować równocennością chemiczną, w efekcie manifestując tylko jeden komplet linii rezonansowych. W rzeczy samej, wiele podobnych związków opisanych w literaturze spełniało to kryterium.[86,160,161] Jednakże, były to widma zarejestrowane w rozpuszczalnikach niepolarnych takich jak CD_2Cl_2 czy $CDCl_3$, co od początku sugerowało, iż polarna i koordynująca natura DMSO może mieć z tym związek. Podczas przeszukiwania literatury napotkano na sprzeczne informacje, gdyż odnaleziono dokładnie te same dane spektroskopowe przypisane do dwóch różnych związków.

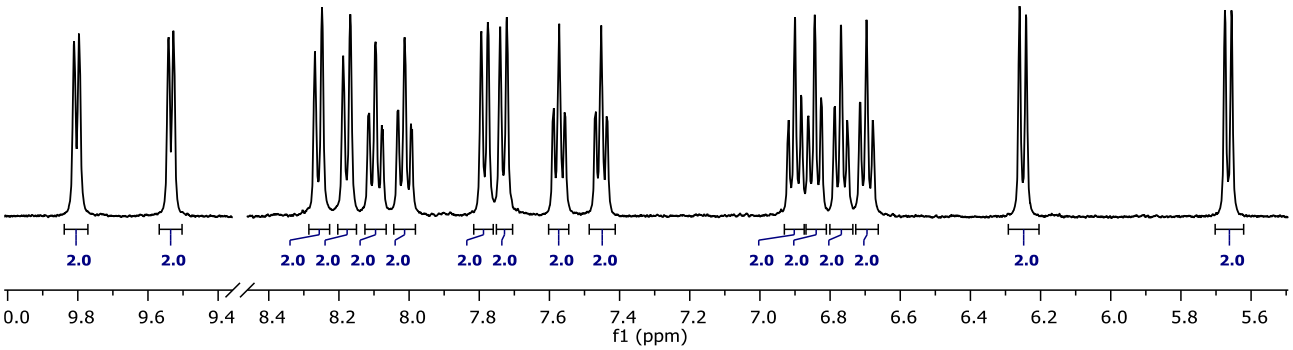

Rys. 51. *Fragment widma ^{1}H NMR związku **[Ir(*μ*-Cl)(ppy)$_2$]$_2$-P5** rozpuszczonego w DMSO-d$_6$.*

Pierwsze źródło raportowało ten sam zestaw linii rezonansowych na widmie ^{1}H NMR związku $[Ir(ppy)_2(DMSO)_2]PF_6$,[162] z kolei drugie przypisywało je **[Ir(μ-Cl)(ppy)$_2$]$_2$-P5**, lecz bez wyjaśnienia przyczyny podwojenia ilości zarejestrowanych sygnałów.[84] W pracy [**P5**] podjęto się wyjaśnienia napotkanych rozbieżności i ustalenia co faktycznie odpowiada za taki obraz spektroskopowy. Do badań wyselekcjonowano nie tylko DMSO, ale także ACN, który również jest znany z właściwości koordynujących, a jego lotność umożliwia zastosowanie w ESI-MS, w odróżnieniu od DMSO.

Analiza dostępnej literatury na temat dwurdzeniowych μ-chlorkowych kompleksów rodu(III) i irydu(III) naprowadziła na trop, że przyczyną badanego fenomenu może być rozszczepienie mostków μ-chlorkowych przez rozpuszczalniki koordynujące, w rezultacie dające kompleksy monordzeniowe o strukturze [Ir(C^N)$_2$Cl(rozpuszczalnik)].[83,163] Jednakże, nie zostało to w pełni potwierdzone z uwagi na odwracalność tego procesu i odtwarzanie oryginalnego dimeru w trakcie izolacji.[164] Z tego względu, najlepszym sposobem izolacji produktów rozszczepienia była krystalizacja, proces wręcz wymagający obecności rozpuszczalnika w trakcie formowania kryształów produktu. W rezultacie opisanych w pracy starań udało się otrzymać monokryształy form monordzeniowych zawierających skoordynowane cząsteczki zarówno ACN jak i DMSO. Rozwiązane struktury krystaliczne przedstawiono na Rys. 52. Otrzymane struktury cechują się brakiem elementów symetrii, co powinno być przyczyną podwojenia ilości obserwowanych linii rezonansowych na zarejestrowanych widmach ^{1}H NMR. Ponadto, ligandy ppy powinny być różnicowane przez dysproporcję w efekcie *trans* anionów chlorkowych oraz cząsteczek ACN i DMSO. W pracy podjęto także krótką dyskusję parametrów sieci krystalicznych.

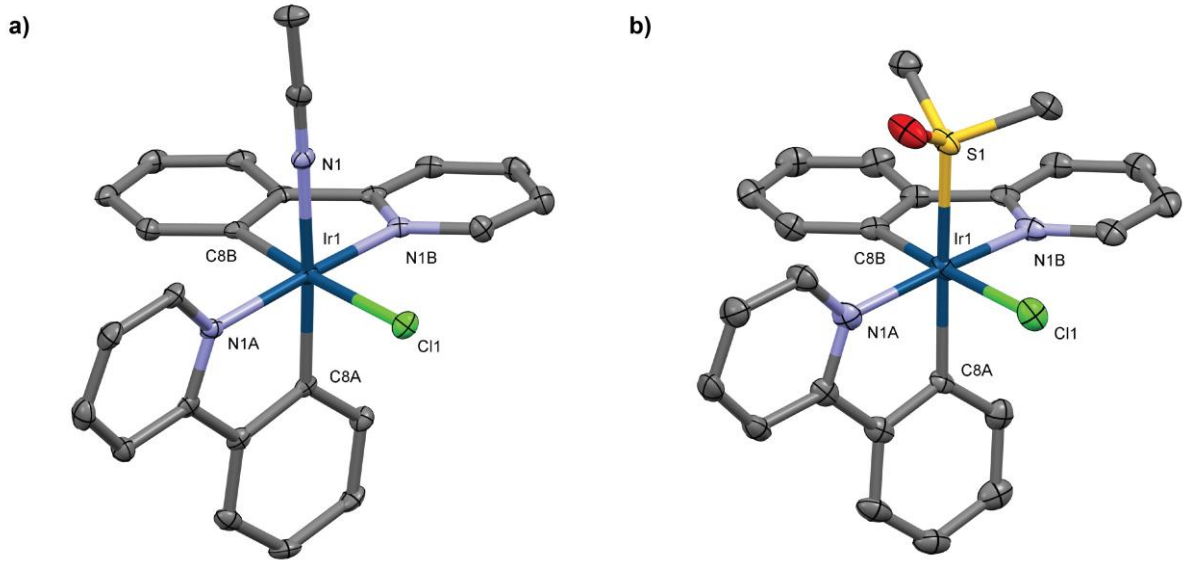

Rys. 52. *Struktury krystaliczne rozszczepionych kompleksów* ***[Ir(ppy)$_2$Cl(ACN)]-P5*** *(a) oraz* ***[Ir(ppy)$_2$Cl(DMSO)]-P5*** *(b).*

Po potwierdzeniu przebiegu procesu rozszczepienia mostków μ-chlorkowych przez rozpuszczalniki koordynujące przy pomocy techniki XRD, postanowiono powiązać ten rezultat z obrazem w spektroskopii ^{1}H NMR. W tym celu kryształy **[Ir(ppy)$_2$Cl(ACN)]-P5** i **[Ir(ppy)$_2$Cl(DMSO)]-P5** rozpuszczono w CD_2Cl_2 i zarejestrowano widma ^{1}H NMR dla otrzymanych roztworów, oczekując zaobserwowania także sygnałów pochodzących od cząsteczek rozpuszczalników. Nieoczekiwanie, stwierdzono bardzo duże różnice w obrazie spektroskopowym analizowanych związków. W przypadku **[Ir(ppy)$_2$Cl(ACN)]-P5** zaobserwowano jedynie jeden komplet sygnałów odpowiadających ppy oraz singlet odpowiadający wolnej cząsteczce ACN. Świadczyło to o całkowitym odtworzeniu μ-chlorkowego kompleksu dwurdzeniowego. Nawet dodatek kolejnych porcji ACN do próbki nie zmieniał stanu równowagi. Z kolei w przypadku **[Ir(ppy)$_2$Cl(DMSO)]-P5** rezultat analizy

^{1}H NMR był znacznie bardziej skomplikowany. Na widmie można było zaobserwować nawet więcej niż dwa komplety sygnałów odpowiadających różnocennym ligandom ppy, co świadczyło o znacznie bardziej zbalansowanej równowadze pomiędzy formą monordzeniową i dwurdzeniową, niż w przypadku ACN. W celu zilustrowania przejścia pomiędzy obiema formami, przeprowadzono miareczkowanie **[Ir(μ-Cl)(ppy)$_2$]$_2$-P5** z użyciem DMSO, monitorując proces przy użyciu techniki ^{1}H NMR (Rys. 53). Jako pierwsze zaprezentowano widmo związku **[Ir(μ-Cl)(ppy)$_2$]$_2$-P5** zarejestrowane w czystym CD_2Cl_2. Każde kolejne widmo przedstawia analizę wykonaną po dodaniu 2 eq DMSO do roztworu badanego kompleksu dwurdzeniowego.

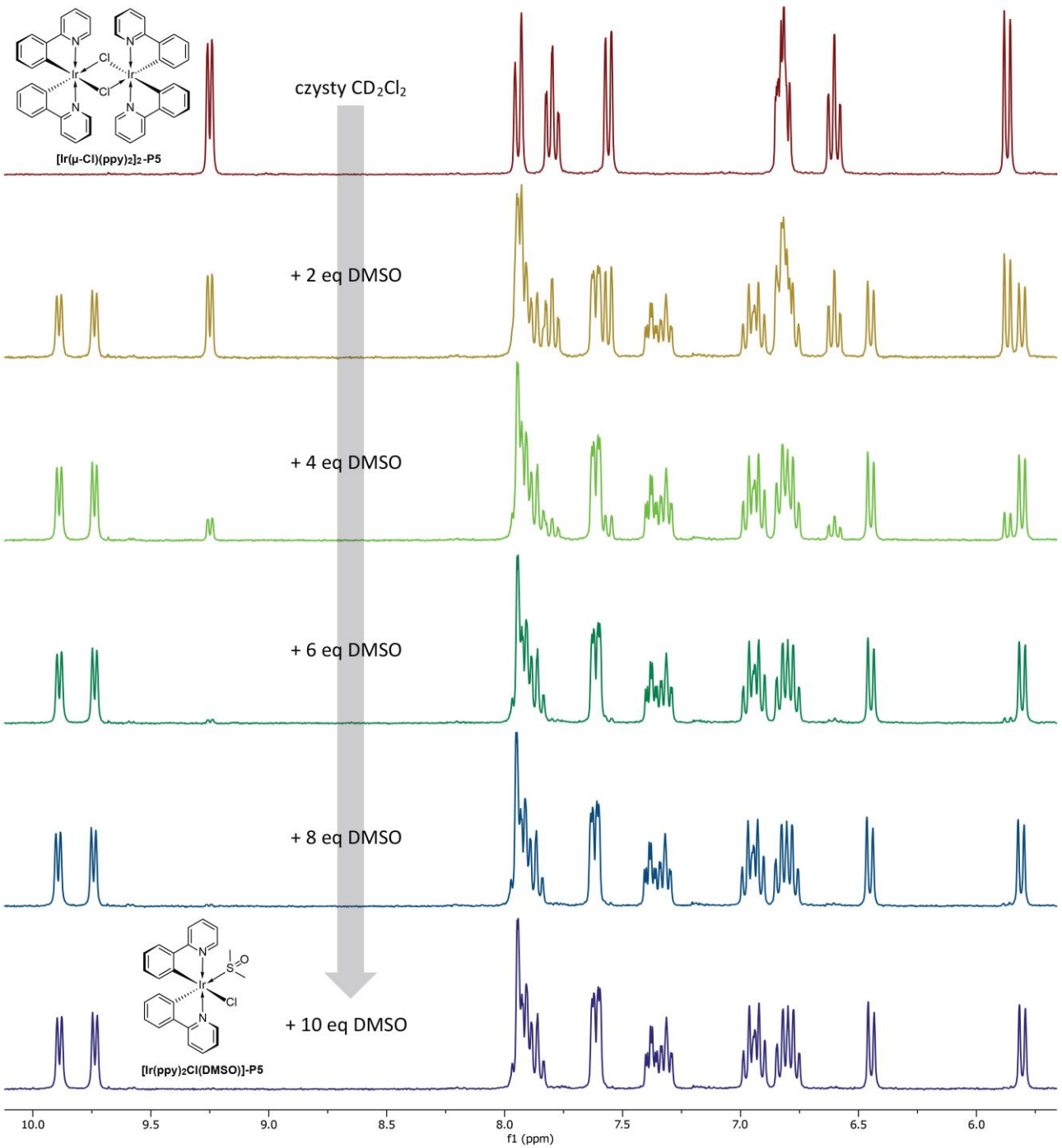

Rys. 53. *Miareczkowanie ^{1}H NMR próbki **[Ir(μ-Cl)(ppy)$_2$]$_2$-P5** rozpuszczonej w CD_2Cl_2. Każde kolejne widmo zostało zarejestrowane po dodaniu 2 eq DMSO i wytrząsaniu przez 5 minut w temperaturze pokojowej.*

Już od pierwszego punktu widać, że intensywność sygnałów formy dwurdzeniowej ulegała obniżeniu, a w zamian pojawiały się dodatkowe linie rezonansowe. Wraz z kolejnymi porcjami DMSO równowaga wyraźnie ulegała przesunięciu w kierunku produktu monordzeniowego, aż do momentu dodania 10 eq będącego punktem końcowym miareczkowania. Na ostatnim widmie można wyraźnie zaobserwować zduplikowanie ilości sygnałów pochodzących od ppy. Proces rozszczepienia można było także obserwować śledząc sygnały pochodzące od DMSO w obszarze wysokiego pola. Oprócz linii odpowiadającej nieskoordynowanej cząsteczce DMSO zaobserwowano także dwa dodatkowe sygnały, przesunięte o około 0,5 ppm w górę i w dół pola. Te dwa sygnały pochodziły od grup metylowych skoordynowanej cząsteczki DMSO, a ich integracja korelowała z integracją sygnałów z zakresu aromatycznego. Oczywiście, sygnały te nigdy nie były widoczne w trakcie analiz wszystkich dimerów w DMSO-d_6, gdyż za rozszczepienie odpowiadały molekuły rozpuszczalnika deuterowanego, który nie jest obserwowany na widmach ^{1}H NMR. Jako dowód ustalania równowagi pomiędzy tymi samymi formami mono- i dwurdzeniowymi zachodzącej w trakcie krystalizacji służy fakt, iż dokładnie te same linie rezonansowe odpowiadające **[Ir(*μ*-Cl)(ppy)$_2$]$_2$-P5** oraz **[Ir(ppy)$_2$Cl(DMSO)]-P5** zaobserwowanym w trakcie miareczkowania, zostały zarejestrowane podczas analizy kryształów **[Ir(ppy)$_2$Cl(DMSO)]-P5** rozpuszczonych w CD_2Cl_2. W ten sposób dostarczono bardzo przekonujących dowodów, że dwurdzeniowe *μ*-chlorkowe kompleksy irydu(III) rzeczywiście ulegają odwracalnemu rozszczepieniu w obecności DMSO i ACN (Rys. 54), przy czym ten drugi wykazuje zdecydowanie niższe powinowactwo do irydu w tym procesie. Uzyskane wyniki jednoznacznie świadczą o tym, że autorzy pracy opublikowanej w *Journal of American Chemical Society* mylnie założyli otrzymanie [Ir(ppy)$_2$(DMSO)$_2$]PF$_6$, w rzeczywistości dysponując **[Ir(ppy)$_2$Cl(DMSO)]-P5** lub **[Ir(*μ*-Cl)(ppy)$_2$]$_2$-P5**.[162] Tym samym można stwierdzić, że trwałe usunięcie anionu chlorkowego z wewnętrznej sfery koordynacyjnej **[Ir(*μ*-Cl)(ppy)$_2$]$_2$-P5** z wykorzystaniem monodentnego liganda może być niemożliwe bez użycia soli srebra, np. AgPF$_6$.[165,166]

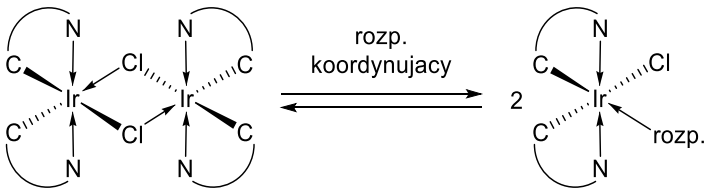

Rys. 54. *Rozszczepienie [Ir(μ-Cl)(C^N)$_2$]$_2$ w obecności rozpuszczalnika koordynującego.*

W trakcie analizy ESI-MS także znaleziono dowody potwierdzające rozszczepianie *μ*-chlorkowych kompleksów irydu(III) w koordynującym rozpuszczalniku (ACN). Zastosowana technika jonizacji jest zaliczana do tzw. „miękkich", czyli takich, które nie powodują daleko idącej fragmentacji jonizowanych cząsteczek, zatem dobrze odzwierciedla równowagę panującą w roztworze. Ponieważ wśród obserwowanych jonów wyraźnie dominowały te odpowiadające wartościom *m/z* form monordzeniowych pozbawionych anionu chlorkowego, stąd wywnioskowano, że rozszczepienie dimerów w ACN rzeczywiście ma miejsce. W trakcie wykonywania analiz na dwóch różnych spektrometrach zaobserwowano wyraźną różnicę w obrazie spektroskopowym analizowanych związków. Po zgłębieniu problemu ustalono, że za tę różnicę odpowiada wartość przyłożonego DP, która mogła być modyfikowana za pośrednictwem oprogramowania jednego z aparatów wykorzystywanych do pomiarów, natomiast w drugim nie była zależna od ustawień operatora. Parametr ten reguluje przyspieszenie jonów w strefie średniego ciśnienia w źródle, tym samym pozwalając użytkownikowi kontrolować stopień CID (kolizyjnie indukowanej dysocjacji). Zjawisko to polega na zderzaniu się jonów z cząsteczkami gazu tła (najczęściej stosowany jest azot), powodując rozbicie klastrów składających się ze zjonizowanego analitu otoczonego cząsteczkami rozpuszczalnika. Zjawisko to generalnie jest pożądane i wykorzystywane m. in. do uwalniania jonów polipeptydów od silnie związanych z nimi cząsteczek wody, aczkolwiek bywa też przyczyną usuwania neutralnych ligandów ze związków kompleksowych.[167,168]

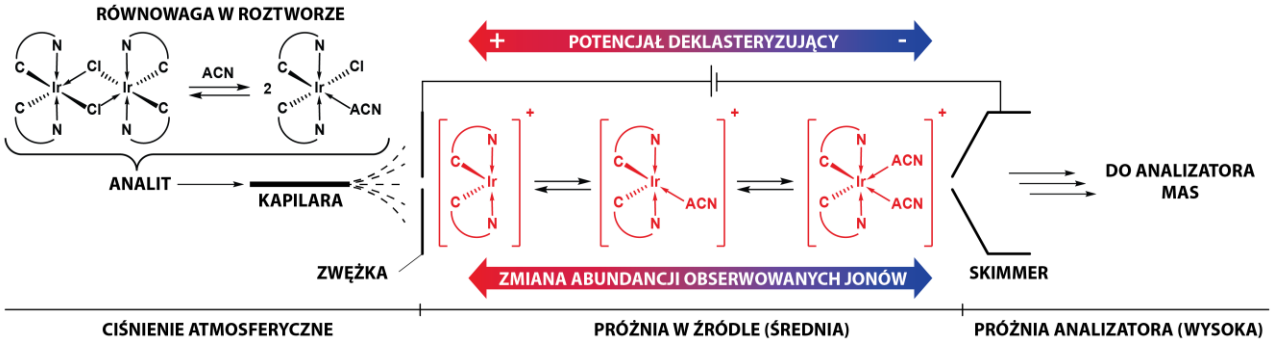

Rys. 55. *Uproszczony schemat źródła jonów spektrometru ESI-MS, ilustrujący zależność pomiędzy potencjałem deklasteryzacji i obserwowanymi jonami.*

Podobnie w przypadku związku analizowanego w pracy [**P5**], wartość DP wpływała na zmianę intensywności obserwowanych jonów, które różniły się o wartość *m/z* odpowiadającą cząsteczce ACN. Gdy przyłożony potencjał był wysoki, dominowały jony o strukturze $[Ir(C^N)_2]^+$. Wraz z obniżaniem napięcia abundancja tych jonów ulegała zmniejszeniu, a rosła intensywność $[Ir(C^N)_2(ACN)]^+$. Zmiana napięcia jeszcze bardziej w kierunku ujemnym powodowała uzyskiwanie obrazu spektroskopowego, na którym wyraźnie dominowały jony o strukturze $[Ir(C^N)_2(ACN)_2]^+$. Proces ten został schematycznie przedstawiony na Rys. 55. Kontynuując analizy na innym spektrometrze, który nie był wyposażony w możliwość zmiany DP, obserwowano wyłącznie jony typu $[Ir(C^N)_2]^+$. Uzyskanie tak różnych wyników może doprowadzić do odmiennej interpretacji danych i wyciągania błędnych wniosków, jak choćby stwierdzenia zdolności rozpuszczalników koordynujących do substytucji obu anionów chlorkowych w dwurdzeniowych μ-chlorkowych kompleksach irydu(III). Przypuszcza się, że ten fakt również mógł mieć znaczenie przy błędnej identyfikacji otrzymanego materiału jako $[Ir(ppy)_2(DMSO)_2]PF_6$.[162] Identyfikacja tego zagrożenia stanowiła niewątpliwą wartość omawianej publikacji, wzbogacając stan wiedzy w dziedzinie chemii związków irydu.

Podsumowując, w artykule [**P5**] przedstawiono zalety wynikające z zastosowania promieniowania mikrofalowego jako medium grzewczego w syntezie związków metaloorganicznych irydu(III). Opracowana metodologia umożliwiła szybką i wydajną syntezę szeregu dwurdzeniowych μ-chlorkowych kompleksów irydu(III) stabilizowanych ligandami wyposażonymi w grupy elektronodonorowe, elektronoakceptorowe oraz wspomagające przewodnictwo dziurowe. Otrzymane związki zostały dokładnie scharakteryzowane technikami NMR, XRD i ESI-MS, oraz zbadano ich zachowanie w obecności rozpuszczalników koordynujących (DMSO i ACN). Wyniki tych kompleksowych badań pozwoliły udowodnić zachodzenie procesu rozszczepiania mostków μ-chlorkowych przez rozpuszczalniki koordynujące, które w literaturze nie było jednoznacznie wyjaśnioną kwestią. Wiedza ta okazała się przydatna w zrewidowaniu wcześniej opublikowanych doniesień literaturowych.

7.6. Związki kompleksowe irydu(III) zawierające 5-funkcjonalizowane pochodne bzq

Ostatni rozdział sekcji omówienia wyników dotyczy monordzeniowych kompleksów irydu(III) zawierających 5-funkcjonalizowane ligandy benzo[*h*]chinolinianowe, stanowiących materiał nieopublikowany. W ramach tego zagadnienia podjęto się syntezy heteroleptycznych kompleksów o strukturze $[Ir(C\hat{}N)_2(N\hat{}N)]PF_6$ i homoleptycznych kompleksów o strukturze $[Ir(C\hat{}N)_3]$ oraz analizy ich niektórych właściwości fotofizycznych, które zostały dotąd przebadane przez współpracowników.

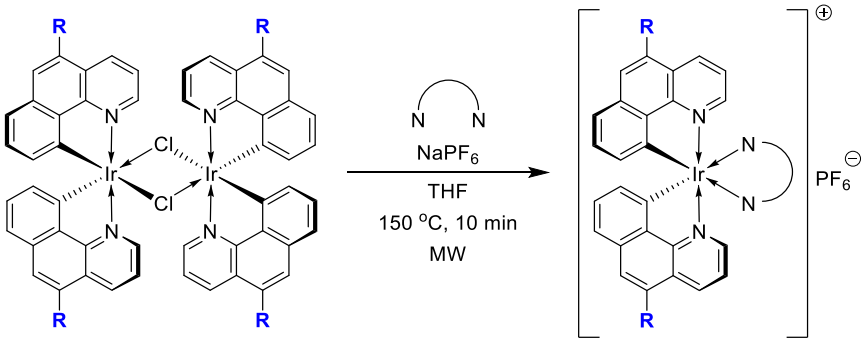

N N	R = ~Br	R = 2,3,5,6-tetrafluorophenyl	R = O-phenyl	R = 4-(*N*-diphenylamino)phenyl
2-phenylpyridine	**[Ir(5-Brbzq)$_2$(ppy)]PF$_6$** 90 %	**[Ir(5-F$_5$C$_6$bzq)$_2$(ppy)]PF$_6$** 87 %	**[Ir(5-PhObzq)$_2$(ppy)]PF$_6$** 74 %	**[Ir(5-(Ph$_2$NC$_6$H$_4$)bzq)$_2$(ppy)]PF$_6$** 77 %
1,10-phenanthroline	**[Ir(5-Brbzq)$_2$(phen)]PF$_6$** 90 %	**[Ir(5-F$_5$C$_6$bzq)$_2$(phen)]PF$_6$** 72 %	**[Ir(5-PhObzq)$_2$(phen)]PF$_6$** 94 %	**[Ir(5-(Ph$_2$NC$_6$H$_4$)bzq)$_2$(phen)]PF$_6$** 84 %

Rys. 56. *Schemat otrzymywania, struktury i wydajności kompleksów jonowych typu* $[Ir(C\hat{}N)_2(N\hat{}N)]PF_6$.

W pierwszej kolejności otrzymano szereg związków jonowych wyposażonych w bpy i phen w roli ligandów pomocniczych oraz dwa cyklometalujące ligandy oparte na rdzeniu bzq. Otrzymane związki zawierały grupy funkcyjne o zróżnicowanym charakterze elektronowym (bromo, pentafluorofenylo, fenoksy, 4-(*N*-difenyloamino)fenylo). Syntezy wszystkich z nich wykonano według metodologii opisanej w pracy [**P1**], co zaowocowało bardzo dobrymi wydajnościami i możliwością przeprowadzenia reakcji w czasie jedynie dziesięciu minut (Rys. 56). Krótką charakterystykę właściwości fotofizycznych czterech kompleksów w roztworze chlorobenzenowym oraz filmie PVK:PBD zebrano w postaci Tabeli 7. Nie zaobserwowano wyraźnej korelacji pomiędzy wydajnościami kwantowymi fotoluminescencji, a strukturą chemiczną badanych związków, jednakże okazały się one niższe od referencyjnych kompleksów **2AA'-P1** oraz **2FA'-P1**. Z drugiej strony, zaobserwowano wyraźny efekt przestrajania długości fali emitowanego promieniowania. Obecność grupy 4-(*N*-difenyloamino)fenylo powodowała zmniejszenie przerwy energetycznej (zwiększenie λ_{max}) poprzez zwiększenie stopnia koniugacji, z kolei obecność grupy pentafluorofenylowej zwiększała przerwę energetyczną (zmniejszała λ_{max}). Efekt ten jest tym bardziej wyraźny, jeśli weźmie się pod uwagę wartości dla niemodyfikowanych kompleksów **2AA'-P1** ($\lambda_{max\ roztwór}$ = 610, $\lambda_{max\ film}$ = 547) oraz **2FA'-P1** ($\lambda_{max\ roztwór}$ = 588, λ_{max}

$_{film}$ = 544). Tym razem również zaobserwowano wyraźne skrócenie długości emitowanej fali w filmie względem pomiaru w roztworze, co może być spowodowane większą sztywnością otoczenia emitera i przyjęcia przez niego innej konfiguracji.

Tabela 7. *Parametry fotofizyczne wybranych kompleksów jonowych.*

Związek	Wydajność kwantowa [%]		λ_{max} fotoluminescencji [nm]	
	Roztwór	Film	Roztwór	Film
[Ir(5-F_5C_6bzq)$_2$(ppy)]PF_6	2.5	10.2	575	533
[Ir(5-F_5C_6bzq)$_2$(phen)]PF_6	1.0	9.3	577	535
[Ir(5-($Ph_2NC_6H_4$)bzq)$_2$(ppy)]PF_6	<1.0	5.8	623	576
[Ir(5-($Ph_2NC_6H_4$)bzq)$_2$(phen)]PF_6	1.0	3.0	610	565

Kolejnym poruszonym zagadnieniem były kompleksy homoleptyczne, wyposażone w trzy takie same ligandy. Związki te zostały otrzymane w reakcji rozszczepiania kompleksów dwurdzeniowych otrzymanych w pracy [**P5**] z użyciem pochodnych benzo[*h*]chinoliny, w obecności zasady w glicerynie (Rys. 57). Związki te otrzymano według literaturowych procedur, uzyskując bardzo zróżnicowane wydajności.[62,169]

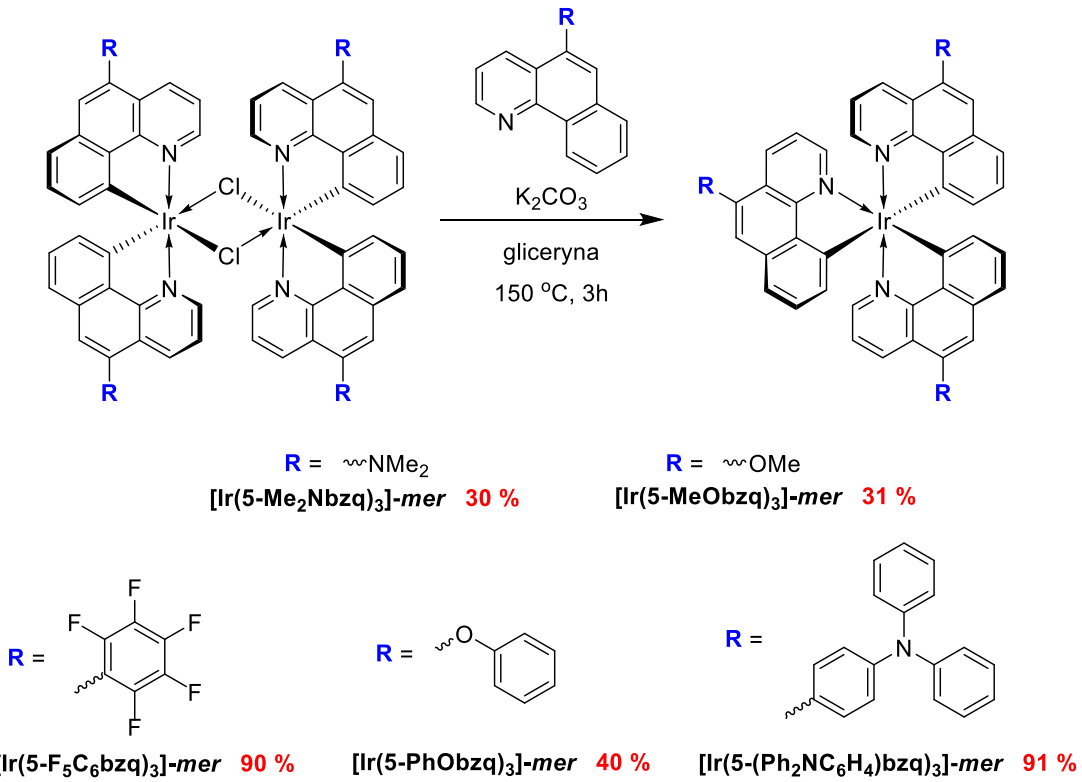

Rys. 57. *Schemat otrzymywania kompleksów meridionalnych typu [Ir(C^N)$_3$].*

Seria związków meridionalnych została poddana badaniom fotofizycznym oraz dodatkowo, na ich bazie zostały wytworzone diody w konfiguracji ITO/PEDOT:PSS/60 % PVK + 40 % PBD+1 % Emiter/Ca/Ag. Wyniki analiz i charakterystyki diod zostały zebrane w Tabeli 8. Niestety, nie udało się uzyskać do porównania diod z ***mer***-[**Ir(bzq)$_3$**], ze względu na jego bardzo niską rozpuszczalność w chlorobenzenie, stąd pozostało dokonać dyskusji parametrów w obrębie badanej grupy związków. Jak można zauważyć, kompleksy cechowały się bardzo niską wydajnością fotoluminescencji w roztworze, która ulegała znacznej poprawie w filmie.

Tabela 8. *Zestawienie wybranych parametrów emiterów meridionalnych.*

Związek	Luminancja (15 V) [cd/m^2]	Wydajność prądowa [cd/A]	Wydajność kwantowa [%]		λ_{max} fotoluminescencji [nm]		λ_{max} elektroluminescencji [nm]
			Roztwór	Film	Roztwór	Film	
mer-[Ir(5-Me$_2$Nbzq)$_3$]	205	2.2	<1.0	4.0	608	585	580
mer-[Ir(5-MeObzq)$_3$]	1800	4.4	<1.0	8.2	600	575	575
mer-[Ir(5-F$_5$C$_6$bzq)$_3$]	2700	3.5	<1.0	16.6	615	595	600
mer-[Ir(5-PhObzq)$_3$]	4000	5.0	<1.0	15.5	615	590	595
mer-[Ir(5-(Ph$_2$NC$_6$H$_4$)bzq)$_3$]	4200	4.0	<1.0	15.6	600	590	595

Najwyższymi wydajnościami kwantowymi charakteryzowały się związki wyposażone w ugrupowania aromatyczne, a najniższymi emitery wyposażone w grupy metoksylową i dimetyloaminową. Podobnie do wcześniej opisanych kompleksów jonowych, badane związki wykazywały zauważalne hipsochromowe przesunięcie pasma emisji w filmie względem pomiarów w roztworze. Zaobserwowano także niewielki wpływ podstawników na przestrajanie emitowanej długości fali w filmie oraz w elektroluminescencji. Najkrótsze długości emitowanych fal zanotowano dla kompleksów wyposażonych w elektronodonorowe podstawniki metoksylowe i dimetyloaminowe, z kolei największą długość fali emitował kompleks wyposażony w pentafluorofenylowe ugrupowanie elektronowyciągające. Wnioski te są zgodne z wcześniej przeprowadzonymi obliczeniami kwantowo-chemicznymi.[72] Najwyższą luminancję zanotowała dioda bazująca na emiterze wyposażonym w grupę 4-(*N*-difenyloamino)fenylową, co mogłoby potwierdzać tezę o pozytywnym wpływie właściwości półprzewodzących typu *p* ugrupowania trifenyloaminowego.

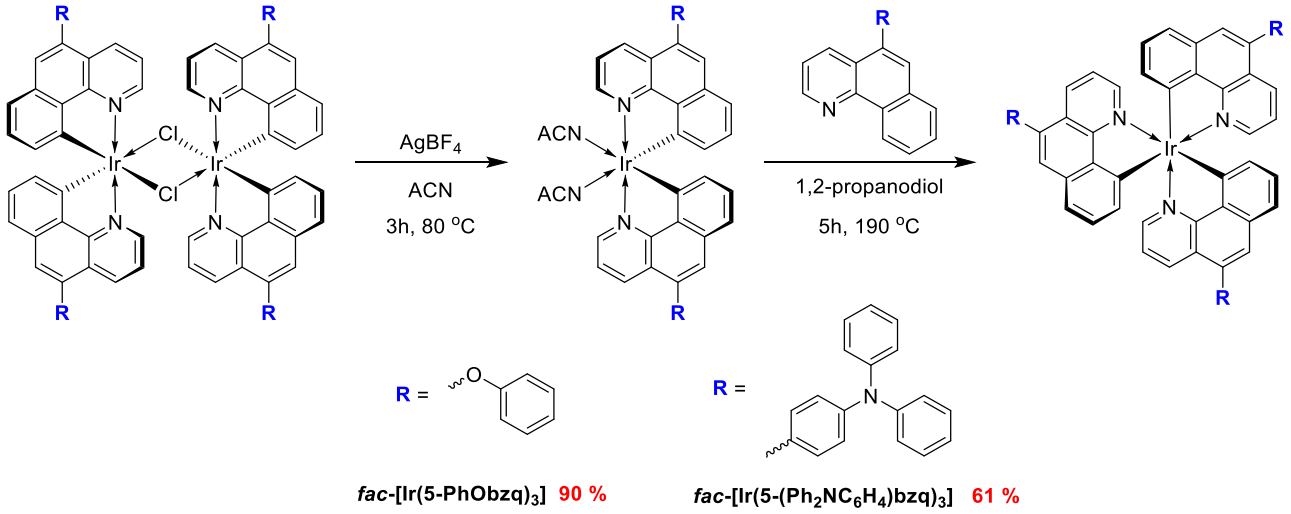

Rys. 58. *Skuteczny szlak syntetyczny prowadzący do otrzymania facjalnych kompleksów typu [Ir(C^N)$_3$].*

Po otrzymaniu i zbadaniu kompleksów meridionalnych, skierowano uwagę w kierunku izomerów facjalnych. W celu ich otrzymania przetestowano wiele znanych z literatury sposobów, włączając w to prowadzenie reakcji rozszczepiania dimerów w temperaturach powyżej 200 °C,[170] oraz izomeryzację kompleksów meridionalnych pod wpływem ogrzewania w stopionym fenolu[169] lub naświetlania promieniowaniem UV w rozpuszczalnikach koordynujących.[32] Niestety, każda z tych procedur okazała się być nieskuteczna, prowadząc w najlepszym razie do odzyskania wyjściowych materiałów, a w większości przypadków do degradacji całej mieszaniny.

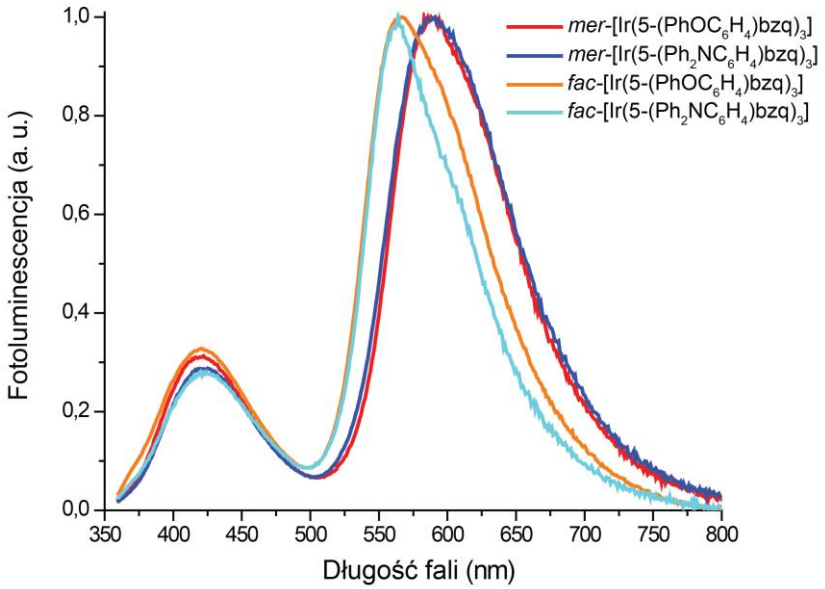

Rys. 59. *Znormalizowane widma fotoluminescencji kompleksów homoleptycznych wyposażonych w grupy fenoksy oraz 4-(N-difenyloamino)fenylo, w filmie PVK:PBD.*

Jedynym skutecznym rozwiązaniem okazało się zastosowanie procedury opisanej w patencie, która wymagała syntezy kompleksu pośredniego, zawierającego skoordynowane cząsteczki ACN.[171] Odbywało się to poprzez rozszczepienie dimeru z użyciem ACN, z jednoczesnym usunięciem anionu chlorkowego z wewnętrznej sfery koordynacyjnej w obecności soli srebra. Dopiero tak uzyskany kompleks pośredni był podatny na zastąpienie ligandów ACN i selektywne przekształcenie w izomer facjalny oczekiwanego produktu (Rys. 58). W ten sposób udało się otrzymać dwa przykłady kompleksów facjalnych, a mianowicie ***fac*-[Ir(5-PhObzq)$_3$]** oraz ***fac*-[Ir(5-(Ph$_2$NC$_6$H$_4$)bzq)$_3$]**. Związki te zostały wyselekcjonowane na podstawie wyników badań kompleksów meridionalnych, gdyż to diody bazujące na emiterach wyposażonych w grupy fenoksy oraz 4-(*N*-difenyloamino)fenylo cechowały się najwyższymi wartościami luminancji. Porównanie ich widm fotoluminescencji w filmie przedstawiono na Rys. 59. Maksimum emisji kompleksów facjalnych przypadało w okolicach 565 nm, z kolei meridionalnych w okolicach 590 nm. Na widmach można także zaobserwować pasmo od matrycy, będące oznaką niecałkowitego transferu energii do emitera. Różnice we właściwościach fotofizycznych izomerów są wyraźne i wynikają z odmiennej symetrii, co zostało przewidziane we wcześniej omówionej pracy teoretycznej.[72] Różnica ta ma swoje odzwierciedlenie także w analizie NMR, w której symetryczny izomer facjalny daje uproszczony obraz spektroskopowy względem niesymetrycznego izomeru meridionalnego, z uwagi na chemiczną równocenność cyklometalujących ligandów (Rys. 60).

Podsumowując, w ramach prac opisanych w tym rozdziale podjęto się otrzymania związków kompleksowych o ogólnych wzorach [Ir(C^N)$_2$(N^N)]PF$_6$ oraz [Ir(C^N)$_3$], zawierających 5-funkcyjne skoordynowane pochodne bzq otrzymane w ramach pracy [**P4**]. Częściowa charakterystyka właściwości fotofizycznych i elektroluminescencyjnych badanych związków udowodniła możliwość wpływu na parametry emisyjne poprzez zmianę struktury liganda cyklometalującego oraz potencjał tych związków w zastosowaniu w roli emiterów OLED.

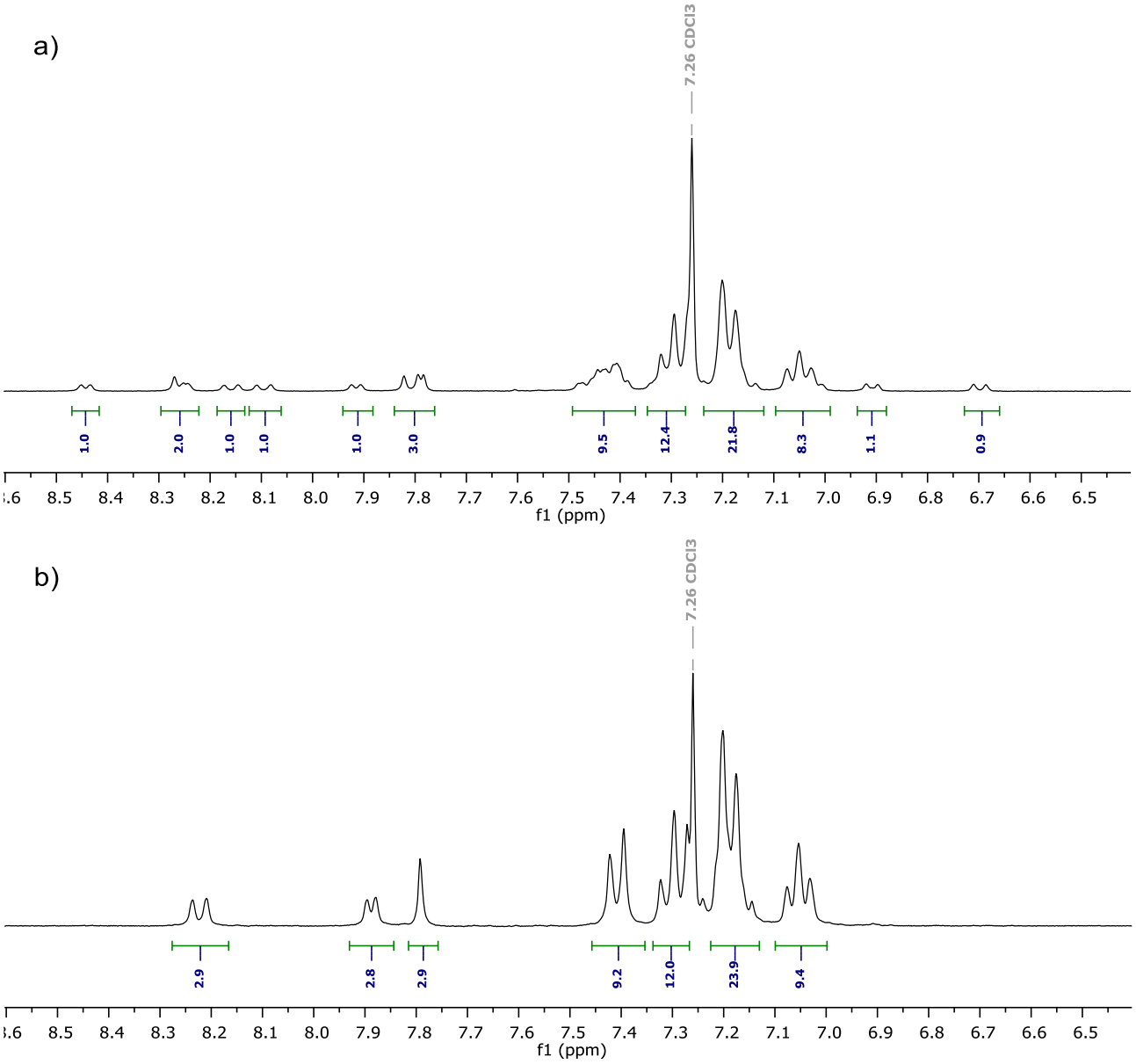

Rys. 60. *Fragmenty widm ^{1}H NMR kompleksów* ***mer-[Ir(5-(Ph$_2$NC$_6$H$_4$)bzq)$_3$]*** (a) oraz ***fac-[Ir(5-(Ph$_2$NC$_6$H$_4$)bzq)$_3$]*** (b).

8. Podsumowanie i wnioski

Celem niniejszej rozprawy doktorskiej było zaprojektowanie, opracowanie efektywnych metod otrzymywania i charakterystyka spektroskopowa nowych koordynacyjnych związków irydu(III) zawierających w swojej strukturze motyw benzo[*h*]chinoliny; określenie relacji pomiędzy budową chemiczną otrzymanych kompleksów oraz ich właściwościami; a także zademonstrowanie potencjału aplikacyjnego nowych prekursorów ligandów *C,N*-donorowych w syntezie cyklometalowanych kompleksów irydu(III).

Przedmiotem pracy [**P1**] było zaprojektowanie, optymalizacja i przeprowadzenie syntez kompleksów jonowych irydu(III) o ogólnym wzorze $[Ir(bzq)_2(N\hat{}N)]^+A^-$, zawierających *N,N*-donorowe ligandy pomocnicze o zróżnicowanej strukturze oraz właściwościach elektronowych. Implementacja niekonwencjonalnego źródła energii w postaci promieniowania mikrofalowego pozwoliła na znaczne skrócenie czasu reakcji oraz uproszczenia całego procesu syntezy tego typu związków względem metod dotychczas opisanych w literaturze, dzięki zastosowaniu metodologii *one-pot*, zapewniającej tym samym wysoką wydajność syntez. Struktury otrzymanych kompleksów zostały potwierdzone przy użyciu spektroskopii NMR oraz analizy rentgenostrukturalnej. Analiza rezultatów badań elektrochemicznych, fotofizycznych i kwantowo-chemicznych wykazała, że struktura chemiczna otrzymanych substancji ma wpływ na ich właściwości, co wynikało głównie z lokalizacji poziomu LUMO w obrębie liganda *N,N*-donorowego. Wprowadzenie do struktury 2,2-bipirydyny ugrupowań o charakterze elektronodonorowym (metylo oraz metoksy) prowadziło do hipsochromowego przesunięcia maksimów emisji fotoluminescencji, z kolei rozbudowa układu aromatycznego liganda powodowała przesunięcie batochromowe. Był to efekt oczekiwany, gdyż zwiększanie/zmniejszanie gęstości elektronowej na ligandzie pomocniczym powinno destabilizować/stabilizować zlokalizowany tam poziom LUMO, tym samym zwiększając/zmniejszając przerwę energetyczną HOMO-LUMO determinującą długość emitowanej fali. Ostatecznie, przykładowe diody skonstruowane w oparciu o nowe związki osiągały luminancję na poziomie 10 000 cd/m^2, potwierdzając ich potencjał do zastosowania w technologii OLED jako emiterów fosforescencyjnych.

W pracy [**P2**] poruszono tematykę kompleksów neutralnych o strukturze $[Ir(bzq)_2(N\hat{}O)]$, wyposażonych w fluorowane *β*-ketoiminianowe ligandy pomocnicze. Zaprojektowane struktury kompleksów różniły się stopniem oraz regioizomerią podstawienia pierścienia fenylowego liganda pomocniczego atomami fluoru. Podobnie jak w przypadku syntezy połączeń jonowych, również i tym razem wykorzystano wspomagający efekt promieniowania mikrofalowego do efektywnego przeprowadzenia syntezy docelowych kompleksów. Analiza rezultatów badań elektrochemicznych oraz obliczeń kwantowo-chemicznych potwierdziła, że modyfikacja chemiczna w obrębie liganda pomocniczego w głównej mierze wpływa na poziom HOMO, aczkolwiek obserwowany wpływ był relatywnie niewielki. Wynikało to głównie z nieznacznego udziału podstawionego pierścienia fenylowego w przestrzeni zajmowanej przez poziom HOMO, wobec czego możliwy był jedynie niewielki wpływ indukcyjny na szkielet ketoiminowy, na którym obecność HOMO była znacząca. Tym samym, zaobserwowany w badaniach fotofizycznych wpływ modyfikacji chemicznych na przestrajanie pasma emisji był nieznaczny. Zaskakująco, zmiana struktury chemicznej miała bardzo duży wpływ na parametry pracy diod skonstruowanych w oparciu o nowe emitery. Najwyższymi wartościami luminancji i wydajności prądowej charakteryzowały się diody zawierające emitery wyposażone w atomy fluoru w pozycji *para* oraz *orto*, przewyższając emiter referencyjny niefunkcjonalizowany atomami fluoru.

Praca [**P3**] była kontynuacją tematyki kompleksów *β*-ketoiminianowych o strukturze $[Ir(bzq)_2(N\hat{}O)]$, tym razem wyposażonych w grupy metoksy, nitrylo, nitro i 5-metylo-2-benzotiazylo przyłączone do podstawnika *N*-fenylowego, a także podstawniki *N*-naftylowe i *N*-antracenylowe. Ideą artykułu była ocena wpływu struktury chemicznej podstawnika arylowego przyłączonego do ketoiminianowego atomu

azotu na właściwości elektrochemiczne, fotofizyczne i elektroluminescencyjne badanych związków, przy wsparciu modelowania kwantowo-chemicznego. W pierwszej fazie prac zostały zaprojektowane i otrzymane wybrane prekursory ligandów oraz docelowe związki kompleksowe irydu(III), które następnie zostały przebadane przez współpracowników. Badania elektrochemiczne wykazały zauważalną odmienność kompleksów zawierających grupę nitrową w aspekcie powinowactwa elektronowego. Jednakże, udało się zidentyfikować ten fenomen przy użyciu innych metod jako redukcję grupy nitrowej, niemającej drastycznego wpływu na zmianę maksimum emitowanej długości fali. Zgodnie z wnioskami płynącymi z pracy [**P2**], tym razem również zaobserwowano jedynie niewielki efekt przestrajania maksimum emisji, a wszystkie kompleksy okazały się emiterami barwy zielonej. Jednakże, stwierdzono bardzo duży wpływ rodzaju podstawnika *N*-arylowego na wydajność fotoluminescencji oraz elektroluminescencji, co może być spowodowane wspomaganiem pułapkowania nośników ładunku na cząsteczkach emitera. Zdecydowanie najgorsze parametry zaobserwowano dla emiterów zawierających grupy antracenylowe, gdyż ulegały one szybkiej foto- i elektrodegradacji. Prosta dioda sporządzona metodą roztworową przy użyciu najlepszego emitera (zawierającego podstawnik 1-naftylowy) osiągnęła maksymalną luminancję na poziomie 16 000 cd/m^2, wydajność prądową zbliżoną do 12 cd/A oraz zewnętrzną wydajność kwantową w okolicach 3.2 %, co było bardzo dobrym wynikiem jak na urządzenie o tak prostej budowie.

W przedostatniej pracy [**P4**] cyklu opracowano szlaki syntetyczne umożliwiające syntezę szeregu nowych pochodnych benzo[*h*]chinoliny podstawionych różnymi grupami funkcyjnymi w pozycji 5. Spektrum tych grup obejmowało podstawniki elektronodonorowe (metoksy, fenoksy, amino, dimetyloamino), elektronowyciągające (fluoro, pentafluorofenylo, bromo), ugrupowania wspomagające przewodnictwo dziurowe (*N*-difenyloamino, *N*-fenotiazylo, *N*-karbazolilo, 4-(*N*-difenyloamino)fenylo) oraz ugrupowanie POSS o dużej zawadzie sterycznej. W większości przypadków reakcje prowadzono w reaktorze mikrofalowym, osiągając bardzo wysokie wydajności oczekiwanych produktów w bardzo krótkim czasie. Wszystkie otrzymane związki posiadają kieszeń koordynacyjną zdolną do *C,N*-cyklometalacji, dzięki czemu stanowią potencjalne prekursory do otrzymywania związków koordynacyjnych metali przejściowych. Jest to szczególnie atrakcyjny materiał do konstrukcji fosforescencyjnych emiterów platynowych lub irydowych stosowanych w technologii OLED, z uwagi na możliwość modyfikacji właściwości kompleksów poprzez odpowiedni dobór grupy funkcyjnej cyklometalującego liganda.

W ramach pracy [**P5**] potwierdzono pozytywny efekt zastosowania ogrzewania mikrofalowego w syntezie cyklometalowanych μ-chlorkowych dwurdzeniowych kompleksów irydu(III) oraz znaczenie wody w tym procesie. W rezultacie przeprowadzonej optymalizacji dobrano warunki reakcji umożliwiające otrzymanie docelowych związków w niezwykle krótkim czasie, stosując bardzo prostą procedurę izolacji. W zoptymalizowanych warunkach dokonano syntezy szeregu znanych oraz nowych dimerów z bardzo dobrymi wydajnościami, których czystość potwierdzono spektroskopowo. W reakcjach otrzymano szereg związków zawierających ligandy oparte o motyw 2-fenylopirydynianowy, benzo[*h*]chinolinianowy oraz 2-fenoksypirydynianowy; wyposażone w grupy o charakterze elektronodonorowym (metylo, metoksy, fenoksy), elektronowyciągającym (fluoro, bromo, trifulorometylo, pentafluorofenylo) oraz ugrupowania wspomagające półprzewodnictwo dziurowe (*N*-difenyloamino, 4-(*N*-difenyloamino)fenylo). W przypadku związku wyposażonego w grupę dimetyloaminową zaproponowano alternatywny szlak syntetyczny, wykluczający wydzielanie HCl w toku reakcji. Badania spektroskopowe NMR otrzymanych dimerów przeprowadzone w DMSO-d_6 i ACN-d_3 ujawniły przebieg reakcji chemicznej pomiędzy związkami koordynacyjnymi, a wymienionymi rozpuszczalnikami koordynującymi. Proces ten zidentyfikowano jako rozszczepienie mostków μ-chlorkowych w kompleksach dwurdzeniowych, prowadzący do utworzenia związków monordzeniowych. Dodatkowych dowodów dostarczyła analiza rentgenostrukturalna wyhodowanych kryształów kompleksów o

ogólnym wzorze $[Ir(ppy)_2Cl(rozpuszczalnik)]$. Zwieńczeniem badań nad procesem rozszczepienia była analiza ESI-MS otrzymanych dimerów, która również potwierdziła przebieg takiego procesu. Ponadto, przeprowadzone badania wykazały istotny wpływ wartości przyłożonego potencjału deklasteryzującego na uzyskiwane widmo masowe analizowanych dimerów, który to w znaczący sposób determinuje interpretację rezultatów. Wnioski wyciągnięte z przeprowadzonych badań pozwoliły na ujawnienie błędu jaki popełnili autorzy pracy opublikowanej w *Journal of American Chemical Society* z 2011 roku, którzy nieprawidłowo interpretując uzyskane dane spektroskopowe, niewłaściwie przypisali wzór $[Ir(ppy)_2(DMSO)_2]PF_6$ otrzymanemu związkowi będącemu podstawą tego artykułu.

Oprócz wyżej wymienionych prac, przedstawiono także nieopublikowany materiał eksperymentalny dotyczący syntezy kompleksów jonowych typu $[Ir(C^N)_2(N^N)]PF_6$ oraz homoleptycznych o ogólnym wzorze $[Ir(C^N)_3]$, zawierających 5-funkcjonalizowane pochodne bzq. W przypadku otrzymywania wymienionych klas koordynacyjnych związków irydu(III) również potwierdzono wysoką skuteczność promieniowania mikrofalowego, aczkolwiek część syntez przeprowadzono także wykorzystując klasyczne źródła ciepła. Szczególnie ważne było znalezienie skutecznej metodologii otrzymywania kompleksów facjalnych, gdyż ich synteza według procedur opracowanych dla analogicznych kompleksów 2-fenylopirydynianowych okazała się niemożliwa. Niemniej jednak, analiza jeszcze niekompletnego materiału eksperymentalnego z zakresu charakterystyki właściwości fotofizycznych i elektroluminescencyjnych wykazała, że związki te mają potencjał do dalszych, szczegółowych badań zorientowanych na zastosowanie ich w roli emiterów OLED.

Podsumowując, w ramach zaprezentowanych publikacji naukowych dokonano syntezy szeregu związków zawierających w swojej strukturze motyw benzo[*h*]chinoliny oraz ich szeroko rozumianej charakterystyki. Przedstawiono metodologie otrzymywania związków kompleksowych irydu(III) stabilizowanych dwoma ligandami bzq i różnej klasy ligandami pomocniczymi oraz określono relacje pomiędzy ich strukturą chemiczną, a właściwościami. Ponadto, zaprezentowano potencjał aplikacyjny pochodnych benzo[*h*]chinoliny w syntezie nowych *C,N*-cyklometalowanych kompleksów irydu(III), który stanowi punkt wyjścia do pełnej oceny wpływu modyfikacji struktury chemicznej głównych ligandów cyklometalujących w ramach przyszłych badań.

9. Literatura

[1] A. Bernanose, M. Comte, P. Vouaux, *J. Chim. Phys.* **1953**, *50*, 64-68 (DOI: 10.1051/jcp/1953500064).
[2] A. Bernanose, P. Vouaux, *J. Chim. Phys.* **1953**, *50*, 261-263 (DOI: 10.1051/jcp/1953500261).
[3] A. Bernanose, *J. Chim. Phys.* **1955**, *52*, 396-400 (DOI: 10.1051/jcp/1955520396).
[4] H. Kallmann, M. Pope, *J. Chim. Phys.* **1960**, *32*, 300-301 (DOI: 10.1063/1.1700925).
[5] H. Kallmann, M. Pope, *Nature* **1960**, *186* , 31-33 (DOI: 10.1038/186031a0).
[6] C. W. Tang, S. A. VanSlyke, *Appl. Phys. Lett.* **1987**, *51*, 913-915 (DOI: 10.1063/1.98799).
[7] Y. Sato, S. Ichinosawa, H. Kanai, *IEEE J. Sel. Top. Quantum Electron.* **1998**, *4*, 40-48 (DOI: 10.1109/2944.669464).
[8] C. David, M. Piens, G. Geuskens, *Eur. Polym. J.* **1972**, *8*, 1291-1297 (DOI: 10.1016/0014-3057(72)90064-X).
[9] M. Uchida, Y. Ohmori, C. Morishima, K. Yoshino, *Synth. Met.* **1993**, *57* 4168-4173 (DOI: 10.1016/0379-6779(93)90576-I).
[10] G. Grem, G. Ledetzky, G. Leising, *Adv. Mater.* **1992**, *4*, 36-37 (DOI: 10.1002/adma.19920040107).
[11] J. H. Burroughes, D. D. C. Bradley, A. R. Brown, R. N. Marks, K. Mackay, R. H. Friend, P. L. Burns, A. B. Holmes, *Nature* **1990**, *347*, 539–541 (DOI: 10.1038/347539a0).
[12] S.R. Tseng, Y.S. Chen, H.F. Meng, H.C. Lai, C.H. Yeh, S.F. Horng, H.H. Liao, C.S. Hsu, *Synth. Met.* **2009**, *159*, 137-141 (DOI: 10.1016/j.synthmet.2008.08.017).
[13] Y. Li, J.-Y. Liu, Y.-D. Zhao, Y.-C. Cao, *Mater. Today* **2017**, *20*, 258-266 (DOI: 10.1016/j.mattod.2016.12.003).
[14] H. Zhang, X. Sun, S. Chen, *Adv. Funct. Mater.* **2017**, *27*, 1603007 (DOI: 10.1002/adfm.201700610).
[15] S.-J. Zou, Y. Shen, F.-M. Xie, J.-D. Chen, Y.-Q. Li, J.-X. Tang, *Mater. Chem. Front.* **2020**, *4*, 788-820 (DOI: 10.1039/C9QM00716D).
[16] M. Segal, M. A. Baldo, R. J. Holmes, S. R. Forrest, Z. G. Soos, *Phys. Rev. B* **2003**, *68*, 075211 (DOI: 10.1103/PhysRevB.68.075211).
[17] X. Yang, G. Zhou, W.-Y. Wong, *Chem. Soc. Rev.* **2015**, *44*, 8484-8575 (DOI: 10.1039/C5CS00424A).
[18] C. Adachi, M. A. Baldo, M. E. Thompson, S. R. Forrest, *J. Appl. Phys.* **2001**, *90*, 5048-5051 (DOI: 10.1063/1.1409582).
[19] Z. Yang, Z. Mao, Z. Xie, Y. Zhang, S. Liu, J. Zhao, J. Xu, Z. Chi, M. P. Aldred, *Chem. Soc. Rev.* **2017**, *46*, 915-1016 (DOI: 10.1039/C6CS00368K).
[20] D. Zhou, W.-P. To, Y. Kwak, Y. Cho, G. Cheng, G. S. M. Tong, C.-M. Che, *Adv. Sci.* **2019**, *6*, 1802297 (DOI: 10.1002/advs.201802297).
[21] P. J. Conaghan, C. S. B. Matthews, F. Chotard, S. T. E. Jones, N. C. Greenham, M. Bochmann, D. Credgington, A. S. Romanov, *Nat. Commun.* **2020,** *11***,** 1758 (DOI: 10.1038/s41467-020-15369-8).
[22] D. Di, A. S. Romanov, L. Yang, J. M. Richter, J. P. H. Rivett, S. Jones, T. H. Thomas, M. A. Jalebi, R. H. Friend, M. Linnolahti, M. Bochmann, D. Credgington, *Science* **2017**, *356*, 159-163 (DOI: 10.1126/science.aah4345).
[23] J.-H. Lee, C.-H. Chen, P.-H. Lee, H.-Y. Lin, M.-K. Leung, T.-L. Chiu, C.-F. Lin, *J. Mater. Chem. C* **2019**, *7*, 5874-5888 (DOI: 10.1039/C9TC00204A).
[24] *Highly Efficient OLEDs with Phosphorescent Materials*, ed. H. Yersin, John Wiley & Sons: Newark, NJ, **2008**.
[25] B. Minaev, G. Baryshnikov, H. Agren, *Phys. Chem. Chem. Phys.* **2014**, *16*, 1719-1758 (DOI: 10.1039/C3CP53806K).
[26] *Iridium(III) in Optoelectronic and Photonics Applications*, ed. E. Zysman-Colman, John Wiley & Sons: Newark, NJ, **2017**.
[27] A. F. Henwood, E. Zysman-Colman, *Chem. Commun.* **2017**, *53*, 807-826 (DOI: 10.1039/C6CC06729H).
[28] K. A. King, P. J. Spellane, R. J. Watts, *J. Am. Chem. Soc.* **1985**, *107*, 1431-1432 (DOI: 10.1021/ja00291a064).
[29] T. Sajoto, P. I. Djurovich, A. B. Tamayo, J. Oxgaard, W. A. Goddard, M. E. Thompson, *J. Am. Chem. Soc.* **2009**, *131*, 9812-9822 (DOI: 10.1021/ja903317w).
[30] T.-Y. Li, J. Wu, Z.-G. Wu, Y.-X. Zheng, J.-L. Zuo, Y. Pan, *Coord. Chem. Rev.* **2018**, *374*, 55-92 (DOI: 10.1016/j.ccr.2018.06.014).
[31] A. Tsuboyama, H. Iwawaki, M. Furugori, T. Mukaide, J. Kamatani, S. Igawa, T. Moriyama, S. Miura, T. Takiguchi, S. Okada, M. Hoshino, K. Ueno, *J. Am. Chem. Soc.* **2003**, *125*, 12971-12979 (DOI: 10.1021/ja034732d).

[32] J. M. Fernandez-Hernandez, J. I. Beltran, V. Lemaur, M.-D. Galvez-Lopez, C.-H. Chien, F. Polo, E. Orselli, R. Frohlich, J. Cornil, L. De Cola, *Inorg. Chem.* **2013**, *52*, 1812-1824 (DOI: 10.1021/ic3018419).
[33] K.-Y. Lu, H.-H. Chou, C.-H. Hsieh, Y.-H. O. Yang, H.-R. Tsai, H.-Y. Tsai, H.-Y. Tsai, L.-C. Hsu, C.-Y. Chen, I-C. Chen, C.-H. Cheng, *Adv. Mater.* **2011**, *23,* 4933-4937 (DOI: 10.1002/adma.201102886).
[34] R. J. Holmes, S. R. Forrest, T. Sajoto, A. Tamayo, P. I. Djurovich, M. E. Thompson, *Appl. Phys. Lett.* **2005**, *87*, 243507 (DOI: 10.1063/1.2143128).
[35] J. Lee, H.-F. Chen, T. Batagoda, C. Coburn, P. I. Djurovich, M. E. Thompson, S. R. Forrest, *Nature Mater.* **2016**, *15*, 92-98 (DOI: 10.1038/nmat4446).
[36] M. Nonoyama, *B. Chem. Soc. Jpn.* **1974**, *47*, 767-768 (DOI: 10.1246/bcsj.47.767).
[37] S. Lamansky, P. Djurovich, D. Murphy, F. Abdel-Razzaq, R. Kwong, I. Tsyba, M. Bortz, B. Mui, R. Bau, M. E. Thompson, *Inorg. Chem.* **2001**, *40*, 1704-1711 (DOI: 10.1021/ic0008969).
[38] I. Takashi, K. Hideo, S. Yoshiro, *U. S. Patent Application* US2013/203997A1 **2013**.
[39] B. Carlson, G. D. Phelan, W. Kaminsky, L. Dalton, X. Jiang, S. Liu, A. K.-Y. Jen, *J. Am. Chem. Soc.* **2002**, *124*, 14162-14172 (DOI: 10.1021/ja0176705).
[40] S. Bernhard, X. Gao, G. G. Malliaras, H. D. Abruna, *Adv. Mater.* **2002**, 14, 433–436 (DOI: 10.1002/1521-4095(20020318)14:6<433::AID-ADMA433>3.0.CO;2-W).
[41] J. Slinker, D. Bernards, P. L. Houston, H. D. Abruna, S. Bernhard, G. G. Malliaras, *Chem. Commun.* **2003**, 2392–2399 (DOI: 10.1039/B304265K).
[42] F. G. Gao, A. J. Bard, *J. Am. Chem. Soc.* **2000**, *122*, 7426–7427 (DOI: 10.1021/ja000666t).
[43] H. Rudmann, S. Shimada, M. F. Rubner, *J. Am. Chem. Soc.* **2002**, *124*, 4918–4921 (DOI: 10.1021/ja012721j).
[44] M. Buda, G. Kalyuzhny, A. J. Bard, *J. Am. Chem. Soc.* **2002**, *124*, 6090–6098 (DOI: 10.1021/ja017834h).
[45] S. Bernhard, J. A. Barron, P. L. Houston, H. D. Abruna, J. L. Ruglovsky, X. Gao and G. G. Malliaras, *J. Am. Chem. Soc.* **2002**, *124*, 13624–13628 (DOI: 10.1021/ja0270524).
[46] P. Reveco, R. H. Schmehl, W. R. Cherry, F. R. Fronczek, J. Selbin, *Inorg. Chem.* **1985**, *24*, 4078–4082 (DOI: 10.1021/ic00218a023).
[47] X. Gong, P. K. Ng, W. K. Chan, Adv. Mater., 1998, 10, 1337–1340 (DOI: 10.1002/(SICI)1521-4095(199811)10:16<1337::AID-ADMA1337>3.0.CO;2-D).
[48] P. Spellane, R. J. Watts and A. Vogler, *Inorg. Chem.* **1993**, *32*, 5633–5636 (DOI: 10.1021/ic00076a036).
[49] G. Li, Q. Lin, L. Ji, H. Chao, *J. Mater. Chem. B* **2014**, *2*, 7918–7926 (DOI: 10.1039/C4TB01251H).
[50] K.-W. K. Lo, C.-K. Chung, T. K.-M. Lee, L.-H. Lui, K. H.-K. Tsang, N. Zhu, *Inorg. Chem.* **2003**, *42*, 6886–6897 (DOI: 10.1021/ic0346984).
[51] K. K.-W. Lo, D. Ch.-M. Ng, Ch.-K. Chung, *Organometallics* **2001**, *20*, 4999–5001 (DOI: 10.1021/om300706c).
[52] K. K.-W. Lo, A. H.-H. Leung, *Sci. China: Chem.* **2010**, *53*, 2091–2098 (DOI: 10.1007/s11426-010-4120-y).
[53] W. H.-T. Law, L. C.-C. Lee, M.-W. Louie, H.-W. Liu, T. W.-H. Ang, K. K.-W. Lo, *Inorg. Chem.* **2013**, *52*, 13029–13041 (DOI: 10.1021/ic401714p).
[54] T. Hu, L. He, L. Duan, Y. Qiu, *J. Mater. Chem.* **2012**, *22*, 4206–4210 (DOI: 10.1039/C2JM16185K).
[55] F. Dumur, D. Bertin, D. Gigmes, *Int. J. Nanotechnol.* **2012**, *9*, 377–395 (DOI: 10.1504/IJNT.2012.045343).
[56] J. Wu, F. Li, Q. Zeng, C. Nie, P. C. Ooi, T. Guo, G. Shan, Z. Su, *Org. Electron.* **2016**, *28*, 314–318 (DOI: 10.1016/j.orgel.2015.11.014).
[57] J. D. Slinker, A. A. Gorodetsky, M. S. Lowry, J. Wang, S. Parker, R. Rohl, S. Bernhard, G. G. Malliaras, *J. Am. Chem. Soc.* **2004**, *126*, 2763–2767 (DOI: 10.1021/ja0345221).
[58] H. Tang, Y. Li, Q. Chen, B. Chen, Q. Qiao, W. Yang, H. Wu, Y. Cao, *Dyes Pigm.* **2014**, *100*, 79-86 (DOI: 10.1016/j.dyepig.2013.07.029).
[59] F. Dumur, G. Nasr, G. Wantz, C. R. Mayer, E. Dumas, A. Guerlin, F. Miomandre, G. Clavier, D. Bertin, D. Gigmes, *Org. Electron.* **2011**, *12*, 1683-1694 (DOI: 10.1016/j.orgel.2011.06.014).
[60] C. Wu, H.-F. Chen, K.-T. Wong, M. E. Thompson, *J. Am. Chem. Soc.* **2010**, *132*, 3133–3139 (DOI: 10.1021/ja9097725).
[61] S. Lamansky, P. Djurovich, D. Murphy, F. Abdel-Razzaq, H.-E. Lee, C. Adachi, P. E. Burrows, S. R. Forrest, M. E. Thompson, *J. Am. Chem. Soc.* **2001**, *123*, 4304–4312 (DOI: 10.1021/ja003693s).

[62] A. B. Tamayo, B. D. Alleyne, P. I. Djurovich, S. Lamansky, I. Tsyba, N. N. Ho, R. Bau, M. E. Thompson, *J. Am. Chem. Soc.* **2003**, *125*, 7377-7387 (DOI: 10.1021/ja034537z).
[63] P. J. Hay, *J. Phys. Chem. A* **2002**, *106*, 1634-1641 (DOI: 10.1021/jp013949w).
[64] D.-F. Huang, T. J. Chow, C.-Y. Wu, S.-S. Sun, S.-H. Tsai, Y.-S. Wen, S. Polosan, T. Tsuboi, J. Chin. Chem. Soc. **2008**, *55*,439-448 (DOI: 10.1002/jccs.200800066).
[65] C. Yi, C.-J. Yang, J. Liu, M. Xu, J.-H. Wang, Q.-Y. Cao, X.-C. Gao, *Inorg. Chim. Acta* **2007**, *360*, 3493-3498 (DOI: 10.1016/j.ica.2007.04.017).
[66] A. F. Rausch, M. E. Thompson, H. Yersin, *Inorg. Chem.* **2009**, *48*, 1928–1937 (DOI: 10.1021/ic801250g).
[67] Y. K. Radwan, A. Maity, T. S. Teets, *Inorg. Chem.* **2015**, *54*, 7122–7131 (DOI: 10.1021/acs.inorgchem.5b01401).
[68] R. A. Maya, A. Maity, T. S. Teets, *Organometallics* **2016**, *35*, 2890–2899 (DOI: 10.1021/acs.organomet.6b00453).
[69] C. Adachi, R. C. Kwong, P. Djurovich, V. Adamovich, M. A. Baldo, M. E. Thompson, S. R. Forrest, *Appl. Phys. Lett.* **2001**, *79*, 2082-2084 (DOI: 10.1063/1.1400076).
[70] E. Baranoff, B. F. E. Curchod, *Dalton Trans.* **2015**, *44*, 8318-8329 (DOI: 10.1039/C4DT02991G).
[71] J. Frey, B. F. E. Curchod, R. Scopelliti, I. Tavernelli, U. Rothlisberger, M. K. Nazeeruddin, E. Baranoff, *Dalton Trans.* **2014**, *43*, 5667-5679 (DOI: 10.1039/C3DT52739E).
[72] I. Grzelak, B. Orwat, I. Kownacki, M. Hoffmann, *J. Mol. Model.* **2019**, *25*, 154 (DOI: 10.1007/s00894-019-4035-2).
[73] C. Zhou, Y. Shi, X. Ding, M. Li, J. Luo, Z. Lu, D. Xiao, *Anal. Chem.* **2013**, *85*, 1171–1176 (DOI: 10.1021/ac303107d).
[74] K. Teegardin, J. I. Day, J. Chan, J. Weaver, *Org. Process Res. Dev.* **2016**, *20*, 1156–1163 (DOI: 10.1021/acs.oprd.6b00101).
[75] Z. A. Page, B. Narupai, C. W. Pester, R. Bou Zerdan, A. Sokolov, D. S. Laitar, S. Mukhopadhyay, S. Sprague, A. J. McGrath, J. W. Kramer, P. Trefonas, C. J. Hawker, *ACS Cent. Sci.* **2017**, *3*, 654–661 (DOI: 10.1021/acscentsci.7b00165).
[76] J. Han, K.-M. Tang, S.-C. Cheng, C.-O. Ng, Y.-K. Chun, S.-L. Chan, S.-M. Yiu, M.-K. Tse, V. A. L. Roy, C.-C. Ko, *Inorg. Chem. Front.* **2020**, *7*, 786–794 (DOI: 10.1039/C9QI01278H).
[77] C. Li, H. Wang, J. Shen, B. Tang, *Anal. Chem.* **2015**, *87*, 4283–4291 (DOI: 10.1021/ac5047032).
[78] J.-H. Zhu, B.-Z. Tang, K. K.-W. Lo, *Chem. - Eur. J.* **2019**, *25*, 10633–10641 (DOI: 10.1002/chem.201901029).
[79] M. Velusamy, K. R. J. Thomas, C.-H. Chen, J. T. Lin, J. Y. S. Wen, W.-T. Hsieh, C.-H. Lai, P.-T. Chou, *Dalton Trans.* **2007**, 3025–3034 (DOI: 10.1039/B618311E).
[80] A. S. Ionkin, W. J. Marshall, D. C. Roe, Y. Wang, *Dalton Trans.* **2006**, 2468–2478 (DOI: 10.1039/B514797B).
[81] C.-H. Yang, K.-H. Fang, W.-L. Su, S.-P. Wang, S.-K. Su, I.-W. Sun, *J. Organomet. Chem.* **2006**, *691*, 2767–2773 (DOI: 10.1016/j.jorganchem.2006.02.034).
[82] F.-M. Hwang, H.-Y. Chen, P.-S. Chen, C.-S. Liu, Y. Chi, C.-F. Shu, F.-I. Wu, P.-T. Chou, S.-M. Peng, G.-H. Lee, *Inorg. Chem.* **2005**, *44*, 1344-1353 (DOI: 10.1021/ic0489443).
[83] S. Sprouse, K. A. King, P. J. Spellane, R. J. Watts, *J. Am. Chem. Soc.* **1984**, *106*, 6647-6653 (DOI: 10.1021/ja00334a031).
[84] S. Soman, G. S. Bindra, A. Paul, R. Groarke, J. C. Manton, F. M. Connaughton, M. Schulz, D. Dini, C. Long, M. T. Pryce, J. G. Vos, *Dalton Trans.* **2012**, *41*, 12678-12680 (DOI: 10.1039/C2DT32028B).
[85] L. Mosca, R. S. Khnayzer, M. S. Lazorski, E. O. Danilov, F. N. Castellano, P. Anzenbacher Jr., *Chem.: Eur. J.* **2015**, *21*, 4056-4064 (DOI: 10.1002/chem.201405717).
[86] R. V. Kiran, C. F. Hogan, B. D. James, D. V. D. Wilson, *Eur. J. Inorg. Chem.* **2011**, *2011*, 4816-4825 (10.1002/ejic.201100639).
[87] D. Ramlot, M. Rebarz, L. Volker, M. Ovaere, D. Beljonne, W. Dehaen, L. V. Meervelt, C. Moucheron, A. K.-D. Mesmaeker, *Eur. J. Inorg. Chem.* **2013**, *2013*, 2031-2040 (DOI: 10.1002/ejic.201201427).
[88] I. R. Laskar, S.-F. Hsu, T.-M. Chen, *Polyhedron* **2006**, *25*, 1167-1176 (DOI: 10.1016/j.poly.2005.08.033).
[89] Y.-T. Huang, T.-H. Chuang, Y.-L. Shu, Y.-C. Kuo, P.-L. Wu, C.-H. Yang, I-W. Sun, *Organometallics* **2005**, *24*, 6230-6238 (DOI: 10.1021/om050638p).
[90] T. M. Monos, A. C. Sun, R. C. McAtee, J. J. Devery III, C. R. J. Stephenson, *J. Org. Chem.* **2016**, *81*, 6988-6994 (DOI: 10.1021/acs.joc.6b00983).
[91] P. Alam, I. R. Laskar, C. Climent, D. Casanova, P. Alemany, M. Karanam, A. R. Choudhury, J. R. Butcher, *Polyhedron*, **2013**, *53*, 286-294 (10.1016/j.poly.2013.01.045).
[92] F. Scarpelli, A. Ionescu, L. Ricciardi, P. Plastina, I. Aiello, M. L. Deda, A. Crispini, M. Ghedini, N. Godbert, *Dalton Trans.* **2016**, *45*, 17264-17273 (DOI: 10.1039/C6DT02976K).

[93] C. A. Echeverry-Gonzalez, C. E. Puerto-Galvis, C. H. Borca, M. A. Mosquera, A. F. Luis-Robles, V. V. Kouznetsov, *Org. Chem. Front.* **2019**, *6*, 3374-3382 (DOI: 10.1039/C9QO00870E).
[94] K. K.-W. Lo, D. Ch.-M. Ng, Ch.-K. Chung, *Organometallics* **2001**, *20*, 4999–5001 (DOI: 10.1021/om010652b).
[95] E. A. Plummer, A. van Dijken, J. W. Hofstraat, L. De Cola, K. Brunner, *Adv. Funct. Mater.* **2005**, *15*, 281–289 (DOI: 10.1002/adfm.200400218).
[96] K. K.-W. Lo, J. S.-W. Chan, C.-K. Chung, V. W.-H. Tsang and N. Zhu, *Inorg. Chim. Acta* **2004**, *357*, 3109–3118 (DOI: 10.1016/j.ica.2004.01.029).
[97] M. S. Lowry, W. R. Hudson, R. A. Pascal Jr., S. Bernhard, *J. Am. Chem. Soc.* **2004**, *126*, 14129–14135 (DOI: 10.1021/ja047156%2B).
[98] S. Salinas, M. A. Soto-Arriaza, B. Loeb, Polyhedron, 2011, 30, 2863–2869 (DOI: 10.1016/j.poly.2011.08.010).
[99] C. Dragonetti, A. Valore, A. Colombo, S. Righetto, V. Trifiletti, *Inorg. Chim. Acta* **2012**, *388*, 163–167 (DOI: 10.1016/j.ica.2012.03.028).
[100] K. Huang, I. W. Bulik, A. A. Marti, *Chem. Commun.* **2012**, *48*, 11760–11762 (DOI: 10.1039/C2CC36588J).
[101] K.-H. Leung, H.-Z. He, V. P.-Y. Ma, H.-J. Zhong, D. S.-H. Chan, J. Zhou, J.-L. Mergny, C.-H. Leung, D.-L. Ma, *Chem. Commun.* **2013**, *49*, 5630–5632 (DOI: 10.1039/C3CC41129J).
[102] D.-L. Ma, L.-J. Liu, K.-H. Leung, Y.-T. Chen, H.-J. Zhong, D. S.-H. Chan, H.-M. D. Wang, C.-H. Leung, *Angew. Chem., Int. Ed.* **2014**, *53*, 9178–9182 (DOI: 10.1002/anie.201404686).
[103] H. Ahmad, A. Wragg, W. Cullen, C. Wombwell, A. J. H. M. Meijer, J. A. Thomas, *Chem. – Eur. J.* **2014**, *20*, 3089–3096 (DOI: 10.1002/chem.201304053).
[104] Z. Wu, J. Mu, Q. Wang, X. Chen, L. Jensen, Ch. Yi, M.-J. Li, *J. Organomet. Chem.* **2015**, *791*, 175–182 (DOI: 10.1016/j.jorganchem.2015.05.035).
[105] Y. Ohsawa, S. Sprouse, K. A. King, M. K. De Armond, K. W. Hanck, R. J. Watts, *J. Phys. Chem.* **1987**, *91*, 1047–1054 (DOI: 10.1021/j100289a009).
[106] A. de la Hoz, Á. Díaz-Ortiz, A. Moreno, *Chem. Soc. Rev.* **2005**, *34*, 164–178 (DOI: 10.1039/B411438H).
[107] N. Yoshikawa, Y. Masuda, T. Matsumura-Inoue, *Chem. Lett.* **2000**, *29*, 1206–1207 (DOI: 10.1246/cl.2000.1206).
[108] S. L. Van Atta, B. A. Duclos, D. B. Green, *Organometallics* **2000**, *19*, 2397–2399 (DOI: 10.1021/om990977g).
[109] B. I. K. Oxana, V. Kharissova, U. O. Mendez, *Advances in Induction and Microwave Heating of Mineral and Organic Materials*, *InTech*, **2011**, p. 766 (DOI: 10.5772/562).
[110] H. Phetmung, M. Wateh, C. Pakawatchai, *Turk. J. Chem.* **2012**, *36*, 556–566 (DOI: 10.3906/kim-1104-30).
[111] J. Lhoste, N. Henry, T. Loiseau, F. Abraham, *Inorg. Chem. Commun.* **2011**, *14*, 1525–1527 (DOI: 10.1016/j.inoche.2011.06.013).
[112] T. Abe, A. Miyazawa, Y. Kawanishi, H. Konno, *Mini-Rev. Org. Chem.* **2011**, *8*, 315–333 (DOI: 10.2174/157019311796197346).
[113] J.-R. Li, Z.-L. Xie, B. Hu, X.-Y. Huang, *Inorg. Chem. Commun.* **2011**, *14*, 265–267 (DOI: 10.1016/j.inoche.2010.11.010).
[114] X. Shen, Y. Zhang, M. Xue, Q. Shen, *Dalton Trans.* **2012**, *41*, 3668–3674 (DOI: 10.1039/C2DT12176J).
[115] R. Dalpozzo, A. De Nino, M. Nardi, B. Russo, A. Procopio, *Synthesis* **2006**, *7*, 1127–1132 (DOI: 10.1055/s-2006-926378).
[116] I. Glowacki, Z. Szamel, *J. Phys. D: Appl. Phys.* **2010**, *43*, 295101 (DOI: 10.1088/0022-3727/43/29/295101).
[117] P.-N. Lai, C. H. Brysacz, M. K. Alam, N. A. Ayoub, T. G. Gray, J. Bao, T. S. Teets, *J. Am. Chem. Soc.* **2018**, *140*, 10198–10207 (DOI: 10.1021/jacs.8b04841).
[118] D. Buu-Hoi, C. R. Guettier, *Hebd. Seances Acad. Sci.* **1946**, *222*, 665–666.
[119] Y. Kitahara, M. Mochii, M. Mori, A. Kubo, *Tetrahedron* **2003**, *59*, 2885–2891 (DOI: 10.1016/S0040-4020(03)00349-1).
[120] W. P. Utermohlen Jr., C. S. Hamilton, *J. Am. Chem. Soc.* **1941**, *63*, 156–159 (DOI: 10.1021/ja01846a038).
[121] W. E. Parham, D. C. Egberg, S. Salgar, *J. Org. Chem.* **1972**, *37*, 3248–3254 (DOI: 10.1021/jo00986a013).
[122] C. J. Evoniuk, G. dos Passos Gomes, M. Ly, F. D. White, I. V. Alabugin, *J. Org. Chem.* **2017**, *82*, 4265–4278 (DOI: 10.1021/acs.joc.7b00262).
[123] Y. Zhang, M. Wang, P. Li, L. Wang, *Org. Lett.* **2012**, *14*, 2206–2209 (DOI: 10.1021/ol300391t).
[124] Z. Zheng, G. Deng, Y. Liang, *RSC Adv.* **2016**, *6*, 103478–103481 (DOI: 10.1039/C6RA23858K).
[125] D. K. O'Dell, K. M. Nicholas, *J. Org. Chem.* **2003**, *68*, 6427–6430 (DOI: 10.1021/jo034447c).

[126] C.-Z. Luo, P. Gandeepan, Y.-C. Wu, W.-C. Chen, C.-H Cheng, *RSC Adv.* **2015**, *5*, 106012–106018 (DOI: 10.1039/C5RA23065A).
[127] H. Lee, C. S. Yi, *Organometallics* **2016**, *35*, 1973–1977 (DOI: 10.1021/acs.organomet.6b00273).
[128] A.I. Tochilkin, I.R. Kovel'man, E.P. Prokof'ev, I. N. Gracheva, M. V. Levinskii, *Chem. Heterocycl. Compd.* **1988**, *24*, 892–897 (DOI: 10.1007/BF00479345).
[129] Y. Furusho, A. Tsunoda, T. Aida, *J. Chem. Soc. Perkin Trans.* **1996**, *1*, 183–190 (DOI: 10.1039/P19960000183).
[130] P. Dash, M. Janni, S. Peruncheralathan, *Eur. J. Org. Chem.* **2012**, *2012*, 4914–4917 (DOI: 10.1002/ejoc.201200753).
[131] J. Huang, Y. Chen, J. Chan, M. L. Ronk, R. D. Larsen, M. M. Faul, *Synlett* **2011**, *10*, 1419–1422 (DOI: 10.1055/s-0030-1260761).
[132] Y. Liu, S. Zhang, *Synlett* **2011**, *2*, 268–272 (DOI: 10.1055/s-0030-1259291).
[133] E. Sperotto, J. G. de Vries, G. P. M. van Klink, G. van Koten, *Tetrahedron Lett.* **2007**, *48*, 7366–7370 (DOI: 10.1016/j.tetlet.2007.08.026).
[134] J. Ju, R. Hua, J. Su, *Tetrahedron* **2012**, *68*, 9364–9370 (DOI: 10.1016/j.tet.2012.09.035).
[135] H. Xua, C. Wolf, *Chem. Commun.* **2009**, 3035– 3037 (DOI: 10.1039/B904188E).
[136] A. Nobutaka, U. Masatsugu, *U. S. Patent Application* US2016/190487 A1 **2016**.
[137] N. Xia, M. Taillefer, *Angew. Chem. Int. Ed.* **2009**, *48*, 337–339 (DOI: 10.1002/anie.200802569).
[138] J. P. Wolfe, J. Ahman, J. P. Sadighi, R. A. Singer, S. L. Buchwald, *Tetrahedron Lett.* **1997**, *38*, 6367–6370 (DOI: 10.1016/S0040-4039(97)01465-2).
[139] G. A. Grasa, M. S. Viciu, J. Huang, S. P. Nolan, *J. Org. Chem.* **2001**, *66*, 7729–7737 (DOI: 10.1021/jo010613+).
[140] X. Huang, S. L. Buchwald, *Org. Lett.* **2001**, *3*, 3417–3419 (DOI: 10.1021/ol0166808).
[141] D.-Y. Lee, J. F. Hartwig, *Org. Lett.* **2005**, *7*, 1169–1172 (DOI: 10.1021/ol050141b).
[142] S. Bhagwanth, A. G. Waterson, G. M. Adjabeng, K. R. Hornberger, *J. Org. Chem.* **2009**, *74*, 4634–4637 (DOI: 10.1021/jo9004537).
[143] R. A. Green, J. F. Hartwig, *Org. Lett.* **2014**, *16*, 4388–4391 (DOI: 10.1021/ol501739g).
[144] P. L. Pickard, T. L. Tolbert, *J. Org. Chem.* **1961**, *26*, 4886–4888 (DOI: 10.1021/jo01070a025).
[145] K. K. Laali, V. J. Gettwert, *J. Fluorine Chem.* **2001**, *107*, 31–34 (DOI: 10.1016/S0022-1139(00)00337-7).
[146] R. M. Adhikari, D. C. Neckers, B. K. Shah, *J. Org. Chem.* **2009**, *74*, 3341–3349 (DOI: 10.1021/jo9002757).
[147] G. Schansker, S. Z. Tóth, L. Kovács, A. R. Holzwarth, G. Garab, *Biochim. Biophys. Acta* **2011**, *1807*, 1032–1043 (DOI: 10.1016/j.bbabio.2011.05.022).
[148] J.-Y. Shen, X.-L. Yang, T.-H. Huang, J. T. Lin, T.-H. Ke, L.-Y. Chen, C.-C. Wu, M.-C. P. Yeh, *Adv. Funct. Mater.* **2007**, *17*, 983–995 (DOI: 10.1002/adfm.200600921).
[149] K. Nozaki, K. Takahashi, K. Nakano, T. Hiyama, H.-Z. Tang, M. Fujiki, S. Yamaguchi, K. Tamao, *Angew. Chem. Int. Ed.* **2003**, *42*, 2051–2053 (DOI: 10.1002/anie.200250648).
[150] G. Cheng, N. R. Vautravers, R. E. Morrisa, D. J. Cole-Hamilton, *Org. Biomol. Chem.* **2008**, *6*, 4662–4667 (DOI: 10.1039/B812140K).
[151] B. Marciniec, J. Guliński, W. Urbaniak, Z.W. Kornetka, *Comprehensive Handbook on Hydrosilylation 1st ed.* (Ed.: B. Marciniec), *Pergamon Press*, Oxford, **1992**.
[152] W. Tejchman, B. Orwat, I. Korona-Głowniak, A. Barbasz, I. Kownacki, G. Latacz, J. Handzlik, E. Żesławska, A. Malm, *RSC Adv.* **2019**, *9*, 39367-39380 (DOI: 10.1039/C9RA08690K).
[153] B. Orwat, E. Witkowska, I. Kownacki, M.-J. Oh, M. Hoffmann, M. Kubicki, I. Grzelak, B. Marciniec, I. Głowacki, B. Łuszczyńska, G. Wiosna-Sałyga, J. Ulański, P. Ledwoń, M. Łapkowski, *Dalton Trans.* **2017**, *426*, 9210-9226 (DOI: 10.1039/C7DT01372H).
[154] B. Orwat, M.-J. Oh, M. Kubicki, I. Kownacki; *Adv. Synth. Catal.* **2018**, *360*, 3331-3344 (DOI: 10.1002/adsc.201800286).
[155] E. Baranoff, B. F. E. Curchod, J. Frey, R. Scopelliti, F. Kessler, I. Tavernelli, U. Rothlisberger, M. Grätzel, M. K. Nazeeruddin, *Inorg. Chem.* **2012**, *51*, 215-224 (DOI: 10.1021/ic202162q).
[156] C. Hierlinger, A. K. Pal, F. Stella, T. Lebl, D. B. Cordes, A. M. Z. Slawin, D. Jacquemin, V. Guerchais, E. Zysman-Colman, *Inorg. Chem.* **2018**, *57*, 2023-2034 (DOI: 10.1021/acs.inorgchem.7b02940).
[157] C. Hierlinger, D. B. Cordes, A. M. Z. Slawin, D. Jacquemin, V. Guerchais, E. Zysman-Colman. *Dalton Trans.* **2018**, *47*, 10569-10577 (DOI: 10.1039/C8DT00467F).

[158] Y.-H. Song, Y.-C. Chiu, Y. Chi, Y.-M. Cheng, C.-H. Lai, P.-T.Chou, K.-T. Wong, M.-H. Tsai, C.-C. Wu, *Chem. Eur. J.* **2008**, *14*, 5423-5434 (DOI: 10.1002/chem.200800050).
[159] C.-F. Chang, Y.-M. Cheng, Y. Chi, Y.-C. Chiu, C.-C. Lin, G.-H. Lee, P.-T. Chou, C.-C. Chen, C.-H. Chang, C.-C. Wu, *Angew. Chem. Int. Ed.* **2008**, *47*, 4542-4545 (DOI: 10.1002/anie.200800748).
[160] M. S. Lowry, W. R. Hudson, R. A. Pascal, S. Bernhard, *J. Am. Chem. Soc.* **2004**, *126*, 14129-14135 (DOI: 10.1021/ja047156+).
[161] F. O. Garces, K. A. King, R. J. Watts, *Inorg. Chem.* **1988**, *27*, 3464-3471 (DOI: 10.1021/ic00293a008).
[162] C. Li, M. Yu, Y. Sun, Y. Wu, C. Huang, F. Li, *J. Am. Chem. Soc.* **2011**, *133*, 11231-11239 (DOI: 10.1021/ja202344c).
[163] G. A. Carlson, P. I. Djurovich, R. J. Watts, *Inorg. Chem.* **1993**, *32*, 4483-4484 (DOI: 10.1021/ic00073a001).
[164] B. Schmid, F. O. Garces, R. J. Watts, *Inorg. Chem.* **1994**, *33*, 9-14 (DOI: 10.1021/ic00079a005).
[165] P.-L. T. Boudreault, M. A. Esteruelas, E. Mora, E. Oñate, J.-Y. Tsai, *Organometallics* **2018**, *37*, 3770-3779 (DOI: 10.1021/acs.organomet.8b00500).
[166] D.-L. Ma, W.-L. Wong, W.-H. Chung, F.-Y. Chan, P.-K. So, T.-S. Lai, Z.-Y. Zhou, Y.-C. Leung, K.-Y. Wong, *Angew. Chem. Int. Edit.* **2008**, *47*, 3735-3739 (DOI: 10.1002/anie.200705319).
[167] B. A. Thompson, *J. Am. Soc. Mass. Spectrom.* **1997**, *8*, 1053-1058 (DOI: 10.1016/S1044-0305(97)00129-3).
[168] M. A. Henderson, S. Kwok, J. S. McIndoe, *J. Am. Soc. Mass. Spectrom.* **2009**, *20*, 658-666 (DOI: 10.1016/j.jasms.2008.12.006).
[169] A. R. McDonald, M. Lutz, L. S. von Chrzanowski, G. P. M. van Klink, A. L. Spek, G. van Koten, *Inorg. Chem.* **2008**, *47*, 6681–6691 (DOI: 10.1021/ic800169n).
[170] K. Ono, M. Joho, K. Saito, M. Tomura, Y. Matsushita, S. Naka, H. Okada, H. Onnagawa, *Eur. J. Inorg. Chem.* **2006**, *2006*, 3676–3683 (DOI: 10.1002/ejic.200600285).
[171] J. C. Deaton, *European Patent* EP1762123 B1 **2007**

10. Oświadczenia współautorów

Oświadczenia współautorów dotyczące wkładu w powstanie publikacji:

[P1] **B. Orwat**, E. Witkowska, I. Kownacki*, M.-J. Oh, M. Hoffmann, M. Kubicki, I. Grzelak, B. Marciniec, I. Głowacki, B. Łuszczyńska, G. Wiosna-Sałyga, J. Ulański, P. Ledwoń, M. Łapkowski; *Microwave-assisted one-pot synthesis of new ionic cyclometalated iridium complexes of $[Ir(bzq)_2(N^N)]^+A^-$ type and their selected electroluminescent properties*; *Dalton Transactions* **2017**, vol. 426, p. 75

Imię i nazwisko	Zakres merytoryczny wkładu	Podpis współautora
Bartosz Orwat	- zaprojektowanie struktur badanych związków - optymalizacja warunków syntez związków koordynacyjnych - otrzymanie związków 2AA' – 2IA' oraz 2IC' - charakterystyka ^{1}H NMR wszystkich związków - udział w korelowaniu struktur emiterów z ich właściwościami i dyskusji wyników - przygotowanie części manuskryptu i suplementu dotyczących syntez oraz udział w przygotowaniu pozostałych sekcji artykułu	Bartosz Orwat
Ewelina Witkowska	- udział w badaniach fotofizycznych - projektowanie, wytwarzanie, wyznaczenie i analiza podstawowych parametrów pracy OLEDów - udział w analizie uzyskanych wyników i opracowaniu manuskryptu	Ewelina Witkowska
Ireneusz Kownacki	- ogólna koncepcja badań - korespondencja z Edytorem i Recenzentami - koordynowanie prac nad przygotowaniem manuskryptu	
Myong Joon Oh	- synteza związków 2AB' – 2IB'	Myong Joon Oh
Marcin Hoffmann	- ogólna koncepcja obliczeń kwantowo-chemicznych - udział w przygotowaniu części manuskryptu dotyczącej obliczeń teoretycznych	Hoffmann
Maciej Kubicki	- analiza rentgenostrukturalna - przygotowanie opisu struktur krystalicznych	Maciej Kubicki

Oświadczenia współautorów dotyczące wkładu w powstanie publikacji:

[**P2**] E. Witkowska, G. Wiosna-Sałyga*, I. Głowacki, **B. Orwat**, M.-J. Oh, I. Kownacki*, M. Kubicki, B. Gierczyk, M. Dutkiewicz, P. Cieszko, B. Łuszczyńska, J. Ulański, I. Grzelak, M. Hoffmann, P. Ledwoń, M. Łapkowski; *Effect of fluorine substitution of the b-ketoiminate ancillary ligand on photophysical properties and electroluminescence ability of new iridium(III) complexes*; *Journal of Materials Chemistry C* **2018**, vol. 6, p. 8688

Imię i nazwisko	Zakres merytoryczny wkładu	Podpis współautora
Bartosz Orwat	- zaprojektowanie struktur badanych związków - oczyszczanie związków 3b – 3f - synteza związków 5b – 5f - analiza ^{1}H NMR wszystkich związków koordynacyjnych - wyhodowanie kryształów 3f i 5e - udział w korelowaniu struktur emiterów z ich właściwościami i dyskusji wyników - przygotowanie części manuskryptu i suplementu dotyczących syntez oraz udział w przygotowaniu pozostałych sekcji artykułu - udział w korespondencji z Edytorem i Recenzentami	Bartosz Orwat
Ewelina Witkowska	- udział w badaniach fotofizycznych oraz pomiarach termoluminescencji - projektowanie, wytwarzanie i analiza parametrów pracy OLEDów - udział w analizie uzyskanych wyników i opracowaniu manuskryptu	Ewelina Witkowska
Gabriela Wiosna-Sałyga	- zaplanowanie oraz udział w wykonaniu i analizie wyników badań fotofizycznych - udział w analizie wyników badań termo- oraz elektroluminescencji - udział w tworzeniu manuskryptu - udział w korespondencji z Edytorem i Recenzentami	G. Wiosna-Sałyga
Ireneusz Głowacki	- udział w pomiarach termoluminescencji i w wyznaczeniu podstawowych parametrów pracy OLEDów - udział w dyskusji ostatecznych wyników oraz w opracowaniu manuskryptu	I. Głowacki
Myong Joon Oh	- synteza związków 5a i 5g	Myong Joon Oh
Ireneusz Kownacki	- ogólna koncepcja badań - koordynowanie prac nad przygotowaniem artykułu - udział w korespondencji z Edytorem i Recenzentami	I. Kownacki

Oświadczenia współautorów dotyczące wkładu w powstanie publikacji:

[P3] E. Witkowska, **B. Orwat**, M.-J. Oh, G. Wiosna-Sałyga*, I. Głowacki, I. Kownacki*, K. Jankowska, M. Kubicki, B. Gierczyk, M. Dutkiewicz, I. Grzelak, M. Hoffmann, J. Nawrocik, G. Krajewski, J. Ulański, P. Ledwoń, M. Łapkowski; *Effect of β-Ketoiminato Ancillary Ligand Modification on Emissive Properties of New Iridium Complexes*; *Inorganic Chemistry* **2019**, vol. 58, p. 15671

Imię i nazwisko	Zakres merytoryczny wkładu	Podpis współautora
Bartosz Orwat	- zaprojektowanie struktur badanych związków - oczyszczanie związków 3b, 3c, 3h, 3i - synteza związków 3j-l, 5d-f i 5h-l - analiza ^{1}H NMR wszystkich związków kompleksowych - wyhodowanie kryształów 3h, 3j, 3l, 5j, 5l - udział w korelowaniu struktur emiterów z ich właściwościami i dyskusji wyników - przygotowanie części manuskryptu i suplementu dotyczących syntez oraz udział w przygotowaniu pozostałych sekcji artykułu - udział w korespondencji z Edytorem i Recenzentami	Bartosz Orwat
Ewelina Witkowska	- udział w badaniach właściwości fotofizycznych - optymalizacja składu i badania warstw typu gospodarz-gość - wyznaczenie parametrów transferu energii - udział w pomiarach termoluminescencji i w wyznaczeniu podstawowych parametrów pracy OLEDów - udział w analizie wyników i tworzeniu manuskryptu	Ewelina Witkowska
Myong Joon Oh	- oczyszczanie ketoimin 3d-f, - synteza związków 5a-c	Myong Joon Oh
Ireneusz Głowacki	- udział w pomiarach termoluminescencji i w wyznaczeniu podstawowych parametrów pracy OLEDów - udział w analizie i interpretacji zjawisk pułapkowania nośników ładunku - udział w dyskusji ostatecznych wyników i w opracowaniu manuskryptu	I. Głowacki
Gabriela Wiosna-Sałyga	- koncepcja badań fotofizcznych w roztworze i filmie oraz interpretacja uzyskanych wyników - udział w analizie wyników badań termo- oraz elektroluminescencji - udział w tworzeniu i korekcie manuskryptu - udział w korespondencji z Edytorem i Recenzentami	G. Wiosna-Sałyga
Ireneusz Kownacki	- ogólna koncepcja badań - koordynowanie prac nad przygotowaniem artykułu - udział w korespondencji z Edytorem i Recenzentami	I. Kownacki

Oświadczenia współautorów dotyczące wkładu w powstanie publikacji:

[P4] **B. Orwat**, M.-J. Oh, M. Kubicki, I. Kownacki*; *Synthesis of 5-Substituted Benzo[h]quinoline Derivatives via Reactions Involving C(sp^2)-Br Bond Activation; Advanced Synthesis & Catalysis* **2018**, vol. 360, p. 3331

Imię i nazwisko	Zakres merytoryczny wkładu	Podpis współautora
Bartosz Orwat	- synteza i optymalizacja warunków otrzymywania związków 1-8 i 10-13 - charakterystyka spektroskopowa (NMR, MS) wszystkich związków - wyhodowanie kryształów do pomiarów rentgenostrukturalnych - przygotowanie manuskryptu i suplementu oraz współudział w ich korekcie - współudział w korespondencji z Edytorem i Recenzentami	Bartosz Orwat
Myong Joon Oh	- synteza związku 9	Myong Joon Oh
Maciej Kubicki	- analiza rentgenostrukturalna - przygotowanie opisu struktur krystalicznych	Maciej Kubicki
Ireneusz Kownacki	- koordynowanie prac nad przygotowaniem artykułu - współudział w korespondencji z Edytorem i Recenzentami	Ireneusz Kownacki

Oświadczenia współautorów dotyczące wkładu w powstanie publikacji:

[P5] **B. Orwat***, M.-J. Oh, M. Zaranek, M. Kubicki, R. Januszewski, I. Kownacki*; *Microwave-accelerated C,N-cyclometalation as a route to chloro-bridged iridium(III) binuclear precursors of phosphorescent materials: optimization, synthesis, and studies of the Ir(III) dimers behavior in coordinating solvents; Inorganic Chemistry* **2020**, DOI: 10.1021/acs.inorgchem.0c01071

Imię i nazwisko	Zakres merytoryczny wkładu	Podpis współautora
Bartosz Orwat	- optymalizacja warunków syntezy dimerów - synteza wszystkich związków oprócz $[Ir(\mu\text{-}Cl)(5\text{-}Ph_2Nbzq)_2]_2$, $[Ir(\mu\text{-}Cl)(PhOPyMe)_2]_2$ oraz $[Ir(\mu\text{-}Cl)(F_3CPhOPy)_2]_2$ - charakterystyka spektroskopowa (NMR, MS) wszystkich związków z wyjątkiem $[Ir(\mu\text{-}Cl)(PhOPyMe)_2]_2$ oraz $[Ir(\mu\text{-}Cl)(F_3CPhOPy)_2]_2$ - wyhodowanie kryształów do pomiarów rentgenostrukturalnych - wyjaśnienie procesu rozszczepienia dimerów w obecności rozpuszczalników koordynujących - wykonanie pomiarów ESI-HRMS i udowodnienie wpływu parametrów analizy na wynik oznaczenia - opracowanie koncepcji pracy, przygotowanie manuskryptu i suplementu oraz współudział w ich korekcie - współudział w korespondencji z Edytorem i Recenzentami	Bartosz Orwat
Myong Joon Oh	- synteza $[Ir(\mu\text{-}Cl)(5\text{-}Ph_2Nbzq)_2]_2$	Myong Joon Oh
Maciej Zaranek	- synteza i charakterystyka spektroskopowa $[Ir(\mu\text{-}Cl)(PhOPyMe)_2]_2$ oraz $[Ir(\mu\text{-}Cl)(F_3CPhOPy)_2]_2$	Maciej Zaranek
Maciej Kubicki	- analiza rentgenostrukturalna - przygotowanie opisu struktur krystalicznych	Maciej Kubicki
Rafał Januszewski	- pomoc w opracowaniu ilustracji do pracy	Januszewski Rafał
Ireneusz Kownacki	- koordynowanie prac nad przygotowaniem artykułu - współudział w korespondencji z Edytorem i Recenzentami	Ireneusz Kownacki

11. Kopie publikacji wchodzących w skład rozprawy

Dalton Transactions

PAPER

View Article Online
View Journal | View Issue

Cite this: *Dalton Trans.*, 2017, **46**, 9210

Microwave-assisted one-pot synthesis of new ionic iridium complexes of $[Ir(bzq)_2(N\hat{}N)]^+A^-$ type and their selected electroluminescent properties†

B. Orwat,[a] E. Witkowska,[b] I. Kownacki, *[a] M.-J. Oh,[a] M. Hoffmann,[a] M. Kubicki,[a] I. Grzelak,[a] B. Marciniec,[a,c] I. Glowacki,[b] B. Luszczynska,[b] G. Wiosna-Salyga,[b] J. Ulanski,[b] P. Ledwon[d] and M. Lapkowski[d,e]

Received 15th April 2017,
Accepted 16th June 2017

DOI: 10.1039/c7dt01372h

rsc.li/dalton

Iridium *C*,*N*-cyclometalated complexes with an ionic structure are considered to be promising candidates for application in host/guest solid-state phosphorescent single-layer devices because the employment of such dopants offers the possibility of reducing their concentration in organic matrices as well as allows obtaining organic light emitting devices (OLEDs) with interesting emission parameters. We report herein a methodology enabling the synthesis of cyclometalated ionic iridium(III) complexes of the type $[Ir(C\hat{}N)_2(N\hat{}N)]^+A^-$ according to a three-component one-pot strategy involving the acceleration of the reaction *via* microwave irradiation. The developed protocol allowed efficient synthesis of a series of new cationic iridium(III) coordination derivatives, which were isolated and spectroscopically characterized, while the structures of two of them were determined by the X-ray method. Moreover, the iridium(III) derivatives were subjected to the cyclic voltammetry studies in order to determine the energies of the HOMO and LUMO levels as well as to estimate their electrochemical properties and to predict some electronic properties. Additionally, the ONIOM calculation scheme that was used to predict HOMO–LUMO gaps for the studied Ir(III) complexes showed a good correlation between the experimental and calculated values. In order to determine the influence of the structure and nature of the ancillary ligand on the location of the maximum emission band, the photophysical properties of the synthesized iridium complexes were characterized. Finally, the selected compounds were used as emitters for the construction of polymer light emitting diodes (PLEDs) based on a poly(*N*-vinylcarbazole)/2-(4-*tert*-butylphenyl)-5-(4-biphenyl)-1,3,4-oxadiazole (PVK/PBD) matrix. The highest luminance, above 10 000 cd m^{-2}, was recorded for the device containing only 1.0 wt% of $[Ir(bzq)_2(1,10\text{-phenanthroline})]^+PF_6^-$ in the PVK/PBD. The fabricated PLEDs exhibit current efficiency in the range of 1.0 to 2.2 cd A^{-1}.

Introduction

Organic Light-Emitting Diodes (OLEDs) show great potential for application as alternatives to traditional inorganic devices, mainly due to the fact that thin-layer technologies for their fabrication are relatively simple, they require a small amount of organic components, and they can offer significant energy savings, which makes them environmentally friendly.[1] In view of the above, the synthesis of new phosphorescence emitters for OLEDs belongs to the hottest research areas on the world scale in chemistry and materials engineering. The growing interest in host/guest phosphorescent systems follows from the fact that the inner quantum yield of OLEDs with an emission layer made of fluorescence materials cannot be higher than 25%. This restriction can be overcome if the emission source is a phosphorescent material, in particular those based on

[a]*Faculty of Chemistry, Adam Mickiewicz University in Poznan, St. Umultowska 89b, 61-614 Poznan, Poland. E-mail: Ireneusz.Kownacki@amu.edu.pl*
[b]*Department of Molecular Physics, Lodz University of Technology, 90-924 Lodz, Zeromskiego 116, Poland*
[c]*Center for Advanced Technologies, Adam Mickiewicz University in Poznan, St. Umultowska 89c, 61-614 Poznan, Poland*
[d]*Silesian University of Technology, Faculty of Chemistry, St. Marcina Strzody 9, 44-100 Gliwice, Poland*
[e]*Centre of Polymer and Carbon Materials, Polish Academy of Sciences, Curie-Sklodowskiej 34, 41-819 Zabrze, Poland*

†Electronic supplementary information (ESI) available: X-ray crystallographic data for **2AA′** and **2FA′** (CIF). Structure refinement data for **2AA′** and **2FA′** as well as full computational details and Cartesian coordinates (PDF). CCDC 1518625 and 1518624. For ESI and crystallographic data in CIF or other electronic format see DOI: 10.1039/c7dt01372h

heavy metal coordination compounds in which the central metal atom is surrounded by organic ligands, mostly *C*,*N*-cyclometalated ligands.[2,3] Such compounds are usually introduced as dopants into the matrix to avoid concentration induced emission quenching. Among the heavy transition metals (TM), the metal most often used for this purpose is iridium but attempts at using other TM such as Pt, Os or Pd have also been reported.[4] Such materials are characterized by a very strong spin–orbit coupling, which causes a mutual isoenergetic transition from the singlet to the triplet state and *vice versa*, known as intersystem crossing (ISC).[5] Because of this effect, there is a theoretical possibility of getting an inner quantum yield of 100%. However, at the moment, mainly fluorescent OLEDs are commercially available because as yet no efficient and stable blue phosphorescence emitter has been designed; the consequence is the lack of a complete set of red–green–blue (RGB) or red–green–blue–white (RGBW) displays.[6] The reason is that, unfortunately, the hitherto discovered blue emitters have several tens of thousands of times shorter lifespan than the emitters responsible for other colours, which means that OLEDs based on such emitters over time significantly lose the ability to properly display images.[7]

Nevertheless, most of the studies concerning this subject have been focused on the synthesis and photophysical properties as well as potential applications of neutral iridium compounds.[1–3] However, in view of the recent literature, a growing interest in ionic TM-complexes as promising candidates for application in host/guest solid-state phosphorescent devices is observed. The reason for using such systems is like that in the case of neutral complexes, *i.e.* to reduce the emitter concentration in order to avoid the emission quenching effect.[8]

However, these studies have been mainly related to the use of ionic coordination derivatives of osmium(II),[9] ruthenium(II),[10] and rhenium(I)[11] as phosphorescent emitters in single-layer devices.

Attempts at the application of cationic iridium(III) complexes in electroluminescent devices have been made by Slinker and co-workers, who observed efficient yellow emission from a single-layer polymer matrix based on the $[Ir(ppy)_2(dtbbpy)]PF_6$ complex as a phosphorescent dopant (where ppy = 2-phenylpyridine; dtbbpy = 4,4′-di-*tert*-butyl-2,2′-dipyridyl).[12] However, in view of the reports published in the past few years, such iridium coordination compounds have been intensively studied in the aspect of the possibility of using them in biological systems as fluorescent markers[13] and light-emitting electrochemical cells (LECs).[14] Very recently, several reports have appeared on the preparation and examination of organic emission layers in the prototypes of OLEDs[15] and LECs[14] created on the basis of iridium cationic phosphorescent emitters (organometallic soft salts), in which different types of 2N-donating aromatic compounds as ancillary ligands were used for the stabilization of the metallic centre bearing cyclometalated phenylpyridine and its derivatives.

As mentioned above, most of the reports published so far have focused on the synthesis of neutral and ionic iridium(III) systems, in particular those stabilized with various types of cyclometalated ligands built on the basis of phenylpyridine or phenylpyridine like cores, and their optoelectronic properties. This fact has prompted us to develop a new and efficient method for the synthesis of ionic iridium(III) cyclometalated complexes and extend the studies to the synthesis and photophysical properties of systems formed on the basis of bis(benzo[*h*]quinolino)iridium(III) cores.

Experimental section

All syntheses and manipulations were carried out under argon using standard Schlenk-line and vacuum techniques. The microwave-assisted reactions were performed using a CEM Discover microwave pressure system (max. power 300 W, magnetron frequency 2455 MHz, max. pressure 20 bars). The chemicals were obtained from the following sources: $IrCl_3{\cdot}3H_2O$ from Pressure Chemicals, acetone, Et_2O, MeOH, DMSO-D_6, $CDCl_3$, 1,2-dichloroethane, THF, 2,2′-bipyridine, 4,4′-dimethyl-2,2′-bipyridine, 6,6′-dimethyl-2,2′-bipyridine, 4,4′-dimethoxy-2,2′-bipyridine, 2,2′-biquinoline, 1,10-phenanthroline, 4,7-diphenyl-1,10-phenanthroline, 2,9-dimethyl-4,7-diphenyl-1,10-phenanthroline from Aldrich, and benzo[*h*]quinoline (bzqH) from ABCR. The complex $[\{Ir(\mu\text{-}Cl)(bzq)_2\}_2]$ (**1**)[16,17] and benzo[*i*]dipyrido[3,2-*a*:2′,3′-*c*]phenazine[18] were synthesized according to a published method. All solvents and liquid reagents were dried and distilled under argon prior to use. The NMR spectra in liquid phase were recorded in $CDCl_3$ or DMSO-D_6 using a 300 MHz spectrometer and were referenced to the residual protonated solvent peaks (^1H δ_H = 7.26 ppm, for $CDCl_3$ and ^1H δ_H = 2.50 ppm for DMSO-D_6). TGA measurements were carried out on a Q50-TGA (TA Instruments, Inc.) thermogravimetric analyser under N_2 at a flow rate of 60 mL min^{-1}. Samples (8–10 mg) were loaded on a platinum pan and heated from ambient temperature to 1000 °C at a rate of 10 °C min^{-1}. DSC measurements were carried out on a DSC-1 (Mettler-Toledo) differential scanning calorimeter under N_2 at a flow rate of 20 mL min^{-1} at a heating/cooling rate of 10 °C min^{-1} in the range of 25 to 150 or 250 °C (depending on the sample). Samples (7–10 mg) were placed in 40 μL aluminum pans with a pierced lid.

X-ray crystallography

Diffraction data were collected at 100(1) K by the ω-scan technique on an Agilent Technologies Xcalibur four-circle diffractometer with an Eos CCD detector and graphite-monochromated MoK_α radiation (λ = 0.71069 Å). The data were corrected for Lorentz-polarization as well as for absorption effects.[19] Precise unit-cell parameters were determined by the least-squares fit of reflections of the highest intensity (4547 for **1**, 5535 for **2**), chosen from the whole experiment (see the ESI†). The structures were solved using SIR92[20] and refined by the full-matrix least-squares procedure on F^2 using SHELXL-2013.[21] All non-hydrogen atoms were refined anisotropically, hydrogen atoms were placed at idealized positions and

refined as a 'riding model' with isotropic displacement parameters set at 1.2 times the U_{eq} of appropriate carrier atoms. In the structure of **1** there are solvent – methanol – molecules, disordered across the twofold axis of symmetry. The crystals of **2** appeared to be twinned, which was taken into account during both data reduction and refinement procedures. The BASF factor, showing relative shares of both components, was refined at 0.4681(7). Some restraints had to be applied on ADPs of certain atoms in **2**.

Crystallographic data (excluding structure factors) for the structural analysis have been deposited with the Cambridge Crystallographic Data Centre, no. CCDC 1518625 (**1**) and 1518624 (**2**).

Electrochemical property determination

Cyclic voltammetry (CV) measurements were performed on a CH Instruments model 620 electrochemical analyser in acetonitrile (MeCN) (Carlo Erba, Acetonitrile RS – For HPLC PLUS Gradient – ACS – Reag. Ph. Eur. – Reag. USP) using 0.1 M tetrabutylammonium hexafluorophosphate ($[Bu_4N]PF_6$) (TCI, >98%) as a supporting electrolyte. Measurements were performed in a classic three electrode assembly. A Pt wire was the working electrode, a Pt spiral was the counter electrode, and an Ag wire was the pseudo-reference electrode. Potentials were estimated using ferrocene as an internal standard.

Computational methods

Full geometry optimizations of the iridium compounds in their singlet ground state were carried out using density functional theory (DFT) with Becke's three-parameter hybrid method combined with the Lee–Yang–Parr correlation functional (B3LYP).[22,23] The SDD[24] basis set was used to treat the Ir atom, whereas the 6-31G(d)[25] basis set was used to treat C, H, N and O atoms. In order to assess the influence of basis sets on the results, further calculations were performed with different basis sets and with ONIOM calculations. To date many theoretical studies have been carried out using the two-layer ONIOM scheme for various systems.[26,27] This computational technique models large molecules by defining two layers within the structure that are treated at different levels of accuracy. In our studies of the high-level system containing an Ir(III) central metal atom together with its neighbouring atoms, the WB97XD functional was used. The SDD basis set was used for the iridium atom and the 6-311++G(d,p) basis set – for the remaining atoms. For the low layer, we used the simplest HF/LanL2MB.[28] In order to determine the solvent effects, calculations were also performed within the self-consistent reaction field (SCRF) theory using the polarized continuum model (PCM)[29–31] in acetonitrile (CH_3CN) medium to analyse the interaction with the solvent used in experimental measurements. All calculations were performed using the Gaussian 09 software package[32] in PL-Grid infrastructure.

Spectroscopic measurements

UV–Vis spectra were recorded on a Carry 5000 (Varian) spectrometer, whereas the photoluminescence spectra were recorded on an FLS980 (Edinburgh Instruments) fluorescence spectrometer equipped with a Xe-lamp as an excitation source and an R-928 photomultiplier detector, featuring a spectral sensitivity range of 200–870 nm for the detector, respectively. The absolute fluorescence quantum yields (QY) of the compounds studied were determined using an integrating sphere, with BENFLEC inside coating, from Edinburgh Instruments. All compounds were dissolved in chlorobenzene. In order to eliminate luminophore self-quenching effects, dilute solutions of the investigated molecules were measured. The same equipment was used for the determination of the spectroscopic properties of thin films of poly(*N*-vinylcarbazole)/2-(4-*tert*-butylphenyl)-5-(4-biphenyl)-1,3,4-oxadiazole (PVK/PBD) blends (70 : 30 weight ratio) doped with iridium complexes. The thin films (about 100 nm) were deposited on quartz plates by spin coating. The thickness of the thin films was determined by means of a profilometer (Dektak XT, Bruker).

Preparation and characterization of PLEDs

The PLEDs were manufactured on glass substrates with indium tin oxide (ITO) coated with a ~30 nm layer of poly(3,4-ethylenedioxythiophene) and poly(styrenesulfonate) (PEDOT:PSS) mixture. The emissive layers (~80 nm) were fabricated by means of the spin coating method from a chlorobenzene solution of PVK/PBD blends, doped with 1 wt% of emitter molecules. To remove the residual amounts of the solvent, the deposited emissive layers were annealed at 90° C for 30 min under a nitrogen atmosphere. In the next step the cathode was vacuum evaporated through a shadow mask. The complete device stack was ITO/PEDOT:PSS/PVK:PBD+emitter/Ca/Ag. These devices were encapsulated with epoxy resin and glass inside a glove box under a nitrogen atmosphere. After encapsulation, they were characterized under ambient conditions. The electroluminescence spectra were recorded using a MicroHR spectrometer and a CCD camera 3500 (Horiba Jobin Yvon). Current density–voltage–luminance characteristics were determined by using a Keithley 2400 source measurement unit and a Minolta CS-200 camera.

Optimization of the reaction conditions

In a Schlenk reactor of 15 mL capacity, equipped with a Rotaflo® valve, portions of 100.00 mg (0.086 mmol) of $[\{Ir(bzq)_2(\mu\text{-}Cl)\}_2]$ (**1**) and 0.188 mmol of the selected N^N donating ligand (**C**, **E**, **H**) and 31.35 mg (0.188 mmol) of $Na[PF_6]$ were placed under an inert atmosphere, and then an anhydrous and deoxygenated solvent ($ClCH_2CH_2Cl$ or THF) was introduced. The reaction was conducted for 12 h at 65 °C or for 10 minutes at 150 °C. After this time, the solvent was fully evaporated from the post-reaction mixture under reduced pressure. The remaining crude product was analyzed by ^1H NMR.

Synthesis of iridium complexes

$[Ir(bzq)_2(2,2'\text{-bipyridine})]^+PF_6^-$ (2AA'). In a pressure glass vessel of 10 mL capacity, portions of 200.00 mg (0.171 mmol) of $[\{Ir(bzq)_2(\mu\text{-}Cl)\}_2]$ (**1**), 54.98 mg (0.350 mmol) of 2,2′-bipyri-

dine (**A**) and 58.33 mg (0.350 mmol) of Na[PF_6] were placed under an inert atmosphere and then 5 mL of anhydrous and deoxygenated THF was introduced. The reactor was sealed using a plastic cap equipped with an elastic membrane and then placed in the chamber of a microwave radiation source. The thus prepared reaction system was sealed with the encapsulating head, equipped with a pressure sensor. The reaction was conducted for 10 minutes at 150 °C, irradiating the mixture with microwaves (150 W and frequency 2445 MHz). After this time, the solvent was fully evaporated from the post-reaction mixture under reduced pressure. The remaining crude product was washed with water (3 × 5 mL), cold MeOH (2 × 2 mL), and finally with cold Et_2O (2 × 2 mL). In the next step, the remaining solid material was purified by flash-chromatography using a column with silica and acetone as the eluent. The purified material was dried under vacuum for 4 hours. The desired product **2AA′** was obtained in a yield of 86% (250 mg, 0.294 mmol). Elemental anal. calculated for $C_{36}H_{24}F_6IrN_4P$: C 50.88; H 2.85; found C 50.94 H 2.93; ^{1}H NMR (300 MHz, DMSO-D_6, 300 K) δ (ppm) = 8.92 (d, $^3J_{H-H}$ = 8.34 Hz, 2H); 8.58 (d, $^3J_{H-H}$ = 7.89 Hz, 2H); 8.25 (m, $^3J_{H-H}$ = 9.00 Hz, 2H); 8.08 (d, $^3J_{H-H}$ = 6.00 Hz, 2H); 7.92 (m, 7H); 7.57 (m, 7H); 6.21 (d, $^3J_{H-H}$ = 6.00 Hz, 2H).

[Ir(bzq)$_2$(4,4′-dimethyl-2,2′-bipyridine)]$^+$PF$_6^-$ (2BA′). Following the procedure used for the preparation of compound **2AA′** (Table 2), the reaction was carried out with 200.00 mg (0.171 mmol) of **1**, 64.23 mg (0.350 mmol) of 4,4′-dimethyl-2,2′-bipyridine (**B**) and 58.78 mg (0.350 mmol) of Na[PF_6] (**A′**). The desired product **2BA′** was obtained in a yield of 80% (240 mg, 0.273 mmol). Elemental anal. calculated for $C_{38}H_{28}F_6IrN_4P$: C 51.99; H 3.22; found C 52.06 H 3.28; ^{1}H NMR (300 MHz, DMSO-D_6, 300 K) δ (ppm) = 8.77 (s, 2H); 8.56 (d, $^3J_{H-H}$ = 9.00 Hz, 2H); 8.07 (d, $^3J_{H-H}$ = 6.00 Hz, 2H); 7.97 (d, $^3J_{H-H}$ = 9.00 Hz, 2H); 7.92 (m, 4H); 7.87 (m, $^3J_{H-H}$ = 9.00 Hz, 2H); 7.62 (m, 4H); 7.53 (m, $^3J_{H-H}$ = 9.00 Hz, 2H); 7.41 (d, $^3J_{H-H}$ = 6.00 Hz, 2H); 7.16 (t, $^3J_{H-H}$ = 9.00 Hz, 2H); 6.21 (d, $^3J_{H-H}$ = 6.00 Hz, 2H); 2.50 (s, 6H, −Me together with residues protons from DMSO-D_6); ^{1}H NMR (300 MHz, $CDCl_3$, 300 K) δ (ppm) = 2.60 (s, 6H, −Me).

[Ir(bzq)$_2$(6,6′-dimethyl-2,2′-bipyridine)]$^+$PF$_6^-$ (2CA′). Following the procedure used for the preparation of compound **2AA′** (Table 2), the reaction was carried out with 200.00 mg (0.171 mmol) of **1**, 64.23 mg (0.350 mmol) of **C** and 58.78 mg (0.350 mmol) of salt **A′**. The desired product **2CA′** was obtained in a yield of 64% (192 mg, 0.226 mmol). Elemental anal. calculated for $C_{38}H_{28}F_6IrN_4P$: C 51.99; H 3.22; found C 52.09 H 3.30; ^{1}H NMR (300 MHz, DMSO-D_6, 300 K) δ (ppm) = 8.62 (t, $^3J_{H-H}$ = 9.00 Hz, 4H); 8.30 (d, $^3J_{H-H}$ = 6.00 Hz, 2H); 8.09 (t, $^3J_{H-H}$ = 9.00 Hz, 2H); 7.89 (m, 4H); 7.65 (m, 2H); 7.38 (t, $^3J_{H-H}$ = 9.00 Hz, 4H); 6.93 (t, $^3J_{H-H}$ = 6.00 Hz, 2H); 5.81 (d, $^3J_{H-H}$ = 6.00 Hz, 2H); 1.56 (s, 6H, −Me).

[Ir(bzq)$_2$(4,4′-dimethoxy-2,2′-bipyridine)]$^+$PF$_6^-$ (2DA′). Following the procedure used for the preparation of compound **2AA′** (Table 2), the reaction was carried out with 160.00 mg (0.137 mmol) of **1**, 61.00 mg (0.281 mmol) of **D** and 47.19 mg (0.281 mmol) of salt **A′**. The desired product **2DA′** was obtained in a yield of 80% (200 mg, 0.220 mmol). Elemental anal. calculated for $C_{38}H_{28}F_6IrN_4O_2P$: C 50.16; H 3.10; found C 50.23 H 3.19; ^{1}H NMR (300 MHz, DMSO-D_6, 300 K) δ (ppm) = 8.57 (d, $^3J_{H-H}$ = 9.00 Hz, $^3J_{H-H}$ = 6.00 Hz, 2H); 8.48 (s, 2H); 8.13 (d, 2H); 7.96 (d, $^3J_{H-H}$ = 6.00 Hz, H); 7.88 (d, $^3J_{H-H}$ = 9.00 Hz, 2H); 7.57 (m, 6H); 7.17 (m, 4H); 6.21 (d, $^3J_{H-H}$ = 6.00 Hz, 2H); 3.96 (s, 6H, −OMe).

[Ir(bzq)$_2$(2,2′-biquinoline)]$^+$PF$_6^-$ (2EA′). Following the procedure used for the preparation of compound **2AA′** (Table 2), the reaction was carried out with 200.00 mg (0.171 mmol) of **1**, 89.36 mg (0.350 mmol) of **E** and 58.78 mg (0.350 mmol) of salt **A′**. The desired product **2EA′** was obtained in a yield of 78% (254 mg, 0.270 mmol). Elemental anal. calculated for $C_{44}H_{28}F_6IrN_4P$: C 55.63; H 2.97; found C 55.73 H 3.06; ^{1}H NMR (300 MHz, DMSO-D_6, 300 K) δ (ppm) = 9.10 (d, $^3J_{H-H}$ = 9.00 Hz, 2H), 8.93 (d, $^3J_{H-H}$ = 9.00 Hz, 2H); 8.55 (d, $^3J_{H-H}$ = 9.00 Hz, 2H); 8.24 (d, $^3J_{H-H}$ = 6.00 Hz, 2H); 8.05 (d, $^3J_{H-H}$ = 9.00 Hz, 2H); 7.87 (m, 6H); 7.51 (m, 6H); 7.07 (t, $^3J_{H-H}$ = 9.00 Hz, 2H); 6.92 (t, $^3J_{H-H}$ = 9.00 Hz, 2H); 5.96 (d, $^3J_{H-H}$ = 6.00 Hz, 2H).

[Ir(bzq)$_2$(2,2′-bipyridine)]$^+$BPh$_4^-$ (2AB′). Following the procedure used for the preparation of compound **2AA′** (Table 2), the reaction was carried out with 200.00 mg (0.171 mmol) of **1**, 54.92 mg (0.350 mmol) of **A** and 119.78 mg (0.350 mmol) of the salt Na[BPh_4] (**B′**). The desired product **2AB′** was obtained in a yield of 63% (220 mg, 0.214 mmol). Elemental anal. calculated for $C_{60}H_{44}BIrN_4$: C 70.37; H 4.33; found C 70.50 H 4.45; ^{1}H NMR (300 MHz, DMSO-D_6, 300 K) δ (ppm) = 8.91 (d, $^3J_{H-H}$ = 8.34 Hz, 2H); 8.57 (d, $^3J_{H-H}$ = 7.89 Hz, 2H); 8.25 (t, $^3J_{H-H}$ = 9.00 Hz, 2H); 8.07 (d, $^3J_{H-H}$ = 6.00 Hz, 2H); 7.94 (m, 7H); 7.58 (m, 7H); 7.17 (m, 8H, BPh_4^-); 6.91 (t, $^3J_{H-H}$ = 9.00, Hz, 8H, BPh_4^-); 6.78 (t, $^3J_{H-H}$ = 6.00 Hz, 4H, BPh_4^-); 6.21 (d, $^3J_{H-H}$ = 6.00 Hz, 2H).

[Ir(bzq)$_2$(4,4′-dimethyl-2,2′-bipyridine)]$^+$BPh$_4^-$ (2BB′). Following the procedure used for the preparation of compound **2AA′** (Table 2), the reaction was carried out with 200.00 mg (0.171 mmol) of **1**, 64.23 mg (0.350 mmol) of **B** and 119.78 mg (0.350 mmol) of salt **B′**. The desired product **2BB′** was obtained in a yield of 71% (256 mg, 0.243 mmol). Elemental anal. calculated for $C_{62}H_{48}BIrN_4$: C 70.78; H 4.60; found C 70.91 H 4.71; ^{1}H NMR (300 MHz, DMSO-D_6, 300 K) δ (ppm) = 8.76 (s, 2H); 8.55 (d, $^3J_{H-H}$ = 9.00 Hz, 2H); 8.06 (d, $^3J_{H-H}$ = 6.00 Hz, 2H); 7.96 (d, $^3J_{H-H}$ = 9.00 Hz, 2H); 7.87 (d, $^3J_{H-H}$ = 9.00 Hz, 2H); 7.65 (d, $^3J_{H-H}$ = 6.00 Hz, 2H); 7.59 (m, 3H), 7.54 (d, $^3J_{H-H}$ = 6.00 Hz, 2H); 7.39 (m, 3H); 7.17 (m, 8H, BPh_4^-); 6.91 (t, $^3J_{H-H}$ = 9.00 Hz, 8H); 6.77 (t, $^3J_{H-H}$ = 6.00 Hz, 4H, BPh_4^-); 6.21 (d, $^3J_{H-H}$ = 6.00 Hz, 2H); 2.50 (s, 6H, −Me together with residue protons from DMSO-D_6); ^{1}H NMR (300 MHz, $CDCl_3$, 300 K) δ (ppm) = 2.60 (s, 6H, −Me).

[Ir(bzq)$_2$(6,6′-dimethyl-2,2′-bipyridine)]$^+$BPh$_4^-$ (2CB′). Following the procedure used for the preparation of compound **2AA′** (Table 2), the reaction was carried out with 200.00 mg (0.171 mmol) of **1**, 64.23 mg (0.350 mmol) of **C** and 119.78 mg (0.350 mmol) of salt **B′**. The desired product **2CB′** was obtained in a yield of 69% (248 mg, 0.236 mmol). Elemental anal. calculated for $C_{62}H_{48}BIrN_4$: C 70.78; H 4.60; found C 70.88 H 4.67;

^{1}H NMR (300 MHz, DMSO-D$_6$, 300 K) δ (ppm) = 8.61 (t, $^3J_{H-H}$ = 9.00 Hz 4H); 8.29 (d, $^3J_{H-H}$ = 6.00 Hz, 2H); 8.08 (t, $^3J_{H-H}$ = 9.00 Hz, 2H); 7.89 (m, 4H); 7.64 (m, 2H); 7.38 (m, 4H); 7.18 (m, 8H, BPh_4^-); 6.91 (t, $^3J_{H-H}$ = 9.00 Hz, 10H, 8H BPh_4^- + 2H bzq); 6.78 (m, $^3J_{H-H}$ = 6.00 Hz, 4H, BPh_4^-); 5.81 (d, $^3J_{H-H}$ = 6.00 Hz, 2H); 1.58 (s, 6H, −Me).

[Ir(bzq)$_2$(4,4′-dimethoxy-2,2′-bipyridine)]$^+$BPh$_4^-$ (2DB′). Following the procedure used for the preparation of compound **2AA′** (Table 2), the reaction was carried out with 160.00 mg (0.137 mmol) of **1**, 61.00 mg (0.281 mmol) of **D** and 97.16 mg (0.281 mmol) of salt **B′**. The desired product **2DB′** was obtained in a yield of 80% (240 mg, 0.221 mmol). Elemental anal. calculated for $C_{62}H_{48}BIrN_4O_2$: C 68.69; H 4.46; found C 68.85 H 4.53; ^{1}H NMR (300 MHz, DMSO-D$_6$, 300 K) δ (ppm) = 8.56 (d, $^3J_{H-H}$ = 6.00 Hz, 2H); 8.48 (s, 2H); 8.13 (d, $^3J_{H-H}$ = 6.00 Hz, 2H); 7.96 (m, $^3J_{H-H}$ = 9.00 Hz, 2H); 7.87 (d, $^3J_{H-H}$ = 9.00 Hz, 2H); 7.59 (m, 6H); 7.52 (d, $^3J_{H-H}$ = 9.00 Hz, 2H); 7.17 (m, 12H, 8H BPh_4^- + 4H); 7.91 (t, $^3J_{H-H}$ = 9.00 Hz, 8H, BPh_4^-); 6.78 (t, $^3J_{H-H}$ = 6.00 Hz, 4H, BPh_4^-); 6.22 (d, $^3J_{H-H}$ = 6.00 Hz, 2H); 3.96 (s, 6H, −OMe).

[Ir(bzq)$_2$(2,2′-biquinoline)]$^+$BPh$_4^-$ (2EB′). Following the procedure used for the preparation of compound **2AA′** (Table 2), the reaction was carried out with 200.00 mg (0.171 mmol) of **1**, 89.36 mg (0.350 mmol) of **E** and 119.78 mg (0.350 mmol) of salt **B′**. The desired product **2EB′** was obtained in a yield of 76% (290 mg, 0.257 mmol). Elemental anal. calculated for $C_{68}H_{48}BIrN_4$: C 72.65; H 4.30; found C 72.85 H 4.40; ^{1}H NMR (300 MHz, DMSO-D$_6$, 300 K) δ (ppm) = 9.09 (d, $^3J_{H-H}$ = 9.00 Hz, 2H), 8.92 (d, $^3J_{H-H}$ = 9.00 Hz, 2H); 8.54 (d, $^3J_{H-H}$ = 6.00 Hz, 2H); 8.23 (d, $^3J_{H-H}$ = 6.00 Hz, 2H); 8.05 (d, $^3J_{H-H}$ = 9.00 Hz, 2H); 7.85 (m, 6H); 7.49 (m, 6H); 7.16 (m, 8H), 7.07 (t, $^3J_{H-H}$ = 9.00 Hz, 2H); 6.92 (m, 10 H, 8H BPh_4^- + 2H); 6.78 (t, $^3J_{H-H}$ = 6.00 Hz, 4H BPh_4^-); 6.94 (d, $^3J_{H-H}$ = 6.00 Hz, 2H).

[Ir(bzq)$_2$(1,10-phenanthroline)]$^+$PF$_6^-$ (2FA′). Following the procedure used for the preparation of compound **2AA′** (Table 2), the reaction was carried out with 200.00 mg (0.171 mmol) of **1**, 63.07 mg (0.350 mmol) of **F** and 58.78 mg (0.350 mmol) of salt **A′**. The desired product **2FA′** was obtained in a yield of 76% (290 mg, 0.332 mmol). Elemental anal. calculated for $C_{38}H_{24}F_6IrN_4P$ C 52.23; H 2.77; found C 52.33; H 2.80; ^{1}H NMR (300 MHz, DMSO-D$_6$, 300 K) δ (ppm) = 8.90 (d, $^3J_{H-H}$ = 9.00 Hz, 2H); 8.51 (d, $^3J_{H-H}$ = 9.00 Hz, 2H); 8.42 (s, 2H); 8.20 (d, $^3J_{H-H}$ = 6.00 Hz, 2H); 7.93 (m, 6H); 7.59 (d, $^3J_{H-H}$ = 9.00 Hz, 2H); 7.45 (d, $^3J_{H-H}$ = 6.00 Hz, 1H); 7.41 (d, $^3J_{H-H}$ = 6.00 Hz, 1H); 7.23 (t, $^3J_{H-H}$ = 6.00 Hz, 2H); 6.35 (d, $^3J_{H-H}$ = 6.00 Hz, 2H).

[Ir(bzq)$_2$(4,7-diphenyl-1,10-phenanthroline)]$^+$PF$_6^-$ (2GA′). Following the procedure used for the preparation of compound **2AA′** (Table 2), the reaction was carried out with 200.00 mg (0.171 mmol) of **1**, 116.34 mg (0.350 mmol) of **G** and 58.78 mg (0.350 mmol) of salt **A′**. The desired product **2GA′** was obtained in a yield of 71% (250 mg, 0.244 mmol). Elemental anal. calculated for $C_{50}H_{32}F_6IrN_4P$ C 58.53; H 3.14; found C 58.68; H 3.23; ^{1}H NMR (300 MHz, DMSO-D$_6$, 300 K) δ (ppm) = 8.56 (d, $^3J_{H-H}$ = 9.00 Hz, 2H); 8.27 (d, $^3J_{H-H}$ = 6.00 Hz, 2H); 8.22 (s, 2H); 8.11 (d, $^3J_{H-H}$ = 6.00 Hz, 2H); 8.02 (d, $^3J_{H-H}$ = 9.00 Hz, 2H) 7.93 (m, 4H); 7.62 (m, 12H, 10H –Ph + 2H); 7.53 (m, 2H); 7.24 (t, $^3J_{H-H}$ = 9.00 Hz, 2H); 6.34 (d, $^3J_{H-H}$ = 9.00 Hz, 2H).

[Ir(bzq)$_2$(2,9-dimethyl-4,7-diphenyl-1,10-phenanthroline)]$^+$PF$_6^-$ (2HA′). Following the procedure used for the preparation of compound **2AA′** (Table 2), the reaction was carried out with 200.00 mg (0.171 mmol) of **1**, 126.16 mg (0.350 mmol) of **H** and 58.78 mg (0.350 mmol) of salt **A′**. The desired product **2HA′** was obtained in a yield of 77% (278 mg, 0.264 mmol). Elemental anal. calculated for $C_{52}H_{36}F_6IrN_4P$ C 59.25; H 3.44; found C 59.50; H 3.52; ^{1}H NMR (300 MHz, DMSO-D$_6$, 300 K) δ (ppm) = 8.59 (d, $^3J_{H-H}$ = 9.00 Hz, 2H); 8.20 (d, $^3J_{H-H}$ = 6.00 Hz, 2H); 8.06 (s, 2H); 7.91 (m, 4H), 7.76 (m, 4H); 7.59 (m, 10H, −Ph); 7.42 (d, $^3J_{H-H}$ = 9.00 Hz, 2H); 6.96 (t, $^3J_{H-H}$ = 9.00 Hz, 2H); 5.89 (d, $^3J_{H-H}$ = 9.00 Hz, 2H); 1.93 (s, 6H, −Me).

[Ir(bzq)$_2$(1,10-phenanthroline)]$^+$BPh$_4^-$ (2FB′). Following the procedure used for the preparation of compound **2AA′** (Table 2), the reaction was carried out with 200.00 mg (0.171 mmol) of **1**, 63.07 mg (0.350 mmol) of **F** and 119.78 mg (0.350 mmol) of salt **B′**. The desired product **2FB′** was obtained in a yield of 74% (268 mg, 0.256 mmol). Elemental anal. calculated for $C_{62}H_{44}BIrN_4$ C 71.05; H 4.23; found C 71.34; H 4.34; ^{1}H NMR (300 MHz, DMSO-D$_6$, 300 K) δ (ppm) = 8.88 (d, $^3J_{H-H}$ = 9.00 Hz, 2H); 8.52 (d, $^3J_{H-H}$ = 9.00 Hz, 2H); 8.40 (s, 2H); 8.19 (d, $^3J_{H-H}$ = 6.00 Hz, 2H); 7.95 (m, 6H); 7.60 (d, $^3J_{H-H}$ = 9.00 Hz, 2H); 7.46 (d, $^3J_{H-H}$ = 6.00 Hz, 1H); 7.43 (d, $^3J_{H-H}$ = 6.00 Hz, 1H); 7.20 (m, 10H, 8H BPh_4^- + 2H); 6.95 (t, $^3J_{H-H}$ = 9.00 Hz, 8H); 6.79 (t, $^3J_{H-H}$ = 6.00 Hz, 4H); 6.33 (d, $^3J_{H-H}$ = 6.00 Hz, 2H).

[Ir(bzq)$_2$(4,7-diphenyl-1,10-phenanthroline)]$^+$BPh$_4^-$ (2GB′). Following the procedure used for the preparation of compound **2AA′** (Table 2), the reaction was carried out with 200.00 mg (0.171 mmol) of **1**, 116.34 mg (0.350 mmol) of **G** and 119.78 mg (0.350 mmol) of salt **B′**. The desired product **2GB′** was obtained in a yield of 70% (285 mg, 0.237 mmol). Elemental anal. calculated for $C_{74}H_{52}BIrN_4$ C 74.05; H 4.37; found C 74.31; H 4.46; ^{1}H NMR (300 MHz, DMSO-D$_6$, 300 K) δ (ppm) = 8.55 (d, $^3J_{H-H}$ = 9.00 Hz, 2H); 8.27 (d, $^3J_{H-H}$ = 6.00 Hz, 2H); 8.22 (s, 2H); 8.10 (d, $^3J_{H-H}$ = 6.00 Hz, 2H); 8.00 (d, $^3J_{H-H}$ = 9.00 Hz, 2H); 7.91 (m, 4H); 7.62 (m, 12H, 10H –Ph + 2H); 7.50 (m, 2H); 7.24 (t, $^3J_{H-H}$ = 9.00 Hz, 2H); 7.17 (m, 8H, BPh_4^-); 6.90 (t, $^3J_{H-H}$ = 6.00 Hz, 8H, BPh_4^-); 6.77 (t, $^3J_{H-H}$ = 6.00 Hz, 4H, BPh_4^-); 6.35 (d, $^3J_{H-H}$ = 6.00 Hz, 2H).

[Ir(bzq)$_2$(2,9-dimethyl-4,7-diphenyl-1,10-phenanthroline)]$^+$BPh$_4^-$ (2HB′). Following the procedure used for the preparation of compound **2AA′** (Table 2), the reaction was carried out with 200.00 mg (0.171 mmol) of **1**, 126.16 mg (0.350 mmol) of **H** and 119.78 mg (0.350 mmol) of salt **B′**. The desired product **2HB′** was obtained in a yield of 60% (250 mg, 0.203 mmol). Elemental anal. calculated for $C_{76}H_{56}BIrN_4$ C 71.31; H 4.60; found C 71.46; H 4.65; ^{1}H NMR (300 MHz, DMSO-D$_6$, 300 K) δ (ppm) = 8.57 (d, $^3J_{H-H}$ = 9.00 Hz, 2H); 8.19 (d, $^3J_{H-H}$ = 6.00 Hz, 2H); 8.06 (s, 2H); 7.91 (m, 4H), 7.75 (m, 4H); 7.59 (m, 10H); 7.43 (d, $^3J_{H-H}$ = 9.00 Hz, 2H); 7.18 (m, 8H, BPh_4^-): 6.97 (t, $^3J_{H-H}$ = 9.00 Hz, 2H); 6.91 (t, $^3J_{H-H}$ = 6.00 Hz, 8H, BPh_4^-); 6.77 (t, $^3J_{H-H}$ = 9.00 Hz, 4H, BPh_4^-); 5.89 (d, $^3J_{H-H}$ = 9.00 Hz, 2H); 1.93 (s, 6H, −Me).

[Ir(bzq)$_2$(benzo[*i*]dipyrido[3,2-*a*:2′,3′-*c*]phenazine)]$^+$PF$_6^-$ (2IA′). Following the procedure used for the preparation of com-

pound **2AA′** (Table 2), the reaction was carried out with 120.00 mg (0.103 mmol) of **1**, 70.13 mg (0.211 mmol) of **I** and 35.43 mg (0.211 mmol) of salt **A′**. The desired product **2IA′** was obtained in a yield of 74% (156 mg, 152 mmol). Elemental anal. calculated for $C_{48}H_{28}F_6IrN_4P$ C 56.19; H 2.75; found C 56.39; H 2.82; ^{1}H NMR (300 MHz, DMSO-D_6, 300 K) δ (ppm) = 9.62 (d, $^3J_{H-H}$ = 9.00 Hz, 2H); 9.13 (s, 2H); 8.57 (d, $^3J_{H-H}$ = 9.00 Hz, 2H); 8.36 (m, 2H); 8.25 (d, $^3J_{H-H}$ = 6.00 Hz, 2H); 8.19 (d, $^3J_{H-H}$ = 6.00 Hz, 2H), 8.02 (m, 4H); 7.91 (d, $^3J_{H-H}$ = 9.00 Hz, 2H); 7.72 (m, 2H); 7.61 (d, $^3J_{H-H}$ = 6.00 Hz, 2H); 7.55 (d, $^3J_{H-H}$ = 9.00 Hz, 1H); 7.53 (d, $^3J_{H-H}$ = 9.00 Hz, 1H); 7.25 (t, $^3J_{H-H}$ = 9.00 Hz, 2H); 6.33 (d, $^3J_{H-H}$ = 6.00 Hz, 2H).

[Ir(bzq)$_2$(benzo[*i*]dipyrido[3,2-*a*:2′,3′-*c*]phenazine)]$^+$BPh$_4^-$ (2IB′). Following the procedure used for the preparation of compound **2AA′** (Table 2), the reaction was carried out with 120.00 mg (0.103 mmol) of **1**, 70.13 mg (0.211 mmol) of **I** and 72.21 mg (0.211 mmol) of salt **B′**. The desired product **2IB′** was obtained in a yield of 80% (198 mg, 0.162 mmol). Elemental anal. calculated for $C_{72}H_{48}BIrN_6$: C 72.05; H 4.03; found C 72.37 H 4.15; ^{1}H NMR (300 MHz, DMSO-D_6, 300 K) δ (ppm) = 9.57 (d, $^3J_{H-H}$ = 9.00 Hz, 2H); 9.08 (s, 2H); 8.55 (d, $^3J_{H-H}$ = 9.00 Hz, 2H); 8.31 (m, 2H); 8.24 (d, $^3J_{H-H}$ = 6.00 Hz, 2H); 8.18 (d, $^3J_{H-H}$ = 6.00 Hz, 2H), 8.02 (m, 4H); 7.90 (m, 2H); 7.67 (m, 2H); 7.61 (d, $^3J_{H-H}$ = 6.00 Hz, 2H); 7.52 (m, 2H); 7.22 (m, 10H, 8H BPh$_4^-$ + 2H); 6.91 (t, $^3J_{H-H}$ = 9.00 Hz, 8H, BPh$_4^-$); 6.78 (t, $^3J_{H-H}$ = 9.00 Hz, 4H, BPh$_4^-$); 6.34 (d, $^3J_{H-H}$ = 6.00 Hz, 2H).

[Ir(bzq)$_2${benzo[*i*]dipyrido[3,2-*a*:2′,3′-*c*]phenazine}]$^+$[B(C$_6$F$_5$)$_4$]$^-$ (2IC′). Following the procedure used for the preparation of compound **2AA′** (Table 2), the reaction was carried out with 120.00 mg (0.103 mmol) of **1**, 70.13 mg (0.211 mmol) of **I** and 168.38 mg (0.211 mmol) of salt **B′**. The desired product **2IB′** was obtained in a yield of 68% (217 mg, 0.139 mmol). Elemental anal. calculated for $C_{72}H_{28}BF_{20}IrN_6$: C 55.43; H 1.81; found C 55.56; H 1.93; ^{1}H NMR (300 MHz, DMSO-D_6, 300 K) δ (ppm) = 9.56 (d, $^3J_{H-H}$ = 9.00 Hz, 2H); 9.05 (s, 2H); 8.55 (d, $^3J_{H-H}$ = 9.00 Hz, 2H); 8.28 (m, 4H); 8.20 (d, $^3J_{H-H}$ = 6.00 Hz, 2H); 8.00 (m, 4H); 7.90 (m, 4H); 7.59 (d, $^3J_{H-H}$ = 9.00 Hz, 2H); 7.54 (d, $^3J_{H-H}$ = 9.00 Hz, 1H); 7.52 (d, $^3J_{H-H}$ = 9.00 Hz, 1H); 7.24 (t, $^3J_{H-H}$ = 6.00 Hz, 2H); 6.34 (d, $^3J_{H-H}$ = 9.00 Hz, 2H).

Results and discussion

In view of the available literature, most of the *C*,*N*-cyclometalated ionic iridium(III) complexes of the type [Ir(C^N)$_2$(N^N)]PF$_6$ (where C^N = *C*,*N*-cyclometalated ligand; N^N = N,N-donating ligand)[13a,b,15,33] have been prepared according to the methodology reported by Oshawa, which consisted in carrying out a sequence of consecutive reactions, *i.e.* transformation of the initial precursor [{Ir(C^N)$_2$(μ-Cl)}$_2$] into the corresponding mononuclear intermediate [Ir(C^N)$_2$(N^N)]Cl *via* a reaction of the former with an appropriate N^N-donating ligand and then conversion of the latter in a reaction with AgPF$_6$ salt into the desired complex such as [Ir(C^N)$_2$(N^N)]PF$_6$.[34] By this method many different iridium(III) cationic complexes were synthesized, particularly with the employment of 2,2′-pyridine and 1,10-phenanthroline, including some of their derivatives, as N^N-donating ligands.[12–15,33] From our point of view, the protocol developed by Oshawa and its further variants[33,34] have a fundamental flaw; firstly, it is very time consuming because it requires to carry out two steps with the separation of intermediate compounds, in most cases; secondly, it is not efficient enough, particularly when sterically crowded N^N-ligands are applied in the reaction because of the thermal initiation of [Ir(C^N)$_2$(N^N)]Cl derivative formation.

Therefore, in order to improve the methodology for the synthesis of cyclometalated ionic iridium(III) complexes, we developed a one-pot strategy for [Ir(C^N)$_2$(N^N)]$^+$A$^-$ compound formation, involving acceleration of the reaction *via* microwave irradiation that would allow the efficient synthesis of new cationic iridium(III) coordination derivatives. For many years, microwave-assisted processes have been commonly used in organic synthesis and have proved to be very attractive, because they have brought about spectacular acceleration of many types of reactions as a result of a high heating rate, which cannot be achieved by using the classical heating methods, with a combination of the selective absorption of electromagnetic radiation by the polar substances.[35] Therefore, higher yields can be achieved under milder reaction conditions and in shorter reaction times; thus many processes can be improved and even reactions that do not occur on conventional heating can be performed using microwaves.[36] The use of microwave radiation is not limited to organic reactions. It has been successfully applied for the acceleration of processes leading to a wide gamut of inorganic compounds and nanomaterials[37] or coordination compounds.[38] The above results encouraged us to apply microwaves as an energy carrier which is able to promote the transformation of the initial reaction components into desired iridium(III) complexes of the structure [Ir(bzq)$_2$(N^N)]$^+$A$^-$, *i.e.* stabilized with both *C*,*N*-cyclometalated ligands and N,N-donating heterocyclic derivatives.

However, at the beginning, our studies focused on the development of an efficient three-component one-pot route for the preparation of cationic iridium(III) complexes according to a literature method under the reaction conditions given therein[34] with various N,N-donating heterocyclic aromatic compounds used as ligands, *e.g.* 2,2′-bipyridine (**A**), 4,4′-dimethyl-2,2′-bipyridine (**B**), 6,6′-dimethyl-2,2′-bipyridine (**C**), 4,4′-dimethoxy-2,2′-bipyridine (**D**), 2,2′-biquinoline (**E**), 1,10-phenanthroline (**F**), 4,7-diphenyl-1,10-phenanthroline (**G**), 2,9-dimethyl-4,7-diphenyl-1,10-phenanthroline (**H**) and benzo[*i*]dipyrido[3,2-*a*:2′,3′-*c*]phenazine (**I**). Therefore, initially the one-pot reactions were carried out in the pathway, presented in Scheme 1, that contrary to the reported methods,[12–15,33,34] all the initial solid materials and a polar solvent were placed in a reactor, which was then heated using a classical source of heat, *i.e.* an oil bath.

As shown in the above scheme, the testing reactions of the initial iridium(III) precursor (**1**) were conducted with the selected N,N-donating ligands **C**, **E**, **H**, which are characterized by a relatively high steric hindrance. In the studied system, the above-mentioned *N*,*N*-based aromatic derivatives as well as the

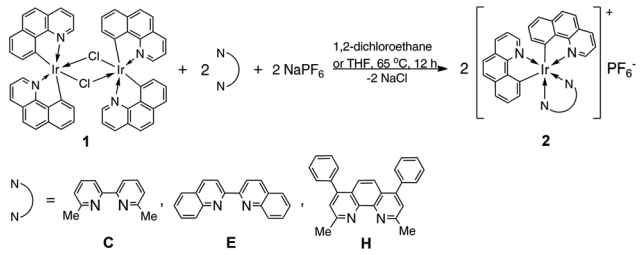

Scheme 1 One-pot protocol using a classical source of heat.

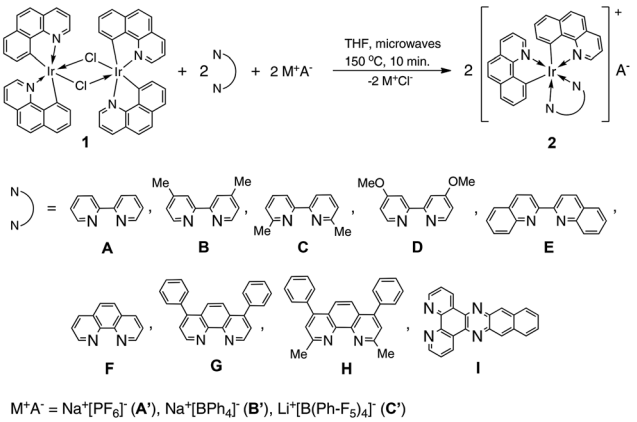

Scheme 2 The microwave-assisted reaction of precursor **1** with various N^N ligands.

salt $NaPF_6$ (**A′**) were used in a moderate excess in relation to complex **1**, *i.e.* with 20% molar excess. All the processes were carried out for 12 hours at 65 °C in two different polar solvents, namely the non-coordinating 1,2-dichloroethane and coordinating THF. Unfortunately, for all the employed *N*,*N*-bidentate ligands, the yields of the isolated materials of type 2 did not exceed 36% as shown in Table 1. Moreover, the ^{1}H NMR spectra recorded for these substances have indicated the presence of other iridium species as impurities.

Thus, in view of the above results, we decided to apply, to the system studied, microwave radiation as a heat carrier as well as a source of energy increasing the frequency of collisions between polar and non-polar reagents. Therefore, to improve the efficiency of the one-pot protocol for the preparation of cationic complexes of the type $[Ir(bzq)_2(N^N)]^+A^-$ (**2**), in the subsequent phase of the study, the reactions of the initial precursor $[\{Ir(bzq)_2(\mu\text{-}Cl)\}_2]$ (**1**) with various N,N-donating compounds, namely 2,2′-bipyridine (**A**) or 1,10-phenanthroline (**F**) and their derivatives (**A–E** and **GI**) as well as selected salts M^+A^- (**A′–C′**), were carried out with the support of microwaves and in a THF environment (see Scheme 2).

This solvent was chosen because of a better solubility of the initial materials and products in it and its relatively high absorbance of microwave electromagnetic radiation. Additionally, we expected that in the studied system, THF, being in large excess in relation to complex **1**, can act as a ligand, supporting dissociation of the initial precursor followed by the formation of labile iridium species $[Ir(bzq)_2(THF)_2]PF_6$, similarly as takes place in the reactions of binuclear iridium complexes $[\{Ir(C^N)_2(\mu\text{-}Cl)\}_2]$ with $AgBF_4$ in an acetonitrile environment, in which $[Ir(C^N)_2(NCMe)_2]BF_4$ complexes were synthesized.[39]

A microwave pressure reactor used for testing the one-pot protocol enabled carrying out the reactions in THF as a solvent at a temperature higher than its boiling point, *i.e.* at 150 °C. The parameters of the process such as the molar ratio of the starting components, the temperature as well as the process time were optimized for the model reagent system based on the initial precursor **1** in combination with 6,6′-dimethyl-2,2′-bipyridine (**C**) and the salt $Na[PF_6]$ (**A′**). In a series of attempts made using the above-mentioned sterically hindered 6,6′-substituted bipyridine (**C**) under various conditions, it was found that the process ran smoothly at 150 °C and the time required for the complete conversion of the initial components did not exceed 10 minutes, giving expected product in good yield.

Moreover, in comparison with the previously used classical heating method, irradiation of the reaction mixture with microwaves allowed the reduction in the amounts of bidentate ligand (N^N) and M^+A^-. Under optimum conditions, complete transformation of neutral cyclometalated binuclear iridium(III)

Table 1 Optimization of the reaction conditions

Ligand (L)	Solvent	Molar ratio of reagents 1 : L : $NaPF_6$	Temp. [°C]	Time [h]	Yield [%]
C	$ClCH_2CH_2Cl$	1 : 2.2 : 2.2	65	12	26
	THF	1 : 2.2 : 2.2	65	12	36
		1 : 2.05 : 2.05	150	0.167	12
		1 : 2.05 : 2.05	150	0.167	64[a]
E	$ClCH_2CH_2Cl$	1 : 2.2 : 2.2	65	12	19
	THF	1 : 2.2 : 2.2	65	12	28
		1 : 2.05 : 2.05	150	0.167	78[a]
H	$ClCH_2CH_2Cl$	1 : 2.2 : 2.2	65	12	24
	THF	1 : 2.2 : 2.2	65	12	33
		1 : 2.05 : 2.05	150	0.167	77[a]
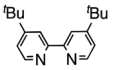	$HOCH_2CH_2OH$	1 : 2.2 : 5.95	150	18	70[b]

[a] The microwave-assisted reaction. [b] See ref. 33*d* and *e* (the reaction was carried out through a two-step protocol).

precursor into the desired cationic compound $[Ir(bzq)_2(6,6'\text{-}Me_2\text{-}2,2'\text{-}bpy)]^+PF_6^-$ (**2CA′**) with the use of **C** and **A′** in a small excess, *i.e.* 5 mol% of each compound in relation to complex **1**, allowed obtaining it with a yield of 64%. The results presented in Table 1 clearly illustrate the advantage of the protocol using microwave radiation in comparison with the classical method for obtaining this type of compound as well as those described in the literature.[33d,e] Therefore, in the next step, the same conditions were applied to the preparation of cationic complexes of the type $[Ir(bzq)_2(N\text{^}N)]^+A^-$ (**2**), using the combinations of precursor **1** with a wide gamut of *N*,*N*-aromatic donors and salts **A′**–**C′**, presented in Scheme 2. The developed one-pot method has proved to be versatile and quite efficient in the systems of the components studied, leading to the desired known (**2AA′**[33d], **2FA′**[33d,34]) as well as a series of new cationic iridium(III) coordination derivatives **2** with good yields in the range 60–86% in relatively short times.[40]

All complexes were isolated and characterized by ^{1}H NMR; additionally, the structures of two of them were determined by X-ray methods. In both structures the Ir cation is 6-coordinated (by four nitrogen and two carbon atoms – *cf.* Fig. 1) in a regular, octahedral fashion. In **2FA′**, the Ir atom lies on the twofold axis, and the whole complex therefore has C_2-symmetry. Bond lengths are typical; Table 2 lists some relevant geometrical parameters. It should be noted that the very nature of the complex allows a disorder; in **2AA′** the benzo[*h*]quinoline fragment is disordered over two positions, rotated by 180°. In the crystal structures, besides the cations and PF_6 counterions, the solvent molecules (disordered over the centre of inversion), methanol in **2FA′** and 1,2-dichloroethane in **2AA′**, fill the voids (Fig. 2).

Table 2 A list of some relevant geometrical parameters

	2AA′	2FA′
Ir1-N15A	2.051(6)	2.036(3)
Ir1-C12A	2.013(8)	2.077(4)
Ir1-N1A	2.067(6)	2.084(3)
Ir1-C26A	2.012(8)	
Ir1-N29A	2.143(6)	
Ir1-N36A	2.129(6)	
C12A-Ir1-C12A[a]		172.50(12)
N1A-Ir1-N15A[a]		173.04(8)
N1A-Ir1-N15A	172.1(3)	
C26A-Ir1-N29A	176.1(3)	
C12A-Ir1-N36A	176.1(3)	

[a] $1-x, y, 1/2-z$.

Thermal analysis

The thermal properties of type 2 synthesized complexes were examined by thermogravimetric analysis (TGA) under a nitrogen stream and the temperatures of 5% weight loss are compiled in Table 3 (see Fig. 2Sa and b in the ESI†). Considering that the thermal stability of complexes depends on the type of counterion used, generally for pairs of complexes having the same ligands, higher stability was observed for the derivatives with the **A′** anion than for the **B′** series. While taking into account the influence of the type of N,N-donating ligand bonded to the iridium center on the thermal properties of the

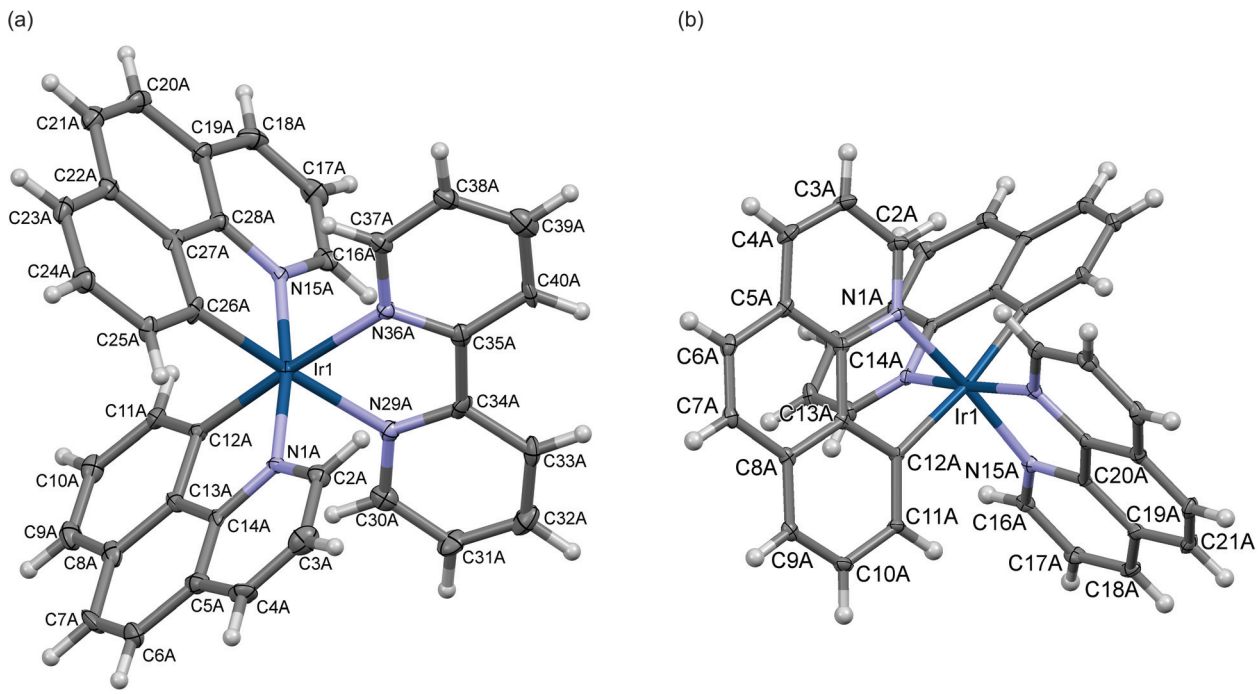

Fig. 1 Anisotropic-ellipsoid representation of complexes **2AA′** (a) and **2FA′** (b); ellipsoids are drawn at the 50% probability level; hydrogen atoms are shown as spheres of arbitrary radii. In **2AA′** only one of the possible positions of Ir-bonded C and N atoms in the benzo[*h*]quinoline moiety has been shown for clarity. In **2FA′** the unlabeled atoms are related to the labelled ones by the symmetry operation $-x+1, y, -z+1/2$.

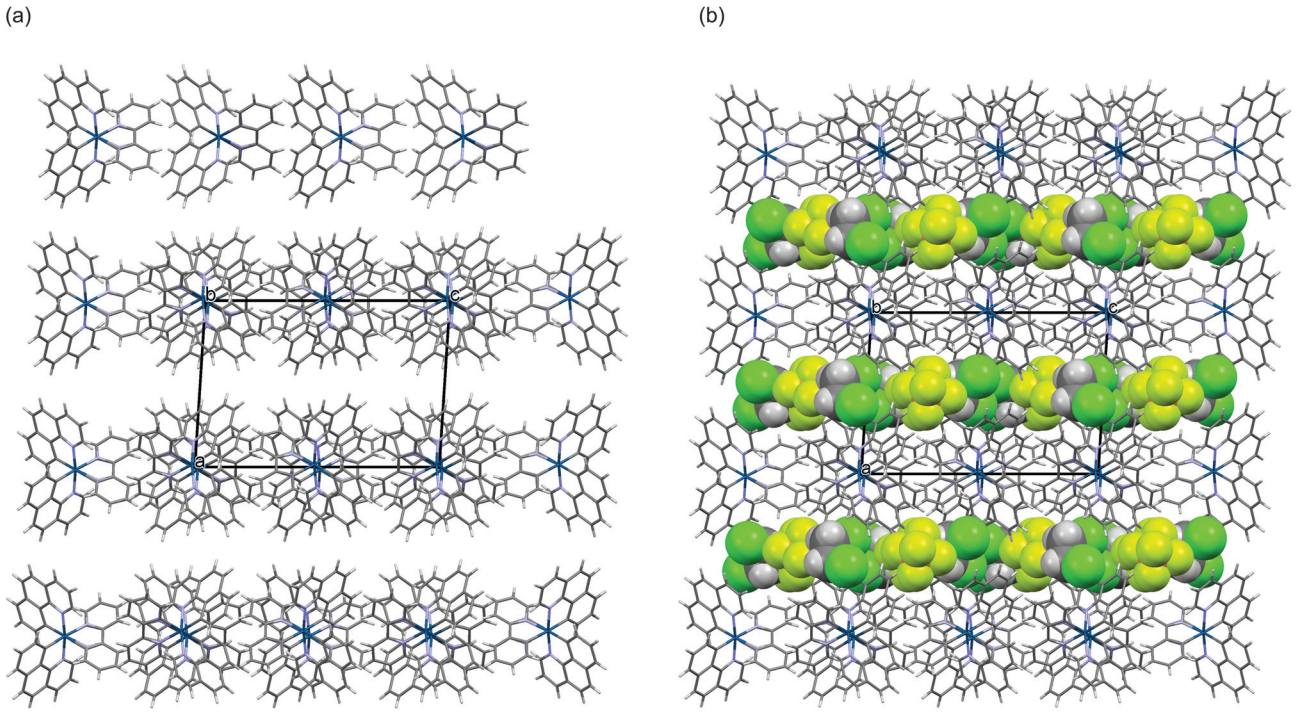

Fig. 2 A crystal packing in the structure of **2AA′** without (a) and with (b) the anions and solvent molecules, shown in van der Waals radii representation.

Table 3 Data of thermogravimetric measurements (TGA)

Sample	Temperature of 5% weight loss [°C]	Residue at 996 °C [%]
2AA′	183.5	38.7
2BA′	278.3	46.1
2CA′	308.7	33.8
2DA′	275.9	50.2
2EA′	219.1	39.1
2FA′	174.7	25.8
2GA′	217.7	46.8
2HA′	216.9	41.0
2IA′	131.6	46.9
2AB′	138.7	35.1
2BB′	215.0	14.6
2CB′	158.1	18.5
2DB′	213.7	43.0
2EB′	124.3	36.3
2FB′	181.1	45.9
2GB′	155.3	26.5
2HB′	269.2	12.1
2IB′	180.0	36.7
2IC′	242.9	10.7

examined ionic iridium(III) complexes, it was found that the type 2 compounds with the series of ligands **A–E** *i.e.* bearing bipyridine motifs and **A′** counterions are thermally more stable than those with the **F**, **G**, **H** series. On the other hand, in a series of cationic iridium compounds stabilized with the benzo[*i*]dipyrido[3,2-*a*:2′,3′-*c*]phenazine ligand (**I**), *i.e.* **2IA′**, **2IB′**, **2IC′**, an increase in thermal stability was observed in the following order of counterions: **A′**, **B′**, **C′**.

In the next step, selected materials *i.e.* **2FA′**, **2FB′**, **2HB′**, and **2IC′** were subjected to DSC analysis in order to determine the melting and crystallization temperatures. Unfortunately, although for **2FB′** the signal corresponding to the melting point was observed at *ca.* 200 °C upon heating, no signal from the crystallization process was observed upon sample cooling. When **2FA′**, **2HB′**, and **2IC′** were subjected to DSC analysis, no signs of any transitions were observed for these materials in the temperature range determined by TGA measurements. This fact may indicate that the samples examined have crystallization points above their degradation temperature or they undergo irreversible transformations on melting.

Determination of electrochemical properties

Cyclic voltammetry experiments were performed in order to estimate the electrochemical properties and to predict some electronic properties of the synthesized iridium(III) derivatives. The values of potentials allowed the calculation of the Ionization Potential (IP) and Energy Affinity (EA) which are related to the energies of the highest occupied molecular orbital (HOMO) and the lowest unoccupied molecular orbital (LUMO).

Iridium(III) complexes with PF_6^- as a counterion were subjected to CV measurements. PF_6^- was chosen as a common anion in Ir complexes and in the supporting electrolyte Bu_4NPF_6. Cationic complexes with BPh_4^- are not shown and discussed because of the low oxidation potential of this counterion. BPh_4^- underwent the oxidation process in a lower potential range than most of the studied Ir complexes.

Therefore, the low oxidation potential excluded the use of BPh_4^- as the anion of the supporting electrolyte. CV curves recorded in MeCN are presented in Fig. 3. Irreversible or quasi reversible oxidation peaks for all the studied compounds are observed in the anodic range. Similar features have been reported earlier for model **2FA′** and **2AA′** compounds.[34] They are assigned to the redox couple Ir(III)/Ir(IV) with orbitals contributed by the iridium centre and ligands.[41,42] Comparison of the oxidation onset potentials ($E_{ox\ onset}$) reveals clear differences depending on the structure of the complexes (Table 4). In both the series of **2FA′** and **2AA′** derivatives, the influence of the ligand substitution with phenyl, methyl and methoxyl groups was observed. The values 0.2 V and 0.22 V of $E_{ox\ onset}$ were observed as a result of the electron donating character of these groups. Addition of the subsequent groups to **2HA′** results in a further 0.1 V reduction of $E_{ox\ onset}$. Ionization potential (IP) related to the removal of electrons from the HOMO orbital was estimated from the $E_{ox\ onset}$ value. The 0.2 eV shift of IP was obtained for both series of **2FA′** and **2AA′** derivatives with two symmetrical groups substituted for the ligands. The 0.3 eV shift was estimated for **2HA′** with four groups, two phenyl and two methyl groups. As reported earlier, a strong contribution of the ligand structure to the HOMO orbital of Ir complexes was confirmed.[41,43,44] In the series of **2FA′** derivatives only a small shift of the reduction onset potential ($E_{red\ onset}$) was observed. Substitution by phenyl and methyl groups had a marginal influence $E_{red\ onset}$. A similar behaviour was observed for **2AA′** derivatives except **2EA′**. The replacement of **A** by **E** as the ancillary ligand led to a significant shift of $E_{red\ onset}$., which results in a change in the electron affinity (EA) related to the delivery of an electron to the LUMO. The EA estimated for all the studied compounds is 3.4 eV except for **2EA′**.

The value 3.8 eV of EA indicates that the presence of **E** ligand significantly modifies the LUMO. In accordance with the previously published DFT calculations for similar iridium complexes, it has been shown that the LUMO orbital is localized mainly to the ligands. However, it has also been reported that the contribution of the main cyclometalated ligands and the ancillary ligand in the LUMO orbital depends on their structures.[42,44–46] The dependences indicate that the modification of the ancillary ligand can lead to significant changes in both the LUMO and HOMO.

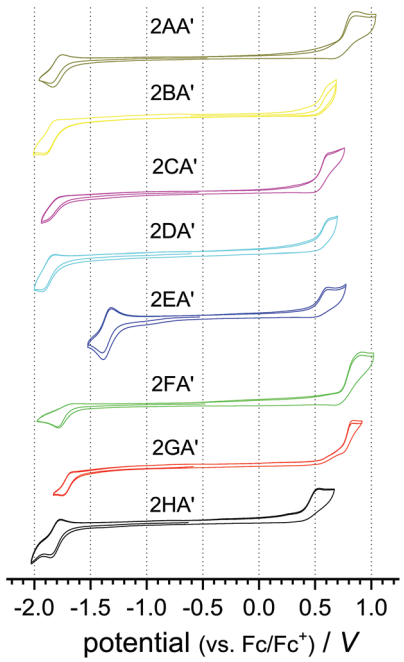

Fig. 3 Cyclic voltammetry of compounds with PF_6^- as a counterion recorded in MeCN with 0.1 M Bu_4NPF_6 as a supporting electrolyte (scan rate 100 mV s^{-1}; concentration 1 mM) or saturated solutions of compounds with lower solubility at a temperature of 298 K.

Theoretical considerations

Molecular geometries in the ground state. The geometries of the ground state structures were fully optimized without imposition of symmetry restrictions. Table 1S (ESI†) gives the Ir-ligand bond lengths and bond angles in the gas phase and the acetonitrile environment. The maximum difference in bond distances between coordinating atoms and Ir(III) was 0.003 Å, while the changes in valence angles were less than 1.0°. This means that solvent effects have a minor influence on the optimized geometries of these complexes. For the compounds investigated herein, the use of a more flexible basis set, includ-

Table 4 Electrochemical and electronic properties of the studied compounds

Compound	$E_{ox\ onset}$ [V]	E_{ox} [V]	$E_{red\ onset}$ [V]	E_{red} [V]	E_g [eV]	IP [eV]	EA [eV]
2AA′	0.69	0.88	−1.71	−1.84	2.40	5.8	3.4
2BA′	0.47	0.62	−1.74	−1.90	2.21	5.6	3.4
2CA′	0.47	0.63	−1.73	−1.90	2.20	5.6	3.4
2DA′	0.49	0.58	−1.75	−1.98	2.24	5.6	3.4
2EA′	0.47	0.61	−1.26	−1.40	1.73	5.6	3.8
2FA′	0.73	0.92	−1.67	−1.79	2.40	5.8	3.4
2GA′	0.51	0.85	−1.66	−1.75	2.17	5.6	3.4
2HA′	0.41	0.57	−1.68	−1.82	2.09	5.5	3.4

Potentials were estimated using the ferrocene redox couple as an internal standard; E_g – electrochemical energy gap was estimated from the equation $E_g = E_{ox\ onset} + E_{red\ onset}$; IP – ionization potential – from the equation IP = $|e| - |(5.1 + E_{ox\ onset})$; EA – electron affinity – from the equation EA = $|e| - |(5.1 - E_{red\ onset})$.

ing diffuse functions, showed no significant changes in the main geometrical features (Table 2S in the ESI†). The representative optimized structure of complex **2FA′** in the ground state (S_0) at the B3LYP level is shown in Fig. 4 along with the numbering of the key atoms.

The main optimized geometry parameters for complex **2FA′** in the S_0 state and the X-ray crystal structure data are summarized in Table 2. It can be seen that the geometry of each of the complexes is pseudo-octahedral (see valence angles in Table 5), similarly to that obtained for other Ir(III) complexes reported in the literature.[33e,44] The optimized bond distances are in good agreement with the available experimental data (Table 5); the deviation is less than 2%. However, the differences between the theoretically calculated and the experimentally obtained geometrical parameters arise not only from the fact that the former were obtained for complex molecules in the environment of CH_3CN as a solvent, while the latter were obtained from X-ray analysis of single crystals in which the molecules are closely packed in the crystal lattice. These types of differences also stem from the fact that the method used, B3LYP, overestimates the bond lengths in transition metal complexes.[47]

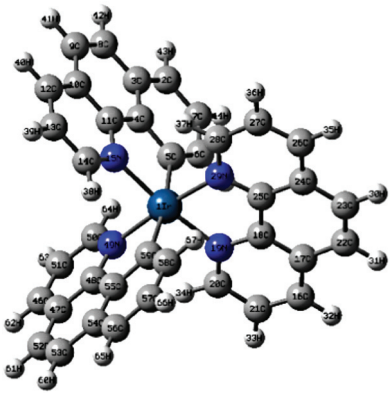

Fig. 4 Optimized structure of the **2FA′** cation part in the ground state.

Table 5 Selected bond distances and valence angles from the optimized geometries and the experimental values for 2FA′

	X-ray	B3LYP
Bond lengths (Å)		
Ir-N15	2.084	2.104
Ir-N19	2.036	2.073
Ir-N29	2.036	2.073
Ir-N49	2.084	2.105
Ir-C5	2.077	2.123
Ir-C59	2.077	2.123
Valence angles (deg)		
N15-Ir-N49	87.84	88.6
C5-Ir-N19	94.26	95.4
C5-Ir-N29	91.45	90.2
N15-Ir-C5	79.51	79.6
N15-Ir-N19	173.04	173.5
N29-Ir-N49	173.04	173.5
C5-Ir-C59	172.49	172.7
N15-Ir-N29	95.85	96.0

Frontier molecular orbital analysis

It is well known that the photophysical properties of cyclometalated Ir(III) complexes strongly depend on the character of their frontier molecular orbitals (FMOs), HOMO and LUMO. Previous results indicated that the selection of the B3LYP functional in DFT calculations yielded good quantitative agreement with the experiment.[33k,48,49] Therefore, we initially adopted this approach for the preliminary studies and the obtained results for eight Ir complexes are collected in Table 3S.† The absolute values of the HOMO and LUMO energies (DFT) are different from the electrochemical data obtained by us. Although the earlier work of Skorka and co-workers gives good correlation between $E_g^{teor.}$ and the experimental ones,[49] in our experiment the results show insufficient correlation between the variables (R^2 = 0.16). The calculated energy gaps between the HOMO and LUMO decrease from 3.51 eV to 2.84 eV when the experimental values decrease from 2.40 eV to 1.73 eV. Our results showed that the B3LYP functional resulted in an increase in the HOMO–LUMO gap values of approximately 1 eV and in some cases, even more (**2EA′**: 1.54 eV, **2HA′**: 1.25 eV and **2GA′**: 1.17 eV). On the basis of these unexpected results and recent findings from theoretical calculations, the next calculations were carried out with the M06 functional.[50,51] However, after further analysis of the data, a poor correlation between $E_g^{teor.}$ and $E_g^{exp.}$ was still observed (R^2 = 0.55), and the detailed data are listed in Table 4S.† Thus, the change in the functional from B3LYP to M06 did not give reasonable results. Considering the above, another way of calculation has been proposed which includes the ONIOM approach. In this paper, on the basis of the experimental data for eight Ir(III) complexes, a relationship was established between the ONIOM calculated HOMO–LUMO gaps at the WB97XD/SDD/6-311++G(d,p) level and the experimental ones (see eqn (1S) and Table 5S in the ESI†). The energies were calculated by using the ONIOM method and are treated at different levels of accuracy. Then we found good agreement between theory and experiment. As shown in Fig. 5, the obtained correlation coefficient between the theoretical energies computed *via* ONIOM and electrochemical data was much higher and equalled 0.79.

Additionally, we tried to model the oxidation potential of the studied compounds. The linear combination of ONIOM calculated energies for complexes bearing +1 and +2 charge resulted in oxidation potentials that correlated well with the experimental $E_{oxonset}$ values – the determination coefficient value was slightly above 0.90 (see Table 14S and Fig. 1S in the ESI†).

Description of photophysical properties

The absorption spectra of the complexes studied in chlorobenzene, measured at room temperature, are presented in Fig. 6a ($[Ir(bzq)_2(bpy)]^+A^-$ type) and 6b ($[Ir(bzq)_2(phen)]^+A^-$ type) complexes.

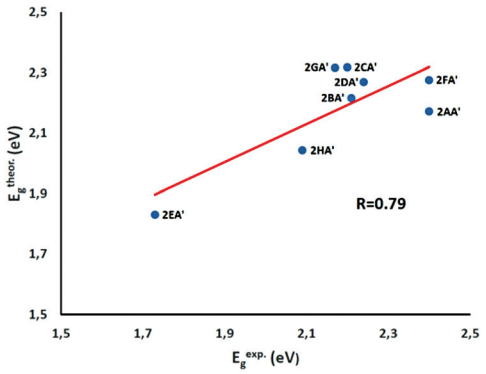

Fig. 5 Theoretical E_g calculated *via* the WB97XD/SDD/6-311++G(d,p) level of theory by using the ONIOM method *vs.* experimental values.

The lowest energy absorption band is observed at *ca.* 420 nm and is assigned to spin-forbidden MLCT transitions related to the electron transfer from an Ir-centred d orbital to a π* orbital localized on one of the ligands. All the spectra display intense absorption bands below 400 nm which are assigned to ligand (N^N and C^N) centered ^{1}LC transitions.[34] As shown in Fig. 7, the HOMO orbital of the complexes studied mainly resides on the Ir(d) and benzo[*h*]quinoline (π) part of the molecule and the LUMO (π*) is localized on the ancillary ligand, so the lowest energy HOMO–LUMO transition may be MLCT or LLCT in character. When the methyl group is attached at positions 6 and 6′ in both ancillary ligands an additional weak transition located at 460 nm in the absorption spectrum appears. The photoluminescence spectra recorded are depicted in Fig. 8a and b. In Fig. 8a,† the emission band of complexes **2AA′–2EA′** can be significantly shifted from 550 to 660 nm *via* modification of the 2,2′-bipyridine ligand. It is well known that the phosphorescent iridium complexes can emit light in the full visible spectrum by modification of the ligand structure and by the incorporation of ancillary ligands.[52] The emission of the studied compounds is red shifted with extension of the conjugation length of the N^N ligand (**2EA′**). The fusion of phenyl rings into the ancillary ligand probably stabilizes the CT states which are mainly responsible for emission. The emissive, low-lying T_1 states can be either MLCT or LC based excited states, depending on the ligands.

The broad and structureless bands observed for the compounds studied suggest rather the MLCT character of emission. The vibronic structure of the **2DA′** emission spectrum indicates electronic mixing between the MLCT and the LC states, very often observed for iridium(III) complexes, because of strong spin–orbit coupling.[53,54]

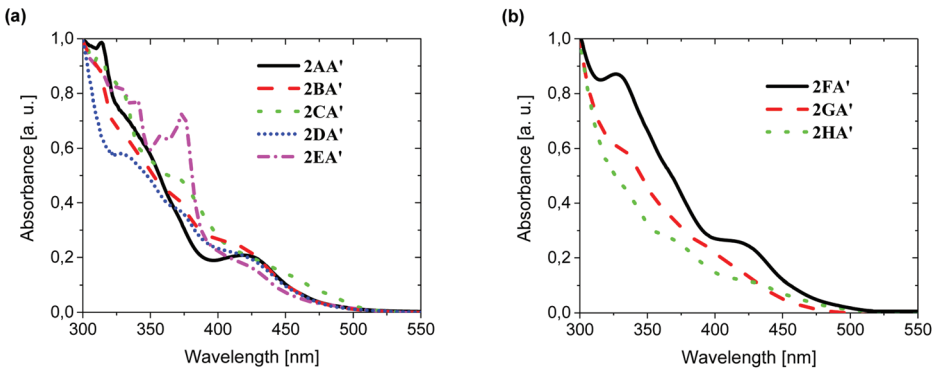

Fig. 6 Normalized absorption spectra of the investigated compounds in chlorobenzene: **2AA′–2EA′** (a) and **2FA′–2HA′** (b).

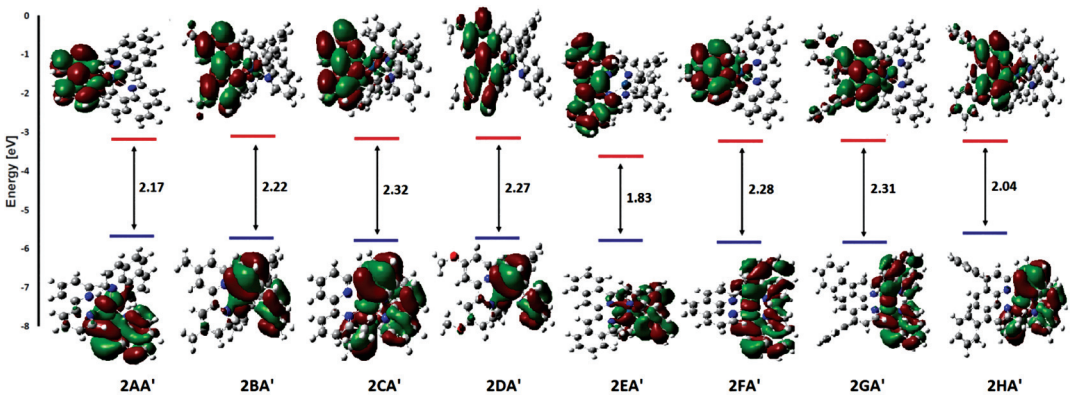

Fig. 7 Molecular orbital diagram of iridium(III) complexes along with the HOMO/LUMO plots computed at the WB97XD/SDD/6-31++G(d,p) level of theory.

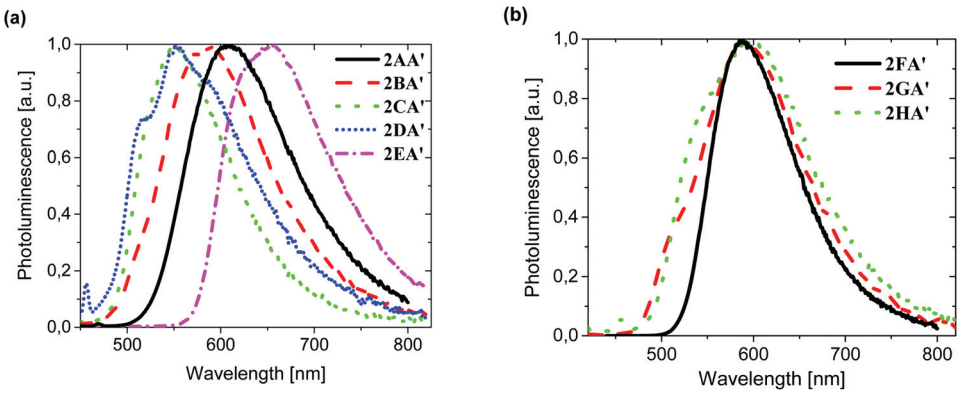

Fig. 8 Normalized photoluminescence spectra of the investigated compounds in chlorobenzene: **2AA′**–**2EA′** (a) and **2FA′**–**2HA′** (b).

Upon the introduction of methyl groups into positions 4,4′ in 2,2′-bipyridine (**2BA′**), the triplet excited state experiences a blue shift of 54 nm in the PL peak. The substitution of the same groups at positions 6,6′ resulted in an additional blue shift of a few nm. This may indicate that the substitution of electron-donating groups on the ancillary ligand leads to destabilization of the LUMO.[55] The colour tuning effect is not found in complexes **2FA′**–**2HA′**, when the ancillary ligand is 1,10-phenanthroline (**F**) and modification of this ligand does not change the position of the emission band. Only a shoulder in the higher energy range is observed as a consequence of implementation of phenyl rings and methyl groups into the N^N ligand.

Complex **2EA′** exhibits the highest QY of emission; however, as shown in Table 6, the value of QY strongly depends on the oxygen present in the solvent, which is typical of phosphorescent emitters.

Degassing of the solvent results in an increase in QY from 2.8 to 16% and from 3.5 to 28% for **2AA′** and **2FA′**, respectively. The lower emission efficiency of **2DA′** may be related to a stronger contribution of the π–π* emissive state. It is known that the value of the radiative rate constant of emission from the ^{3}MLCT-based excited state is two or three orders of magnitude higher than that of the rate constant of emission from the ^{3}π–π* excited state.[16,56] Moreover, the determined emission QY values may suggest that the C–H bonds vibrations in methyl or methoxyl groups in **B**, **C**, **D** and **H** ligands may have an impact on the intensity of emitted light. Generally, from among the complexes studied, those with **F** as the N^N ligand seem to show better emissive properties in solution than those with 2,2′-bipyridine as the ancillary ligand. The comparison of the emission decay time for the most efficient emitters (**2AA′**, **2EA′**, **2FA′**, **2GA′**) reveals that the longest living emissive state (1 μs) was observed for **2FA′**. The phosphorescence of **2AA′**, **2EA′**, **2GA′** decays faster, within 0.4, 0.6, and 0.5 μs, respectively. Additionally, the negative influence of oxygen on the emissive properties is best visible for **2FA′**. This might suggest a significant contribution of the triplet component to the emitting states.

Table 6 UV-Vis absorption and photoluminescence spectral data of the investigated compounds

Compound	$\lambda_{max.\ abs.}$ [nm]	$\lambda_{max.\ emission}$ [nm]	Quantum yield Φ [%]
2AA′	420, 374, 341, 314	610	2.8 16.0[a]
2BA′	420, 374, 327, 314	558	1.0
2CA′	460, 420, 374, 327	552	0.3
2DA′	420, 374, 327	552	0.3
2EA′	420, 374, 357, 341, 327	655	9.0 13.5[a]
2FA′	420, 374, 327	588	3.5 28.0[a]
2GA′	420, 327	592	6.6 22.3[a]
2HA′	460, 420, 374	596	2.8

[a] In a degassed solution.

Selected complexes were tested as emitters in the emission layer for application in polymer light-emitting diodes (PLEDs). To avoid the concentration induced emission quenching, known for iridium complexes, the host–guest systems were used. Such systems contain a polymer matrix and a small-molecule emitter.[1a] A commonly used host matrix is made of a mixture of poly(*N*-vinylcarbazole) (PVK) and 2-(4-*tert*-butylphenyl)-5-(4-biphenyl)-1,3,4-oxadiazole (PBD).[57] The PVK and PVK/PBD blends are particularly useful as host matrices for the phosphorescent guest molecules because PVK ensures hole transport and PBD electron transport, and additionally the high triplet exciton energy of PVK prevents the crossing of the triplet guest exciton back to the host triplet state.[58]

Results for the layers of PVK/PBD blends doped with complexes **2AA′** and **2FA′** are shown in Fig. 9. The PVK/PBD matrix fulfils the condition of an overlap of its emission spectrum and the guest absorption spectrum, necessary for the Förster energy transfer to occur (see Fig. 9).

The values of the spectral overlap integral (J, calculated according to a well-known published procedure[59]) between the host and the guest were determined to be 8.43 and 7.57 × 10^{13} nm^4 mol^{-1} cm^{-1} and consequently the Förster radii (Ro) were 1.8 and 1.9 nm for **2AA′** and **2FA′**, respectively. Thus, one can

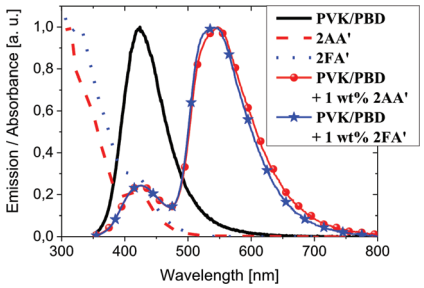

Fig. 9 Normalized absorption spectra of **2AA′** and **2FA′** compounds recorded in chlorobenzene and normalized photoluminescence spectra of thin layers: the neat PVK/PBD matrix and PVK/PBD doped with 1 wt% of emitter molecules (excitation with light of 340 nm).

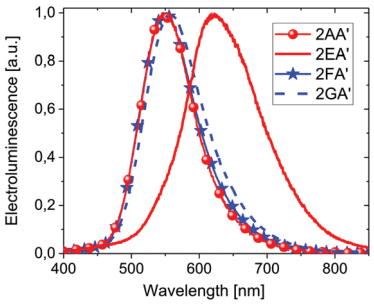

Fig. 10 Normalized electroluminescence spectra of PLEDs with an emitting layer created on the basis of the PVK/PBD matrix doped with 1 wt% of emitter molecules (**2AA′**, **2EA′**, **2FA′** or **2GA′**).

assume a Förster mechanism of energy transfer in the systems. However, in both cases the exciton transfer from PVK/PBD to emitter molecules is incomplete.

Upon excitation with light at a wavelength of 340 nm, corresponding to the lowest energy absorption band of the PVK/PBD matrix, the photoluminescence spectra of the thin layers display two emission bands. Besides the emission band associated with emitter molecules, a band with a maximum around 430 nm is observed, assigned to the matrix.

Moreover, the maxima of emitter emission are shifted by about 50 nm toward shorter wavelengths as compared to their positions in the spectra in solution. The effect can be caused by the rigidity of the matrix and can be treated as confirmation of MLCT character of the emissive state. A similar effect was usually observed for transition metal complexes.[41,60]

Studies on the determination of basic work parameters of the single-layer PLEDs with an emitting layer created on the basis of the PVK/PBD matrix with the synthesized cationic iridium(III) complexes as dopants confirm their potential application as emitters.

Electroluminescence (EL) spectra recorded for PLEDs with selected emitters correspond to their PL spectra (*cf.* Fig. 8 and 10). The colour tuning effect is clearly observed for the modified bipyridine complexes. In contrast to the PL spectra, in the EL spectra no matrix emission is observed, which indicates the influence of charge carrier trapping in the EL phenomenon.[58a] The basic characteristics of the constructed PLEDs are shown in Fig. 11. The so-called switching voltage of the diodes (the value for which the luminance reaches 1 cd m^{-2}) is about 7 V and the devices work stably up to

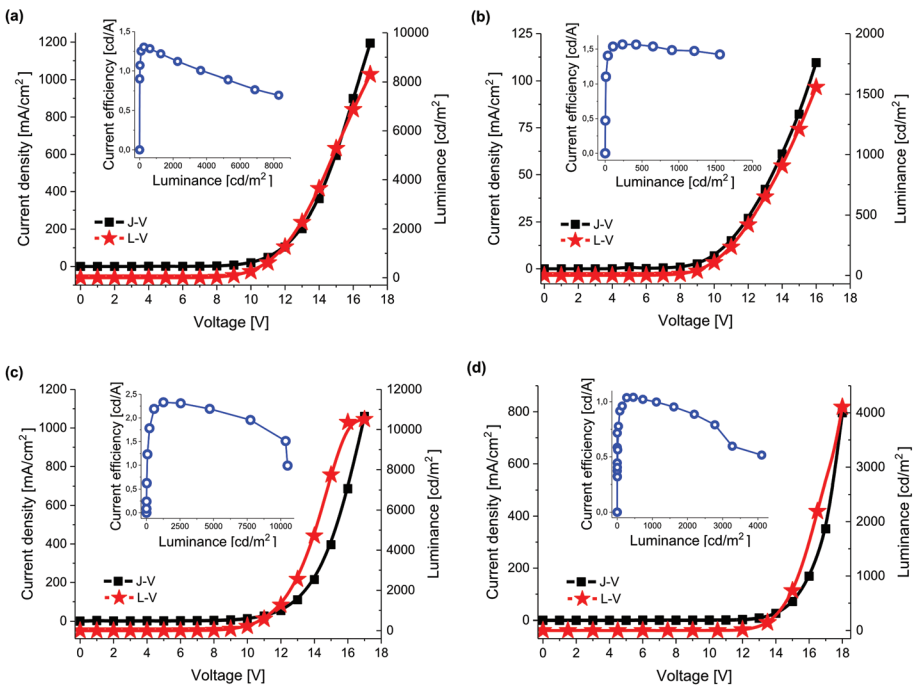

Fig. 11 Current density–luminance–voltage (J–L–U) characteristics of PLEDs with the emitting layer made of PVK/PBD doped with 1 wt% of emitter molecules: **2AA′** (a), **2EA′** (b), **2FA′** (c) or **2GA′** (d). Insets present their current efficiency–luminance dependencies.

18 volts. The highest luminance values, exceeding 8000 and 10 000 cd m^{-2}, were recorded for the device based on $[Ir(bzq)_2(2,2'\text{-bipyridine})]^+PF_6^-$ (**2AA′**) and $[Ir(bzq)_2(1,10\text{-phenanthroline})]^+PF_6^-$ (**2FA′**), respectively (see Fig. 11a and c). The fabricated PLEDs exhibit current efficiency in the range of 1.0 to 2.2 cd A^{-1}. These parameters were obtained for the device containing only 1.0 wt% of emitter molecules. Increasing the emitter's concentration to 2 wt% did not improve the performance of the devices. Hence, it can be assumed that optimal concentrations are in the range of 1 to 2 wt%. It should be underlined that these preliminary results were obtained for PLEDs with a simple structure, without additional transporting and/or charge carrier blocking layers.

Conclusions

Comparing the synthetic protocols described in the literature, leading to iridium complexes with an ionic structure in which the metallic centre is stabilized with both *C*,*N*-cyclometalated and N^N-donating ligands, with the method proposed by us, it seems that our methodology for the preparation of such iridium derivative ($[Ir(C^N)_2(N^N)]^+A^-$) structures based on a one-pot protocol with the support of microwave radiation is definitely more efficient and less time-consuming, requiring up to 10 min reaction time. The microwave-assisted synthetic pathway successfully enabled the synthesis of a wide range of iridium(III) ionic complexes bearing in their structure coordinated molecules such as 2,2′-bipyridine or 1,10-phenantrioline and their sterically hindered derivatives besides two bonded cyclometalated benzo[*h*]quinoline ligands as well as various counterions. All of the synthesized complexes were characterized by NMR spectroscopy; moreover, the structures of two of them were determined by single crystal X-ray analysis. Additionally, cyclic voltammetry experiments (CV) allowed the calculation of Ionization Potential (IP) and Energy Affinity (EA), thereby the determination of the HOMO and LUMO energies and consequently the band gap. However, it was possible only for iridium compounds with PF_6^- counterions, because for complexes with BPh_4^-, the oxidation process of this anion took place in a lower potential range than most of the iridium coordinating cations stabilized with N^N ligands. Employing the ONIOM approach at the WB97XD/SDD/6-311++G(d,p) level for the energy calculations of the HOMO/LUMO orbitals we found good agreement between theory and experimental data, obtaining satisfactory correlation coefficient between theoretical energies of the above-mentioned orbitals and those calculated on the basis of electrochemical experiments. The constructed simple PLEDs based on the selected emitters molecularly dispersed in the PVK/PBD matrix exhibit luminance in the range from 1500 to above 10 000 cd m^{-2}, which indicates that these iridium complexes are suitable candidates for host/guest type light emitting diodes. The EL spectra recorded for PLEDs with different complexes of the type $[Ir(bzq)_2(N^N)]^+A^-$ show that by a simple modification of the bipyridine structure the colour of emitted light can be tuned.

Acknowledgements

This work was supported by the National Science Centre through grant no UMO-2013/11/B/ST5/01334. This research was supported in part by the PL-Grid Infrastructure. Przemyslaw Ledwon acknowledges award no. 04/040/RGJ17/0055 from the Rector of the Silesian University of Technology for research and development achievements.

Notes and references

1 (*a*) Z. Li and H. Meng, in *Organic light-emitting materials and devices*, ed. Z. Li and H. Meng, Taylor and Francis, Boca Raton, 2007; (*b*) J. Kalinowski, in *Organic Light-Emitting Diodes; Principles, Characteristics, and Processes*, ed. J. Kalinowski, Marcel Dekker, New York, 2005.
2 S. Miyata and H. S. Nalawa, in *Organic Electroluminescent Materials and Devices*, ed. S. Miyata and H. S. Nalawa, CRC Press, London, 1997, p. 496.
3 (*a*) Z. R. Li, in *Organic Light-Emitting Materials and Devices*, ed. Z. R. Li, CRC Press, Boca Raton, FL, 2nd edn, 2015, p. 813; (*b*) L. F. R. Pereira, in *Organic Light Emitting Diodes: the Use of Rare Earth and Transition Metals*, ed. L. F. R. Pereira, CRC Press, Hoboken, NJ, 2012, p. 341.
4 H. Yersin, in *Highly Efficient OLEDs with Phosphorescent Materials*, ed. H. Yersin, Wiley-VCH Verlag GmbH and KGaA, Weinheim, 2008, p. 438.
5 F. Xu, J.-H. Kim, H. U. Kim, D. Mi, Y. J. Cho, J. Y. Lee, U. Ch. Yoon and D.-H. Hwang, *Synth. Met.*, 2013, **178**, 10–17.
6 S. Scholz, D. Kondakov, B. Lüssem and K. Leo, *Chem. Rev.*, 2015, **115**, 8449–8503.
7 (*a*) E. Baranoff, H. J. Bolink, F. De Angelis, S. Fantacci, D. Di Censo, K. Djellab, M. Grätzel and Md. K. Nazeeruddin, *Dalton Trans.*, 2010, **39**, 8914–8918; (*b*) V. Sivasubramaniam, F. Brodkorb, S. Hanning, H. P. Loebl, V. van Elsbergen, H. Boerner, U. Scherf and M. Kreyenschmidt, *J. Fluorine Chem.*, 2009, **130**, 640–649.
8 B. Carlson, G. D. Phelan, W. Kaminsky, L. Dalton, X. Jiang, S. Liu and A. K.-Y. Jen, *J. Am. Chem. Soc.*, 2002, **124**, 14162–14172.
9 S. Bernhard, X. Gao, G. G. Malliaras and H. D. Abruna, *Adv. Mater.*, 2002, **14**, 433–436.
10 (*a*) J. Slinker, D. Bernards, P. L. Houston, H. D. Abruna, S. Bernhard and G. G. Malliaras, *Chem. Commun.*, 2003, 2392–2399; (*b*) F. G. Gao and A. J. Bard, *J. Am. Chem. Soc.*, 2000, **122**, 7426–7427; (*c*) H. Rudmann, S. Shimada and M. F. Rubner, *J. Am. Chem. Soc.*, 2002, **124**, 4918–4921; (*d*) M. Buda, G. Kalyuzhny and A. J. Bard, *J. Am. Chem. Soc.*, 2002, **124**, 6090–6098; (*e*) S. Bernhard, J. A. Barron, P. L. Houston, H. D. Abruna, J. L. Ruglovsky, X. Gao and G. G. Malliaras, *J. Am. Chem. Soc.*, 2002, **124**, 13624–13628; (*f*) S. Lamansky, P. Djurovich, D. Murphy, F. Abdel-Razzaq, R. Kwong, I. Tsyba, M. Bortz, B. Mui, R. Bau and M. E. Thompson, *Inorg. Chem.*, 2001, **40**, 1704–1711;

(*g*) P. Reveco, R. H. Schmehl, W. R. Cherry, F. R. Fronczek and J. Selbin, *Inorg. Chem.*, 1985, **24**, 4078–4082.

11 (*a*) X. Gong, P. K. Ng and W. K. Chan, *Adv. Mater.*, 1998, **10**, 1337–1340; (*b*) P. Spellane, R. J. Watts and A. Vogler, *Inorg. Chem.*, 1993, **32**, 5633–5636.

12 J. D. Slinker, A. A. Gorodetsky, M. S. Lowry, J. Wang, S. Parker, R. Rohl, S. Bernhard and G. G. Malliaras, *J. Am. Chem. Soc.*, 2004, **126**, 2763–2767.

13 (*a*) G. Li, Q. Lin, L. Ji and H. Chao, *J. Mater. Chem. B*, 2014, **2**, 7918–7926; (*b*) K.-W. K. Lo, C.-K. Chung, T. K.-M. Lee, L.-H. Lui, K. H.-K. Tsang and N. Zhu, *Inorg. Chem.*, 2003, **42**, 6886–6897; (*c*) K. K.-W. Lo, D. Ch.-M. Ng and Ch.-K. Chung, *Organometallics*, 2001, **20**, 4999–5001; (*d*) K. K.-W. Lo and A. H.-H. Leung, *Sci. China: Chem.*, 2010, **53**, 2091–2098; (*e*) W. H.-T. Law, L. C.-C. Lee, M.-W. Louie, H.-W. Liu, T. W.-H. Ang and K. K.-W. Lo, *Inorg. Chem.*, 2013, **52**, 13029–13041.

14 (*a*) T. Hu, L. He, L. Duan and Y. Qiu, *J. Mater. Chem.*, 2012, **22**, 4206–4210; (*b*) F. Dumur, D. Bertin and D. Gigmes, *Internet J. Nanotechnol.*, 2012, **9**, 377–395.

15 (*a*) J. Wu, F. Li, Q. Zeng, C. Nie, P. C. Ooi, T. Guo, G. Shan and Z. Su, *Org. Electron.*, 2016, **28**, 314–318; (*b*) H. Tang, L. Wei, G. Meng, Y. Li, G. Wang, F. Yang, H. Wu, W. Yang and Y. Cao, *Opt. Mater.*, 2014, **37**, 679–687; (*c*) H. Tang, Y. Li, Q. Chen, B. Chen, Q. Qiao, W. Yang, H. Wu and Y. Cao, *Dyes Pigm.*, 2014, **100**, 79–86; (*d*) L. He, L. Duan, J. Qiao, D. Zhang, G. Dong, L. Wang and Y. Qiu, *Synth. Met.*, 2013, **166**, 52–56; (*e*) F. Dumur, G. Nasr, G. Wantz, C. R. Mayer, E. Dumas, A. Guerlin, F. Miomandre, G. Clavier, D. Bertin and D. Gigmes, *Org. Electron.*, 2011, **12**, 1683–1694; (*f*) C. Wu, H.-F. Chen, K.-T. Wong and M. E. Thompson, *J. Am. Chem. Soc.*, 2010, **132**, 3133–3139; (*g*) F. Dumur, D. Bertin, C. R. Mayer, A. Guerlin, G. Wantz, G. Nasr, E. Dumas, F. Miomandre, G. Clavier and D. Gigmes, *Synth. Met.*, 2011, **161**, 1934–1939.

16 S. Suprouse, K. A. King, P. J. Spellane and R. J. Watts, *J. Am. Chem. Soc.*, 1984, **106**, 6647–6653.

17 M. Nonoyama, *Bull. Chem. Soc. Jpn.*, 1974, **47**, 767–768.

18 Z. Molphy, A. Prisecaru, C. Slator, N. Barron, M. McCann, J. Colleran, D. Chandran, N. Gathergood and A. Kellett, *Inorg. Chem.*, 2014, **53**, 5392–5404.

19 *CrysAlisPro 1.171.38.34a*, Rigaku OD, 2015.

20 A. Altomare, G. Cascarano, C. Giacovazzo and A. Gualardi, *J. Appl. Crystallogr.*, 1993, **26**, 343–350.

21 G. M. Sheldrick, *Acta Crystallogr., Sect. C: Cryst. Struct. Commun.*, 2015, **71**, 3–8.

22 C. Lee, W. Yang and R. Parr, *Phys. Rev. B: Condens. Matter Mater. Phys.*, 1988, **37**, 785–789.

23 A. D. Becke, *J. Chem. Phys.*, 1993, **98**, 5648–5652.

24 T. H. Dunning Jr. and P. J. Hay, *Modern Theoretical Chemistry*, Plenum, New York, 1976, pp. 1–28.

25 M. M. Francl, *J. Chem. Phys.*, 1982, **77**, 3654–3665.

26 S. Dapprich, I. Komáromi, K. S. Byun, K. Morokuma and M. J. Frisch, *J. Mol. Struct.: THEOCHEM.*, 1999, **461–462**, 1–21.

27 L. W. Chung, W. M. C. Sameera, R. Ramozzi, A. J. Page, M. Hatanaka, G. P. Petrova, T. V. Harris, X. Li, Z. Ke, F. Liu, H.-B. Li, L. Ding and K. Morokuma, *Chem. Rev.*, 2015, **115**, 5678–5796.

28 W. J. Hehre, R. F. Stewart and J. A. Pople, *J. Chem. Phys.*, 1969, **51**, 2657–2664.

29 E. Cancès, B. Mennucci and J. Tomasi, *J. Chem. Phys.*, 1997, **107**, 3032–3041.

30 B. Mennucci and J. Tomasi, *J. Chem. Phys.*, 1997, **106**, 5151–5158.

31 M. Cossi, V. Barone, B. Mennucci and J. Tomasi, *Chem. Phys. Lett.*, 1998, **286**, 253–260.

32 M. Frisch, G. Trucks, H. Schlegel, G. Scuseria, M. Robb, J. Cheeseman, G. Scalmani, V. Barone, B. Mennucci, G. Petersson, H. Nakatsuji, M. Caricato, X. Li, H. Hratchian, A. Izmaylov, J. Bloino, G. Zheng, J. Sonnenberg, M. Hada, M. Ehara, K. Toyota, R. Fukuda, J. Hasegawa, M. Ishida, T. Nakajima, Y. Honda, O. Kitao, H. Nakai, T. Vreven, J. Montgomery, J. Peralta, F. Ogliaro, M. Bearpark, J. Heyd, E. Brothers, K. Kudin, V. Staroverov, R. Kobayashi, J. Normand, K. Raghavachari, A. Rendell, J. Burant, S. Iyengar, J. Tomasi, M. Cossi, N. Rega, J. Millam, M. Klene, J. Knox, J. Cross, V. Bakken, C. Adamo, J. Jaramillo, R. Gomperts, R. Stratmann, O. Yazyev, A. Austin, R. Cammi, C. Pomelli, J. Ochterski, R. Martin, K. Morokuma, V. Zakrzewski, G. Voth, P. Salvador, J. Dannenberg, S. Dapprich, A. Daniels, F. J. Foresman, J. Ortiz, J. Cioslowski and D. Fox, *Gaussian 09, Revision B.01*,Gaussian Inc., Wallingford CT, 2009.

33 (*a*) E. A. Plummer, A. van Dijken, J. W. Hofstraat, L. De Cola and K. Brunner, *Adv. Funct. Mater.*, 2005, **15**, 281–289; (*b*) K. K.-W. Lo, C.-K. Chung, T. K.-M. Lee, L.-H. Lui, K. H.-K. Tsang and N. Zhu, *Inorg. Chem.*, 2003, **42**, 6886–6897; (*c*) K. K.-W. Lo, J. S.-W. Chan, C.-K. Chung, V. W.-H. Tsang and N. Zhu, *Inorg. Chim. Acta*, 2004, **357**, 3109–3118; (*d*) M. S. Lowry, W. R. Hudson, R. A. Pascal Jr. and S. Bernhard, *J. Am. Chem. Soc.*, 2004, **126**, 14129–14135; (*e*) S. Salinas, M. A. Soto-Arriaza and B. Loeb, *Polyhedron*, 2011, **30**, 2863–2869; (*f*) C. Dragonetti, A. Valore, A. Colombo, S. Righetto and V. Trifiletti, *Inorg. Chim. Acta*, 2012, **388**, 163–167; (*g*) K. Huang, I. W. Bulik and A. A. Marti, *Chem. Commun.*, 2012, **48**, 11760–11762; (*h*) K.-H. Leung, H.-Z. He, V. P.-Y. Ma, H.-J. Zhong, D. S.-H. Chan, J. Zhou, J.-L. Mergny, C.-H. Leung and D.-L. Ma, *Chem. Commun.*, 2013, **49**, 5630–5632; (*i*) D.-L. Ma, L.-J. Liu, K.-H. Leung, Y.-T. Chen, H.-J. Zhong, D. S.-H. Chan, H.-M. D. Wang and C.-H. Leung, *Angew. Chem., Int. Ed.*, 2014, **53**, 9178–9182; (*j*) H. Ahmad, A. Wragg, W. Cullen, C. Wombwell, A. J. H. M. Meijer and J. A. Thomas, *Chem. – Eur. J.*, 2014, **20**, 3089–3096; (*k*) Z. Wu, J. Mu, Q. Wang, X. Chen, L. Jensen, Ch. Yi and M.-J. Li, *J. Organomet. Chem.*, 2015, **791**, 175–182.

34 Y. Ohsawa, S. Sprouse, K. A. King, M. K. De Armond, K. W. Hanck and R. J. Watts, *J. Phys. Chem.*, 1987, **91**, 1047–1054.

35 (*a*) A. Loupy, in *Microwaves in Organic Synthesis*, ed. A. Loupy, Wiley-VCH, Weinheim, 1st edn, 2002, p. 499; (*b*) A. Loupy, in *Microwaves in Organic Synthesis*, ed.

A. Loupy, Wiley-VCH Verlag GmbH, Weinheim, Germany, 2nd edn, 2008, p. 1007; (*c*) J. P. Tierney and P. Lidstrom, in *Microwave Assisted Organic Synthesis*, ed. J. P. Tierney and P. Lidstrom, Blackwell Publishing, Oxford, U.K., 2005, pp. xi+280.

36 A. de la Hoz, Á. Díaz-Ortiz and A. Moreno, *Chem. Soc. Rev.*, 2005, **34**, 164–178.

37 (*a*) R. Xu and Y. Xu, in *Modern Inorganic Synthetic Chemistry*, ed. R. Xu and Y. Xu, Elsevier Science, 2nd edn, 2017, p. 808; (*b*) R. Xu, W. Pang and Q. Huo, in *Modern Inorganic Synthetic Chemistry*, ed. R. Xu, W. Pang and Q. Huo, Elsevier, 1st edn, 2011, p. 590.

38 (*a*) N. Yoshikawa, Y. Masuda and T. Matsumura-Inoue, *Chem. Lett.*, 2000, **29**, 1206–1207; (*b*) S. L. Van Atta, B. A. Duclos and D. B. Green, *Organometallics*, 2000, **19**, 2397–2399; (*c*) B. I. K. Oxana, V. Kharissova and U. O. Mendez, in *Advances in Induction and Microwave Heating of Mineral and Organic Materials*, InTech, 2011, p. 766; (*d*) H. Phetmung, M. Wateh and C. Pakawatchai, *Turk. J. Chem.*, 2012, **36**, 556–566; (*e*) J. Lhoste, N. Henry, T. Loiseau and F. Abraham, *Inorg. Chem. Commun.*, 2011, **14**, 1525–1527; (*f*) T. Abe, A. Miyazawa, Y. Kawanishi and H. Konno, *Mini-Rev. Org. Chem.*, 2011, **8**, 315–333; (*g*) J.-R. Li, Z.-L. Xie, B. Hu and X.-Y. Huang, *Inorg. Chem. Commun.*, 2011, **14**, 265–267; (*h*) H. Konno, T. Ito and Y. Sugita, Method for producing complex of trisortho-metalated iridium, light-emitting material using said complex, and light-emitting element. *Jpn. Pat* 5881216, 2016.

39 J. C. Deaton, Synthesis of organometallic cyclometallated transition metal complexes, Kodak Ltd., *EP* 1762123(B1), 2008.

40 (*a*) I. Kownacki, B. Orwat, B. Marciniec, G. Wiosna-Sałyga, B. Łuszczyńska, I. Głowacki and J. Ulański, New ionic iridium(III) complexes and a method for their synthesis and their use as phosphorescent emitters, *Pat. Appl* PL418615, 2016; (*b*) I. Kownacki, B. Orwat and B. Marciniec, A method for the synthesis of iridium(III) ionic complexes, *Pat. Appl* PL418616, 2016; (*c*) G. Wiosna-Sałyga, B. Łuszczyńska, I. Głowacki, J. Ulański, I. Kownacki, B. Orwat and B. Marciniec, Organic light emitting diodes with the new emission layers, *Pat. Appl* PL418617, 2016.

41 S. Kammer, I. Starke, A. Pietrucha, A. Kelling, W. Mickler, U. Schilde, C. Dosche, E. Kleinpeter and H.-J. Holdt, *Dalton Trans.*, 2012, **41**, 10219–10227.

42 K. Hasan, A. K. Bansal, I. D. W. Samuel, C. Roldán-Carmona, H. J. Bolink and E. Zysman-Colman, *Sci. Rep.*, 2015, **5**, 12325, DOI: 10.1038/srep12325.

43 A. M'hamedi, A. S. Batsanov, M. A. Fox, M. R. Bryce, K. Abdullah, H. A. Al-Attar, *et al.*, *J. Mater. Chem.*, 2012, **22**, 13529–13540.

44 Z.-G. Niu, D. Liu, D.-C. Li, J. Zuo, J.-M. Yang, Y.-H. Su, *et al.*, *Inorg. Chem. Commun.*, 2014, **43**, 146–150.

45 Q.-L. Xu, C.-C. Wang, T.-Y. Li, M.-Y. Teng, S. Zhang, Y.-M. Jing, *et al.*, *Inorg. Chem.*, 2013, **52**, 4916–4925.

46 G.-N. Li, C.-W. Gao, H. Xie, H.-H. Chen, D. Liu, W. Sun, *et al.*, *Chin. Chem. Lett.*, 2016, **27**, 428–432.

47 P. Hirva, M. Haukka, M. Jakonen and M. A. Moreno, *J. Mol. Model.*, 2008, **14**, 171–181.

48 E. Baranoff, B. F. E. Curchod, F. Monti, F. Steimer, G. Accorsi, I. Tavernelli, U. Rothlisberger, R. Scopelliti, M. Grätzel and M. K. Nazeeruddin, *Inorg. Chem.*, 2012, **51**, 799–811.

49 X. Shang, D. Han, D. Li and Z. Wu, *Chem. Phys. Lett.*, 2013, **565**, 12–17.

50 Ł. Skórka, M. Filapek, L. Zur, J. G. Malecki, W. Pisarski, M. Olejnik, W. Danikiewicz and S. Krompiec, *J. Phys. Chem. C*, 2016, **120**, 7284–7294.

51 S. Xu, J. Wang, H. Xia, F. Zhao and Y. Wang, *J. Mol. Model.*, 2015, **21**, 943–910.

52 C. S. K. Mak, A. Hayer, S. I. Pascu, S. E. Watkins, A. B. Holmes, A. Köhler and R. H. Friend, *Chem. Commun.*, 2005, 4708–4710.

53 Y. You and W. Nam, *Chem. Soc. Rev.*, 2012, **41**, 7061–7084.

54 H. Yersin, A. F. Rausch, R. Czerwieniec, T. Hofbeck and T. Fischer, *Coord. Chem. Rev.*, 2011, **255**, 2622–2652.

55 F. De Angelis, S. Fantacci, N. Evans, C. Klein, S. M. Zakeeruddin, J.-E. Moser, K. Kalyanasundaram, H. J. Bolink, M. Gratzel and M. K. Nazeeruddin, *Inorg. Chem.*, 2007, **46**, 5989–6001.

56 G. A. Crosby, *Acc. Chem. Res.*, 1975, **8**, 231–238.

57 (*a*) B. Luszczynska, E. Dobruchowska, I. Glowacki, J. Ulanski, F. Jaiser, X. Yang, D. Neher and A. Danel, *J. Appl. Phys.*, 2006, **99**, 24505, DOI: 10.1063/1.2162268; (*b*) I. Glowacki and Z. Szamel, *J. Phys. D: Appl. Phys.*, 2010, **43**, 295101–295110.

58 (*a*) I. Glowacki, Z. Szamel and G. Wiosna–Salyga, *Org. Electron.*, 2016, **31**, 127–135; (*b*) I. Glowacki, Z. Szamel and G. Wiosna–Salyga, *Synth. Met.*, 2016, **220**, 213–220; (*c*) B. Luszczynska, E. Dobruchowska, I. Glowacki, A. Danel and J. Ulanski, *J. Lumin.*, 2009, **129**, 1215–1218.

59 A. Visser, E. Vysotsky and J. Lee, *Critical Transfer Distance Determination Between FRET Pairs*, 2011.

60 P. Dreyse, B. Loeb, M. Barrera and I. Gonzalez, *J. Chil. Chem. Soc.*, 2014, **59**, 2628–2631.

Electronic Supplementary Information

Microwave-assisted one-pot synthesis of new ionic iridium complexes of $[Ir(bzq)_2(N\hat{}N)]^+A^-$ type and their selected electroluminescent properties

B. Orwat,[a] E. Witkowska,[b] I. Kownacki,*[a] M.-J. Oh,[a] M. Hoffmann,[a] M. Kubicki,[a] I. Grzelak,[a] B. Marciniec,[a,c] I. Głowacki,[b] B. Luszczynska,[b] G. Wiosna-Salyga,[b] J. Ulanski,[b] P. Ledwon,[d] M. Lapkowski,[d,e]

[a] *Faculty of Chemistry, Adam Mickiewicz University in Poznan, St. Umultowska 89b, 61-614 Poznan, Poland, E-mail: Ireneusz.Kownacki@amu.edu.pl*

[b] *Department of Molecular Physics, Lodz University of Technology, 90-924 Lodz, Zeromskiego 116, Poland*

[c] *Center for Advanced Technologies, Adam Mickiewicz University in Poznan, St. Umultowska 89c, 61-614 Poznan, Poland*

[d] *Silesian University of Technology, Faculty of Chemistry, St. Marcina Strzody 9, 44-100 Gliwice, Poland*

[e] *Centre of Polymer and Carbon Materials, Polish Academy of Sciences, Curie-Sklodowskiej 34, 41-819 Zabrze, Poland*

E-mail: Ireneusz.Kownacki@amu.edu.pl

Table of contents

Table 1S. Selected optimized ground-state parameters of 2FA' in gas phase and CH_3CN media at B3LYP/SDD level **3**

Table 2S. Selected optimized ground-state parameters of 2FA' in CH_3CN media using B3LYP functional containing different basis sets **4**

Table 3S. The energy levels and HOMO-LUMO energy gaps for the studied complexes (in eV) calculated at the B3LYP/LANL2DZ/6-311++G(d,p) level of theory together with the experimental results **5**

Table 4S. The energy levels and HOMO-LUMO energy gaps for the studied complexes (in eV) calculated at the M06/LANL2DZ/6-311++G(d,p) level of theory together with the experimental results **6**

Table 5S. The HOMO-LUMO energy gaps for the studied complexes (in eV) calculated by ONIOM method using WB97XD functional containing different basis sets **7**

Table 6S. Cartesian coordinates from the optimized structures of S_0 in CH_3CN media for **2FA'** **8**

Table 7S. Cartesian coordinates from the optimized structures of S_0 in CH_3CN media for **2GA'** **10**

Table 8S. Cartesian coordinates from the optimized structures of S_0 in CH_3CN media for **2HA'** **12**

Table 9S. Cartesian coordinates from the optimized structures of S_0 in CH_3CN media for **2AA'** **15**

Table 10S. Cartesian coordinates from the optimized structures of S_0 in CH_3CN media for **2CA'** **17**

Table 11S. Cartesian coordinates from the optimized structures of S_0 in CH_3CN media for **2BA'** **19**

Table 12S. Cartesian coordinates from the optimized structures of S_0 in CH_3CN media for **2DA'** **21**

Table 13S. Cartesian coordinates from the optimized structures of S_0 in CH_3CN media for **2EA'** **23**

Equation 1S. **25**

Table 14S. **26**

Figure 1S. Calculated oxidation potential (vertical) *vs* experimental oxidation onset potential (horizontal) for studied compounds. **27**

Table 15S. Crystal data, data collection and structure refinement **28**

Figure 2S. TGA curves **29**

Table 1S. Selected optimized ground-state parameters of 2FA' in gas phase and CH_3CN media at B3LYP/SDD level.

	gas	CH_3CN
	Bond lengths (Å)	
Ir-N15	2.104	2.104
Ir-N29	2.070	2.073
Ir-C49	2.125	2.123
	Bond angles (deg)	
N15-Ir-N49	88.4	88.6
C5-Ir-N19	96.0	95.4
C5-Ir-N29	89.9	90.2
N15-Ir-C5	79.6	79.6
N15-Ir-N19	174.0	173.5
N29-Ir-N49	173.9	173.5
C5-Ir-C59	172.3	172.5
N15-Ir-N29	96.1	96.0

Table 2S. Selected optimized ground-state parameters of 2FA' in CH_3CN media using B3LYP functional containing different basis sets

	Basis sets	Bond lengths (Å)
Ir-N15	6-31G*	2.104
	6-31++G**	2.104
	6-311++G**	2.104
Ir-N29	6-31G*	2.073
	6-31++G**	2.073
	6-311++G**	2.073
Ir-C49	6-31G*	2.105
	6-31++G**	2.105
	6-311++G**	2.105
	Basis sets	Valence angle (deg)
N15-Ir-N49	6-31G*	88.6
	6-31++G**	88.6
	6-311++G**	88.6
C5-Ir-N19	6-31G*	95.4
	6-31++G**	95.4
	6-311++G**	95.4
C5-Ir-N29	6-31G*	90.2
	6-31++G**	90.2
	6-311++G**	90.2
N15-Ir-C5	6-31G*	79.6
	6-31++G**	79.6
	6-311++G**	79.6
N15-Ir-N19	6-31G*	173.5
	6-31++G**	173.5
	6-311++G**	173.5
N15-Ir-N29	6-31G*	96.0
	6-31++G**	96.0
	6-311++G**	96.0
N29-Ir-N49	6-31G*	173.5
	6-31++G**	173.5
	6-311++G**	173.5
C5-Ir-C59	6-31G*	172.7
	6-31++G**	172.7
	6-311++G**	172.7

Table 3S. The energy levels and Homo-Lumo energy gaps for the studied complexes (in eV) calculated at the B3LYP/LANL2DZ/6-311++G(d,p) level of theory together with the experimental results.

compound	HOMO [eV]	LUMO [eV]	$E_g^{theor.}$ [eV]	$E_g^{exp.}$ [eV]
2AA’	-5,75	-2,48	3,27	2.40
2BA’	-5,72	-2,42	3,29	2.21
2CA’	-5,79	-2,44	3,35	2.20
2DA’	-5,69	-2,38	3,31	2.24
2EA’	-5,59	-2,32	3,27	1.73
2FA’	-5,84	-2,44	3,40	2.40
2GA’	-5,82	-2,47	3,34	2.17
2HA’	-5,77	-2,43	3,34	2.09

Table 4S. The energy levels and Homo-Lumo energy gaps for the studied complexes (in eV) calculated at the M06/LANL2DZ/6-311++G(d,p) level of theory together with the experimental results.

compound	HOMO [eV]	LUMO [eV]	$\Delta E_{theor.}$ [eV]	$\Delta E_{exp.}$ [eV]
2AA’	-8,06	-5,22	2,84	2.40
2BA’	-8,15	-4,76	3,39	2.21
2CA’	-8,21	-4,82	3,39	2.20
2DA’	-8,10	-4,78	3,32	2.24
2EA’	-8,07	-4,59	3,47	1.73
2FA’	-8,03	-5,14	2,89	2.40
2GA’	-7,92	-4,66	3,25	2.17
2HA’	-8,00	-4,50	3,51	2.09

Table 5S. The HOMO-LUMO energy gaps for the studied complexes (in eV) calculated by ONIOM method using WB97XD functional containing different basis sets.

compound	E_1 [eV]	E_2 [eV]	E_3 [eV]	$E_g^{teor.}$ [eV]	$E_g^{exp.}$ [eV]
2AA’	9.62	6.21	9.13	2.17	2.40
2BA’	9.68	6.23	9.14	2.22	2.21
2CA’	9.53	6.30	9.05	2.32	2.20
2DA’	9.73	6.24	9.18	2.27	2.24
2EA’	9.80	6.04	9.10	1.83	1.73
2FA’	9.55	6.32	8.84	2.28	2.40
2GA’	9.46	6.10	8.85	2.32	2.17
2HA’	9.51	6.22	8.82	2.04	2.09

Table 6S. Cartesian coordinates from the optimized structures of S_0 in CH_3CN media for **2FA'**.

Atom symbol	X	Y	Z
Ir	-0.04074265	-0.00041241	0.00005571
C	0.67372352	-4.39211403	-2.21606153
C	1.39406753	-3.96446035	-1.07822972
C	1.08915394	-2.68275189	-0.54445639
C	0.10531347	-1.81291059	-1.09526249
C	-0.57199609	-2.29084914	-2.21677343
C	-0.29082481	-3.56320364	-2.76805893
C	2.41340163	-4.75661981	-0.44267781
C	3.09156471	-4.30475701	0.65289019
C	2.80966455	-3.01304571	1.21738014
C	1.80570489	-2.22201657	0.60418346
C	3.46905801	-2.48383757	2.34463729
C	3.12060945	-1.22770838	2.81217491
C	2.11658236	-0.50128657	2.15803636
N	1.47212836	-0.97997218	1.08638983
C	-4.00901040	1.60821962	-2.31862031
C	-4.07749341	0.79638652	-1.16585796
C	-2.85581538	0.39261501	-0.58242881
N	-1.63649291	0.75514275	-1.08671679
C	-1.60113535	1.52448307	-2.17858177
C	-2.77014882	1.96681475	-2.81784162
C	-5.30391187	0.35961656	-0.55777116
C	-5.29897962	-0.42746080	0.55703077
C	-4.06721527	-0.84876013	1.16522816
C	-2.85066487	-0.42934244	0.58213160
C	-3.98863831	-1.65997311	2.31778287
C	-2.74539290	-2.00264540	2.81732881
C	-1.58195908	-1.54517343	2.17851968
N	-1.62689853	-0.77626206	1.08668482
H	-6.23219545	-0.75073552	1.00686437
H	-6.24111695	0.67113090	-1.00764493
H	-4.92220653	1.94198902	-2.80040629
H	-2.67877270	2.58857005	-3.70073132
H	-0.62095339	1.79158820	-2.55255440
H	-4.89762699	-2.00566890	2.79914611
H	-2.64627858	-2.62339995	3.70008768
H	-0.59855439	-1.79985557	2.55276980
H	1.81527359	0.48132454	2.49836289
H	3.60768892	-0.79120722	3.67638789
H	4.24395491	-3.06395623	2.83712261

H	3.85867450	-4.91480942	1.12051728
H	2.64047689	-5.73607918	-0.85545874
H	0.88266770	-5.36655317	-2.64888470
H	-0.84287304	-3.89643725	-3.64371120
H	-1.33778307	-1.68246109	-2.69471217
C	3.43693632	2.52870959	-2.34399353
C	2.77037254	3.04931242	-1.21696890
C	1.77671841	2.24521752	-0.60395664
N	1.45954937	0.99883809	-1.08611492
C	2.11072466	0.52847086	-2.15743996
C	3.10527026	1.26800247	-2.81136566
C	3.03511372	4.34469264	-0.65258011
C	2.35074257	4.78778331	0.44269967
C	1.34179464	3.98234894	1.07813224
C	1.05397779	2.69662888	0.54450014
C	0.61558762	4.40066362	2.21571410
C	-0.33793904	3.55912281	2.76774228
C	-0.60207463	2.28303917	2.21665916
C	0.08165168	1.81394165	1.09531037
H	2.56483203	5.77019153	0.85541323
H	3.79432013	4.96468217	-1.12004107
H	4.20425371	3.11890134	-2.83637661
H	3.59841470	0.83781141	-3.67529962
H	1.82282874	-0.45817962	-2.49773007
H	0.81145016	5.37791360	2.64832258
H	-0.89459866	3.88520224	3.64316794
H	-1.35990245	1.66465013	2.69446558

Table 7S. Cartesian coordinates from the optimized structures of S_0 in CH_3CN media for **2GA'**.

Atom symbol	X	Y	Z
C	-4.37617909	3.71944412	-2.06713798
C	-4.05358308	3.05917198	-0.83163171
C	-3.03145770	2.07687492	-0.84724833
C	-2.33615523	1.74117657	-2.05139728
C	-2.67990010	2.41409777	-3.25556031
C	-3.71755091	3.41045348	-3.22257271
C	-1.97786787	2.06225858	-4.43012443
C	-0.99262204	1.08846859	-4.37393084
C	-0.67317267	0.43268591	-3.16171160
C	-4.69013047	3.32893442	0.39620848
C	-4.30264553	2.63827599	1.53223399
C	-3.28251566	1.68164496	1.44455978
H	-5.15794854	4.47310987	-2.05958374
H	-3.97493564	3.92116240	-4.14683913
H	0.10821986	-0.32508513	-3.17959028
H	-2.21632791	2.55749423	-5.36733154
H	-0.45405827	0.82156975	-5.28020499
H	-5.47805399	4.07503284	0.44250431
H	-4.77142630	2.82135736	2.49212257
H	-2.95166502	1.12595341	2.31289089
C	-4.28273688	-2.77769181	-1.34518055
C	-4.58169451	-3.48118917	-0.19035300
C	-3.29574967	-1.78359940	-1.31229045
C	-3.88991456	-3.18658528	1.00137596
C	-4.12038824	-3.85661776	2.25216030
C	-2.90504404	-2.16759563	0.96196966
C	-3.41111477	-3.52256278	3.37005012
C	-2.15722683	-1.80574074	2.12640223
C	-2.40980046	-2.48938954	3.34691832
C	-1.65745926	-2.11115953	4.48148833
C	-0.48497154	-0.43583190	3.14511336
C	-0.71328885	-1.10179860	4.37235929
H	-4.79600701	-2.97922819	-2.27824891
H	-5.34232199	-4.25645275	-0.19463921
H	-4.87362315	-4.63806984	2.28679702
H	-3.03318487	-1.21656017	-2.19654749
H	-3.59892199	-4.04107751	4.30661278
H	-1.82564159	-2.61399289	5.42984759
H	0.26707362	0.35098572	3.12110101
H	-0.13624729	-0.81424956	5.24812829
Ir	-1.12792435	-0.01248321	0.00694070
H	1.41614752	4.36406862	1.22299433

H	-0.59781832	2.98863113	0.82502594
C	0.38973913	2.56547041	0.69333912
C	1.53721382	3.33470768	0.90607839
C	2.81068975	2.79271392	0.75299489
N	0.45015056	1.27888660	0.33985270
C	2.89248453	1.42995808	0.33308860
C	1.68423427	0.71638730	0.15303002
N	0.47371427	-1.24753338	-0.41551754
C	1.69697416	-0.65329199	-0.25727238
C	4.11513887	0.74401350	0.02385836
C	0.43748363	-2.52021511	-0.81908104
C	2.91808050	-1.32629359	-0.49656957
H	-0.54174014	-2.96595809	-0.93773062
C	4.12711314	-0.56265526	-0.37051255
C	1.59917195	-3.25765893	-1.06499368
C	2.86219526	-2.69615208	-0.89696762
H	1.49774916	-4.29439500	-1.36423153
C	4.00525184	3.63149146	1.02075421
C	4.10186563	4.91233156	0.44978819
C	5.20151436	5.72653229	0.71881023
C	6.21433540	5.27953263	1.57095363
C	6.12224649	4.01310030	2.15329778
C	5.02838078	3.19212520	1.87937289
H	3.32221402	5.25972378	-0.22148557
H	5.26746382	6.70886244	0.26101959
H	7.06882039	5.91531040	1.78209291
H	6.89930232	3.66435211	2.82664397
H	4.95357628	2.21902717	2.35464170
C	4.07286962	-3.52002554	-1.13898159
C	5.09820128	-3.61267831	-0.18131083
C	6.20788642	-4.42608007	-0.41083831
C	6.31388623	-5.15251542	-1.59932734
C	5.29899698	-5.06957721	-2.55577799
C	4.18357064	-4.26498142	-2.32581984
H	5.01343939	-3.06979393	0.75488296
H	6.98671611	-4.49561783	0.34245101
H	7.18079345	-5.78145539	-1.77774455
H	3.40244109	-4.19563279	-3.07692001
H	5.37549362	-5.62973890	-3.48273653
H	5.04769125	1.29072985	0.08596495
H	5.06873732	-1.03666097	-0.61750085
C	-1.19599633	-0.76344921	1.99077298
N	-2.62050624	-1.48465394	-0.19522153
N	-2.65864932	1.40633476	0.29206400
C	-1.33181626	0.73457911	-1.96989786

Table 8S. Cartesian coordinates from the optimized structures of S_0 in CH_3CN media for 2HA'.

Atom symbol	X	Y	Z
C	4.83341604	2.55261455	-2.98207193
C	3.60503050	1.82072905	-3.14334864
C	2.93255255	1.34474917	-1.98450027
C	3.48538315	1.63050700	-0.69614407
C	4.69325679	2.35877856	-0.55385179
C	5.35804776	2.80653678	-1.74732302
N	2.77513009	1.19288020	0.39386006
C	5.16258940	2.60892313	0.75096788
C	4.43757979	2.14664467	1.83661689
C	3.24661285	1.43990597	1.62149188
C	3.02362346	1.54624680	-4.40115994
C	1.83394929	0.83650504	-4.46490889
C	1.19249623	0.36558147	-3.29546407
C	1.72056300	0.59456553	-2.02402810
H	5.34595632	2.90683395	-3.87258653
H	6.28614708	3.36053468	-1.64292105
H	2.65256639	1.07053408	2.44775655
H	6.08525160	3.16334042	0.89536685
H	4.76871079	2.32240856	2.85355136
H	3.51142170	1.89566192	-5.30689918
H	1.38647478	0.63225116	-5.43480275
H	0.26505339	-0.19279844	-3.40909738
C	4.44506254	-2.82835655	-0.45682533
C	4.40474825	-3.50564168	0.75027681
C	3.49692771	-1.83170773	-0.71928224
C	3.42987290	-3.15907820	1.70623240
C	3.32208387	-3.77550761	3.00013685
C	2.51210627	-2.12823935	1.37730966
C	2.38129715	-3.36267520	3.89891477
C	1.53234810	-1.67644573	2.31552864
C	1.46851384	-2.29299023	3.59538300
C	0.69925707	-0.59256860	1.91798362
C	0.51394261	-1.80538812	4.51523987
C	-0.21247268	-0.14731586	2.87602302
C	-0.30574276	-0.74797749	4.15335248
N	2.53927425	-1.50310096	0.15585853
H	5.18965112	-3.05783111	-1.21015713
H	5.12143608	-4.29117987	0.97102016
H	4.01439187	-4.57418952	3.24917256
H	3.49256305	-1.29867342	-1.66114451

H	2.31837165	-3.83616023	4.87517039
H	0.43697844	-2.25666014	5.50056281
H	-0.87794455	0.68499935	2.65717883
H	-1.03332636	-0.36798745	4.86663913
Ir	1.08957826	0.01983970	-0.08312040
H	-1.49592286	4.58352787	0.58551921
C	-0.42608828	2.77363356	0.19418142
C	-1.59768817	3.51417843	0.44322175
C	-2.85472078	2.93937244	0.47815031
N	-0.47932877	1.44184962	-0.00696686
C	-2.92705083	1.53938440	0.22575913
C	-1.71940561	0.84334806	-0.03618865
N	-0.56259700	-1.15118584	-0.67600283
C	-1.76415420	-0.54520070	-0.39360934
C	-4.15225470	0.80055275	0.25903985
C	-0.58364594	-2.39773384	-1.18436849
C	-3.01112366	-1.21150649	-0.49241347
C	-4.19313803	-0.51592941	-0.08451069
C	-1.79731615	-3.09878613	-1.32164859
C	-3.01876253	-2.55432102	-0.96997688
H	-1.75729990	-4.09693239	-1.74192972
C	-4.04380441	3.78938134	0.74351712
C	-4.05413054	4.63854255	1.86328376
C	-5.14288677	5.47500091	2.10853273
C	-6.23068274	5.48609945	1.23227500
C	-6.22484904	4.65525795	0.10924715
C	-5.14198462	3.81012126	-0.13393496
H	-3.21354857	4.62817084	2.55076020
H	-5.14082972	6.11693942	2.98424954
H	-7.07658623	6.13998218	1.42167383
H	-7.06126554	4.66777865	-0.58298837
H	-5.13664702	3.18419157	-1.02079439
C	-4.25662366	-3.35993249	-1.13263767
C	-5.34613619	-2.88777666	-1.88522610
C	-6.47781455	-3.68318760	-2.06569485
C	-6.54147187	-4.95627278	-1.49405494
C	-5.46281829	-5.43563747	-0.74707526
C	-4.32572738	-4.64691333	-0.57253794
H	-5.29714015	-1.90853767	-2.35109143
H	-7.30736026	-3.30909943	-2.65803454
H	-7.42514956	-5.57189231	-1.63238075
H	-3.49193676	-5.02022191	0.01462193
H	-5.50550872	-6.42363638	-0.29873200
H	-5.05804264	1.30860221	0.56456157
H	-5.13135975	-1.05509315	-0.05398862
C	0.87026600	3.52459352	0.13025586

H	1.45023693	3.22657291	-0.74274729
H	1.47651726	3.35259359	1.02272469
H	0.66891049	4.59485155	0.06539819
C	0.67252988	-3.06682239	-1.65784250
H	1.32205908	-2.35521224	-2.16715246
H	0.41603774	-3.86965414	-2.35158386
H	1.22688066	-3.51182306	-0.82762666

Table 9S. Cartesian coordinates from the optimized structures of S_0 in CH_3CN media for **2AA'**.

Atom symbol	X	Y	Z
Ir	0.03254530	0.19326957	0.01063120
C	-4.40781011	-0.27612737	-2.23171768
C	-4.02543670	-1.04112653	-1.11065692
C	-2.73261223	-0.81956257	-0.57172360
N	-1.87404266	0.09797345	-1.10987770
C	-2.26297548	0.80929066	-2.17064157
C	-3.52549351	0.65029342	-2.76173665
C	-4.86304974	-2.02729205	-0.48630998
C	-4.42370088	-2.73349212	0.59593874
C	-3.11484716	-2.52368331	1.15687220
C	-2.25971739	-1.55354998	0.56500551
C	-2.63746290	-3.24061017	2.27640283
C	-1.36601551	-2.98324395	2.76232330
C	-0.53056653	-2.01344862	2.16330702
C	-0.94879567	-1.27129496	1.05815928
C	1.74062658	4.22936232	-2.29096564
C	0.93471352	4.29084265	-1.15759815
C	0.48828695	3.10482767	-0.56623304
N	0.82897336	1.89713429	-1.08531570
C	1.60913933	1.84108888	-2.17737585
C	2.08614319	2.98331863	-2.81189538
C	-0.81674984	4.20446533	1.30121678
C	-0.36690702	3.05946672	0.63818187
C	-1.61675350	4.08233871	2.43261164
C	-1.95447424	2.80799733	2.88309884
C	-1.48069722	1.70300689	2.18679433
N	-0.70505347	1.81622530	1.08996169
H	2.09328410	5.14276162	-2.75748685
H	2.71281795	2.88894568	-3.69103342
H	1.84914825	0.84923388	-2.54246580
H	-1.96780542	4.96783942	2.95095123
H	-2.57386223	2.65962804	3.75987471
H	-1.71016988	0.69298745	2.49931269
H	0.45667541	-1.84807097	2.58439013
H	-0.99949540	-3.53683175	3.62323942
H	-3.27196834	-3.98731018	2.74554359
H	-5.06859361	-3.47642629	1.05778748
H	-5.85420017	-2.19873470	-0.89576919
H	-5.39082161	-0.41979482	-2.67082026

H	-3.78947668	1.25328036	-3.62296726
H	-1.54889336	1.52427356	-2.56542939
C	2.50647574	-3.30448687	-2.33565835
C	3.02612280	-2.64219231	-1.20542620
C	2.22312422	-1.64461171	-0.60215370
N	0.98314252	-1.31552414	-1.08579183
C	0.51197967	-1.96251827	-2.15821870
C	1.24968292	-2.96169484	-2.80852945
C	4.31381924	-2.90727198	-0.62261638
C	4.74469014	-2.21927252	0.47648269
C	3.93605191	-1.20411515	1.09983240
C	2.66121087	-0.92058125	0.54430897
C	4.33552376	-0.46903567	2.23795111
C	3.48333015	0.49033525	2.76482673
C	2.21683690	0.75507708	2.19408860
C	1.76951818	0.05645516	1.07284610
H	5.72127878	-2.43505970	0.90169913
H	4.93926536	-3.66935035	-1.07795794
H	3.09132802	-4.07694222	-2.82617565
H	0.82021984	-3.45250514	-3.67416419
H	-0.47290441	-1.67460329	-2.50444729
H	5.30448312	-0.65970651	2.69050987
H	3.79404941	1.05512647	3.64035384
H	1.59209406	1.51621220	2.65398665
H	0.66136402	5.25235260	-0.74257847
H	-0.54420620	5.18654814	0.93745912

Table 10S. Cartesian coordinates from the optimized structures of S_0 in CH_3CN media for 2CA'.

Atom symbol	X	Y	Z
C	5.27918101	0.28711164	0.42432224
C	4.17907582	-0.36984078	1.07909311
C	2.87209388	-0.22317249	0.53886084
C	2.69832385	0.54787492	-0.65373391
C	3.79386260	1.18163261	-1.29225841
C	5.09757042	1.03283455	-0.70483749
N	1.42741003	0.61663091	-1.16686208
C	3.53855863	1.90888561	-2.47182994
C	2.24660318	1.97451942	-2.96648165
C	1.21249238	1.31619594	-2.28725993
C	4.32712802	-1.16243782	2.23890309
C	3.21308323	-1.76709965	2.80104913
C	1.92273439	-1.59562157	2.24734149
C	1.70705221	-0.81408605	1.11132102
H	6.27398568	0.17817924	0.84823525
H	5.93886329	1.52129566	-1.18722931
H	0.19249608	1.34183148	-2.64938165
H	4.35491182	2.40849129	-2.98521525
H	2.01568069	2.52294961	-3.87234719
H	5.31231997	-1.29500557	2.67729973
H	3.33192795	-2.38306232	3.68931306
H	1.08620499	-2.09110815	2.73670000
C	0.64337296	3.60716595	2.02300233
C	-0.41615463	4.37253649	1.56635405
C	0.75709055	2.27327811	1.61236833
C	-1.34330693	3.80554038	0.67024738
C	-2.45736099	4.52155779	0.11219948
C	-1.15361726	2.45383992	0.28238045
C	-3.29229464	3.92899501	-0.79043954
C	-2.01129708	1.82703638	-0.67460214
C	-3.08831756	2.57349709	-1.22675699
C	-1.70121782	0.48954544	-1.05269188
C	-3.89840653	1.94377846	-2.19765553
C	-2.52722999	-0.06973805	-2.02847622
C	-3.61167929	0.64571983	-2.58859680
N	-0.12547042	1.69752012	0.78732139
H	1.38448885	4.01346165	2.70143020
H	-0.53274228	5.40513289	1.88207436
H	-2.61388425	5.55085000	0.42058790
H	1.56290684	1.64680849	1.97156993

H	-4.12597905	4.48762321	-1.20766428
H	-4.73159158	2.48602287	-2.63602334
H	-2.35107600	-1.08192159	-2.38549355
H	-4.22919219	0.16673910	-3.34472294
Ir	-0.04691756	-0.28233910	0.04177989
C	0.45292485	-2.75210429	-1.87029931
C	0.01081435	-3.91737071	-2.50698173
C	-1.16895173	-4.53428418	-2.11930495
N	-0.27343044	-2.18715098	-0.86606787
C	-1.87089547	-3.99294995	-1.05264652
C	-1.40012185	-2.83360611	-0.43397174
N	-1.44824711	-1.19641687	1.33181503
C	-2.04888255	-2.28739124	0.76861542
C	-1.87048910	-0.77541525	2.55444880
C	-3.16215492	-2.89543207	1.34993114
C	-2.97602134	-1.37183147	3.17172754
C	-3.65130797	-2.41490114	2.55686822
H	-2.77245927	-4.47436525	-0.70203220
H	-3.63965501	-3.74201209	0.87715138
H	0.61423331	-4.32772822	-3.30799434
H	-1.52297406	-5.42972985	-2.61822787
H	-4.52066468	-2.86843511	3.02015676
H	-3.28901963	-1.00157791	4.14101074
C	1.75502902	-2.15634553	-2.31581296
H	2.37451839	-1.88756901	-1.46126422
H	1.59910682	-1.26308909	-2.92492733
H	2.29590820	-2.88357886	-2.92345749
C	-1.14819869	0.31638006	3.28709456
H	-0.07197857	0.24058572	3.13630939
H	-1.36164779	0.23420482	4.35474501
H	-1.47838086	1.30525229	2.95995454

Table 11S. Cartesian coordinates from the optimized structures of S_0 in CH_3CN media for 2BA'.

Atom symbol	X	Y	Z
C	1.66411842	5.00039285	1.03502629
C	1.73466730	3.65929015	1.55409153
C	1.05924286	2.62668700	0.85242268
C	0.33601812	2.94682269	-0.33326767
C	0.27206967	4.26989338	-0.83292894
C	0.96711412	5.29519505	-0.10257846
N	-0.28934034	1.89975528	-0.95985974
C	-0.46812757	4.48865837	-2.01206735
C	-1.09731477	3.41944316	-2.62960856
C	-0.98949912	2.13619890	-2.07528561
C	2.43768964	3.30639942	2.72729408
C	2.44403771	1.98443969	3.14753162
C	1.76211603	0.97270663	2.43285508
C	1.04974887	1.26407080	1.26903711
H	2.18206171	5.79060031	1.57208651
H	0.92592688	6.31369340	-0.47683968
H	-1.47257118	1.28278795	-2.53474232
H	-0.54145618	5.48959641	-2.42709161
H	-1.67609473	3.55326412	-3.53613332
H	2.96651623	4.07023048	3.29039389
H	2.98628209	1.71574178	4.05084731
H	1.79969183	-0.04364305	2.81621720
C	-3.44367015	1.16547150	2.59058652
C	-4.49459114	0.52128400	1.95833241
C	-2.12412570	1.08750280	2.09073598
C	-4.24929562	-0.23003964	0.78751155
C	-5.28746783	-0.92865924	0.07626240
C	-2.91572953	-0.29548527	0.29748938
C	-5.02516290	-1.65091289	-1.05189156
C	-2.65389335	-1.05557099	-0.88925787
C	-3.69022475	-1.73791788	-1.57596202
N	-1.35865578	-1.08447971	-1.32518156
C	-3.34217880	-2.45996439	-2.73614092
C	-1.05769456	-1.77646307	-2.42614905
C	-2.02435748	-2.47921856	-3.16131932
C	-1.81982332	0.35789179	0.94069634
H	-3.63425679	1.74444110	3.49090070
H	-5.50509246	0.58708598	2.35189359
H	-6.30255861	-0.87142135	0.46024885
H	-1.33500646	1.60905848	2.62426329

H	-5.82222066	-2.17188496	-1.57421097
H	-4.10998532	-2.99456866	-3.28795612
H	-0.01772467	-1.76795948	-2.73443481
H	-1.72547298	-3.02429151	-4.04934717
Ir	-0.01627989	0.06312428	0.01091133
C	2.44289752	0.12251765	-1.98448667
C	3.62378158	-0.32805892	-2.55645868
C	4.21097482	-1.51376449	-2.09290909
N	1.82187705	-0.53624000	-0.99071222
C	3.55704729	-2.18846608	-1.05869253
C	2.36883651	-1.68545869	-0.52149132
N	0.48704817	-1.70748295	0.98651289
C	1.62085917	-2.34141629	0.57259837
C	-0.23654676	-2.25875859	1.98280560
C	2.02688838	-3.53844859	1.16671739
C	0.12602504	-3.44365866	2.60300846
C	1.28586919	-4.11798107	2.19868430
H	3.98312089	-3.10795292	-0.67643203
H	2.92944202	-4.02948126	0.82496175
H	4.08024704	0.24436464	-3.35699152
H	-0.49883162	-3.83460881	3.39891893
H	1.96632630	1.03556559	-2.32203437
H	-1.12465064	-1.71457067	2.27624451
C	5.49366546	-2.03182597	-2.68493042
H	5.38929615	-2.17774529	-3.76499860
H	5.78944369	-2.98133445	-2.23447558
H	6.30452016	-1.31114394	-2.53420810
C	1.71111590	-5.40505828	2.85072475
H	2.61360010	-5.81038588	2.38903520
H	0.91673358	-6.15506633	2.77805631
H	1.90927963	-5.24823917	3.91642521

Table 12S. Cartesian coordinates from the optimized structures of S_0 in CH_3CN media for 2DA'.

Atom symbol	X	Y	Z
C	-2.73905343	-4.59399362	-1.36086477
C	-1.72053156	-3.69581133	-1.83008341
C	-1.44210522	-2.53616350	-1.06254711
C	-2.14870942	-2.25588328	0.15306591
C	-3.15036392	-3.16724909	0.58801040
C	-3.42010137	-4.33678702	-0.20629380
C	-1.80780534	-1.07301793	0.87866177
C	-3.83775436	-2.88183148	1.78852184
C	-3.52155718	-1.73729797	2.50213396
C	-2.52237010	-0.84351492	2.05547083
C	-0.97687662	-3.89343468	-3.01181342
C	-0.01659013	-2.96587005	-3.37962911
C	0.19721308	-1.84277071	-2.56595943
N	-0.49215290	-1.62964361	-1.44308088
H	-2.95607082	-5.48269588	-1.94611404
H	-4.18798971	-5.02574055	0.13565257
H	-2.31259504	0.03942277	2.65183156
H	-4.60735653	-3.56266228	2.14138438
H	-4.05169630	-1.51855503	3.42585045
H	-1.16291061	-4.77081648	-3.62460766
H	0.57116547	-3.08911119	-4.28209190
H	0.93856719	-1.09549293	-2.82796999
C	-3.44962574	1.85917715	-2.49209157
C	-3.74512099	3.01668742	-1.78969540
C	-2.47229396	0.98088572	-2.00317281
C	-3.05652921	3.29507223	-0.59205155
C	-3.27202332	4.46015802	0.22281847
C	-2.08300263	2.36166389	-0.16185496
C	-2.55960019	4.65803841	1.37187937
C	-1.33397260	2.55624454	1.03505502
C	-1.56724915	3.71574566	1.81970526
C	-0.38370279	1.54993469	1.37442890
C	-0.80766668	3.87481838	2.99991212
C	0.34044084	1.76081893	2.54854995
C	0.12583292	2.90867525	3.34597534
N	-1.80151504	1.22212657	-0.87073493
H	-3.96119892	1.61483991	-3.41584865
H	-4.49993706	3.70762805	-2.15337638
H	-4.01636288	5.18335790	-0.09697948
H	-2.22116051	0.06858888	-2.52968778

H	-2.73817548	5.54570174	1.97299857
H	-0.95932388	4.74967622	3.62581771
H	1.08280323	1.03710766	2.87551547
H	0.70944788	3.03413762	4.25477673
Ir	-0.31967036	0.03529058	0.00938913
C	1.16844214	-1.92485246	1.82724065
C	2.25108140	-2.57450911	2.38299803
C	3.54558805	-2.21322582	1.97508126
N	1.28981212	-0.94508173	0.90241327
C	3.67951762	-1.19682693	1.02116683
C	2.54024333	-0.57907262	0.50496920
N	1.40791588	0.96474447	-0.93535951
C	2.60729880	0.50671457	-0.50243807
C	1.38393370	1.95422542	-1.85063569
C	3.81054715	1.03242478	-0.97758134
C	2.52814451	2.52418972	-2.37281817
C	3.77837782	2.05987807	-1.92981684
H	4.65752693	-0.89266180	0.67992942
H	4.75359579	0.65557182	-0.61029413
H	2.10827297	-3.35459963	3.12093892
H	2.47091509	3.31868729	-3.10706116
H	0.15704001	-2.17651009	2.11785784
H	0.40295834	2.29087603	-2.16489103
O	4.56399273	-2.87880344	2.53758018
O	4.85941080	2.64949053	-2.46177812
C	5.90811793	-2.55229259	2.15357875
H	6.54691610	-3.21353215	2.73710893
H	6.14068281	-1.51013027	2.39310740
H	6.06513488	-2.73663849	1.08634009
C	6.16464544	2.22459277	-2.04356880
H	6.32941055	1.17020094	-2.28591251
H	6.30474099	2.39010746	-0.97093728
H	6.86565554	2.84210841	-2.60322883

Table 13S. Cartesian coordinates from the optimized structures of S_0 in CH_3CN media for 2EA'.

Atom symbol	X	Y	Z
C	-3.83251042	2.66542632	-2.94478520
C	-2.78693262	1.68163963	-3.02719842
C	-1.99626259	1.46127990	-1.87365638
C	-2.21412387	2.18687782	-0.66588598
C	-3.25486799	3.15033226	-0.61233154
C	-4.05338635	3.36356358	-1.79124373
C	-1.35692396	1.88966634	0.43304461
C	-3.44549662	3.84617911	0.60209791
C	-2.62263622	3.56998952	1.68395798
C	-1.58899686	2.60786175	1.60643884
C	-2.49209056	0.92126780	-4.17674290
C	-1.45773925	-0.00000162	-4.13713276
C	-0.72079938	-0.16519538	-2.95583611
N	-0.97870498	0.54307472	-1.85085859
H	-4.44585250	2.84175090	-3.82343378
H	-4.84975314	4.10192259	-1.74959821
H	-0.97295598	2.43878440	2.48556433
H	-4.23304931	4.59041058	0.67938933
H	-2.77136358	4.10795173	2.61698782
H	-3.07411487	1.06206954	-5.08270885
H	-1.20397013	-0.59993613	-5.00338858
H	0.09440041	-0.87611353	-2.89793795
C	2.62265508	3.56997079	-1.68397095
C	3.44551638	3.84616183	-0.60211192
C	1.58901214	2.60784720	-1.60644795
C	3.25488501	3.15032070	0.61232038
C	4.05340414	3.36355372	1.79123174
C	2.21413714	2.18687054	0.66587878
C	3.83252548	2.66542200	2.94477607
C	1.99627270	1.46127878	1.87365229
C	2.78694368	1.68163990	3.02719339
N	0.97871113	0.54307784	1.85085835
C	2.49209861	0.92127384	4.17674093
C	0.72080297	-0.16518712	2.95583857
C	1.45774373	0.00000827	4.13713445
C	1.35693624	1.88965768	-0.43305069
H	2.77138464	4.10792848	-2.61700306
H	4.23307197	4.59038991	-0.67940639
H	4.84977381	4.10190945	1.74958325
H	0.97297083	2.43876831	-2.48557283

H	4.44586829	2.84174776	3.82342391
H	3.07412362	1.06207676	5.08270624
H	-0.09439959	-0.87610233	2.89794318
H	1.20397241	-0.59992196	5.00339260
Ir	0.00000261	0.42984503	0.00000032
C	-2.47669229	-1.22317591	1.00626712
C	-3.27861889	-2.35248569	1.28996988
C	-2.72082863	-3.64177647	1.03262552
N	-1.24639001	-1.30323149	0.52096437
C	-1.40617171	-3.69886556	0.51440568
C	-0.68978479	-2.54402686	0.26839498
N	1.24638393	-1.30324171	-0.52095612
C	0.68976822	-2.54403252	-0.26838710
C	2.47668734	-1.22319646	-1.00625769
C	1.40614551	-3.69887718	-0.51439783
C	3.27860449	-2.35251297	-1.28996057
C	2.72080302	-3.64179913	-1.03261737
C	-4.59399039	-2.23942096	1.80972067
C	-5.32746931	-3.37714723	2.06322875
C	-4.77639747	-4.65998226	1.80816167
C	-3.50140313	-4.79619954	1.30372228
C	3.50136757	-4.79622876	-1.30371489
C	4.59397706	-2.23945919	-1.80971095
C	5.32744613	-3.37719162	-2.06321983
C	4.77636319	-4.66002210	-1.80815393
H	-5.00792835	-1.25391097	2.00097298
H	-6.33434724	-3.29859923	2.46029898
H	-5.37200862	-5.54365086	2.01506086
H	-3.08208109	-5.77860058	1.10935555
H	5.37196676	-5.54369563	-2.01505379
H	3.08203703	-5.77862635	-1.10934912
H	5.00792363	-1.25395265	-2.00096239
H	6.33432486	-3.29865199	-2.46028981
H	-2.85759277	-0.22309268	1.18815267
H	-0.97257135	-4.67069145	0.31212877
H	0.97253683	-4.67069941	-0.31212122
H	2.85759673	-0.22311645	-1.18814235

Equation 1S.

$$E_g^{exp.} = 0.228*E1 + 2.144*E2 + 0,349*E3 - 16,532$$

E1- energies for the real system with the low method

E2 - energies for the high layer with the high method

E3 - energies for the high layer with the low method

Table 14S.

Absolute energies computed within ONIOM scheme for the studied compounds with charge +1 (E_1-E_3) and with charge +2 (E_4-E_6) together with calculated oxidation potential $E_{ox\ calc.}$ and experimental oxidation onset potential $E_{ox\ onset}$

Compound	E_1 [a] [hartree]	E_2 [b] [hartree]	E_3 [c] [hartree]	E_4 [d] [hartree]	E_5 [e] [hartree]	E_6 [f] [hartree]	$E_{ox\ calc.}$ [g] [V]	$E_{ox\ onset}$ [V]
2AA'	-1679,371355	-635,0301737	-624,4302032	-1679,231263	-634,9573767	-624,4800436	0.69	0.69
2BA'	-1756,580234	-635,208135	-624,6914546	-1756,402985	-634,9582285	-624,4798084	0.51	0.47
2CA'	-1756,536345	-635,1744322	-624,662409	-1756,421302	-634,923416	-624,4813829	0.46	0.47
2DA'	-1904,252478	-635,2086723	-624,6926713	-1904,155965	-634,9588083	-624,483638	0.45	0.49
2EA'	-1981,002555	-635,1930058	-624,6733771	-1980,852125	-634,9227543	-624,4621099	0.49	0.47
2FA'	-1754,232229	-635,1960287	-624,6805641	-1754,042816	-634,9388459	-624,5364009	0.71	0.73
2GA'	-2207,703412	-635,1760963	-624,6561876	-2207,513396	-634,9196263	-624,5077704	0.46	0.51
2HA'	-2284,898198	-635,1827756	-624,6702564	-2284,76386	-634,9209821	-624,53894	0.46	0.41

[a] E_1- energy for the real system at the low accuracy method for a complex with charge +1

[b] E_2 - energies for the real system at the high accuracy method for a complex with charge +1

[c] E_3 - energies for the small model system at the low accuracy method for a complex with charge +1

[d] E_4- energies for the real system at the low accuracy method for a complex with charge +2

[e] E_5- energies for the real system at the high accuracy method for a complex with charge +2

[f] E_6- energies for the small model system at the low accuracy method for a complex with charge +2

[g] $E_{ox\ calc.} = c_0 + \sum_{i=1}^{6} c_i E_i$ where c_0=-2194.95, c_1=-0.059, c_2=5.085, c_3=-3.208, c_4=0.059, c_5=-17.875, c_6=12.698

Figure 1S. Calculated oxidation potential (vertical) *vs* experimental oxidation onset potential (horizontal) for studied compounds.

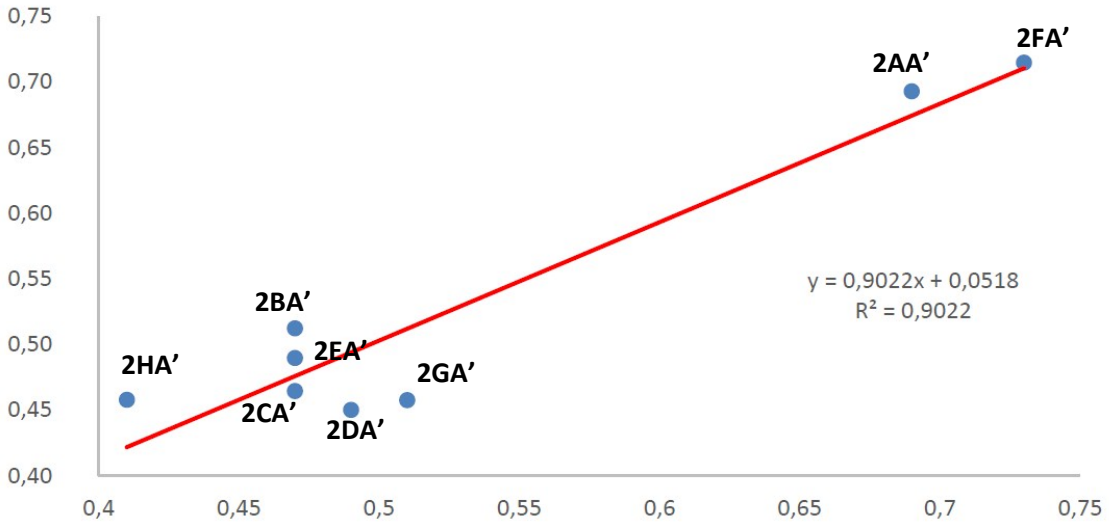

Table 15S. Crystal data, data collection and structure refinement

Compound	**2AA'**	**2FA'**
Formula	$C_{36}H_{24}IrN_4 \cdot PF_6 \cdot C_2H_4Cl_2$	$C_{38}H_{24}IrN_4 \cdot PF_6 \cdot CH_3OH$
Formula weight	948.71	905.82
Crystal system	monoclinic	monoclinic
Space group	$P2_1/c$	C2/c
a(Å)	12.7207(5)	12.1984(5)
b(Å)	14.4809(6)	14.8577(5)
c(Å)	18.6448(12)	18.2375(7)
β(º)	93.662(5)	101.868(4)
V(Å^3)	3427.5(3)	3234.7(2)
Z	4	4
D_x(g cm^{-3})	1.84	1.86
F(000)	1856	1776
μ(mm^{-1})	4.17	4.25
Θ range (^{0})	3.13 – 26.79	3.41 – 28.27
Reflections:		
collected	7381	11744
unique (R_{int})	8471 (0.021)	3565 (0.015)
with I>2σ(I)	7235	3141
R(F) [I>2σ(I)]	0.039	0.021
wR(F^2) [I>2σ(I)]	0.089	0.069
R(F) [all data]	0.047	0.025
wR(F^2) [all data]	0.091	0.0732
Goodness of fit	1.10	1.04
max/min Δρ (e Å^{-3})	1.96/-1.63	1.37/-0.96

Figure 2S. TGA curves

a)

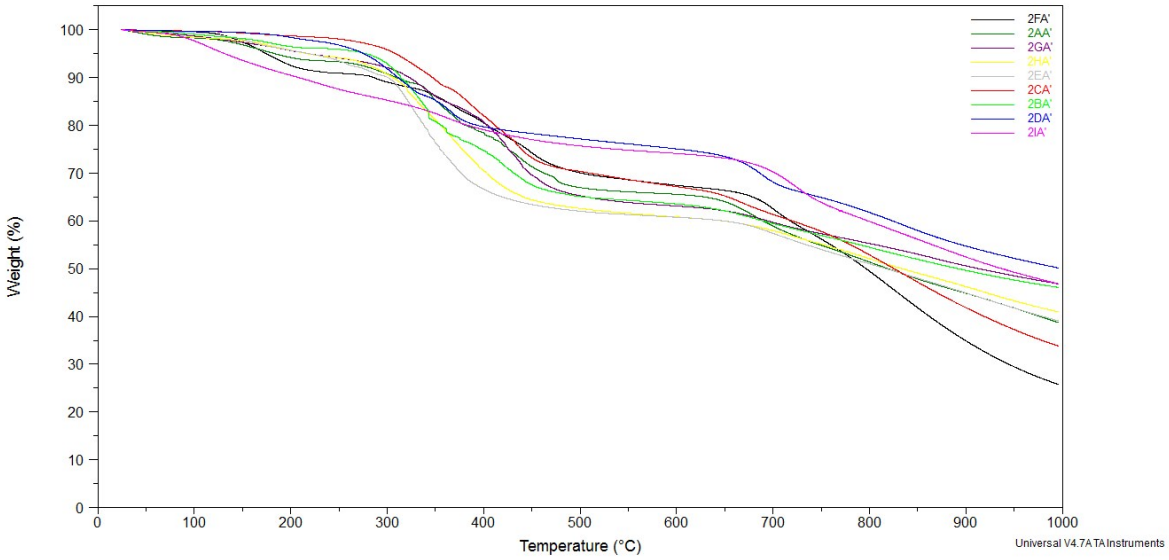

b)

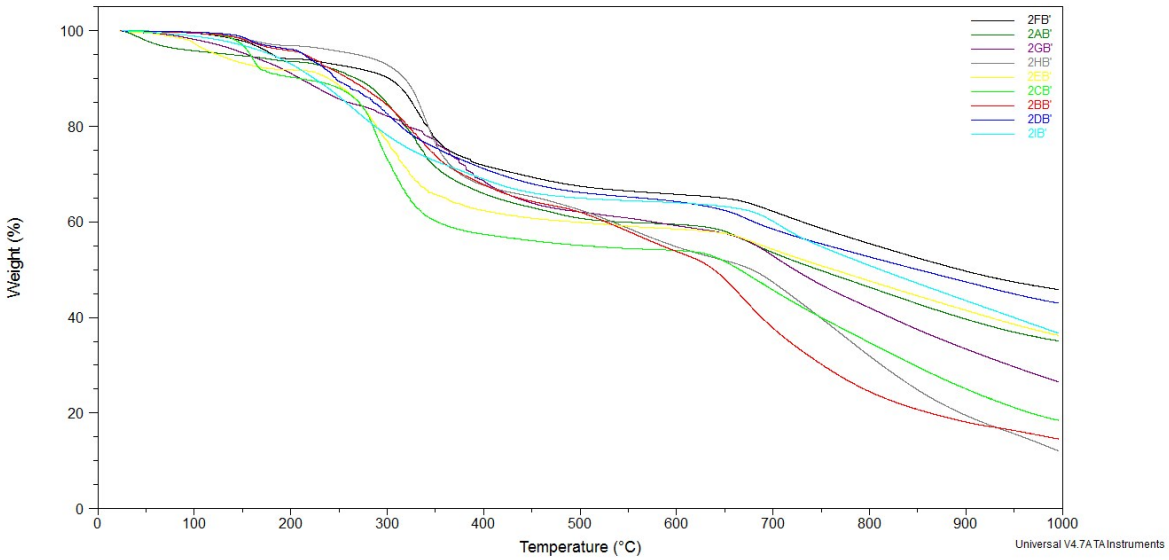

Journal of Materials Chemistry C

PAPER

View Article Online
View Journal | View Issue

Cite this: J. Mater. Chem. C, 2018, 6, 8688

Effect of fluorine substitution of the β-ketoiminate ancillary ligand on photophysical properties and electroluminescence ability of new iridium(III) complexes†

Ewelina Witkowska,[a] Gabriela Wiosna-Salyga,*[a] Ireneusz Glowacki,[a] Bartosz Orwat,[bc] Myong-joon Oh,[bc] Ireneusz Kownacki,*[bc] Maciej Kubicki,[b] Blazej Gierczyk,[b] Michal Dutkiewicz,[cd] Pawel Cieszko,[bc] Beata Luszczynska,[a] Jacek Ulanski,[a] Izabela Grzelak,[b] Marcin Hoffmann,[b] Przemyslaw Ledwon[e] and Mieczyslaw Lapkowski[ef]

Received 12th June 2018,
Accepted 10th July 2018

DOI: 10.1039/c8tc02890g

rsc.li/materials-c

In this paper we report studies of the electronic structure as well as photophysical and emissive properties of a family of new heteroleptic iridium(III) complexes of the general formula [Ir(bzq)$_2$(N^O)] with N,O-donating β-ketoiminate ligands equipped with different directly fluorinated *N*-aryl moieties. For this purpose, a series of suitable β-ketoimines were prepared and successfully employed in the synthesis of iridium(III) phosphorescent materials. It is worth emphasizing that the developed synthetic strategy, involving the use of microwaves to accelerate the reaction course, allows reduction of the process time by up to 10 minutes. All the obtained complexes were characterized by spectroscopic methods and the structures of three of them were resolved by X-ray methods. The cyclic voltammetry measurements allowed determination of the energies of HOMO and LUMO levels of the studied complexes. Moreover, the HOMO–LUMO gaps predicted for these compounds by DFT methods showed a good correlation with the experimental values. The determined negligible influence of ligand modification on LUMO levels and only small change of HOMO levels explains the observed slight effect of different directly fluorinated *N*-aryl moieties on photophysical properties of the complexes. All Ir complexes were tested in host–guest type organic light emitting diodes (PhOLEDs) with an poly(*N*-vinylcarbazole):2-*tert*-butylphenyl-5-biphenyl-1,3,4-oxadiazole matrix. The PhOLEDs based on all studied iridium complexes emitted green light. The most efficient phosphorescent emitter turned out to be the iridium complex with one fluorine atom substituted in the *para* position in the phenyl ring of the ancillary ligand. Diodes with the emissive layer containing 1 wt% of this emitter showed the best operating parameters: luminance of about 13 000 cd m^{-2} and current efficiency close to 10 cd A^{-1}. A comparison of photoluminescence, electroluminescence and spectrally resolved thermoluminescence spectra of the investigated systems revealed an important role of charge carrier trapping in the TL phenomena.

Introduction

In the quest for highly efficient organic light emitting diodes (OLEDs), the search for new phosphorescent materials is motivated by the limited inner quantum yield of OLEDs based on fluorescent materials which cannot be higher than 25%. This limitation can be overcome by employing phosphorescent materials which allow harvesting triplet states, constituting 75% of all formed excitons.[1,2] The most popular phosphorescent systems are based on coordination compounds of heavy metals such as Ir, Pt, Os or Pd[3] in which the central metal atom is stabilized by cyclometalated organic ligands of various structures, such as C,N-[1,2,4] donating compounds, but also C,C-[5] or

[a] Department of Molecular Physics, Lodz University of Technology, 90-924 Lodz, Zeromskiego 116, Poland. E-mail: Gabriela.Wiosna-Salyga@p.lodz.pl
[b] Faculty of Chemistry, Adam Mickiewicz University in Poznan, St. Umultowska 89b, 61-614 Poznan, Poland. E-mail: Ireneusz.Kownacki@amu.edu.pl
[c] Center for Advanced Technology, Adam Mickiewicz University in Poznan, St. Umultowska 89c, 61-614 Poznan, Poland
[d] Poznan Science and Technology Park, Adam Mickiewicz University Foundation, ul. Rubiez 46, Poznan, Poland
[e] Silesian University of Technology, Faculty of Chemistry, St. Marcina Strzody 9, 44-100 Gliwice, Poland
[f] Centre of Polymer and Carbon Materials, Polish Academy of Sciences, Curie-Sklodowskiej 34, 41-819 Zabrze, Poland

† Electronic supplementary information (ESI) available. CCDC 1814938 (**3f**), 1814939 (**5b**), 1814940 (**5e**), and 1814941 (**5g**). For ESI and crystallographic data in CIF or other electronic format see DOI: 10.1039/c8tc02890g

C,P-chelating[6] systems. In particular, iridium complexes deserve much attention because of their attractive photophysical properties,[7] in part due to efficient triplet emission as an effect of very strong spin–orbit coupling, which causes mutual isoenergetic transition from the singlet to the triplet state and conversely, known as intersystem crossing (ISC).[8] In fact, the iridium cyclometalated coordination derivatives have been found to be so far the best light emitting species for phosphorescent organic light emitting diodes (PhOLEDs).[1–4,7,9–11] In addition, Ir complexes proved to be convenient fluorescent markers for biological systems,[12–21] as well as photocatalysts in light accelerated processes.[22–24] Generally, neutral triscyclometallated $[Ir(C\hat{}E)_3]$ type complexes (where C^E is a C,E-donating ligand, E = C, N, P), also termed homoleptic, have been intensively studied for years. In particular, complexes with selected C,N-cyclometalating ligands, and among them those based on a 2-phenylpyridine (ppyH) moiety, have gained an opinion of highly phosphorescent organometallic materials and are potential candidates for phosphorescent dopants for PhOLED technology.[7,25,26]

Nevertheless, heteroleptic complexes of the type $[Ir(C\hat{}E)_2(LL')]$, in which LL′ denotes a bidentate ligand or two monodentate ligands, have also been intensively studied. The above-mentioned iridium six-coordinated systems include both cationic as well as neutral compounds, depending on the type and charge of the ancillary ligand. Thus, the cleavage of binuclear precursors $[\{Ir(\mu\text{-}Cl)(C\hat{}E)_2\}_2]$ with neutral ligands (LL′) such as N^N[7,27] or C^C[28] yields soft salt derivatives $[Ir(C\hat{}E)_2(LL')]^+A^-$, while employment of ancillary ligands in anionic form ($^-$LL′), *e.g.* N^O$^-$,[29] $^-$N^N,[30] leads to formation of neutral complexes of the type $[Ir(C\hat{}E)_2(LL')]$. The neutral complexes $[Ir(C\hat{}N)_2(O\hat{}O)]$ in which O^O denotes an acetylacetonate (acac) or acac-like ligand[3,9,31] were in the past one of the most extensively studied iridium complexes, mainly because of their better solubility as well as low influence of such an O^O ancillary ligand on HOMO/LUMO orbitals located on the $[Ir(C\hat{}N)_2]^+$ core.[32] Therefore, for this type of complex the observed changes in electrochemical and photophysical properties were associated only with the alteration of the C,E-donating ligands structure.[9,26,32]

Nevertheless, on the basis of many examples of different iridium compounds, it has also been shown that incorporation of ancillary ligands of various stereoelectronic properties into the metal coordination sphere can lead to a significant modification of the electronic structure of a metal coordination system.[3,10,27*d*,33] Summarizing, for heteroleptic systems of the type $[Ir(C\hat{}E)_2(LL')]$, the decoration of a C^E-donating ligand with substituents of various electronic characters induces the energy change in the unoccupied ligand-centered π* level, while the introduction of ancillary ligands (LL′) with various electronic properties in a metal coordination sphere affects the energy of the metal-centered HOMO level. Moreover, the spatial arrangement of this orbital in the emitter molecule influences the extent to which MLCT and LC states contribute to the emissive excited state.

Although there is abundant literature on the synthesis and properties of heteroleptic phosphorescence dopants, the reports concerning the use of β-ketoiminate or β-diketiminate as the acac-like ancillary ligands to stabilize cyclometalated organometallic phosphors are very scarce.

Nonetheless, the 2,4-O,N- or 2,4-N,N-donating ligands formed on the basis of the acac skeleton have found wide application as supporting ligands for stabilization of various coordination systems[34] based on the main-group elements or transition metals, reported as active species employed in catalysis of polymerization processes[35–39] or reactions occurring through activation of small molecules.[40–45]

Teets and co-workers very recently have reported[46,47] on the preparation of a series of β-ketoiminate- and β-diketiminate-stabilized iridium(III) coordination compounds and examination of their photophysical properties: absorption and emission in solution. Additionally, they provided a discussion on the influence of these two types of ancillary ligands on the properties of excited states generated in iridium-coordination systems. In the designed complexes, they used 2-phenylpridine (ppy) and 2-phenylbenzothiazole (bt) as the C,N-donating ligands in combination with different ancillary (L^X) ligands such as an *N*-phenyl-substituted β-ketoiminate ($acNac^{Me}$), an *N*-phenyl-substituted β-diketiminate ($NacNac^{Me}$) as well as fluorinated versions of the latter, by introduction of $-CF_3$ substituents into the ligand backbone and/or *N*-aryl substituents. They found that the above-mentioned L^X ligands bonded to the metal center stabilized with ppy and bt ligands,[46] strongly affecting the energy of the Ir-centered HOMO. In particular, the increase in π-donating ability of the ligand with increasing number of nitrogen donors was observed in the sequence acac → acNac → NacNac. This resulted in higher HOMO energies and less positive oxidation potentials for the studied C,N-cyclometalated iridium compounds, while fluorofunctionalization of the weaker-field NacNac and acNac ligands caused an increase in the energy of the metal-centered HOMO, in the following order $NacNac^{CF_3} < acNac^{Me} < NacNac^{Me}$. Moreover, on the basis of the photophysical properties studied for these complexes, the authors hypothesized that when ppy is used as the C^N ligand and acac is substituted by the nitrogen-containing acNac or NacNac ligands, an increase in the MLCT character in the excited states is observed. In contrast, the replacement of ppy with bt enhances the LC character, resulting in a strong increase in the emission quantum yield, as demonstrated for $[Ir(bt)_2(acNac^{Me})]$.[46] On the other hand, they revealed that the introduction of $-CF_3$ moieties into different sites of such ligand skeletons, including the =N–Ph moiety,[47] led to substantial changes in the electrochemical and photophysical properties. They found also that the redox potential was much more sensitive to fluorination of such a ligand backbone than to substitution of the *N*-aryl substituent with $-CF_3$ moieties. Furthermore, fluorination of the backbone of the acNac ligand suppressed luminescence altogether, whereas the backbone fluorination of the NacNac ligand induced dramatic changes in the excited-state properties which was particularly evident at low temperatures.

Taking into account the latest of Teets' reports,[46,47] particularly those concerning detailed studies of the electrochemical and photophysical properties of iridium(III) coordination compounds stabilized with β-ketoiminate and β-diketiminate bidentate

ligands and their fluorinated analogues, it seems that the aforementioned properties of organometallic phosphors strongly depend on the presence and collocation of fluorine atoms in the structure of examined types of ancillary ligands. However, looking at the structures of fluoro-substituted β-ketoiminate ligands reported by Teets,[46,47] it can be concluded that the authors in their research notably focused on determination of the effects related to the introduction of fluorine atoms to the acNac backbone as well as $-CF_3$ moieties to the phenyl ring bonded to the N-imine atom. Nevertheless, it is well documented that $-CF_3$ substituents attached to the phenyl system have significantly weaker Hammett parameters than the fluorine atom directly bonded to sp^2-aromatic carbon. Moreover, the $-CF_3$ group non-specifically acts on *meta*- and *para*-positions in aromatic systems.[48] Considering the above, it is expected that incorporation of fluorine atoms directly into the *N*-bonded aryl group will cause changes in photophysical as well as emissive properties of targeted iridium complexes.

The effects described above, associated with the presence of fluorine atoms in the ancillary N,O-, N,N-donating ligands, encouraged us to extend the knowledge on the effects related to the presence of the directly fluorinated *N*-aryl moiety, in the structure of the N,O-type ligand, *i.e.* its influence on electronic structure, electrochemical and photophysical properties. It will be particularly important to determine the influence of the presence of such fluorofunctionalized ligands on the electronic structure of iridium(III) complexes $[Ir(C^N)_2(N^O)]$, their emissive properties in thin layers as well as on operating parameters of single layer PhOLEDs created on the basis of such emitters. In a number of reports concerning the synthesis and luminescence properties of transition metal complexes, iridium materials created with employment of ppy and ppy-like cyclometalated systems dominate.[1–4,7] Notwithstanding, iridium(III) neutral homoleptic $[Ir(bzq)_3]$[49] and heteroleptic $[Ir(acac)(bzq)_2]$[31] as well as the soft-salt type compounds $[Ir(bzq)_2(N^N)]^+A^-$ [27] were also characterized as highly phosphorescent materials, however less explored than the former, but in our opinion they seem to be very interesting due to their photophysical properties, similar to those of ppy-based compounds.

The work undertaken is aimed at determination of the correlation between the number of fluorine atoms, their location at various positions of the *N*-phenyl substituent in the β-ketoiminate ancillary ligand and electronic structure, electrochemical and photophysical properties of iridium phosphorescent materials bearing in their structure such ligands as $[Ir(bzq)_2(\beta\text{-ketoiminato})]$. Particular attention is paid to their emissive properties in thin layers as well as PhOLEDs.

Results and discussion

Synthesis of the ligands

A series of selected 4-arylimino-2-pentanones (**3a–f**) were synthesized according to the methodology described in the literature.[50] Namely, appropriate aryl amines (**2**) bearing in their structure one fluorine atom at the phenyl ring in three possible positions (**b**, **c**, **d**) or $-CF_3$ group in the 4-position (**e**) were refluxed with 2,4-pentanedione (acacH) in the presence of *p*-$TolSO_3H$ in benzene as the reaction medium and using Dean–Stark apparatus until water stopped being generated. However, in the case of perfluorinated aniline (**f**), instead of *p*-$TolSO_3H$, $Er(OTf)_3$[51] was applied as a catalyst and the condensation process in toluene environment was carried out with assistance of microwave radiation as an energy carrier (Scheme 1).

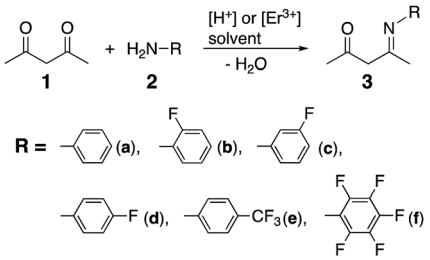

Scheme 1 Synthesis of 4-arylimino-2-pentanones.

The synthesized materials were readily characterized by ^1H, $^{13}C\{^1H\}$ and ^{19}F NMR spectroscopy as well as the HRMS technique (see ESI†). In the ^1H NMR spectra recorded for all 4-arylimino-2-pentanones (**3a–f**), the presence of characteristic resonances coming from N–H–O and ═CH– moieties, namely a singlet for the N–H–O system in the region *ca.* 11.6–12.6 ppm, a singlet for –(O–)C═CHC(═N)– between values 5.0 and 5.6 ppm, and two inequivalent singlets for CH_3–C(═N)– and CH_3–C(–O)– systems in the region from 1.5 to 2.5 ppm, confirms that the keto–enol equilibrium is shifted completely toward the enol form.

The structure of compound (3*Z*)-4-[(pentafluorophenyl)-amino]pent-3-en-2-one (**3f**) was also determined by X-ray analysis. **3f** is an example of the family of ligand molecules, which in the solid state adopt the *Z* conformation stabilized by intramolecular N–H···O hydrogen bonding (Table 2S, ESI;† Fig. 1a). The correct tautomeric form was determined on the basis of localization of the NH hydrogen atom in the difference Fourier map (see Fig. 1S, ESI†) and successful refinement of this atom. In **3f** the chain C–N–C═C–C═O is almost planar (maximum deviation from the least-squares plane is 0.0527(12) Å) and makes a dihedral angle of 61.61(5)° with the phenyl ring. Table 3S presented in the ESI† lists the important geometrical parameters, including relevant torsion and dihedral angles, for all molecules. In the crystal structure molecules of **3f** are connected into centrosymmetric hydrogen bonded dimers; notably this intermolecular hydrogen bond is also of NH···O type, between the same atoms as the intramolecular one (Fig. 1b and Table 3S, ESI†). A similar sequence (intra/intermolecular) of secondary C–H···F hydrogen bonding is also observed in the structure. The selected geometrical data are compiled in Table 3S (see ESI†).

Preparation of new iridium(III) phosphors

All previously obtained 4-arylimino-2-pentanone derivatives (**3a–f**) were applied as N,O-donating ligands in the synthesis of neutral heteroleptic iridium(III) C,N-cyclometalated complexes of type **5** (Scheme 2).

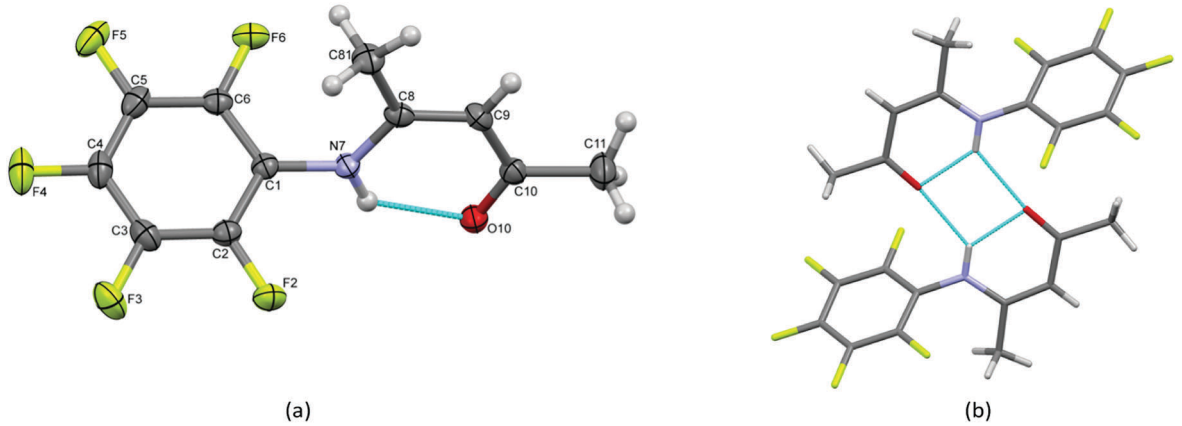

Fig. 1 (a) Perspective view of molecule **3f** with labelling scheme; ellipsoids are drawn at the 50% probability level, hydrogen atoms are represented by spheres of arbitrary radii, intramolecular hydrogen bond is shown as dashed blue line; (b) centrosymmetric NH···O hydrogen bonded dimer in the crystal structure of **1**; intra- and intermolecular hydrogen bonds are shown as dashed blue lines.

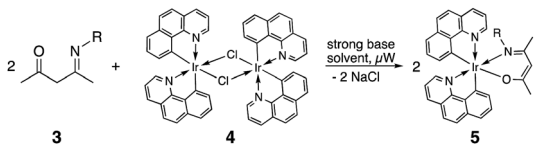

Scheme 2 Synthesis of [Ir(bzq)$_2$(β-ketoiminate)] (**5**) complexes.

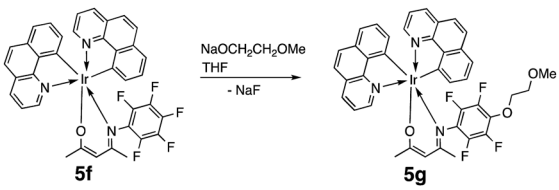

Scheme 3 Conversion of compound **5f** to complex **5g**.

The methodology leading to the iridium derivatives **5** was carried out with the cleavage of binuclear precursor **4** by interaction with 4-arylimino-2-pentanonalate anion, *in situ* generated in the reaction of the corresponding derivative **3** with the most commonly used strong bases, *i.e.* NaOMe or NaH in a THF environment. Taking into account numerous literature reports on employment of microwaves in syntheses of inorganic[52] or coordination compounds[53] as well as results of our earlier work concerning the synthesis of iridium(III) cationic complexes with assistance of such an unconventional type of energy carrier,[27a] in current studies, the processes of ancillary ligand introduction into the iridium coordination system were conducted with the support of microwaves. As for ionic iridium(III) compounds,[27a] the use of such a heat source enabled efficient preparation of desired iridium materials in a relatively short reaction time and with good yields, achieving 65–76%.

However, for compound **5g**, several synthetic attempts have been carried out to get the target iridium compound. Most of them were intended to obtain a suitable ligand of appropriate structure, which in the further step could be introduced to the iridium coordination sphere in the reaction with **4**. Unfortunately, these attempts failed. All these failures prompted us to change the synthesis strategy. In this particular case, formation of **5g** derivative was based on the well-known reactivity of the $-C_6F_5$ moiety in the nucleophilic substitution of the fluorine atom in the *para*-position especially by O-nucleophiles.[54] Thus, nucleophilic reagent $NaOCH_2CH_2OMe$ was generated in THF solution prior to use and then employed in the reaction with **5f**, giving finally the desired **5g** with moderate yield 68% (Scheme 3).

All the synthesized iridium materials were characterized by spectroscopic methods and the structures of three of them were resolved by X-ray analysis.

In all three complexes **5b**, **5e**, and **5g**, the Ir cation is six-coordinated (C_2N_3O pattern) by N7 and O10 atoms from the β-ketoiminate ligand molecule and by N and C atoms from two benzo[*h*]quinoline ligands (Fig. 2a, 3a and 4). The coordination geometry is a quite regular octahedral one (Table 3S (ESI†) contains the appropriate bond lengths as well as values of the three largest angles around Ir cations).

In the crystal structure of **5b** there are two symmetry-independent molecules of very similar geometry (Fig. 2b). In one of these molecules (B), the 2-fluorophenyl fragment is disordered – the two alternative rings are almost parallel but rotated by approximately 180°. Disordered solvent molecules (modelled as methanol) fill up the voids in the structure of **5e** (Fig. 3b). In both **5e** and **5g** compounds, some weak hydrogen-bond-type interactions as well as π···π (between benzo[*h*]quinoline molecules) and C–H···π interactions take part in the determination of crystal packing.

Thermal analysis

Prepared complexes **5a–5g** were subjected to thermogravimetric analysis to determine the boundary temperature of their thermal stability. Analysis of the obtained TG curves presented in Fig. 5 reveals that regardless of the chemical structure of the measured samples they are thermally stable up to 270 °C at which the first decomposition step begins. For all the measured samples, two or three (for samples **5c** and **5e**, respectively)

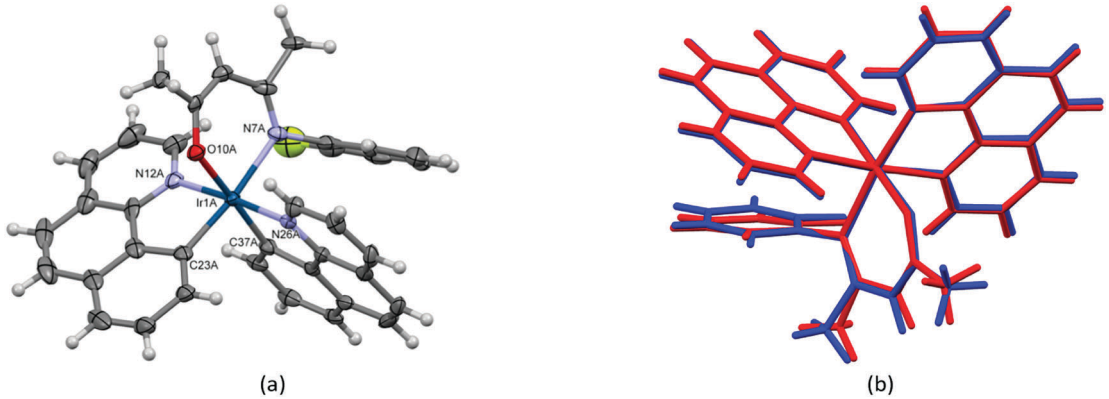

Fig. 2 (a) Perspective view of the complex molecule **5bA**; ellipsoids are drawn at the 50% probability level, hydrogen atoms are shown as spheres of arbitrary radii; (b) a comparison of two symmetry-independent molecules of **5b**, the higher-occupied alternative of **5bB** is shown.

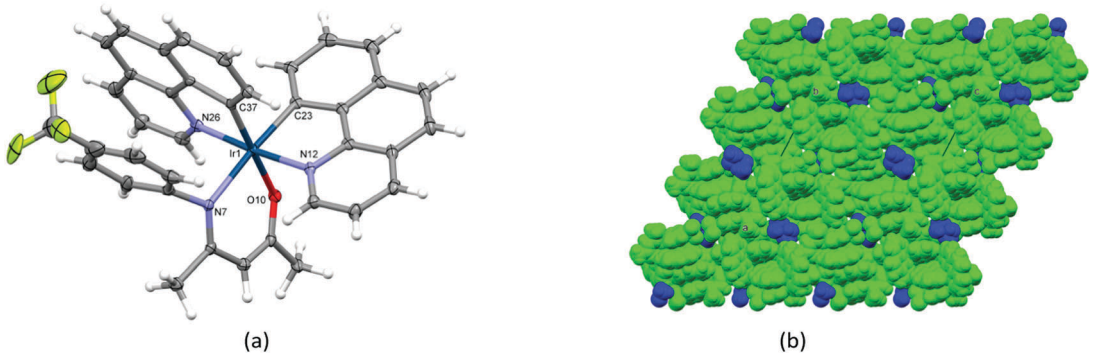

Fig. 3 (a) Perspective view of the complex molecule **5e**; ellipsoids are drawn at the 50% probability level, hydrogen atoms are shown as spheres of arbitrary radii; (b) van der Waals representation of a fragment of crystal packing of complex **5e** (green) with solvent molecules shown in blue.

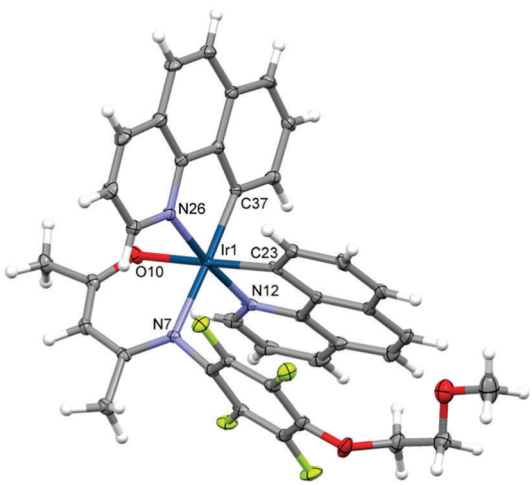

Fig. 4 Perspective view of the complex molecule **5g**; ellipsoids are drawn at the 50% probability level, hydrogen atoms are shown as spheres of arbitrary radii.

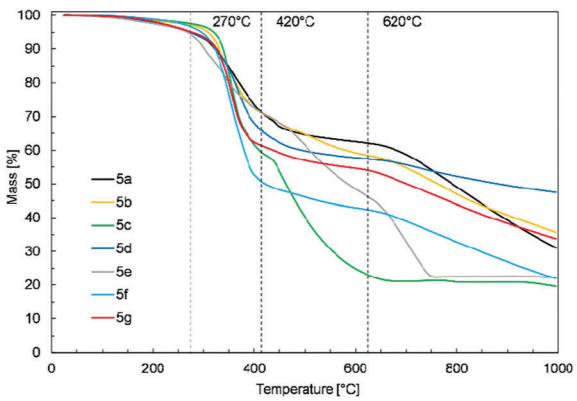

Fig. 5 TG curves of all complexes.

distinct decomposition steps were observed, beginning at 270, 420 and 620 °C and T_{max} temperatures were in the range of 330–370 °C, 460–500 °C and 700–790 °C, respectively. The residues after pyrolysis at 1000 °C ranged from 20 to 48% of the starting samples mass. No direct correlation between the samples' chemical structure and their thermal stability was observed.

TG and DTG curves for all the measured samples as well as detailed results of TG and DTG analysis are given in the ESI.†

Subsequently, complexes **5a–5g** were subjected to DSC analysis to evaluate their melting and crystallization temperatures.

The upper limit (270 °C) of the temperature program was established on the basis of TG experiments. Unfortunately, for no complexes tested except **5g** were the transitions characteristic

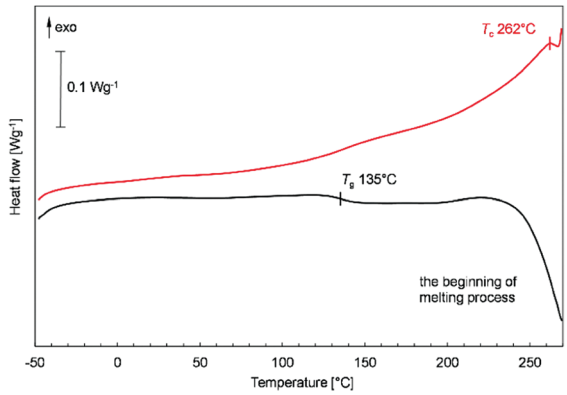

Fig. 6 DSC curves of second heating and cooling run for sample **5g**.

of melting or crystallization processes observed in the applied temperature range. As shown in Fig. 6, only for sample **5g** a glass transition at 135 °C and the beginning of the melting process above 225 °C were observed. Also, the crystallization of partially molten sample was noted at 262 °C on the second cooling curve. The results of TG and DSC analyses lead to the conclusion that the synthesized complexes melt with decomposition above 270 °C. All the measured DSC curves are available in the ESI.†

Determination of electrochemical properties

Electrochemical measurements were made in order to estimate the influence of ligand structure on Ir complex properties. The measurements were made in a solution of the studied compounds in Bu_4NBF_4/CH_2Cl_2 as an electrolyte. Electrochemical results are collected in Table 1.

Cyclic voltammetry curves reveal quasi-reversible oxidation peaks in the anodic range (Fig. 12S, ESI†). This behavior is observed for all compounds. This redox couple is related to the oxidation of the Ir(III) complex to an Ir(IV) one. $E_{ox\,onset}$ changes with the modification of ligand structure. The fluorine atom slightly increases the $E_{ox\,onset}$ of **5b**, **5c** and **5d** in comparison to that of **5a**. However, the effect associated with the fluorine substituent's location in the phenyl moiety on the value of $E_{ox\,onset}$ is minor. Introduction of additional fluorine atoms, as for example **5f** and **5g** causes an even greater increase in $E_{ox\,onset}$ as a result of the electron acceptor character of these atoms. For similar complexes with 2-phenyl-pridine (ppy) and phenyl-substituted β-ketoiminate as ancillary ligands, a slight shift of oxidation potential is observed.[47] The shift of the potential depends on phenyl substitution. However, the shifts of the oxidation potential are smaller than those taking place as a result of different substitution of β-ketoiminate ligands. This indicates that the effect of various phenyl substituents is lower than that of direct substitution of β-ketoiminate.

Table 1 Basic electrochemical properties

Compound	$E_{ox\,onset}$ [V]	$E_{red\,onset}$ [V]	E_g [V]	IP [eV]	EA [eV]
5a	0.14	−2.44	2.58	5.2	2.7
5b	0.21	−2.42	2.63	5.3	2.7
5c	0.18	−2.39	2.57	5.3	2.7
5d	0.18	−2.43	2.62	5.3	2.7
5e	0.12	−2.36	2.48	5.2	2.7
5f	0.32	−2.41	2.73	5.4	2.7
5g	0.30	−2.39	2.69	5.4	2.7

Irreversible reduction peaks are observed in the cathodic range. Cyclic voltammetry of the compounds studied reveals only a slight effect of fluorine atom substitution on $E_{red\,onset}$. All compounds show similar values of reduction potential. The results reveal that the studied compounds undergo a reduction process at lower potentials than iridium complexes with 2-phenylpridine (ppy) and 2-phenylbenzothiazole (bt) ligands and phenyl-substituted β-ketoiminate or phenyl-substituted β-diketiminate as ancillary ligands.[46] Ionization potential (IP) and energy affinity (EA) were estimated on the basis of the reduction and oxidation onset potentials. IP values increase with substitution of fluorine atoms. The incorporation of one atom changes the IP from 5.2 eV to 5.3 eV, whilst the incorporation of 5 or 4 atoms leads to molecules with an IP of 5.4 eV. It indicates a weak contribution of fluorine atoms to the HOMO. This effect is lower for the LUMO. The EA of all the studied compounds is 2.7 eV. It indicates a lower contribution of fluorine atoms to the LUMO of the studied compounds. The presented results confirm that the introduction of different fluorine-based groups to the phenyl moiety leads to the modification of electronic properties of iridium complexes. Different substitution groups impact mainly IP as a result of the modification of the HOMO.

Theoretical considerations

Molecular geometries in the ground state. The representative optimized structure of the studied complex **5b** in the ground state (S_0) is shown in Fig. 7. The geometries of the ground state structures were fully optimized without imposition of symmetry restrictions. The main optimized geometry parameters for **5b** in the gas phase and chlorobenzene environment are summarized in Table 2. All the studied complexes (the corresponding parameters are provided in the ESI†) show pseudo-octahedral coordination around the Ir metal centers, similar to that of the reported Ir(III) complexes, owing to the d^6 configuration. For all complexes, the two N atoms (N1 and N2) are at the *trans*

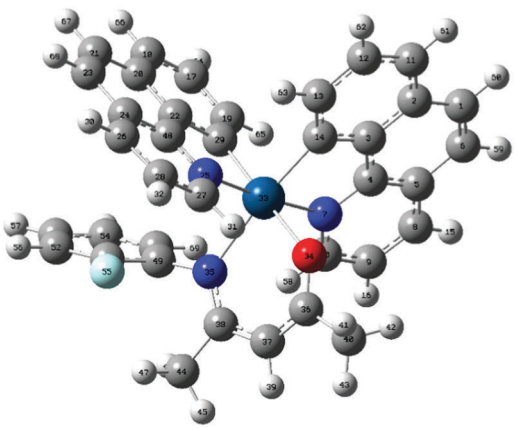

Fig. 7 The optimized structure of **5b** in the ground state.

Table 2 Selected bond distances and valence angles from the optimized geometries and the experimental values for **5b**

	Gas	C_6H_5Cl	X-ray
Bond lengths (Å)			
Ir–N1	2.093	2.098	2.065
Ir–N2	2.078	2.082	2.043
Ir–N3	2.244	2.240	2.153
Ir–C13	2.038	2.040	2.008
Ir–C25	2.030	2.029	1.996
Ir–O	2.185	2.192	2.133
Bond angles (deg)			
C13–Ir–C25	88.1	88.5	90.2
C13–Ir–N2	95.1	94.4	95.2
C25–Ir–N2	80.8	80.8	81.7
C13–Ir–N1	80.6	80.6	81.4
C25–Ir–N1	97.4	97.1	96.3
N2–Ir–N1	175.4	174.7	176.2
C13–Ir–N3	173.5	173.6	173.3
C25–Ir–N3	97.0	96.8	94.8
N2–Ir–N3	89.7	90.0	89.8
N1–Ir–N3	94.7	95.1	93.7
C13–Ir–O	88.9	88.7	86.9
C25–Ir–O	174.0	174.6	174.1
N2–Ir–O	94.3	94.8	93.4
N1–Ir–O	87.2	87.0	88.3
N3–Ir–O	86.3	86.3	88.4

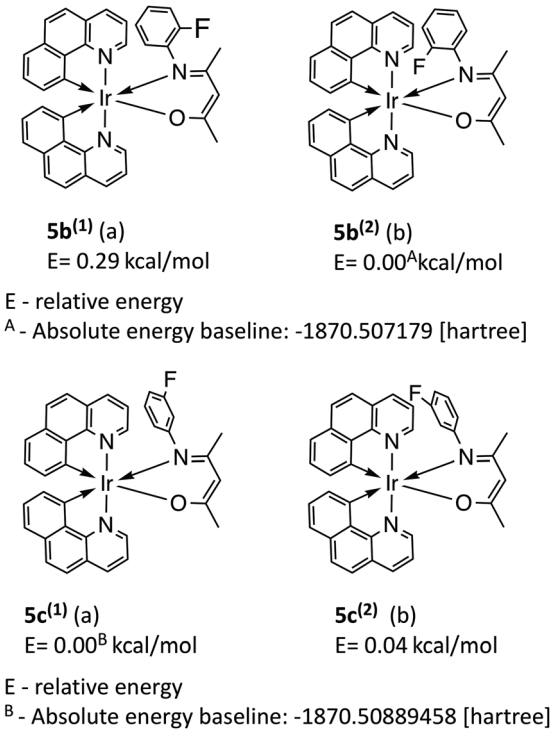

Fig. 8 Structures of conformers of **5b** and **5c** complexes.

position, while the C atoms (C13 and C25) are at the *cis* position. From Table 2, it is seen that the calculated Ir–N, Ir–C and Ir–O bond lengths are slightly greater in the chlorobenzene environment than in the gas phase. The maximum deviation in bond distances between the coordinating atoms and Ir(III) is 0.006 Å for **5b**, while changes in bond angles are less than 1.0°. However, the geometries of all the complexes present similar features, indicating that the solvent does not have a strong effect on the geometry of the complexes when compared to the isolated molecules.

A comparison of DFT computed and X-ray derived values of the geometry parameters is made in Table 2. The results show that the calculated Ir–N, Ir–C and Ir–O bond lengths are slightly greater than the corresponding experimental data. The differences between the calculated and the experimental values are in the range from 0.03 to 0.08 Å. Similarly, the optimized valence angles of **5b** are in good agreement with the experimental data and a deviation less than 2.0° is achieved.

One should note that for complexes **5b** and **5c**, two conformers with different orientation of fluorine atoms at the phenyl ring should be investigated (see Fig. 8). In both cases the energy differences between the two conformers are very small (less than 1 kcal mol^{-1}). It may suggest that for complexes **5b** and **5c** both structures are likely to be observed in the mixture of conformers. According to the results, the crystal structure of $\mathbf{5b^{(2)}}$ has slightly lower energy than that of $\mathbf{5b^{(1)}}$ (the difference is close to 0.29 kcal mol^{-1}).

Frontier molecular orbitals

Density functional theory (DFT) calculations helped us to investigate the frontier molecular orbitals (FMOs): the HOMO and LUMO. Seven calculated energy gaps between the HOMO and LUMO were correlated with their experimental values obtained by cyclic voltammetry measurements. The results of DFT calculation using different functionals: B3LYP, M06 and WB97XD were indeed in good correlation with experimental values.

As shown in Fig. 9, the HOMO–LUMO energy gaps ($E_g^{theor.}$) calculated using the WB97XD functional at the basis set composed of 6-311++G(d,p) and SDD for the Ir atom gave good correlation with the experimental values obtained from cyclic voltammetry measurements, which was characterized by an acceptable value of the correlation coefficient R = 0.905 in contrast to the results obtained by the other calculation methods.

The HOMO and LUMO distribution of energy levels and HOMO–LUMO energy gaps of the studied complexes are plotted in Fig. 10. The calculated energy gaps between the HOMO and LUMO were between 2.65 eV and 2.52 eV while the experimental ones were between 2.73 eV and 2.48 eV. The energies of FMOs calculated with the use of different methods are listed in Tables 6S–8S (ESI†).

Photophysical properties of the investigated Ir(III) complexes

The absorption spectra of the studied complexes **5a–5g** in chlorobenzene solution, under ambient conditions are presented in Fig. 11a and b. The examined complexes have similar absorption spectra. For all of them, one can distinguish broad absorption bands in the short-wavelength range (300–420 nm) and long-wavelength bands in the range of 420–550 nm. The lower energy ones, with lower extinction, for all studied complexes have a very similar shape and can be attributed to the MLCT transitions (mixture of both singlet and triplet character).[7]

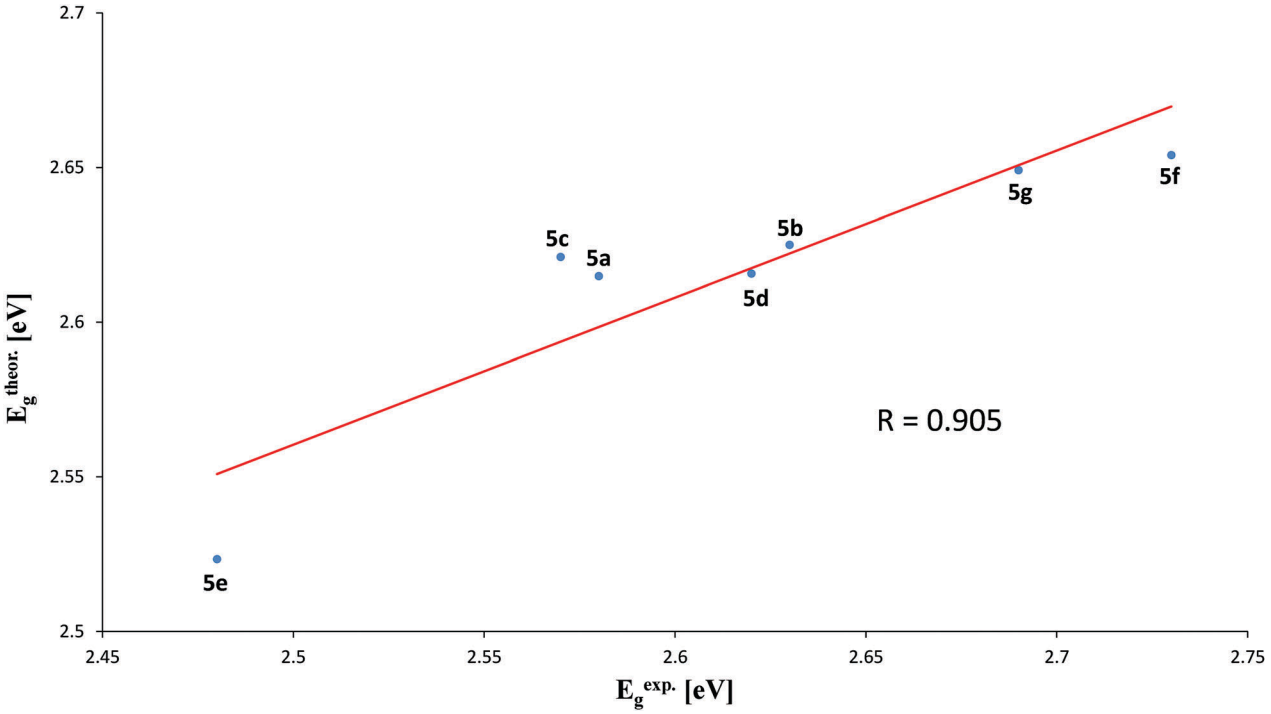

Fig. 9 Theoretical E_g values calculated at the WB97XD/SDD/6-311++G(d,p) level of theory *vs* experimental values.

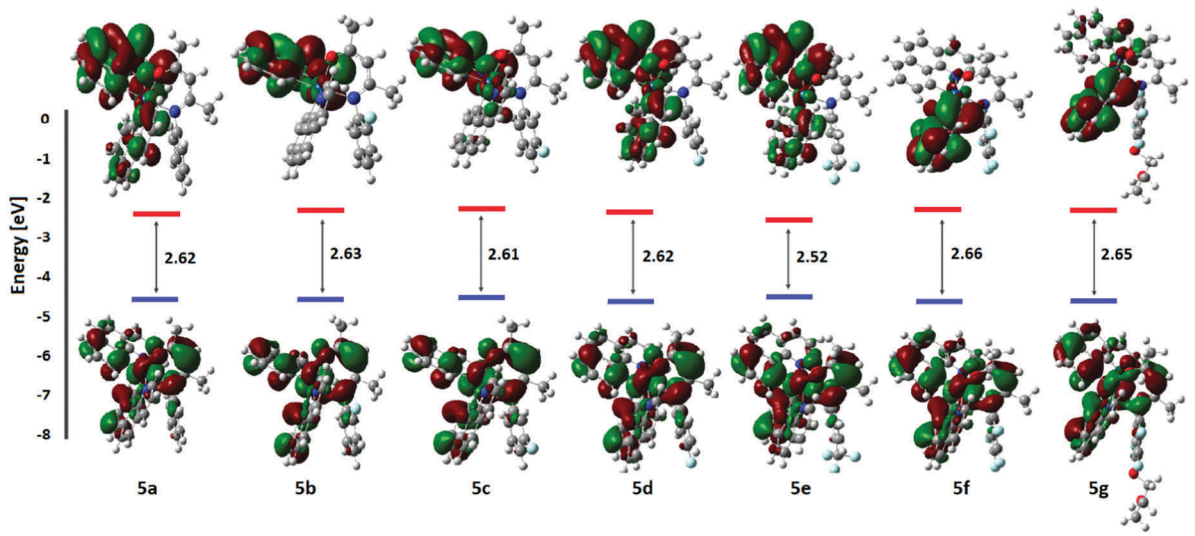

Fig. 10 Molecular orbital diagram of iridium(III) complexes along with the HOMO/LUMO plots computed at the WB97XD/SDD/6-31++G(d,p) level of theory.

The higher energy bands observed at about 325, 350 and 395 nm are assigned to the ligand centered (LC) transitions and their maxima positions and shapes differ slightly for the studied complexes. The bands with the maxima at 350 and 395 nm are better visible for the complexes with the largest number (5, 4 and 3) of introduced fluorine atoms into the phenyl ring in the ancillary ligand. The normalized photoluminescence (PL) spectra of the studied complexes in dilute chlorobenzene solutions are shown in Fig. 12. Excitation with the wavelength corresponding to the MLCT bands at 440 nm of the complexes **5a–5e**, resulted in a broad emission band in the range of 500–750 nm, with a maximum at 579 nm for the reference complex **5a**, and in only slightly shifted maxima of emission at ~570 nm for the complexes **5b–5e** with one or three incorporated fluorine atoms. The results obtained are consistent with those previously presented for Ir(III) complexes with β-ketoiminate as ancillary ligands.[46,47] The optical properties, mainly the color of emitted light, is not changed drastically as a result of fluorination on the *N*-aryl substituent in the β-ketoiminate group. The electronic structure and character

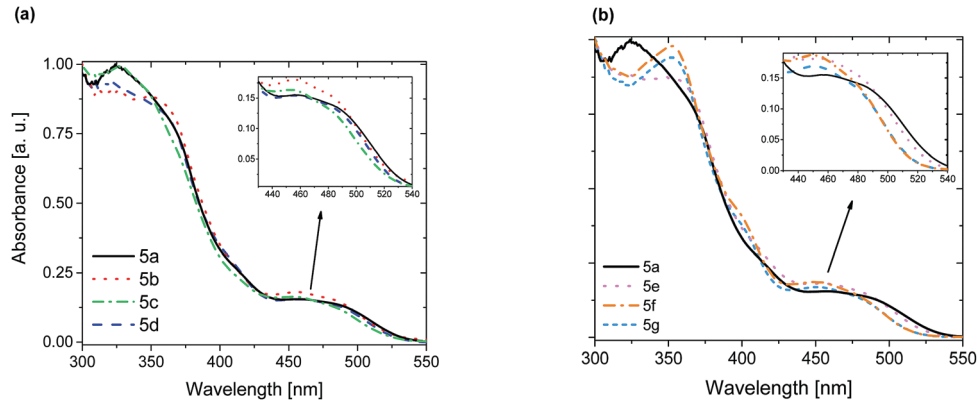

Fig. 11 Normalized absorption spectra of the investigated complexes in chlorobenzene: **5b**, **5c**, **5d** compared with **5a** (a), and **5e**, **5f**, **5g** compared with **5a** (b).

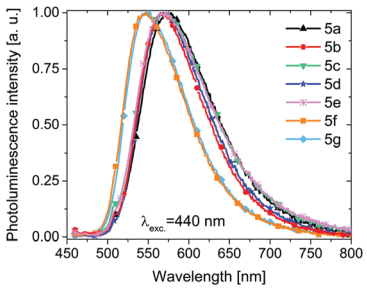

Fig. 12 Normalized photoluminescence spectra of the investigated complexes in chlorobenzene.

of emissive states are much more influenced by the substitution of fluorine atoms in the backbone of such ancillary ligands and this effect is more visible for β-diketiminate ligands.[46,47]

Only for the complexes with a sufficiently large number, four (**5g**) or five (**5f**), of fluorine atoms introduced into the ancillary ligand structure, the emission maximum is more shifted towards shorter wavelengths, by about 20 nm (λ_{max} ~ 550 nm). It correlates with theoretical results which predict that a significant part of the HOMO is localized on the ketoiminate ligand, while the LUMO is embedded on a completely different part of the molecule. Therefore, it is expected that functionalization of the ancillary ligand phenyl ring should have much stronger impact on the HOMO than LUMO energy levels. As shown by both calculations and electrochemical data, discrete changes are observed in the maximum position of the emission spectra (Table 3). In view of the above, they should be related to the effect of the electron withdrawing nature of the fluorine substituents on the HOMO energies (Table 1), thus shifting λ_{max} towards the blue. An inductive effect of fluorine substituents on the HOMO energy is related to the number of substituents since complexes **5f** and **5g** (bearing at least 4 fluorine substituents) emit at 546–547 nm, compounds **5b**, **5c** and **5d** (bearing one F atom) emit at 567–568 nm, while non-fluorinated compound **5a** emits at 577 nm. An exception is the complex **5e** with a CF_3 group which does not fit this trend (λ_{max} = 569 nm). The incorporation of fluorine into the phenyl ring of the ancillary ligand *via* a carbon atom has much less effect on the electronic structure of investigated complexes than the fluorine atoms introduced directly to the phenyl ring. The observed broad and unstructured phosphorescence bands suggest the emission is mainly from the MLCT states of these complexes.[55] These results are in line with the increased MLCT character of the complexes containing *N*-donating β-ketoiminate and β-ketiminate ligands in comparison to that of their previously reported acac analogues.[46] To explain the observed effects, one should take into account that when the complexes are heteroleptic and possess different chromophoric ligands, the orbitals involved in the lowest energy transitions can be located on both of them or mostly centered on one of them. In the studied complexes

Table 3 UV-Vis absorption and photoluminescence spectra data of the investigated compounds (dissolved in chlorobenzene). HOMO and LUMO levels are calculated on the basis of cyclic voltammetry experiments

Compound	$\lambda_{max\,Abs}$ [nm]	$\lambda_{max\,PL}$ [nm]	Quantum yield [%]	HOMO [eV]	LUMO [eV]
5a	~325, ~450, ~485	577	<1	−5.2	−2.7
5b	~320, ~350, ~400, ~450, ~485	567	<1	−5.3	−2.7
5c	~325, ~350, ~450, ~485	567	<1	−5.3	−2.7
5d	~318, ~350, ~450, ~485	568	<1 44.1[a]	−5.3	−2.7
5e	~325, ~350, ~400, ~450, ~485	569	<1	−5.2	−2.7
5f	~350, ~400, ~450, ~485	547	<1	−5.4	−2.7
5g	~350, ~400, ~450, ~485	546	<1 27.5[a]	−5.4	−2.7

[a] Degassed.

the HOMOs have similar shapes and are delocalized on almost the whole molecule, including the fluorine-functionalized ketoiminate ancillary ligand (*cf.* Fig. 10). Electrochemical studies proved that their energy is slightly changed for modified complexes, while the LUMO energies seem to be insensitive to modification of ligand (Table 1). However, the shapes of the LUMOs look different for the studied complexes. For **5a**, **5d** and **5e**, the electron density is moved from the ketoimine part towards the bzq ligands. In the complexes with a fluorine atom positioned *ortho* (**5b**) and *meta* (**5c**), upon excitation, the whole charge is transferred to the bzq group located further from the phenyl ring of the ancillary ligand. When the number of F atoms substituted to the phenyl ring is higher (**5f** and **5g**), the electrons are shifted to the second bzq ligand, which is in the proximity of the phenyl ring. However, in all cases the LUMO is not located on the ancillary ligand so modification of this part of the complex mainly influences the HOMOs as shown by electrochemical studies.

In Table 3 absorption and emission data for all complexes dissolved in chlorobenzene are summarized. HOMO and LUMO levels, calculated on the basis of CV experiments, are also displayed.

Interestingly, a lack of a fluorine regiosubstitution effect on the electrochemical and photophysical properties of the studied complexes was observed. As one can see, there are no significant differences between complexes **5b**, **5c** and **5d**, bearing fluorine in *ortho*, *meta* and *para* positions respectively. The absence of the regiofuncionalization effect on PL λ_{max} should be emphasized as it is in contrast to the state of the art, which claims that a correlation between regiosubstitution and emitted wavelength is well known.[2–4,7]

The photoluminescence quantum yield (QY) of all the examined complexes in solution is low (below 1%) although, as shown in Table 3, QY values depend on the presence of oxygen in the solution, which is typical of the phosphorescent emitters. Degassing of the solutions results in an increase in QY up to 44.1% and to 27.5% for complexes **5d** and **5g**, respectively.

Photoluminescence of the host–guest layers for application in PhOLEDs

To avoid the concentration induced emission quenching, the active layers in PhOLEDs are usually host–guest systems, in which the emitters are molecularly dispersed in a polymer matrix.[3,7,56] In this work we used the well-known composite of poly(*N*-vinylcarbazole) (PVK) and 2-(4-*tert*-butylphenyl)-5-(4-biphenylyl)-1,3,4-oxadiazole (PBD) as an ambipolar matrix.[57]

In this composite, PVK ensures hole transport and PBD supplies electron transport. Both components of the PVK/PBD mixture are characterized by wide energy gaps, which is necessary to ensure the energy transfer of the exciton from the matrix to the guest molecules whose LUMO and HOMO levels should be situated in the energy gap of the matrix.[58] The PL spectra of thin PVK/PBD films doped with 1 wt% of studied emitters upon excitation with the wavelength corresponding to the lowest absorption band of the PVK/PBD matrix (λ_{ex} = 340 nm), are presented in Fig. 13. One can see that the main photoluminescence bands are similar to those detected for solutions of the

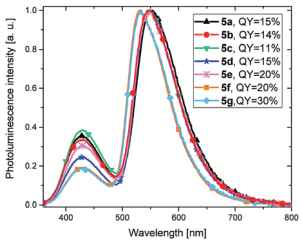

Fig. 13 Normalized photoluminescence spectra of thin layers of the PVK/PBD blend doped with 1 wt% of emitter molecules (**5a–5g**). Excitation wavelength was 340 nm.

emitters, (just blue shifted by about 20 nm), which indicates energy transfer from the matrix to the emitter molecules. However, in addition to the dopant emission, another band, originating from singlet exciplexes formed between the carbazole group and oxadiazole molecule (λ_{max} ~ 430 nm), is also observed.[57b] It is known that the oxadiazole and the carbazole groups form the excited state complexes and the PL maximum at around 430 nm has been assigned to the singlet exciplexes, which are created rapidly after the excitation of the PVK/PBD matrix.[57b,59–61] This interpretation was supported also by an observation that the intensity of this PL band increases for higher PBD content.[59] A contribution of the matrix emission indicates incomplete energy transfer from the matrix to the emitters. Efficiency of such an energy transfer influences the photoluminescence quantum yield (QY), which for the investigated layers ranges between 11% and 30% (see Fig. 13). As can be observed in this figure, the relative emission intensity from the PVK/PBD exciplexes is the lowest for the layers with the emitters substituted with 5 or 4 fluorine atoms (**5f** and **5g**) and it corresponds to higher QY values, 15% and 30%, respectively. Among the emitters with one fluorine atom, the one with substitution in the *para* position (emitter **5d**) displays the most efficient energy transfer from the matrix to the emitter.

Dominant contribution of the dopant emission in the investigated layers may arise from long range Förster and/or from short range Dexter energy transfer. The Dexter mechanism is less likely due to low emitter concentration; however, the exciton diffusion can enhance this path of energy transfer. Both mechanisms of energy transfer can operate effectively only when the emission spectrum of the donor and the absorption spectrum of the acceptor overlap considerably. For the tested emitters, the degree of spectral overlap is comparable (see Fig. 11 and 14).

Nevertheless, there are significant differences in experimental efficiency of exciton transfer energy, resulting from different matrix emission contribution in the PL spectra (see Fig. 13 and 14). Analysis of the Förster mechanism allowed determination of the theoretical (η_F) and real ($\eta_{exp.}$) efficiency of this process in the PVK/PBD matrix doped with 1 wt% of **5a**, **5d** or **5g** emitter. As shown in Table 4, there is a big discrepancy between the theoretical (~20%) and the experimental (~70%) values. It can be explained by the exciton diffusion effect, allowing excitons created on the matrix to approach the emitter molecules to a distance smaller than the average distance between the host and the guest molecules in the layer (see Table 4).

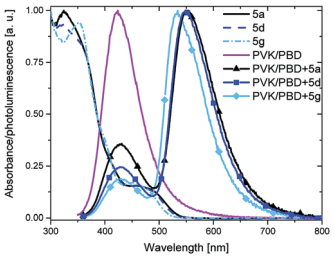

Fig. 14 Normalized absorption spectra of three selected compounds in chlorobenzene solutions and normalized photoluminescence spectra of thin layers: the neat PVK/PBD blend and PVK/PBD doped with 1 wt% of the selected emitter molecule (**5a**, **5d** or **5g**). Excitation wavelength was 340 nm.

Table 4 Photoluminescence quantum yield of thin layers (QY_{films}) and experimental efficiency of energy transfer ($\eta_{exp.}$) for PVK/PBD doped with 1 wt% of three selected emitters, and the parameters of Förster energy transfer for the systems: R_0 – Förster radii, R_{DA} – average distance between the host and the guest molecules, η_F – efficiency of energy transfer by Förster mechanism

Compound	QY_{films} [%]	$\eta_{exp.}$ [%]	R_0 [nm]	R_{DA} [nm]	η_F [%]
5a	15	71.9	2.045	2.576	20.0
5d	15	72.1	2.063	2.595	20.2
5g	30	65.6	1.981	2.737	12.6

Electroluminescent properties

The electroluminescence ability of the iridium complexes was tested in PhOLEDs with the simplest structure, *i.e.* a device with one active layer produced from solution (Fig. 15). Such a simple structure is a requirement from the point of view of the printing technique since printing of multilayer structures is very difficult. Additionally, such a minimalistic approach offers a screening procedure enabling quick selection of the most promising emitters.

The emissive layers of fabricated PhOLEDs were based on the same matrix–emitter systems as for the PL investigations described above. It should be noted that the mentioned PVK/PBD blend with 0.6 : 0.4 wt ratio is characterized by balanced transport capabilities for carriers of both types, which is required to obtain the efficient so-called single-layer OLEDs.[3,57a] Electroluminescence (EL) spectra recorded for the devices with investigated emitters are presented in Fig. 16. EL spectra obtained for PhOLEDs based on emitters **5a–5e** are very similar to each other and similar to their PL spectra. The maximum emission occurs at 555 nm and is only slightly red shifted by *ca.* 5 nm in relation to the PL spectra (compare the spectra in Fig. 13 and 16).

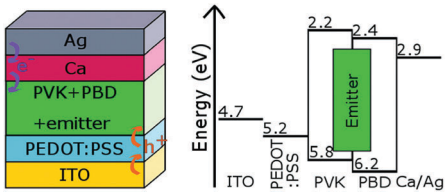

Fig. 15 PhOLED architecture and energy levels of the used materials.

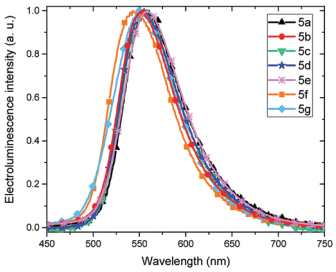

Fig. 16 Normalized electroluminescence spectra of PhOLEDs with PVK/PBD doped with 1 wt% of the investigated emitter molecules as emission layers.

Similarly like the PL bands, the EL bands for PhOLEDs with the emitters **5f** and **5g** are slightly shifted in comparison to those with the other emitters. Nevertheless, the shift observed in the EL spectra (by *ca.* 10 nm) is less noticeable than that in the PL spectra (over 20 nm). However, the most important difference between the EL and PL spectra is the lack of emission from the matrix in the EL spectra. The red shift of the EL spectra and disappearance of the band originating from the matrix have a direct effect on the *x*, *y* color coordinates of the emitted light according to the CIE 1931 diagram. It is presented in Fig. 17a and b for the samples with 1 wt% of emitter **5g**.

The lack of the matrix contribution in the EL spectra may indicate a considerable role of charge carriers trapped in the electroluminescence phenomenon, which can promote formation of excitons on the dopant molecules.[62] Current density–voltage (*J*–*V*) and luminance–voltage (*L*–*V*) characteristics of PhOLEDs, based on all tested emitters, are shown in Fig. 18.

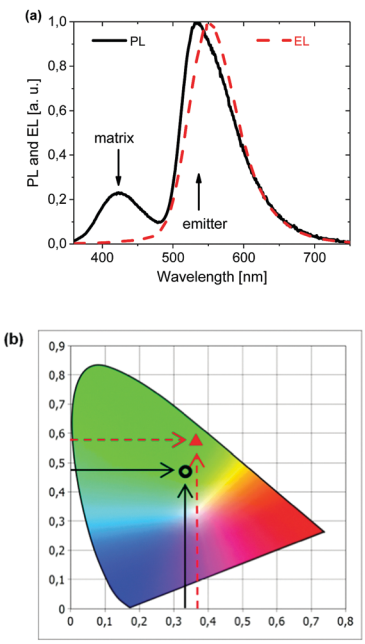

Fig. 17 Photoluminescence and electroluminescence spectra of the PVK/PBD layer doped with 1 wt% of emitter **5g** (a), and the CIE 1931 diagram with points indicating the color of the emitted light (PL marked as circle and EL as filled triangle) (b).

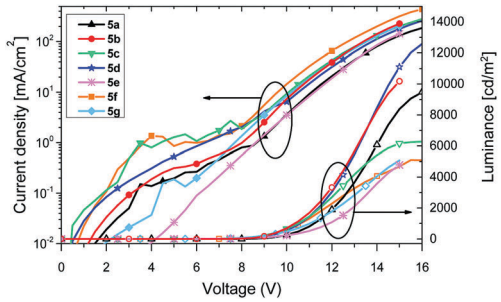

Fig. 18 Current density–luminance–voltage (*J–L–V*) characteristics of PhOLEDs with PVK/PBD doped with 1 wt% of emitter molecules. Full symbols: current density–voltage characteristics; empty symbols: luminance–voltage characteristics.

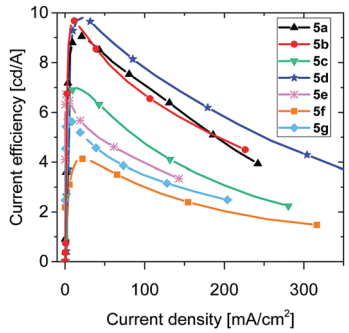

Fig. 19 Current efficiency–current density dependencies of PhOLEDs with emitting layer made of PVK/PBD doped with 1 wt% of all the tested Ir complexes.

These dependencies exhibit the typical shape in the range up to 16 V. The obtained luminance values are in the range from 5000 to over 12 000 cd m^{-2} at 16 V. The turn-on voltage (defined as voltage at which the detected luminance value is 1 cd m^{-2}) is between 6.5 and 8 V. In Fig. 19, the current efficiencies are plotted *versus* current density for the tested devices. The highest value (almost 10 cd A^{-1}) was obtained for PhOLEDs with emitter **5d**, which has a fluorine atom substituted in the *para* position of the phenyl ring. Only slightly lower performance was shown by the devices with emitter **5a**, *i.e.* complex without a fluorine atom or with emitter **5b** with a fluorine atom in the *ortho* position. Definitely the least efficient in electroluminescence turns out to be emitter **5f**; the devices with this emitter show a current efficiency of only 4 cd A^{-1}. A comparison of the parameters determined for all tested Ir complex-based devices is shown in Table 5. It should be noted that although these diodes were not encapsulated, they were stable over a series of measurements performed in air, lasting up to 8 hours. One should keep in mind that the lifetime of the diodes strongly depends on all of its components and not only on the emitter stability. However, the stability of the emitter might be verified in the course of CIE chromaticity monitoring, during the device operation. For all reported diodes, the colour of emitted light remained unchanged under applied voltages in the range of 8 to 16 V. For example, the diode based on complex **5d** exhibited average coordinates of the emitted light x = 0.428 and y = 0.559, with standard deviation 0.004 and 0.003 respectively, in the voltage range of 8 to 16 V. This indicates that the electroluminescence properties of the reported iridium complexes are relatively stable. For more detailed analysis of the fabricated PhOLEDs performance, we have selected devices with emitter **5a** (as a reference without a fluorine atom), with emitter **5d** (yielding the best PhOLEDs) and with emitter **5f** (yielding the least efficient devices). Fig. 20 shows the basic characteristics of these devices. The characteristic shapes are similar, but the current density values at 16 V are different: 180 mA cm^{-2} for emitter **5a**, *ca.* 250 mA cm^{-2} for emitter **5d** and over 400 mA cm^{-2} for emitter **5f**. The highest luminance values, above 11 000 and 9000 cd m^{-2}, were obtained for the devices based on emitters **5d** and **5a**, respectively. Their high performance is confirmed also by the current efficiency–luminance characteristics presented in the insets in Fig. 20. PhOLEDs based on the best emitter **5d** (Fig. 20b), show the current efficiency of 9.8 cd A^{-1} at a luminance of over 2100 cd m^{-2}, and 5.5 cd A^{-1} at a luminance of over 12 000 cd m^{-2}.

Table 5 Parameters of PhOLEDs with PVK/PBD layers doped with 1 wt% of all the tested Ir complexes

Compound	L_{max} [cd m^{-2}]	η_{max} [cd A^{-1}]	EQE [%]	EL peak position [nm]
5a	9500	9.1	2.71	560
5b	10 000	9.7	2.75	553
5c	6200	7.0	1.80	556
5d	13 000	9.8	2.68	554
5e	4800	6.7	1.99	559
5f	5000	4.1	1.13	543
5g	5000	5.8	1.65	550

It should be emphasized that the best devices exhibit quite good parameters, considering that the diodes have the simplest structure (single layer) and are produced using solution methods. The performance of the PhOLEDs depends on the concentration of the emitter in the active layer. To determine this dependence, a series of devices were prepared with different contents (from 0.5 to 5.0 wt%) of emitter **5g**, which embedded in the PVK/PBD matrix exhibits the highest quantum photoluminescence efficiency (30%).

It should be added that we controlled morphology and surface roughness of the emissive layers using polarized microscopy, AFM (ESI†) and a profilometer. We have not found any influence of addition of the emitter, even at a concentration of 5 wt%, or of annealing, on morphology and on surface roughness of the polymer matrix. Fig. 21 shows the *J–V* and *L–V* characteristics of these PhOLEDs. There is a significant decrease in the value of the current density, by about one order of magnitude, for the voltage of 16 V with increasing emitter concentration. The maximum luminance values (at 16 V) are in the range from *ca.* 4000 cd m^{-2} for a concentration of 0.5 wt% to over 7000 cd m^{-2} for 2 wt%. The maximum value of current efficiency (about 7.4 cd A^{-1}) was obtained for the devices with emitter concentration of 3 and 5 wt% (see Fig. 22). A slightly lower value (about 6.4 cd A^{-1}), but with lower dynamics of its decrease for higher values of current density, was observed for the diodes with the emission layer with 2% content of this emitter.

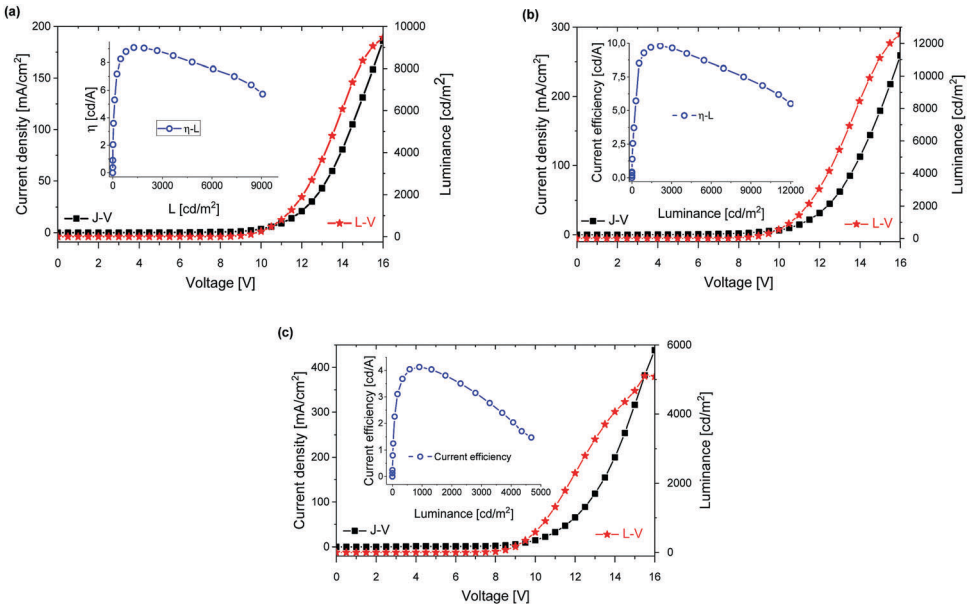

Fig. 20 Current density–luminance–voltage (*J*–*L*–*V*) characteristics of PhOLEDs with emitting layer made of PVK/PBD doped with 1 wt% of emitter molecules: **5a** (a), **5d** (b) and **5f** (c). Insets show their current efficiency–luminance dependencies.

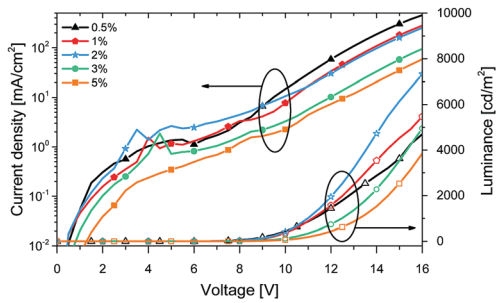

Fig. 21 Current density–luminance–voltage (*J*–*L*–*V*) characteristics of PhOLEDs with emitting layer made of PVK/PBD doped with different concentrations (from 0.5 to 5 wt%) of emitter **5g**. Full symbols: current density–voltage characteristics; empty symbols: luminance–voltage characteristics.

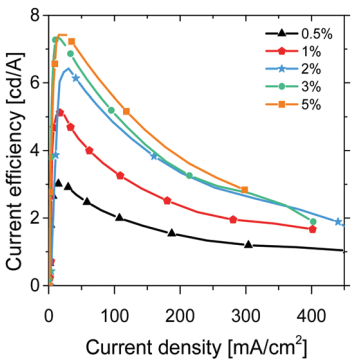

Fig. 22 Current efficiency–current density dependency of PhOLEDs with emitting layer made of PVK/PBD doped with different concentration (from 0.5 to 5 wt%) of **5g** emitter.

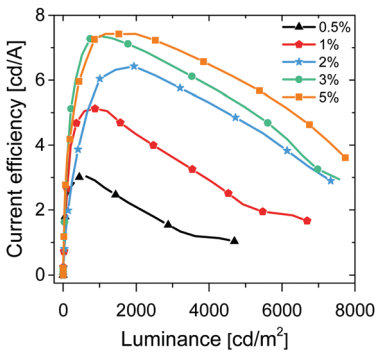

Fig. 23 Current efficiency–luminance dependency of PhOLEDs with emitting layer made of PVK/PBD doped with **5g** in different concentrations (from 0.5 to 5 wt%).

However, the current efficiency–luminance characteristics shown in Fig. 23 indicate that the best performance was exhibited by the devices with the emitter concentration of 5 wt%. The reduction in current density (Fig. 21) and higher current efficiency (Fig. 22 and 23) observed for the diodes with higher emitter concentration may be caused by two effects. The first one may be an increase in the probability of direct injection of holes into the emitter molecules in the near-anode area. It seems to be possible due to the small barrier between the HOMO levels of PEDOT/PSS (5.2 eV) and the emitter (5.4 eV). In such a scenario, the transfer of the exciton from the matrix to the emitter is omitted. The second reason may be the presence of deep trap states, both for holes (approximately 0.4 eV) and electrons (approximately 0.3 eV), located on the emitter molecules in the whole volume of the emissive layer. In Fig. 24, the EL and PL spectra for PhOLEDs and layers with different concentration of emitter **5g** are compared. As one can see, in contrast to the PL spectra almost complete quenching of PVK/PBD emission in EL occurs even for the lowest concentration

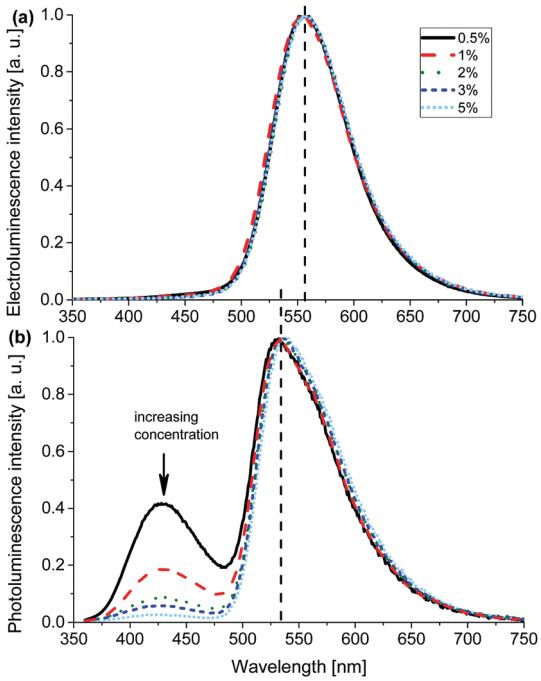

Fig. 24 Comparison of the electroluminescence (a) and photoluminescence (b) spectra of emitting layer made of PVK/PBD doped with **5g** in different concentrations (from 0.5 to 5 wt%).

(0.5 wt%) of emitter **5g**. In addition, the EL spectra have a slightly different shape and the maximum emission is a bit red shifted (about 10 nm) compared to the PL band. In order to elucidate the possible role of trapping phenomena in the electroluminescence process, for the best emissive layer, PVK/PBD with 1 wt% emitter **5d**, the spectrally resolved thermoluminescence (SRTL) studies were performed.[60] Previously published SRTL results for the host–guest system with another iridium complex have shown that trapping of charge carriers on the emitter molecules competes with the trapping on the matrix; in the electroluminescence process such trapping results in efficient formation of excitons on the emitter and finally in elimination of emission from the matrix.[57b,58a] Fig. 25 shows the SRTL results for the undoped PVK/PBD matrix and for the PVK/PBD matrix doped with **5d** iridium complex. Comparison of both SRTL spectra indicates that the emitter molecules create deeper and more efficient traps as compared to the traps present in the undoped PVK/PBD matrix. The TL intensity is about twice as high as the TL intensity for neat matrix (compare the non-normalized isothermal spectra shown in Fig. 25c). Comparison of the monochromatic spectra for neat PVK/PBD and for PVK/PBD with 1 wt% of emitter **5d** (Fig. 25b) leads to a conclusion that incorporation of the emitter results in an increased relative intensity of the TL signal in the high temperature range. This indicates the presence of deeper traps located on the emitter's molecules, which is expected taking into account the positions of HOMO and LUMO levels of emitter **5d** in relation to the levels of PVK/PBD matrix [see Table 3 and Fig. 15].

Comparison of the isothermal spectra of light emitted close to the TL maximum temperature, *i.e.* at about 105 K, reveals not

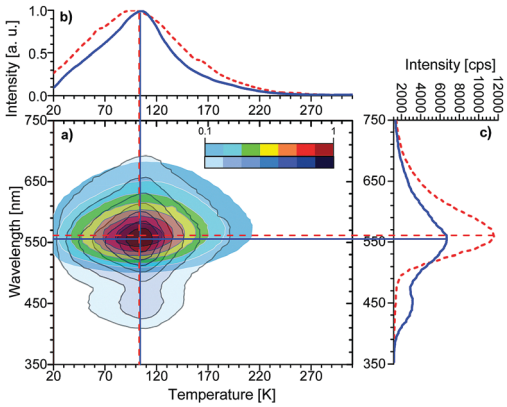

Fig. 25 The SRTL spectra for undoped PVK/PBD layer and for PVK/PBD layer doped with 1 wt% of emitter **5d**: the TL maps (a); normalized monochromatic TL curves recorded at $\lambda \sim 560$ nm (b); non-normalized isothermal spectra of emitted light recorded at *ca.* 105 K (c). Straight lines on the SRTL map indicate: selected wavelength for monochromatic TL curves (horizontal lines) and selected temperature for isothermal spectra of emitted light (vertical lines).

only the large difference in the TL intensity discussed above, but also a clear difference in the shape of the emission curves (Fig. 25c). The spectrum obtained for neat PVK/PBD has two characteristic broad bands: the dominant one with a maximum at 550 nm and the second one with a maximum at ~430 nm. These bands are assigned to the exciplexes formed between the carbazole group and oxadiazole molecule: the dominant band originates from the triplet exciplexes, and the band at 430 nm can be related to the singlet exciplexes.[57b]

Due to the fact that the emission band typical of the matrix with a maximum at 550 nm is very close to the emission band of the complex molecules (maximum at 560 nm), it is difficult to clearly identify the active center of radiative recombination in the TL experiment. However, one can see that the spectrum of PVK/PBD doped with **5d** has no short-wavelength band and the main emission band with a maximum at ~560 nm is much more intensive and it has a smaller half-width than that for undoped PVK/PBD matrix. Taking into account the differences, it can be assumed that in the TL spectrum of PVK/PBD doped with emitter **5d** the emission from the iridium complex dominates. Hence, one can conclude that introduction of the iridium complex molecules results in formation of new, deeper trapping states which promote creation of radiative recombination centers directly on the Ir complex molecule. It is worth noting that the spectrum of light emitted in the TL experiment for PVK/PBD doped with **5d** shown in Fig. 25c is similar in the shape and in the maximum position to the EL spectrum for this system (*cf.* Fig. 16), indicating that in both TL and EL phenomena the same emission centers operate. This effect has been already observed for other iridium complexes embedded in PVK and PVK/PBD.[58a,b,63]

Conclusions

In summary, a rapid and efficient method involving microwaves as a non-classical energy carrier has been successfully

applied in the synthesis of a series of novel heteroleptic iridium(III) cyclometalated complexes ([Ir(bzq)$_2$(O^N)]) stabilized with fluorinated β-ketoiminate ancillary ligands. The effects of aryl imine moiety fluorination on the electronic structure, and the electrochemical and photophysical properties of new iridium complexes were studied. For this purpose, appropriate aryl substituents equipped with a different number of fluorine atoms located at various positions of the phenyl ring were introduced into the examined ancillary ligands. TG analysis showed that the studied complexes are thermally stable up to 270 °C and there is no correlation between chemical structure of iridium materials and their thermal stability. Cyclic voltammetry measurements of new iridium(III) coordination compounds have revealed that fluorination of phenyl-substituted β-ketoiminate ligands leads to an increase in the oxidation and ionization potentials of the studied iridium(III) complexes, however for the reduction process the effect of structure modification of the ancillary ligand was negligible. These results were supported by the quantum chemistry calculations based on DFT methods – we found good agreement between the calculated HOMO/LUMO energies and the experimental data.

The photophysical studies have shown, as expected, that the effect of fluorine substitution on optical properties of the Ir complexes increases with the growing number of fluorine atoms. The strongest (although still relatively weak) effect, *ca.* 20 nm blue-shift of the emission maximum, was found for the Ir complexes with four or five fluorine atoms substituted to the phenyl ring of the ancillary ligand.

One can conclude that the theoretical as well as the electrochemical and photophysical studies yield a coherent picture explaining why fluorination of phenyl-substituted β-ketoiminate ligands does not modify substantially the electronic properties of iridium complexes. By contrast, the electroluminescence performance of the host–guest systems, PVK/PBD layers doped with 1 wt% of studied complexes, depends strongly on the structure of the fluorinated ligands. While the PL spectra show the presence of emission bands from both the Ir complex and from the PVK/PBD matrix, demonstrating incomplete matrix–emitter energy transfer, in the EL spectra only the emission from the dopant is visible. Although all PhOLEDs based on the studied emitters showed electroluminescence spectra of similar shapes (according to the CIE 1931 diagram, all studied complexes can be qualified as green-yellow emitters), the maximum current efficiency and the maximum luminance values are very different for Ir complexes with varied fluorinated ligands. The maximum values, current efficiency of 9.8 cd A^{-1} and luminance of 13 000 cd m^{-2}, were obtained for the Ir complex with one fluorine atom substituted in the *para* position in the phenyl ring of the ancillary ligand, which turned out to be the most efficient emitter among the studied Ir complexes. The SRTL experiments performed for the PVK/PBD matrix doped with the most efficient emitter indicate that the emitter molecules create deep trapping states. On the basis of the SRTL, PL and EL results, one can conclude that the introduction of iridium complex molecules results in efficient formation of excitons on the emitter and in the quenching of matrix emission seen in the EL phenomenon.

Experimental

General information

All synthesis and manipulations were carried out under argon using standard Schlenk-line and vacuum techniques. The microwave-assisted reactions were performed with use of a CEM Discover microwave pressure system (Power max. 300 W, magnetron frequency 2455 MHz, pressure max. 20 bars). The chemicals were obtained from the following sources: $IrCl_3 \cdot 3H_2O$ from Pressure Chemicals, acetone, acetylacetone (acacH), Et_2O, MeOH, $CDCl_3$, 1,2-dichloroethane, THF, arylamines from Aldrich, benzo[*h*]quinoline (bzqH) from ABCR. The complex [{Ir(μ-Cl)(bzq)$_2$}$_2$] (**4**)[64] was synthesized according to the published method. All solvents and liquid reagents were dried and distilled under argon prior to use. The NMR spectra for 4-arylimino-2-pentanones were recorded in $CDCl_3$ on a 300 MHz spectrometer at 298 K, using $SiMe_4$ as internal standard for ^{1}H and ^{13}C measurements and $CFCl_3$ for ^{19}F measurements. For iridium complexes, the chemical shifts were referenced to the residual protonated solvent peaks (^{1}H δ_H = 7.26 ppm, for $CDCl_3$). HRMS data were obtained on an AMD 402 two-sector mass spectrometer of B/E geometry.

X-ray crystallography

Diffraction data were collected using the ω-scan technique, at 100(1) K on a Rigaku Xcalibur four-circle diffractometer with Eos CCD detector and graphite-monochromated MoK_α radiation (λ = 0.71069 Å). The data were corrected for Lorentz-polarization as well as for absorption effects.[65] Precise unit-cell parameters were determined by a least-squares fit of reflections of the highest intensity (3596 for **3f**, 10 921 for **5b**, 6785 for **5e**, 5737 for **5g**), chosen from the whole experiment. The structures were solved with SHELXT[66] and refined with the full-matrix least-squares procedure on F^2 by SHELXL-2013.[66] All non-hydrogen atoms were refined anisotropically, hydrogen atoms in **3f** were found in difference Fourier maps and freely isotropically refined, in all other structures were placed in idealized positions and refined as a 'riding model' with isotropic displacement parameters set at 1.2 (1.5 for methyl groups) times U_{eq} of appropriate carrier atoms. In one of the symmetry-independent molecules of **5b** the phenyl ring was found to be disordered, the s.o.f. converged at 62.3(14)/37.7(14)%. In **5e** the CF_3 group was found in two alternative positions with occupations of 65.4(8)% and 34.6(8)% for more and less occupied positions, respectively. In both cases the restraints were applied to the geometry (SAME in **5b**, DFIX in **5e**) and displacement ellipsoids (ISOR, RIGU) of disordered fragments. In **5e**, additionally, a disordered solvent molecule was found, which was modelled as methanol with s.o.f. fixed at 1/2. Table 1S (ESI†) lists the relevant crystallographic and refinement data.

Crystallographic data for the structural analysis have been deposited with the Cambridge Crystallographic Data Centre, CCDC 1814938 (**3f**), 1814939 (**5b**), 1814940 (**5e**), and 1814941 (**5g**).

Thermal analysis

Thermogravimetric analysis (TGA) of the prepared complexes was carried out using a Q50-TGA thermobalance (TA Instruments, Inc.)

under N_2 flow of 60 mL min^{-1}. Samples (3–7 mg) to be studied were loaded on a platinum pan and heated from RT to 1000 °C at a rate of 10 °C min^{-1}.

DSC measurements of prepared complexes were carried out on samples (3–6 mg) placed in 40 μL aluminum pans with a pierced lid, in an N_2 atmosphere at a flow rate of 20 mL min^{-1} in a temperature range from −50 to 270 °C at a heating/cooling rate of 10 °C min^{-1} using a Mettler-Toledo DSC-1 differential scanning calorimeter.

Electrochemical properties measurement

Cyclic voltammetry (CV) measurement was performed on an Autolab PGSTAT 100N using platinum wire as a working electrode, a platinum spiral as a counter electrode and silver wire as a pseudo-reference electrode calibrated using ferrocene as an internal standard. Measurement was carried out in dichloromethane (Sigma Aldrich, HPLC grade) with 0.2 M tetrabutylammonium tetrafluoroborate (Bu_4NBF_4) (TCI, purity >98%) as a supporting electrolyte. Bu_4NBF_4 was dried in a vacuum drier for at least 24 hours before use. 2 mM solutions of studied compounds were used. The solutions were deoxidized by argon bubbling prior to measurement. Oxidation onset potential ($E_{ox\,onset}$) and reduction onset potential ($E_{red\ \ onset}$) were estimated from the intersections of tangential lines of redox peaks and background line. Ionization potential (IP) and electron affinity (EA) and electrochemical energy gap (E_g) were estimated from the equations IP = $(5.1 + E_{ox\,onset})|e^-|$ and EA = $(5.1 + E_{red\,onset})|e^-|$, $E_g = E_{ox\,onset} - E_{red\,onset}$.

Computational methods

All the molecular geometries of the iridium compounds in their singlet ground state were optimized using density functional theory (DFT)[67] with B3LYP – the hybrid Becke's three parameter functional and Lee–Young–Parr exchange–correlation potential.[68] B3LYP is one of the most popular functionals and can be applied for different systems.[69] The calculations were performed using the 6-31G(d) basis set for H, C, N, O and F atoms.[70] For the Ir metal center the SDD basis set was selected as it contains an effective core pseudopotential.[71] After preliminary calculations the basis set was extended from 6-31G(d) to 6-311++G(d,p). The DFT calculations using the B3LYP,[68] M06,[72] WB97XD[73] functionals based on the optimized S_0 geometries were performed to obtain the energies of the highest occupied molecular orbital (HOMO) and the lowest unoccupied orbital (LUMO). The presence of solvent was included within the SCRF (self-consistent reaction field) theory using the polarized continuum model (PCM)[74] in chlorobenzene (C_6H_5Cl)-medium which was used in experimental measurements. All calculations were carried out with the Gaussian09 software package[75] in PL-Grid infrastructure.

Spectroscopic measurements

Absorbance measurements were performed using a Carry 5000 (Varian) spectrometer, whereas photoluminescence was measured on an Edinburgh Instruments FLS980 spectrofluorometer. The luminescence quantum yields of the studied compounds were detected using an integrating sphere, with BENFLEC inside coating. The spectra were recorded with a spectral resolution of 1 nm. For the spectroscopic studies, the standard 1 cm path length quartz cuvette was used. All compounds were measured in dilute solutions ($\sim 10^{-5}$ M) of chlorobenzene. The same equipment was used for thin film spectroscopic studies of PVK/PBD blend (0.6 : 0.4 weight ratio) doped with iridium complexes. About 60 nm thin films were deposited on quartz plates by means of a spin-coating and their thicknesses were determined by a profilometer (Dektak XT, Bruker). This profilometer was used also to determine surface roughness of the samples in area of a few mm^2, while for a smaller area (*ca.* 10 × 10 μm) atomic force microscope (FlexAFM with C3000 controller, Nanosurf) was employed. The homogeneity of the dispersion of the emitter molecules in the PVK/PBD matrix was controlled by observation of thin films under the AFM and a polarizing microscope.

Samples of layers (thickness in a 4–5 μm range) for SRTL experiments were obtained by drop casting from chlorobenzene solutions onto stainless steel substrates at room temperature. The samples of PVK/PBD doped with 1 wt% of the tested complexes were placed between a thermostated stage and sapphire plate, squeezed together with the aid of a brazen frame anchored thermally to the stage, in a vacuum chamber (closed-cycle cryogenic system APD Cryogenics, type Displex). The SRTL measurements were carried out in the 15–325 K temperature range under a heating rate of 7 K min^{-1} after photoexcitation at 15 K for 10 min by a pulsed nitrogen laser (λ = 337 nm) PTI, model GL-3300. Light emitted during the SRTL experiment was detected by a specially designed detection system consisting of an optical collector, optical-fiber cable, a Micro HR Imaging Spectrograph and a CCD camera (Horriba Jobin-Yvon). The detailed SRTL experimental procedure was described previously.[57b,63]

Fabrication and characterization of PhOLEDs

The PhOLEDs were manufactured on glass substrates using a spin-coating method followed by a physical evaporation technique. The active layers were spin-coated from chlorobenzene solutions of PVK/PBD with dopant. Different emitters were added to the matrix with the same 1 wt% concentration. The dopant concentration influence on the device parameters were checked only for **5g** in the range of 0.5–5 wt%. These active layers were deposited on the top of a poly(3,4-ethylenedioxythiophene) and poly(styrenesulfonate) mixture (PEDOT:PSS) layer spin coated on an ITO electrode. The emissive layers in the devices had a thickness of about 60 nm and surface roughness of a satisfactory level. Measurements using AFM (on a surface of 10 × 10 μm) indicated that the root square roughness was in the range of 0.6–1.0 nm. The values of this parameter determined using the profilometer on a distance similar to the size of OLEDs (about 2 mm) do not exceed 10 nm. In the next step the cathode materials were patterned through a shadow mask with vacuum evaporation. The complete device stack was ITO/PEDOT:PSS/PVK:PBD+emitter/Ca/Ag as shown in Fig. 15. The devices were characterized by a Minolta CS-200 camera connected with a Keithley 2400 source measurement

unit, whereas the electroluminescence spectra were recorded by a CCD camera 3500 (Horiba Jobin Yvon).

Procedures

Synthesis of N,O-donating ligands – 4-arylimino-2-pentanones

*4-Phenylimino-2-pentanone (**3a**).* To a solution of 5.0 g of acacH (**1**) (0.05 mol) in benzene, 4.2 g of aniline (**2a**) (0.045 mol) and 20 mg of *p*-toluenesulfonic acid were added. The obtained mixture was refluxed using Dean–Stark apparatus, until no further water was generated (*ca.* 10 h). Then the solvent was evaporated and the oily residue was crystallized from hexane. The product was filtered off and dried in vacuum at r.t. Yield: 7.1 g (40.06 mmol, 90%), m.p. 47–49 °C.

HRMS (*m*/*z*): cal. for $C_{11}H_{13}NO$: 175.0997, found: 175.0971.

^{1}H NMR ($CDCl_3$): δ 12.47 (bs, 1H; N**H**); 7.32 (t, 2H, J = 7.7 Hz; $C_{Ar3,5}$**H**); 7.17 (t, 1H, J = 7.7 Hz; C_{Ar4}**H**); 7.09 (d, 2H, J = 7.7 Hz; $C_{Ar2,6}$**H**); 5.18 (s, 1H; =C**H**); 2.09 (s, 3H; C(=O)C**H**$_3$); 1.98 (s, 3H; =CC**H**$_3$). ^{13}C NMR ($CDCl_3$): δ 196.0 (C=O); 160.1 (=C–N); 138.7 (N-**C**$_{Ar1}$); 129.0 (**C**$_{Ar2,6}$); 125.5 (**C**$_{Ar4}$); 124.7 (**C**$_{Ar3,5}$); 97.5 (=**C**H); 29.1 (C(=O)**C**H$_3$); 19.8 (=C**C**H$_3$).

*4-(2-Fluorophenyl)imino-2-pentanone (**3b**).* 5.1 g (0.046 mol) of 2-fluoroaniline (**2b**) was used. Yield: 7.3 g (37.39 mmol, 82%), m.p. 47–48 °C.

HRMS (*m*/*z*): cal. for $C_{11}H_{12}FNO$: 193.0903, found: 193.0888.

^{1}H NMR ($CDCl_3$): δ 12.23 (bs, 1H; N**H**); 7.17 (m, 2H; $C_{Ar3,5}$**H**); 7.11 (m, 2H; $C_{Ar4,6}$**H**); 5.25 (s, 1H; =C**H**); 2.10 (s, 3H; C(=O)C**H**$_3$); 1.93 (s, 3H; =CC**H**$_3$). ^{13}C NMR ($CDCl_3$): δ 196.7 (C=O); 160.4 (=C–N); 156.6 (d, J = 248.1 Hz; **C**$_{Ar2}$F); 127.2 (d, J = 7.7 Hz; **C**$_{Ar4}$); 127.1 (**C**$_{Ar5}$); 126.8 (d, J = 12.8 Hz; N-**C**$_{Ar1}$); 124.3 (d, J = 4.0 Hz; **C**$_{Ar6}$); 116.2 (d, J = 20.3 Hz; **C**$_{Ar3}$); 98.1 (=**C**H); 29.2 (C(=O)**C**H$_3$); 19.5 (d, J = 2.6 Hz; =C**C**H$_3$). ^{19}F NMR ($CDCl_3$): −123.0 (ddd, J = 12.4, 8.1 & 5.2 Hz).

*4-(3-Fluorophenyl)imino-2-pentanone (**3c**).* 5.1 g (0.046 mol) of 3-fluoroaniline (**2c**) was used. Yield: 6.9 g (35.35 mmol, 78%), m.p. 38–40 °C.

HRMS (*m*/*z*): cal. for $C_{11}H_{12}FNO$: 193.0903, found: 193.0914.

^{1}H NMR ($CDCl_3$): δ 12.49 (bs, 1H; N**H**); 7.27 (td, 1H, J = 8.1 & 6.7 Hz; C_{Ar5}**H**); 6.86 (m, 2H; $C_{Ar2,4}$**H**); 6.81 (dt, 1H, J = 10.0 & 2.1 Hz; C_{Ar6}**H**); 5.20 (s, 1H; =C**H**); 2.09 (s, 3H; C(=O)C**H**$_3$); 2.02 (s, 3H; =CC**H**$_3$). ^{13}C NMR ($CDCl_3$): δ 196.6 (C=O); 162.8 (d, J = 247.1 Hz; **C**$_{Ar3}$F); 159.3 (=C–N); 140.4 (d, J = 10.0 Hz; N-**C**$_{Ar1}$); 130.2 (d, J = 9.4 Hz; **C**$_{Ar5}$); 119.9 (d, J = 3.1 Hz; **C**$_{Ar6}$); 112.0 (d, J = 21.1 Hz; **C**$_{Ar2}$); 111.4 (d, J = 23.4 Hz; **C**$_{Ar4}$); 98.4 (=**C**H); 29.2 (C(=O)**C**H$_3$); 19.9 (=C**C**H$_3$). ^{19}F NMR ($CDCl_3$): −112.1 (ddd, J = 10.0, 7.6 & 6.7 Hz).

*4-(4-Fluorophenyl)imino-2-pentanone (**3d**).* 4.9 g (0.044 mol) of 4-fluoroaniline (**2d**) was used. Yield: 6.5 g (33.30 mmol, 76%), m.p. 45–46 °C.

HRMS (*m*/*z*): cal. for $C_{11}H_{12}FNO$: 193.0903, found: 193.0927.

^{1}H NMR ($CDCl_3$): δ 12.33 (bs, 1H; N**H**); 7.06 (m, 2H; C_{Ar2}**H**); 7.02 (m, 2H; C_{Ar3}**H**); 5.17 (s, 1H; =C**H**); 2.08 (s, 3H; C(=O)C**H**$_3$); 1.91 (s, 3H; =CC**H**$_3$). ^{13}C NMR ($CDCl_3$): δ 196.3 (C=O); 160.6 (d, J = 245.8 Hz; **C**$_{Ar4}$F); 160.4 (=C–N); 134.7 (d, J = 3.2 Hz; N-**C**$_{Ar1}$); 126.8 (d, J = 8.4 Hz; **C**$_{Ar2,6}$); 115.8 (d, J = 22.6 Hz; **C**$_{Ar3,5}$); 97.5 (=**C**H); 29.1 (C(=O)**C**H$_3$); 19.6 (=C**C**H$_3$). ^{19}F NMR ($CDCl_3$): −116.9 (ttd, J = 8.1, 5.1 & 0.7 Hz).

*4-(4-Trifluoromethylphenyl)imino-2-pentanone (**3e**).* 7.3 g (0.045 mol) of 4-trifluoromethylaniline (**2e**) was used. Yield: 9.9 g (40.37 mmol, 90%), m.p. 70–71 °C.

HRMS (*m*/*z*): cal. for $C_{12}H_{12}F_3NO$: 243.0871, found: 243.0879.

^{1}H NMR ($CDCl_3$): δ 12.61 (bs, 1H; N**H**); 7.57 (d, 2H, J = 8.4 Hz; $C_{Ar3,5}$**H**); 7.18 (m, 2H, 8.4 Hz; $C_{Ar2,6}$**H**); 5.25 (s, 1H; =C**H**); 2.11 (s, 3H; C(=O)C**H**$_3$); 2.07 (s, 3H; =CC**H**$_3$).

^{13}C NMR ($CDCl_3$): δ 197.1 (C=O); 158.6 (=C–N); 142.2 (N-**C**$_{Ar1}$); 126.7 (q, J = 33.1 Hz; **C**$_{Ar4}$CF); 126.3 (q, J = 3.4 Hz; **C**$_{Ar3,5}$); 124.0 (q, J = 271.4 Hz; **C**F$_3$); 123.5 (**C**$_{Ar2,6}$); 99.3 (=**C**H); 29.3 (C(=O)**C**H$_3$); 20.1 (d, J = 2.6 Hz; =C**C**H$_3$). ^{19}F NMR ($CDCl_3$): −62.7 (s).

*4-(2,3,4,5,6-Pentafluorophenyl)imino-2-pentanone (**3f**).* In a pressure glass vessel of 10 mL capacity, equipped with a magnetic stirrer, 0.87 g (4.84 mmol, 1 eq.) of $C_6F_5NH_2$ (**2f**), 2.42 g (24.22 mmol; *ca.* 5 eq.) of acacH (**1**), 29.7 mg (0.0484 mmol) of $Er(OTf)_3$ and 3.00 mL of dried and deoxygenated toluene were placed. The reactor was sealed by a plastic cap equipped with elastic membrane and then placed in the chamber of a microwave radiation source. The thus prepared reaction system was sealed with the encapsulating head, equipped with a pressure sensor. The reaction was conducted for 10 minutes at 150 °C, irradiating the mixture with microwaves (150 W and frequency 2445 MHz). After this time, the solvent and excess of acacH were fully evaporated from the post-reaction mixture under reduced pressure. The remaining crude product was purified by column chromatography using silica as the solid phase. The reaction mixture was applied on the top of the column and separation was carried out using a *n*-hexane/DCM mixture (9 : 1, v/v). The purified material was dried *in vacuo* for 4 hours. The desired product **3f** was obtained in 85% yield (1.1 g, 4.12 mmol), m.p. 93–95 °C.

HRMS (*m*/*z*): cal. for $C_{11}H_8F_5NO$: 265.0526 found: 265.0525.

^{1}H NMR ($CDCl_3$): δ 11.90 (bs, 1H; N**H**); 5.38 (s, 1H; =C**H**); 2.12 (s, 3H; C(=O)C**H**$_3$); 1.84 (s, 3H; =CC**H**$_3$).

^{13}C NMR ($CDCl_3$): δ 198.1 (C=O); 159.8 (=C–N); 143.5 (ddq, J = 248.9, 11.6 & 4.1 Hz; **C**$_{Ar2,6}$F); 139.9 (dtt, J = 254.8, 13.3 & 4.2 Hz; **C**$_{Ar4}$F); 137.8 (ddddd, J = 252.4, 16.0, 12.6, 5.0 & 3.2; **C**$_{Ar3,5}$F); 114.5 (t; J = 13.9 Hz; N-**C**$_{Ar1}$); 99.6 (=**C**H); 29.3 (C(=O)**C**H$_3$); 18.8 (d, J = 2.6 Hz; =C**C**H$_3$). ^{19}F NMR ($CDCl_3$): −146.6 (m; $C_{Ar2,6}$**F**); −156.8 (t, 1F, J = 21.3 Hz; C_{Ar4}**F**); −162.4 (m; $C_{Ar3,5}$**F**).

Synthesis of iridium(III) complexes

*[Ir(bzq)$_2${MeC(O)=CHC(=NPh)Me}] (**5a**).* In a Schlenk vessel equipped with a magnetic stirrer, 60.0 mg (1.505 mmol; *ca.* 8.8 eq.) of NaH (60% dispersion in mineral oil) was placed and washed with *n*-pentane (3 × 3 mL), then 3 mL of dried and deoxygenated THF was added. In the next step, to the stirred NaH suspension, 66.0 mg (0.377 mmol; 2.2 eq.) of **3a** was introduced. The reaction was conducted until hydrogen evolution ceased. The mixture obtained was transferred by a

syringe equipped with a syringe-filter disc to a pressure glass vessel of 10 mL capacity, in which a portion of 200.00 mg (0.171 mmol, 1.0 eq.) of [{Ir(bzq)$_2$(μ-Cl)}$_2$] (**4**) and 5 mL of anhydrous and deoxygenated THF were placed under inert atmosphere. The reactor was sealed by a plastic cap equipped with elastic membrane and then placed in the chamber of a microwave radiation source. The thus prepared reaction system was sealed with an encapsulating head, equipped with a pressure sensor. The reaction was conducted for 15 minutes at 80 °C, irradiating the mixture with microwaves (150 W and frequency 2445 MHz). After this time, the solvent was fully evaporated from the post-reaction mixture under reduced pressure. The remaining crude product was purified by column chromatography using silica as the solid phase. At the beginning, the reaction mixture applied on the top of the column was washed with a *n*-hexane/DCM mixture (1 : 3, v/v). After washing off the excess of pure ligand, separation was carried out using pure DCM as the eluent. The purified material was dried *in vacuo* for 4 hours. The desired product **5a** was obtained in 65% yield (160 mg, 0.222 mmol). HRMS (EI) calc. for $C_{37}H_{28}IrN_3O$: $[M]^+$ 723.1862, found 723.1870. ^{1}H NMR (300 MHz, $CDCl_3$, 300 K) δ (ppm) = 9.32 (d, $^3J_{H-H}$ = 6.00 Hz, 1H); 9.12 (d, $^3J_{H-H}$ = 6.00 Hz); 8.23 (d, $^3J_{H-H}$ = 9.00 Hz, 1H); 8.15 (d, $^3J_{H-H}$ = 6.00 Hz, 1H); 7.73 (d, $^3J_{H-H}$ = 9.00 Hz, 2H); 7.59 (m, 4H); 7.23 (d, $^3J_{H-H}$ = 9.00 Hz, 2H); 6.91 (m, 2H); 6.61 (t, $^3J_{H-H}$ = 6.00 Hz, 1H); 6.31 (m, 4H); 5.97 ($^3J_{H-H}$, 2H); 4.87 (s, 1H, =CH–); 4.71 (d, $^3J_{H-H}$ = 9.00 Hz, 1H); 1.70 (s, 3H, –CH_3); 1.60 (s, 3H, –CH_3).

*[Ir(bzq)$_2${MeC(O)=CHC(=N(2-F-C$_6$H$_4$))Me}] (**5b**).* Following the procedure used for preparation of **5a**, the reaction was carried out with 158.00 mg (0.135 mmol, 1.0 eq.) of **4**, 48.00 mg (1.188 mmol, 8.8 eq.) of NaH and 58.00 mg (0.297 mmol, 2.2 eq.) of **3b**. The remaining crude product was purified by column chromatography using silica as the solid phase. At the beginning the reaction mixture applied on the top of the column was washed with a *n*-hexane/DCM mixture (1 : 1, v/v). After washing off the excess of pure ligand, separation was carried out using pure DCM as the eluent. The desired product **5b** was obtained in 72% yield (144 mg, 0.194 mmol).

HRMS (EI) calc. for $C_{37}H_{27}FIrN_3O$: $[M]^+$ 741.1767, found 741.1772; ^{1}H NMR (300 MHz, $CDCl_3$, 300 K) δ (ppm) = 9.24 (dd, $^3J_{H-H}$ = 9.00 Hz, J = 5.22 Hz, 1H); 9.09 (t, $^3J_{H-H}$ = 6.00 Hz, 1H); 8.23 (m, 1H); 8.16 (m, $^3J_{H-H}$ = 8.00 Hz, 1H); 7.59 (m, 3H); 7.49 (d, $^3J_{H-H}$ = 9.00 Hz, 2H); 7.24 (d, $^3J_{H-H}$ = 9.00 Hz, 1H); 6.93 (m, 2H); 6.66 (dt, $^3J_{H-F}$ = 25.00 Hz, $^3J_{H-H}$ = 9.00 Hz; 1H); 6.39–5.85 (m, 5H); 4.87 (s, 1H, =CH–); 4.45 (m, 1H); 1.70 (s, 3H, –CH_3); 1.61 (s, 3H, –CH_3).

*[Ir(bzq)$_2${MeC(O)=CHC(=N(3-F-C$_6$H$_4$))Me}] (**5c**).* Following the procedure used for preparation of **5a**, the reaction was carried out with 158.00 mg (0.135 mmol, 1.0 eq.) of **4**, 48.00 mg (1.188 mmol, 8.8 eq.) of NaH and 58.00 mg (0.297 mmol, 2.2 eq.) of **3c**. The remaining crude product was purified by column chromatography using silica as the solid phase. At the beginning the reaction mixture applied on the top of the column was washed with a *n*-hexane/DCM mixture (1 : 1, v/v). After washing off the excess of pure ligand, separation was carried out using a *n*-hexane/DCM mixture (1 : 3, v/v). The desired product **5c** was obtained in 66% yield (132 mg, 0.178 mmol) – mixture of two isomers 40/60.

HRMS (EI) calc. for $C_{37}H_{27}FIrN_3O$: $[M]^+$ 741.1767, found 741.1774; ^{1}H NMR (300 MHz, $CDCl_3$, 300 K) δ (ppm) = ^{1}H NMR (300 MHz, $CDCl_3$, 300 K) δ (ppm) = 9.45 (dd, $^3J_{H-H}$ = 6.00 Hz, J = 5.22 Hz, 1H, first isomer); 9.29 (d, $^3J_{H-H}$ = 6.00 Hz, 1H, second isomer) 9.14 (t, $^3J_{H-H}$ = 6.00 Hz, 1H, first isomer); 9.06 (d, $^3J_{H-H}$ = 6.00 Hz, 1H, second isomer); 8.20 (m, 4H); 7.73 (m), 7.58 (m), 7.45 (m) (12H); 7.22 (d, $^3J_{H-H}$ = 6.00 Hz, 2H); 6.91 (m, 4H); 6.62 (m, 2H); 6.40–6.05 (m, 7H); 5.96 (d, $^3J_{H-H}$ = 6.00 Hz, 1H); 5.81 (m); 5.68 (m, 1H); 4.94 (s, 1H, =CH–, second isomer); 4.87 (s, 1H, =CH–, first isomer); 4.61 (t, $^3J_{H-H}$ = 9.00 Hz, 1H); 1.72 (s, 3H, –CH_3, second isomer); 1.68 (s, 3H, –CH_3, first isomer); 1.63 (s, 3H, –CH_3, second isomer); 1.61 (s, 3H, –CH_3, first isomer).

*[Ir(bzq)$_2${MeC(O)=CHC(=N(4-F-C$_6$H$_4$))Me}] (**5d**).* Following the procedure used for preparation of **5a**, the reaction was carried out with 158.00 mg (0.135 mmol, 1.0 eq.) of **4**, 48.00 mg (1.188 mmol, 8.8 eq.) of NaH and 58.00 mg (0.297 mmol, 2.2 eq.) of **3d**. The remaining crude product was purified by column chromatography using silica as the solid phase. At the beginning the reaction mixture applied on the top of the column was washed with a *n*-hexane/DCM mixture (1 : 1, v/v). After washing off the excess of pure ligand, separation was carried out using pure DCM as the eluent. The desired product **5d** was obtained in 66% yield (180 mg, 0.243 mmol).

HRMS (EI) calc. for $C_{37}H_{27}FIrN_3O$: $[M]^+$ 741.1767, found 741.1770; ^{1}H NMR (300 MHz, $CDCl_3$, 300 K) δ (ppm) = 9.26 (d, $^3J_{H-H}$ = 6.00 Hz, 1H); 9.11 (d, $^3J_{H-H}$ = 6.00 Hz, 1H); 8.23 (d, $^3J_{H-H}$ = 9.00 Hz, 1H); 8.15 (d, $^3J_{H-H}$ = 9.00 Hz, 1H); 7.74 (d, $^3J_{H-H}$ = 9.00 Hz, 1H); 7.58 (m, 3H); 7.48 (m, 2H); 7.24 (d, $^3J_{H-H}$ = 9.00 Hz, 1H); 6.94 (m, 2H); 6.64 (t, $^3J_{H-H}$ = 6.00 Hz; 1H); 6.32 (d, $^3J_{H-H}$ = 9.00 Hz, 1H); 6.25 (m, 1H); 6.05 (dt, $^3J_{H-H}$ = 9.00 Hz, $^3J_{H-H}$ = 3.00 Hz, 1H); 5.96 (d, $^3J_{H-H}$ = 9.00 Hz, 1H); 5.65 (dt, $^3J_{H-H}$ = 9.00 Hz, J = 3.00 Hz, 1H); 4.86 (s, 1H, =CH–); 4.63 (m, 1H); 1.69 (s, 3H, –CH_3); 1.59 (s, 3H, –CH_3).

*[Ir(bzq)$_2${MeC(O)=CHC(=N(4-CF$_3$-C$_6$H$_4$))Me}] (**5e**).* Following the procedure used for preparation of **5a**, the reaction was carried out with 150.00 mg (0.128 mmol, 1.0 eq.) of **4**, 46.00 mg (1.126 mmol, 8.8 eq.) of NaH and 68.00 mg (0.282 mmol, 2.2 eq.) of **3e**. The remaining crude product was purified by column chromatography using silica as the solid phase. At the beginning the reaction mixture applied on the top of the column was washed with a *n*-hexane/DCM mixture (1 : 1, v/v). After washing off the excess of pure ligand, separation was carried out using pure DCM as the eluent. The desired product **5e** was obtained in 65% yield (130 mg, 0.166 mmol).

HRMS (EI) calc. for $C_{38}H_{27}F_3IrN_3O$: $[M]^+$ 791.1735, found 791.1744; ^{1}H NMR (300 MHz, $CDCl_3$, 300 K) δ (ppm) = 9.26 (d, $^3J_{H-H}$ = 6.00 Hz, 1H); 9.09 (d, $^3J_{H-H}$ = 6.00 Hz, 1H); 8.25 (d, $^3J_{H-H}$ = 9.00 Hz, 1H); 8.15 (d, $^3J_{H-H}$ = 6.00 Hz, 1H); 7.75

(d, $^3J_{H-H}$ = 9.00 Hz, 1H); 7.61 (d, $^3J_{H-H}$ = 9.00 Hz, 1H); 7.59 (m, 2H); 7.43 (s, 2H); 7.25 (d, $^3J_{H-H}$ = 6.00 Hz, 1H); 6.94 (m, 2H); 6.64 (t, $^3J_{H-H}$ = 9.00 Hz, 1H); 6.55 (d, $^3J_{H-H}$ = 9.00 Hz, 1H); 6.33 (m, 2H); 6.18 (d, $^3J_{H-H}$ = 9.00 Hz); 5.94 (d, $^3J_{H-H}$ = 6.00 Hz, 1H); 4.90 (s, 1H, =CH–); 4.75 (d, $^3J_{H-H}$ = 9 Hz, 1H); 1.70 (s, 3H, $-CH_3$); 1.61 (s, 3H, $-CH_3$).

*[Ir(bzq)$_2${MeC(O)=CHC(=NC$_6$F$_5$)Me}] (**5f**).* Following the procedure used for preparation of **5a**, the reaction was carried out with 360.00 mg (0.308 mmol, 1.0 eq.) of **4**, 108.00 mg (2.710 mmol, 8.8 eq.) of NaH and 180.00 mg (0.677 mmol, 2.2 eq.) of **3f**. The remaining crude product was purified by column chromatography using silica as the solid phase and a *n*-hexane/DCM mixture (1 : 2, v/v). After washing off the excess of pure ligand, separation was carried out using pure DCM as the eluent. The desired product **5f** was obtained in 76% yield (380 mg, 0.4683 mmol).

HRMS (EI) calc. for $C_{37}H_{23}F_5IrN_3O$: $[M]^+$ 813.1391, found 813.1402; ^{1}H NMR (300 MHz, $CDCl_3$, 300 K) δ (ppm) = 9.26 (m, 1H); 9.02 (d, J = 6 Hz, 1H); 8.23 (dt; J = 6 Hz, 2H); 7.74 (d, J = 9 Hz, 1H); 7.58 (m, 5 H); 7.27 (d, J = 6 Hz, 1H); 7.07 (d, J = 6 Hz, 1H); 6.95 (t, J = 9 Hz; 1H); 6.79 (t, J = 6 Hz, 1H); 6.27 (d, J = 9 Hz, 1H); 6.16 (dd, J = 9 Hz, J = 3 Hz, 1H); 5.03 (s, 1H, =CH–); 1.74 (s, 3H, $-CH_3$); 1.65 (s, 3H, $-CH_3$).

*[Ir(bzq)$_2${MeC(O)=CHC(=N(4-MeOCH$_2$CH$_2$OC$_6$F$_4$))Me}] (**5g**).* In a Schlenk vessel equipped with a magnetic stirrer, 200.00 mg (0.246 mmol, 1.00 eq.) of **5f** and 6 mL of dried and deoxygenated THF were placed, then 12.00 mg (*ca.* 0.313 mmol, 1.27 eq.) of NaH (60% dispersion in mineral oil) was added. In the next step, to the vigorously stirred mixture, 40 μL (0.507 mmol, 2.1 eq.) of $MeOCH_2$-CH_2OH was slowly introduced. The reaction was conducted for 72 h at 80 °C. After this time all volatile ingredients were evaporated under reduced pressure. The remaining crude product was dissolved in a small amount of 1,2-dichloroethane (DCE), then the solution obtained was applied on top of a column with silica. Separation was carried out using a *n*-hexane/DCE mixture (2 : 3, v/v). The purified material was dried *in vacuo* for 6 hours. The desired product **5g** was obtained in 68% yield (145 mg, 0.167 mmol).

HRMS (EI) calc. for $C_{40}H_{30}F_4IrN_3O_3$: $[M]^+$ 869.1853, found 869.1859; ^{1}H NMR (300 MHz, $CDCl_3$, 300 K) δ (ppm) = 9.29 (m, 1H); 9.03 (d, $^3J_{H-H}$ = 6.00 Hz, 1H); 8.23 (dd, $^3J_{H-H}$ = 6.00 Hz, 2H); 7.73 (d, $^3J_{H-H}$ = 6.00 Hz, 1H); 7.60 (d, $^3J_{H-H}$ = 6.00 Hz, 1H); 7.56 (m, 4H); 7.24 (d, $^3J_{H-H}$ = 6.00 Hz, 1H); 7.00 (d, $^3J_{H-H}$ = 9.00 Hz, 1H); 6.93 (t, $^3J_{H-H}$ = 9.00 Hz, 1H); 6.77 (t, $^3J_{H-H}$ = 9.00 Hz, 1H); 6.20 (m, 2H); 5.02 (s, 1H, =CH–); 3.86 (m, 2H, $-CH_2-$); 3.57 (t, 2H, $-CH_2-$); 3.41 (s, 3H, $-OCH_3$); 1.73 (s, 3H, $-CH_3$); 1.65 (s, 3H, $-CH_3$).

Conflicts of interest

There are no conflicts to declare.

Acknowledgements

This work was supported by the National Science Centre (Poland) through grant no. UMO-2013/11/B/ST5/01334. This research was supported in part by the PL-Grid Infrastructure. E. Witkowska acknowledges the financial support of the National Science Centre (Poland) through the grant no. UMO-2017/24/T/ST5/00017.

References

1 S. Miyata and H. S. Nalawa, in *Organic Electroluminescent Materials and Devices*, ed. S. Miyata and H. S. Nalawa, CRC Press, London, 1997, p. 496.
2 Z. R. Li, in *Organic Light-Emitting Materials and Devices*, ed. Z. R. Li, CRC Press, Boca Raton, FL, 2nd edn, 2015, p. 813.
3 H. Yersin, in *Highly Efficient OLEDs with Phosphorescent Materials*, ed. H. Yersin, Wiley-VCH Verlag GmbH and KgaA, Weinheim, 2008, p. 438.
4 L. F. R. Pereira, in *Organic Light Emitting Diodes: the Use of Rare Earth and Transition Metals*, ed. L. F. R. Pereira, CRC Press, Hoboken, NJ, 2012, p. 341.
5 (*a*) T. Sajoto, P. I. Djurovich, A. B. Tamayo, M. Yousufuddin, R. Bau, M. E. Thompson, R. J. Holmes and S. R. Forrest, *Inorg. Chem.*, 2005, **44**, 7992–8003; (*b*) C.-H. Chien, S. Fujita, S. Yamoto, T. Hara, T. Yamagata, M. Watanabe and K. Mashima, *Dalton Trans.*, 2008, 916–923; (*c*) J. Lee, H.-F. Chen, T. Batagoda, C. Coburn, P. I. Djurovich, M. E. Thompson and S. R. Forrest, *Nat. Mater.*, 2016, **15**, 92–98; (*d*) R. J. Holmes, S. R. Forrest, T. Sajoto, A. Tamayo, P. I. Djurovich, M. E. Thompson, J. Brooks, Y.-J. Tung, B. W. D'Andrade, M. S. Weaver, R. C. Kwong and J. J. Brown, *Appl. Phys. Lett.*, 2005, **87**, 243507; (*e*) H. Sasabe, J.-I. Takamatsu, T. Motoyama, S. Watanabe, G. Wagenblast, N. Langer, O. Molt, E. Fuchs, C. Lennartz and J. Kido, *Adv. Mater.*, 2010, **22**, 5003–5007.
6 (*a*) Y.-C. Chiu, C.-H. Lin, J.-Y. Hung, Y. Chi, Y.-M. Cheng, K.-W. Wang, M.-W. Chung, G.-H. Lee and P.-T. Chou, *Inorg. Chem.*, 2009, **48**, 8164–8172; (*b*) C.-H. Lin, Y.-Y. Chang, J.-Y. Hung, C.-Y. Lin, Y. Chi, M.-W. Chung, C.-L. Lin, P.-T. Chou, G.-H. Lee, C.-H. Chang and W.-C. Lin, *Angew. Chem., Int. Ed.*, 2011, **50**, 3182–3186.
7 E. Zysman-Colman, *Iridium(III) in optoelectronic and photonics applications*, John Wiley & Sons, Newark, NJ, 2017.
8 F. Xu, J.-H. Kim, H. U. Kim, D. Mi, Y. J. Cho, J. Y. Lee, U. Ch. Yoon and D.-H. Hwang, *Synth. Met.*, 2013, **178**, 10–17.
9 S. Lamansky, P. Djurovich, D. Murphy, F. Abdel-Razzaq, H.-E. Lee, C. Adachi, P. E. Burrows, S. R. Forrest and M. E. Thompson, *J. Am. Chem. Soc.*, 2001, **123**, 4304–4312.
10 M. K. Nazeeruddin, R. Humphry-Baker, D. Berner, S. Rivier, L. Zuppiroli and M. Graetzel, *J. Am. Chem. Soc.*, 2003, **125**, 8790–8797.
11 R. Tao, J. Qiao, G. Zhang, L. Duan, L. Wang and Y. Qiu, *J. Phys. Chem. C*, 2012, **116**, 11658–11664.
12 Q. Zhao, C. Huang and F. Li, *Chem. Soc. Rev.*, 2011, **40**, 2508–2524.
13 E. Baggaley, J. A. Weinstein and J. A. G. Williams, *Coord. Chem. Rev.*, 2012, **256**, 1762–1785.
14 Y. Yang, Q. Zhao, W. Feng and F. Li, *Chem. Rev.*, 2013, **113**, 192–270.

15 A. Maity, J.-S. Choi, T. S. Teets, N. Deligonul, A. J. Berdis and T. G. Gray, *Chem. – Eur. J.*, 2013, **19**, 15924–15932.
16 G. Li, Q. Lin, L. Ji and H. Chao, *J. Mater. Chem. B*, 2014, **2**, 7918–7926.
17 L. C.-C. Lee, J. C.-W. Lau, H.-W. Liu and K. K.-W. Lo, *Angew. Chem., Int. Ed.*, 2016, **55**, 1046–1049.
18 K.-W. K. Lo, C.-K. Chung, T. K.-M. Lee, L.-H. Lui, K. H.-K. Tsang and N. Zhu, *Inorg. Chem.*, 2003, **42**, 6886–6897.
19 K. K.-W. Lo, D. Ch.-M. Ng and Ch.-K. Chung, *Organometallics*, 2001, **20**, 4999–5001.
20 K. K.-W. Lo and A. H.-H. Leung, *Sci. China: Chem.*, 2010, **53**, 2091–2098.
21 W. H.-T. Law, L. C.-C. Lee, M.-W. Louie, H.-W. Liu, T. W.-H. Ang and K. K.-W. Lo, *Inorg. Chem.*, 2013, **52**, 13029–13041.
22 C. K. Prier, D. A. Rankic and D. W. C. MacMillan, *Chem. Rev.*, 2013, **113**, 5322–5363.
23 Z. Zuo, D. T. Ahneman, L. Chu, J. A. Terrett, A. G. Doyle and D. W. C. MacMillan, *Science*, 2014, **345**, 437–440.
24 T. P. Yoon, M. A. Ischay and J. Du, *Nat. Chem.*, 2010, **2**, 527–532.
25 K. Dedeian, P. I. Djurovich, F. O. Garces, G. Carlson and R. J. Watts, *Inorg. Chem.*, 1991, **30**, 1685–1687.
26 A. B. Tamayo, B. D. Alleyne, P. I. Djurovich, S. Lamansky, I. Tsyba, N. N. Ho, R. Bau and M. E. Thompson, *J. Am. Chem. Soc.*, 2003, **125**, 7377–7387.
27 (*a*) B. Orwat, E. Witkowska, I. Kownacki, M.-J. Oh, M. Hoffmann, M. Kubicki, I. Grzelak, B. Marciniec, I. Glowacki, B. Luszczynska, G. Wiosna-Salyga, J. Ulanski, P. Ledwon and M. Lapkowski, *Dalton Trans.*, 2017, **46**, 9210; (*b*) E. A. Plummer, A. van Dijken, J. W. Hofstraat, L. De Cola and K. Brunner, *Adv. Funct. Mater.*, 2005, **15**, 281–289; (*c*) K. K.-W. Lo, C.-K. Chung, T. K.-M. Lee, L.-H. Lui, K. H.-K. Tsang and N. Zhu, *Inorg. Chem.*, 2003, **42**, 6886–6897; (*d*) K. K.-W. Lo, J. S.-W. Chan, C.-K. Chung, V. W.-H. Tsang and N. Zhu, *Inorg. Chim. Acta*, 2004, **357**, 3109–3118; (*e*) M. S. Lowry, W. R. Hudson, R. A. Pascal Jr. and S. Bernhard, *J. Am. Chem. Soc.*, 2004, **126**, 14129–14135; (*f*) S. Salinas, M. A. Soto-Arriaza and B. Loeb, *Polyhedron*, 2011, **30**, 2863–2869; (*g*) C. Dragonetti, A. Valore, A. Colombo, S. Righetto and V. Trifiletti, *Inorg. Chim. Acta*, 2012, **388**, 163–167; (*h*) K. Huang, I. W. Bulik and A. A. Marti, *Chem. Commun.*, 2012, **48**, 11760–11762; (*i*) K.-H. Leung, H.-Z. He, V. P.-Y. Ma, H.-J. Zhong, D. S.-H. Chan, J. Zhou, J.-L. Mergny, C.-H. Leung and D.-L. Ma, *Chem. Commun.*, 2013, **49**, 5630–5632; (*j*) D.-L. Ma, L.-J. Liu, K.-H. Leung, Y.-T. Chen, H.-J. Zhong, D. S.-H. Chan, H.-M. D. Wang and C.-H. Leung, *Angew. Chem., Int. Ed.*, 2014, **53**, 9178–9182; (*k*) H. Ahmad, A. Wragg, W. Cullen, C. Wombwell, A. J. H. M. Meijer and J. A. Thomas, *Chem. – Eur. J.*, 2014, **20**, 3089–3096; (*l*) Z. Wu, J. Mu, Q. Wang, X. Chen, L. Jensen, Ch. Yi and M.-J. Li, *J. Organomet. Chem.*, 2015, **791**, 175–182.
28 (*a*) S. B. Meier, W. Sarfert, J. M. Junquera-Hernández, M. Delgado, D. Tordera, E. Ortí, H. J. Bolink, F. Kessler, R. Scopelliti, M. Grätzel, M. K. Nazeeruddin and E. Baranoff, *J. Mater. Chem. C*, 2013, **1**, 58; (*b*) C.-H. Yang, J. Beltran, V. Lemaur, J. Cornil, D. Hartmann, W. Sarfert, R. Fröhlich, C. Bizzarri and L. De Cola, *Inorg. Chem.*, 2010, **49**, 9891–9901.
29 (*a*) Y. You and S. Y. Park, *J. Am. Chem. Soc.*, 2005, **127**, 12438–12439; (*b*) Y. You, K. S. Kim, T. K. Ahn, D. Kim and S. Y. Park, *J. Phys. Chem. C*, 2007, **111**, 4052–4060.
30 (*a*) P.-T. Chou and Y. Chi, *Chem. – Eur. J.*, 2007, **13**, 380–395; (*b*) P.-C. Wu, J.-K. Yu, Y.-H. Song, Y. Chi, P.-T. Chou, S.-M. Peng and G.-H. Lee, *Organometallics*, 2003, **22**, 4938; (*c*) C. Di Pietro, S. Serroni, S. Campagna, T. Gandolfi, R. Ballardini, S. Fanni, W. R. Browne and J. G. Vos, *Inorg. Chem.*, 2002, **41**, 2871; (*d*) J. G. Vos and J. M. Kelly, *Dalton Trans.*, 2006, 4869.
31 S. Lamansky, P. Djurovich, D. Murphy, F. Abdel-Razzaq, R. Kwong, I. Tsyba, M. Bortz, B. Mui, R. Bau and M. E. Thompson, *Inorg. Chem.*, 2001, **40**, 1704–1711.
32 P. J. Hay, *J. Phys. Chem. A*, 2002, **106**, 1634–1641.
33 (*a*) M. S. Lowry and S. Bernhard, *Chem. – Eur. J.*, 2006, **12**, 7970–7977; (*b*) J. Li, P. I. Djurovich, B. D. Alleyne, M. Yousufuddin, N. N. Ho, J. C. Thomas, J. C. Peters, R. Bau and M. E. Thompson, *Inorg. Chem.*, 2005, **44**, 1713–1727; (*c*) N. M. Shavaleev, F. Monti, R. Scopelliti, A. Baschieri, L. Sambri, N. Armaroli, M. Grätzel and M. K. Nazeeruddin, *Organometallics*, 2013, **32**, 460–467.
34 L. Bourget-Merle, M. F. Lappert and J. R. Severn, *Chem. Rev.*, 2002, **102**, 3031–3066.
35 B. M. Chamberlain, M. Cheng, D. R. Moore, T. M. Ovitt, E. B. Lobkovsky and G. W. Coates, *J. Am. Chem. Soc.*, 2001, **123**, 3229–3238.
36 P. G. Hayes, W. E. Piers and R. McDonald, *J. Am. Chem. Soc.*, 2002, **124**, 2132–2133.
37 X.-F. Li, K. Dai, W.-P. Ye, L. Pan and Y.-S. Li, *Organometallics*, 2004, **23**, 1223–1230.
38 C. Cui, H. W. Roesky, H.-G. Schmidt, M. Noltemeyer, H. Hao and F. Cimpoesu, *Angew. Chem., Int. Ed.*, 2000, **39**, 4274–4276.
39 M. Driess, S. Yao, M. Brym, C. van Wüllen and D. Lentz, *J. Am. Chem. Soc.*, 2006, **128**, 9628–9629.
40 P. L. Holland and W. B. Tolman, *J. Am. Chem. Soc.*, 1999, **121**, 7270–7271.
41 K. C. MacLeod, D. J. Vinyard and P. L. Holland, *J. Am. Chem. Soc.*, 2014, **136**, 10226–10229.
42 F. Basuli, B. C. Bailey, J. Tomaszewski, J. C. Huffman and D. J. Mindiola, *J. Am. Chem. Soc.*, 2003, **125**, 6052–6053.
43 R. Thompson, C.-H. Chen, M. Pink, G. Wu and D. J. Mindiola, *J. Am. Chem. Soc.*, 2014, **136**, 8197–8200.
44 E. Kogut, H. L. Wiencko, L. Zhang, D. E. Cordeau and T. H. Warren, *J. Am. Chem. Soc.*, 2005, **127**, 11248–11249.
45 E. S. Jang, C. L. McMullin, M. Käß, K. Meyer, T. R. Cundari and T. H. Warren, *J. Am. Chem. Soc.*, 2014, **136**, 10930–10940.
46 Y. K. Radwan, A. Maity and T. S. Teets, *Inorg. Chem.*, 2015, **54**, 7122–7131.
47 R. A. Maya, A. Maity and T. S. Teets, *Organometallics*, 2016, **35**, 2890–2899.
48 J. E. Leffler and E. Grunwald, *Rates and Equilibria of Organic Reactions*, Wiley, 1963, (Dover reprint).
49 H. Konno, T. Ito and Y. Sugita, *Method for producing complex of trisortho-metalated iridium, light-emitting materiał using said complex, and light-emitting element, US Pat.* 2013/0203997 A1, 2013.

50 X. Shen, Y. Zhang, M. Xuea and Q. Shen, *Dalton Trans.*, 2012, **41**, 3668–3674.
51 R. Dalpozzo, A. De Nino, M. Nardi, B. Russo and A. Procopiob, *Synthesis*, 2006, 1127–1132.
52 (*a*) R. Xu and Y. Xu, in *Modern Inorganic Synthetic Chemistry*, ed. R. Xu and Y. Xu, Elsevier Science, 2nd edn, 2017, p. 808; (*b*) R. Xu, W. Pang and Q. Huo, in *Modern Inorganic Synthetic Chemistry*, ed. R. Xu, W. Pang and Q. Huo, Elsevier, 1st edn, 2011, p. 590.
53 (*a*) N. Yoshikawa, Y. Masuda and T. Matsumura-Inoue, *Chem. Lett.*, 2000, 1206–1207; (*b*) S. L. Van Atta, B. A. Duclos and D. B. Green, *Organometallics*, 2000, **19**, 2397–2399; (*c*) B. I. K. Oxana, V. Kharissova and U. O. Mendez, *Advances in Induction and Microwave Heating of Mineral and Organic Materials*, InTech, 2011, p. 766; (*d*) H. Phetmung, M. Wateh and C. Pakawatchai, *Turk. J. Chem.*, 2012, **36**, 556–566; (*e*) J. Lhoste, N. Henry, T. Loiseau and F. Abraham, *Inorg. Chem. Commun.*, 2011, **14**, 1525–1527; (*f*) T. Abe, A. Miyazawa, Y. Kawanishi and H. Konno, *Mini-Rev. Org. Chem.*, 2011, **8**, 315–333; (*g*) J.-R. Li, Z.-L. Xie, B. Hu and X.-Y. Huang, *Inorg. Chem. Commun.*, 2011, **14**, 265–267; (*h*) H. Konno, T. Ito and Y. Sugita, *Method for producing complex of trisortho-metalated iridium, light-emitting material using said complex, and light-emitting element, Jpn Pat.* 5881216, 2016.
54 (*a*) J. G. Allen, J. Burdon and J. C. Tatlow, *J. Chem. Soc.*, 1965, **0**, 1045–1051; (*b*) H. Amii and K. Uneyama, *Chem. Rev.*, 2009, **109**, 2119–2183.
55 (*a*) Y. You and W. Nam, *Chem. Soc. Rev.*, 2012, **41**, 7061–7084; (*b*) K. P. S. Zanoni, R. L. Coppo, R. C. Amaral and N. Y. M. Iha, *Dalton Trans.*, 2015, **44**, 14559–14573.
56 S. Reineke, M. Thomschke, B. Lüssem and K. Leo, *Rev. Mod. Phys.*, 2013, **85**, 1245–1294.
57 (*a*) B. Luszczynska, E. Dobruchowska, I. Glowacki, J. Ulanski, F. Jaiser, X. Yang, D. Neher and A. Danel, *J. Appl. Phys.*, 2006, **99**, 24505; (*b*) I. Glowacki and Z. Szamel, *J. Phys. D: Appl. Phys.*, 2010, **43**, 295101.
58 (*a*) I. Glowacki, Z. Szamel and G. Wiosna-Salyga, *Org. Electron.*, 2016, **31**, 127–135; (*b*) I. Glowacki, Z. Szamel and G. Wiosna-Salyga, *Synth. Met.*, 2016, **220**, 213–220; (*c*) B. Luszczynska, E. Dobruchowska, I. Glowacki, A. Danel and J. Ulanski, *J. Lumin.*, 2009, **129**, 1215–1218.
59 X. Jiang, R. A. Register, K. A. Killen, M. E. Thompson, F. Pschenitzka, T. R. Heber and J. C. Sturm, *J. Appl. Phys.*, 2002, **91**, 6717–6724.
60 X. Gong, S.-H. Lim, J. C. Ostrowski, D. Moses, Ch. J. Bardeen and G. C. Bazan, *J. Appl. Phys.*, 2004, **95**, 948–953.
61 R. A. Negres, X. Gong, J. C. Ostrowski, G. C. Bazan, D. Moses and A. J. Heeger, *Phys. Rev. B: Condens. Matter Mater. Phys.*, 2003, **68**, 115209.
62 I. Glowacki, J. Jung, G. Wiosna-Sałyga Gabriela, M. Chapran, A. Łuczak, B. Dupont, B. Łuszczyńska and J. Ulanski, *Display and Imaging*, 2017, **2**, 279–319.
63 I. Glowacki and Z. Szamel, *Org. Electron.*, 2015, **24**, 288–296.
64 (*a*) S. Suprouse, K. A. King, P. J. Spellane and R. J. Watts, *J. Am. Chem. Soc.*, 1984, **106**, 6647–6653; (*b*) M. Nonoyama, *Bull. Chem. Soc. Jpn.*, 1974, **47**, 767–768.
65 CrysAlisPro 1.171.38.34a, Rigaku OD, 2015.
66 G. M. Sheldrick, *Acta Crystallogr., Sect. C: Struct. Chem.*, 2014, **71**, 3–8.
67 A. D. Becke, *J. Chem. Phys.*, 1993, **98**, 5648–5652.
68 (*a*) P. J. Stephens, F. J. Devlin, C. F. Chabalowski and M. J. Frisch, *J. Phys. Chem.*, 1994, **98**, 11623–11627; (*b*) K. Kim and K. D. Jordan, *J. Phys. Chem.*, 1994, **98**, 10089–10094; (*c*) T. Clark, J. Chandrasekhar, G. W. Spitznagel and P. V. R. Schleyer, *J. Comput. Chem.*, 1993, **4**, 294–301.
69 (*a*) J. Miao, W. Xu, B. Zhu and Y. Gao, *Phys. Lett. A*, 2017, **381**, 2363–2366; (*b*) D. R. Glowacki, W. J. Rodgers, R. Shannon, S. H. Robertson and J. N. Harvey, *Philos. Trans. R. Soc., A*, 2017, **375**, 20160206; (*c*) N. Dechamps, R. Flammang, P. Gerbaux, P.-C. Nam and M.-T. Nguyen, *J. Am. Soc. Mass Spectrom.*, 2006, **17**, 807–814.
70 M. M. Francl, *J. Chem. Phys.*, 1982, **77**, 3654.
71 T. H. Dunning Jr and P. J. Hay, *Modern Theoretical Chemistry*, Plenum, New York, 1976.
72 Y. Zhao and D. G. Truhlar, *Theor. Chem. Acc.*, 2008, **120**, 215.
73 J.-D. Chai and M. Head-Gordon, *J. Chem. Phys.*, 2008, **128**, 084106.
74 (*a*) E. Cancès, B. Mennucci and J. Tomasi, *J. Chem. Phys.*, 1997, **107**, 3032–3041; (*b*) B. Mennucci and J. Tomasi, *J. Chem. Phys.*, 1997, **106**, 5151–5158; (*c*) M. Cossi, V. Barone, B. Mennucci and J. Tomasi, *Chem. Phys. Lett.*, 1998, **286**, 253–260.
75 M. Frisch, G. Trucks, H. Schlegel, G. Scuseria, M. Robb, J. Cheeseman, G. Scalmani, V. Barone, B. Mennucci, G. Petersson, H. Nakatsuji, M. Caricato, X. Li, H. Hratchian, A. Izmaylov, J. Bloino, G. Zheng, J. Sonnenberg, M. Hada, M. Ehara, K. Toyota, R. Fukuda, J. Hasegawa, M. Ishida, T. Nakajima, Y. Honda, O. Kitao, H. Nakai, T. Vreven, J. Montgomery, J. Peralta, F. Ogliaro, M. Bearpark, J. Heyd, E. Brothers, K. Kudin, V. Staroverov, R. Kobayashi, J. Normand, K. Raghavachari, A. Rendell, J. Burant, S. Iyengar, J. Tomasi, M. Cossi, N. Rega, J. Millam, M. Klene, J. Knox, J. Cross, V. Bakken, C. Adamo, J. Jaramillo, R. Gomperts, R. Stratmann, O. Yazyev, A. Austin, R. Cammi, C. Pomelli, J. Ochterski, R. Martin, K. Morokuma, V. Zakrzewski, G. Voth, P. Salvador, J. Dannenberg, S. Dapprich, A. Daniels, Ö. Farkas, J. Foresman, J. Ortiz, J. Cioslowski and D. Fox, *Gaussian 09, Revision B.01*, Gaussian Inc., Wallingford, CT, 2009.

Electronic Supplementary Information

Effect of fluorine substitution of the *β*-ketoiminate ancillary ligand on photophysical properties and electroluminescent ability of new iridium(III) complexes

Ewelina Witkowska,[a] Gabriela Wiosna-Salyga,[a]* Ireneusz Glowacki,[a] Bartosz Orwat,[b,c] Myong-joon Oh,[b,c] Ireneusz Kownacki,[b,c]** Maciej Kubicki,[b] Blazej Gierczyk,[b] Michal Dutkiewicz,[c,d] Pawel Cieszko,[b,c] Beata Luszczynska,[a] Jacek Ulanski,[a] Izabela Grzelak,[b] Marcin Hoffmann,[b] Przemyslaw Ledwon,[e] Mieczyslaw Lapkowski[e,f]

[a] Department of Molecular Physics, Lodz University of Technology, 90–924 Lodz, Zeromskiego 116, Poland, E–mail: Gabriela.Wiosna-Salyga@p.lodz.pl

[b] Faculty of Chemistry, Adam Mickiewicz University in Poznan, St. Umultowska 89b, 61–614 Poznan, Poland

[c] Center for Advanced Technology, Adam Mickiewicz University in Poznan, St. Umultowska 89c, 61–614 Poznan, Poland

[d] Poznan Science and Technology Park, Adam Mickiewicz University Foundation, ul. Rubiez 46, Poznan, Poland

[e] Silesian University of Technology, Faculty of Chemistry, St. Marcina Strzody 9, 44–100 Gliwice, Poland

[f] Centre of Polymer and Carbon Materials, Polish Academy of Sciences, Curie-Sklodowskiej 34, 41–819 Zabrze, Poland

* *E-mail: Gabriela.Wiosna-Salyga@p.lodz.pl*

** *E-mail: Ireneusz.Kownacki@amu.edu.pl*

Table of contents

1. Spectroscopic data of 4-arylimino-2-pentanones	**S3**
2. Crystallographic data	**S14**
3. Thermal analysis data	**S17**
4. Cyclic voltammetry measurements	**S23**
5. DFT calculation data	**S24**
6. AFM data	**S46**

1. Spectroscopic data of 4-arylimino-2-pentanones

4-Phenylimino-2-pentanone (3a)

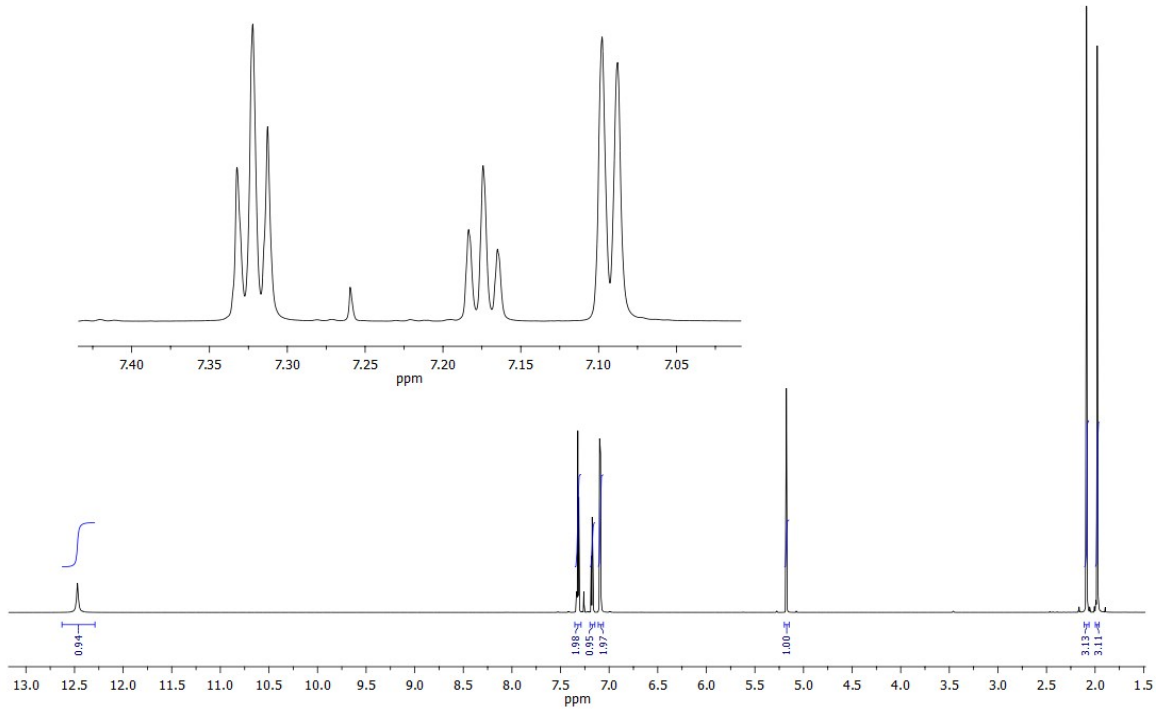

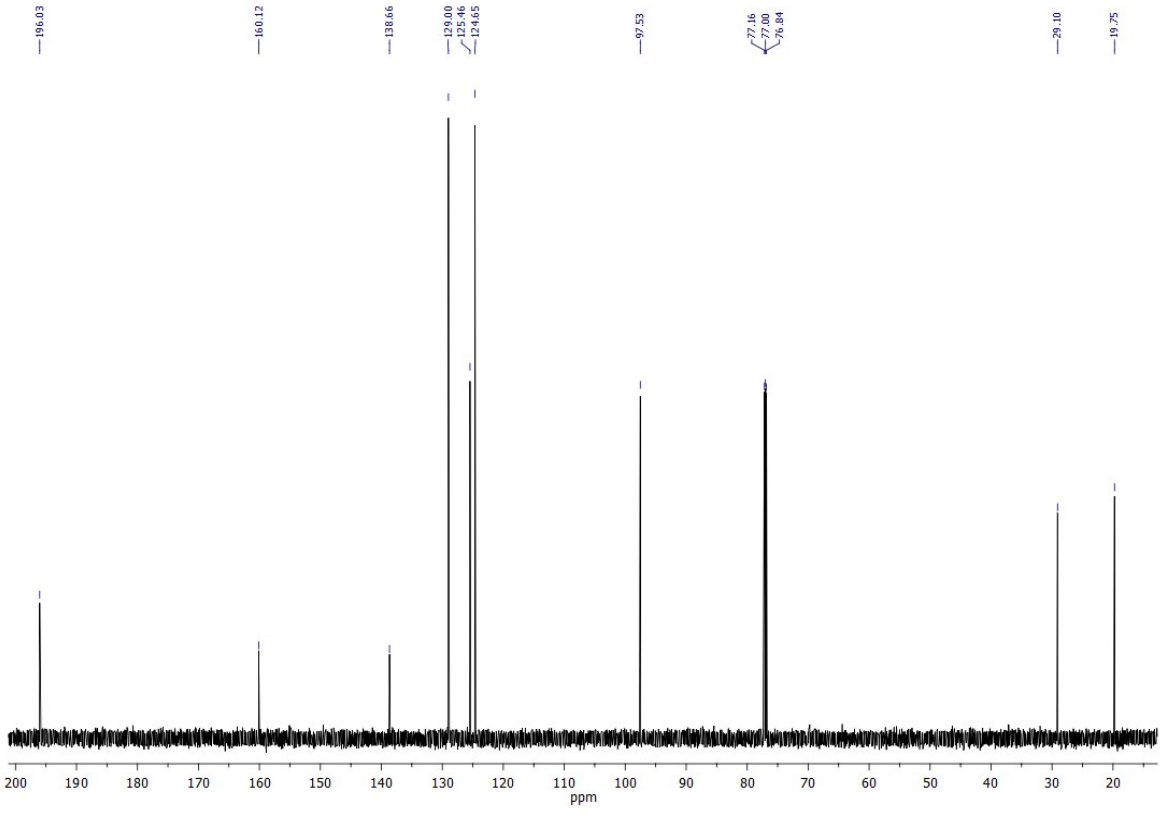

4-(2-Fluorophenyl)imino-2-pentanone (3b)

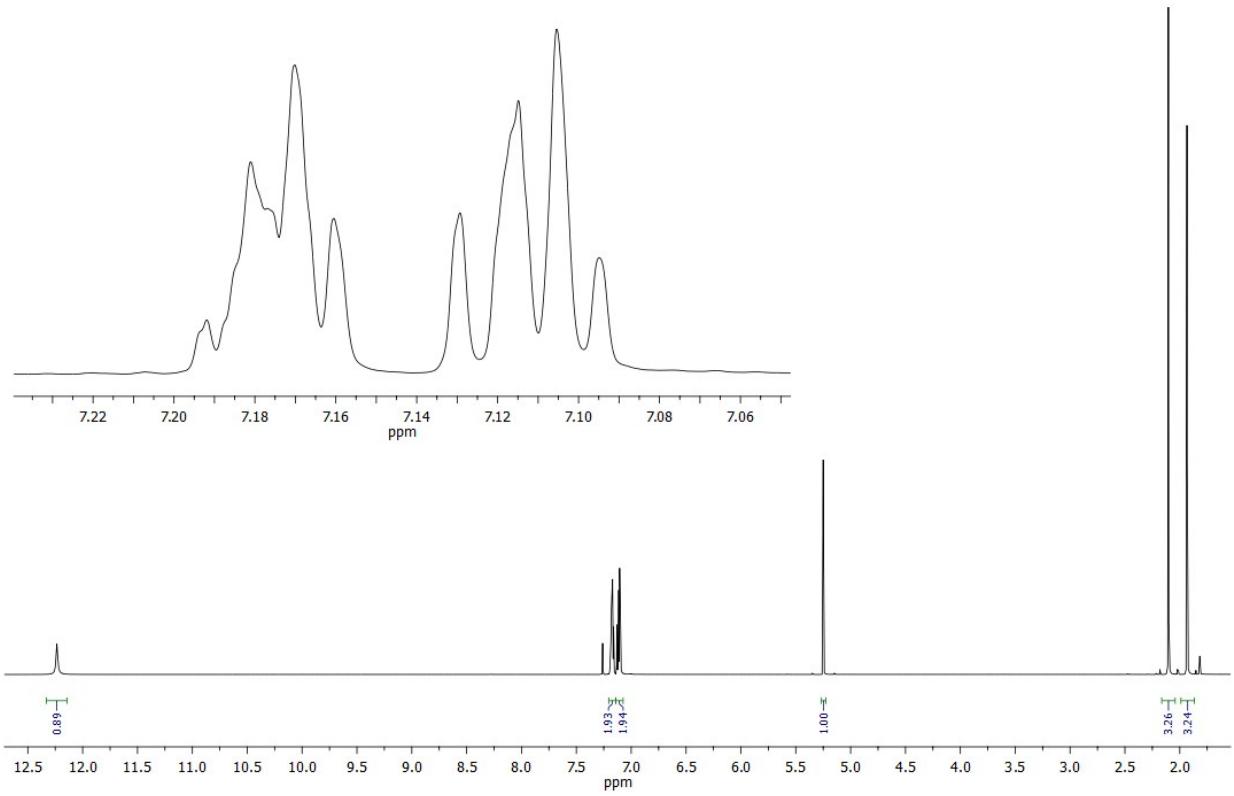

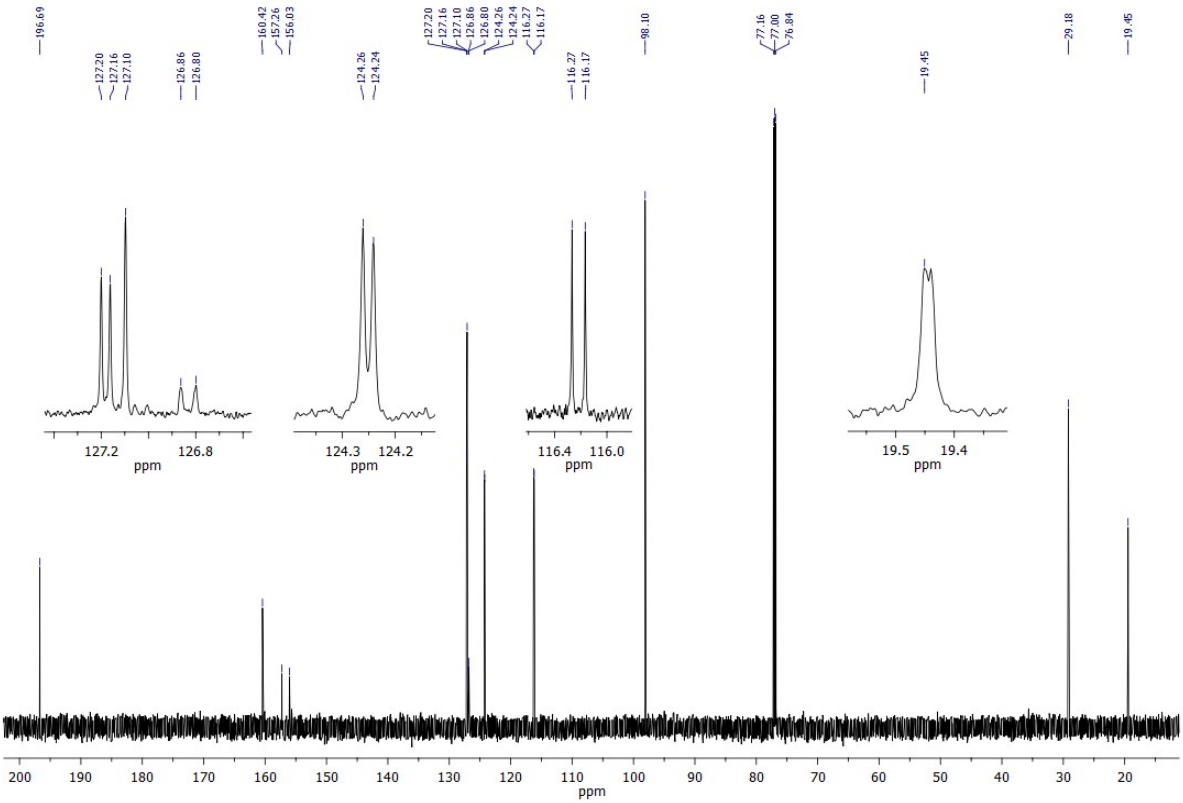

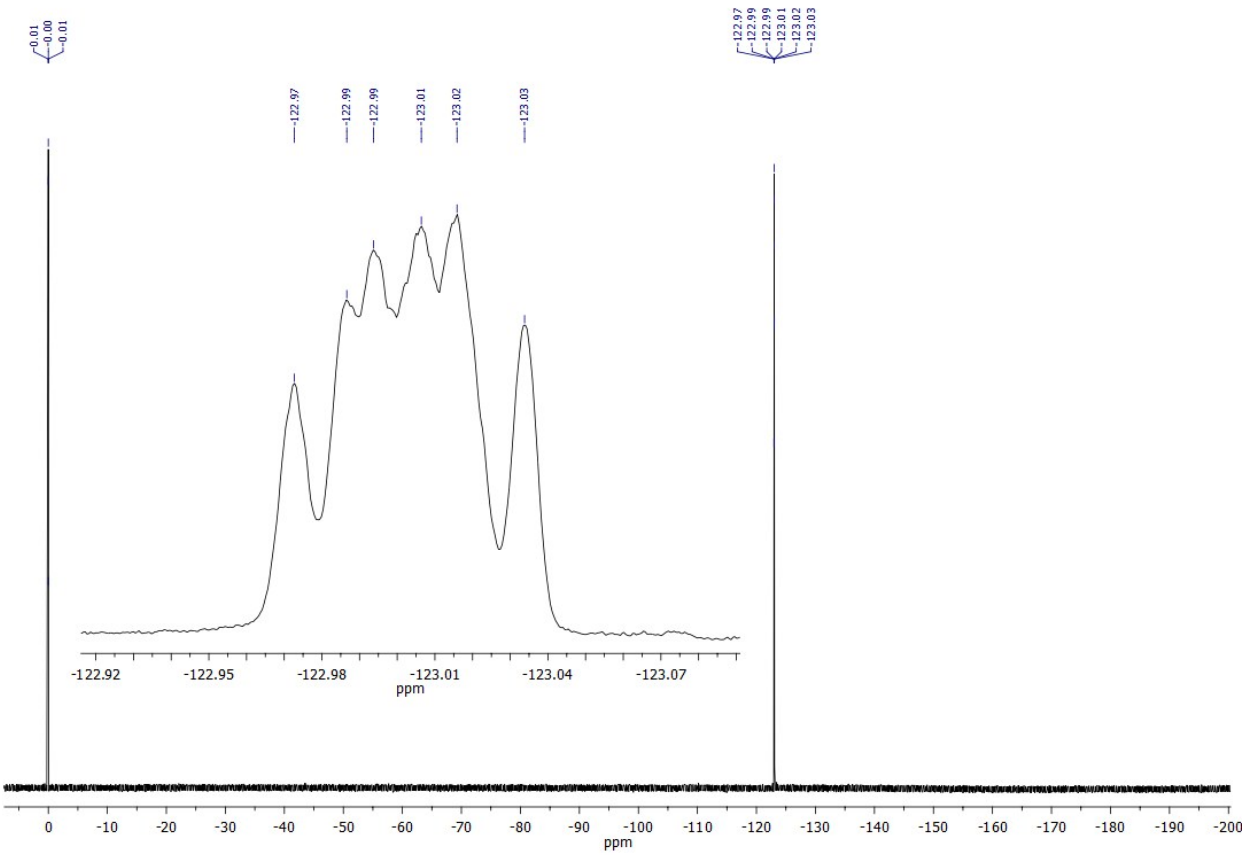
-0.01
-0.00
-0.01
-122.97
-122.99
-122.99
-123.01
-123.02
-123.03
-122.97
-122.99
-122.99
-123.01
-123.02
-123.03
-122.92
-122.95
-122.98
-123.01
-123.04
-123.07
ppm
0
-10
-20
-30
-40
-50
-60
-70
-80
-90
-100
-110
-120
-130
-140
-150
-160
-170
-180
-190
-200
ppm

4-(3-Fluorophenyl)imino-2-pentanone (3c)

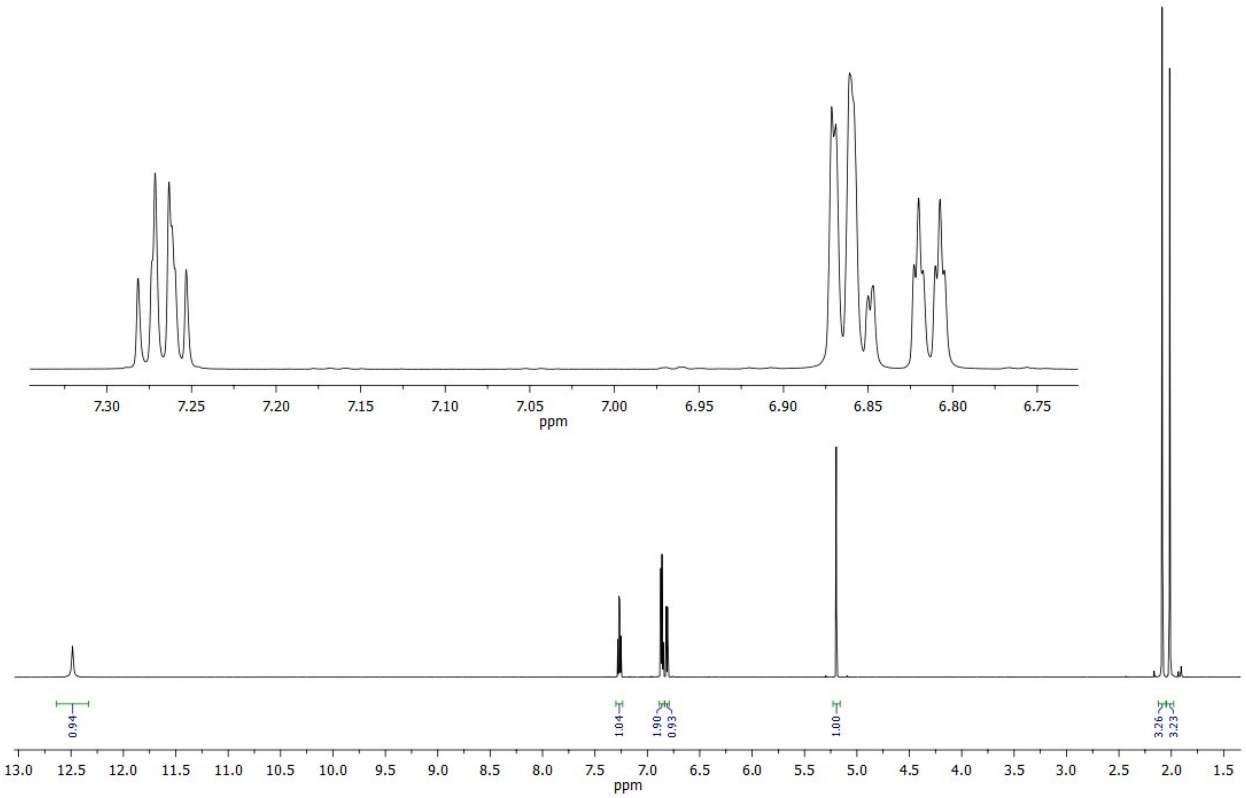

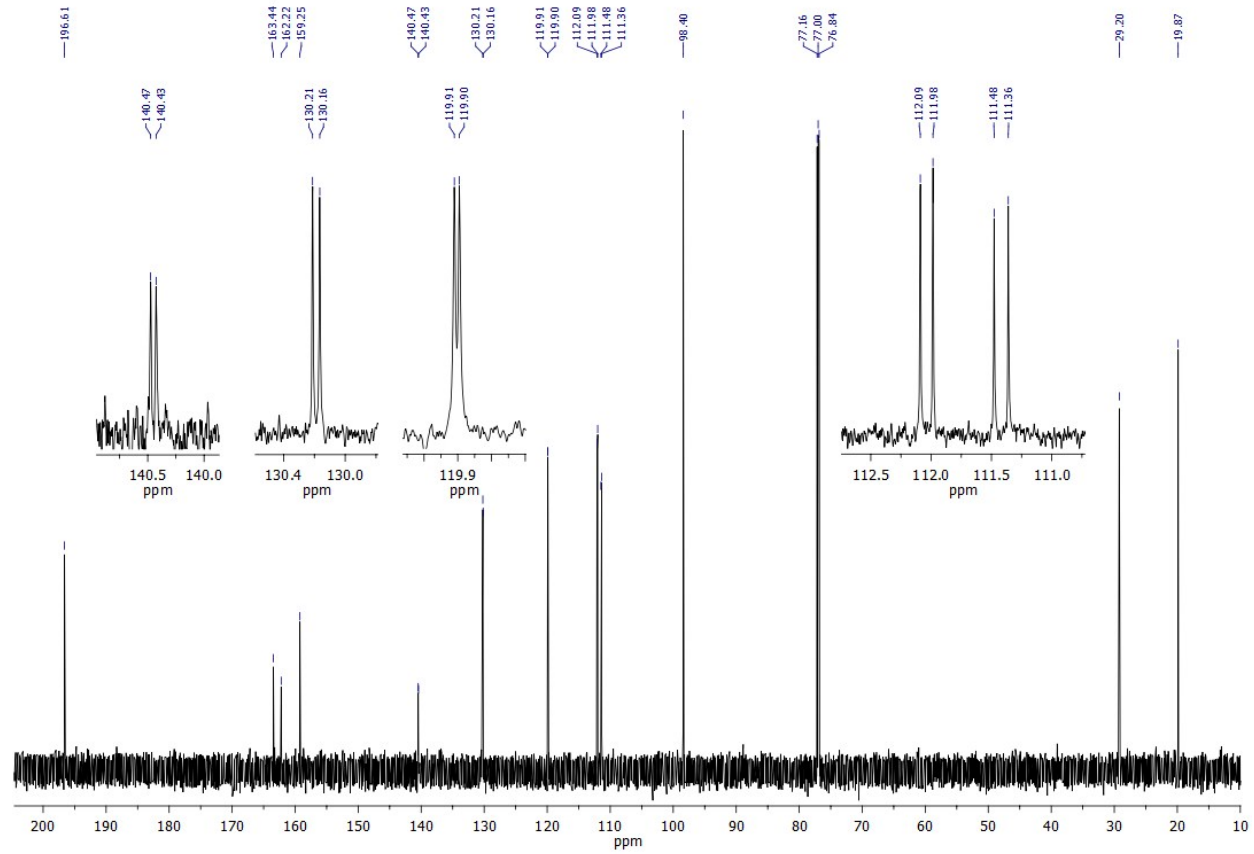

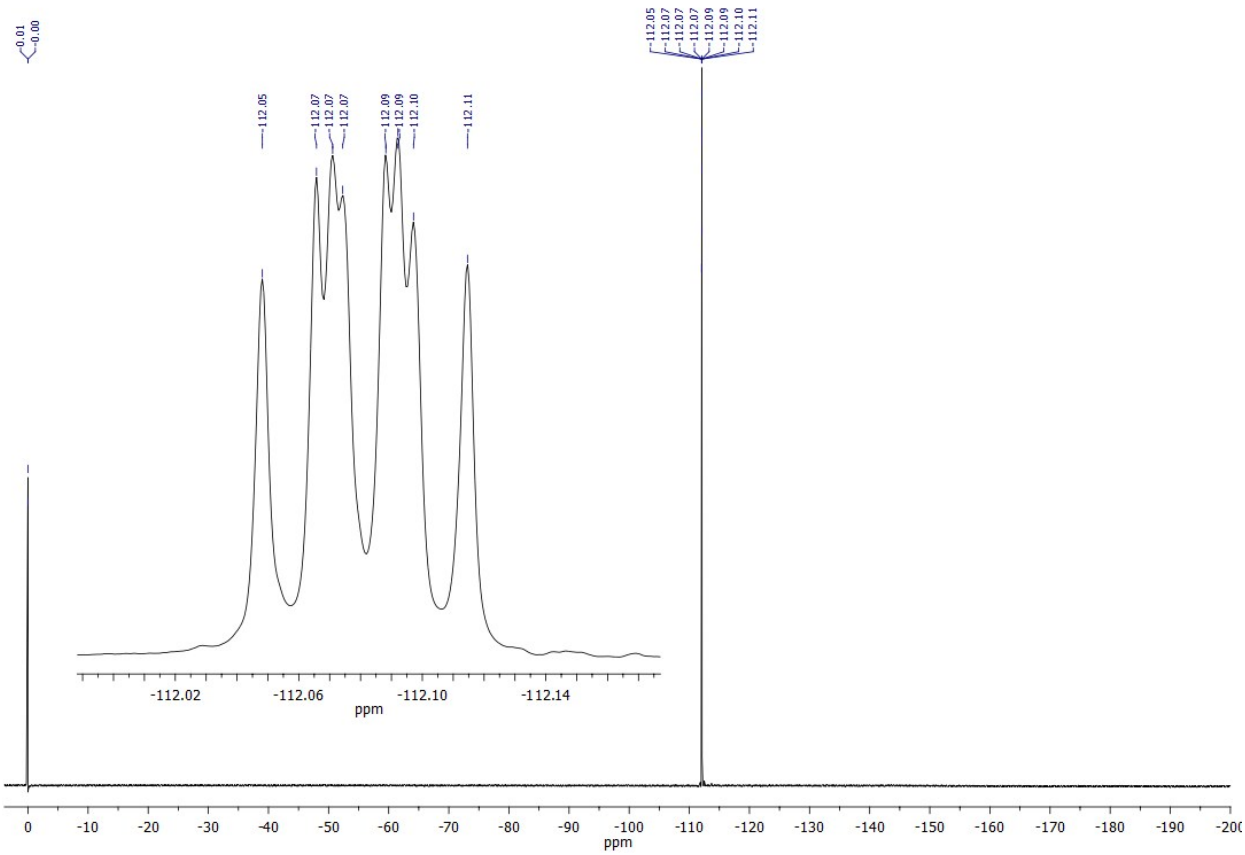
0.01
0.00
-112.05
-112.07
-112.07
-112.07
-112.09
-112.09
-112.10
-112.11
-112.02
-112.06
-112.10
-112.14
ppm
0
-10
-20
-30
-40
-50
-60
-70
-80
-90
-100
-110
-120
-130
-140
-150
-160
-170
-180
-190
ppm

4-(4-Fluorophenyl)imino-2-pentanone (3d)

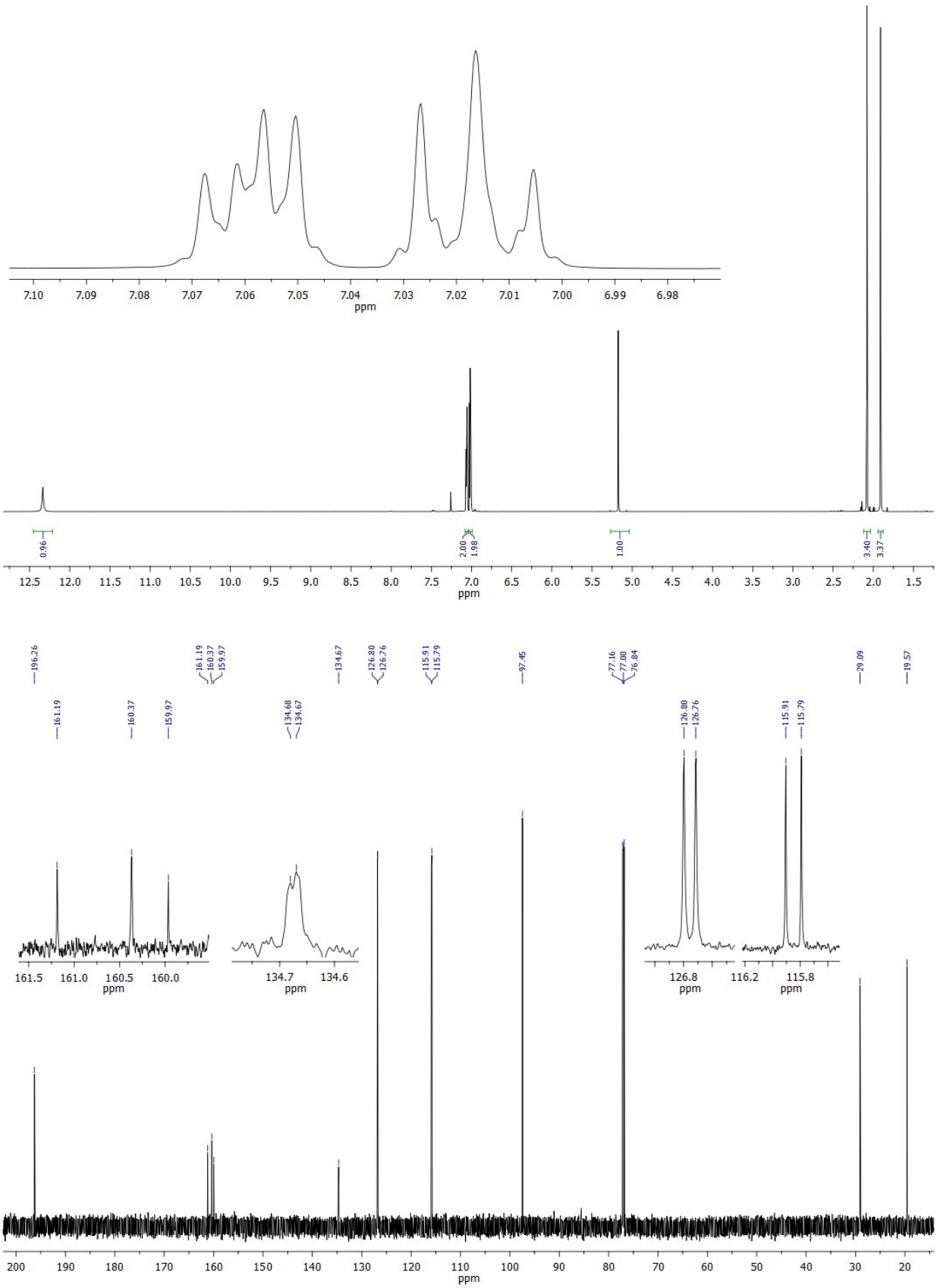

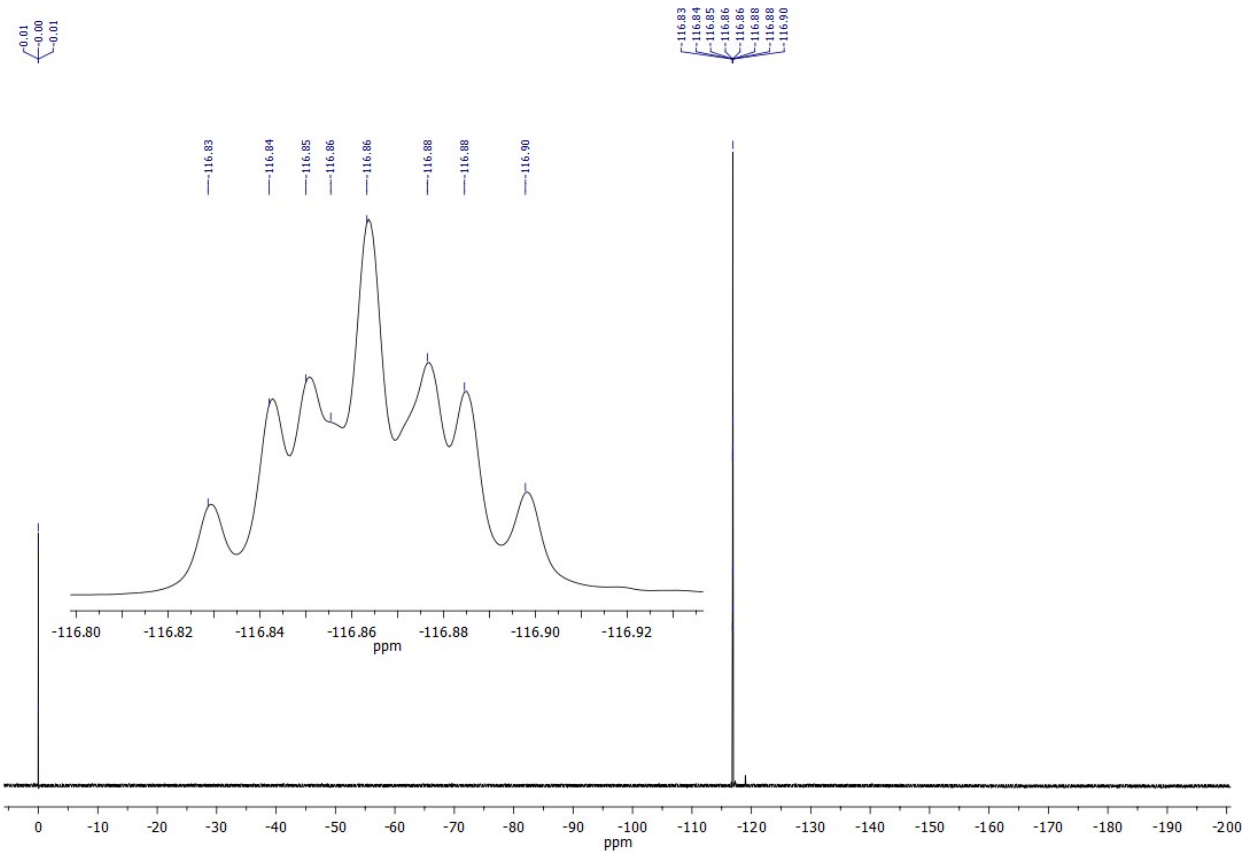
0.01
0.00
-0.01
-116.83
-116.84
-116.85
-116.86
-116.86
-116.88
-116.88
-116.90
-116.80
-116.82
-116.84
-116.86
-116.88
-116.90
-116.92
ppm
0
-10
-20
-30
-40
-50
-60
-70
-80
-90
-100
-110
-120
-130
-140
-150
-160
-170
-180
-190
-200
ppm

4-(4-Trifluoromethylphenyl)imino-2-pentanone (3e)

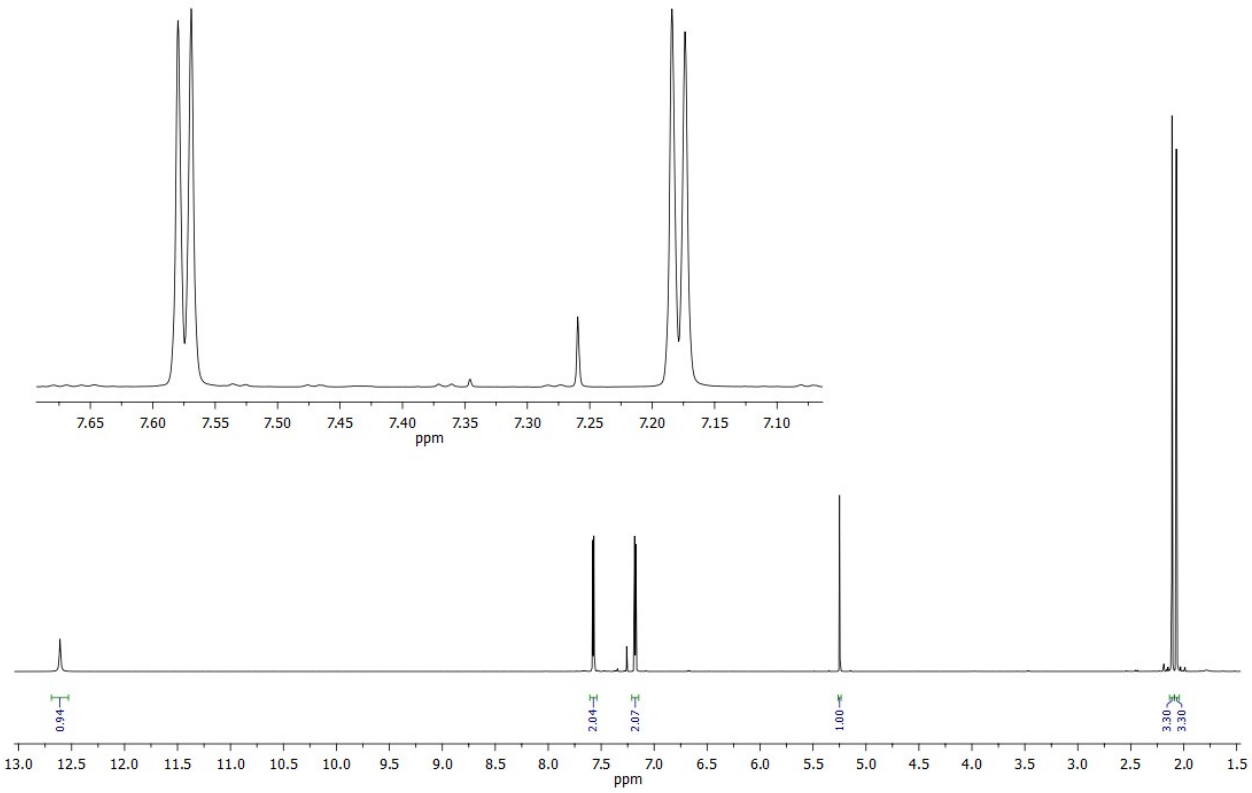

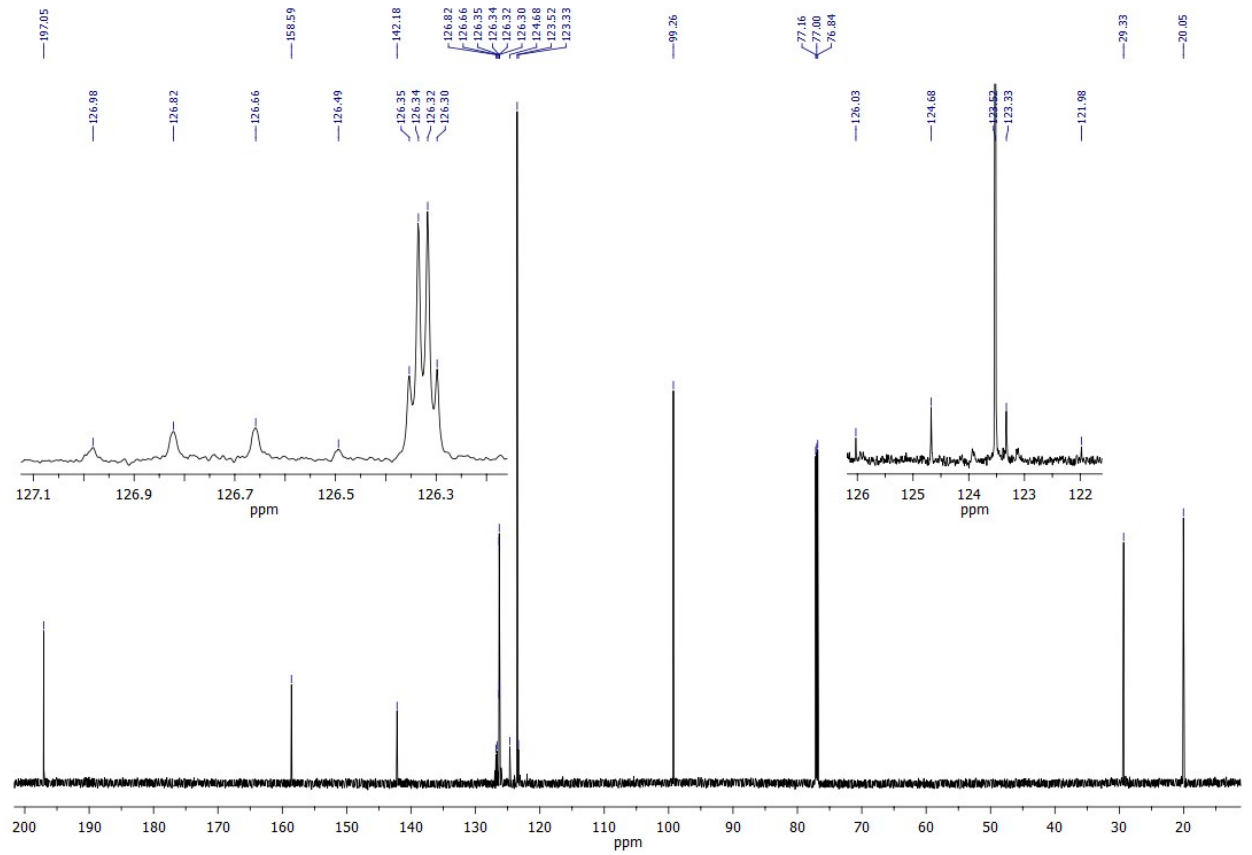

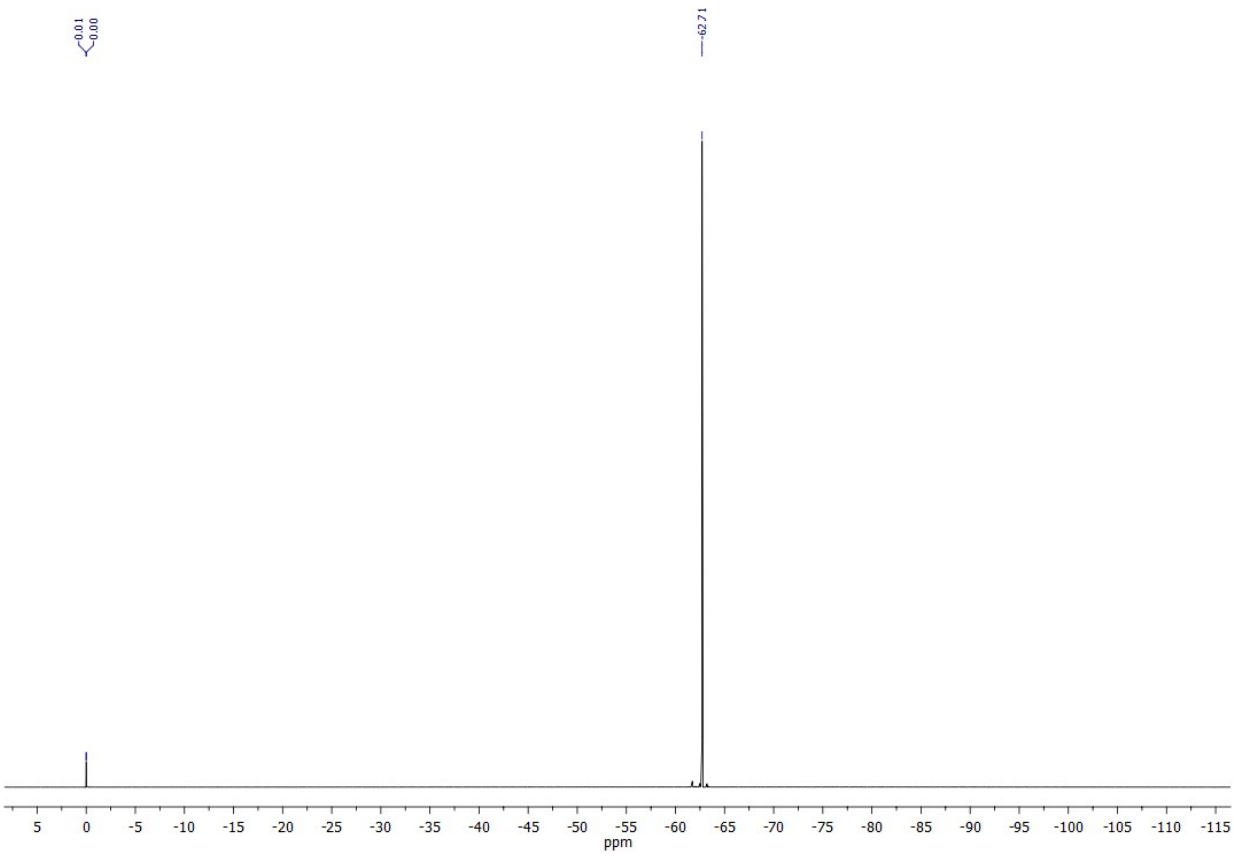
0.01
0.00
62.71
5
0
-5
-10
-15
-20
-25
-30
-35
-40
-45
-50
-55
-60
-65
-70
-75
-80
-85
-90
-95
-100
-105
-110
-115
ppm

4-(2,3,4,5,6-Pentafluorophenyl)imino-2-pentanone (3f)

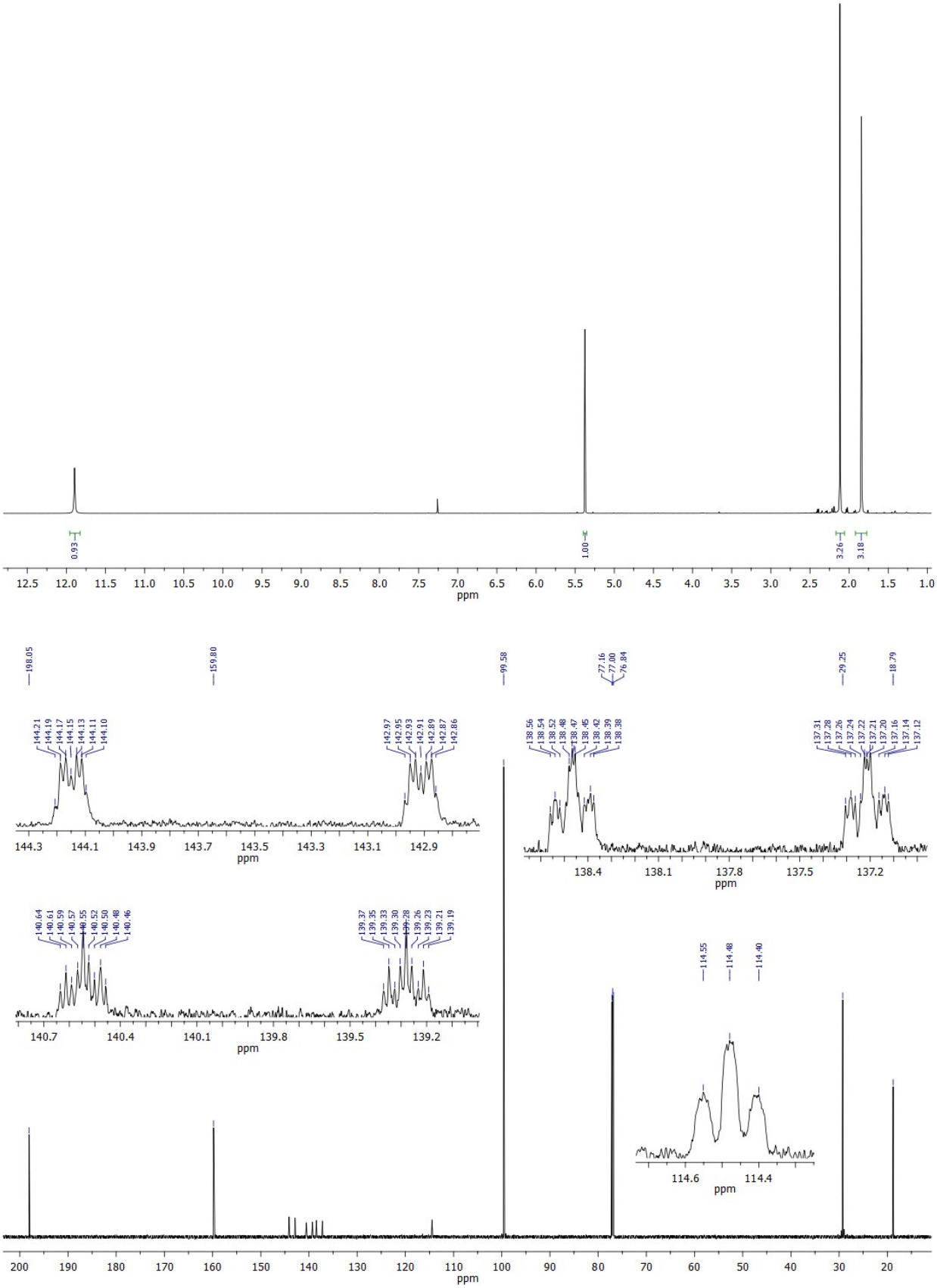

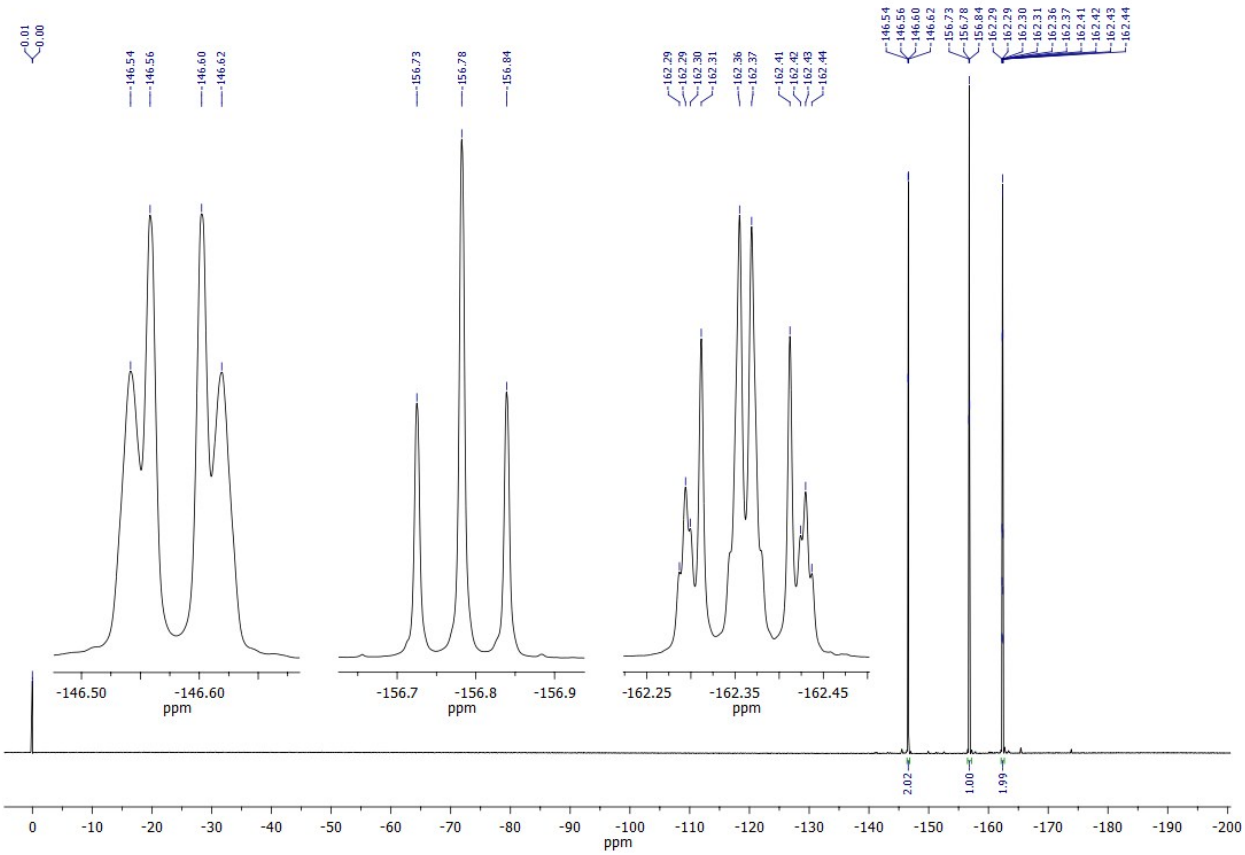
0.01
0.00
146.54
146.56
146.60
146.62
156.73
156.78
156.84
162.29
162.29
162.30
162.31
162.36
162.37
162.41
162.42
162.43
162.44
-146.50
-146.60
ppm
-156.7
-156.8
-156.9
ppm
-162.25
-162.35
-162.45
ppm
2.02
1.00
1.99
0
-10
-20
-30
-40
-50
-60
-70
-80
-90
-100
-110
-120
-130
-140
-150
-160
-170
-180
-190
-200
ppm

2. Crystallographic data

Table 1S. Crystal data, data collection and structure refinement

Compound	**3f**	**5b**	**5e**	**5g**
Formula	$C_{11}H_8F_5NO$	$C_{37}H_{27}FIrN_3O$	$C_{38}H_{27}F_3IrN_3O_2 \cdot 1/2(CH_3OH)$	$C_{40}H_{30}F_4IrN_3O$
Formula weight	265.18	740.81	806.85	868.87
Crystal system	monoclinic	monoclinic	monoclinic	monoclinic
Space group	$P2_1/c$	$P2_1/c$	C2/c	I2/a
a(Å)	10.8061(4)	16.3067(4)	27.6629(10)	16.4734(6)
b(Å)	8.7128(3)	18.7491(4)	9.1355(2)	12.7322(5)
c(Å)	11.6109(4)	19.7051(5)	29.0965(11)	31.2845(11)
α(°)	90	90	90	90
β(º)	90.422(3)	108.847(3)	117.344(5)	99.973(3)
γ(°)	90	90	90	90
V(Å^3)	1093.15(7)	5701.5(3)	6531.5(5)	6462.5(4)
Z	4	8	8	8
D_x(g cm^{-3})	1.61	1.73	1.64	1.79
F(000)	536	2912	3176	3424
μ(mm^{-1})	0.16	4.73	4.14	4.20
Θ range (^{0})	3.47 – 27.03	3.06 – 26.52	3.06 – 27.01	2.95 – 28.31
Reflections:				
collected	7398	24228	14409	14925
unique (R_{int})	2234 (0.014)	10919 (0.037)	6545 (0.022)	6750 (0.021)
with I>2σ(I)	2042	8514	5874	5971
R(F) [I>2σ(I)]	0.032	0.047	0.035	0.026
wR(F^2) [I>2σ(I)]	0.084	0.094	0.100	0.068
R(F) [all data]	0.036	0.067	0.041	0.033
wR(F^2) [all data]	0.086	0.102	0.105	0.072
Goodness of fit	1.05	1.05	1.07	1.01
max/min Δρ (e Å^{-3})	0.20/-0.20	2.87/-1.81	1.16/-0.85	2.09/-1.06

Table 2S. Hydrogen bond data (Å, °)

D	H	A	D-H	H···A	D···A	D-H···A
3f						
N7	H7	O10	0.881(18)	1.978(17)	2.6669(14)	134.0(15)
N7	H7	O10^{i}	0.881(18)	2.293(18)	2.9749(14)	134.1(14)
C81	H81A	F2	0.96(2)	2.431(19)	3.0451(17)	121.2(14)
C81	H81A	F2^{ii}	0.96(2)	2.53(2)	3.2224(16)	128.3(14)

Symmetry codes: ^{i} 1-x,1-y,1-z; ^{ii} 1-x,1-y,-z;

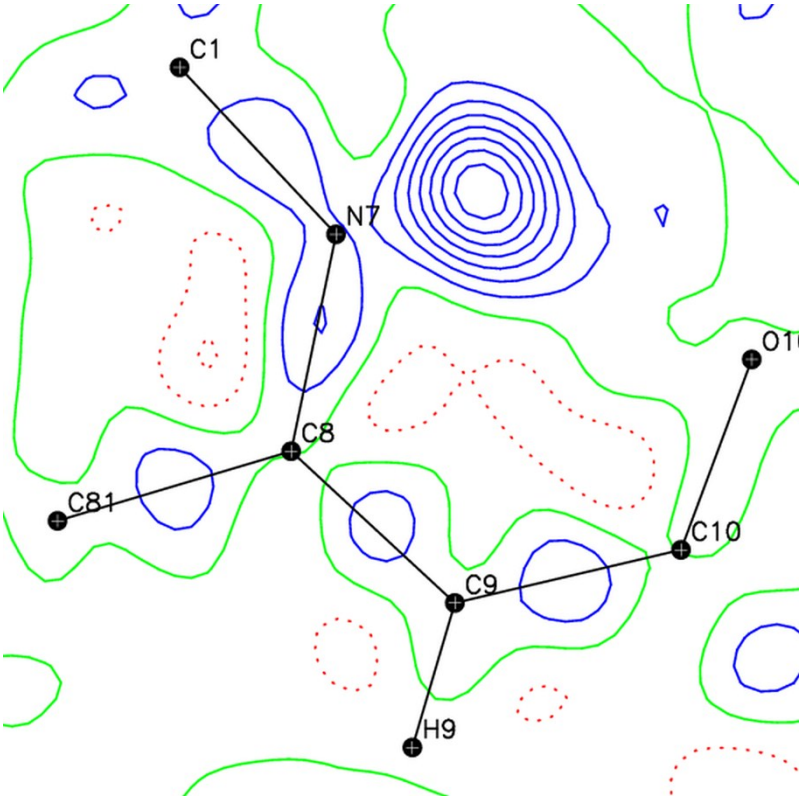

Figure 1S.

Table 3S. Selected geometrical data (Å,º) with s.u.'s in parentheses (second line, if exists, refers to alternative, less-occupied part). A and B denote least squares planes of aromatic ring and chain.

	3f	**5bA**	**5bB**	**5e**	**5g**
Ir1-N7		2.154(8)	2.171(6)	2.173(4)	2.153(3)
Ir1-O10		2.133(6)	2.152(6)	2.144(3)	2.133(3)
Ir1-N12		2.065(7)	2.037(6)	2.048(4)	2.037(3)
Ir1-C23		2.008(9)	2.006(8)	2.012(5)	1.970(3)
Ir1-N26		2.042(7)	2.045(6)	2.035(4)	2.049(3)
Ir1-C37		1.996(8)	2.016(8)	1.992(4)	2.012(3)
N7-Ir1-C23		173.3(3)	173.4(3)	175.18(15)	176.58(11)
O10-Ir1- C37		174.1(3)	175.2(3)	176.37(15)	175.58(11)
N12-Ir1-N26		176.2(3)	174.9(3)	175.34(15)	174.20(11)
C1-N7-C8	125.00(11)	118.3(8)	117.7(10) 119.9(13)	119.1(4)	119.1(3)
C13-N12-C25		120.1(8)	118.7(7)	118.1(4)	118.9(3)
C22-C23-C24		114.5(9)	115.5(8)	116.3(4)	114.0(3)
C27-N26-C39		119.3(7)	118.5(7)	118.0(4)	118.6(3)
C36-C37-C38		115.7(8)	115.8(7)	114.8(4)	116.2(3)
C2-C1-N7-C8	63.17(17)	-94.8(11)	-112.7(17) 78(3)	-72.5(6)	83.4(4)
C6-C1-N7-C8	-120.14(14)	87.2(10)	70(2) -107(3)	114.8(5)	-106.7(4)
C1-N7-C8-C9	-177.59(12)	-167.1(8)	-163.5(9) -177.2(9)	165.7(4)	-172.3(3)
C1-N7-C8-C81	4.93(19)	12.7(12)	13.6(12) 0.0(13)	-12.6(6)	9.1(5)
N7-C8-C9-C10	-0.6(2)	13.4(14)	15.3(14(	-16.4(8)	10.7(6)
C8-C9-C10-C11	-174.20(13)	165.6(8)	170.8(8)	-169.5(5)	173.9(3)
C8-C9-C10-O10	4.4(2)	-12.9(14)	-6.3(14)	6.8(8)	-5.3(6)
A/B	61.61(5)	74.2(5)	88.0(6) 88.0(8)	87.8(2)	88.40(13)

3. Thermal analysis data

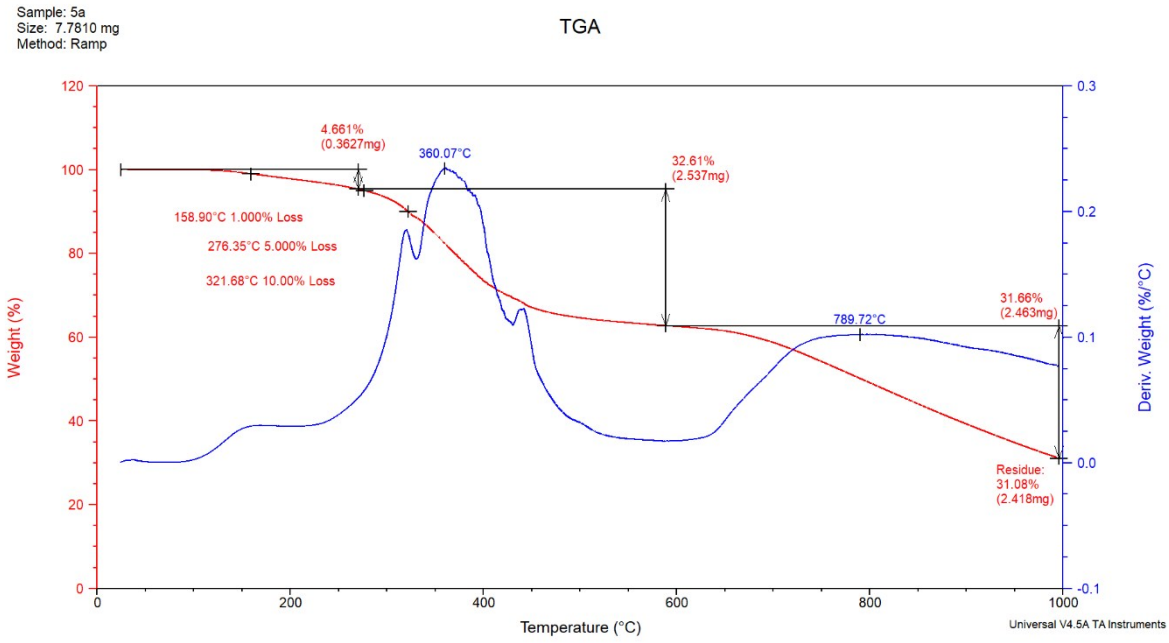

Figure 2S. TG and DTG curve of **5a** sample.

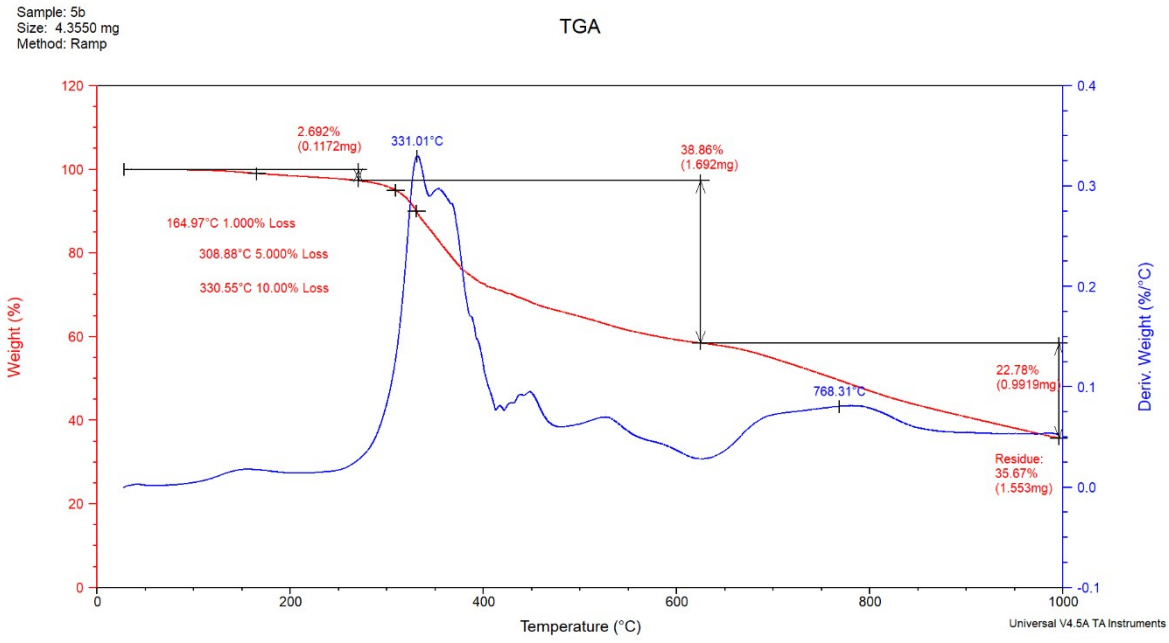

Figure 3S. TG and DTG curve of **5b** sample.

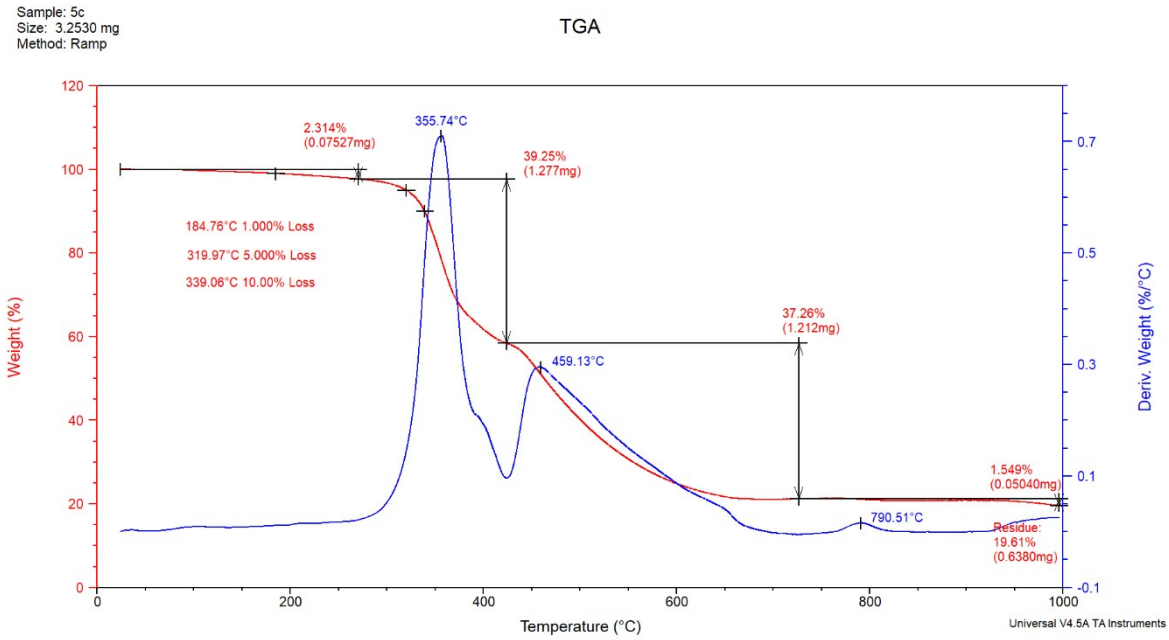

Figure 4S. TG and DTG curve of **5c** sample.

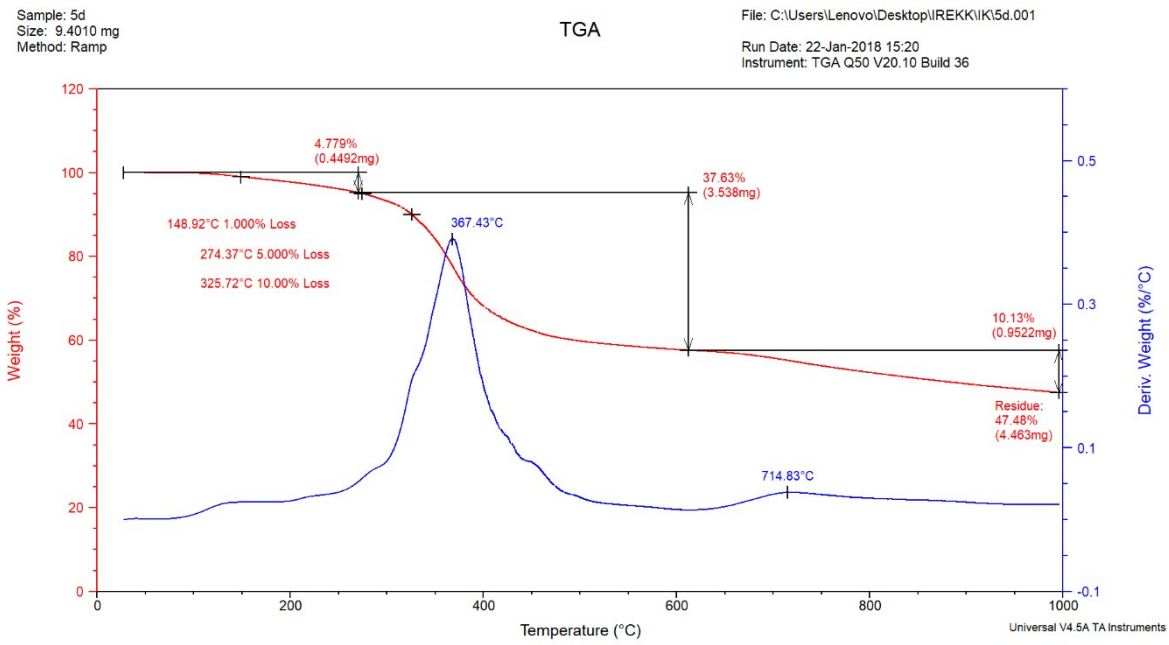

Figure 5S. TG and DTG curve of **5d** sample.

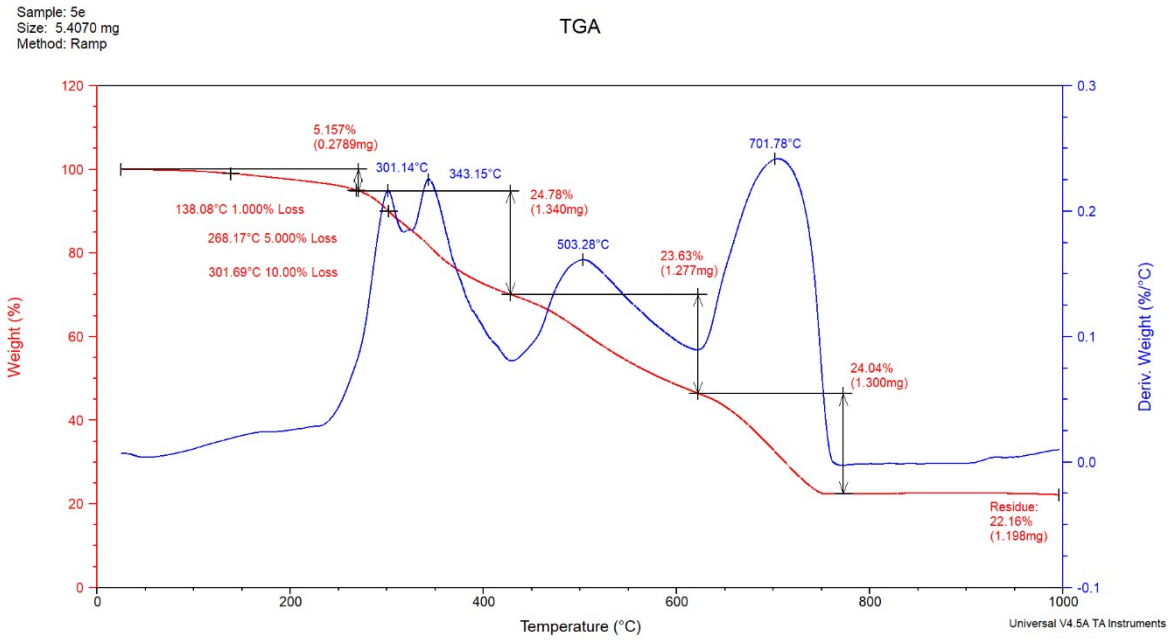

Figure 6S. TG and DTG curve of **5e** sample.

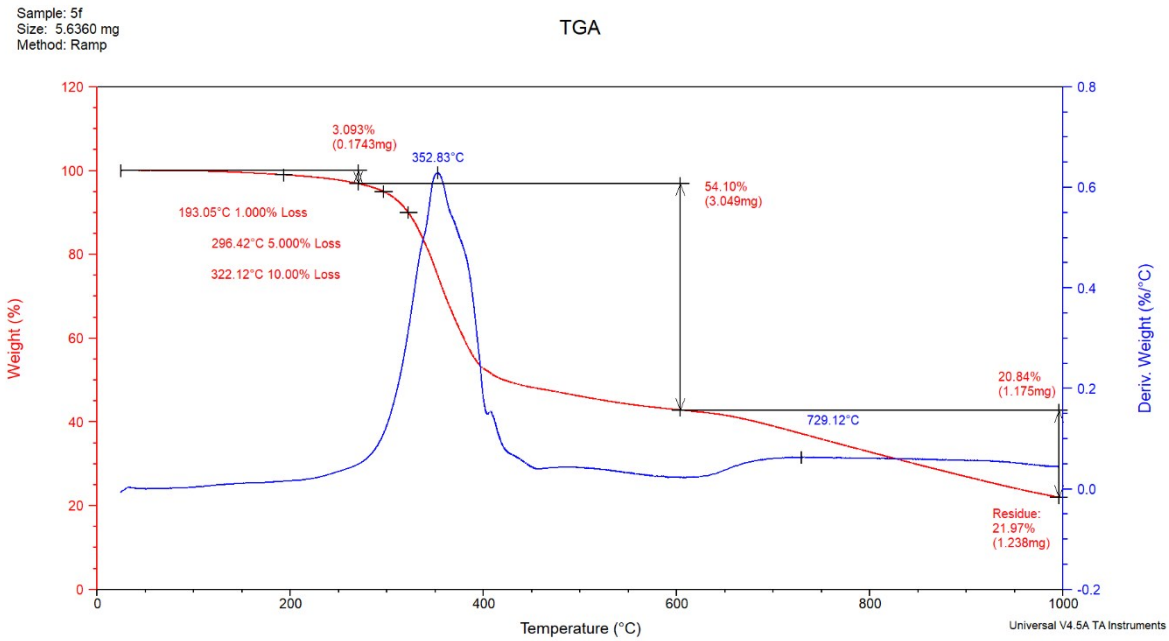

Figure 7S. TG and DTG curve of **5f** sample.

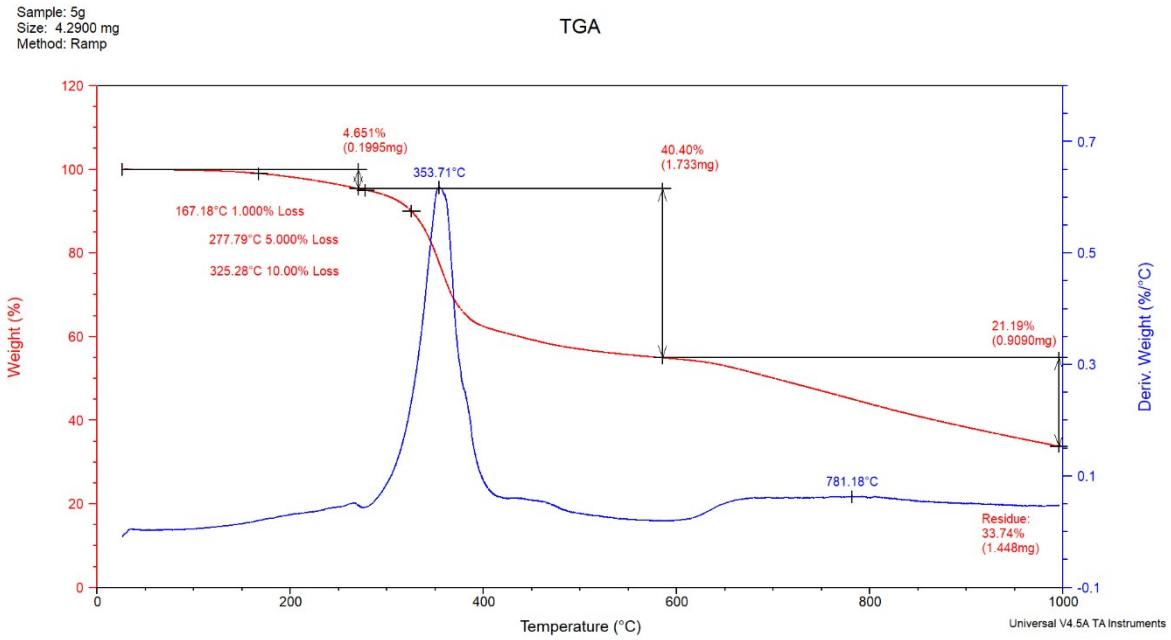

Figure 8S. TG and DTG curve of **5f** sample.

Table 4S. Results of TG and DTG analysis.

Sample	Weight Loss Temperature [°C]			Decomposition Temperature [°C]				Residue at 1000 °C [%]
	$T_{1\%}$	$T_{5\%}$	$T_{10\%}$	T_{Onset}	$T_{Max\ 1}$	$T_{Max\ 2}$	$T_{Max\ 3}$	
5a	159	276	322	286	360	-	790	31
5b	165	309	331	303	331	-	768	36
5c	185	320	339	328	356	459	791	20
5d	149	274	326	312	367	-	715	48
5e	138	268	302	268	301/343	503	702	22
5f	193	296	322	313	353	-	729	21
5g	167	278	325	319	354	-	781	34

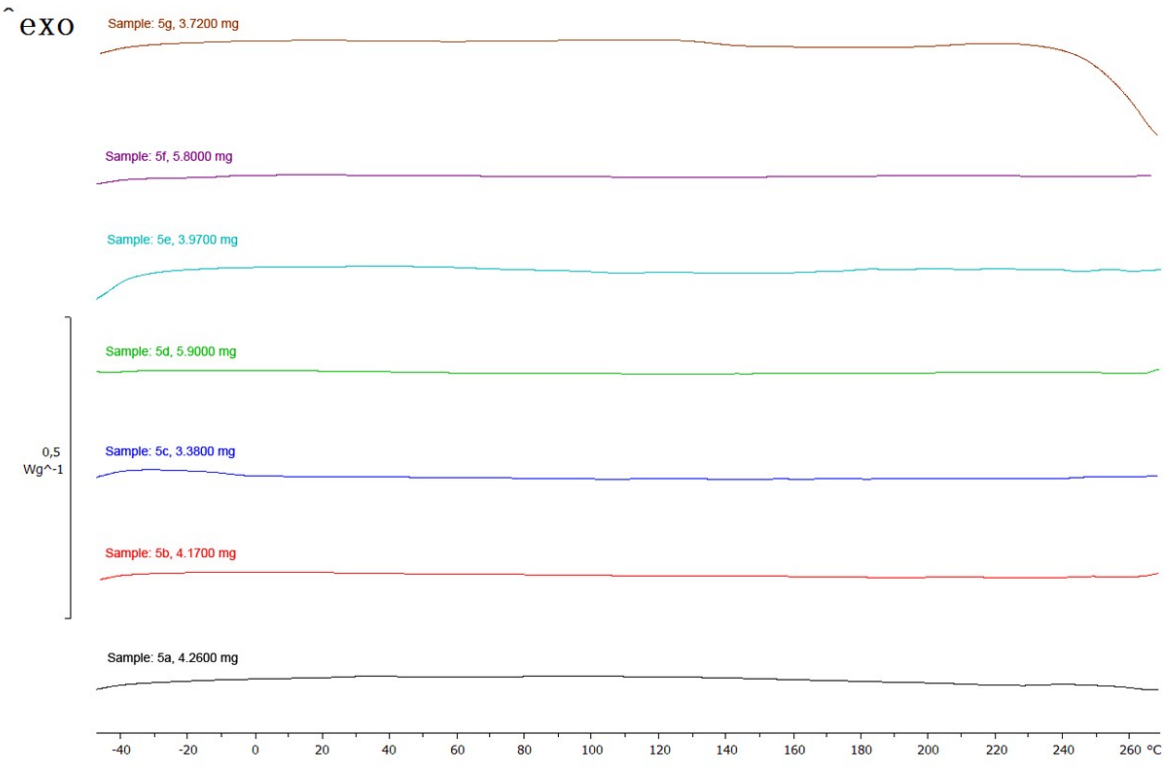

Figure 9S. DSC curves of second heating run for **5a**-**5g** samples.

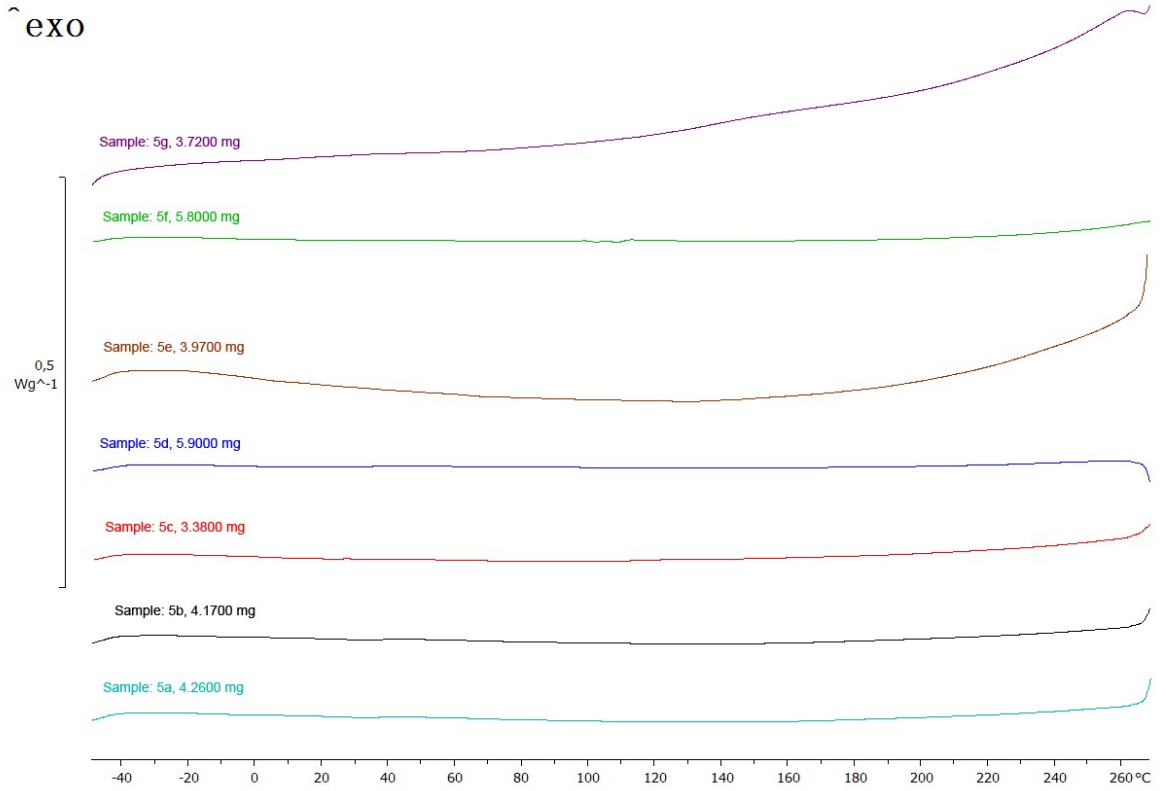

Figure 10S. DSC curves of second cooling run for **5a**-**5g** samples.

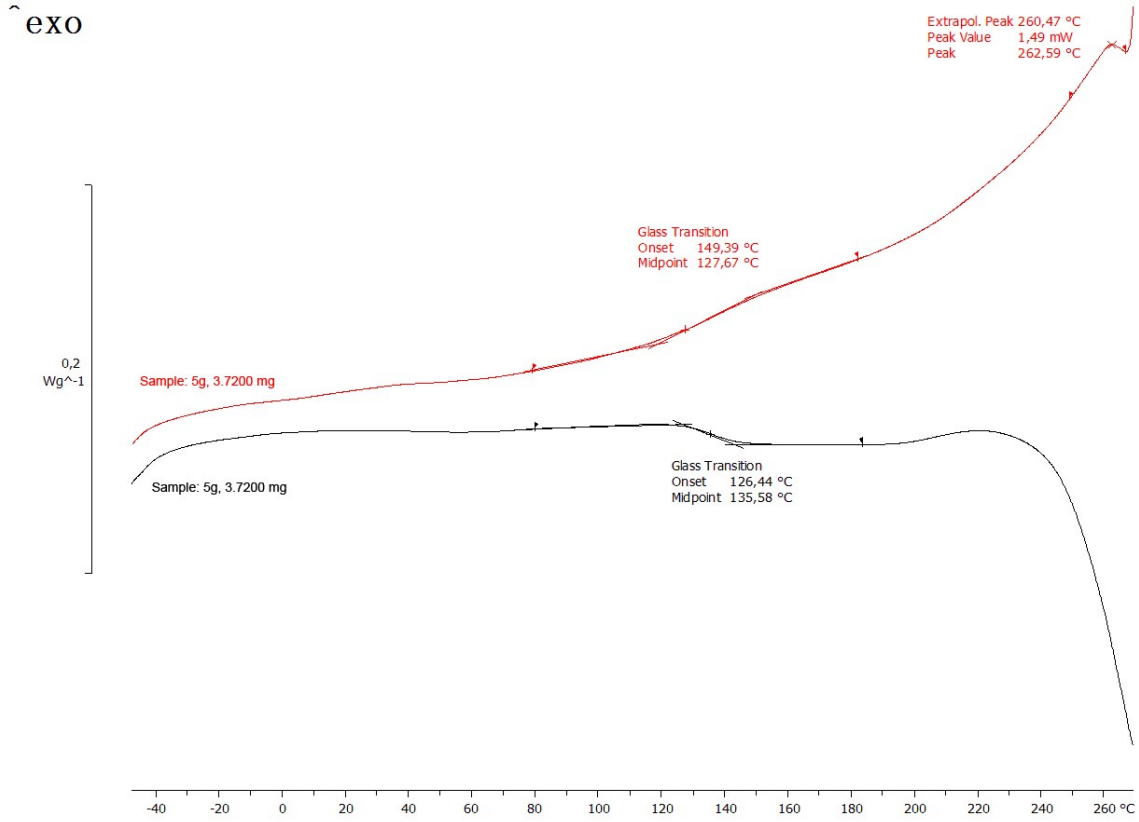

Figure 11S. DSC curves of second heating and cooling run for **5g** sample.

4. Cyclic voltammetry measurements

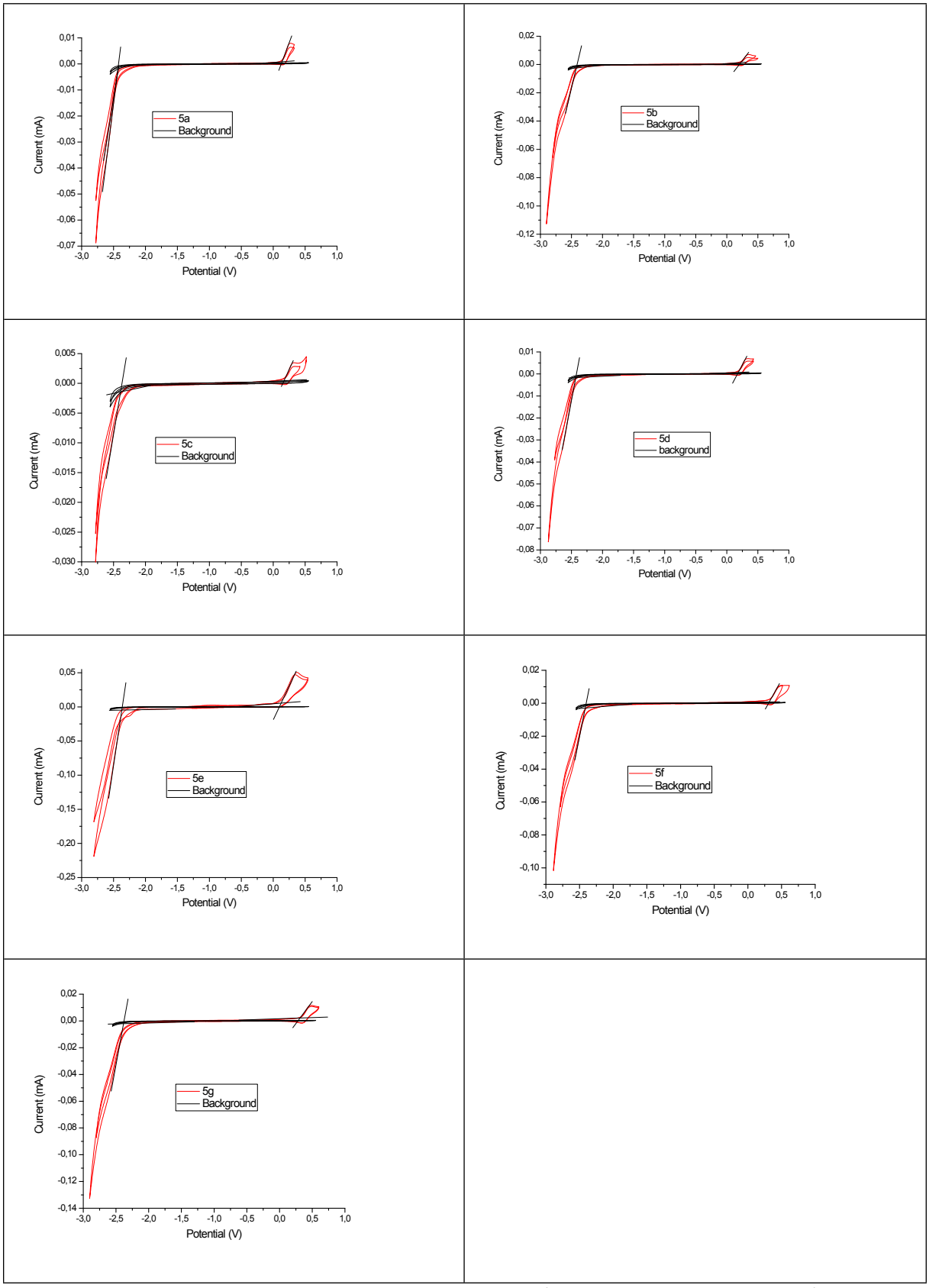

Figure 12S. Cyclic voltammetry of studied compounds in Bu_4NBF_4/CH_2Cl_2 solutions; scan rate 0.1V/s; concentration 2 mM. Intersections of tangential lines mark oxidation and reduction onset potentials.

5. DFT calculation data

Table 5S. The energy of optimized structures of iridium(II) complexes.

compound	Energy [hartree]
5a	-1771.23859192
5b$^{(1)}$	-1870.50717896
5b$^{(2)}$	-1870.50764600
5c$^{(1)}$	-1870.50889458
5c$^{(2)}$	-1870.50883848
5d	-1870.50778500
5e	-2108.39128637
5f	-2267.54834837
5g	-2436.72050752

Table 6S. The energy levels and Homo-Lumo energy gaps for the studied complexes (in eV) calculated at the B3LYP/SDD/6-311++G(d,p) level of theory together with the experimental results.

compound	HOMO [eV]	LUMO [eV]	$E_g^{theor.}$ [eV]	$E_g^{exp.}$ [eV]
5a	-5,28	-1,97	-3,31	2,58
5b$^{(1)}$	-5,32	-1,99	-3,33	2,63
5b$^{(2)}$	-5,30	-1,98	-3,32	2,63
5c$^{(1)}$	-5,32	-1,99	-3,33	2,57
5c$^{(2)}$	-5,32	-1,99	-3,33	2,57
5d	-5,30	-1,99	-3,31	2,62
5e	-5,36	-2,01	-3,34	2,48
5f	-5,43	-2,02	-3,41	2,73
5g	-5,38	-1,98	-3,41	2,69

Table 7S. The energy levels and Homo-Lumo energy gaps for the studied complexes (in eV) calculated at the M06/SDD/6-311++G(d,p) level of theory together with the experimental results.

compound	HOMO [eV]	LUMO [eV]	$E_g^{theor.}$ [eV]	$E_g^{exp.}$ [eV]
5a	-5,55	-1,86	-3,69	2,58
5b$^{(1)}$	-5,57	-1,88	-3,70	2,63
5b$^{(2)}$	-5,54	-1,88	-3,66	2,63
5c$^{(1)}$	-5,59	-1,88	-3,70	2,57
5c$^{(2)}$	-5,58	-1,89	-3,69	2,57
5d	-5,59	-1,89	-3,70	2,62
5e	-5,63	-1,92	-3,71	2,48
5f	-5,70	-1,92	-3,77	2,73
5g	-5,66	-1,91	-3,75	2,69

Table 8S. The energy levels and Homo-Lumo energy gaps for the studied complexes (in eV) calculated at the WB97XD/SDD/6-311++G(d,p) level of theory together with the experimental results.

compound	$E_g^{theor.}$ [eV]	$E_g^{theor.*}$ [eV]	$E_g^{exp.}$ [eV]
5a	6,87	2,61	2,58
5b	6,90	2,63	2,63
5c	6,89	2,62	2,57
5d	6,87	2,62	2,62
5e	6,63	2,52	2,48
5f	6,97	2,65	2,73
5g	6,96	2,64	2,69

$E_g^{thero^*}$= 0.38* $E_g^{theor.}$

Table 9S. Cartesian coordinates from the optimized structures of S_0 in C_6H_5Cl media for **5e**

Atom symbol	X	Y	Z
C	5.52148	0.57121	-2.15322
C	4.60221	1.28562	-1.30856
C	3.42613	0.62287	-0.87726
C	3.19118	-0.71972	-1.29067
C	4.10319	-1.41131	-2.12057
C	5.28690	-0.71451	-2.54224
N	2.03598	-1.29650	-0.83648
C	3.79057	-2.73741	-2.47212
C	2.62321	-3.30762	-1.99745
C	1.76991	-2.55769	-1.17891
C	4.80285	2.61504	-0.88238
C	3.85655	3.21875	-0.07025
C	2.69233	2.53899	0.34543
C	2.44582	1.22460	-0.04133
H	4.46516	-3.30215	-3.10640
H	2.35506	-4.32716	-2.24284
C	-1.05321	1.42853	-3.25269
C	-1.88374	2.41364	-2.74128
C	-0.21045	0.65959	-2.42381
C	-1.88412	2.66410	-1.35345
C	-2.69598	3.66905	-0.71999
C	-1.02788	1.88064	-0.54139
C	-2.65209	3.88646	0.62616
C	-1.78392	3.11500	1.47244
N	-0.12709	1.33509	1.57605
C	-1.66310	3.27936	2.86486
C	-0.02725	1.51238	2.89439
C	-0.78372	2.47684	3.57152
C	-0.17963	0.85339	-1.04446
H	-2.25436	4.03296	3.37366
H	0.67824	0.87299	3.40868
H	-0.66468	2.58189	4.64220
Ir	0.91375	-0.04132	0.41292
O	2.10731	-0.80624	2.08548
N	-0.58711	-1.61558	0.95576
C	1.93423	-1.92272	2.67961
C	0.83890	-2.78134	2.54852
C	-0.36588	-2.59324	1.82046

H	0.87730	-3.68080	3.14774
C	3.04521	-2.30618	3.63723
H	3.15819	-1.52486	4.39459
H	3.99131	-2.36288	3.09122
H	2.86230	-3.25886	4.13479
C	-1.44934	-3.62508	2.09133
H	-1.02528	-4.50377	2.57574
H	-1.95144	-3.93424	1.17300
H	-2.21596	-3.21429	2.75454
C	-0.98901	2.11998	0.86068
C	-1.89815	-1.46227	0.42260
C	-2.19010	-1.85788	-0.88834
C	-2.91016	-0.86713	1.18733
C	-4.18466	-0.68625	0.66317
C	-4.46544	-1.09463	-0.64178
C	-3.46377	-1.68458	-1.41543
H	-2.69089	-0.54181	2.19722
H	0.85573	-2.97767	-0.78290
H	5.99350	-1.23542	-3.17897
H	6.42221	1.07930	-2.48254
H	5.69168	3.15365	-1.19286
H	4.01199	4.24278	0.25531
H	1.98810	3.06658	0.97967
H	-1.04914	1.24236	-4.32245
H	0.41840	-0.09518	-2.88485
H	-2.52576	2.99255	-3.39632
H	-3.35628	4.26586	-1.34105
H	-3.27216	4.65126	1.08088
H	-3.67292	-1.99869	-2.43050
H	-1.41280	-2.30122	-1.49710
H	-4.95400	-0.22075	1.26692
C	-5.85097	-0.95035	-1.19037
F	-6.51153	0.11286	-0.67048
F	-6.63120	-2.03994	-0.92459
F	-5.86860	-0.80274	-2.53714

Table 10S. Cartesian coordinates from the optimized structures of S_0 in C_6H_5Cl media for **5a**.

Atom symbol	X	Y	Z
C	-5.13087	-1.75439	-0.73518
C	-3.92862	-2.08424	-0.01784
C	-2.84487	-1.17188	-0.05963
C	-2.97823	0.03526	-0.80396
C	-4.16643	0.34877	-1.50314
C	-5.24777	-0.59542	-1.44419
N	-1.89195	0.86826	-0.80074
C	-4.20955	1.56718	-2.20558
C	-3.10691	2.40174	-2.18295
C	-1.96501	2.02085	-1.46760
C	-3.76375	-3.26913	0.72934
C	-2.56545	-3.49660	1.38667
C	-1.49987	-2.57398	1.32889
C	-1.60768	-1.38743	0.60794
H	-5.10307	1.84429	-2.75437
H	-3.10755	3.34880	-2.70705
C	1.02043	-1.97794	-3.28502
C	2.11622	-2.68103	-2.80870
C	0.26475	-1.12499	-2.45490
C	2.48442	-2.54990	-1.45382
C	3.59532	-3.24058	-0.85469
C	1.70787	-1.69054	-0.63843
C	3.90642	-3.09427	0.46555
C	3.12888	-2.23844	1.31884
N	1.23305	-0.71845	1.46463
C	3.36853	-2.03735	2.69088
C	1.47874	-0.54612	2.76440
C	2.54150	-1.19082	3.40937
C	0.58991	-0.94637	-1.11185
H	4.19396	-2.54676	3.17632
H	0.80393	0.11445	3.29324
H	2.69735	-1.01819	4.46652
Ir	-0.29323	0.15171	0.34947
O	-1.19862	1.16275	2.06902
N	0.95791	1.98947	0.09734
C	-1.11158	2.41090	2.32893
C	-0.26558	3.33764	1.71712
C	0.75269	3.12250	0.74643

H	-0.33903	4.35092	2.08824
C	-2.02529	2.88680	3.44151
H	-1.81169	2.32255	4.35404
H	-3.06495	2.67967	3.17162
H	-1.91620	3.95168	3.64896
C	1.64303	4.32593	0.47768
H	1.17909	5.23486	0.85913
H	1.84350	4.44874	-0.58779
H	2.61035	4.20786	0.97389
C	2.03944	-1.55077	0.73821
C	2.11920	1.88948	-0.73275
C	2.01870	2.00244	-2.12365
C	3.37506	1.64640	-0.16423
C	4.50858	1.53820	-0.96841
C	4.40430	1.66732	-2.35299
C	3.15324	1.89731	-2.92551
H	3.45793	1.54396	0.91191
H	5.47390	1.35098	-0.51058
H	5.28541	1.58278	-2.97888
H	-1.08996	2.65377	-1.42419
H	-6.16400	-0.36543	-1.97696
H	-5.96034	-2.45355	-0.70275
H	-4.57185	-3.99065	0.78411
H	-2.44017	-4.40920	1.96147
H	-0.58584	-2.81168	1.86262
H	0.73357	-2.08625	-4.32672
H	-0.58252	-0.60305	-2.88715
H	2.68587	-3.33089	-3.46425
H	4.19394	-3.89526	-1.48012
H	4.74731	-3.62772	0.89529
H	1.04905	2.17380	-2.57504
H	3.05781	1.99197	-4.00176

Table 11S. Cartesian coordinates from the optimized structures of S_0 in C_6H_5Cl media for **5b**[1].

Atom symbol	X	Y	Z
C	5.31132	-1.55628	0.58307
C	4.10928	-1.92114	-0.11749
C	2.98210	-1.06831	-0.01464
C	3.07299	0.11551	0.77212
C	4.26099	0.46343	1.45516
C	5.38728	-0.42031	1.33359
N	1.94637	0.89125	0.82553
C	4.25996	1.65532	2.20288
C	3.11631	2.43228	2.23802
C	1.97796	2.02050	1.53428
C	3.98535	-3.08451	-0.90520
C	2.78324	-3.34958	-1.54103
C	1.67411	-2.48593	-1.42268
C	1.74113	-1.32183	-0.66150
H	5.15178	1.95754	2.74103
H	3.08219	3.35794	2.79802
C	-0.80386	-2.16649	3.25190
C	-1.88495	-2.88853	2.77094
C	-0.09220	-1.26058	2.43890
C	-2.28219	-2.72475	1.42756
C	-3.37739	-3.43503	0.82267
C	-1.55012	-1.81193	0.62934
C	-3.71144	-3.26038	-0.48855
C	-2.97588	-2.35310	-1.32585
N	-1.14021	-0.75951	-1.44904
C	-3.23624	-2.12606	-2.69028
C	-1.40355	-0.56511	-2.74145
C	-2.44686	-1.23349	-3.39395
C	-0.44923	-1.04672	1.10935
H	-4.04788	-2.65224	-3.18102
H	-0.76101	0.13455	-3.25977
H	-2.61899	-1.03969	-4.44483
Ir	0.36158	0.14093	-0.32321
O	1.19085	1.25735	-2.01576
N	-0.96876	1.91343	0.01816
C	1.02341	2.50124	-2.24694
C	0.13549	3.36383	-1.59759
C	-0.84295	3.07261	-0.61090
H	0.14128	4.38660	-1.94905
C	1.88173	3.05522	-3.36744
H	1.67359	2.50501	-4.28973

H	2.93735	2.89570	-3.12929
H	1.71133	4.11782	-3.54229
C	-1.78999	4.21666	-0.28952
H	-1.38044	5.16154	-0.64475
H	-1.98127	4.29454	0.78195
H	-2.75366	4.06381	-0.78431
C	-1.90648	-1.64163	-0.73811
C	-2.09094	1.73272	0.87493
C	-1.96421	1.72586	2.26959
C	-3.37138	1.50404	0.36414
C	-4.48223	1.29015	1.16344
C	-4.32678	1.29885	2.54802
C	-3.06408	1.51774	3.09779
F	-3.54583	1.50313	-0.98752
H	-5.44575	1.12161	0.69774
H	-5.18536	1.13281	3.18769
H	1.07204	2.61014	1.53408
H	6.30417	-0.16306	1.85258
H	6.17424	-2.20969	0.50352
H	4.82739	-3.76065	-1.00721
H	2.68923	-4.24587	-2.14660
H	0.75978	-2.75093	-1.94275
H	-0.49384	-2.30127	4.28384
H	0.74626	-0.72632	2.87359
H	-2.42020	-3.57946	3.41338
H	-3.94342	-4.12943	1.43545
H	-4.53864	-3.81071	-0.92352
H	-0.98352	1.88669	2.69933
H	-2.93261	1.52237	4.17352

Table 12S. Cartesian coordinates from the optimized structures of S_0 in C_6H_5Cl media for **5b²**.

Atom symbol	X	Y	Z
C	5.16794	1.62942	-0.98013
C	3.97405	2.07035	-0.31031
C	2.87795	1.17606	-0.22336
C	2.98961	-0.12251	-0.79802
C	4.16891	-0.54341	-1.45381
C	5.26412	0.38377	-1.52639
N	1.89184	-0.93232	-0.67836
C	4.19058	-1.84516	-1.98815
C	3.07568	-2.65126	-1.85264
C	1.94218	-2.16249	-1.19043
C	3.82867	3.34849	0.26841
C	2.63703	3.68119	0.89163
C	1.55912	2.77387	0.96537
C	1.64872	1.49849	0.41452
H	5.07719	-2.20556	-2.49863
H	3.05793	-3.65824	-2.24924
C	-1.10839	1.51046	-3.47668
C	-2.16743	2.31024	-3.07552
C	-0.33222	0.78245	-2.55151
C	-2.48118	2.40348	-1.70389
C	-3.55436	3.20536	-1.17892
C	-1.68774	1.66359	-0.79336
C	-3.81827	3.26901	0.15808
C	-3.02780	2.53113	1.10458
N	-1.16163	0.99895	1.41448
C	-3.22413	2.54011	2.49807
C	-1.36546	1.02656	2.73257
C	-2.39119	1.78679	3.30786
C	-0.60069	0.83108	-1.18498
H	-4.02130	3.13657	2.92837
H	-0.68704	0.43371	3.33221
H	-2.51393	1.77583	4.38324
Ir	0.32013	-0.04923	0.39474
O	1.27460	-0.82732	2.20822
N	-0.94851	-1.89451	0.44701
C	1.19476	-2.02593	2.63878
C	0.32693	-3.02448	2.18618
C	-0.72249	-2.93524	1.23377

H	0.40838	-3.97666	2.69227
C	2.14050	-2.35106	3.77842
H	1.95238	-1.66857	4.61245
H	3.17134	-2.18413	3.45289
H	2.03888	-3.37819	4.12967
C	-1.63429	-4.14868	1.15699
H	-1.21630	-4.97983	1.72307
H	-1.78675	-4.46855	0.12398
H	-2.62012	-3.91750	1.56961
C	-1.97322	1.73822	0.59856
C	-2.14587	-1.88537	-0.32423
C	-2.16932	-2.28025	-1.66263
C	-3.35704	-1.43552	0.21738
C	-4.52113	-1.38746	-0.54590
C	-4.50108	-1.78862	-1.88093
C	-3.31049	-2.24182	-2.44591
H	-3.36925	-1.12044	1.25422
H	-5.44202	-1.03317	-0.09742
H	-5.40179	-1.75036	-2.48187
H	1.05302	-2.76410	-1.07638
H	6.17366	0.07019	-2.02702
H	6.00712	2.31458	-1.04581
H	4.64676	4.05922	0.22109
H	2.52675	4.66615	1.33506
H	0.65208	3.09425	1.46668
H	-0.86658	1.44211	-4.53304
H	0.48484	0.17570	-2.92730
H	-2.75196	2.86222	-3.80369
H	-4.16346	3.77257	-1.87560
H	-4.63186	3.88237	0.52980
F	-1.02204	-2.75495	-2.22489
H	-3.25585	-2.56638	-3.47796

Table 13S. Cartesian coordinates from the optimized structures of S_0 in C_6H_5Cl media for **5c**[1].

Atom symbol	X	Y	Z
C	-5.33335	-1.52038	-0.78401
C	-4.15475	-1.91173	-0.05838
C	-3.02620	-1.05510	-0.08962
C	-3.09277	0.15867	-0.83186
C	-4.25746	0.53174	-1.54127
C	-5.38581	-0.35633	-1.49229
N	-1.96657	0.93679	-0.81713
C	-4.23272	1.75063	-2.24361
C	-3.08970	2.52871	-2.21087
C	-1.97545	2.09137	-1.48444
C	-4.05508	-3.10513	0.68675
C	-2.87462	-3.39459	1.35187
C	-1.76357	-2.52661	1.30482
C	-1.80710	-1.33428	0.58701
H	-5.10609	2.07191	-2.80065
H	-3.03778	3.47433	-2.73497
C	0.85540	-2.00803	-3.28745
C	1.91332	-2.76214	-2.80355
C	0.12301	-1.13381	-2.45857
C	2.26625	-2.66229	-1.44193
C	3.33826	-3.40552	-0.83477
C	1.51393	-1.78021	-0.62805
C	3.63506	-3.28707	0.49144
C	2.88132	-2.40851	1.34305
N	1.05075	-0.80974	1.47877
C	3.10878	-2.23284	2.72064
C	1.28311	-0.66355	2.78426
C	2.30730	-1.36052	3.43710
C	0.43473	-0.98527	-1.10874
H	3.90516	-2.78151	3.21164
H	0.62892	0.01872	3.31141
H	2.45437	-1.20659	4.49835
Ir	-0.41795	0.13995	0.35001
O	-1.29508	1.18660	2.06401
N	0.91985	1.92229	0.12707
C	-1.15334	2.42636	2.33477
C	-0.25802	3.31795	1.73838
C	0.76008	3.06175	0.78040
H	-0.28890	4.33108	2.11572

C	-2.05460	2.93603	3.44234
H	-1.86772	2.36290	4.35521
H	-3.09968	2.76842	3.16625
H	-1.90590	3.99558	3.65210
C	1.70989	4.22214	0.52869
H	1.27806	5.15268	0.89521
H	1.94140	4.33127	-0.53200
H	2.65803	4.06401	1.05041
C	1.83100	-1.66883	0.75472
C	2.08424	1.76561	-0.68309
C	2.01508	1.87632	-2.07688
C	3.31311	1.46090	-0.08477
C	4.42559	1.29226	-0.89128
C	4.38731	1.40844	-2.27027
C	3.15608	1.70441	-2.85614
H	3.40001	1.35606	0.98921
F	5.61641	0.99758	-0.29195
H	5.28506	1.26607	-2.85808
H	-1.07066	2.68010	-1.43192
H	-6.28491	-0.07928	-2.03178
H	-6.19732	-2.17674	-0.75886
H	-4.89875	-3.78530	0.73371
H	-2.79972	-4.31394	1.92462
H	-0.86656	-2.81120	1.84432
H	0.58036	-2.09234	-4.33455
H	-0.69508	-0.57181	-2.89703
H	2.46512	-3.42776	-3.45853
H	3.91856	-4.07743	-1.45909
H	4.44682	-3.85921	0.92714
H	1.06533	2.09687	-2.54662
H	3.08889	1.79749	-3.93390

Table 14S. Cartesian coordinates from the optimized structures of S_0 in C_6H_5Cl media for **5c²**.

Atom symbol	X	Y	Z
C	5.20959	1.34513	-1.32228
C	4.08502	1.86484	-0.59150
C	2.95878	1.02643	-0.39838
C	2.97503	-0.29565	-0.92812
C	4.08687	-0.79469	-1.64485
C	5.21385	0.07806	-1.82624
N	1.85472	-1.04907	-0.70239
C	4.01409	-2.11414	-2.12833
C	2.87789	-2.86402	-1.88421
C	1.81763	-2.29950	-1.16479
C	4.03618	3.16755	-0.05316
C	2.90515	3.57694	0.63442
C	1.79492	2.72480	0.81202
C	1.78968	1.42827	0.30446
H	4.84595	-2.53354	-2.68368
H	2.79049	-3.88383	-2.23616
C	-1.15870	1.45755	-3.42393
C	-2.18425	2.28755	-2.99814
C	-0.35886	0.73559	-2.51447
C	-2.43421	2.42326	-1.61693
C	-3.46459	3.26357	-1.06688
C	-1.61667	1.68979	-0.72260
C	-3.66244	3.37327	0.27855
C	-2.84159	2.64822	1.20905
N	-0.99565	1.08429	1.47704
C	-2.96639	2.70778	2.60948
C	-1.13110	1.16016	2.80185
C	-2.10930	1.96283	3.40163
C	-0.56932	0.81989	-1.13970
H	-3.72792	3.33603	3.05866
H	-0.43555	0.57149	3.38572
H	-2.17706	1.99041	4.48158
Ir	0.39180	-0.05271	0.42103
O	1.39943	-0.80099	2.21899
N	-0.94472	-1.83831	0.59784
C	1.28549	-1.97647	2.70441
C	0.35687	-2.95104	2.33030
C	-0.72919	-2.85365	1.41871
H	0.42193	-3.88749	2.86762

C	2.26432	-2.29714	3.81702
H	2.13065	-1.58293	4.63494
H	3.28676	-2.17563	3.44803
H	2.14233	-3.30835	4.20609
C	-1.68216	-4.03860	1.43143
H	-1.19755	-4.90829	1.87427
H	-2.02401	-4.29484	0.42777
H	-2.57054	-3.81180	2.02770
C	-1.83167	1.81451	0.67824
C	-2.17105	-1.80302	-0.13034
C	-2.18954	-2.09206	-1.49955
C	-3.36501	-1.43546	0.50367
C	-4.55678	-1.37028	-0.21432
C	-4.58730	-1.66347	-1.57749
C	-3.39168	-2.01746	-2.18047
H	-3.35173	-1.19908	1.56079
H	-5.47287	-1.08453	0.28974
H	-5.50037	-1.61529	-2.15690
H	0.92016	-2.86262	-0.94934
H	6.07251	-0.29411	-2.37428
H	6.07158	1.98790	-1.46984
H	4.87992	3.83709	-0.18110
H	2.86915	4.58053	1.04722
H	0.93815	3.10449	1.35842
H	-0.96417	1.35865	-4.48754
H	0.42886	0.10282	-2.91010
H	-2.78944	2.83273	-3.71441
H	-4.09430	3.82308	-1.75131
H	-4.44437	4.01528	0.66930
H	-1.28631	-2.36582	-2.02754
F	-3.39378	-2.30892	-3.51398

Table 15S. Cartesian coordinates from the optimized structures of S_0 in C_6H_5Cl media for **5d**.

Atom symbol	X	Y	Z
C	-5.27241	-1.40587	-1.22496
C	-4.15967	-1.85311	-0.43088
C	-3.02392	-1.01193	-0.32467
C	-3.02066	0.24278	-0.99849
C	-4.12133	0.67134	-1.77565
C	-5.25740	-0.20355	-1.86821
N	-1.89325	1.00448	-0.84804
C	-4.02967	1.92869	-2.40077
C	-2.88716	2.68929	-2.23013
C	-1.83868	2.19646	-1.44381
C	-4.13147	-3.08675	0.25226
C	-3.01104	-3.42842	0.99228
C	-1.89106	-2.57515	1.08096
C	-1.86478	-1.34539	0.42861
H	-4.85251	2.29288	-3.00629
H	-2.78613	3.66344	-2.69105
C	1.06937	-1.82447	-3.27706
C	2.07899	-2.62420	-2.76418
C	0.28698	-0.99062	-2.45201
C	2.33024	-2.61305	-1.37652
C	3.34433	-3.40991	-0.73855
C	1.53015	-1.76915	-0.56784
C	3.54393	-3.37561	0.61065
C	2.74182	-2.53490	1.45621
N	0.92881	-0.91427	1.55372
C	2.87080	-2.44256	2.85451
C	1.06858	-0.84549	2.87848
C	2.03275	-1.59716	3.56145
C	0.49881	-0.92869	-1.07620
H	3.62100	-3.03375	3.36840
H	0.38740	-0.18103	3.39405
H	2.10455	-1.50703	4.63771
Ir	-0.44503	0.11946	0.38260
O	-1.43236	1.06738	2.09517
N	0.92040	1.88959	0.36468
C	-1.31125	2.29239	2.43600
C	-0.37889	3.21026	1.94693
C	0.71207	2.99534	1.06026
H	-0.43718	4.20408	2.36977

C	-2.28405	2.74735	3.50633
H	-2.14831	2.13574	4.40329
H	-3.30868	2.58559	3.15955
H	-2.15740	3.79741	3.77114
C	1.68284	4.16049	0.94666
H	1.22011	5.07658	1.31242
H	2.01121	4.31434	-0.08231
H	2.57886	3.97575	1.54610
C	1.74725	-1.74427	0.83819
C	2.15630	1.75898	-0.34231
C	2.21301	1.92442	-1.73060
C	3.32902	1.42198	0.34393
C	4.53809	1.26731	-0.33231
C	4.55350	1.45058	-1.70428
C	3.41415	1.77624	-2.42082
H	3.29420	1.27834	1.41736
H	5.44906	1.00636	0.19221
F	5.73313	1.30075	-2.37597
H	-0.93639	2.77016	-1.28333
H	-6.10764	0.11494	-2.46142
H	-6.14145	-2.05095	-1.30633
H	-4.98277	-3.75642	0.19367
H	-2.99138	-4.37851	1.51751
H	-1.04287	-2.90059	1.67383
H	0.87289	-1.83970	-4.34493
H	-0.48940	-0.39021	-2.91460
H	2.67038	-3.25738	-3.41674
H	3.95989	-4.05419	-1.35822
H	4.31289	-3.98778	1.06918
H	1.31201	2.17226	-2.27713
H	3.46634	1.90536	-3.49485

Table 16S. Cartesian coordinates from the optimized structures of S_0 in C_6H_5Cl media for **5f**.

Atom symbol	X	Y	Z
C	5.59389	0.77833	-1.59357
C	4.53184	1.49229	-0.93727
C	3.35155	0.78526	-0.59748
C	3.25228	-0.59984	-0.91368
C	4.30514	-1.29060	-1.55564
C	5.48933	-0.54862	-1.88935
N	2.08358	-1.21784	-0.55751
C	4.12306	-2.66107	-1.81807
C	2.94179	-3.27201	-1.44018
C	1.94286	-2.51977	-0.80954
C	4.59606	2.86268	-0.60919
C	3.51977	3.46153	0.02457
C	2.35482	2.73695	0.35417
C	2.23947	1.38201	0.05699
H	4.90729	-3.22658	-2.30950
H	2.76986	-4.32500	-1.62228
C	-0.87082	1.07063	-3.55149
C	-1.79956	2.04758	-3.22941
C	-0.08820	0.43298	-2.56607
C	-1.96858	2.42341	-1.88041
C	-2.89516	3.43181	-1.43854
C	-1.17252	1.76922	-0.90841
C	-3.01575	3.77082	-0.12261
C	-2.21538	3.12927	0.88378
N	-0.50186	1.46145	1.33895
C	-2.26425	3.42276	2.25951
C	-0.56465	1.75936	2.63709
C	-1.43654	2.73739	3.13131
C	-0.22027	0.75565	-1.21749
H	-2.94576	4.18246	2.62633
H	0.09965	1.20486	3.28683
H	-1.44884	2.94170	4.19410
Ir	0.73847	0.05650	0.42924
O	1.73547	-0.51964	2.29686
N	-0.74991	-1.55961	0.90768
C	1.53026	-1.58736	2.95815
C	0.49531	-2.51586	2.76245
C	-0.60494	-2.45767	1.87935
H	0.49371	-3.35691	3.44189

C	2.51267	-1.83273	4.08556
H	2.48704	-0.98601	4.77754
H	3.52602	-1.88354	3.67723
H	2.30284	-2.74914	4.63717
C	-1.67366	-3.51441	2.08905
H	-1.30608	-4.30771	2.73806
H	-1.99386	-3.95648	1.14308
H	-2.55673	-3.07748	2.56477
C	-1.30855	2.13209	0.46139
C	-1.98219	-1.50480	0.22032
C	-2.12844	-1.98711	-1.08398
C	-3.10973	-0.89114	0.77751
C	-4.30174	-0.74828	0.08125
C	-4.40358	-1.22575	-1.21754
C	-3.31025	-1.85237	-1.79864
F	-3.05654	-0.42128	2.03680
F	-5.35553	-0.14921	0.65625
H	1.00855	-2.96910	-0.50716
H	6.30290	-1.06898	-2.38283
H	6.49747	1.32020	-1.85385
H	5.48365	3.43591	-0.85439
H	3.57086	4.51664	0.27524
H	1.54585	3.26268	0.84959
H	-0.73870	0.78672	-4.59100
H	0.62423	-0.32145	-2.88125
H	-2.39092	2.52596	-4.00259
H	-3.50785	3.93140	-2.18211
H	-3.71935	4.53613	0.18621
F	-1.10872	-2.63286	-1.67427
F	-3.40442	-2.33394	-3.04683
F	-5.54733	-1.08867	-1.90134

Table 17S. Cartesian coordinates from the optimized structures of S_0 in C_6H_5Cl media for **5g**.

Atom symbol	X	Y	Z
C	5.80545	-0.97235	-2.49982
C	5.02042	0.14016	-2.03675
C	3.85608	-0.12568	-1.27387
C	3.49794	-1.47542	-0.99390
C	4.27912	-2.55973	-1.45381
C	5.45538	-2.26075	-2.22270
N	2.35809	-1.65718	-0.25747
C	3.85211	-3.85926	-1.12350
C	2.70457	-4.02418	-0.37036
C	1.98175	-2.89949	0.04737
C	5.34250	1.48825	-2.29894
C	4.52212	2.49114	-1.80907
C	3.36817	2.20233	-1.05034
C	3.00546	0.89039	-0.75889
H	4.42362	-4.71781	-1.45914
H	2.34851	-5.00873	-0.09569
C	-0.82234	-0.03251	-3.45045
C	-1.50047	1.17583	-3.41797
C	0.05202	-0.42431	-2.41514
C	-1.31380	2.04438	-2.32249
C	-1.95941	3.32389	-2.19284
C	-0.43368	1.62866	-1.29347
C	-1.74163	4.13415	-1.11704
C	-0.85135	3.73917	-0.06031
N	0.64952	2.01330	0.77298
C	-0.56046	4.51191	1.07950
C	0.90843	2.76390	1.84424
C	0.31975	4.02097	2.02785
C	0.26632	0.38841	-1.30448
H	-1.02465	5.48379	1.20699
H	1.60308	2.34827	2.56245
H	0.56438	4.59131	2.91464
Ir	1.45129	0.14417	0.32645
O	2.75154	0.08233	2.09179
N	-0.10363	-0.82584	1.62869
C	2.55044	-0.59455	3.15071
C	1.37822	-1.28040	3.50262
C	0.12803	-1.31432	2.84395
H	1.40842	-1.79157	4.45496

C	3.71520	-0.61565	4.12033
H	3.95920	0.40923	4.41468
H	4.59656	-1.02434	3.61812
H	3.50832	-1.20277	5.01517
C	-1.00300	-1.96555	3.61911
H	-0.61372	-2.52396	4.46909
H	-1.58259	-2.64423	2.98980
H	-1.68976	-1.20648	4.00495
C	-0.21630	2.48260	-0.17591
C	-1.44057	-0.77096	1.17216
C	-1.93908	-1.65433	0.21143
C	-2.32771	0.22172	1.60140
C	-3.61418	0.33481	1.09763
C	-4.09928	-0.55130	0.13423
C	-3.22720	-1.55308	-0.29387
F	-1.93138	1.10612	2.53879
F	-4.40952	1.32950	1.54033
O	-5.33211	-0.42108	-0.42394
H	1.07792	-2.99627	0.63032
H	6.06194	-3.08569	-2.58011
H	6.69754	-0.76840	-3.08331
H	6.22577	1.72928	-2.88058
H	4.77097	3.52803	-2.01333
H	2.76564	3.03143	-0.69540
H	-0.96569	-0.69801	-4.29614
H	0.55723	-1.38036	-2.49870
H	-2.16893	1.45767	-4.22426
H	-2.63547	3.64283	-2.97971
H	-2.23865	5.09519	-1.04261
F	-1.16646	-2.66830	-0.22331
F	-3.64138	-2.44413	-1.21073
C	-6.45114	-0.78633	0.42420
C	-7.72658	-0.62357	-0.36444
H	-6.47631	-0.13026	1.29839
H	-6.33064	-1.82377	0.74988
O	-7.82455	-1.64983	-1.33620
H	-7.74325	0.36591	-0.84261
H	-8.57411	-0.67567	0.33532
C	-8.97915	-1.52403	-2.15254
H	-8.96461	-2.35262	-2.86025
H	-8.97253	-0.57677	-2.70701
H	-9.89829	-1.57774	-1.55391

6. AFM data

Images of thin layers:

5 wt% of complex **5g** in PVK:PBD matrix

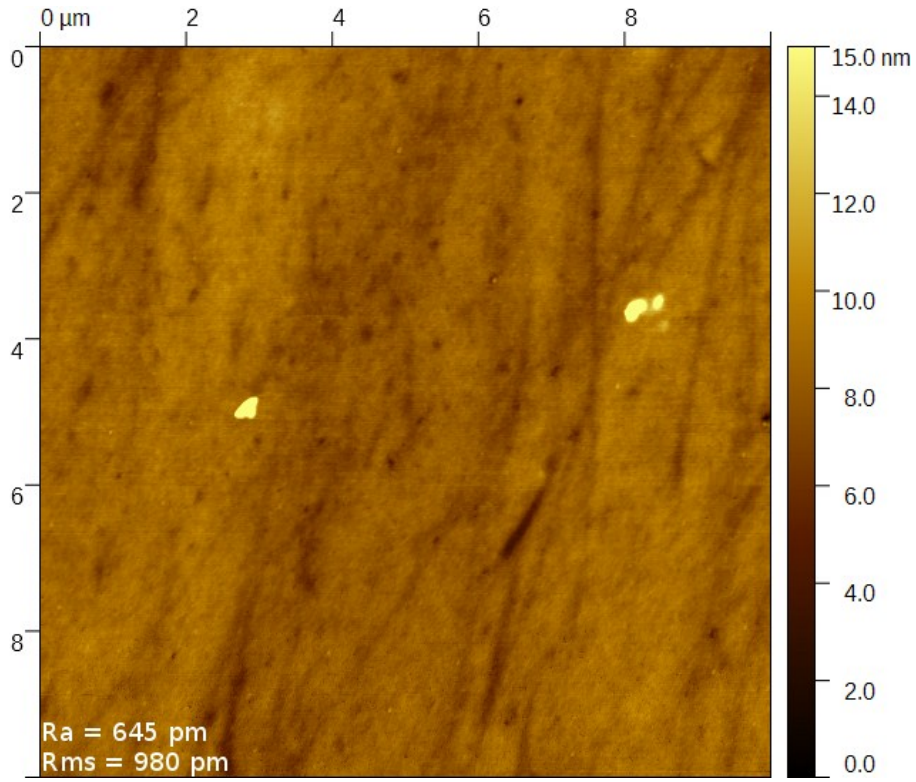

0.5 wt% of complex **5g** in PVK:PBD matrix

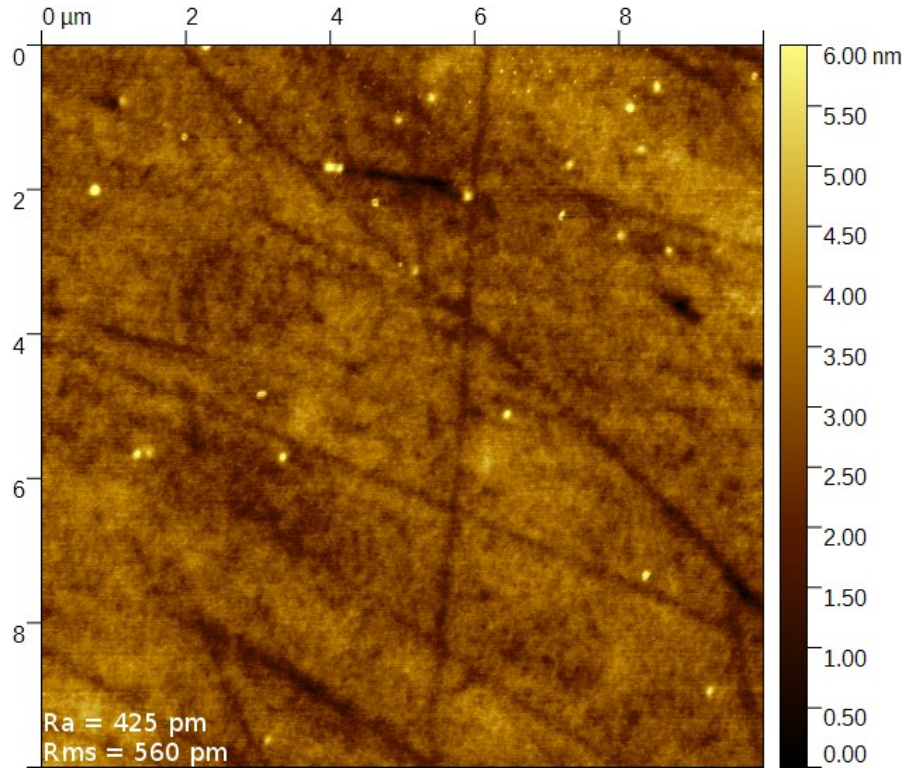
0 µm
2
4
6
8
0
2
4
6
8
6.00 nm
5.50
5.00
4.50
4.00
3.50
3.00
2.50
2.00
1.50
1.00
0.50
0.00
Ra = 425 pm
Rms = 560 pm

Inorganic Chemistry
Article
Cite This: Inorg. Chem. 2019, 58, 15671−15686
pubs.acs.org/IC

Effect of β-Ketoiminato Ancillary Ligand Modification on Emissive Properties of New Iridium Complexes

Ewelina Witkowska,[†] Bartosz Orwat,[‡,§] Myong Joon Oh,[‡,§] Gabriela Wiosna-Salyga,[*,†] Ireneusz Glowacki,[†] Ireneusz Kownacki,[*,‡,§] Kamila Jankowska,[‡,§] Maciej Kubicki,[‡] Blazej Gierczyk,[‡] Michal Dutkiewicz,[§,∥] Izabela Grzelak,[‡] Marcin Hoffmann,[‡] Julita Nawrocik,[‡,§] Grzegorz Krajewski,[‡,§] Jacek Ulanski,[†] Przemyslaw Ledwon,[⊥] and Mieczyslaw Lapkowski[⊥,#]

[†]Department of Molecular Physics, Lodz University of Technology, Zeromskiego 116, 90-924 Lodz, Poland
[‡]Faculty of Chemistry, Adam Mickiewicz University in Poznan, St. Uniwersytetu Poznanskiego 8, 61-614 Poznan, Poland
[§]Center for Advanced Technology, Adam Mickiewicz University in Poznan, St. Uniwersytetu Poznanskiego 10, 61-614 Poznan, Poland
[∥]Poznan Science and Technology Park, Adam Mickiewicz University Foundation, ul. Rubiez 46, 61-612 Poznan, Poland
[⊥]Faculty of Chemistry, Silesian University of Technology, St. Marcina Strzody 9, 44-100 Gliwice, Poland
[#]Center of Polymer and Carbon Materials, Polish Academy of Sciences, Curie−Sklodowskiej 34, 41-819 Zabrze, Poland

Supporting Information

ABSTRACT: A series of new bis(benzo[*h*]quinolinato) Ir(III) complexes with modified β-ketoiminato ancillary ligands were synthesized, and their electrochemical, photophysical properties were determined with the support of theoretical calculations. Moreover, all the synthesized heteroleptic Ir(III) complexes were examined as dopants of the host−guest type emissive layers in solution-processed phosphorescent organic light emitting diodes (PhOLEDs) of a simple structure. As expected on the basis of voltammetry measurements as well as DFT calculations, all the compounds appeared to be green emitters. Their examination showed that alteration of β-ketoiminato ligand structure causes frontier orbitals' energy levels to be slightly changed, while significantly affecting photoluminescence and electroluminescence efficiencies of iridium phosphors containing these ligands. It was also found that modification of ancillary ligands might enhance charge trapping on the dopant, thus increasing its efficiency, especially in electroluminescence. From among the iridium complexes studied, the compound bearing 1-naphthyl group bonded to the nitrogen atom of the ancillary ligand proved to be the most efficient emitter. The PhOLED fabricated on the basis of this dopant has reached a luminance level of 16000 cd/m^2, current efficiency close to 12 cd/A, and an external quantum efficiency around 3.2%.

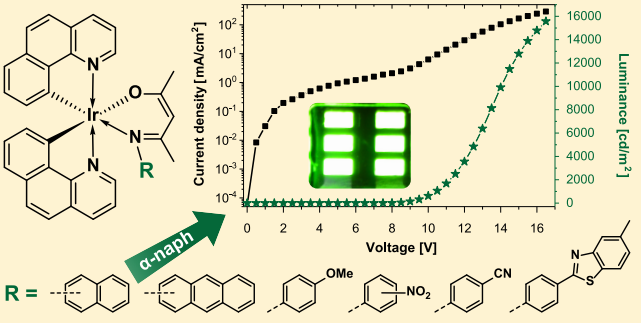

INTRODUCTION

Intensive research into new organic electroluminescent materials has been ongoing since Tang and Van Slake described the first organic light emitting diodes (OLEDs),[1] and the researchers from the Cambridge University presented the first polymer light emitting diode (PLED).[2] In the first generation of electroluminescent devices, emission occurs mainly from singlet states and is related to the phenomenon of fluorescence. Therefore, according to statistical rules, theoretical internal efficiency of such devices can reach maximally 25%. This limit may be overcome by phosphorescent emitters, for which quantum mechanics selection rules can be broken, and theoretically their emission yield can increase up to 100%.[3] Popular phosphorescent materials are heavy metal complexes bearing organic ligands whose properties result from the presence of strong spin−orbit coupling. The complexes of Pt, Pd, or Os metals have been studied, but the most examined are Ir(III) derivatives.[4] Popularity of the iridium compounds is related to their intensive phosphorescence, even at room temperature, that might be tuned within the whole visible spectrum depending on the ligand structure modification. It should be emphasized that 2-phenylpyridine was one of the first ligands successfully used in this role and together with benzo[*h*]quinoline gave rise to a group of iridium complexes characterized by very intense green emission, for instance: tris(2-phenylpyridinato)iridium(III) ([Ir(ppy)$_3$]) and bis(2-phenylpyridinato-$C^{2'}$,N) (acetylacetonato)iridium(III) ([Ir(ppy)$_2$(acac)]),[5] tris(benzo[*h*]quinolinato-C^2,N')iridium(III) ([Ir(bzq)$_3$]), and bis(2-benzo[*h*]quinolinato-C^2,N')(acetyl-

Received: September 18, 2019
Published: November 7, 2019

DOI: 10.1021/acs.inorgchem.9b02785
Inorg. Chem. 2019, 58, 15671−15686

acetonato)iridium(III) ([Ir(bzq)$_2$(acac)]).[5] Although the first iridium(III) complexes for OLEDs were developed over 20 years ago, the synthesis and study of new efficient iridium-based emitters is still considered an attractive topic.[4b,6]

In general, emissive materials show higher photoluminescence yield in solution than in solid state (i.e., thin layer) which is related to the self−quenching of excited states. In order to suppress this effect, a host−guest system can be implemented. In such a system, the emitter molecules are dispersed in an active host, e.g. polymeric matrix, that increases the mean distance between two emitter molecules.[7] On the other hand, this approach emphasizes the importance of the intermolecular energy transfer. The yield of energy transfer from the excited states of the matrix to the dopant (by Förster and/or Dexter mechanism) depends on the overlap of the emission spectrum of the host and the absorption spectrum of the guest.[8] Only when this condition is satisfied, a very efficient energy transfer from the host to the guest can take place. Moreover, the emission originating from the guest molecules can be also caused by the direct charge carrier trapping on the dopant.[9] Thus, the host−guest systems can be successfully applied in the form of an efficient emission layer in phosphorescent OLEDs (PhOLEDs).

Very recently, we have reported the studies concerning new heteroleptic complexes of the general formula [Ir(bzq)$_2$(O∧N)], for which we discussed the impact of the number and distribution of fluorine atoms directly bonded to the *N*-aryl moiety (=NR^1) in *N*,*O*-donating *β*-ketoiminato ligand (RC(=NR^1)CH=C(−O$^-$)R), on the photophysical and emissive properties.[10] We have found that the introduction of fluorine atoms does not significantly modify the optical and electrochemical properties of the iridium complexes, while the electroluminescence performance of PhOLEDs based on them was strongly dependent on the structure of the modified *β*-ketoiminato ligand. The most promising results were obtained for the Ir complex with 4-fluorophenyl substituent in the ancillary ligand structure. Therefore, as a continuation of our research, we decided to explore *para* substitution effect by investigation of Ir(III) heteroleptic complexes with different substituents in the mentioned position of the phenyl moiety in 4-phenylimino-2-pentanonate ancillary ligand. As follows from the available reports on this subject, in particular those by Teets'[11] as well as our recent findings,[10] so far the subjects of studies have been limited to phenyl-based *N*-substituents (=NR^1). Unfortunately, there are no other reports concerning the influence of the higher condensed polycyclic aromatic hydrocarbon used as −R^1 substituents in *N*,*O*-donating *β*-ketoiminato ligand. Therefore, we focused also on the synthesis of 4-arylimino-2-pentanones (MeC(=NR^1)CH$_2$−C(=O)Me) equipped with various polycyclic aromatic moieties −R^1, which were further employed in the preparation of new [Ir(bzq)$_2$(MeC(=NR^1)CH=C(−O)Me)] type complexes. The modification of *β*-ketoiminato ancillary ligand allowed determination of the =NR^1 substitution effect on the emitter photochemical properties. The obtained iridium complexes were applied as dopants in PhOLEDs, whose work parameter analysis allowed identification of the most efficient and promising iridium emitters.

RESULTS AND DISCUSSION

Synthesis. According to recently published protocols,[10] in the initial step a series of 4-arylimino-2-pentanones, bearing aryl substituents of variable stereoelectronic character **3a−l** at nitrogen atom, were successfully synthesized. Some of the desired derivatives (**3a−f**, **h**, **i**) were prepared by the classical manner, i.e. the refluxing of appropriate amines (**2a−f**, **h**, **i**) with 2,4-pentanedione (acacH) in the presence of *p*-toluenesulfonic acid in a benzene environment, using a Dean−Stark apparatus. However, the conversion of more hindered amines (**2g**, **j−l**) required an acceleration with microwave irradiation as a non-classical energy source (Scheme 1). Anyhow, these methods allowed us to obtain *β*-

Scheme 1. Synthesis of Ancillary Ligands

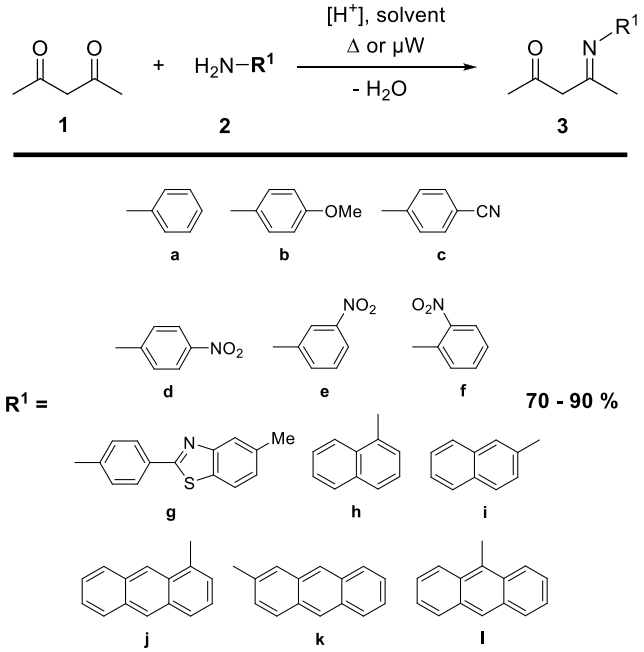

ketoimines equipped with phenyl-based substituents bearing in their structure groups characterized by strong electron withdrawing properties (**3c−f**), including various regioisomers of nitro−substituted derivatives (**3d−f**). Thus, in order to explain the influence of the presence of a strong electron withdrawing group and its position on photophysical properties of final heteroleptic Ir(III) complexes, not only *para*-substituted phenyl *β*-ketoimines, but also the compounds bearing −NO$_2$ group in *meta* and *ortho* positions were synthesized. We assumed that different position of the highly electron withdrawing substituent in the phenyl group could significantly affect the emissive parameters of the target iridium complex, as we have previously described for the phenyl group having one fluorine substituent.[10] Additionally, on the basis of the protocol involving the use of microwaves,[10] 4-arylimino-2-pentanones with selected bulky polycyclic aromatic systems were synthesized (**3g−l**). The purity of all organic materials was confirmed by spectroscopic methods, such ^{1}H, ^{13}C NMR, HRMS (high resolution mass spectrometry) as well as the structures of three of them (**3d, j, l**) were solved using X-ray methods.

In the next stage of our synthetic work, previously prepared 4-arylimino-2-pentanones were employed in the preparation of new iridium(III) complexes, according to the earlier described method.[10] However, this time instead of microwaves, a classical source of heat was used. The protocol applied consisted of two successive steps, namely, generation of 4-arylimino-2-pentanonalate salt in the reaction of *β*-ketoimi-

DOI: 10.1021/acs.inorgchem.9b02785
Inorg. Chem. 2019, 58, 15671−15686

nates **3** with NaH or KH in THF solution and employment of the former for cleavage of binuclear precursor **4** (Scheme 2).

Scheme 2. Synthesis of Heteroleptic *β*-Ketoiminato Iridium(III) Complexes

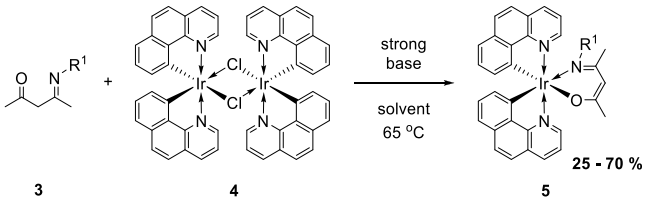

However, due to encountered vulnerability of the initial ketoimine to degradation during the deprotonation process, the use of NaO^{t}Bu as base in a one-pot protocol was required when using **5b** and **5f**. The applied methodologies made it possible to obtain a series of Ir(III)-based phosphors bearing in their structures various types of ancillary ligands (**5a**–**l**).

Compounds **5a**–**l** were obtained with moderate to good yields and characterized by spectroscopic methods. In the ^{1}H NMR spectra, sets of resonance lines characteristic of protons coming from specific parts of ligands were clearly visible, namely, in the region typical of cyclometalated bzq ligand (9.70–9.00 ppm), methine part of *N,O*-donating ancillary ligand (*c.a.* 5.00 ppm), as well as magnetically and chemically non-equivalent methyl groups of ketoiminato ligand (2.00–1.60 ppm). However, the ^{1}H NMR spectra of some of the isolated materials, namely **5c**, **5f**, **5i**, **5k**, and **5l** revealed the presence of two isomeric forms. We suppose that the reaction selectivity toward the formation of one isomer depends on properties of aryl substituents bonded to imine nitrogen atom, such as steric hindrance or its orientation relative to the *C,N*-cyclometalated ligands. In our opinion, the presence of *N*-aryl substituents in close proximity of the cyclometalated ligands may induce their intramolecular $\pi-\pi$ interaction (π-stacking), which might be the driving force for the formation of one of the two possible isomers, as it takes place for complexes **5b**, **5d**, **5g**, **5h**, and **5j**. Heteroleptic octahedral iridium(III) complexes with bidentate ligands may exist in the form of various geometrical isomers, such as *N,N-trans*–*mer, cis*–*fac, cis*–*mer* as well as *C,C-trans*–*mer* and their corresponding enantiomeric forms, as reported for the FIrpic complex.[12] The authors of the cited publication showed that the geometrical isomers do not differ in photophysical properties, thus we decided not to isolate pure isomers but examine their mixtures. Nevertheless, we wanted to determine exactly which of the possible isomers is formed in predominance. Therefore, the structures of five complexes (**5f, g, i, j, l**) were determined by X-ray analysis and are discussed in the next paragraph.

X-Ray Analysis. X-ray diffraction structural analysis confirmed the obtainment of target molecules (Figures 1 and 2 and Figure 23S in the SI). Although the crystal structure of **3d** has been published earlier,[13] for the sake of completeness, we decided to add this structure determination as well. The relevant geometrical parameters are listed in Table 2S (see the SI). In all complexes the Ir atom is six-coordinated in quite a regular octahedral fashion, surrounded by N and O atoms from ketoiminato fragment, and N and C atoms from two benzo[*h*]quinolinato ligands. Table 2S (see the SI) shows that, upon complexation, the C4–N5–C6 angle becomes significantly smaller, while the conformation of the 4-imino-2-pentanone fragment remains stable, although less planar. This observation can be connected with the presence of intramolecular N–H···O hydrogen bonds in free ligand molecules, responsible for planarization (cf. Table 3S, see the SI). What is more, the plane of the aromatic substituent at N5 (Table 2S, the SI) is almost perpendicular to the O=C–C=C–N plane (Table 2S, see the SI) in the coordinated ligands. The conformations of all complexes, whose structural data are collected, are quite similar. This can be shown by a comparison of the dihedral angles between planar fragments: Ir–ketoiminato cycle, two bzq planes, and substituent at N5. Table 2S (see the SI) lists the appropriate values, and the data can be summarized as follows: (i) the Ir–ketoiminato ring plane is almost perpendicular to all of the other planes, (ii)

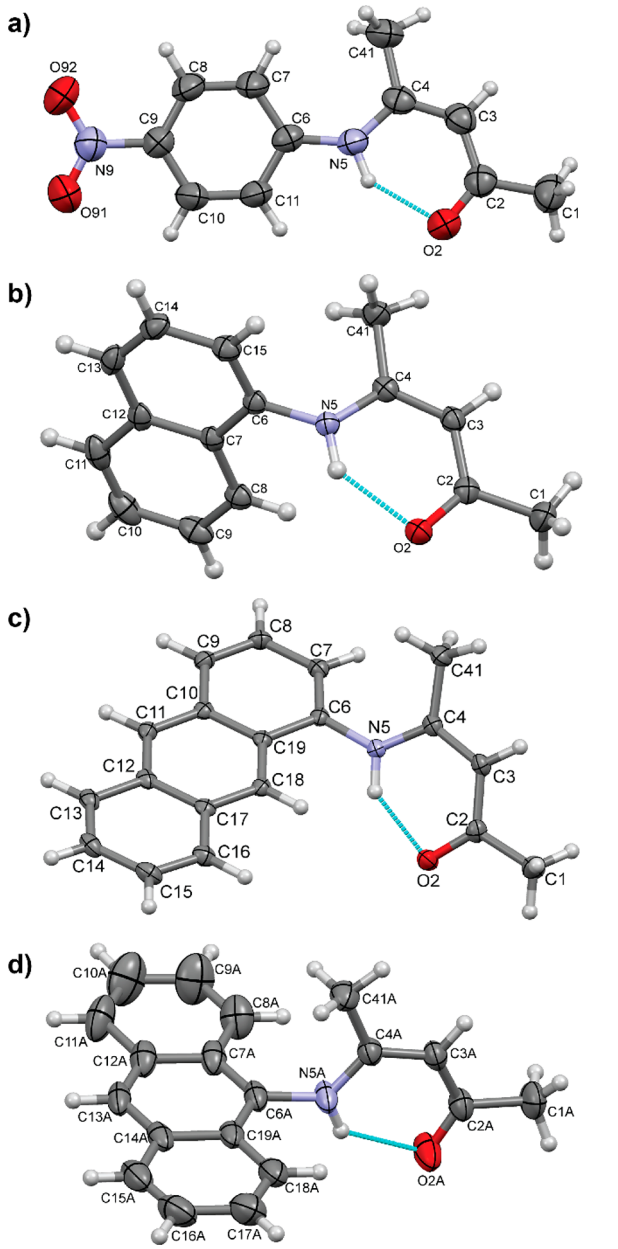

Figure 1. Perspective views of ligands: (**a**) **3d**, (**b**) **3h**, (**c**) **3j**, (**d**) **3l** (molecule A), together with the labeling schemes. Ellipsoids are drawn at the 50% probability level, hydrogen atoms are shown as spheres of arbitrary radii, and intramolecular hydrogen bonds are drawn as dashed blue lines.

DOI: 10.1021/acs.inorgchem.9b02785
Inorg. Chem. 2019, 58, 15671–15686

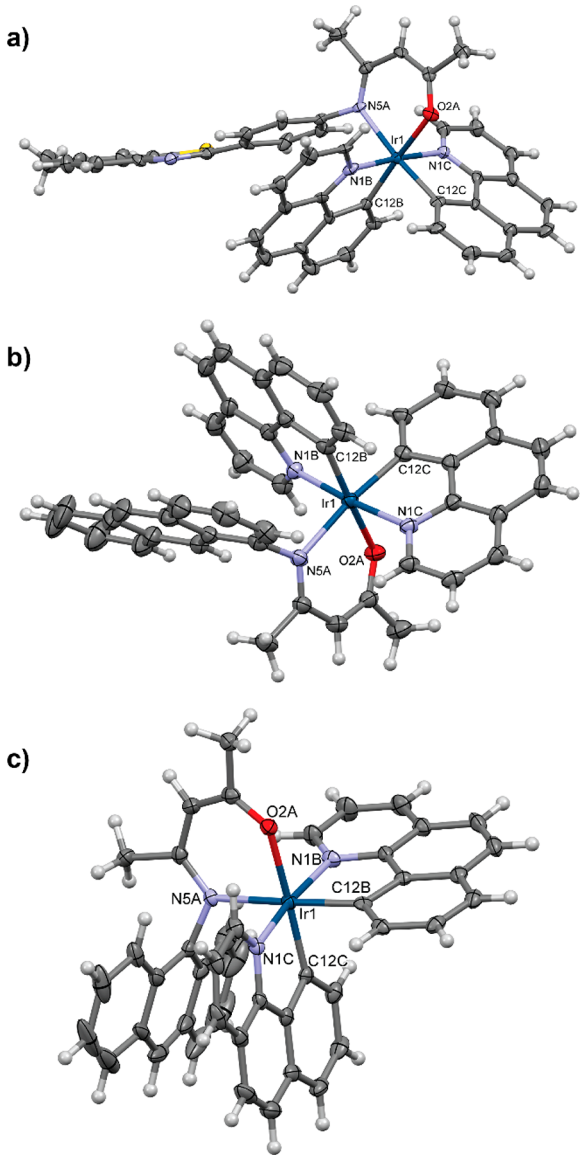

Figure 2. Perspective views of iridium complexes: (**a**) **5g**, (**b**) **5j**, (**c**) **5l**. Only Ir and coordinated atoms are labeled, for clarity. Ellipsoids are drawn at the 50% (**a** and **c**) and 33% (**b**) probability level, and hydrogen atoms are shown as spheres of arbitrary radii.

benzo[*h*]quinolinato planes are almost perpendicular to each other, and (iii) the aromatic substituents at N5 assume positions close to *gauche* with respect to one benzo[*h*]-quinolinato ligand and almost parallel to the other. In all complexes, the tendency toward such a parallel disposition is accompanied by a relatively close interplanar separation (in all cases ca. 3.6−3.7 Å; centroid−to−centroid distances are around 3.8−3.9 Å) which can be connected with the weak intramolecular $\pi\cdots\pi$ interactions.

The crystal structures are defined mainly by weak dispersive forces. Calculations of intermolecular (molecule-to-molecule) potential using UNI force field[14] indicate that the stabilizing energy is the largest for pairs for which $\pi\cdots\pi$ (−57.5 kJ/mol for **5l**, −67.0 kJ/mol for **5g**), C−H$\cdots\pi$ (−65.8 kJ/mol for **5j**), C−H···S (−67.0 kJ/mol in **5g**), or C−H···O (−48.1 kJ/mol in **5f**) intermolecular interactions can be found.

Considering the above, it seems that even weak intramolecular $\pi\cdots\pi$ interactions between the *N*-aryl group and the *C,N*-cyclometalated bzq ligand might induce the selective formation of only one isomer as it takes place for compounds **5b−d** and **5g−j** (see ^{1}H NMR spectra in the SI). On the basis of XRD analysis of single crystals obtained from isomerically pure samples **5g** and **5j**, we assume that for the above-mentioned complexes, *N,N-trans−mer* is the most preferred geometric isomer, which is confirmed by spectroscopic studies. This might be supported by the fact that such a configuration of *C,N*-donating ligands around the metal atom is typical of such a binuclear substrate.[15] However, in the case of any disturbances of this type of interactions related to the mutual arrangement of the above-mentioned elements of the complex molecule, e.g. by introduction of a substituent at position 2 relative to the N−C(Aryl) bond (**5f**) or changing the substitution site of the polyaromatic system (**5i**, **5k**, **5l**) (see ^{1}H NMR spectra in the SI), the formation of another isomer was observed.

Thermal Analysis. Thermal decomposition process of all discussed Ir complexes was essentially multimodal with two or three well-pronounced steps observed. The first decomposition step occurred in the range of 250−450 °C, followed by the second one, less pronounced, in the range of 450−650 °C and the third one which could be observed between 650 and 950 °C. Comparing the results of TG analysis presented in Table 1

Table 1. Results of TG and DTG Analysis

	mass loss temperature [°C]		
sample	$T_{5\%}$	$T_{10\%}$	residue[a] [%]
5a	272	333	23.9
5b	300	340	24.3
5c	238	313	26.2
5d	302	343	24.3
5e	278	338	24.4
5f	217	313	23.5
5g	349	376	25.6
5h	233	318	21.7
5i	339	367	23.2
5j	311	358	23.2
5k	313	351	22.6
5l	238	329	21.1

[a]Measured at 990 °C.

as well as TG curves presented in Figures 24S−33S, it can be concluded that the most thermally stable are complexes **5g** and **5b** with the temperatures of 5% mass loss exceeding 230 °C.

Careful analysis of the obtained data leads to the observation that not only the chemical nature of the functional group present in the phenyl ring (see Figure 24S) influence the thermal stability of examined compounds but also its regiosubstitution. This phenomenon can be easily observed in the example of TG curves of 4-, 3-, and 2-substituted nitrophenyl **5d**, **5e**, and **5f** derivatives presented in Figure 25S. While only slight differences are observed between the thermograms of **5d** and **5g** isomers, the thermal stability of **5f** is significantly lower, which was revealed by a decrease in the temperatures $T_{5\%}$ and $T_{10\%}$ (see Table 1). The influence of regioisomerism on thermal stability of the studied compounds was also confirmed by the results obtained for 1- and 2-naphthyl (**5h**, **5i**), as well as for 1-, 2-, and 9-anthracenyl (**5j**, **5k**, and **5l**) derivatives TG analysis, presented in Figure 26S and 27S, respectively. Comparing the TG curves of the above-mentioned naphthyl and anthracenyl derivatives with phenyl-

DOI: 10.1021/acs.inorgchem.9b02785
Inorg. Chem. 2019, 58, 15671−15686

derived complex (**5a**), it is easy to notice that also the number of condensed aromatic rings present in the structure of R substituent unambiguously influences the complex stability (see Figures 30S−33S). Despite the above-mentioned differences in the thermal stability of the investigated samples, the relative residue at 990 °C was similar. The latter was expected as the iridium should be the main component of the pyrolysis residue, and its content in the examined compounds was comparable.

As a conclusion of this paragraph, it might be said that all the complexes exhibited sufficient thermal stability to be applied as potential phosphorescent emitters.[16]

Electrochemical Properties. In order to determine electrochemical properties of the studied iridium(III) complexes, in particular their correlation with the structure of β-ketoiminato ligand, cyclic voltammetry measurements were performed. On the basis of the onsets of oxidation and reduction potentials, the electron affinity (EA) and ionization potential (IP) were estimated. The measured curves are shown in Figure 34S (SI). The oxidation onset potentials ($E_{ox\ onset}$) of all studied complexes are in the range from 0.12 up to 0.29 V. The oxidation is quasi-reversible and related to the oxidation of Ir(III) to Ir(IV). These results are in good agreement with those reported for the corresponding iridium complexes with β-ketoiminato ligands.[10,11] The incorporation of a methoxy group to the phenyl moiety leads to a slight decrease in $E_{ox\ onset}$ with respect to that of **5a**, while incorporation of nitrile or nitro groups leads to $E_{ox\ onset}$ increase (**5d**, **5e**) or has no effect (**5f**). This is consistent with the electronic effects of these groups, since the methoxy group is electron donating, while nitrile and nitro groups are electron withdrawing. For polycyclic aromatic substituted complexes (**5h**−**l**), the most intensive influence on $E_{ox\ onset}$ was observed for α-naphthyl derived complex. As one can see, the measured reduction onset potentials ($E_{red\ onset}$) were significantly more varied than $E_{ox\ onset}$. In general, most of the complexes were characterized with $E_{red\ onset}$ near −2.3 V, while the values reported for methoxy- and nitrile-derived complexes were slightly more positive. However, the most outstanding values were measured for nitro-derived complexes (**5d**−**f**). The three complexes showed quasi reversible reduction in contrast to the other studied compounds whose reduction was irreversible. These results are similar to those in the other reports concerning iridium complexes equipped with nitro group, in which a drastic change in the reduction potential was also observed.[17]

Electrochemical EA and IP were estimated from $E_{red\ onset}$ and $E_{ox\ onset}$, respectively. EA, which corresponds to the energy level of LUMO (the lowest occupied molecular orbital), was found to be more sensitive toward ancillary ligand chemical modification than IP, corresponding to the HOMO (the highest occupied molecular orbital) energy level. According to Table 2, EA values were within the 2.8−3.4 eV range, while the IP spread was only 0.2 eV. Therefore, the chemical modification had noticeably greater impact on the LUMO energy level. It is worth emphasizing that the complexes equipped with naphthyl or anthracenyl substituents (**5h**−**l**) were characterized by identical EA and IP values as the reference complex **5a**.

Results of electrochemical measurement show that the incorporation of different electron withdrawing or electron donating groups to β-ketoiminato ligand might lead to a change in their electrochemical properties. Obviously, it is a consequence of electron density shift caused by chemical

Table 2. Electrochemical Properties of Studied Compounds

compound	$E_{red\ onset}$ [V]	$E_{ox\ onset}$ [V]	E_g [eV]	EA [eV]	IP [eV]
5a	−2.32	0.17	2.49	2.8	5.3
5b	−2.20	0.12	2.32	2.9	5.2
5c	−2.15	0.21	2.36	3.0	5.3
5d	−1.73	0.26	1.99	3.4	5.4
5e	−1.70	0.26	1.96	3.4	5.4
5f	−1.72	0.17	1.89	3.4	5.3
5g	−2.35	0.29	2.64	2.8	5.4
5h	−2.28	0.23	2.51	2.8	5.3
5i	−2.31	0.16	2.47	2.8	5.3
5j	−2.29	0.20	2.49	2.8	5.3
5k	−2.26	0.18	2.44	2.8	5.3
5l	−2.31	0.15	2.46	2.8	5.3

modifications of the studied complexes and, hence, modification of their HOMO and LUMO energy levels. Our attention was drawn by the most outstanding EA change observed for nitro-derived complexes, that must have come from the presence of $-NO_2$ groups. Thus, we decided to implement computational chemistry methods in order to explore the electronic structure of these three compounds along with the other complexes, intending to explain the origin of the difference.

Theoretical Considerations. As the basis for further theoretical considerations, at first the complexes' geometries were optimized at the B3LYP level without any symmetry constrains. Cartesian coordinates of the ground states (S_0) of the complexes are presented in Tables 10S−21S, while the exemplary perspective view of **5f** structure is shown in Figure 3. Table 3 illustrates the parameters of Ir−ligand bond lengths

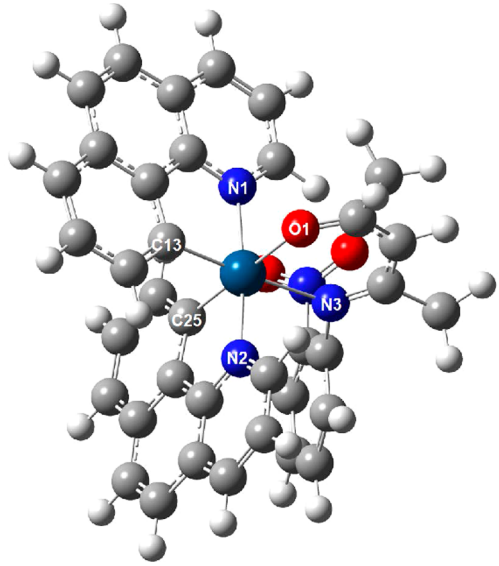

Figure 3. Optimized structure of **5f** in the ground state.

and bond angles *in vacuo* and in the C_6H_5Cl media, together with the X-ray crystal structure data of **5f**. Due to the d^6 configuration of the Ir(III) ion, all complexes have the expected pseudo-octahedral coordination geometry around the iridium center. As presented in Figure 3 and Table 3, two coordinating nitrogen atoms in the bzq ligands (N(1) and N(2)) are in *trans* positions and the valence angles N(1)−Ir−N(2) are nearly 180°, while the coordinating carbon atoms

DOI: 10.1021/acs.inorgchem.9b02785
Inorg. Chem. 2019, 58, 15671−15686

Table 3. Comparison of Selected Bond Lengths and Valence Angles from the Optimized Geometries with the Experimental Values for 5f

	gas	C_6H_5Cl	X-ray
	Bond Lengths (Å)		
Ir−N1	2.102	2.105	1.946
Ir−N2	2.076	2.080	1.899
Ir−N3	2.265	2.271	2.195
Ir−C13	2.034	2.036	2.034
Ir−C25	2.028	2.029	2.009
Ir−O1	2.180	2.191	2.125
	Valence Angles (deg)		
C13−Ir−C25	89.2	88.4	92.5
C13−Ir−N2	93.4	93.6	91.2
C25−Ir−N2	80.9	80.8	81.6
C13−Ir−N1	80.5	80.4	82.7
C25−Ir−N1	98.1	98.0	98.3
N2−Ir−N1	173.8	173.9	173.9
C13−Ir−N3	174.4	174.7	173.8
C25−Ir−N3	95.8	96.2	93.4
N2−Ir−N3	89.9	89.8	91.6
N1−Ir−N3	96.2	96.2	94.5
C13−Ir−O1	89.0	89.5	85.9
C25−Ir−O1	174.8	175.1	177.0
N2−Ir−O1	94.3	94.9	96.0
N1−Ir−O1	86.5	86.0	84.0
N3−Ir−O1	86.2	86.1	88.4

(C(13) and C(25)) are in *cis* positions and the valence angle C(13)−Ir−C(25) is close to 90°. Furthermore, two valence angles between the coordinating atoms from the bzq ligand and the central iridium atom, namely C(13)−Ir−N(1) and C(25)−Ir−N(2) (Table 3 and Figure 3) are nearly identical, ca. 80°. The comparison of the structural parameters calculated in the chlorobenzene environment and *in vacuo* showed that the solvent effects have minor influence on the optimized geometries of these complexes. The calculated Ir−N, Ir−C, and Ir−O bond lengths are slightly longer (up to 0.01 Å) in C_6H_5Cl media, while changes in the bond angles are less than 1.0°.

In general, the DFT (density functional theory) calculation results are in reasonable agreement with the X-ray crystal structure data. The deviations measured by the mean unsigned error are 0.08 Å and 2° for bond lengths and valence angles, respectively. The slight discrepancy between the calculated and the measured values is reasonable, because the former results were obtained adopting the complex molecules *in vacuo*, whereas the latter ones were examined in the crystalline state. The above differences of geometrical parameters were indeed expected as B3LYP method overestimates the bond lengths in transition metal complexes.[18]

Spectral properties are strongly dependent on the frontier molecular orbitals' (FMOs) properties. Therefore, DFT calculations were employed to investigate the HOMO and LUMO of the complexes. The molecular orbitals were calculated assuming the optimized geometry of the ground state. For all complexes, the energy gaps between the HOMO and LUMO were correlated with their experimental values obtained by cyclic voltammetry measurements. In this study, apart from B3LYP, other commonly used functionals, namely M06 and WB97XD with basis set composed of 6-311++G(d,p) for H, C, N, and O and SDD for Ir atom, were tested to obtain the best possible correlation with experimental values. Because the geometries optimized with B3LYP were comparable to those obtained from the experimental XRD results, we initially adopted this approach in our studies. The linear regression coefficient determined, characterizing the strength of the correlation between the theoretical energies and electrochemical data, was 0.86 (Figure 35S SI). From among the other tested functionals, B3LYP was characterized by the best correlation between experimental results and allowed us to explain the unusually low bandgap for **5d−f**; thus, it was chosen for further considerations. This choice was also supported by the fact that B3LYP functional is applicable for prediction with good accuracy of the trend of structural changes effect on the electronic structure of the modified compound with respect to that of the unmodified one.[19] The exemplary HOMO and LUMO contours and HOMO−LUMO energy gaps of the studied complexes are presented in Figure 4, while the full set of the numerical values of orbital distributions are compiled in Table 9S (see the SI).

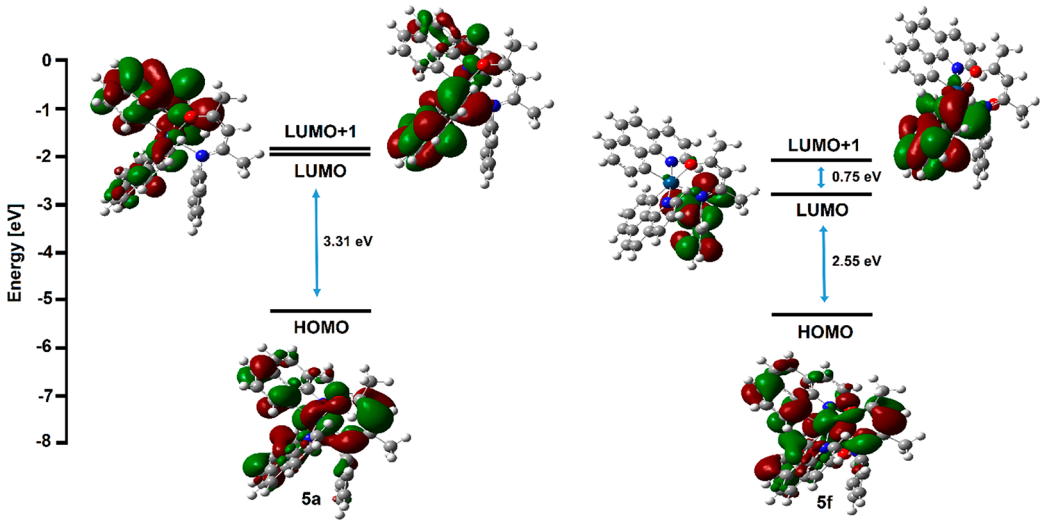

Figure 4. Frontier molecular orbital diagrams of complexes **5a** and **5f** computed at the B3LYP/SDD/6-311++G(d,p) level of theory.

DOI: 10.1021/acs.inorgchem.9b02785
Inorg. Chem. 2019, 58, 15671−15686

As usually observed for cyclometalated cationic iridium(III) complexes,[18,19] the iridium atom brings a significant contribution to HOMO, while being much less involved in LUMO. This fact indicates that HOMO−LUMO transition should be characterized by strong MLCT (metal to ligand charge transfer) character. Therefore, the HOMOs are localized on both types of ligands, but their distribution is limited to the *N,O*-donating atoms of the *β*-ketoiminato ligand and is also spread over the whole bzq ligands, with slight shift of electron density toward the *C*-donating part of bzq. On the contrary, the LUMOs are almost totally present on cyclometalating ligands (except **5d−f**) with less than 5% contribution of the Ir atom. It is worth noting that due to the lack of symmetry constraint in the calculated structures, the two bzq ligands are inequivalent, so their LUMOs are split into two subsequent levels (e.g., LUMO and LUMO + 1) that are very close in energy. However, for complexes **5d−f** equipped with a nitro group, the LUMOs are mainly located on the ancillary ligand, in particular its nitrophenyl moiety, while the successive unoccupied molecular orbitals LUMO + 1 and LUMO + 2 primarily originate from the cyclometalating ligands (see Table 9S in the SI). According to Table 6S, the bandgap values calculated for **5a−c** and **5g−l** are very close, the spread is 0.21 eV, while the respective electrochemical bandgap spread is 0.32 eV. The calculated bandgap spread for **5d−f** is 0.11 eV, while electrochemically determined bandgaps are within 0.1 eV range. This indicates that the electrochemical data and theoretical predictions are well correlated and show that the mentioned complexes should exhibit similar properties related to the bandgap values within the above−specified groups, despite the fact that their LUMO levels are overestimated. Additionally, the calculated **5d−f** bandgaps are lower than the value obtained for the reference **5a** by about 0.8 eV for B3LYP functional (Table 6S). The respective electrochemically determined difference is in the 0.5−0.6 eV range, which indicates good reproducibility of the experimental data by theory. Interestingly, if one calculates HOMO and LUMO + 1 energy level differences for **5d−f**, they will obtain a value close to the calculated HOMO−LUMO bandgap of **5a.** Considering the above, the DFT calculations reproduced the trends observed in electrochemical measurements, confirming that incorporation of $-NO_2$ groups into the ancillary ligand structure is associated with the insertion of its own lowest unoccupied level between the original HOMO and LUMO levels of the unmodified reference complex **5a** (see Figure 4). Therefore, it supports our supposition that $E_{red\ onset}$ decreases for **5d−f** complexes relative to the other complexes which originates from the reduction of the nitro group itself. This conclusion is very important since it indicates that the electrochemically determined bandgaps for these three complexes are flawed. The correlation of electronic structure with photophysical properties of the complexes is further discussed in the following sections.

Photophysical Properties. Absorption spectra of the studied complexes **5a−5l** in chlorobenzene under ambient conditions are presented in Figure 5. The strong spin−orbit coupling of iridium atom makes the formally forbidden triplet metal−ligand charge transfer transitions (^{3}MLCT) possible, and for the examined complexes, they are observed as long-wavelength absorption bands in the range of 440−550 nm. Generally, the bands located around 400 nm can be assigned to the higher extinction singlet ^{1}MLCT, and the bands falling in the short-wavelength range (below 400 nm), to *π*−*π** ligand

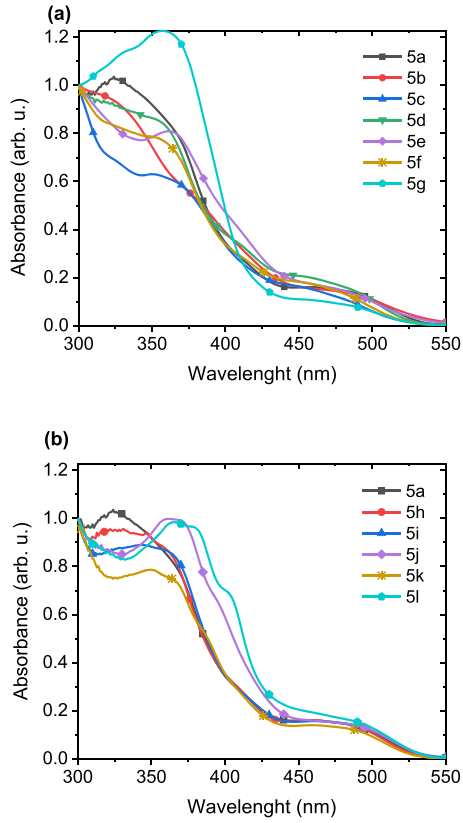

Figure 5. Normalized absorption spectra of the investigated complexes in chlorobenzene: **5a−5g** (a) and **5h−5l** compared with **5a** (b).

centered (^{1}LC) transitions. However, the exact assignment of the lowest energy states may be inaccurate, because it is generally known that they can be a mixture of ^{3}LC, ^{3}MLCT, and ^{1}MLCT.[4b] The fact that for tris(benzo[*h*]quinolinato)-iridium(III) complex ([Ir(bzq)$_3$]) the absorption bands in the 370 nm region were assigned to ^{1}MLCT states might support our interpretation.[20]

As one can see, the performed modifications of *β*-ketoiminato ancillary ligand structure did not affect significantly the absorption spectra of the studied complexes. Nonetheless, the absorption spectra of the complexes equipped with polycyclic aromatic substituents, especially anthracenyl, differ mostly in the range of ^{1}MLCT/LC transitions. Interestingly, the change in anthracenyl regio-substitution from position 2 (**5k**) to 1 or 9 (**5j**, **5l** respectively) resulted in alteration in the probability of these transitions. The bands located around 400 nm are more pronounced for **5j** and **5l** complexes, and the most intense bands (350−380 nm) are slightly red-shifted in comparison to the corresponding signals in the spectra of **5a**, **5h**, **5i**, and **5k**. Interestingly, the absorption onset for **5d−5e** is similar to those of the other complexes and no additional low−energy absorption bands were observed for them. This fact is in contrast to the electrochemically determined energy levels, which suggests a significant decrease in the bandgaps for the nitro-substituted complexes. This indicates that the excitation from HOMO to LUMO levels are not preferable for them. Therefore, it can be supposed that the observed lowest in energy transitions involve the central atom and bzq ligands (corresponding to HOMO → LUMO+1 transition). The reason for that might be the

DOI: 10.1021/acs.inorgchem.9b02785
Inorg. Chem. 2019, 58, 15671−15686

location of LUMO on the nitrophenyl moiety of ancillary ligand, which hampers the electron transition from HOMO mostly located on bzq ligands, due to very poor overlapping of the orbitals.

Normalized photoluminescence (PL) spectra of the studied complexes in chlorobenzene are shown in Figure 6. Excitation

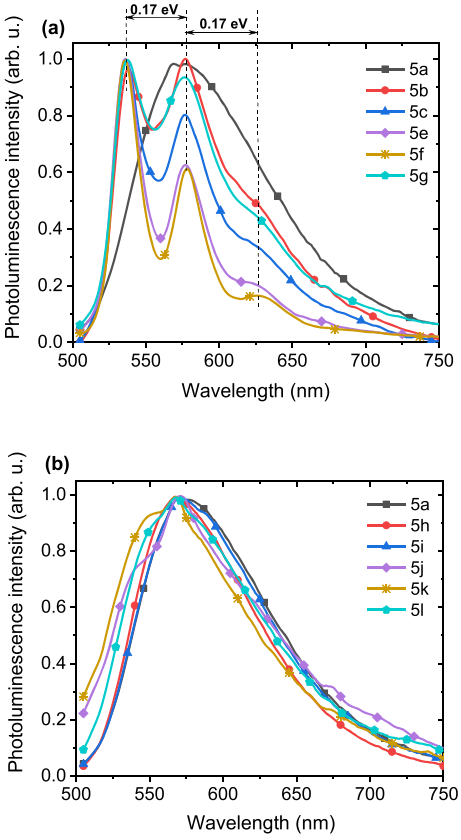

Figure 6. Normalized photoluminescence spectra of the investigated complexes in chlorobenzene (λ_{ex} = 485 nm): **5a**–**5g** (a) and **5h**–**5l** compared with **5a** (b).

at 485 nm, corresponding to the ^{3}MLCT transition of the complexes, resulted in a broad emission band in the range of 500–750 nm with a maximum at ~570 nm for the complexes with phenyl, naphthyl, and anthracenyl substituents (**5a** and **5h**–**5l**). All other complexes (**5b**–**5g**) showed a structured emission with narrow bands located at ~538, ~577, and ~628 nm. The most structured emission spectrum was observed for complexes **5e** and **5f**, equipped with $-NO_2$ groups. Nonetheless, the emission spectra of the complex with $-NO_2$ groups in the *para* position (**5d**) revealed its instability and thus, it was not further examined (see Figure 36S in the SI). As one can see, the most pronounced structure is observed for the complexes bearing electron withdrawing substituents (e.g., $-NO_2$, $-CN$) and less distinct bands are noticed when the electron donating groups (e.g., $-OCH_3$, $-Ph$) are present in the ancillary ligand structure. The structured emission spectra of transition metal complexes often indicate a large contribution of LC in the emissive excited states.[21] Additionally, for the complexes with electron withdrawing group, the most intense is the 0–0 transition that changes a little bit the color of the emitted light and suggests small geometry changes during excitation and relaxation.

Complexes from the first group (**5b**–**5g**) exhibited the structured emission which was a mirror image of the excitation spectra (compare Figures 6a and 7), as relative intensities of

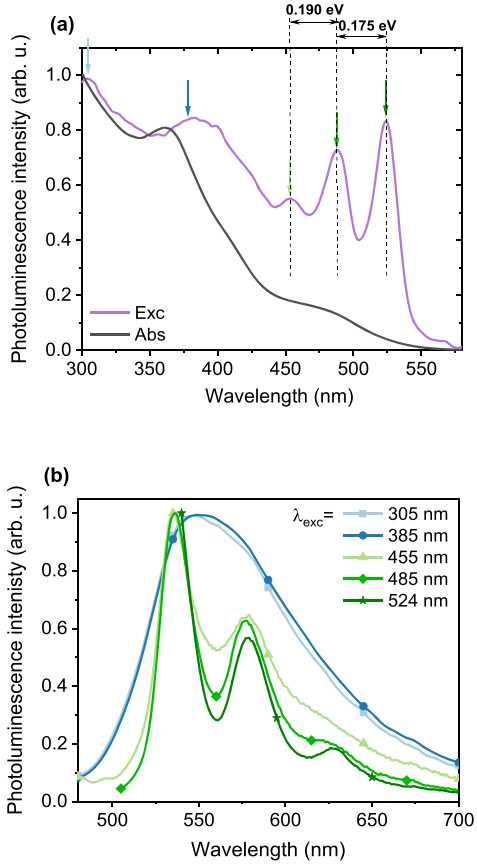

Figure 7. (a) Normalized photoluminescence excitation and absorption spectra of **5e** in chlorobenzene. (b) Normalized photoluminescence spectra of **5e** in chlorobenzene, measured at different excitation wavelengths.

the vibrational peaks in the emission correlated with the excitation spectra (see Figure 37S in the SI for a full data set). Considering the spectra recorded for the nitro-derived complexes **5e** and **5f**, the emission structure is the most visible and the probability of higher energy transition relative to the other bands is higher. For many common fluorophores, the vibrational energy levels spacing is similar for the ground and excited states, which results in the emission spectrum that strongly resembles the mirror image of the absorption spectrum. However, for our complexes, the vibrational mirror image is only visible in the excitation spectra and no structure is observed in the absorption spectra. It may suggest that these two spectra have different excited-state origins. It is supposed that the first absorption band reflects a combination of different transitions to MLCT states, whereas the excitation spectrum comes from the specific state responsible for the emission. In general, MLCT transitions are coupled to low energy vibrations and are more influenced by the molecule's environment, thus the absorption bands should reveal more inhomogeneous broadening with increasing degree of MLCT character. As shown for **5e** (Figure 7), when its molecule was excited at the lowest energy absorption bands observed in the excitation spectra, a structured emission spectrum in photoluminescence was recorded. Nevertheless, when higher energy

DOI: 10.1021/acs.inorgchem.9b02785
Inorg. Chem. 2019, 58, 15671–15686

was supplied to the molecule, a broad and structureless emission spectrum was found. Usually, the structureless spectrum is assigned to the emission from MLCT states, whereas the structured emission indicates that LC emissive excited states play a crucial role in generation of visible light. Therefore, the probable explanation of this behavior could be that upon tuning the excitation energy, the emission from different close lying excited states is observed. However, in order to examine this phenomenon, additional experiments are needed. The strong excitation wavelength dependency of emission have been reported by Hsu et al. for osmium(II) and silver(I) complexes[22] in which the phosphorescence/fluorescence intensity ratio is enhanced when the excitation energy is increased.

Additionally, LC transitions are characterized with higher energy than MLCT transitions.[23] However, our results obtained for the studied iridium complexes suggests almost the same energy for both transitions and a strong mixing of LC and MLCT. Since the structured emission was observed only for the complexes bearing phenyl-based ketoimine ancillary ligands, we expected that this phenomenon would be connected with the presence of this moiety. Surprisingly, with the higher energy applied for excitation of **5e** and **5f**, their emission spectra were almost the same as those of the other compounds. Once again, it proved that the electron transitions involving nitrophenyl moiety are not preferable and rather Ir-bzq are engaged, which correspond to HOMO−LUMO+1 and HOMO−LUMO+2 transitions. This explanation was further supported by the results of electroluminescence studies.

$[Ir(bzq)_3]$ is classified as a complex whose emission originates from the ^{3}MLCT state.[20] A comparison of its emissive properties with the results reported here suggest that β-ketoiminato ancillary ligand plays rather a marginal role in the emission processes that originates mainly from the states in which bzq and iridium are mostly involved. As a consequence, the observed structured photoluminescence spectrum can correspond to the vibronic−sublevel, especially for the electron transition between the orbitals localized mostly on the ligand, when the electronic−vibronic coupling occurs and/or for low energy metal−ligand vibrations, when the metal participation in the electronic state increases. Since electron transitions are much faster than nuclear oscillations, the structured spectra should be observed when a small molecular geometry change takes place in the excited state. The latter was confirmed previously on the basis of the intensity of 0−0 transition. Therefore, taking into account the above considerations, it can be concluded that substitution of *N*-donating atom in the β-ketoiminato with various aryl groups affects only the LC/MLCT excited states contribution to the total emission, while all the studied $[Ir(bzq)_2(N\wedge O)]$ complexes exhibit green emission in the same range. Therefore, it should be expected that the modification of ancillary ligand should influence the luminescence performance, since the emission from the ^{3}MLCT state is expected to be more efficient, but this will not tune the emitted wavelength. Driven by this conclusion, we wanted to examine if the structured emission would occur in photo- and electroluminescence in the solid state.

Photoluminescence of PhOLED Active Layers. In order to avoid the concentration induced emission quenching, for which Ir(III) complexes are known,[24] the host−guest systems are commonly used as an active layer, which means that the emitter is homogeneously dispersed in a polymer matrix. In this work, we used a well-known ambipolar matrix, composed of poly(*N*-vinylcarbazole) (PVK) and 2-(4-*tert*-butylphenyl)-5-(4-biphenylyl)-1,3,4-oxadiazole (PBD), providing hole and electron transport, respectively. The PVK/PBD mixture was selected as a host material due to its wide energy gap in accordance with the general rule that the emitter energy gap should be localized between HOMO and LUMO levels of the matrix to ensure good energy transfer of the excitons from the matrix to the emitter molecules.

The PL spectra of thin PVK/PBD films doped with 1 wt % of the studied emitters upon excitation with the wavelength corresponding to the lowest absorption band of the PVK/PBD matrix (λ_{ex} = 340 nm) are presented in Figure 8. All tested

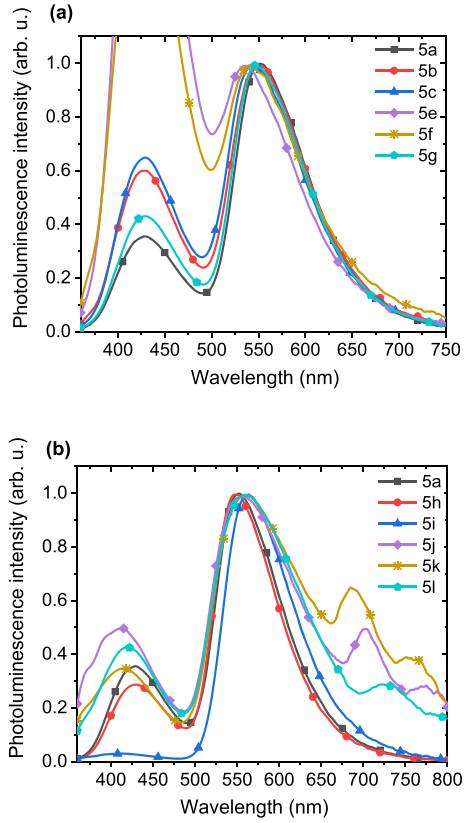

Figure 8. Normalized photoluminescence spectra of thin layers of the PVK/PBD blend doped with 1 wt % of emitter molecules: **5a**−**5g** (a), and **5h**−**5l** compared with **5a** (b). Excitation wavelength was 340 nm, that corresponds to first absorption band of PVK/PBD matrix.

layers showed the emission related to the phosphorescent dopants as well as host component (λ_{max} ∼ 430 nm), originating from singlet exciplexes formed between carbazole moieties and oxadiazole molecules. A contribution of the matrix emission indicates incomplete energy transfer from the matrix to the emitters. The best energy transfer was observed for naphthyl−derived complex (**5i**), whereas the worst efficiency of this process was noted for the complexes characterized by structured emission spectra in solution (primarily **5e**, **5f**). The main photoluminescence bands are generally similar to those detected for the emitters in solution upon high energy excitation. For the neat films, the emission distribution is broadened and less structured, thus indicating that mostly MLCT energy states are responsible for the emission in the examined host−guest systems. Efficiency of such an energy transfer influences the photoluminescence

DOI: 10.1021/acs.inorgchem.9b02785
Inorg. Chem. 2019, 58, 15671−15686

Table 4. Parameters of PhOLEDs Based on PVK/PBD Layers Doped with 1 wt % of All Tested Ir Complexes

compound	λ_{EL} [nm]	L_{max} [cd/m^2]	η_{max} [cd/A]	EQE [%]	λ_{PLfilm} [nm]	QY_{film} [%]
5a	559	9 500	9.1	2.71	552	15
5b	565	1400	2.6	0.83	548	8
5c	559	600	1.5	0.48	545	9
5e	567	180	0.2	0.07	534	2
5f	563	580	0.3	0.10	540	2
5g	559	4200	3.8	1.13	548	12
5h	**556**	**15700**	**12.3**	**3.20**	**549**	**18**
5i	569	5500	4.2	1.45	563	4
5j	587, 715	50	0.02	0.01	554, 703, 775	<1
5k	625, 697, 765	100	0.06	0.03	561, 685, 753	<1
5l	575, 740	70	0.02	0.02	559, 723	<1

quantum yield (QY), which was up to 18% for the investigated layers (Table 4).

The emission spectra of thin layers doped with anthracenyl substituted complexes (**5j**−**5l**) showed additional low energy bands (680−800 nm) that were not visible in the spectra recorded in solution. The presence of these bands is most likely related to the anthracenyl degradation products. These complexes exhibited poor emissive properties (QY < 1%, Table 4), as well as low stability of emissive states that was also observed in further electroluminescence studies. Additionally, incorporation of **5j**−**5l** complexes resulted in a hypsochromic shift of the matrix emission as presented in Figure 8b. It can be attributed to the disruption of exciplex formation between carbazole moieties from PVK and oxadiazole molecules. Therefore, **5j**−**5l** complexes are not good candidates for efficient emitters in the PVK/PBD matrix, even though their energy transfer was acceptable.

Dominant contribution to the emission of dopant introduced to the layers may originate from long-range Förster and/or from short-range Dexter energy transfer. The Dexter mechanism is less likely because of low emitter concentration. However, the exciton diffusion can enhance both paths of energy transfer. Both mechanisms can operate efficiently only when the emission spectrum of the donor and the absorption spectrum of the acceptor overlap considerably. All the studied complexes are characterized by a good spectral overlap of their MLCT absorption bands with the matrix emission spectrum, as shown in Figure 9, for exemplary **5a** and **5h**−**5i** complexes. In the whole group of tested compounds, emitter **5i** stands out in the energy transfer efficiency since only a small contribution of its emission originated from the matrix is visible in the film PL spectrum. However, the photoluminescence QY of this compound in thin film was very low (4%, Table 4). The opposite relationship was observed for **5g**, for which the energy transfer was much less effective, but the compound showed higher QY. Furthermore, **5h** was characterized with the best quantum yield (18%), despite showing noticeable contribution of matrix emission in the photoluminescence spectrum. These observations indicate that aryl-substitution of β-ketoiminato ancillary ligand can tune photoluminescence efficiency of the complexes in a way not fully understood. Nevertheless, the confirmed spectral overlap of the complex absorption and the matrix emission was a good premise to examine the efficiency of energy transfer in electroluminescence studies.

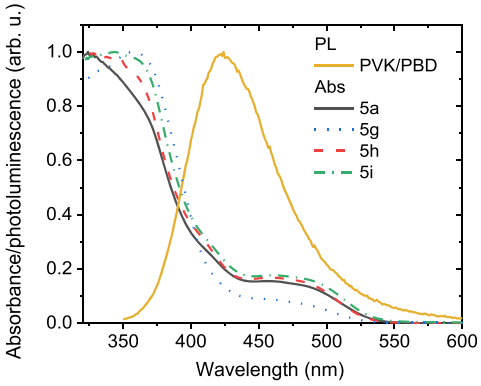

Figure 9. Normalized absorption spectra of four selected compounds (**5a**, **5g**, **5h**, **5i**) in chlorobenzene solutions and normalized photoluminescence spectra of neat PVK/PBD blend.

Electroluminescent Properties. The electroluminescence properties of the iridium complexes were tested in one of the simplest PhOLED structure. The devices with a hole injection layer (HIL) and an emissive layer were produced by a spin-coating technique. Such a simple construction of the device is preferable for manufacturing by economical wet printing techniques. Additionally, this minimalistic approach is an easy screening procedure for emitters' electroluminescent properties. The emissive layers were based on PVK/PBD matrix systems as used in photoluminescence studies. It should be noted that a PVK/PBD blend with a 7:3 weight ratio is characterized by balanced charge transport properties, which is a basic requirement for efficient OLEDs.

Electroluminescence (EL) spectra recorded for the devices based on the investigated emitters are presented in Figure 10. The EL spectra obtained for PhOLEDs doped with emitters **5a**−**5i** were very similar to the PL spectra in thin films. The maxima of emission were in the range of 555−570 nm, with one exception, and were only slightly red-shifted in relation to the PL spectra (compare Figures 8 and 10). It should be emphasized that the matrix emission disappeared in the EL spectra, even when it was predominant in PL of thin films (for complexes **5e** and **5f**). The lack of emission from the matrix in the EL spectra suggests a strong contribution of the charge trapping process in EL phenomenon, which can promote formation of excitons on the dopant molecules.

Similarly to the PL spectra, the EL spectra of PhOLEDs doped with emitters **5j**−**5l** showed long-wavelength bands in addition to the desired ^{3}MLCT bands. For the PhOLED created on the basis of **5k**, this red emission even dominated. During prolonged measurements of these OLED emissions, we observed that the contribution of long-wavelength bands changed irreversibly along with the device operation time (see Figure 38S in the SI). Therefore, it can be concluded that the

DOI: 10.1021/acs.inorgchem.9b02785
Inorg. Chem. 2019, 58, 15671−15686

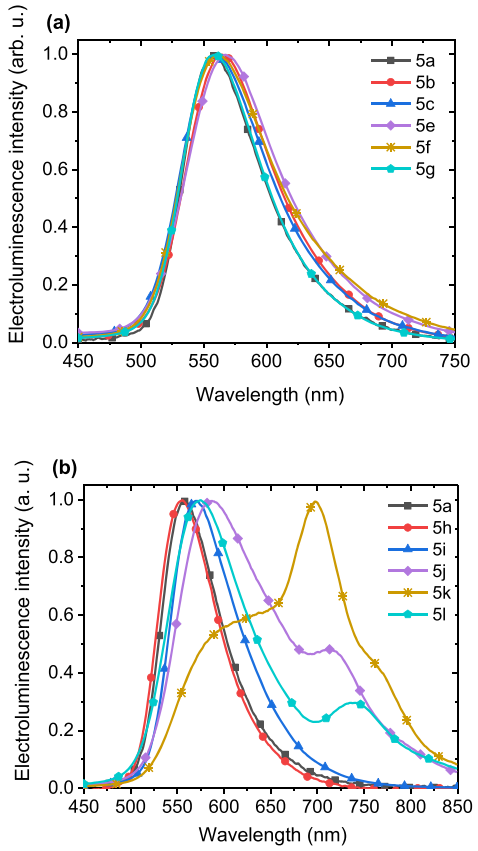

Figure 10. Normalized electroluminescence spectra of PhOLEDs based on PVK/PBD doped with 1 wt % of the investigated emitter molecules: **5a**–**5g** (a) and **5h**–**5l** compared with **5a** (b).

complexes with the anthracenyl substituent (**5j**–**5l**) are unstable. This indicates that the degradation process of anthracenyl groups may occur during the radiative excitation and can be reinforced during operation of the device. Such a scenario is possible because the degradation might be caused, e.g., by trace amounts of oxygen molecules embedded in the bulk of the emissive layer, despite their production in a nitrogen atmosphere.

Current density–voltage (J–V) and luminance–voltage (L–V) characteristics of the best performing PhOLEDs, based on **5a** and **5h** emitters, are shown in Figure 11. These plots represent typical PhOLED characteristics in the range up to 16 V. The obtained luminance values were ∼9500 and ∼16000 cd/m^2 at 16 V for **5a** and **5h** based PhOLEDs, respectively. The turn-on voltage (the voltage value at which the luminance reaches 1 cd/m^2) was around 7 V. Although the **5h**-based PhOLED was characterized by a greater leakage of current; nevertheless, the maximum luminance was higher when compared to the system made with the use of **5a**. In Figure 12, the current efficiencies are plotted versus luminance for the tested devices. The highest value (over 12 cd/A) was obtained for PhOLED with **5h** emitter, derived with a 1-naphthyl substituent. This result correlates well with the fact that the highest photoluminescence QY was measured for thin films with this dopant (Table 4). Moreover, measured current efficiency was relatively stable in the wide luminance range (1500–4000 cd/m^2).

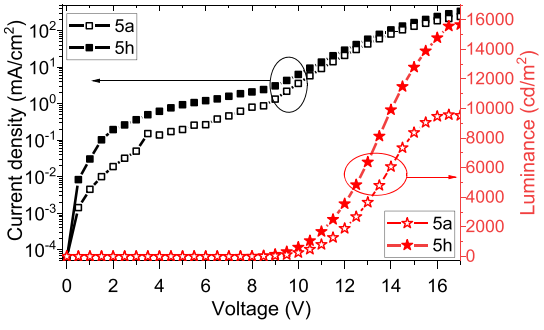

Figure 11. Current density–luminance–voltage (J–L–V) characteristics of PhOLEDs with emitting layer made of PVK/PBD doped with 1 wt % of emitter molecules: **5a** (empty symbols) and **5h** (full symbols).

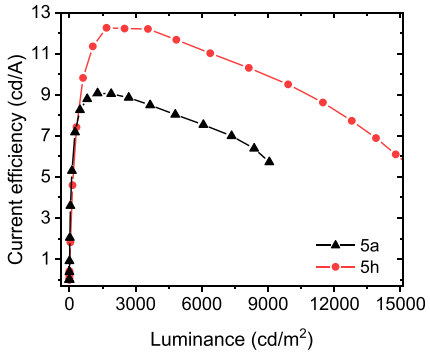

Figure 12. Current efficiency–luminance dependencies of PhOLEDs with emitting layer made of PVK/PBD doped with 1 wt % of **5a** and **5h** complexes.

A comparison of the parameters determined for all tested devices and their emissive layers is shown in Table 4. It should be emphasized that the best devices exhibited good parameters, considering that the diodes had such a simple structure and were produced using solution methods. OLEDs of similar structure, based on [Ir(bzq)$_2$(acac)], exhibited the maximum current efficiency of 4.2 cd/A.[25] Therefore, the obtained current efficiencies of 9.5 and 12.0 cd/A for **5a** and **5h** can be considered to be quite high. Of course, further optimization of the devices' structure by incorporation of additional layers should lead to PhOLEDs of better performance.[26]

The devices that exhibited the best EQE were those with **5a**, **b** and **5g**–**i** phosphorescent dopants (Table 4). As one can see from a comparison of QY$_{film}$ and EQE, they correlate well for all complexes with the exception of **5i**. This deviation might be related to a noticeable impact of the exciton energy transfer on the device performance. Considering the above, it seems that the best external efficiencies were obtained for the emitters equipped with unmodified aromatic moieties (**5a** and **5g**–**i**) and electron-donating methoxy group (**5b**), all rich in electrons. The very low performance of anthracenyl-derived complexes (**5j**–**k**) might deny it at a first glance, but their poor stability in electroluminescence should be kept in mind. Taking into account the above-mentioned details, it is clear that their efficiency might be suppressed by their unexpected instability. In this way, we proved that β-ketoiminato ligands affect the photophysical properties of the examined complexes, in particular luminescence efficiency, although they do not tune the maximum emission wavelength.

DOI: 10.1021/acs.inorgchem.9b02785
Inorg. Chem. 2019, 58, 15671–15686

It is known that the performance of PhOLEDs strongly depends on the concentration of emitter in the active layer. After screening all the emitters as dopants for OLEDs at 1 wt %, we decided to optimize the dopant concentration for the complex with the best−performance, i.e. **5h**. This emitter was chosen *inter alia* because of its highest quantum photoluminescence efficiency (18%). Furthermore, the devices based on it exhibited the highest luminance and current efficiency from among the tested PhOLEDs. To determine the optimal dopant concentration, a series of devices with different emitter content in the PVK/PBD matrix were prepared (from 0.5 to 7.0 wt %). The observed maximum luminance values (at 17 V) were in the range from ∼4000 cd/m^2 (for 7 wt %) to ∼16000 cd/m^2 (for 1 wt %). The maximum value of external quantum efficiency (EQE ∼ 3.2%) was obtained for the devices with 1 wt % emitter additive. A little bit lower value, but with slower reduction of the efficiency with the increase in current density, was observed for the diodes with 2 wt % emitter content (Figure 13). Therefore, it can be assumed that the optimal

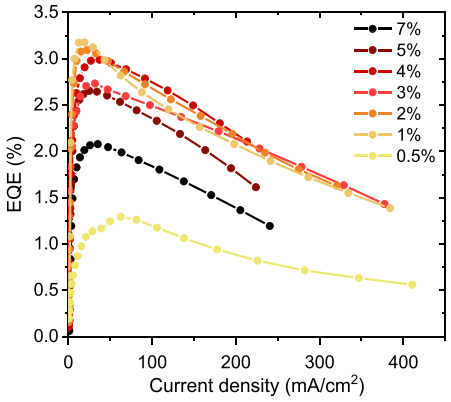

Figure 13. External quantum efficiency−current density dependencies of PhOLEDs with emitting layer made of PVK/PBD doped with different concentrations (from 0.5 to 7 wt %) of **5h** emitter.

emitter content for such PhOLEDs ranges between 1 and 2 wt %. Higher concentration may result in the emitter molecules aggregation process resulting in quenching of emissive states that is a common phenomenon observed in guest−host systems. This might be the reason for the decrease in EQE with increasing emitter concentration from 4 to 7 wt % in the examined case.

In order to compare the energy transfer efficiency in electro- and photoluminescence, the same amounts of **5h** dopant were used in both experiments. The obtained normalized PL spectra are presented in Figure 14. As one can see, the contribution of matrix emission decreases as the dopant concentration increases. However, even for 7 wt % emitter additive, a small emission from the matrix exciplexes was observed, so the energy transfer was still incomplete. It strongly contrasts with the electroluminescence spectra, in which almost complete quenching of PVK/PBD emission was observed for the lowest examined concentration (0.5 wt %) of emitter **5h** (see Figure 39S in the SI). As mentioned above, these results suggest that charge carrier trapping processes play an important role in the electroluminescence phenomenon. EL spectra do not change noticeably with the concentration increase and only a slight shift of the band maximum was observed from 557 nm (0.5 wt %) to 560 (7 wt %) nm. In the dopant concentration−photoluminescence studies, a slightly bigger redshift from 547

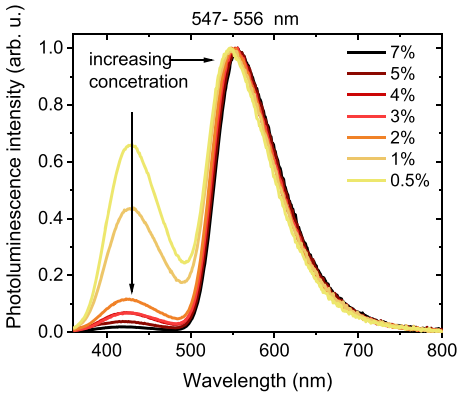

Figure 14. Normalized photoluminescence spectra of emissive layers based on PVK/PBD doped with **5h** in different concentrations (from 0.5 to 7 wt %). The excitation wavelength, corresponding to first absorption band of PVK/PBD matrix, was 340 nm.

nm (0.5 wt %) to 556 nm (7 wt %) was observed, suggesting stronger intermolecular interactions. This is a normal consequence of increasing concentration since it should also reduce the mean distance between emitter's molecules in the emissive layer. It is worth noting that this phenomenon is more visible in photoluminescence and less in electroluminescence. Nevertheless, it is undoubtedly clear that the lower dopant concentration gave better results in OLEDs.

As mentioned above, the charge carrier trapping might play an important role in electroluminescence, therefore this phenomenon was further explored by spectrally resolved thermoluminescence (SRTL) studies in the range of 20−300 K. In recent years, it has been proved that guest and matrix molecules compete in charge carriers trapping in emissive layers based on host−guest systems.[9b,27] To maximize the emitter efficiency, this balance should be shifted toward efficient formation of excitons on guest molecules and quenching of host emission, even for the systems with minor content of the emitter molecules in the matrix.

The SRTL results for the neat PVK/PBD and for the PVK/PBD matrix doped with 1 wt % of **5h** are shown in Figure 15. A comparison of the TL maps showed that doping of **5h** into the PVK/PBD matrix results in a change in the emitted light range. The spectrally resolved luminescence (SRL) recorded close to the TL maximum (115 K) revealed that the emission occurs in the range of 490−730 nm with one very broad band with a maximum at 565 nm (see Figure 15c, red dashed line) which does not change its position with temperature (see Figure 15a). For the neat PVK/PBD matrix (see Figure 15c, blue solid line), the emission occurred in the broader range of 390 to 750 nm. One can see two separated emission bands: a dominant one with a maximum at 550 nm and the second one with a maximum at 450 nm. Both emission bands from the PVK/PBD blend are attributed to the exciplexes formed between carbazolyl group and PBD molecule. The dominant band originates from the triplet exciplexes, and the minor one can be related to the singlet exciplexes and/or monomeric triplet states of carbazolyl groups.[27] However, the identification of the radiative recombination active center in the doped matrix is problematic because the dominant emission band of the matrix (550 nm) is close to the emission originating from the iridium complex molecules (565 nm). Nevertheless, comparing both spectra, one can see that the spectrum of the matrix doped with **5h** is more intensive and has no short-

DOI: 10.1021/acs.inorgchem.9b02785
Inorg. Chem. 2019, 58, 15671−15686

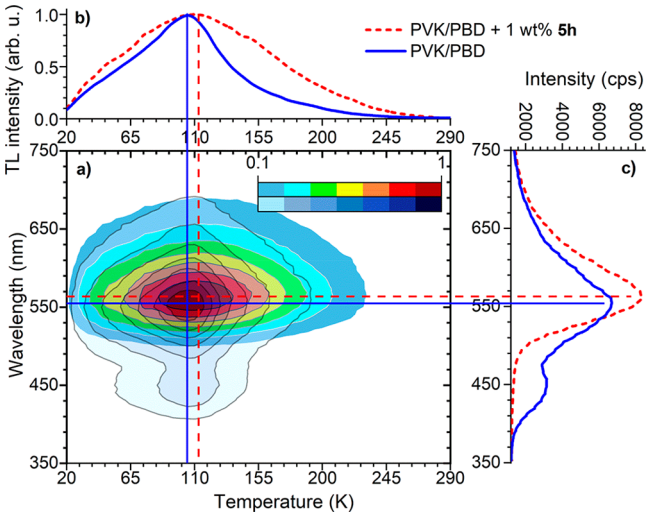

Figure 15. SRTL spectra for PVK/PBD layer doped with 1 wt % of emitter **5h** and for neat PVK/PBD matrix layer: (a) the TL maps; (b) normalized monochromatic TL curves recorded at λ = 565 and 550 nm, respectively; (c) non-normalized isothermal spectra of emitted light recorded at 105 and 115 K, respectively. The red dashed and blue solid curves show results for the doped and neat PVK/PBD matrixes, respectively. Straight lines on the TL maps indicate selected wavelength for monochromatic TL curves (horizontal lines) and selected temperature for isothermal spectra of emitted light (vertical lines).

wavelength band; the main emission band is slightly red-shifted by 15 nm and has a smaller full width at half-maximum (FWHM). Considering the differences, it can be assumed that in doped film the emission from **5h** dominates over PVK/PBD emission. It is clear that the TL intensity of PVK/PBD with 1 wt % of **5h** is significantly higher than the TL intensity of the matrix alone (about 30%). In addition, two normalized monochromatic TL curves shown in Figure 15b differ as well. The monochromatic TL curve of the pure matrix (recorded at λ = 550 nm) has a main maximum at 105 K. Introduction of 1 wt % of **5h** causes an increase in the relative intensity of the TL signal in the high temperature range (above 110 K), as well as TL signal broadening in comparison to that of its pure matrix analogue. In this case, high-temperature TL signal contribution was greater in comparison to the previous TL results obtained for the system doped with the iridium complex containing one fluorine atom in the *para* position of phenyl ring of the β-ketoiminato ligand.[10] This comparison points out the impact of deep traps located on the emitter molecules. The depth of the traps might be approximated to 0.5 eV for holes and 0.4 eV for electrons, on the basis of differences between HOMO and LUMO levels of the emitter (5.3 and 2.8 eV, see Table 1) and the matrix (PVK (5.8, 2.2 eV) and PBD (6.2, 2.4 eV)). However, it should be taken into account that HOMO and LUMO levels obtained from CV experiments might be slightly varied in thin films due to different environment of the molecules (THF as solvent in CV, PVK/PBD in thin films).

It can be concluded that introduction of the iridium complex molecules to PVK/PBD matrix causes formation of new, deeper trapping states that promote radiative recombination on the dopant molecules. In addition, it must be emphasized that the spectrum observed in the TL experiment for PVK/PBD doped with **5h** shown in Figure 15c is similar to the EL spectrum, as far as their shapes and location of the maximum are concerned (cf. Figure 10b). This indicates that in both cases, after optical excitation at low temperatures (SRTL) and during the excitation induced by the current flow at room temperature (EL), the generation mechanism of triplet exciton for the emitter molecules added to PVK/PBD is similar.

CONCLUSIONS

In summary, we reported a synthetic protocol for the obtainment of heteroleptic [Ir(bzq)$_2$(MeC(=NR)CH=C-(−O)Me)] complexes series and studied their electrochemical, photoluminescent, and electroluminescent properties in reference to the structure of β-ketoiminato ligand. The spectrum of investigated R substituents included phenyl with methoxy, cyano, nitro, and 5-methyl-2-benzothiazyl groups in *para* position, as well as all possible regioisomers of naphthyl and anthracenyl moieties. In the case of nitro-substituted complexes, also *ortho* and *meta* isomers were investigated in order to explore in detail their outstanding electrochemical properties. Namely, it was found that the presence of nitro group drastically increases electron affinity. With the aid of theoretical calculations, we proved that this phenomenon was related to the reduction of nitro group and should have rather minor effect on other properties related to the bandgap between the orbitals involved in excitation and emission. Apart from the three nitro-derived complexes, the variation of ancillary ligand structure had only slight impact on the electron affinity and ionization potential.

The photoluminescence studies confirmed the results obtained from electrochemical measurements and theoretical considerations, showing that the ancillary ligand structure modification does not affect the bandgap. As a result, the complexes were found to be green emitters with emission maximum within the range of 30 nm. Surprisingly, it evidenced that the electrochemically determined bandgap for nitro-derived complexes was flawed because of the incorporation of lowest unoccupied orbital of nitro moiety. Therefore, together with theoretical calculations, it proved that HOMO localized mostly on iridium and cyclometalating ligands, and LUMOs present mostly on bzq, are predominantly involved in radiative transitions. It also correlates with the measured photoluminescence spectra, which resemble the typical broad MLCT character of the transition. Additionally, the compounds equipped with polyaromatic substituents exhibited broad and structureless emission, whereas the complexes bearing phenyl-based substituents were characterized by structured emission. The observed structure could correspond to ligand vibrations or low energy metal−ligand vibrations. Additionally, the structured emission spectra were not observed in solid state for thin film layers of PVK/PBD doped with 1 wt % of studied complexes, suggesting that mainly MLCT states were filled by exciton transfer from the host to the guest.

We found that although the structure modification of β-ketoiminato ligand did not allow tuning of the maximum emission wavelength, the other properties related to luminescence efficiency were strongly affected. A particular impact was observed in the photoluminescence quantum yield of PVK/PBD layers doped with 1 wt % of the studied Ir(III) phosphors, which ranged between <1 and 18%. A similar, but less spectacular change, was observed for external quantum efficiencies of the devices based on the same emissive layer, namely from 0.01 to 3.20%. Interestingly, *N*,*O*-donating ligands bearing unsubstituted aromatic moiety seemed to be

DOI: 10.1021/acs.inorgchem.9b02785
Inorg. Chem. 2019, 58, 15671−15686

more promising in the application as dopants for PhOLEDs. However, this does not include the anthracenyl substituents since incorporation of these moieties resulted in instability of the complex upon photo- and electro-excitation.

From the tested devices, the best performance showed the PhOLED doped with the complex bearing 4-(1-naphthyl)-imino-2-pentanonate as an ancillary ligand. The maximum measured work parameters reached 12 cd/A for current efficiency and 16000 cd/m^2 for luminance. It should be emphasized that these values are quite high, considering that diodes were fabricated using solution methods and taking into account the uncomplicated device structure. For reference, a very similar OLED based on [Ir(bzq)$_2$(acac)] exhibited the maximum current efficiency of 4.2 cd/A. In all the examined devices, the electroluminescence spectra demonstrated only the dopant emission, while a significant contribution of the PVK/PBD matrix emission was observed in the photoluminescence of the same emissive layers. This indicated that the charge trapping might be the dominant mechanism of exciton generation in EL phenomenon. In fact, spectrally resolved thermoluminescence studies for the most efficient host−guest system proved that the recombination centers are created on the emitter molecules which simultaneously act as deeper trapping states, than the pure matrix. Therefore, on the basis of our results, it can be concluded that the introduction of the iridium complexes into the matrix causes efficient exciton creation on the emitter molecules in EL phenomenon, proving their applicability in PhOLED technology.

EXPERIMENTAL SECTION

General Information. All syntheses and manipulations were carried out under argon using standard Schlenk-line and vacuum techniques. The microwave-assisted reactions were performed with the use of a CEM Discover microwave pressure system (power max 300 W, magnetron frequency 2455 MHz, pressure max 20 bar). The chemicals were obtained from the following sources: $IrCl_3 \cdot 3H_2O$ from Pressure Chemicals, acetone, acetylacetone (acacH), Et_2O, MeOH, $CDCl_3$, CD_2Cl_2, 1,2-dichloroethane, THF, arylamines from Aldrich, benzo[*h*]quinoline (bzqH) from ABCR, THF 99.5 extra dry from Acros Organics, Bu_4NBF_4 (purity > 98) from TCI. The complex [{Ir(μ-Cl)(bzq)$_2$}$_2$] (**4**)[28] was synthesized according to the published method. All solvents and liquid reagents were dried and distilled under argon prior to use. The NMR spectra for 4-arylimino-2-pentanones were recorded in $CDCl_3$ on 300 MHz spectrometer at 298 K, using $SiMe_4$ as internal standard for ^{1}H and ^{13}C measurements. For iridium complexes, the chemical shifts were referred to the residual protonated solvent peaks (^{1}H δ_H = 7.26 ppm for $CDCl_3$ and ^{1}H δ_H = 5.32 ppm for CD_2Cl_2). The purity of iridium materials was determined by elemental analysis on Flash 2000 (Thermo Scientific). HRMS data were obtained on AMD 402 two−sector mass spectrometer of B/E geometry (EI-MS) and Waters/Micromass Q-tof Premier mass spectrometer equipped with an electrospray ion source (ESI-MS).

Synthesis of Ligands and Complexes. Detailed descriptions of the preparation of ligands and complexes, as well as spectroscopic data, can be found in the Supporting Information.

X-ray Crystallography. Diffraction data were collected by the ω-scan technique, for **5g** and **5l** at 100(1) K, for **3h** and **3j** at 130(1) K, for **3d** and **3l** at room temperature on a Rigaku Xcalibur four-circle diffractometer with an Eos CCD detector and graphite-monochromated Mo Kα radiation (λ = 0.71069 Å), and for **5j** at room temperature on Rigaku SuperNova four-circle diffractometer with Atlas CCD detector and mirror-monochromated Cu Kα radiation (λ = 1.54178 Å). The data were corrected for Lorentz polarization as well as for absorption effects.[29] Precise unit-cell parameters were determined by the least-square fit of reflections of the highest intensity, chosen from the whole experiment. The structures were solved with SHELXT[30] and refined with the full-matrix least-squares procedure on F^2 by SHELXL-2013.[31] All non-hydrogen atoms were refined anisotropically, in **3j** all hydrogen atoms were found in difference Fourier maps, in **3h** NH and OH hydrogen atoms, in **3d** al but methyl group, and these hydrogen atoms were freely, isotropically refined. All other hydrogen atoms were placed in idealized positions and refined as "riding model" with isotropic displacement parameters set at 1.2 (1.5 for methyl groups) times U_{eq} of appropriate carrier atoms. In the structure **3h** the hydrogen atoms of methyl group C1 were found in two alternative positions with 50/50 site occupations.

The structures of two other compounds (**5f** and **5i**) were also confirmed by X-ray diffraction, but—due to the poor quality of crystals and severe disorder—these structures are attached as Supporting Information. Table 1S lists the relevant information about the crystal and refinement data.

Crystallographic data for the structural analysis have been deposited with the Cambridge Crystallographic Data Centre, Nos. CCDC 1865881 (**3d**), 1892376 (**3h**), 1865882 (**3j**), 1865883 (**3l**), 1865883 (**5f**), 1865885 (**5g**), 1865886 (**5i**), 1865887 (**5j**) and 1865888 (**5l**). Copies of this information may be obtained free of charge from The Director, CCDC, 12 Union Road, Cambridge, CB2 1EZ, UK. Fax: + 44(1223)336-033. E-mail: deposit@ccdc.cam.ac.uk. www.ccdc.cam.ac.uk.

Thermogravimetric Analysis (TGA). Thermogravimetric analysis (TGA) of the prepared complexes samples was carried out using a Q50-TGA thermobalance (TA Instruments, Inc.) under an N_2 flow of 60 mL min^{-1}. Samples (3−5 mg) loaded on a platinum pan were heated from RT to 1000 °C at a rate of 10 °C min^{-1}.

Electrochemical Measurements. Electrochemical properties were estimated from cyclic voltammetry (CV) measurement using Electrochemical Analyzer model 620 (CH Instruments). A classic three electrode setup was used with a platinum wire as a working electrode, platinum spiral as a counter electrode, and silver wire as pseudo-reference electrode. Potential was calibrated by ferrocene as an internal standard. Measurement was carried out in THF with Bu_4NBF_4 as a supporting electrolyte. Oxidation onset potential ($E_{ox\ onset}$) and reduction onset potential ($E_{red\ onset}$) were estimated from the intersections of tangential lines of redox peaks and background line. Electrochemical energy gaps (E_g) were estimated from equation $E_g = (E_{ox\ onset} - E_{red\ onset})|e^-|$. Ionization potential (IP) and electron affinity (EA) were estimated from equations IP = $(5.1 + E_{ox\ onset})|e^-|$ and EA = $(5.1 + E_{red\ onset})|e^-|$.[32]

Computational Methods. The full optimizations of all Ir(III) complexes in their singlet ground state were carried out. Initially, the density functional theory (DFT)[33] with B3LYP—the hybrid Becke's three parameter functional—and Lee−Young−Parr exchange-correlation potential were used.[34−36] For the Ir metal center the SDD basis set with Stuttgart−Dresden pseudopotentials[37] were used and the 6-31G(d) basis set for H, C, N, and O atoms.[38] After preliminary calculations more flexible basis sets including diffuse and polarization functions were used variety 6-311++G(d,p). The DFT calculations using the B3LYP,[34,36,36] M06,[39] WB97XD[40] functionals based on the optimized S_0 geometries were performed to obtain the energies of the highest occupied molecular orbital (HOMO) and the lowest unoccupied orbital (LUMO). To investigate solvent effect, the ground−state geometry optimization of iridium compounds was also performed within the SCRF (self-consistent reaction field) theory using the polarized continuum model (PCM)[41−43] in chlorobenzene (C_6H_5Cl) solution to model the interaction with the solvent. All calculations were performed using the Gaussian09 software package in PL-Grid infrastructure.[44]

Spectroscopic Measurements. Photophysical studies of new Ir complexes were performed in a solution as well as for emissive layers. All compounds were diluted (~10^{-5} M) in chlorobenzene and the standard 1 cm path length quartz cuvette was used. Thin films (60 nm) of PVK/PBD blends (7:3 weight ratio) doped with iridium complexes were prepared on quartz substrates by means of spin−coating. Absorption spectra were detected by a Carry 5000 (Varian) spectrometer. The emission spectra were recorded on Edinburgh

DOI: 10.1021/acs.inorgchem.9b02785
Inorg. Chem. 2019, 58, 15671−15686

Instruments FLS980 spectrofluorometer equipped with an integrating sphere used to determine the photoluminescence quantum yields.

Samples of thick layers (few μm), required for SRTL experiments, were prepared by drop−casting from chlorobenzene solutions onto aluminum substrates in ambient conditions. The samples for SRTL studies were placed in the vacuum chamber on a thermostated holder and covered by a sapphire plate. After sample photoexcitation at 15 K for by pulsed nitrogen laser (λ = 337 nm) (PTI, model GL-3300T) the TL measurements were carried out in the temperature range of 20−300 K with heating rate of 7 K/min. Sample thermoluminescence was recorded by a detection system contained an optical collector, an optical−fiber, a Micro HR Imaging Spectrograph and a CCD 3500 camera (Horriba Jobin Yvon).

Fabrication and Characterization of PhOLEDs. The OLEDs were fabricated on glass substrates by means of the spin−coating technique followed by vacuum evaporation. First, the hole injection layer of poly(3,4−ethylenedioxythiophene) and poly-(styrenesulfonate) mixture (PEDOT:PSS) was spin coated on an ITO anode in ambient conditions. Second, the emissive layer of PVK/PBD with 1 wt % Ir complex was spin-coated from a chlorobenzene solution in a glove box. The dopant concentration influence on the device parameters was checked only for **5h** in the range of 0.5−7 wt %. As the last step, the cathode materials were patterned through a shadow mask by physical vacuum deposition technique. The complete device stack can be written as ITO/PEDOT:PSS (20 nm)/PVK:PBD + emitter (60 nm)/Ca (20 nm)/Ag (100 nm). The device *J*−*V*−*L* characteristics were determined with use of Keithley 2400 source measurement unit connected with Minolta CS-200 camera. The EL spectra were recorded by the CCD 3500 camera (Horiba Jobin Yvon).

■ ASSOCIATED CONTENT

Supporting Information

The Supporting Information is available free of charge on the ACS Publications website at DOI: 10.1021/acs.inorgchem.9b02785.

> Procedures for the synthesis of ligands and complexes, NMR spectra of the new compounds, X-ray analysis detailed data, thermal analysis curves, cyclic voltammograms, theoretical and experimental data correlation, frontier orbitals' energy levels and distributions, optimized geometry coordinates, and additional photophysical data (PDF)

Accession Codes

CCDC 1865881−1865888 and 1892376 contain the supplementary crystallographic data for this paper. These data can be obtained free of charge via www.ccdc.cam.ac.uk/data_request/cif, or by emailing data_request@ccdc.cam.ac.uk, or by contacting The Cambridge Crystallographic Data Centre, 12 Union Road, Cambridge CB2 1EZ, UK; fax: +44 1223 336033.

■ AUTHOR INFORMATION

Corresponding Authors

*E-mail: irekk@o365.amu.edu.pl.
*E-mail: gabriela.wiosna-salyga@p.lodz.pl.

ORCID

Ireneusz Kownacki: 0000-0002-5445-760X
Maciej Kubicki: 0000-0001-7202-9169
Przemyslaw Ledwon: 0000-0001-6769-8739

Notes

The authors declare no competing financial interest.

■ ACKNOWLEDGMENTS

This work was supported by the National Science Centre (Poland) through grant no. UMO-2013/11/B/ST5/01334. This research was supported in part by the PL-Grid Infrastructure. E.W. acknowledges the financial support of the National Science Centre (Poland) through the grant no. UMO-2017/24/T/ST5/00017.

■ REFERENCES

(1) Tang, C. W.; Vanslyke, S. A. Organic electroluminescent diodes. *Appl. Phys. Lett.* **1987**, *51*, 913−915.

(2) Burroughes, J. H.; Bradley, D. D. C.; Brown, A. R.; Marks, R. N.; Mackay, K.; Friend, R. H.; Burns, P. I.; Holmes, A. B. Light-emitting diodes based on conjugated polymers. *Nature* **1990**, *347*, 539−541.

(3) (a) Miyata, S.; Nalwa, H. S. *Organic Electroluminescent Materials and Devices*; CRC Press: London, 1997. (b) Li, Z. R. *Organic Light−Emitting Materials and Devices*; CRC Press: Boca Raton, 2015.

(4) (a) Yersin, H. *Highly Efficient OLEDs with Phosphorescent Materials*; Wiley−VCH Verlag GmbH and KgaA: Weinheim, 2008. (b) Zysman-Colman, E. *Iridium(III) in optoelectronic and photonics applications*; John Wiley & Sons: Newark, 2017; pp 753.

(5) Lamansky, S.; Djurovich, P.; Murphy, D.; Abdel-Razzaq, F.; Kwong, R.; Tsyba, I.; Bortz, M.; Mui, B.; Bau, R.; Thompson, M. E. Synthesis and characterization of phosphorescent cyclometalated iridium complexes. *Inorg. Chem.* **2001**, *40*, 1704−1711.

(6) (a) Ko, S. H. *Organic light emitting diode−material, process and devices*; InTech: London, 2011. (b) Pereira, L. F. R. *Organic light emitting diodes: the use of rare earth and transition metals*; CRC Press, Hoboken, 2012. (c) Chi, Y.; Chang, T.-K.; Ganesan, P.; Rajakannu, P. Emissive bis-tridentate Ir(III) metal complexes: Tactics, photophysics and applications. *Coord. Chem. Rev.* **2017**, *346*, 91−100.

(7) Perepichka, D. F.; Meng, H.; Ling, M.-M. Phosphorescent Polymer Light-Emitting Diodes. In *Organic Light-Emitting Materials and Devices*; Li, Z., Meng, H., Eds.; Taylor and Francis: Boca Raton, 2007; pp 413−449.

(8) Xu, H.; Chen, R.; Sun, Q.; Lai, W.; Su, Q.; Huang, W.; Liu, X. Recent progress in metal−organic complexes for optoelectronic applications. *Chem. Soc. Rev.* **2014**, *43*, 3259−3302.

(9) (a) Chen, S.; Wu, Q.; Kong, M.; Zhao, X.; Yu, Z.; Jia, P.; Huang, W. On the origin of the shift in color in white organic light-emitting diodes. *J. Mater. Chem. C* **2013**, *1*, 3508−3524. (b) Glowacki, I.; Szamel, Z.; Wiosna-Salyga, G. Spectrally resolved thermoluminescence versus electroluminescence spectra of PVK doped with 1 wt % of $Ir(btp)_2(acac)$. *Org. Electron.* **2016**, *31*, 127−135.

(10) Witkowska, E.; Wiosna-Salyga, G.; Glowacki, I.; Orwat, B.; Oh, M−j.; Kownacki, I.; Kubicki, M.; Gierczyk, B.; Dutkiewicz, M.; Cieszko, P.; Luszczynska, B.; Ulanski, J.; Grzelak, I.; Hoffmann, M.; Ledwon, P.; Lapkowski, M. Effect of fluorine substitution of the β-ketoiminate ancillary ligand on photophysical properties and electroluminescence ability of new iridium(III) complexes. *J. Mater. Chem. C* **2018**, *6*, 8688−8708.

(11) (a) Radwan, Y. K.; Maity, A.; Teets, T. S. Manipulating the excited states of cyclometalated iridium complexes with β-ketoiminate and β-diketiminate ligands. *Inorg. Chem.* **2015**, *54*, 7122−7131. (b) Maya, R. A.; Maity, A.; Teets, T. S. Fluorination of cyclometalated iridium β-ketoiminate and β-diketiminate complexes: extreme redox tuning and ligand-centered excited states. *Organometallics* **2016**, *35*, 2890−2899. (c) Lai, P.-N.; Brysacz, C. H.; Alam, M. K.; Ayoub, N. A.; Gray, T. G.; Bao, J.; Teets, T. S. Highly efficient red-emitting bis-cyclometalated iridium complexes. *J. Am. Chem. Soc.* **2018**, *140*, 10198−10207.

(12) Citti, C.; Battisti, U. M.; Ciccarella, G.; Maiorano, V.; Gigli, G.; Abbate, S.; Mazzeo, G.; Castiglioni, E.; Longhi, G.; Cannazza, G. Analytical and preparative enantioseparation and main chiroptical properties of Iridium(III) bis(4,6-difluorophenylpyridinato)-picolinato. *J. Chromatogr. A* **2016**, *1467*, 335−346.

(13) Da Silva, M. A. V. R.; Da Silva, M. D. M. C. R.; Paiva, J. P. A.; Nogueira, I. M. C. S.; Damas, A. M.; Berkley, J. V.; Harding, M. M.;

DOI: 10.1021/acs.inorgchem.9b02785
Inorg. Chem. 2019, 58, 15671−15686

Akello, M. J.; Pilcher, G. Thermochemical and Crystallographic Studies of some p-Ketoimine Derivatives. *J. Chem. Soc., Perkin Trans. 2* **1993**, 1765−1769.
(14) (a) Gavezzotti, A. Are Crystal Structures Predictable? *Acc. Chem. Res.* **1994**, *27*, 309−314. (b) Gavezzotti, A.; Filippini, G. J. Geometry of the intermolecular X-H···Y (X, Y = N, O) hydrogen bond and the calibration of empirical hydrogen-bond potentials. *J. Phys. Chem.* **1994**, *98*, 4831−4837.
(15) Chepelin, O.; Ujma, J.; Wu, X.; Slawin, A. M. Z.; Pitak, M. B.; Coles, S. J.; Michel, J.; Jones, A. C.; Barran, P. E.; Lusby, P. J. Luminescent, Enantiopure, Phenylatopyridine Iridium-Based Coordination Capsules. *J. Am. Chem. Soc.* **2012**, *134*, 19334−19337.
(16) (a) Ràfols-Ribé, J.; Will, P.-A.; Hänisch, C.; Gonzalez-Silveira, M.; Lenk, S.; Rodríguez-Viejo, J.; Reineke, S. High-performance organic light-emitting diodes comprising ultrastable glass layers. *Sci. Adv.* **2018**, *4* (5), 1−9. (b) Kwak, K.; Cho, K.; Kim, S. Analysis of thermal degradation of organic light-emitting diodes with infrared imaging and impedance spectroscopy. *Opt. Express* **2013**, *21*, 29558−29559.
(17) Chen, Z.-Q.; Shen, X.; Xu, J.-X.; Zou, H.; Wang, X.; Xu, Y.; Zhu, D.-R. Iridium(III) complexes based on 5-nitro-2-(2′,4′-difluorophenyl)pyridyl: Syntheses, structures and photoluminescence properties. *Inorg. Chem. Commun.* **2015**, *61*, 152−156.
(18) Hirva, P.; Haukka, M.; Jakonen, M.; Moreno, M. A. DFT tests for group 8 transition metal carbonyl complexes. *J. Mol. Model.* **2008**, *14*, 171−181.
(19) Skorka, L.; Filapek, M.; Zur, L.; Malecki, J. G.; Pisarski, W.; Olejnik, M.; Danikiewicz, W.; Krompiec, S. Highly Phosphorescent Cyclometalated Iridium(III) Complexes for Optoelectronic Applications: Fine Tuning of the Emission Wavelength through Ancillary Ligands. *J. Phys. Chem. C* **2016**, *120*, 7284−7294.
(20) Kodate, S.; Suzuka, I. Assignments of Lowest Triplet State in Ir Complexes by Observation of Phosphorescence Excitation Spectra at 6 K. *Jpn. J. Appl. Phys.* **2006**, *45*, 574−578.
(21) (a) Li, J.; Djurovich, P. I.; Alleyne, B. D.; Yousufuddin, M.; Ho, N. N.; Thomas, J. C.; Peters, J. C.; Bau, R.; Thompson, M. E. Synthetic Control of Excited-State Properties in Cyclometalated Ir(III) Complexes Using Ancillary Ligands. *Inorg. Chem.* **2005**, *44*, 1713−1727. (b) Yersin, H.; Rausch, A. F.; Czerwieniec, R.; Hofbeck, T.; Fischer, T. The triplet state of organo-transition metal compounds. Triplet harvesting and singlet harvesting for efficient OLEDs. *Coord. Chem. Rev.* **2011**, *255*, 2622−2652.
(22) Hsu, C.-C; Lin, C.-C.; Chou, P.-T.; Lai, C.-H.; Hsu, C.-W.; Lin, C.-H.; Chi, Y. Harvesting Highly Electronically Excited Energy to Triplet Manifolds: State-Dependent Intersystem Crossing Rate in Os(II) and Ag(I) Complexes. *J. Am. Chem. Soc.* **2012**, *134*, 7715−7724.
(23) You, Y.; Nam, W. Photofunctional triplet excited states of cyclometalated Ir(III) complexes: beyond electroluminescence. *Chem. Soc. Rev.* **2012**, *41*, 7061−7084.
(24) Kawamura, Y.; Goushi, K.; Brooks, J.; Brown, J. J.; Sasabe, H.; Adachi, C. 100% phosphorescence quantum efficiency of Ir(III) complexes in organic semiconductor films. *Appl. Phys. Lett.* **2005**, *86*, 071104−3.
(25) Wu, L−L.; Tsai, S−H.; Guo, T−F.; Yang, Ch−H.; Sun, I−W. Synthesis and green electrophosphorescence of a novel cyclometalated iridium complex in polymer light-emitting diodes. *J. Lumin.* **2007**, *126*, 687−694.
(26) Tang, H.; Li, Y.; Wei, C.; Chen, B.; Yang, W.; Wu, H.; Cao, Y. Novel yellow phosphorescent iridium complexes containing a carbazole−oxadiazole unit used in polymeric light-emitting diodes. *Dyes Pigm.* **2011**, *91*, 413−421.
(27) Glowacki, I.; Szamel, Z. The impact of 1 wt% of $Ir(ppy)_3$ on trapping sites and radiative recombination centres in PVK and PVK/PBD blend seen by thermoluminescence. *Org. Electron.* **2015**, *24*, 288−296.
(28) (a) Sprouse, S.; King, K. A.; Spellane, P. J.; Watts, R. J. Photophysical effects of metal-carbon σ bonds in ortho-metalated complexes of iridium(III) and rhodium(III). *J. Am. Chem. Soc.* **1984**, *106*, 6647−6653. (b) Nonoyama, M. Benzo[*h*]quinolin-10-yl-*N* Iridium(III) Complexes. *Bull. Chem. Soc. Jpn.* **1974**, *47*, 767−768.
(29) CrysAlisPro (Version 1.171.38.41), Rigaku OD, 2015.
(30) Sheldrick, G. M. *SHELXT* − Integrated space-group and crystal-structure determination. *Acta Crystallogr., Sect. A: Found. Adv.* **2015**, *A71*, 3−8.
(31) Sheldrick, G. M. Crystal structure refinement with *SHELXL*. *Acta Crystallogr., Sect. C: Struct. Chem.* **2015**, *C71*, 3−8.
(32) Cardona, C. M.; Li, W.; Kaifer, A. E.; Stockdale, D.; Bazan, G. C. Electrochemical Considerations for Determining Absolute Frontier Orbital Energy Levels of Conjugated Polymers for Solar Cell Applications. *Adv. Mater.* **2011**, *23*, 2367−2371.
(33) Becke, A. D. Density-functional thermochemistry. III. The role of exact exchange. *J. Chem. Phys.* **1993**, *98*, 5648−5652.
(34) Stephens, P. J.; Devlin, F. J.; Chabalowski, C. F.; Frisch, M. J. Ab Initio Calculation of Vibrational Absorption and Circular Dichroism Spectra Using Density Functional Force Fields. *J. Phys. Chem.* **1994**, *98*, 11623−11627.
(35) Kim, K.; Jordan, K. D. Comparison of Density Functional and MP2 Calculations on the Water Monomer and Dimer. *J. Phys. Chem.* **1994**, *98*, 10089−10094.
(36) Clark, T.; Chandrasekhar, J.; Spitznagel, G. W.; Schleyer, P. V. R. Efficient diffuse function-augmented basis sets for anion calculations. III.* The 3-21+G basis set for first-row elements, Li−F. *J. Comput. Chem.* **1983**, *4*, 294−301.
(37) Dunning, T. H.; Hay, P. J. Gaussian Basis Sets for Molecular Calculations. In *Applications of Electronic Structure Theory*; Schaefer III, H. F., Eds.; Plenum: New York, 1976; pp 1−28.
(38) Francl, M. M.; Pietro, W. J.; Hehre, W. J.; Binkley, J. S.; Gordon, M. S.; DeFrees, D. J.; Pople, J. A. Self-consistent molecular orbital methods. XXIII. A polarization-type basis set for second-row elements. *J. Chem. Phys.* **1982**, *77*, 3654−3665.
(39) Zhao, Y.; Truhlar, D. G. The M06 suite of density functionals for main group thermochemistry, thermochemical kinetics, noncovalent interactions, excited states, and transition elements: two new functionals and systematic testing of four M06-class functionals and 12 other functionals. *Theor. Chem. Acc.* **2008**, *120*, 215−241.
(40) Chai, J.−D.; Head-Gordon, M. Long-range corrected hybrid density functionals with damped atom−atom dispersion corrections. *J. Chem. Phys.* **2008**, *128*, 084106.
(41) Cancès, E.; Mennucci, B.; Tomasi, J. A new integral equation formalism for the polarizable continuum model: Theoretical background and applications to isotropic and anisotropic dielectrics. *J. Chem. Phys.* **1997**, *107*, 3032−3041.
(42) Mennucci, B.; Tomasi, J. Continuum solvation models: A new approach to the problem of solute's charge distribution and cavity boundaries. *J. Chem. Phys.* **1997**, *106*, 5151−5158.
(43) Cossi, M.; Barone, V.; Mennucci, B.; Tomasi, J. Ab initio study of ionic solutions by a polarizable continuum dielectric model. *Chem. Phys. Lett.* **1998**, *286*, 253−260.
(44) Frisch, M. J.; Trucks, G. W.; Schlegel, H. B.; Scuseria, G. E.; Robb, M. A.; Cheeseman, J. R.; Scalmani, G.; Barone, V.; Petersson, G. A.; Nakatsuji, H.; Li, X.; Caricato, M.; Marenich, A. V.; Bloino, J.; Janesko, B. G.; Gomperts, R.; Mennucci, B.; Hratchian, H. P.; Ortiz, J. V.; Izmaylov, A. F.; Sonnenberg, J. L.; Williams-Young, D.; Ding, F.; Lipparini, F.; Egidi, F.; Goings, J.; Peng, B.; Petrone, A.; Henderson, T.; Ranasinghe, D.; Zakrzewski, V. G.; Gao, J.; Rega, N.; Zheng, G.; Liang, W.; Hada, M.; Ehara, M.; Toyota, K.; Fukuda, R.; Hasegawa, J.; Ishida, M.; Nakajima, T.; Honda, Y.; Kitao, O.; Nakai, H.; Vreven, T.; Throssell, K.; Montgomery, J. A., Jr.; Peralta, J. E.; Ogliaro, F.; Bearpark, M. J.; Heyd, J. J.; Brothers, E. N.; Kudin, K. N.; Staroverov, V. N.; Keith, T. A.; Kobayashi, R.; Normand, J.; Raghavachari, K.; Rendell, A. P.; Burant, J. C.; Iyengar, S. S.; Tomasi, J.; Cossi, M.; Millam, J. M.; Klene, M.; Adamo, C.; Cammi, R.; Ochterski, J. W.; Martin, R. L.; Morokuma, K.; Farkas, O.; Foresman, J. B.; Fox, D. J. *Gaussian 16*, Revision B.01; Gaussian, Inc.: Wallingford CT, 2016.

DOI: 10.1021/acs.inorgchem.9b02785
Inorg. Chem. 2019, 58, 15671−15686

Supporting Information for

Effect of *β*–ketoiminato ancillary ligand modification on emissive properties of new iridium complexes

Ewelina Witkowska[a], Bartosz Orwat[b,c], Myong Joon Oh[b,c], Gabriela Wiosna–Salyga[a]*, Ireneusz Glowacki[a], Ireneusz Kownacki[b,c]*, Kamila Jankowska[b,c], Maciej Kubicki[b], Błażej Gierczyk[b], Michał Dutkiewicz[c,d], Izabela Grzelak[b], Marcin Hoffmann[b], Julita Nawrocik[b,c], Grzegorz Krajewski[b,c], Jacek Ulanski[a], Przemyslaw Ledwon[e], Mieczyslaw Lapkowski[e,f]

[a] Department of Molecular Physics, Lodz University of Technology, 90–924 Lodz, Zeromskiego 116, Poland, E–mail: Gabriela.Wiosna–Salyga@p.lodz.pl

[b] Faculty of Chemistry, Adam Mickiewicz University in Poznan, St. Uniwersytetu Poznanskiego 8, 61–614 Poznan, Poland

[c] Center for Advanced Technology, Adam Mickiewicz University in Poznan, St. Uniwersytetu Poznanskiego 10, 61–614 Poznan, Poland

[d] Poznan Science and Technology Park, Adam Mickiewicz University Foundation, ul. Rubiez 46, 61–612 Poznan, Poland

[e] Silesian University of Technology, Faculty of Chemistry, St. Marcina Strzody 9, 44–100 Gliwice, Poland

[f] Centre of Polymer and Carbon Materials, Polish Academy of Sciences, Curie–Sklodowskiej 34, 41–819 Zabrze, Poland

Table of contents

1. **Synthesis of ligands and complexes** **3**
2. **NMR spectra of 4-arylimino-2-pentanones** **13**
3. **NMR spectra of iridium(III) complexes** **25**
4. **X-Ray analysis data** **30**
5. **Thermal analysis curves** **35**
6. **Cyclic voltammetry measurements** **40**
7. **DFT calculation data** **41**
8. **Photophysical measurements** **70**

1. Synthesis of ligands and complexes

4-Phenylimino-2-pentanone (**3a**)[1]: To a solution of 0.05 mol of acetylacetone (5.0 g) in benzene, 0.045 mol of aniline (4.2 g) and 20 mg of *p*-toluenesulfonic acid were added. The obtained mixture was refluxed using Dean-Stark apparatus, until no more water was generated (ca. 10 h). Then the solvent was evaporated and the oily residue was crystallized from hexane. The product was filtered off and dried in vacuum at r.t. Yield: 7.1 g (90%), m.p. 47-49°C. Yield: 7.1 g (90%); m.p. 47-49°C; ^{1}H NMR (300 MHz, $CDCl_3$): δ = 12.47 (bs, 1H; N**H**); 7.32 (t, 2H, 7.7 Hz; $C_{Ar3,5}$**H**); 7.17 (t, 1H, 7.7 Hz; C_{Ar4}**H**); 7.09 (d, 2H, 7.7 Hz; $C_{Ar2,6}$**H**); 5.18 (s, 1H; =C**H**); 2.09 (s, 3H; C(=O)C**H**$_3$); 1.98 (s, 3H; =CC**H**$_3$); ^{13}C NMR (75 MHz, $CDCl_3$) δ = 196.0 (C=O); 160.1 (=C-N); 138.7 (N-**C**$_{Ar1}$); 129.0 (**C**$_{Ar2,6}$); 125.5 (**C**$_{Ar4}$); 124.7 (**C**$_{Ar3,5}$); 97.5 (=**C**H); 29.1 (C(=O)**C**H$_3$); 19.8 (=C**C**H3); HRMS (EI): *m/z* calcd for $C_{11}H_{13}NO^+$: 175.0992, found: 175.0971.

Compounds **3b-3i** have been synthesized using the same method as for **3a**:

4-(4-Methoxyphenyl)imino-2-pentanone (**3b**): 0.07 mol (8.6 g) of 4-methoxyaniline was used. Yield: 10.2 g (71%); m.p. 40-42°C; ^{1}H NMR (300 MHz, $CDCl_3$) δ = δ 12.27 (bs, 1H; N**H**); 7.01 (m, 2H; C_{Ar2}**H**); 6.84 (m, 2H; C_{Ar3}**H**); 5.13 (s, 1H; =C**H**); 2.06 (s, 3H; C(=O)C**H**$_3$); 1.88 (s, 3H; =CC**H**$_3$); ^{13}C NMR ($CDCl_3$) δ = 195.7 (C=O); 161.3 (=C-N); 157.6 (**C**$_{Ar4}$O); 131.4 (N-**C**$_{Ar1}$); 126.5 (**C**$_{Ar2,6}$); 114.2 (**C**$_{Ar3,5}$); 96.7 (=**C**H); 28.5 (C(=O)**C**H$_3$); 19.5 (=C**C**H$_3$); HRMS (EI): *m/z* calcd for $C_{12}H_{15}NO_2^+$: 205.1097, found: 205.1109.

4-(4-cyanophenyl)imino-2-pentanone (**3c**): 0.05 mol (5.5 g) of 4-aminobenzonitrile was used. Yield: 8.2 g (88%); m.p. 85-88°C; ^{1}H NMR (300 MHz, $CDCl_3$) δ = δ 12.67 (bs, 1H; N**H**); 7.59 (m, 2H; C_{Ar3}**H**); 7.14 (m, 2H; C_{Ar2}**H**); 5.28 (s, 1H; =C**H**); 2.12 (s, 3H;

C(=O)C**H**$_3$); 2.11 (s, 3H; =CC**H**$_3$); ^{13}C NMR ($CDCl_3$) δ = 197.5 (C=O); 157.5 (=C–N); 143.3 (N–**C**$_{Ar1}$); 133.2 (**C**$_{Ar3,5}$); 122.8 (**C**$_{Ar2,6}$); 118.6 (**C**≡N); 107.2 (**C**$_{Ar4}$CN); 99.9 (=**C**H); 29.5 (C(=O)**C**H$_3$); 20.3 (=C**C**H$_3$); HRMS (EI): *m/z* calcd for $C_{12}H_{12}N_2O^+$: 200.0944, found: 200.0938.

4–(4–Nitrophenyl)imino–2–pentanone (**3d**): 0.04 mol (6.1 g) of 4-nitroaniline was used. Yield: 7.1 g (73%); m.p. 140–142°C; ^{1}H NMR (300 MHz, $CDCl_3$) δ = 12.75 (bs, 1H; N**H**); 8.16 (m, 2H; C$_{Ar3}$**H**); 7.15 (m, 2H; C$_{Ar2}$**H**); 5.31 (s, 1H; =C**H**); 2.17 (s, 3H; C(=O)C**H**$_3$); 2.11 (s, 3H; =CC**H**$_3$); ^{13}C NMR ($CDCl_3$) δ = 197.8 (C=O); 156.9 (=C–N); 145.2 (N–**C**$_{Ar1}$); 143.4 (**C**$_{Ar4}$NO$_2$); 125.1 (**C**$_{Ar3,5}$); 121.8 (**C**$_{Ar2,6}$); 101.1 (=**C**H); 29.5 (C(=O)**C**H$_3$); 20.5 (=C**C**H$_3$); HRMS (EI): *m/z* calcd for $C_{11}H_{12}N_2O_3^+$: 220.0842, found: 220.0840.

4–(3–Nitrophenyl)imino–2–pentanone (**3e**): 0.05 mol (6.8 g) of 3-nitroaniline was used. Yield: 7.8 g (72%); m.p. 76–78°C; ^{1}H NMR (300 MHz, $CDCl_3$) δ = 12.64 (bs, 1H; N**H**); 7.99 (ddd, 1H, 8.1, 2.1 & 0.9 Hz; C$_{Ar4}$**H**); 7.96 (t, 1H, 2.1 Hz; C$_{Ar2}$**H**); 7.50 (t, 1H, 8.1 Hz; C$_{Ar5}$**H**); 7.40 (ddm, 1H, 8.1 & 2.1 Hz; C$_{Ar6}$**H**); 5.28 (s, 1H; =C**H**); 2.12 (s, 3H; C(=O)C**H**$_3$); 2.09 (s, 3H; =CC**H**$_3$); ^{13}C NMR ($CDCl_3$) δ = 197.4 (C=O); 158.3 (=C–N); 148.7 (**C**$_{Ar3}$NO$_2$); 140.3 (N–**C**$_{Ar1}$); 130.0 (C$_{Ar5}$); 129.6 (C$_{Ar6}$); 119.5 (**C**$_{Ar2}$); 118.3 (**C**$_{Ar4}$); 99.6 (=**C**H); 29.4 (C(=O)**C**H$_3$); 19.4 (=C**C**H$_3$); HRMS (EI): *m/z* calcd for $C_{11}H_{12}N_2O_3^+$: 220.0842, found: 220.0857.

4–(2–Nitrophenyl)imino–2–pentanone (**3f**): 0.04 mol (5.2 g) of 2-nitroaniline was used. Yield: 7.3 g (88%); m.p. 58–60°C; ^{1}H NMR (300 MHz, $CDCl_3$) δ = 12.89 (bs, 1H; N**H**); 8.02 (dd, 1H, 8.2 & 1.5 Hz; C$_{Ar3}$**H**); 7.54 (ddd, 1H, 8.4, 7.0 & 1.5 Hz; C$_{Ar5}$**H**); 7.22 (dd, 1H, 8.4 & 1.2 Hz; C$_{Ar6}$**H**); 7.23 (ddd, 1H, 8.2, 7.0 & 1.2 Hz; C$_{Ar4}$**H**); 5.37 (s, 1H; =C**H**); 2.14 (s, 3H; C(=O)C**H**$_3$); 2.03 (s, 3H; =CC**H**$_3$); ^{13}C NMR ($CDCl_3$) δ = δ 197.3 (C=O); 156.2 (=C–N); 142.5 (**C**$_{Ar2}$NO$_2$); 134.0 (N–**C**$_{Ar1}$); 133.4 (C$_{Ar5}$); 126.4 (C$_{Ar3}$); 125.7

(C_{Ar4}); 124.5 (**C**$_{Ar6}$); 101.9 (=**C**H); 29.5 (C(=O)**C**H_3); 19.9 (=C**C**H_3); HRMS (EI): *m/z* calcd for $C_{11}H_{12}N_2O_3^+$: 220.0842, found: 220.0861.

4-(4-(5-Methyl-2-benzothiazyl)phenyl)imino-2-pentanone (**3g**): 0.03 mol (7.8 g) of 2-(4-aminophenyl)-5-methylbenzothiazole was used. Yield: 9.4 g (90%); m.p. 156-158°C; ^{1}H NMR (300 MHz, $CDCl_3$) δ = 12.65 (bs, 1H; N**H**); 8.01 (m, 2H; $C_{Ph3,5}$**H**); 7.91 (d, 1H, 8.3 Hz; C_{Bt7}**H**); 7.66 (s, 1H; C_{Bt4}**H**); 7.28 (d, 1H, 8.2 Hz; C_{Bt6}**H**); 7.18 (m, 2H; $C_{Ph2,6}$**H**); 5.24 (s, 1H; =C**H**); 2.48 (s, 3H; BtC**H**$_3$); 2.12 (s, 3H; C(=O)C**H**$_3$); 2.09 (s, 3H; =CC**H**$_3$); ^{13}C NMR (75 MHz, $CDCl_3$) δ = 196.7 (C=O); 165.9 (C_{Bt2}); 158.8 (=C-N); 152.2 (C_{Bt3a}); 141.2 (N-**C**$_{Ar1}$); 135.3 (C_{Bt5}); 135.1 (C_{Bt7a}); 130.2 (**C**$_{Ar4}$Bt); 128.2 (**C**$_{Ar3,5}$); 127.9 (C_{Bt6}); 123.7 ($C_{Ar2,6}$); 122.6 (C_{Bt7}); 121.3 (C_{Bt4}); 100.0 (=**C**H); 29.3 (C(=O)**C**H_3); 21.5 (Bt**C**H_3); 20.1 (=C**C**H_3); HRMS (EI): *m/z* calcd for $C_{19}H_{18}N_2OS^+$: 322.1134, found: 322.1153.

4-(1-Naphthyl)imino-2-pentanone (**3h**): 0.04 mol (5.8 g) of 1-aminonaphthalene was used. Yield: 6.8 g (75%); m.p. 74-75°C; ^{1}H NMR (300 MHz, $CDCl_3$) δ = 12.75 (bs, 1H; N**H**); 8.03 (d, 1H, 7.9 Hz; C_{Nph8}**H**); 7.87 (d, 1H, 7.5 Hz; C_{Nph5}**H**); 7.77 (d, 1H, 8.2 Hz; C_{Nph4}**H**); 7.53 (m, 2H; $C_{Nph6,7}$**H**); 7.44 (t, 1H, 7.4 Hz; C_{Nph3}**H**); 7.28 (d, 1H, 7.4 Hz; C_{Nph2}**H**); 5.31 (s, 1H; =C**H**); 2.18 (s, 3H; C(=O)C**H**$_3$); 1.88 (s, 3H; =CC**H**$_3$); ^{13}C NMR (75 MHz, $CDCl_3$) δ = 196.4 (C=O); 161.8 (=C-N); 134.8 (N-**C**$_{Nph1}$); 134.2 (**C**$_{Nph10}$); 129.9 (**C**$_{Nph9}$); 128.2 (**C**$_{Nph5}$); 126.9 (**C**$_{Nph6}$); 126.8 (**C**$_{Nph3}$); 126.5 (**C**$_{Nph7}$); 125.2 (**C**$_{Nph8}$); 123.4 (**C**$_{Nph4}$); 122.7 (**C**$_{Nph2}$); 97.4 (=**C**H); 29.1 (C(=O)**C**H_3); 19.6 (=C**C**H_3); HRMS (EI): *m/z* calcd for $C_{15}H_{15}NO^+$: 225.1148, found: 225.1157.

4-(2-Naphthyl)imino-2-pentanone (**3i**): 0.04 mol (5.7 g) of 2-aminonaphthalene was used. Yield: 6.3 g (70%); m.p. 95-97°C; ^{1}H NMR (300 MHz, $CDCl_3$) δ = 12.66 (bs, 1H; N**H**); 7.82 (d, 1H, 7.2 Hz; C_{Nph5}**H**); 7.81 (d, 1H, 8.6 Hz; C_{Nph4}**H**); 7.77 (d, 1H, 8.1 Hz;

C_{Nph8}**H**); 7.54 (d, 1H, 1.9 Hz; C_{Nph1}**H**); 7.49 (t, 1H, 7.2 Hz; C_{Nph7}**H**); 7.45 (d, 1H, 7.2 Hz; C_{Nph6}**H)**; 7.25 (dd, 1H, 8.6 & 1.9 Hz; C_{Nph3}**H**); 5.31 (s, 1H; =C**H**); 2.18 (s, 3H; C(=O)C$\mathbf{H}_3$); 1.88 (s, 3H; =CC$\mathbf{H}_3$); ^{13}C NMR (75 MHz, $CDCl_3$) δ = 196.2 (C=O); 160.1 (=C–N); 136.3 (N–$\mathbf{C}_{Nph1}$); 133.5 ($\mathbf{C}_{Nph9}$); 131.1 ($\mathbf{C}_{Nph10}$); 129.0 ($\mathbf{C}_{Nph4}$); 127.6 ($\mathbf{C}_{Nph5}$); 127.4 ($\mathbf{C}_{Nph7}$); 126.6 ($\mathbf{C}_{Nph7}$); 125.6 ($\mathbf{C}_{Nph8}$); 123.9 ($\mathbf{C}_{Nph6}$); 121.7 ($\mathbf{C}_{Nph3}$); 97.9 (=**C**H); 29.2 (C(=O)**C**H_3); 20.0 (=C**C**H_3); HRMS (EI): *m/z* calcd for $C_{15}H_{15}NO^+$: 225.1148, found: 225.1141.

4–(1–Anthracenyl)imino–2–pentanone (**3j**): to a pressure glass vessel of 10 mL capacity equipped with a magnetic stirrer, 400 mg (2.070 mmol; 1.00 eq.) of 1–aminoanthracene, 2.125 mL of pentane–2,4–dione (20.70 mmol; 10.00 eq.) and a drop of acetic acid were added. The reactor was sealed by a plastic cap equipped with elastic membrane and then placed in the chamber of a microwave radiation source. The thus prepared reaction system was sealed with an encapsulating head, equipped with a pressure sensor. The reaction was conducted for 1 hour at 150 ℃, irradiating the mixture with microwaves (150 W and frequency 2445 MHz). Afterwards, the solvent was fully evaporated from the post–reaction mixture under reduced pressure. The remaining crude product was purified by flash chromatography using silica treated with triethylamine as the solid phase (gradient elution from pure n–hexane to n–hexane:AcOEt = 4:1, v/v). The purified material was dried *in vacuo* for 4 hours. The desired product was obtained in 79 % yield (450.35 mg, 1.637 mmol); m.p. 157–158°C; ^{1}H NMR (300 MHz, $CDCl_3$) δ = 12.86 (bs, 1H; N**H**); 8.58 (s, 1H; C_{Ant10}**H**); 8.45 (s, 1H; C_{Ant9}**H**); 8.06 (m, 1H; C_{Ant8}**H**); 8.00 (m, 1H; C_{Ant5}**H**); 7.92 (d, 1H, 8.5 Hz; C_{Ant4}**H**); 7.49 (m, 2H; $C_{Ant6,7}$**H**); 7.42 (dd, 1H, 8.5 & 7.0 Hz; C_{Ant3}**H**); 7.25 (dt, 1H, 7.0 & 1.0 Hz; C_{Ant2}**H**); 5.37 (s, 1H; =C**H**); 2.23 (s, 3H; C(=O)C$\mathbf{H}_3$); 1.92 (s, 3H; =CC$\mathbf{H}_3$); ^{13}C NMR ($CDCl_3$) δ = 196.5 (C=O); 161.9 (=C–N); 134.8 (N–$\mathbf{C}_{Ant1}$); 132.2 ($\mathbf{C}_{Ant4a}$); 132.0 ($\mathbf{C}_{Ant10a}$); 131.9 ($\mathbf{C}_{Ant8a}$); 128.7 ($\mathbf{C}_{Ant8}$); 128.6

(**C**$_{Ant9a}$); 127.9 (**C**$_{Ant5}$); 127.2 (**C**$_{Ant10}$); 126.8 (**C**$_{Ant7}$); 126.0 (**C**$_{Ant3}$); 125.8 (**C**$_{Ant6}$); 124.4 (**C**$_{Ant9}$); 122.6 (**C**$_{Ant4}$); 121.6 (**C**$_{Ant2}$); 97.7 (=**C**H); 29.2 (C(=O)**C**H$_3$); 19.6 (=C**C**H$_3$); HRMS (ESI): *m/z* calcd for $C_{19}H_{18}NO^+$ ([M+H]$^+$): 276.1383, found: 276.1384.

4-(2-Anthracenyl)imino-2-pentanone (**3k**): Following the procedure used for preparation of **3j**, the reaction was carried out with 0.726 mmol (140 mg) of 1-aminoanthracene and 7.26 mmol pentane-2,4-dione. Yield: 150.17 mg (0.545 mmol, 75%); m.p. 185-188°C; ^{1}H NMR (300 MHz, $CDCl_3$) δ = 12.71 (bs, 1H; N**H**); 8.39 (s, 1H; C$_{Ant9}$**H**); 8.33 (s, 1H; C$_{Ant10}$**H**); 7.99 (dm, 1H, 8.7 Hz; C$_{Ant4}$**H**); 7.97 (dm, 2H, 8.9 Hz; C$_{Ant5,8}$**H**); 7.67 (d, 1H, 2.1 Hz; C$_{Ant1}$**H**); 7.47 (m, 2H; C$_{Ant6,7}$**H**); 7.24 (dd, 1H, 8.7 & 2.1 Hz; C$_{Ant3}$**H**); 5.27 (s, 1H; =C**H**); 2.16 (s, 3H; =CC**H**$_3$); 2.15 (s, 3H; C(=O)C**H**$_3$); ^{13}C NMR ($CDCl_3$) δ = 196.4 (C=O); 159.9 (=C-N); 135.7 (N-**C**$_{Ant2}$); 132.2 (**C**$_{Ant9a}$); 131.5 (**C**$_{Ant8a,10a}$); 129.5 (**C**$_{Ant4}$); 129.4 (**C**$_{Ant4a}$); 128.2 (**C**$_{Ant5}$); 127.9 (**C**$_{Ant8}$); 126.3 (**C**$_{Ant10}$); 125.8 (**C**$_{Ant7}$); 125.6 (**C**$_{Ant6}$); 125.4 (**C**$_{Ant9}$); 124.1 (**C**$_{Ant3}$); 120.5 (**C**$_{Ant1}$); 98.3 (=**C**H); 29.3 (C(=O)**C**H$_3$); 20.2 (=C**C**H$_3$); HRMS (ESI): *m/z* calcd for $C_{19}H_{18}NO^+$ ([M+H]$^+$): 276.1383, found: 276.1473.

4-(9-Anthracenyl)imino-2-pentanone (**3l**): Following the procedure used for preparation of **3j**, the reaction was carried out with 2.070 mmol (400 mg) of 9-aminoanthracene and 20.70 mmol (2.125 mL) of pentane-2,4-dione. Yield: 399.04 mg (1.450 mmol, 70%); m.p. 147-149°C; ^{1}H NMR (300 MHz, $CDCl_3$) δ = 12.67 (bs, 1H; N**H**); 8.44 (s, 1H; C$_{Ant10}$**H**); 8.08 (dq, 2H, 8.5 & 0.9 Hz; C$_{Ant1,8}$**H**); 8.03 (ddt, 2H, 8.3, 1.4 & 0.9 Hz; C$_{Ant4,5}$**H**); 7.52 (m, 2H; C$_{Ant2,7}$**H**); 7.49 (m, 2H; C$_{Ant3,6}$**H**); 5.42 (s, 1H; =C**H**); 2.25 (s, 3H; C(=O)C**H**$_3$); 1.57 (s, 3H; =CC**H**$_3$); ^{13}C NMR ($CDCl_3$) δ = 196.7 (C=O); 163.8 (=C-N); 131.6 (**C**$_{Ant5a,10a}$); 130.3 (N-**C**$_{Ant9}$); 129.1 (**C**$_{Ant10}$); 128.5 (**C**$_{Ant3,6}$); 126.7 (**C**$_{Ant4,5}$); 126.6 (**C**$_{Ant8a,9a}$); 125.6 (**C**$_{Ant2,7}$); 127.2 (**C**$_{Ant1,8}$); 96.7 (=**C**H); 29.3 (C(=O)**C**H$_3$); 19.3

(=C**C**H_3); HRMS (ESI): *m/z* calcd for $C_{19}H_{18}NO^+$ ($[M+H]^+$): 276.1383, found: 276.1410.

[Ir(bzq)$_2${MeC(O)=CHC(=N(C_6H_5))Me}] (**5a**): Complex was synthesized according to previously published procedure.[1]

[Ir(bzq)$_2${MeC(O)=CHC(=N(4–MeO–C_6H_4))Me}] (**5b**): In a Schlenk vessel equipped with a magnetic stirrer, 100 mg (0.0856 mmol, 1.00 eq.) of [{Ir(bzq)$_2$(μ–Cl)}$_2$] (**4**), 70.15 mg (0.342 mmol, 4.00 eq.) of 4–(4–methoxyphenyl)imino–2–pentanone (**3b**) were placed and then 5 mL of dried and deoxygenated THF was introduced. In the next step, to the stirred mixture 41.13 mg (0.428 mmol, 5 eq.) of NaO^{t}Bu was added. The reaction was conducted at ambient condition for 12 hours. Then the solvent was evaporated from the red–orange solution under reduced pressure. The remaining crude product was purified by flash chromatography using silica as the solid phase and chloroform as eluent. After evaporation of the solvent the remaining solid was dried *in vacuo* for 4 hours. The desired product was obtained in 62 % yield (78.90 mg, 0.103 mmol). Elemental anal. calcd for $C_{38}H_{30}IrN_3O_2$, C 60.62; H 4.02; found C 60.70; H 4.06. ^{1}H NMR (300 MHz, $CDCl_3$) δ = 9.28 (dd, *J* = 5.3&1.4 Hz, 1H); 9.11 (dd, *J* = 5.3&1.4 Hz, 1H); 8.23 (dd, *J* = 8.0&1.4 Hz, 1H); 8.14 (dd, *J* = 8.0&1.4 Hz, 1H); 7.75 (d, *J* = 9.2 Hz, 1H); 7.60 (d, *J* = 8.8 Hz, 1H); 7.56 (dd, *J* = 8.0&5.3 Hz, 2H); 7.45 (d, *J* = 1.5 Hz, 2H); 6.93 (ddd, *J* = 7.6&4.0&3.2 Hz, 2H); 6.63 (t, *J* = 7.5 Hz, 1H); 6.34 (dd, *J* = 7.2&0.9 Hz, 1H); 6.19 (dd, *J* = 8.7&2.6 Hz, 1H); 5.96 (dd, *J* = 7.3&0.9 Hz, 1H); 5.89 (dd, *J* = 8.6&2.9 Hz, 1H); 5.48 (dd, *J* = 8.6&2.9 Hz, 1H); 4.85 (s, 1H, =CH–); 4.59 (dd, *J* = 8.6&2.6 Hz, 1H); 3.41 (s, 3H, –OCH_3); 1.68 (s, 3H, –CH_3); 1.61 (s, 3H, –CH_3). HRMS (EI): *m/z* calcd for $C_{38}H_{30}IrN_3O_2^+$: $[M]^+$ 753.1962, found 753.1975.

[Ir(bzq)$_2${MeC(O)=CHC(=N(4-CN-C$_6$H$_4$))Me}] (**5c**): In a Schlenk vessel equipped with a magnetic stirrer, 27.27 mg (0.668 mmol, 10.00 eq.) of NaH (60% dispersion in mineral oil) was placed and washed with anhydrous and deoxygenated toluene (3 x 1.5 mL). In the next step, to the stirred NaH powder, 30.00 mg (0.147 mmol, 2.20 eq.) 4-(4- cyanophenyl)imino-2-pentanone **(3c)** and 4 mL of dried and deoxygenated THF was introduced. The reaction was conducted until hydrogen evolution ceased. The mixture obtained was transferred by a syringe equipped with a syringe-filter disc to a Schlenk vessel of 25 mL capacity, in which a portion of 78.00 mg (0.0667 mmol, 1.00 eq.) of [{Ir(bzq)$_2$(μ-Cl)}$_2$] (**4**) and 2 mL of anhydrous and deoxygenated THF were placed under inert atmosphere. The reaction was conducted at 65℃ for 24 hours. After that, mixture was filtered and concentrated. The remaining crude product was purified by flash chromatography using silica as the solid phase (gradient elution from pure n-hexane to n-hexane:CH_2Cl_2 = 1:2, v/v). Solid material was dried *in vacuo* for 4 hours. The desired product was obtained in 68 % yield (67.87 mg, 0.091 mmol). Elemental anal. calcd for $C_{38}H_{27}IrN_4O$, C 61.03; H 3.64; found C 61.10; H 3.69. ^{1}H NMR (300 MHz, $CDCl_3$) δ = 9.22 (d, *J* = 5 Hz, 1H); 9.06 (d, *J* = 5 Hz, 1H); 8.26 (d, *J* = 8.0 Hz, 1H); 8.17 (d, *J* = 8 Hz, 1H); 7.75 (d, J = 9Hz, 1H); 7.60 (m, 3H); 7.53 (d, *J* = 9 Hz, 1H); 7.48 (d, J = 9Hz, 1H); 6.99 (d, *J* = 8 Hz, 1H); 6.94 (t, J = 8 Hz, 1H); 6.66 (t, J = 8Hz, 1H); 6.60 (d, J = 8Hz, 1H); 6.35 (dd, J = 8 & 2 Hz, 1H); 6.30 (d, J = 7 Hz, 1H); 6.23 (dd, *J* = 8.2 & 1.9 Hz, 1H); 5.94 (d, *J* = 7 Hz, 1H); 4.91 (s, 1H); 4.78 (dd, *J* = 8.1, 2.1 Hz, 1H); 1.70 (s, 3H, -CH_3); 1,59 (s, 3H, - CH_3); HRMS (EI): *m/z* calcd for $C_{38}H_{27}IrN_4O^+$: $[M]^+$ 748.1809, found 748.1825.

[Ir(bzq)$_2${MeC(O)=CHC(=N(4-NO$_2$-C$_6$H$_4$))Me}] (**5d**): Following the procedure used for preparation of **5c**, the reaction was carried out with 200.00 mg (0.171 mmol, 1.00 eq.) of [{Ir(bzq)$_2$(μ-

Cl)}$_2$] (**4**), 68.18 mg (1.713 mmol, 10.00 eq.) of NaH and 82.00 mg (0.377 mmol, 2.20 eq.) of 4-(4-nitrophenyl)imino-2-pentanone **(3d)**. Mixture was filtered and the solvent was fully evaporated from the post-reaction mixture under reduced pressure. The remaining crude product was purified by flash chromatography using silica as the solid phase (gradient elution from pure n-hexane to n-hexane:CH_2Cl_2 = 1:2, v/v). The desired product was obtained in 67 % yield (176.02 mg, 0.229 mmol). Elemental anal. calcd for $C_{37}H_{27}IrN_4O_3$, C 57.88; H 3.54; found C 57.99; H 3.59. ^{1}H NMR (300 MHz, $CDCl_3$) δ = 9.23 (d, J = 6 Hz; 1H); 9.07 (d, J = 6 Hz, 1H); 8.27 (d, J = 9 Hz, 1H); 8.18 (d, J = 6Hz, 1H); 7.75 (d, J = 9Hz, 1H); 7.61 (m, 3H); 7.44 (q, J = 9 Hz, 2H); 7.17 (m, 2H); 6.97 (d, J = 9 Hz, 1H); 6.92 (d, J = 9 Hz, 1H); 6.81 (m, 1H); 6.68 (t, J = 9 Hz, 1H); 6.34 (m, 2H); 5.96 (d, J = 6Hz, 1H); 4.94 (s, 1H, =CH-); 4.80 (dd, 1H); 1.72 (s, 3H, $-CH_3$); 1.62 (s, 3H, $-CH_3$); HRMS (EI): *m/z* calcd for $C_{37}H_{27}IrN_4O_3^+$: $[M]^+$ 768.1707, found 768.1723.

[Ir(bzq)$_2${MeC(O)=CHC(=N(3-NO$_2$-C$_6$H$_4$))Me}] (**5e**): Following the procedure used for preparation of **5c**, the reaction was carried out with 200.00 mg (0.171 mmol, 1.00 eq.) of [{Ir(bzq)$_2$(μ-Cl)}$_2$] (**4**), 68.18 mg (1.713 mmol, 10.00 eq.) of NaH and 82.00 mg (0.377 mmol, 2.20 eq) of 4-(3-nitrophenyl)imino-2-pentanone (**3e**). Mixture was filtered and the solvent was fully evaporated from the post-reaction mixture under reduced pressure. The remaining crude product was purified by flash chromatography using silica as the solid phase (gradient elution from pure n-hexane to n-hexane:CH_2Cl_2 = 1:2, v/v). The desired product was obtained in 80 % yield (210.17 mg, 0.274 mmol). Elemental anal. calcd for $C_{37}H_{27}IrN_4O_3$, C 57.88; H 3.54; found C 58.02; H 3.59. ^{1}H NMR (300 MHz, $CDCl_3$) δ = 9.24 (m, 1H); 9.09 (m, 1H); 8.27 (t, J = 6 Hz, 1H); 8.18 (m, 1H); 7.75 (m, 1H); 7.62 (m, 4H); 7.64 (s, 1H); 7.73 (m, 1H); 7.08 (m, 1H); 6.93 (m, 2H); 6.63 (m, 1H); 6.33 (dd, J = 6 Hz, 1H); 6.07

(m, 1H); 4.93 (s, 1H, =CH–); 1.71 (s, 3H, –CH3); 1.61 (s, 3H, –CH_3); HRMS (EI): *m/z* calcd for $C_{37}H_{27}IrN_4O_3^+$: $[M]^+$ 768.1707, found 768.1725.

[Ir(bzq)$_2${MeC(O)=CHC(=N(2–NO$_2$–C$_6$H$_4$))Me}] (**5f**): In a Schlenk vessel equipped with a magnetic stirrer, 100 mg (0.0856 mmol, 1.00 eq.) of [{Ir(bzq)$_2$(μ–Cl)}$_2$] (**4**), 75.36 mg (0.342 mmol, 4.00 eq.) of 4–(2–nitrophenyl)imino–2–pentanone (**3f**) were placed and then 5 mL of dried and deoxygenated THF was introduced. In the next step, to the stirred mixture 41.13 mg (0.428 mmol, 5 eq.) of NaO^{t}Bu was added. The reaction was conducted at ambient condition for 12 hours. After that, solvent was evaporated under reduced pressure. The remaining crude product was purified by flash chromatography using silica as the solid phase and chloroform as eluent. After evaporation of the solvent the remaining solid was dried *in vacuo* for 4 hours. The desired product was obtained in 60 % yield (78.90 mg, 0.103 mmol). Elemental anal. calcd for $C_{37}H_{27}IrN_4O_3$, C 57.88; H 3.54; found C 57.96; H 3.57. ^{1}H NMR (300 MHz, $CDCl_3$) δ = 9.50 (d, *J* = 5.5 Hz, 1H); 9.18 (d, *J* = 5.5 Hz, 1H); 8.24 (d, *J* = 8.1 Hz, 1H); 8.18 (d, *J* = 8.0 Hz, 1H); 7.76 – 7.56 (m, 4H); 7.47 (d, *J* = 5.0 Hz, 2H); 7.21 (d, *J* = 7.8 Hz, 1H); 7.02 (d, *J* = 7.8 Hz, 1H); 6.96 (d, *J* = 8.2 Hz, 1H); 6.87 (t, *J* = 7.5 Hz, 1H); 6.76 (t, *J* = 7.5 Hz, 1H); 6.24 (t, *J* = 7.8 Hz, 1H); 6.14 – 5.99 (m, 3H); 5.09 (s, 1H); 4.93 (d, *J* = 7.9 Hz, 1H); 1.81 (s, 3H), 1.71 (s, 3H); HRMS (EI): *m/z* calcd for $C_{37}H_{27}IrN_4O_3^+$: $[M]^+$ 768.1707, found 768.1729.

[Ir(bzq)$_2${4–(4–(5–Methyl–2–benzothiazyl)phenyl)imino–2–pentanolato}] (**5g**): Following the procedure used for preparation of **5c**, the reaction was carried out with 134 mg (0.115 mmol, 1 eq.) of [{Ir(bzq)$_2$(μ–Cl)}$_2$] (**4**), 46.1 mg (1.149 mmol; 10 eq.) of KH and 82 mg (0.253 mmol; 2.2 eq.) of (4–(4–(5–Methyl–2–benzothiazyl)phenyl)imino–2–pentanone (**3g**). The crude product was purified by precipitation from DCM/*n*–hexane

mixture and then dried *in vacuo* for 4 hours. The desired product was obtained in 51 % yield (102.07 mg, 0.117 mmol). Elemental anal. calcd for $C_{45}H_{33}IrN_4OS$, C 63.12; H 3.82; found C 62.21; H 3.89. ^{1}H NMR (300 MHz, CD_2Cl_2) δ = 9.35 (dd, 1H, *J* = 5.3 & 1.4 Hz); 9.07 (dd, 1H, *J* = 5.3 & 1.3 Hz); 8.33 (dd, 1H, *J* = 8.0 & 1.4 Hz); 8.25 (dd, 1H, *J* = 8.1 & 1.3 Hz); 7.81 – 7.75 (m, 2H); 7.71 – 7.62 (m, 4H); 7.49 (d, 1H, *J* = 8.8 Hz); 7.35 – 7.23 (m, 3H); 7.02 (dd, 1H, *J* = 8.3 & 2.2 Hz); 6.94 (t, 1H, *J* = 7.5 Hz); 6.85 (d, 1H, *J* = 7.7 Hz); 6.65 (t, 1H, *J* = 7.5 Hz); 6.60 (dd, 1H, *J* = 8.2 & 2.2 Hz); 6.43 (dd, 1H, *J* = 8.3 & 2.2 Hz); 6.31 (dd, 1H, *J* = 7.2 & 1.0 Hz); 5.98 – 5.94 (m, 1H); 4.96 (s, 1H, =CH–); 4.77 (dd, 1H, *J* = 8.2 & 2.2 Hz); 2.47 (s, 3H, $-CH_3$); 1.72 (s, 3H, $-CH_3$); 1.66 (s, 3H, $-CH_3$); HRMS (EI): *m/z* calcd for $C_{45}H_{33}IrN_4OS^+$: $[M]^+$ 870.1999, found 870.2019.

[Ir(bzq)$_2${MeC(O)=CHC(=N(1–Naph))Me}] (**5h**): Following the procedure used for preparation of **5c**, the reaction was carried out with 189 mg (0.162 mmol, 1 eq.) of [{Ir(bzq)$_2$(μ–Cl)}$_2$] (**4**), 64.97 mg (1.620 mmol; 10 eq.) of KH and 80.29 mg (0.356 mmol; 2.2 eq.) of 4–(1–naphthyl)imino–2–pentanone (**3h**). The remaining crude product was purified by flash chromatography using silica as the solid phase (gradient elution from pure n–hexane to n–hexane:CH_2Cl_2 = 1:2, v/v). The desired product was obtained in 64 % yield (160.33 mg, 0.207 mmol). Elemental anal. calcd for $C_{41}H_{30}IrN_3O$, C 63.71; H 3.91; found C 63.86; H 3.97. ^{1}H NMR (300 MHz, $CDCl_3$) δ = 9.47 (d, J = 6 Hz, 1H); 9.35 (d, J = 6Hz, 1H); 9.17 (d, JH = 6 Hz, 1H); 8.27 (d, J = 9 Hz, 2H); 7.74 (m, 4H); 7.48 (m, 1H); 7.22 (m, 2H); 6.90 (m, 2H); 6.67 (t, JH = 9 Hz, 2H); 6.16 (d, J = 6 Hz, 1H); 5.98 (d, J = 9 Hz, 1H); 5.92 (d, J = 6 Hz, 1H); 4.97 (s, 1H, =CH–); 1.78 (s, 3H, $-CH_3$); 1.59 (s, 3H, $-CH_3$); HRMS (EI): *m/z* calcd for $C_{41}H_{30}IrN_3O^+$: $[M]^+$ 773.2013, found 773.2033.

[Ir(bzq)$_2${MeC(O)=CHC(=N(2-Naph))Me}] (**5i**): Following the procedure used for preparation of **5c**, the reaction was carried out with 189 mg (0.162 mmol, 1 eq.) of [{Ir(bzq)$_2$(μ-Cl)}$_2$] (**4**), 64.97 mg (1.620 mmol; 10 eq.) of KH and 80.29 mg (0.356 mmol; 2.2 eq.) of 4-(2-naphthyl)imino-2-pentanone (**3i**). The remaining crude product was purified by flash chromatography using silica as the solid phase (gradient elution from pure n-hexane to n-hexane:CH_2Cl_2 = 1:2, v/v). The desired product was obtained in 70 % yield (174.74 mg, 0.226 mmol). Elemental anal. calcd for $C_{41}H_{30}IrN_3O$, C 63.71; H 3.91; found C 63.83; H 3.96. ^{1}H NMR (300 MHz, $CDCl_3$) δ = 9.44 (d, *J* = 4.8 Hz); 9.37 (d, *J* = 5.2 Hz, 2H); 9.18 (d, *J* = 5.2 Hz, 2H); 9.13 (d, *J* = 4.8 Hz); 8.27 (m, *J* = 6.9 Hz); 8.14 (d, *J* = 7.9 Hz); 7.74 (m); 7.69–7.55 (m); 7.37 (d, *J* = 8.8 Hz); 7.31 (d, *J* = 7.9 Hz); 7.24 – 7.20 (m); 7.18 – 7.13 (m); 7.07 (m); 6.99 (d, *J* = 8.8 Hz); 6.96 – 6.87 (m); 6.78 (d, *J* = 8.8 Hz); 6.66 (m); 6.56 (m); 6.46 – 6.34 (m); 6.30 (d, *J* = 7.2 Hz); 5.98 – 5.91 (m); 4.99 (d, *J* = 2.0 Hz); 4.96 (dd, *J* = 8.6 & 2.1 Hz); 4.91 (s), 4.89 (s, 1H), 1.72 (s), 1.71 (s, 3H), 1.65 (s, 3H), 1.64 (s); HRMS (EI): *m/z* calcd for $C_{41}H_{30}IrN_3O^+$: $[M]^+$ 773.2013, found 773.2029.

[Ir(bzq)$_2${MeC(O)=CHC(=N(1-anthracenyl))Me}] (**5j**): Following the procedure used for preparation of **5c**, the reaction was carried out with 142 mg (0.121 mmol, 1 eq.) of [{Ir(bzq)$_2$(μ-Cl)}$_2$] (**4**), 48.5 mg (1.214 mmol; 10 eq.) of KH and 73.5 mg (0.267 mmol; 2.2 eq.) of 4-(1-anthracenyl)imino-2-pentanone (**3j**). The remaining crude product was purified by flash chromatography using silica treated with triethylamine as the solid phase (gradient elution from pure n-hexane to n-hexane: AcOEt = 6:4, v/v). The purified material was dried *in vacuo* for 4 hours. The desired product was obtained in 25% yield (50.0 mg, 0.061 mmol). Elemental anal. calcd for $C_{45}H_{32}IrN_3O$, C 65.67; H 3.92; found C 65.80; H 3.97. ^{1}H NMR (300 MHz, CD_2Cl_2) δ (ppm) = 9.55

(dd, 1H, *J* = 5.4 & 1.3 Hz); 9.22 (dd, 1H, *J* = 5.4 & 1.4 Hz); 8.35 (dd, 1H, *J* = 8.0 & 1.3 Hz); 7.80 – 7.66 (m, 5H); 7.47 – 7.40 (m, 2H); 7.37 – 7.24 (m, 4H); 7.20 (s, 1H); 7.01 (d, 1H, *J* = 8.8 Hz); 6.97 (d, 1H, *J* = 8.4 Hz); 6.86 (t, 1H, *J* = 7.5 Hz); 6.81 – 6.76 (m, 1H); 6.70 – 6.52 (m, 4H); 6.05 (dd, 1H, *J* = 7.2 & 1.0 Hz); 5.86 (dd, 1H, *J* = 7.2 & 1.0 Hz); 5.09 (s, 1H, =CH–); 1.85 (s, 3H, $-CH_3$); 1.68 (s, 3H, CH_3); HRMS (EI): *m/z* calcd for $C_{45}H_{32}IrN_3O^+$: $[M]^+$ 823.2169, found 823.2197.

[Ir(bzq)$_2${MeC(O)=CHC(=N(2-anthracenyl))Me}] (**5k**): Following the procedure used for preparation of **5c**, the reaction was carried out with 142 mg (0.121 mmol, 1 eq.) of [{Ir(bzq)$_2$(μ-Cl)}$_2$] (**4**), 48.5 mg (1.214 mmol; 10 eq.) of KH and 73.5 mg (0.267 mmol; 2.2 eq.) of 4-(2-anthracenyl)imino-2-pentanone (**3k**). The remaining crude product was purified by flash chromatography using silica treated with triethylamine as the solid phase (gradient elution from pure n-hexane to n-hexane: AcOEt = 6:4, v/v). The purified material was dried *in vacuo* for 4 hours. The desired product was obtained in 38 % yield (74.8 mg, 0.091 mmol). Elemental anal. calcd for $C_{45}H_{32}IrN_3O$, C 65.67; H 3.92; found C 65.77; H 3.96. ^{1}H NMR (300 MHz, $CDCl_3$) δ = 6.49 (d, *J* = 6.0); 9.39 (d, *J* = 5.1 Hz, 1H); 9.21 (d, *J* = 5.1 Hz, 1H); 9.15 (d, *J* = 5.2 Hz), 8.30–8.23 (m); 8.20 – 8.13 (m, 1H); 7.89 (s, 1H); 7.83 – 7.78 (m); 7.77 – 7.71 (m); 7.70 – 7.65 (m); 7.65 – 7.59 (m); 7.39 – 7.31 (m); 7.24 – 7.20 (m); 7.16 (s, 1H); 7.08 (d, *J* = 8.7 Hz, 1H); 6.95 (d, *J* = 8.8 Hz, 1H); 6.92 (t, *J* = 7.5 Hz, 1H); 6.87 (s, 1H); 6.79 (d, *J* = 8.7 Hz, 1H); 6.61 (d, *J* = 8.7 Hz, 1H); 6.58 – 6.53 (m); 6.46 (s); 6.39 (s); 6.28 (t, *J* = 7.0 Hz, 1H); 6.14 (d, *J* = 7.7 Hz, 0H), 5.99 – 5.97 (d, *J* = 7.3 Hz, 1H), 5.12 (s, 1H); 5.01 (dd, *J* = 8.9, 2.0 Hz); 4.94 (s); 4.92 (s, 1H); 1.75 (s); 1.72 (s, 3H); 1.70 (s, 3H); 1.68 (s); HRMS (EI): *m/z* calcd for $C_{45}H_{32}IrN_3O^+$: $[M]^+$ 823.2169, found 823.2198.

[Ir(bzq)$_2${MeC(O)=CHC(=N(9-anthracenyl))Me}] (5l): Following the procedure used for preparation of **5c**, the reaction was carried out with 142 mg (0.121 mmol, 1 eq.) of [{Ir(bzq)$_2$(μ-Cl)}$_2$] (**4**), 48.5 mg (1.214 mmol; 10 eq.) of KH and 73.5 mg (0.267 mmol; 2.2 eq.) of 4-(9-anthracenyl)imino-2-pentanone (**31**). The remaining crude product was purified by flash chromatography using silica treated with triethylamine as the solid phase (gradient elution from pure n-hexane to n-hexane: AcOEt = 6:4, v/v). The purified material was dried *in vacuo* for 4 hours. The desired product was obtained in 63 % yield (127.0 mg, 0.154 mmol). Elemental anal. calcd for $C_{45}H_{32}IrN_3O$, C 65.67; H 3.92; found C 65.82; H 3.97. ^{1}H NMR (300 MHz, CD_2Cl_2) δ = δ 10.08 (d, *J* = 5.3 Hz); 9.98 (d, *J* = 5.5 Hz, 1H); 9.23 (d, *J* = 5.3 Hz); 9.14 (d, *J* = 5.5 Hz, 1H); 8.45 – 8.30 (m, 3H); 7.93 – 7.82 (m); 7.79 – 7.66 (m); 7.65 – 7.53 (m); 7.47 – 7.38 (m); 7.32 (s, 1H); 7.26 (d, *J* = 8.6 Hz); 7.18 (d, *J* = 7.3 Hz); 7.14 – 7.08 (m); 7.01 – 6.88 (m); 6.83 – 6.73 (m); 6.59 (t, *J* = 7.5 Hz, 1H); 6.52 (d, *J* = 8.0 Hz); 6.44 (d, *J* = 7.8 Hz, 1H); 5.94 (t, *J* = 7.2 Hz, 1H); 5.86 (d, *J* = 7.4 Hz, 1H); 5.81 (t, *J* = 7.5 Hz, 1H); 5.61 (s); 5.44 (t, *J* = 6.3 Hz, 1H); 5.24 (s, 1H), 5.02 (s); 2.50 (s), 2.05 (s), 1.85 (s, 3H), 1.62 (s, 3H); HRMS (EI): *m/z* calcd for $C_{45}H_{32}IrN_3O^+$: $[M]^+$ 823.2169, found 823.2193.

References

(1) Witkowska, E.; Wiosna–Salyga, G.; Głowacki, I.; Orwat, B.; Oh, M–j.; Kownacki, I.; Kubicki, M.; Gierczyk, B.; Dutkiewicz, M.; Cieszko, P.; Luszczynska, B.; Ulanski, J.; Grzelak, I.; Hoffmann, M.; Ledwon, P.; Lapkowski, M. Effect of fluorine substitution of the β-ketoiminate ancillary ligand on photophysical properties and electroluminescence ability of new iridium(III) complexes. *J. Mater. Chem. C* **2018**, *6*, 8688–8708.

2. NMR spectra of 4-arylimino-2-pentanones

^{1}H NMR

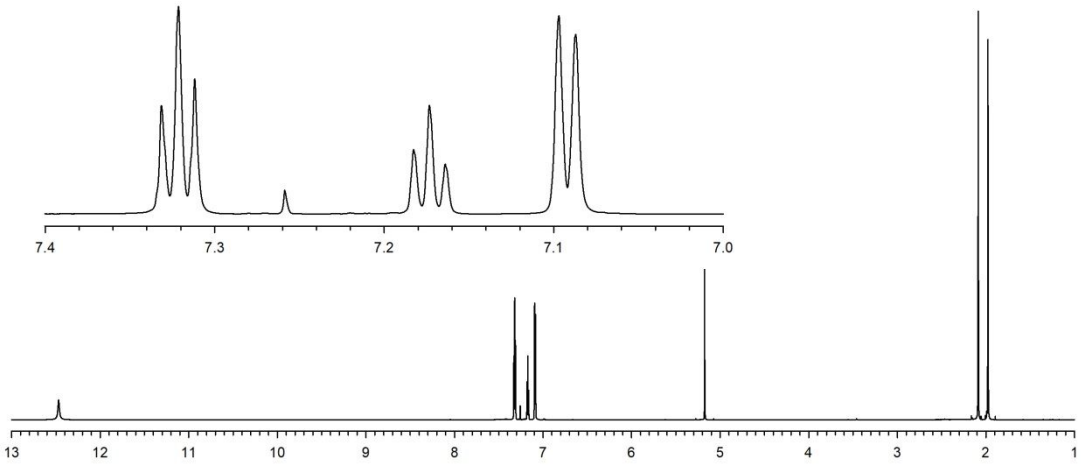

^{13}C NMR

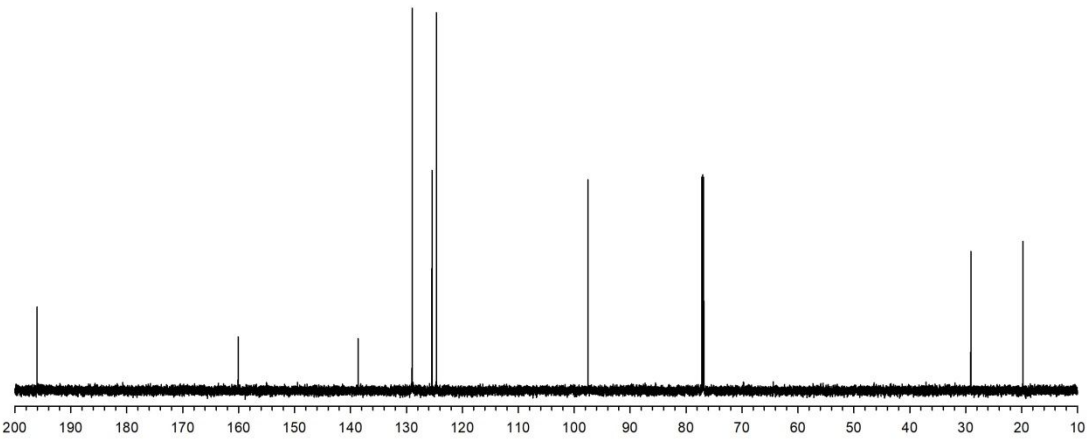

Fig. 1S. NMR spectra of 4-phenylimino-2-pentanone (**3a**)

^{1}H NMR

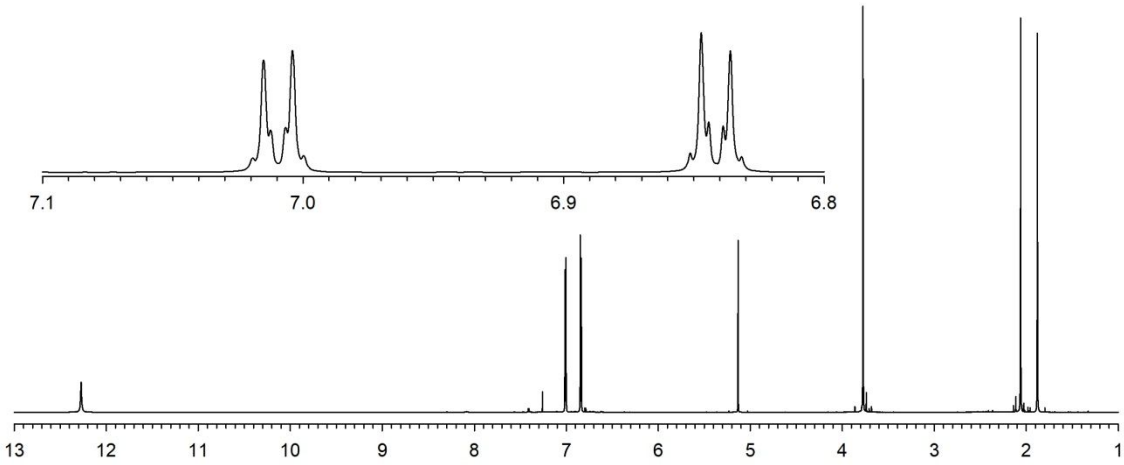

^{13}C NMR

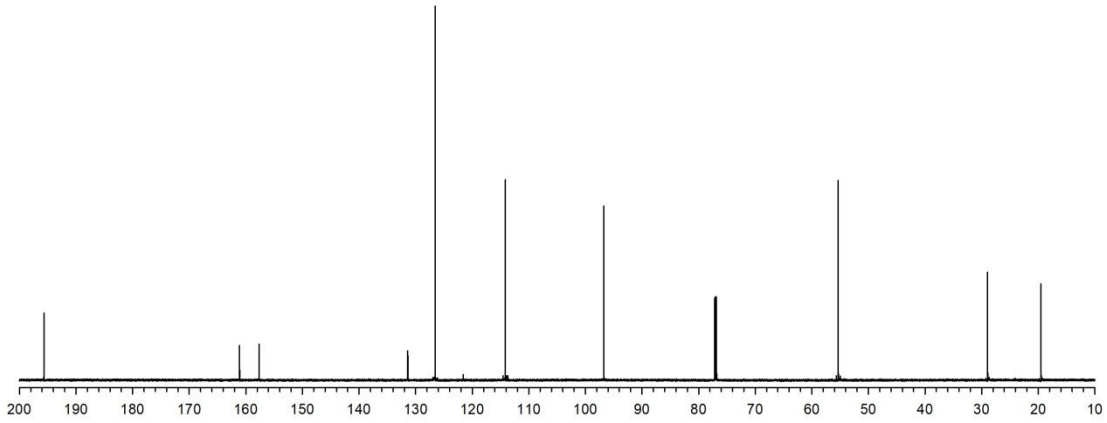

Fig. 2S. NMR spectra of 4-(4-methoxyphenyl)imino-2-pentanone (**3b**)

^{1}H NMR

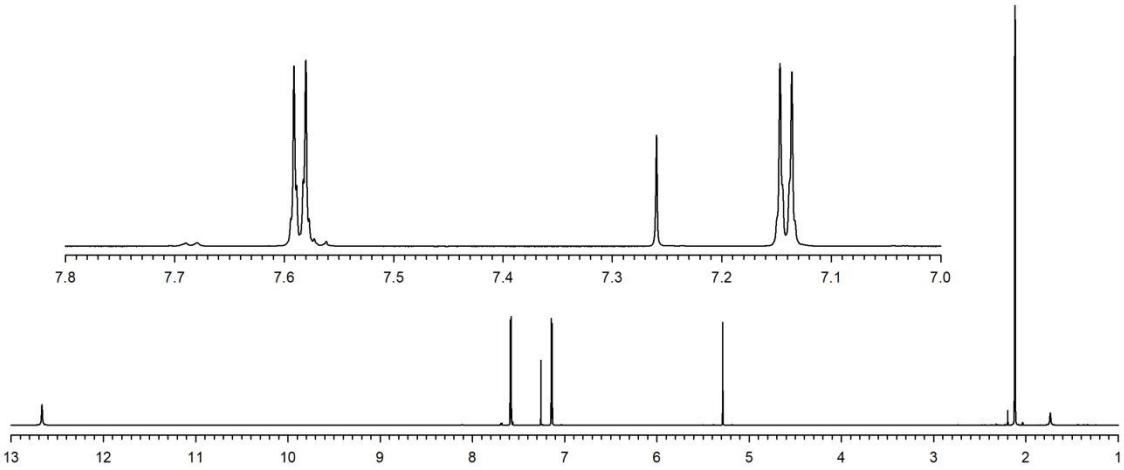

^{13}C NMR

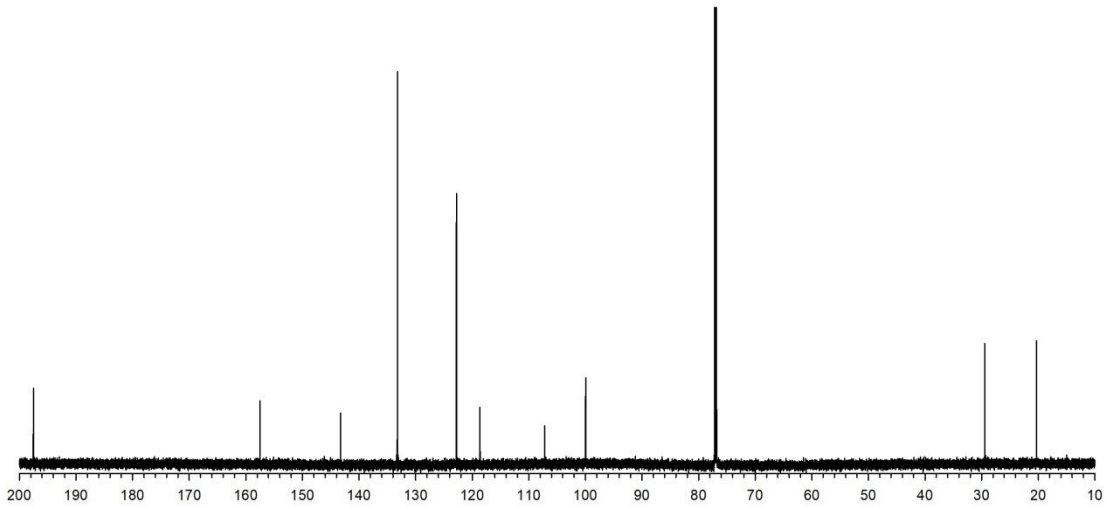

Fig. 3S. NMR spectra of 4-(4-cyanophenyl)imino-2-pentanone (**3c**)

^{1}H NMR

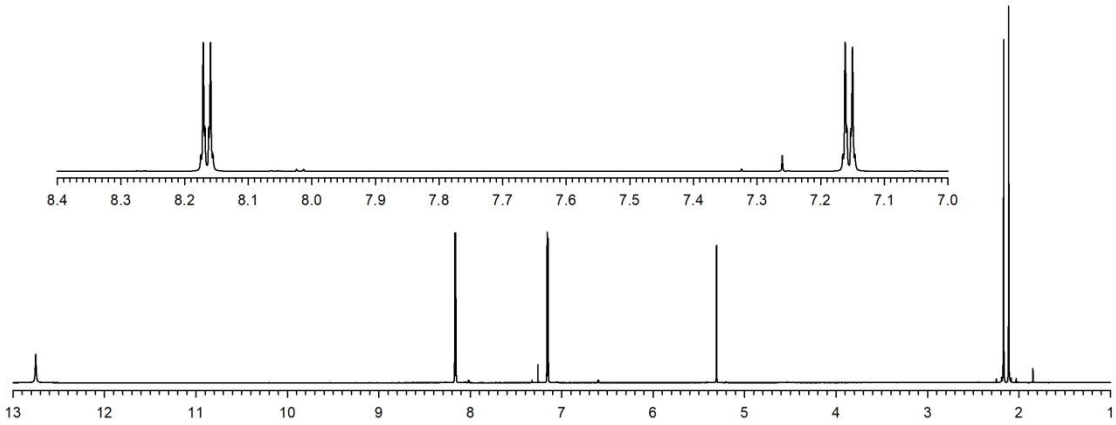

^{13}C NMR

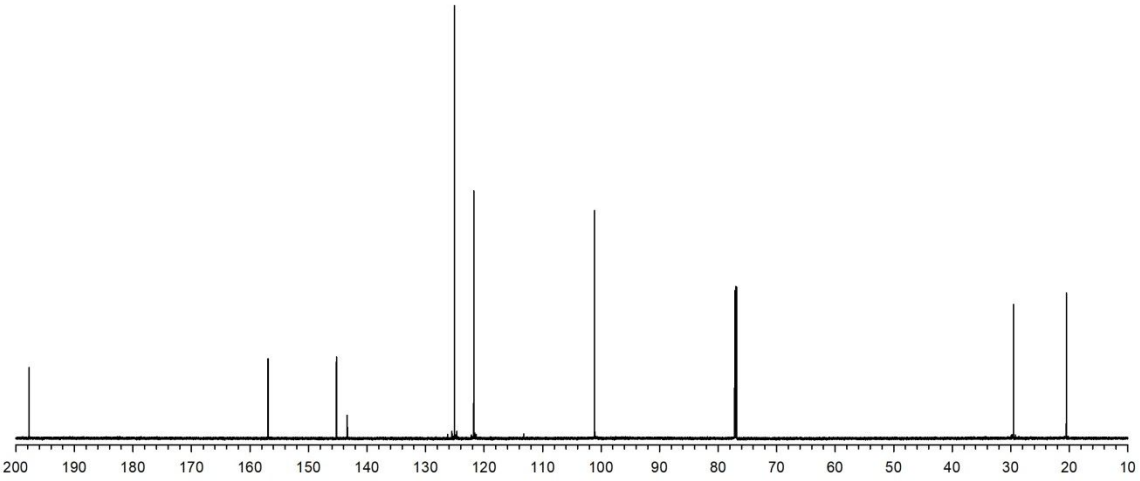

Fig. 4S. NMR spectra of 4-(4-nitrophenyl)imino-2-pentanone (**3d**)

^{1}H NMR

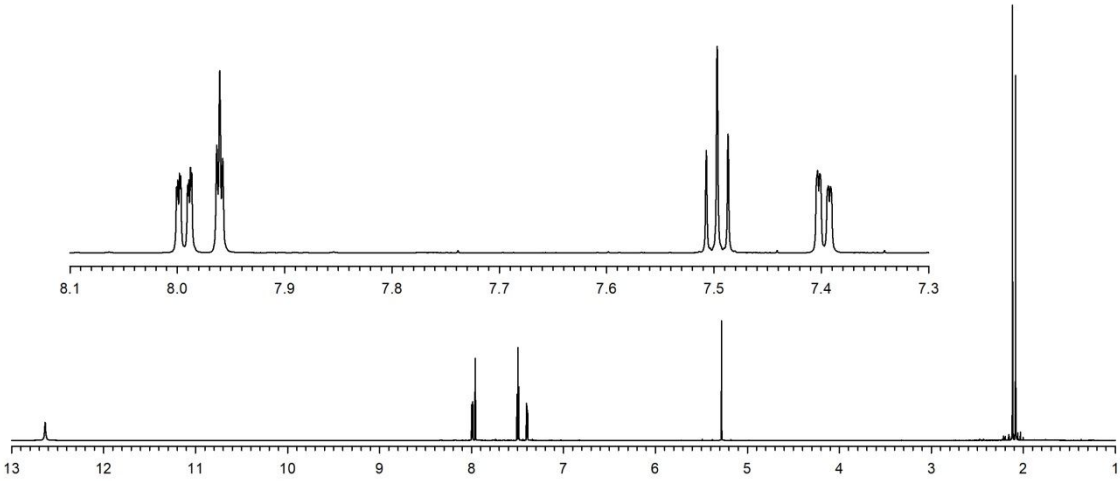

^{13}C NMR

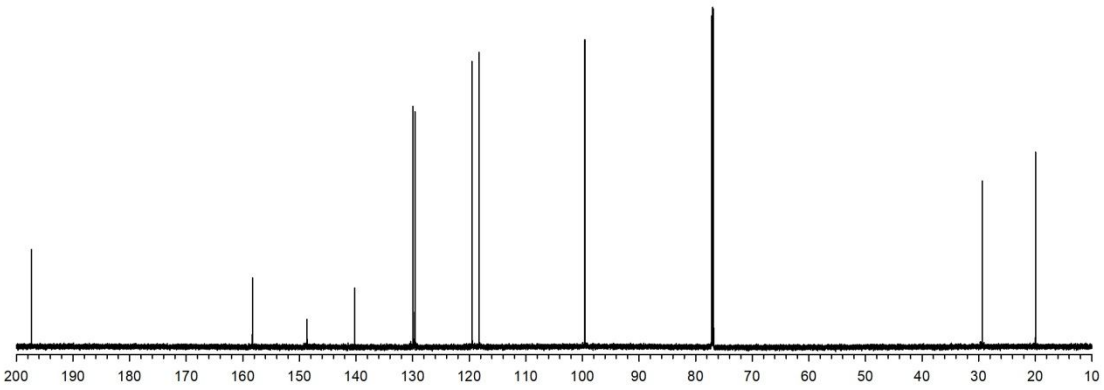

Fig. 5S. NMR spectra of 4-(3-nitrophenyl)imino-2-pentanone (**3e**)

^{1}H NMR

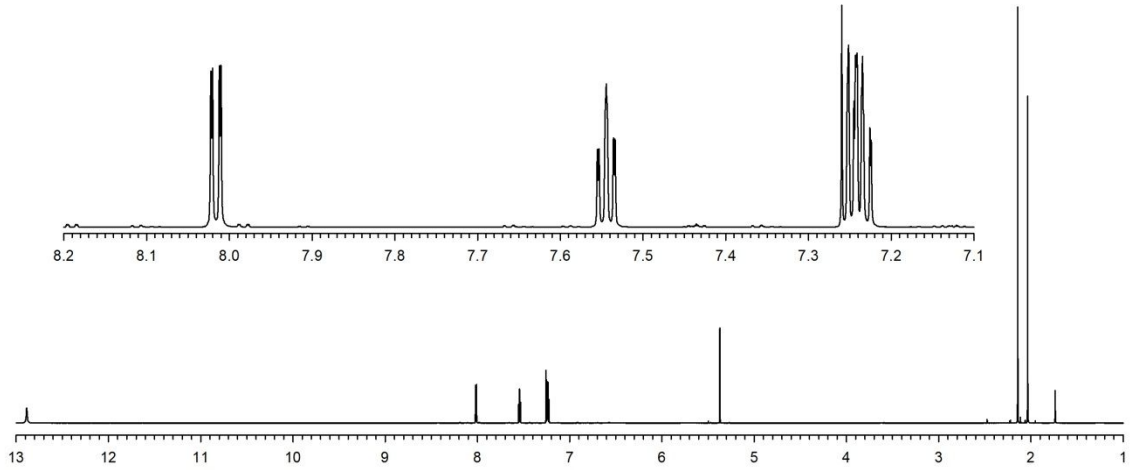

^{13}C NMR

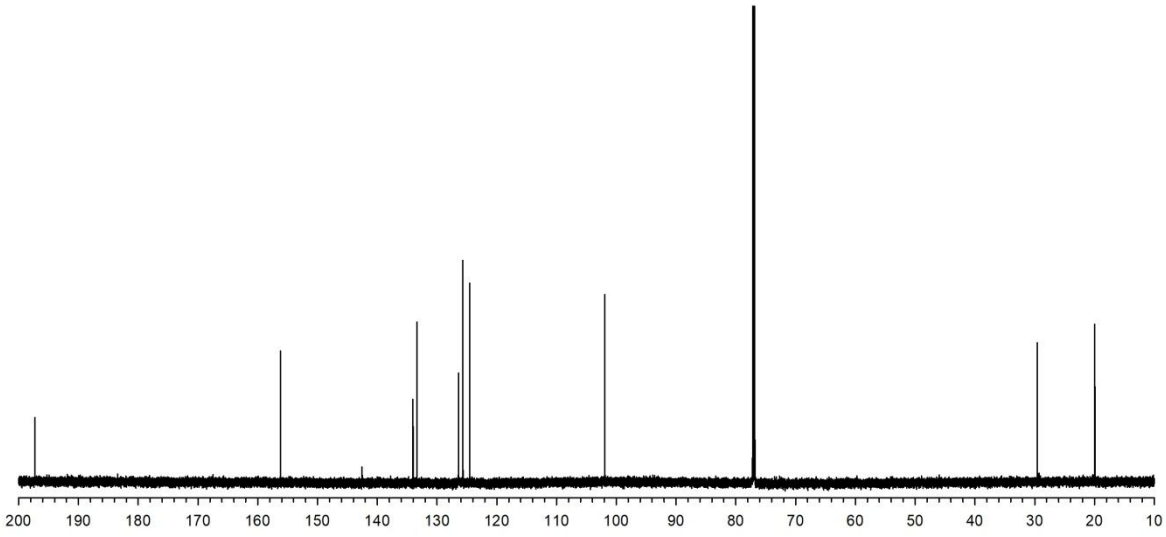

Fig. 6S. NMR spectra of 4-(2-nitrophenyl)imino-2-pentanone (**3f**)

^{1}H NMR

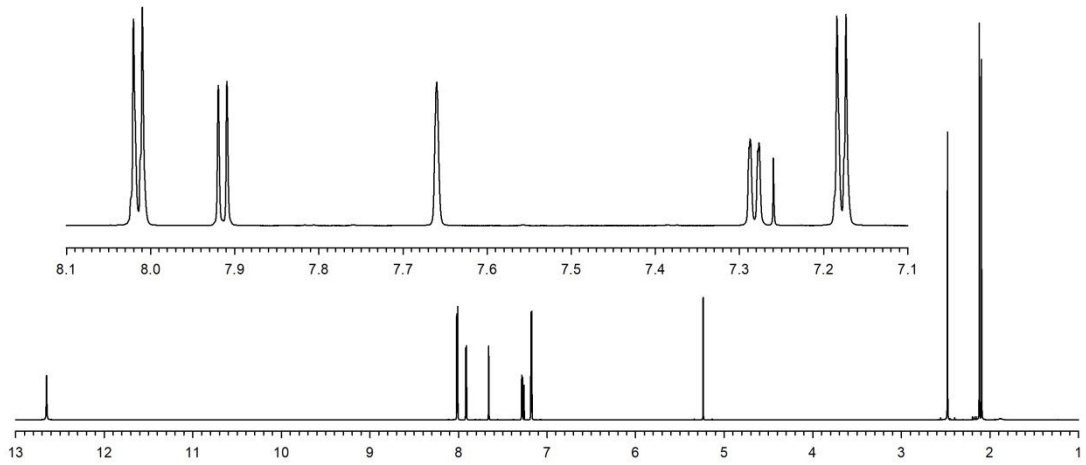

^{13}C NMR

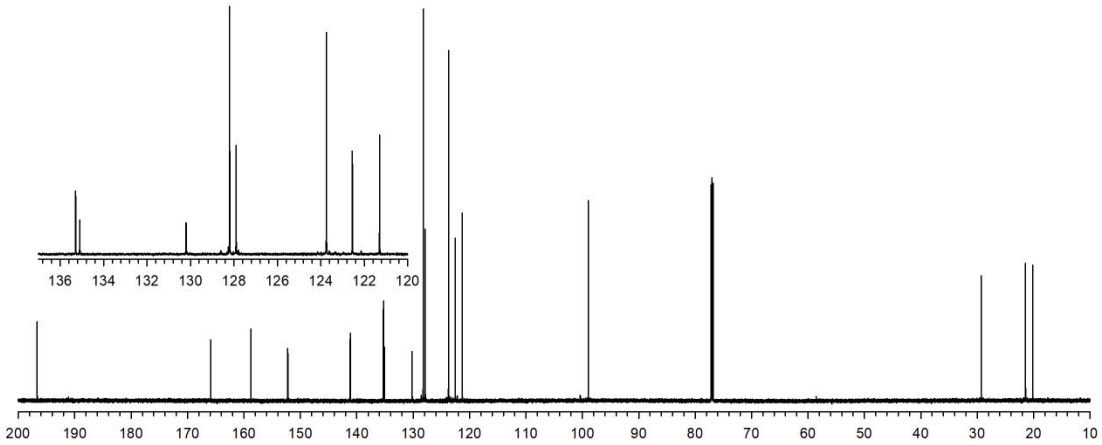

Fig. 7S. NMR spectra of 4-(4-(5-methyl-2-benzothiazyl)phenyl)imino-2-pentanone (**3g**)

^{1}H NMR

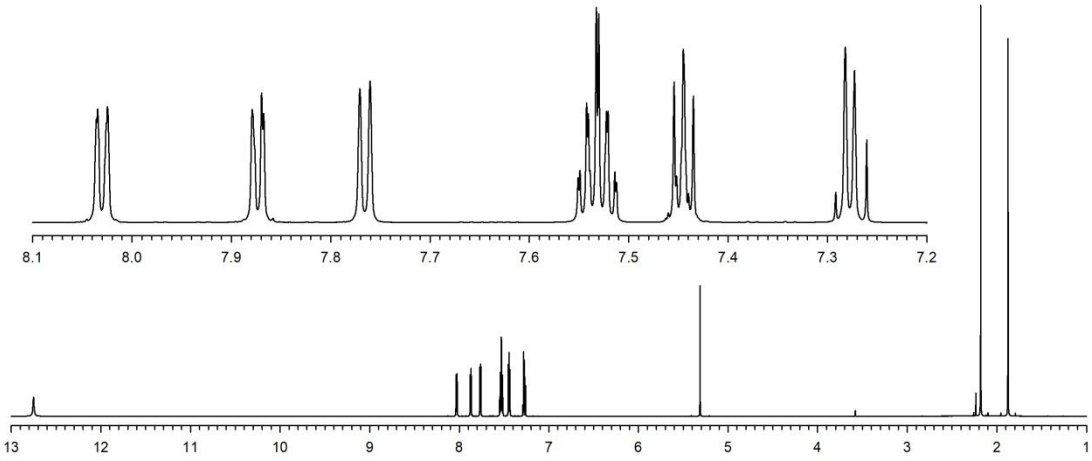

^{13}C NMR

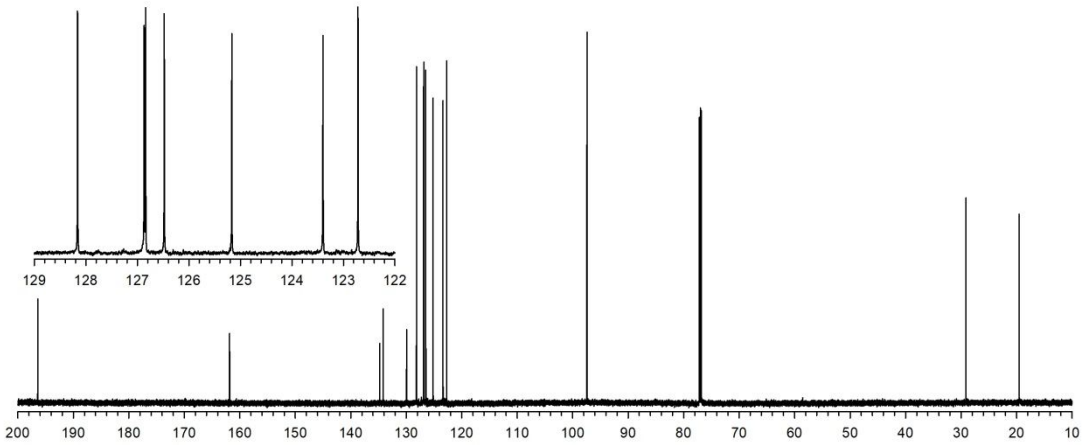

Fig. 8S. NMR spectra of 4-(1-naphthyl)imino-2-pentanone (**3h**)

^{1}H NMR

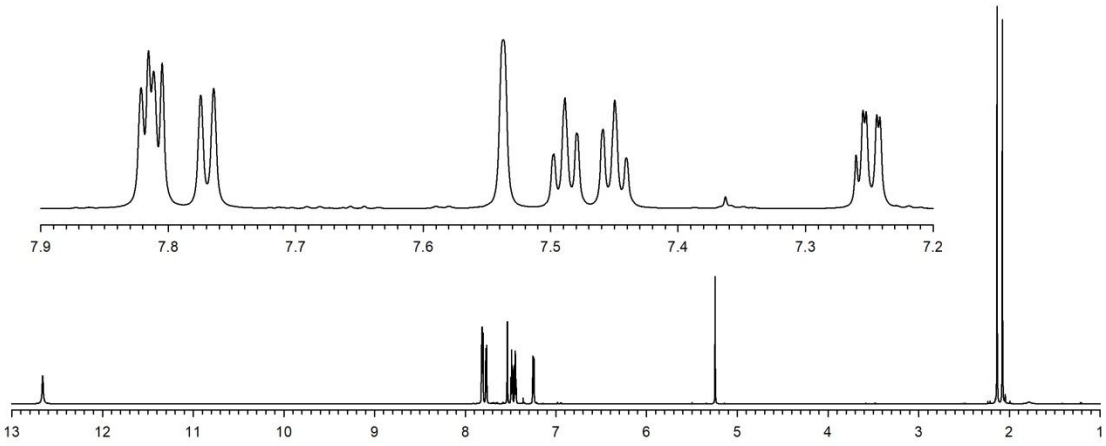

^{13}C NMR

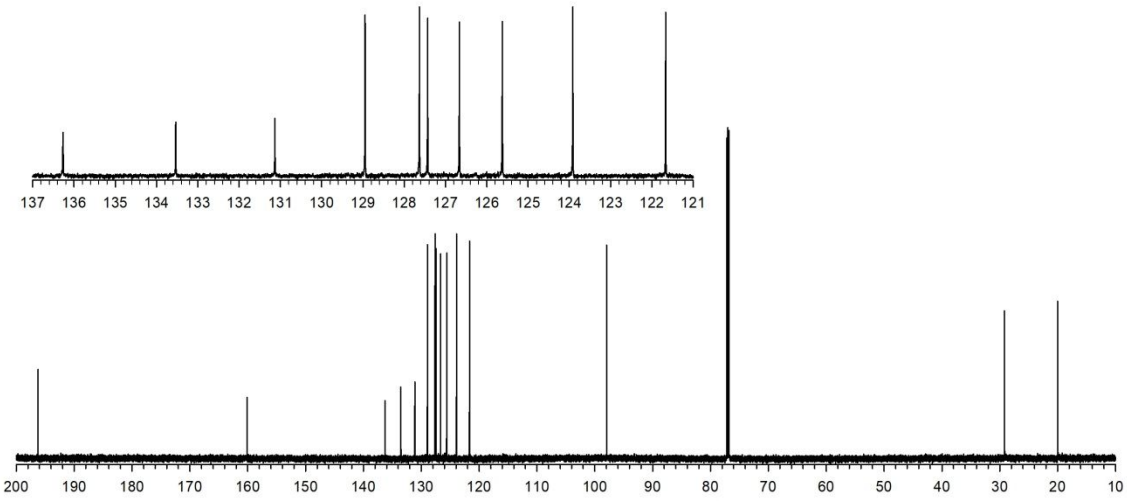

Fig. 9S. NMR spectra of 4-(2-naphthyl)imino-2-pentanone (**3i**)

^{1}H NMR

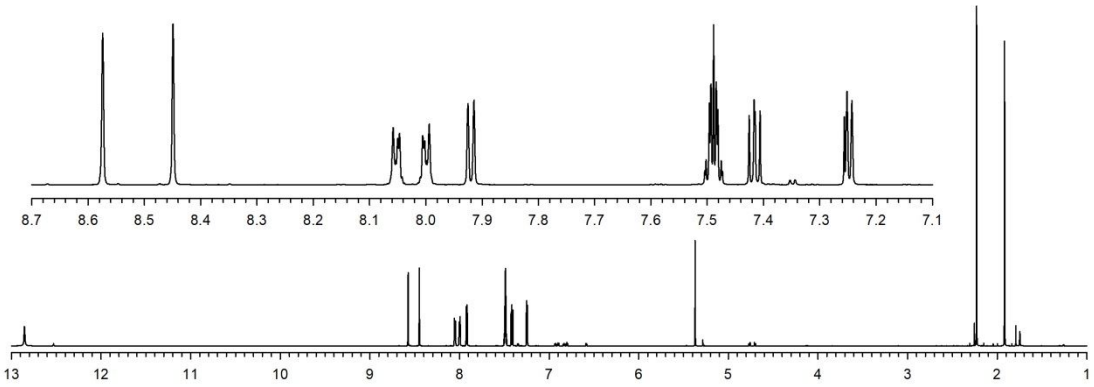

^{13}C NMR

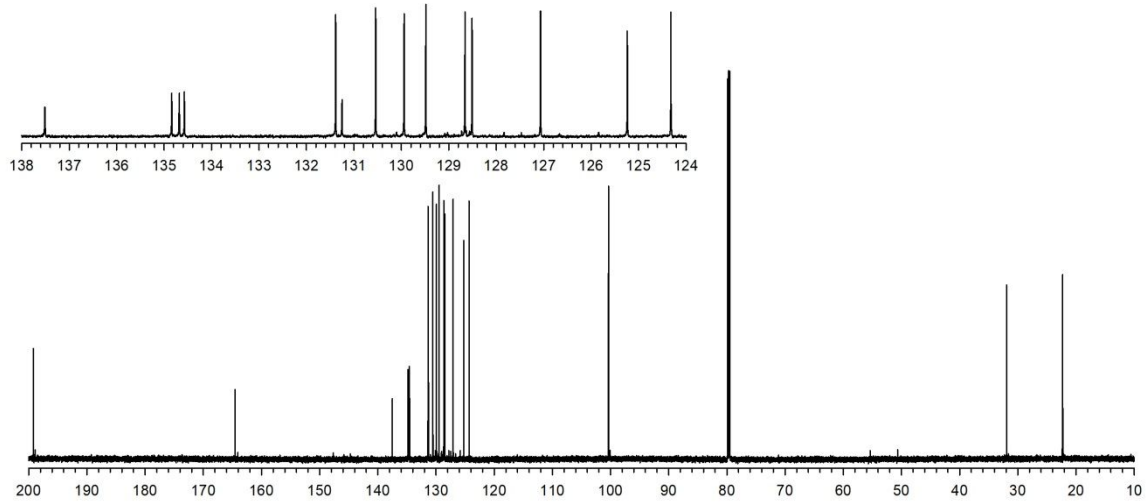

Fig. 10S. NMR spectra of 4-(1-anthracenyl)imino-2-pentanone (**3j**)

^{1}H NMR

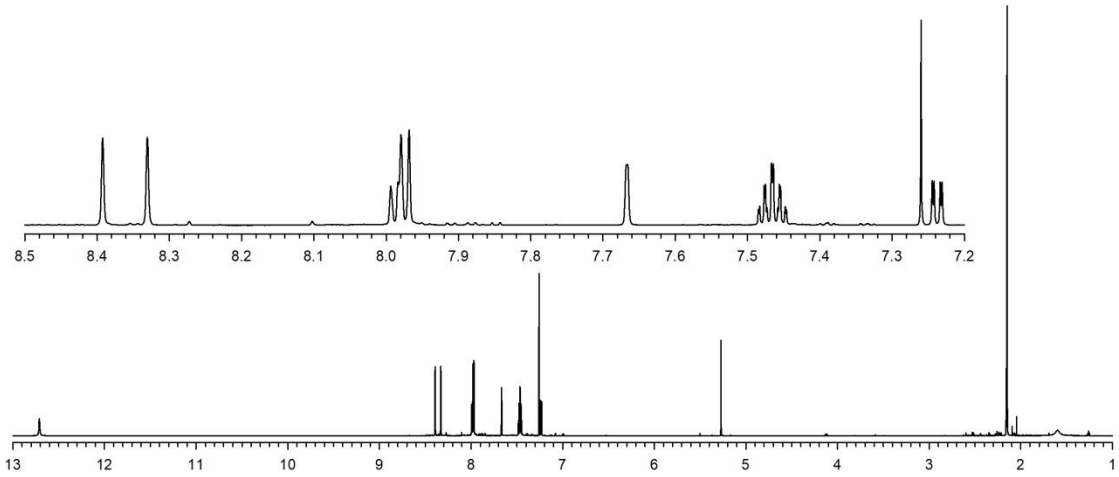

^{13}C NMR

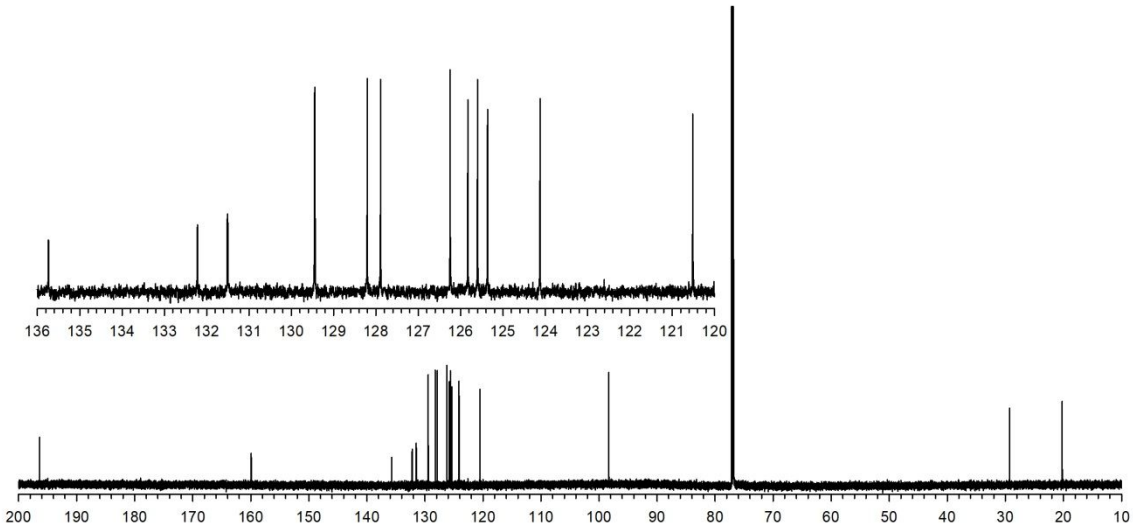

Fig. 11S. NMR spectra of 4-(2-anthracenyl)imino-2-pentanone (**3k**)

^{1}H NMR

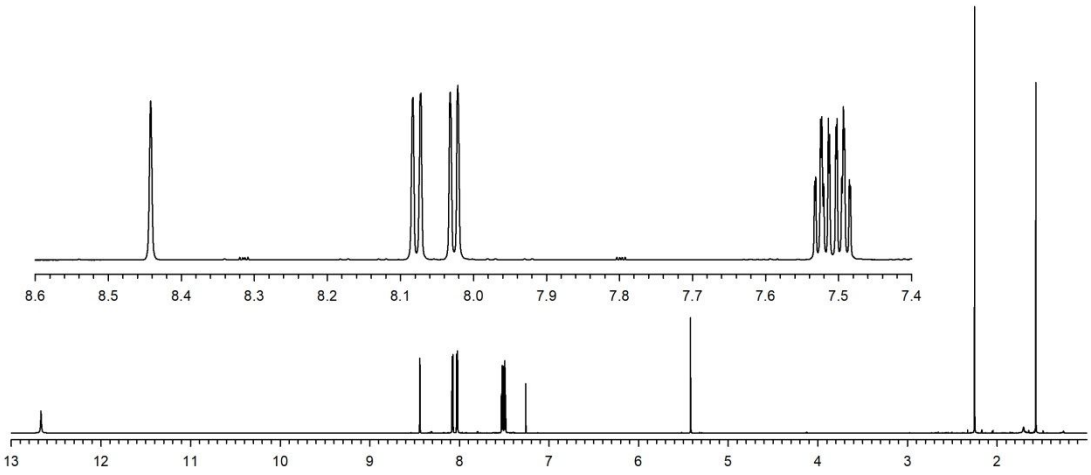

^{13}C NMR

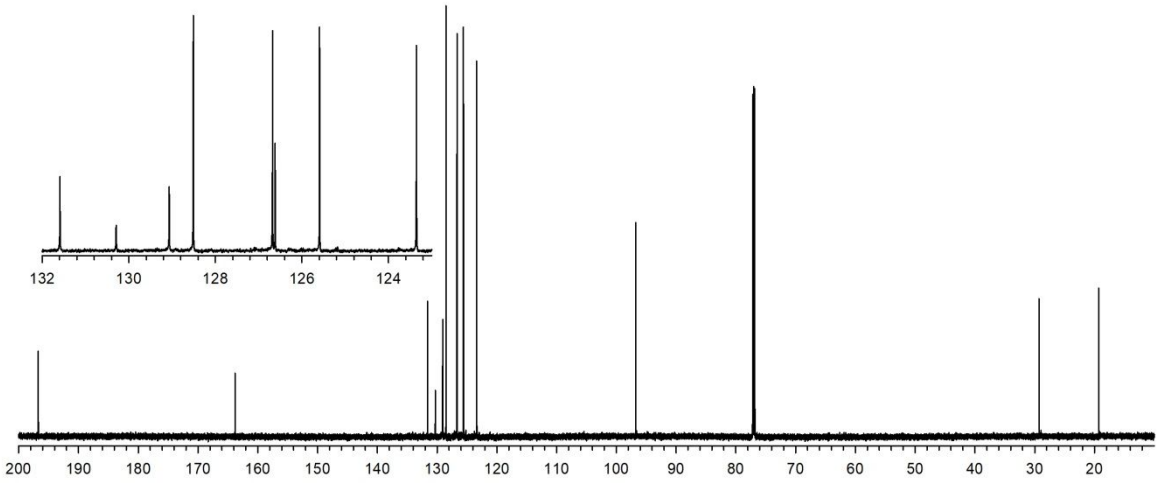

Fig. 12S. NMR spectra of 4-(9-anthracenyl)imino-2-pentanone (**3l**)

3. NMR spectra of iridium(III) complexes

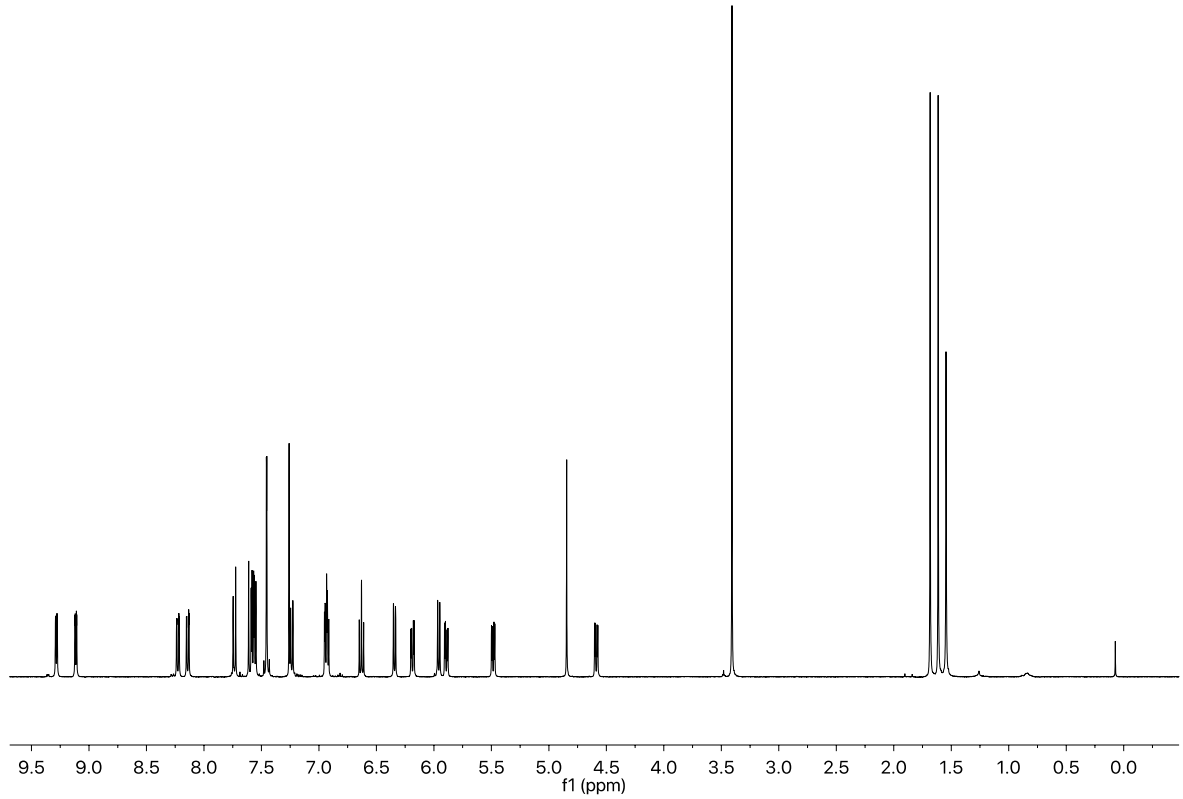

Fig. 13S. ^{1}H NMR spectrum of **5b**

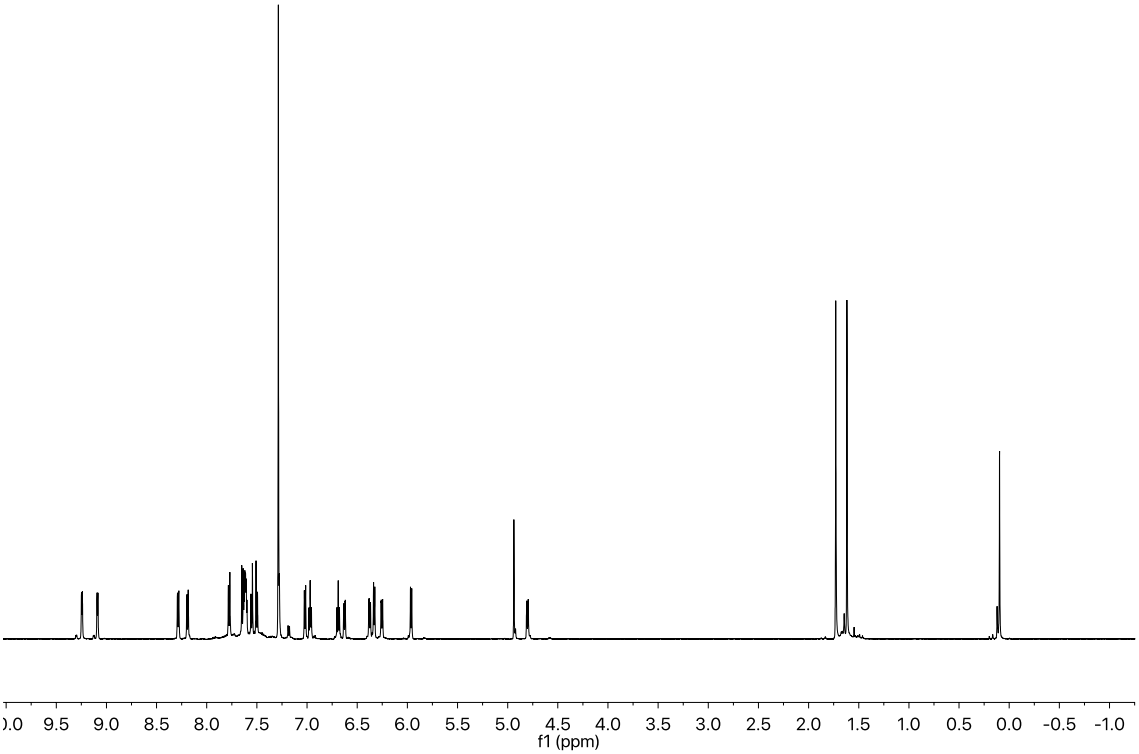

Fig. 14S. ^{1}H NMR spectrum of **5c**

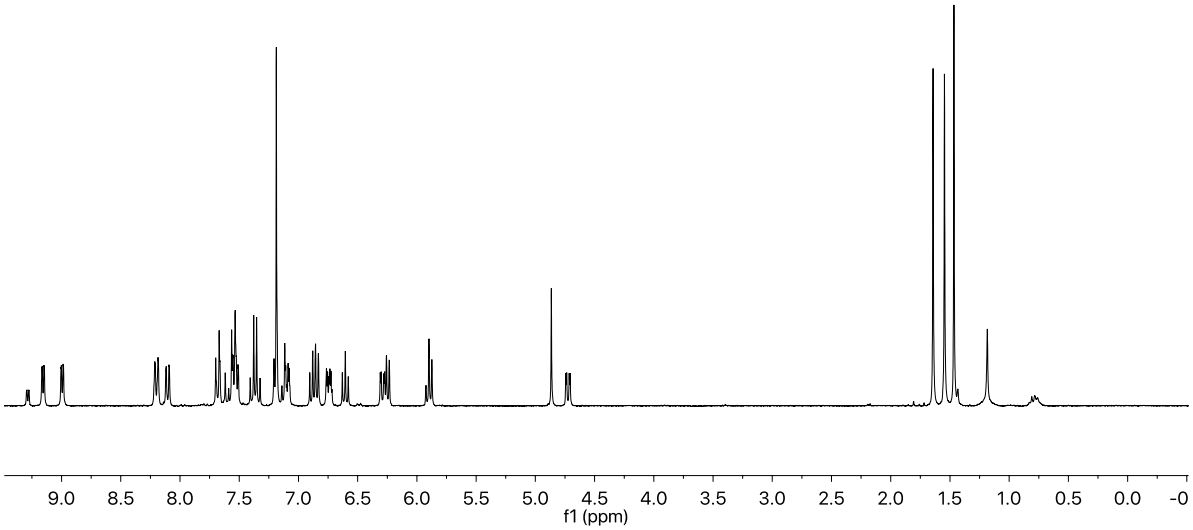

Fig. 15S. ^{1}H NMR spectrum of **5d**

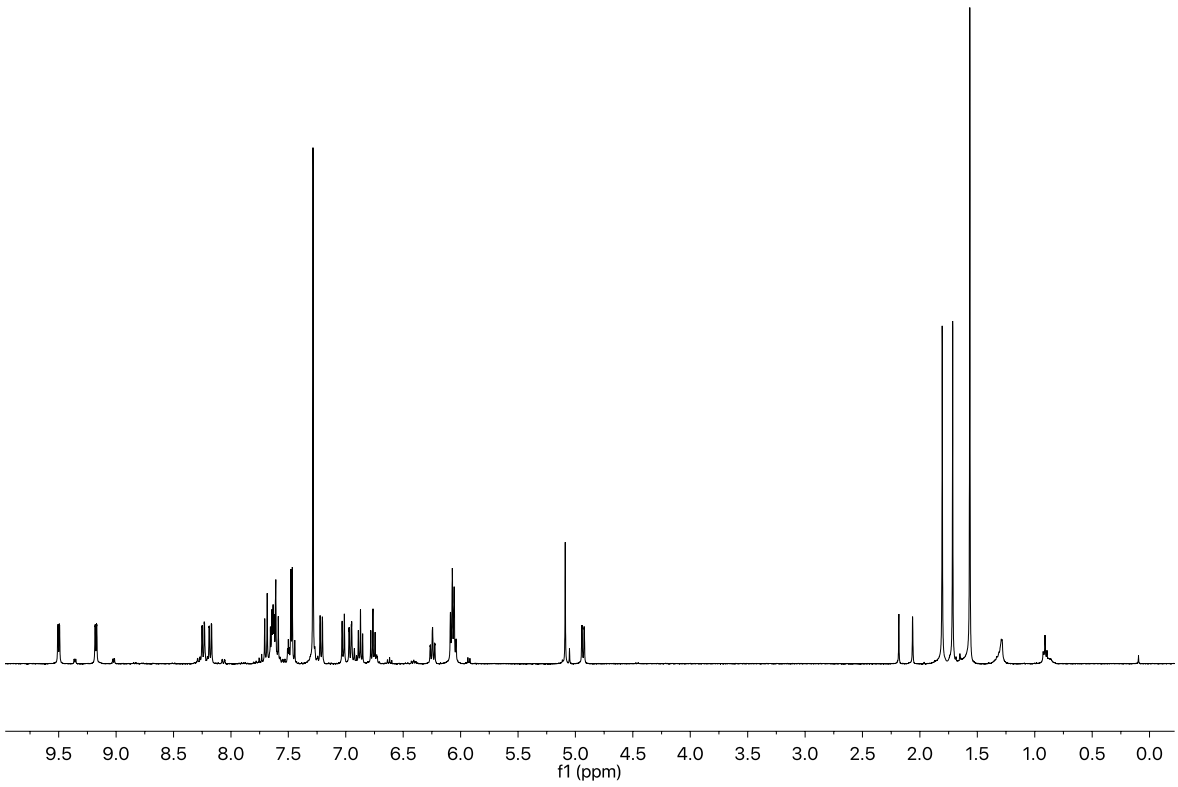

Fig. 16S. ^{1}H NMR spectrum of **5f**

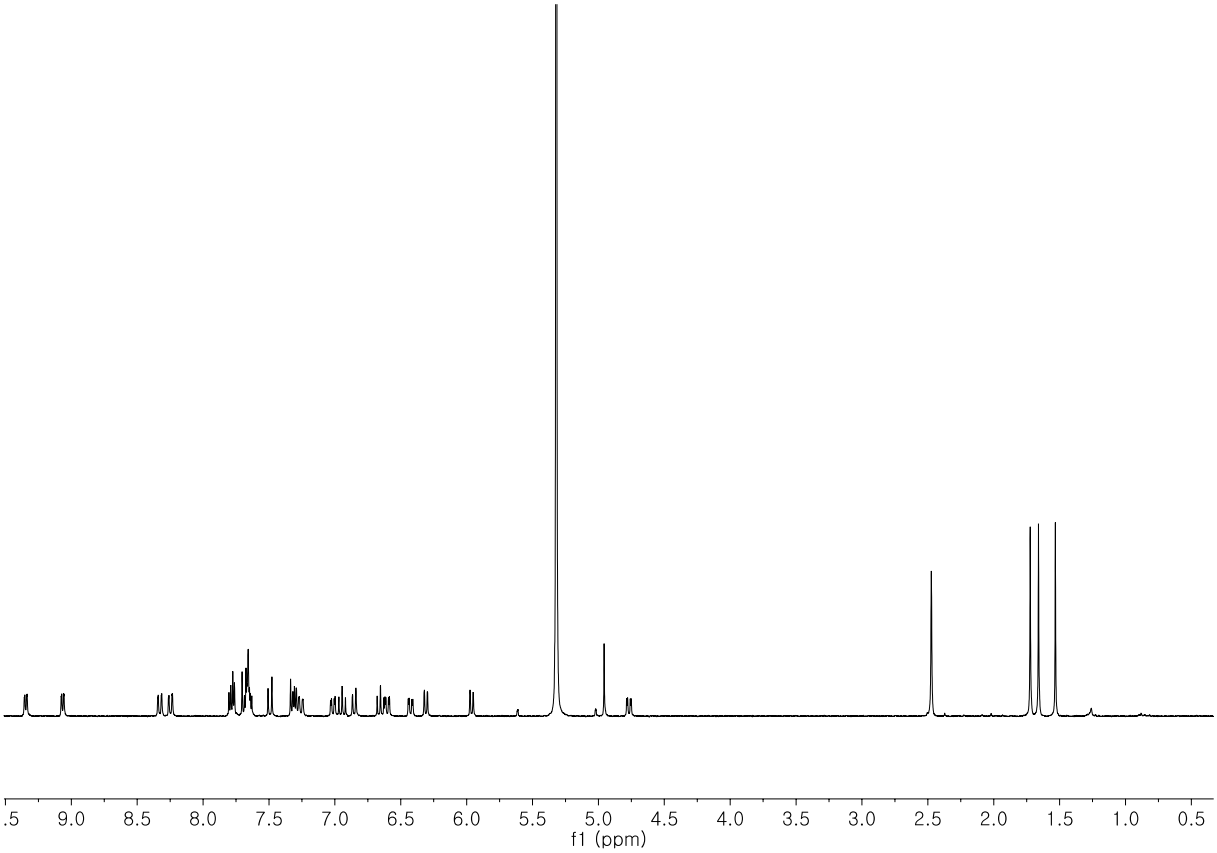

Fig. 17S. ^{1}H NMR spectrum of **5g**

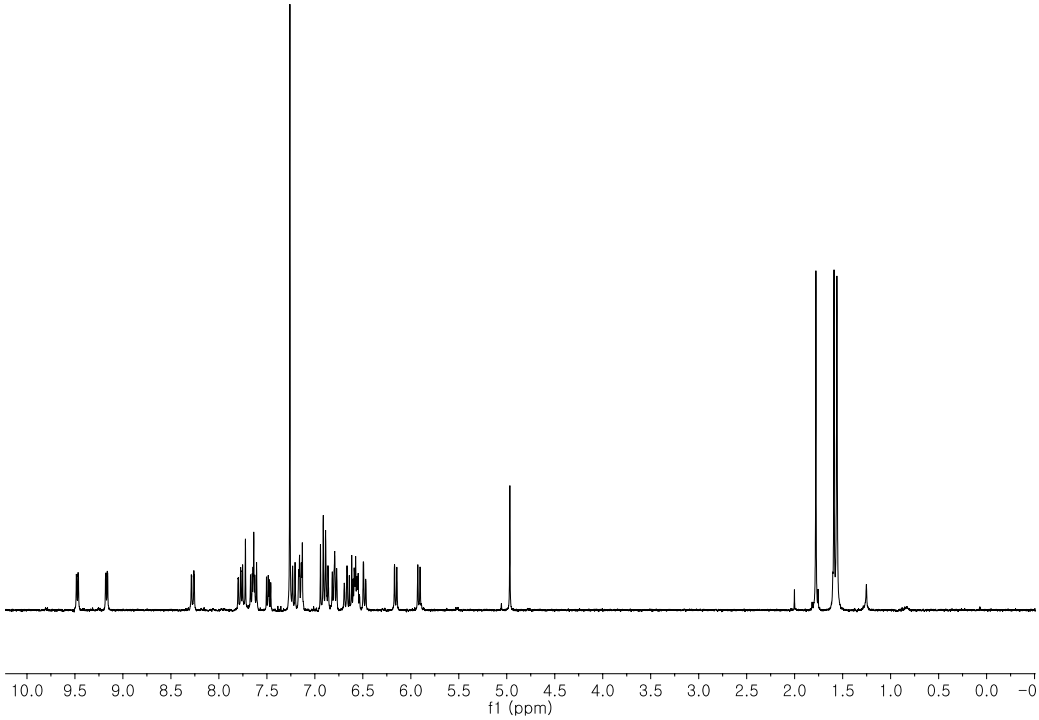

Fig. 18S. ^{1}H NMR spectrum of **5h**

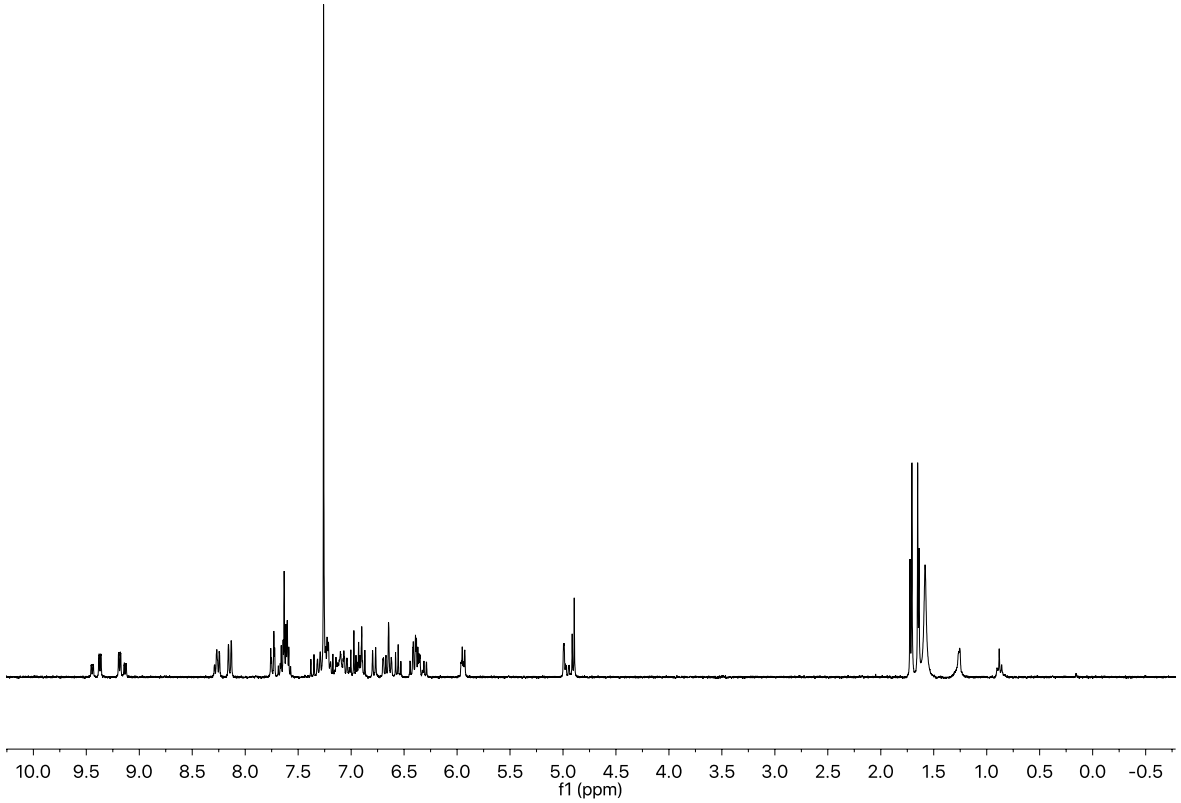

Fig. 19S. ^{1}H NMR spectrum of **5i**

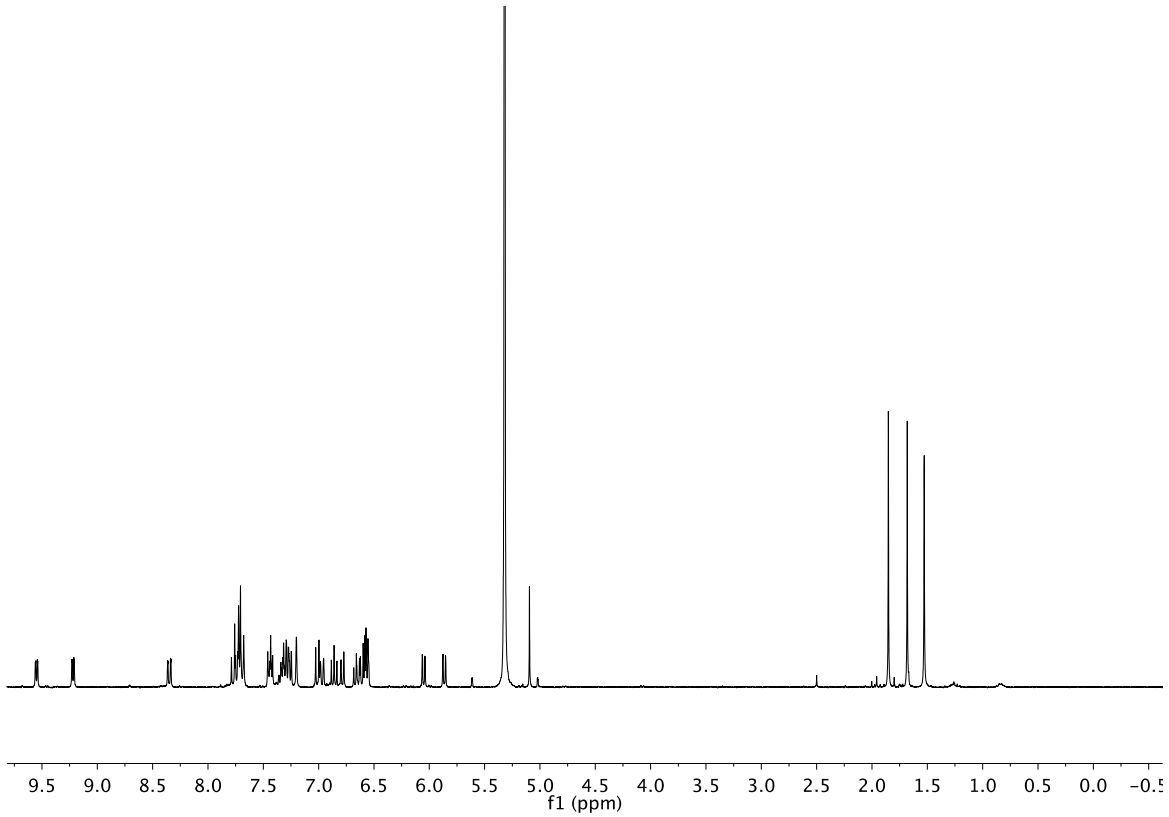

Fig. 20S. ^{1}H NMR spectrum of **5j**

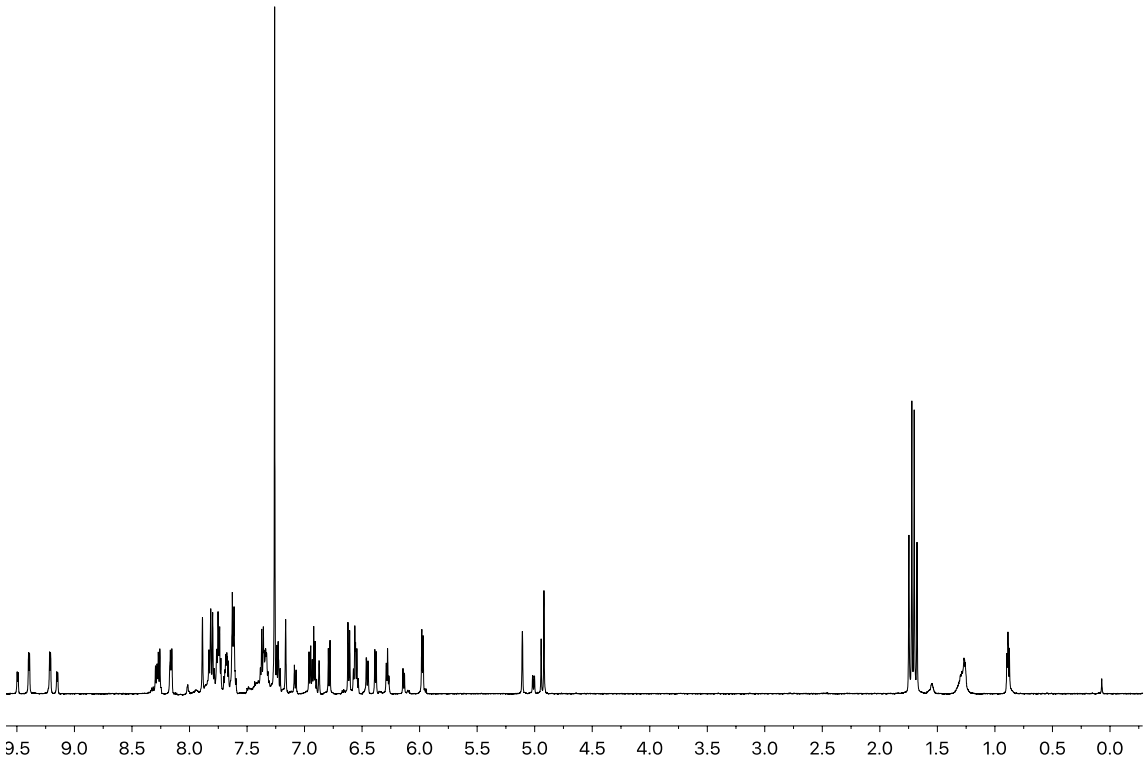

Fig. 21S. ^{1}H NMR spectrum of **5k**

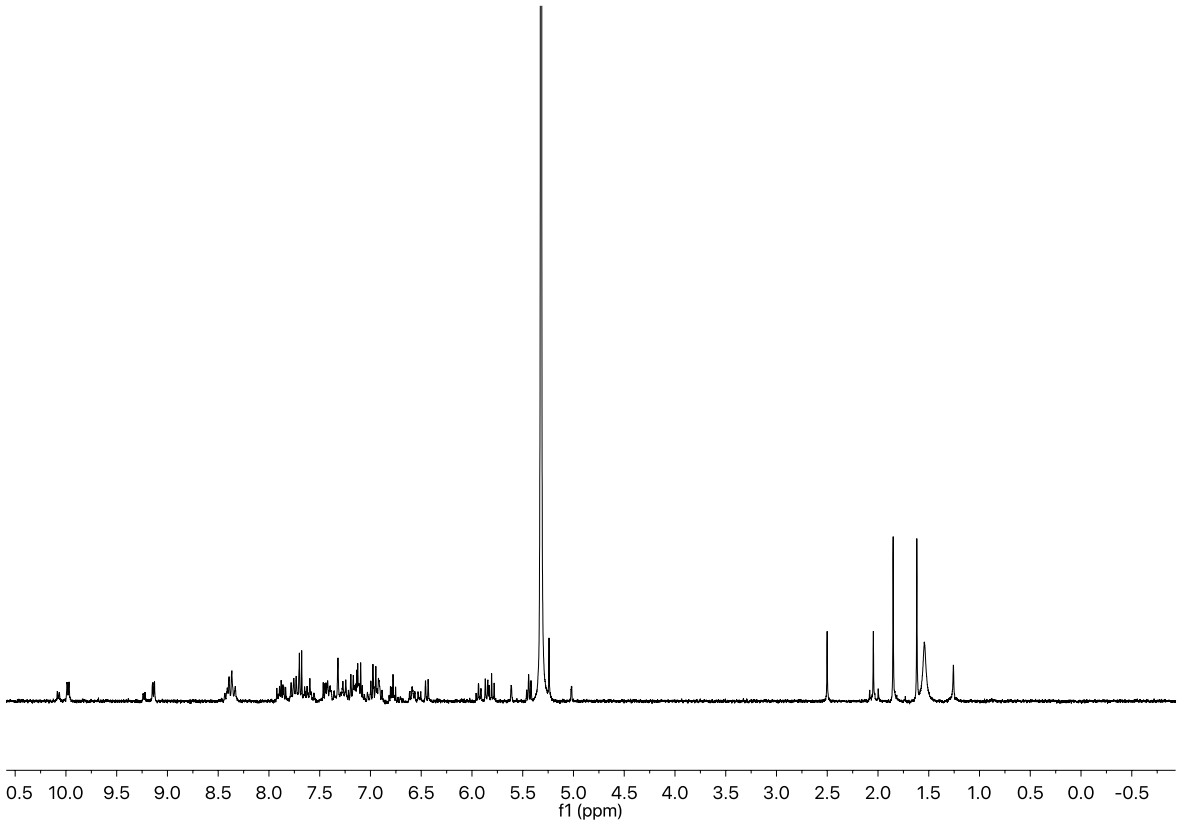

Fig. 22S. ^{1}H NMR spectrum of **5l**

4. X-Ray analysis data

Table 1S. Crystal data, data collection and structure refinement

Compound	**3d**	**3h**	**3j**	**3l**	**5g**	**5j**	**5l**
Formula	$C_{11}H_{12}N_2O_3$	$2(C_{15}H_{15}NO)\cdot H_2O$	$C_{19}H_{17}NO$	$C_{19}H_{17}NO$	$C_{45}H_{33}IrN_4OS$	$C_{45}H_{32}IrN_3O$	$C_{45}H_{32}IrN_3O$
Formula weight	220.23	468.58	275.33	275.33 /c	870.01	822.93	822.93
Crystal system	monoclinic	monoclinic	monoclinic	monoclinic	monoclinic	monoclinic	monoclinic
Space group	$P2_1/n$	I2/a	$P2_1/c$	$P2_1/n$	$P2_1/c$	$P2_1/n$	$P2_1/n$
a(Å)	4.3661(7)	16.8762(4)	7.7643(3)	8.8402(4)	8.7504(2)	15.39264(9)	9.53788(14)
b(Å)	13.1478(18)	8.2994(2)	14.0865(8)	15.0895(4)	32.0328(12)	12.27706(7)	19.5224(3)
c(Å)	18.853(3)	18.2491(5)	13.5190(6)	22.5145(8)	13.1546(5)	19.49316(13)	17.3966(4)
β(º)	93.000(15)	103.665(2)	101.690(4)	97.237(4)	92.144(3)	109.5070(7)	95.4280(17)
V(Å^3)	1080.8(3)	2483.66(11)	1447.93(12)	2979.38(19)	3684.7(2)	3472.30(4)	3224.76(10)
Z	4	4	4	8	4	4	4
D_x(g cm^{-3})	1.353	1.253	1.263	1.228	1.568	1.574	1.695
F(000)	464	1000	584	1168	1728	1632	1632
μ(mm^{-1})	0.100	0.081	0.078	0.076	3.721	7.752	4.184
Reflections:							
collected	4926	12884	6148	27337	21762	33752	14603
unique (R_{int})	1897 (0.019)	2720 (0.013)	2904 (0.016)	5242 (0.035)	7479 (0.057)	7195 (0.035)	6553 (0.029)
with I>2σ(I)	1507	2452	2464	4961	5645	7017	5427
R(F) [I>2σ(I)]	0.0452	0.0350	0.0362	0.0637	0.0529	0.0283	0.0278
wR(F^2) [I>2σ(I)]	0.1296	0.0914	0.0917	0.1679	0.1395	0.0803	0.0517
R(F) [all data]	0.0565	0.0389	0.0443	0.1239	0.0786	0.0288	0.0398
wR(F^2) [all data]	0.1375	0.0945	0.0981	0.1990	0.153	0.0809	0.0553
Goodness of fit	1.079	1.020	1.057	0.882	1.039	1.105	1.033
max/min Δρ (e·Å^{-3})	0.18/-0.17	0.24/-0.24	0.22/-0.18	0.27/-0.18	0.31/-0.22	2.79/-1.43	1.08/-0.61

Table 2S. Relevant geometrical features (Å, º). Max(A) is the maximum deviation from the least-squares plane through C1 – N5 atoms, A is the least-squares plane of keto-iminato fragment, A' – of Ir-ketoiminato group, B – of aromatic substituent at N5, and C and D – of two bzq planes.

	3d	**3h**	**3j**	**3l**	**5g**	**5j**	**5l**
C2=O2	1.237(2)	1.2571(13)	1.2553(15)	1.231(3) 1.231(3)	1.280(10)	1.265(4)	1.283(4)
C4-N5	1.357(2)	1.3430(13)	1.3523(16)	1.327(3) 1.328(3)	1.302(10)	1.313(4)	1.314(4)
N5-C6	1.388(2)	1.4277(13)	1.4169(15)	1.427(3) 1.431(3)	1.424(10)	1.437(4)	1.444(4)
O2-C2-C3-C4	-2.9(3)	1.23(17)	1.0(2)	-4.8(5) 3.5(5)	3.2(6)	4.5(5)	7.9(7)
C2-C3-C4-N5	1.7(3)	1.98(16)	-0.57(19)	2.7(5) -1.3(5)	-9.0(2)	-10.8(5)	-11.9(6)
C3-C4-N5-C6	-178.72(17)	-167.93(9)	176.23(12)	-175.2(3) 177.1(3)	171.8(5)	172.9(3)	165.7(4)
Ir1-O2A					2.135(6)	2.156(2)	2.137(2)
Ir1-N5A					2.157(6)	2.171(3)	2.183(3)
Ir1-N1B					2.028(7)	2.045(2)	2.061(3)
Ir1-N1C					2.050(7)	2.064(3)	2.045(3)
Ir1-C12B					2.006(9)	2.018(3)	2.018(4)
Ir1-C12C					2.009(8)	2.015(3)	2.005(4)
C-N-C	133.27(15)	125.26(9)	129.01(11)	126.2(2) 126.4(2)	118.8(7)	119.3(3)	118.3(3)
angles					175.2(3) 174.3(3) 173.8(3)	175.34(9) 173.97(9) 173.31(10)	176.51(13) 174.72(12) 172.38(11)
Max(A)	0.0216(12)	-0.1224(7)	0.0341(9)	0.057(3) 0.042(3)	0.116(6)	0.118(2)	0.196(3)
A/B	12.36(11)	61.29(5)	47.36(4)	85.10(11) 83.06(11)	89.8(4)	79.17(19)	89.11(14)
A'/B					89.3	80.2	89.9
A'/C					86.2	79.2	85.8
A'/D					72.1	86.9	84.3
B/C					60.3	66.5	78.0
B/D					25.7	30.6	16.5
C/D					82.8	89.2	89.9

Table 3S. Intramolecular hydrogen bonds in the ligand molecules.

D	H	A	D-H	H···A	D···A	D-H···A
3d						
N5	H5	O2	0.90(2)	1.88(2)	2.6497(19)	141.9(17)
3h						
N5	H5	O2	0.911(15)	1.925(15)	2.6716(12)	137.9(12)
3j						
N5	H5	O2	0.918(16)	1.877(16)	2.6496(14)	140.4(14)

31						
N5A	H5A	O2A	0.86	1.97	2.642(3)	134
N5B	H5B	O2B	0.86	1.98	2.650(3)	134

Table 4S. Crystal data, data collection and structure refinement

Compound	**5f**	**5i**
Formula	$C_{37}H_{27}IrN_4O_3$	$C_{41}H_{30}IrN_3O$
Formula weight	767.82	772.88
Crystal system	monoclinic	monoclinic
Space group	C2/c	$P2_1/c$
a(Å)	35.389(2)	16.7335(11)
b(Å)	10.0534(4)	18.7126(16)
c(Å)	19.4276(11)	20.7091(16)
β(º)	105.773(6)	108.945(8)
V(Å^3)	6651.7(6)	6133.3(9)
Z	8	8
D_x(g cm^{-3})	1.533	1.674
F(000)	3024	3056
μ(mm^{-1})	4.055	4.393
Reflections:		
collected	21762	25025
unique (R_{int})	7479 (0.057)	10773 (0.074)
with I>2σ(I)	5645	5738
R(F) [I>2σ(I)]	0.1118	0.0847
wR(F^2) [I>2σ(I)]	0.3216	0.1838
R(F) [all data]	0.1359	0.1693
wR(F^2) [all data]	0.3654	0.2162
Goodness of fit	1.414	0.971
max/min Δρ (e·Å^{-3})	3.06/-4.81	7.13/-1.35
CCDC number	1865883	1865886

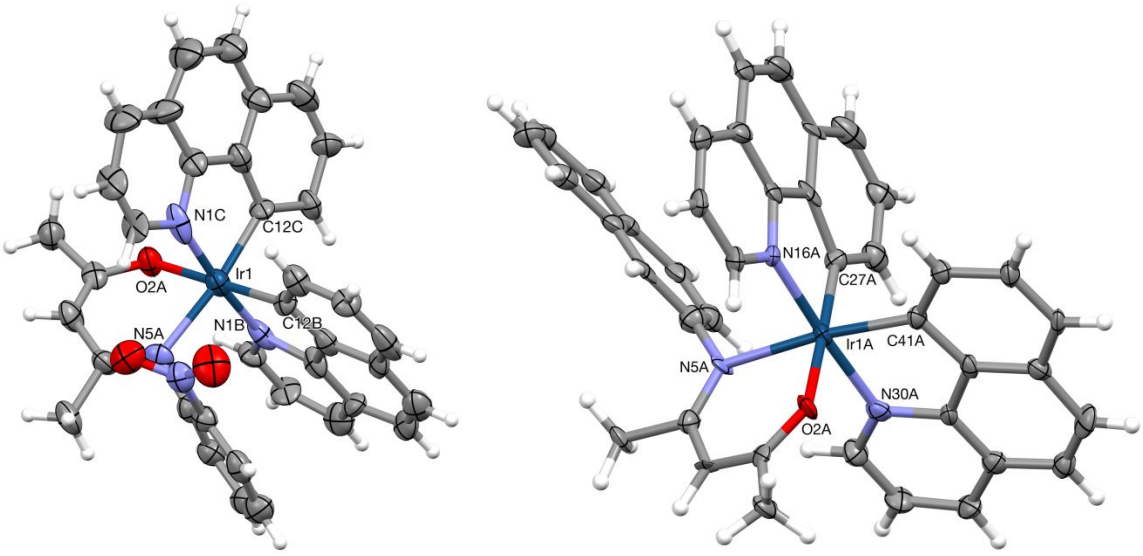

Fig. 23S. Perspective views of the complexes **5f** and **5i**.

Table 5S. Conformations of the **5g** and **5i** complexes; plane codes as in Table 2S.

	5g	**5i**(A)	**5i**(B)
A'/B	83.5	81.4	86.3
A'/C	85.9	83.1	83.4
A'/D	84.8	89.2	87.6
B/C	60.9	57.8	56.1
B/D	26.8	32.5	30.1
C/D	87.1	87.0	85.6

5. Thermal analysis curves

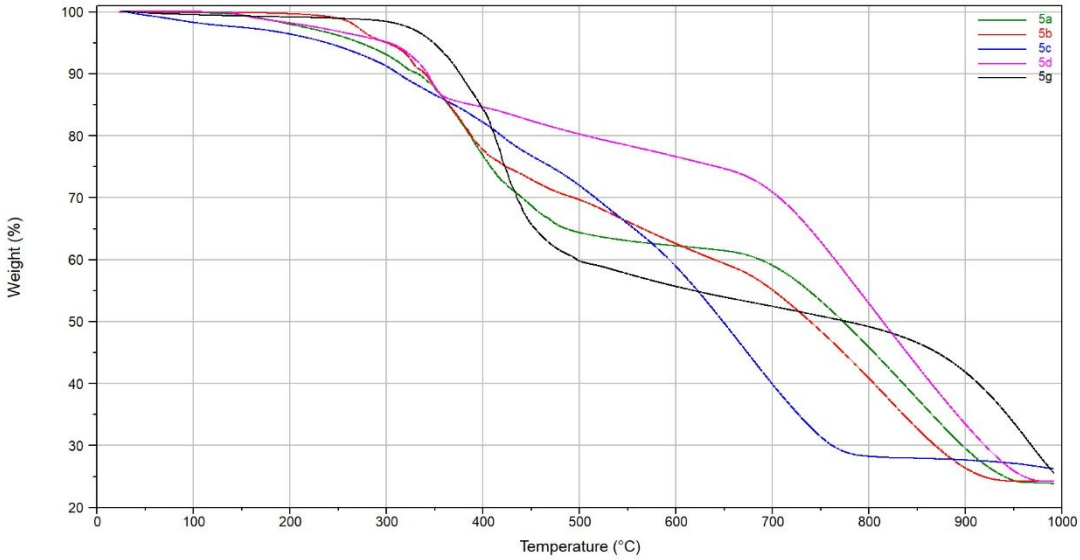

Figure 24S. TG curves of **5a**, **5b**, **5c**, **5d** and **5g** complexes in N_2 atmosphere.

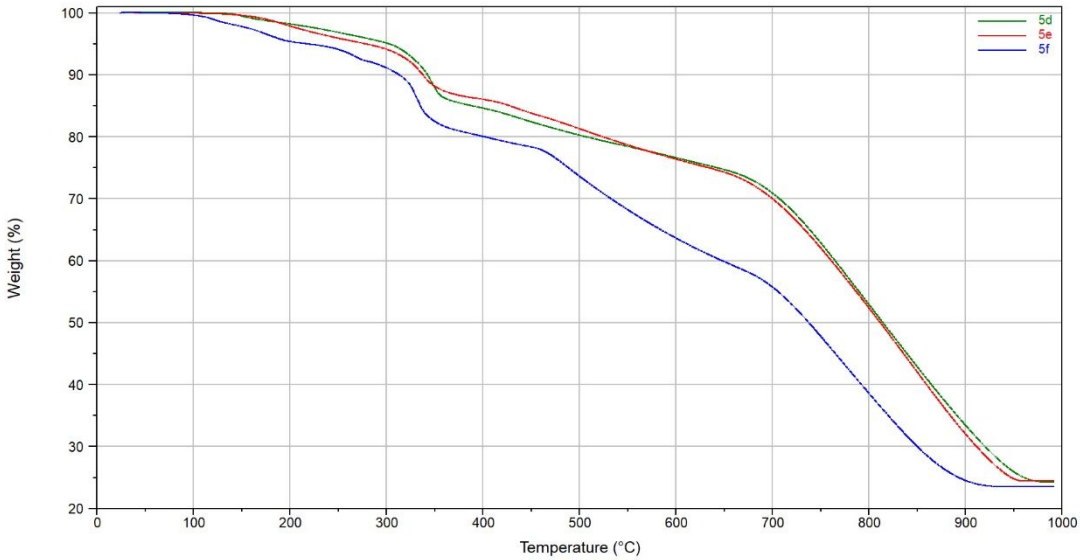

Figure 25S. TG curves of **5d**, **5e** and **5f** complexes in N_2 atmosphere.

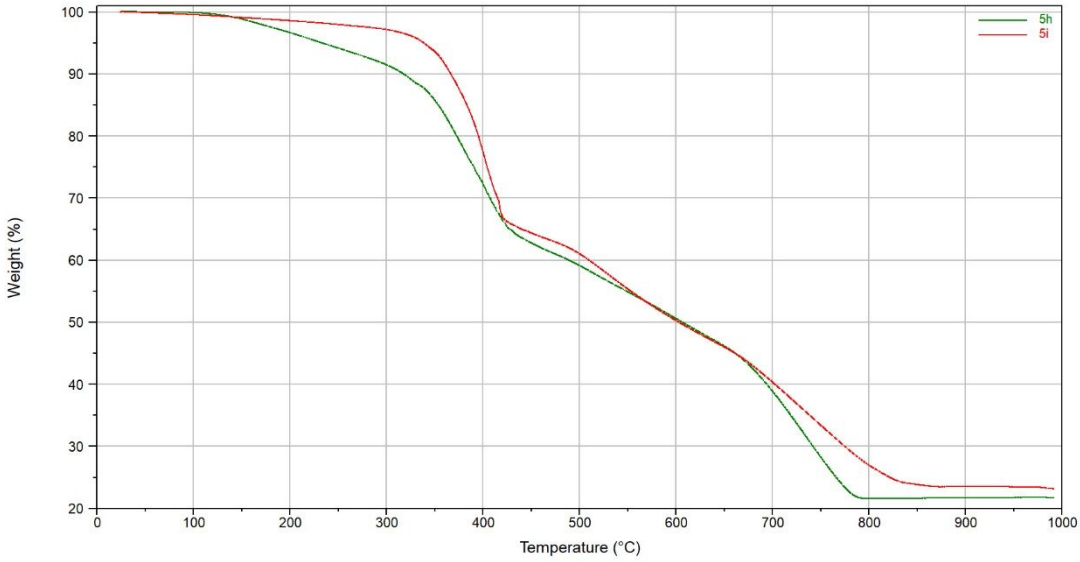

Figure 26S. TG curves of **5h** and **5i** complexes in N_2 atmosphere.

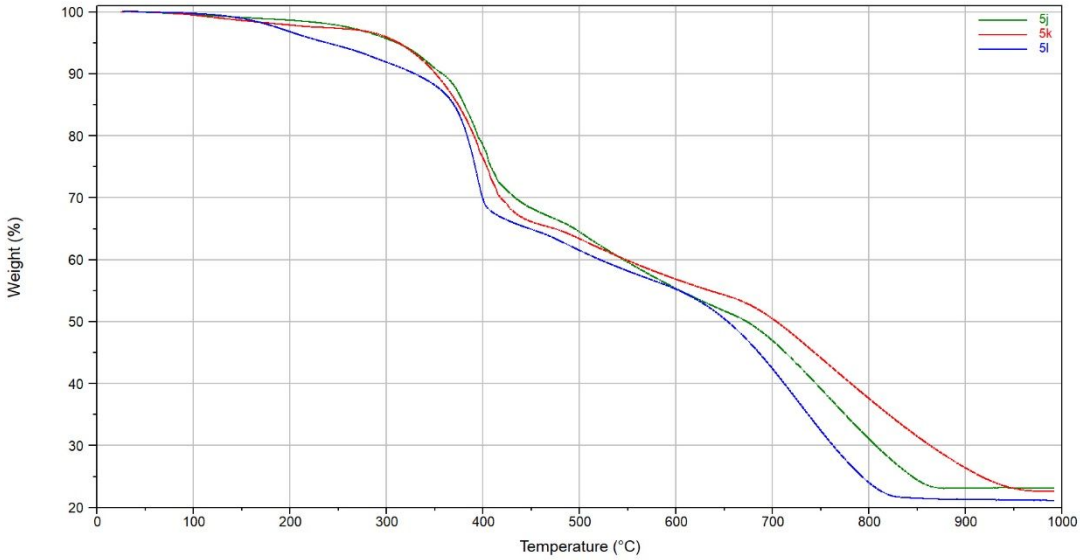

Figure 27S. TG curves of **5j**, **5k** and **5l** complexes in N_2 atmosphere.

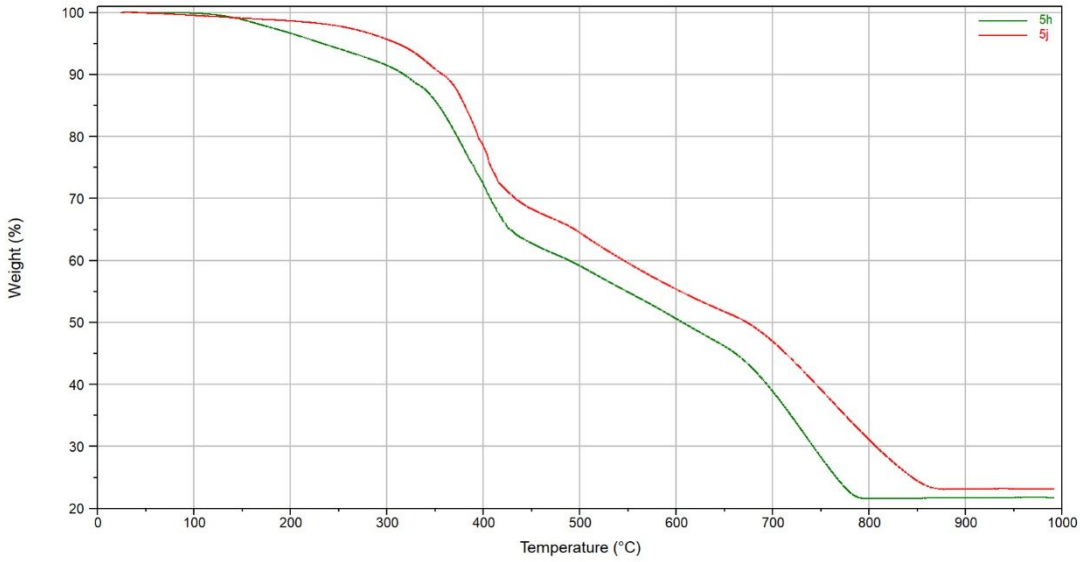

Figure 28S. TG curves of **5h** and **5j** complexes in N_2 atmosphere.

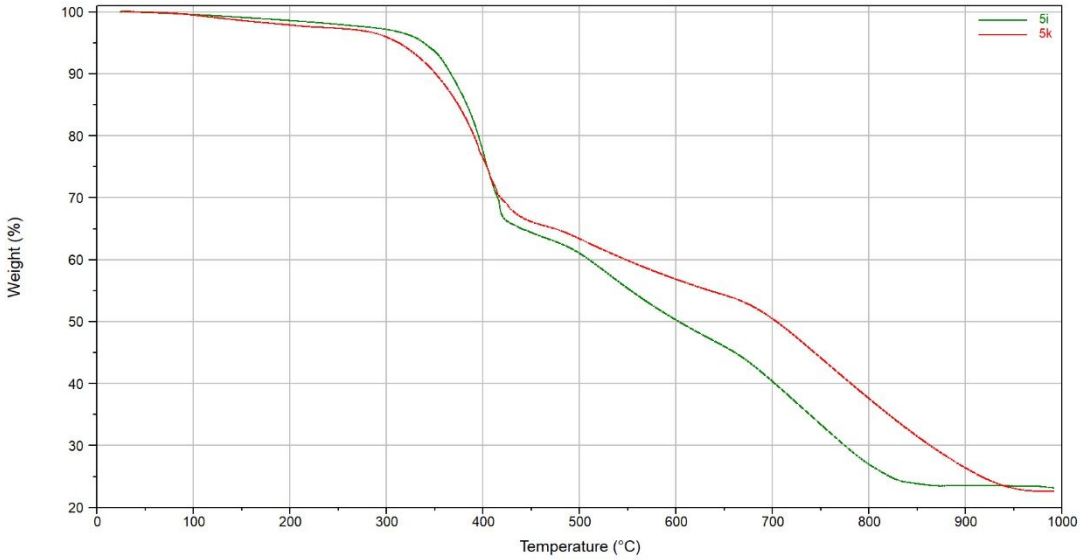

Figure 29S. TG curves of **5i** and **5k** complexes in N_2 atmosphere.

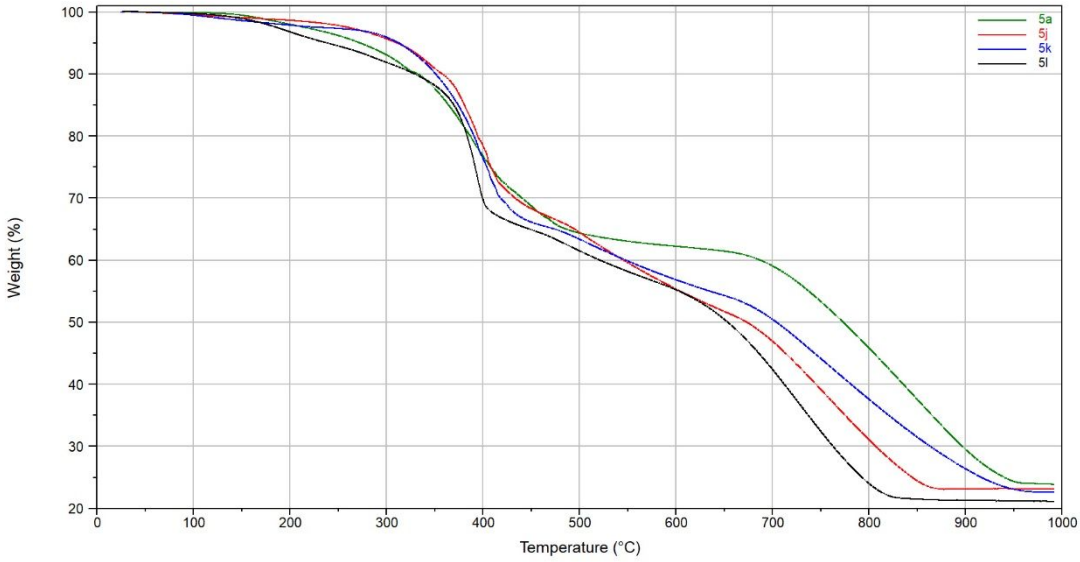

Figure 30S. TG curves of **5a**, **5j**, **5k** and **5l** complexes in N_2 atmosphere.

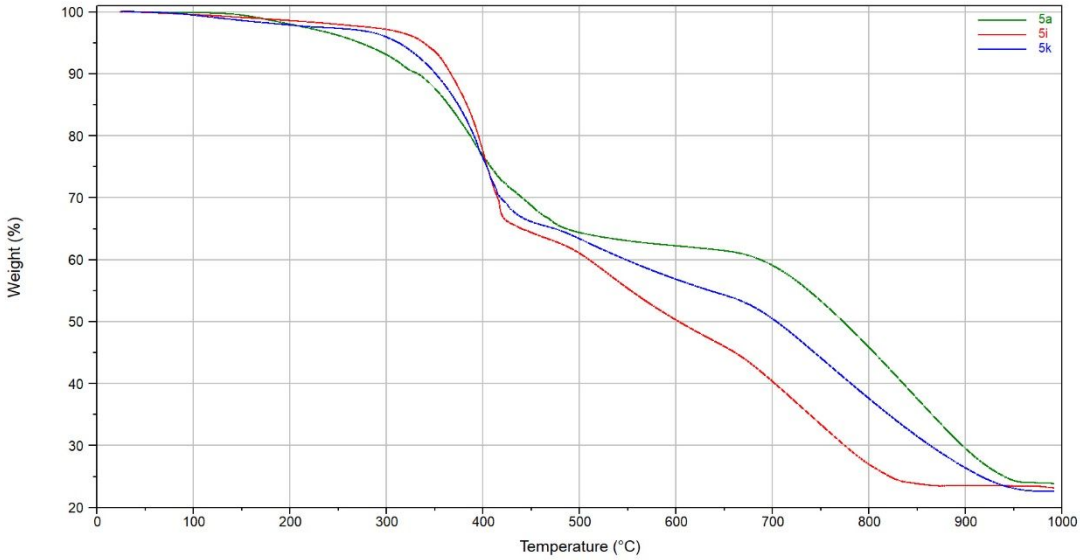

Figure 31S. TG curves of **5a**, **5i** and **5k** complexes in N_2 atmosphere.

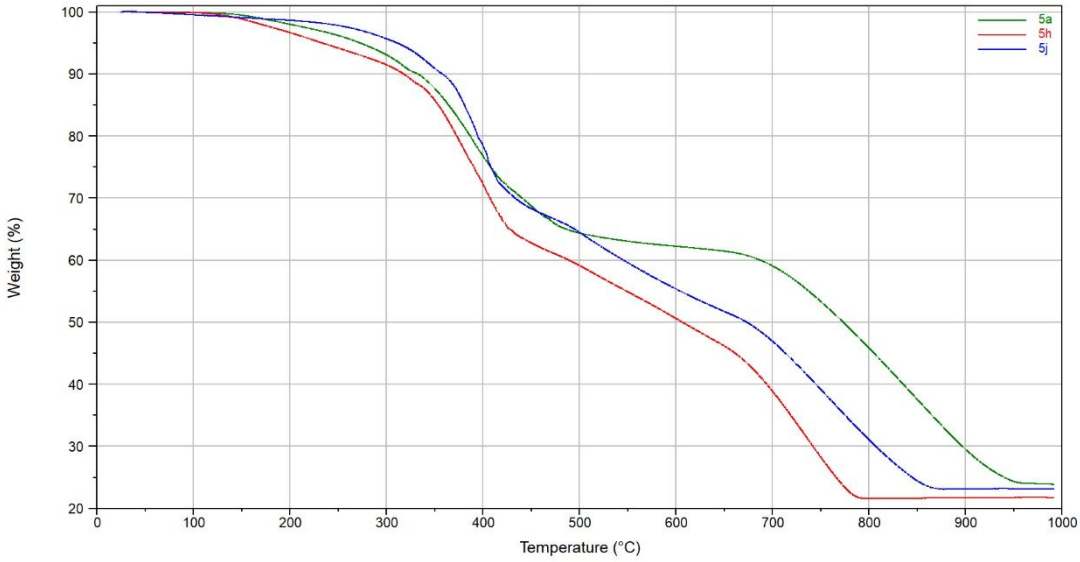

Figure 32S. TG curves of **5a**, **5h** and **5j** complexes in N_2 atmosphere.

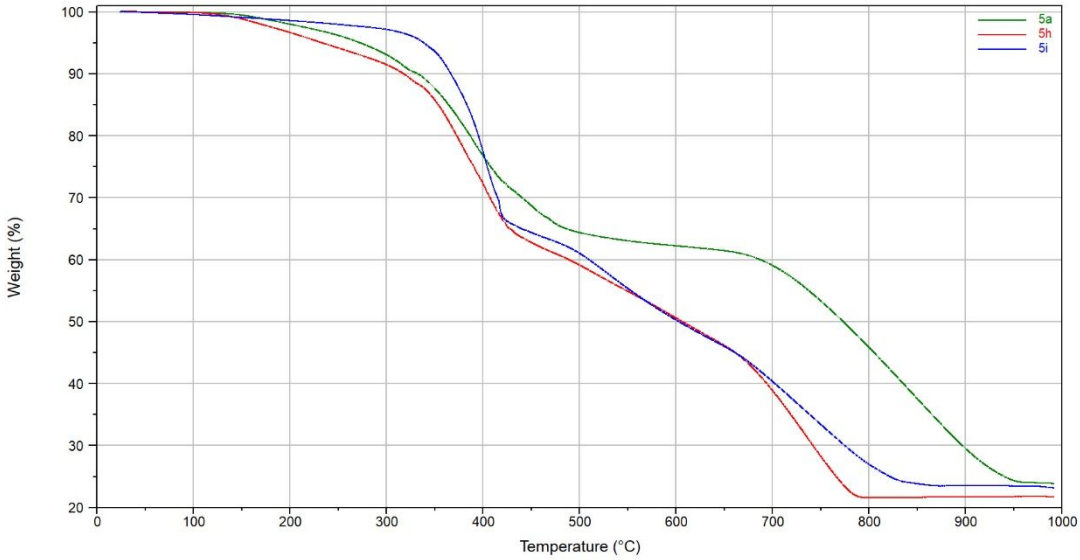

Figure 33S. TG curves of **5a**, **5h** and **5i** complexes in N_2 atmosphere.

6. Cyclic voltammetry measurements

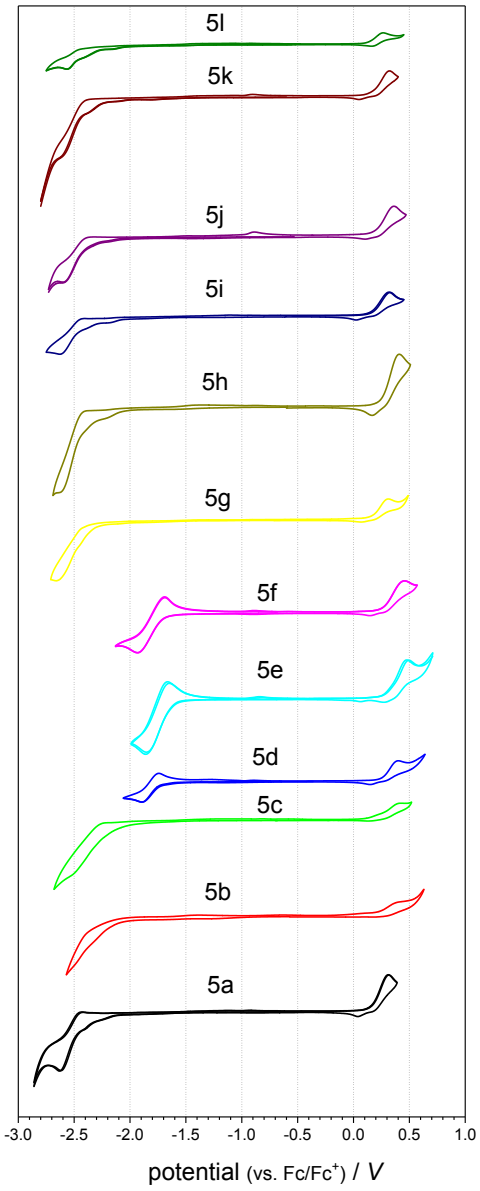

Fig. 34S. Cyclic voltammetry of compounds recorded in THF/0.1 M Bu_4NBF_4 electrolyte; scan rate 100 mV/s; concentration 2 mM.

7. DFT calculation data

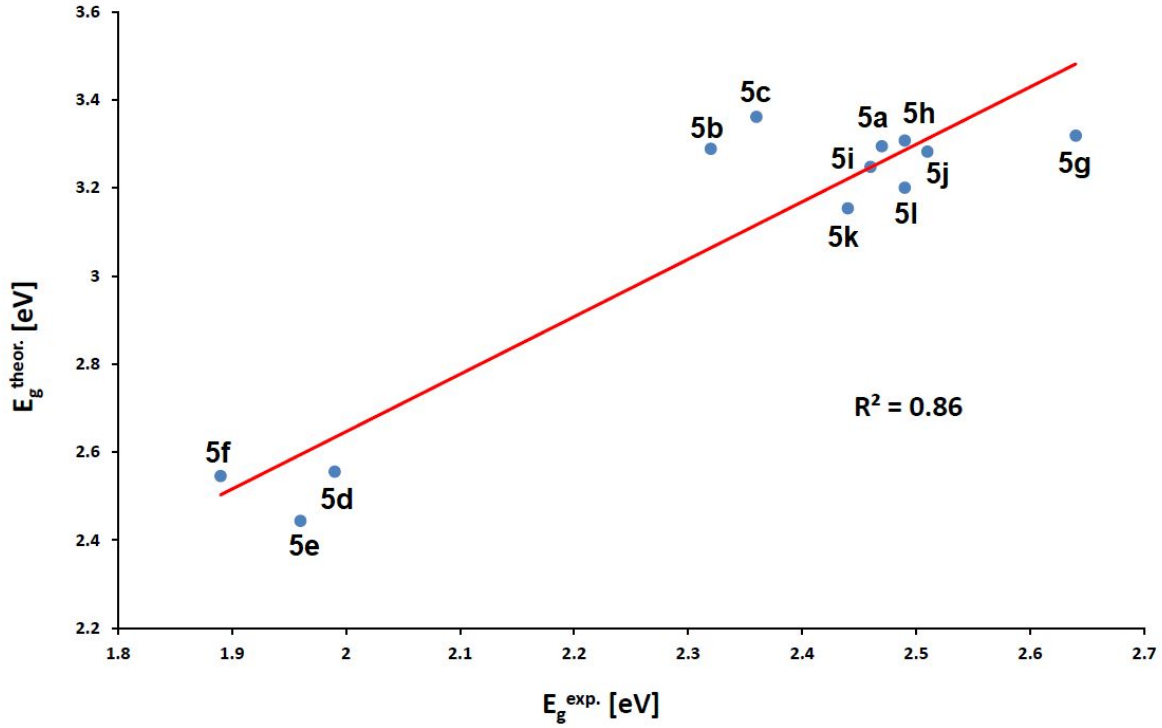

Fig. 35S. Theoretical $E_g^{theor.}$ calculated at the B3LYP/SDD/6-311++G(d,p) level of theory vs experimental values $E_g^{exp.}$.

Table 6S. The energy levels and HOMO-LUMO energy gaps for the studied complexes (in eV) calculated at the B3LYP/SDD/6-311++G(d.p) level of theory together with the experimental results.

compound	HOMO [eV]	LUMO [eV]	LUMO+1 [eV]	LUMO+2 [eV]	$E_g^{theor.}$ [eV]	$E_g^{exp.}$ [eV]
5a	-5.28	-1.97	-1.95	-1.34	3.31	2.49
5b	-5.25	-1.96	-1.94	-1.33	3.29	2.32
5c	-5.39	-2.03	-2.02	-1.62	3.36	2.36
5d	-5.43	-2.87	-2.05	-2.03	2.56	1.99
5e	-5.39	-2.94	-2.03	-2.00	2.44	1.96
5f	-5.34	-2.79	-2.04	-1.92	2.55	1.89
5g	-5.32	-2.00	-1.98	-1.90	3.32	2.64
5h	-5.26	-1.98	-1.95	-1.40	3.28	2.51
5i	-5.27	-1.97	-1.95	-1.40	3.30	2.47
5j	-5.24	-2.04	-1.98	-1.92	3.20	2.49
5k	-5.24	-1.99	-1.99	-1.90	3.25	2.44
5l	-5.18	-2.03	-1.96	-1.94	3.15	2.46

Table 7S. The energy levels and HOMO-LUMO energy gaps for the studied complexes (in eV) calculated at the M06/SDD/6-311++G(d.p) level of theory together with the experimental results.

compound	HOMO [eV]	LUMO [eV]	LUMO+1 [eV]	LUMO+2 [eV]	$E_g^{theor.}$ [eV]	$E_g^{exp.}$ [eV]
5a	-5.55	-1.86	-1.86	-1.24	3.69	2.49
5b	-5.52	-1.86	-1.85	-1.24	3.66	2.32
5c	-5.67	-1.94	-1.92	-1.46	3.73	2.36
5d	-5.71	-2.62	-1.96	-1.94	3.09	1.99
5e	-5.66	-2.70	-1.92	-1.92	2.96	1.96
5f	-5.64	-2.54	-1.95	-1.82	3.10	1.89
5g	-5.60	-1.93	-1.92	-1.79	3.67	2.64
5h	-5.54	-1.88	-1.85	-1.28	3.66	2.51
5i	-5.54	-1.87	-1.86	-1.33	3.67	2.47
5j	-5.55	-1.90	-1.87	-1.83	3.65	2.49
5k	-5.49	-1.89	-1.86	-1.82	3.60	2.44
5l	-5.48	-1.88	-1.86	-1.83	3.60	2.46

Table 8S. The energy levels and HOMO-LUMO energy gaps for the studied complexes (in eV) calculated at the WB97XD/SDD/6-311++G(d,p) level of theory together with the experimental results.

compound	HOMO [eV]	LUMO [eV]	LUMO+1 [eV]	LUMO+2 [eV]	$E_g^{theor.}$ [eV]	$E_g^{exp.}$ [eV]
5a	-7.06	-0.76	-0.74	-0.11	6.30	2.49
5b	-7.01	-0.82	-0.80	-0.17	6.19	2.32
5c	-7.17	-0.92	-0.90	-0.42	6.25	2.36
5d	-7.19	-1.39	-0.79	-0.77	5.80	1.99
5e	-7.23	-1.48	-0.74	-0.72	5.75	1.96
5f	-7.14	-1.05	-0.56	-0.42	6.09	1.89
5g	-7.16	-0.83	-0.83	-0.76	6.33	2.64
5h	-7.06	-0.76	-0.70	-0.14	6.30	2.51
5i	-7.02	-0.75	-0.72	-0.20	6.27	2.47
5j	-7.06	-0.81	-0.70	-0.64	6.25	2.49
5k	-6.97	-0.80	-0.70	-0.61	6.17	2.44
5l	-7.06	-0.89	-0.82	-0.79	6.17	2.46

Table 9S. Set of numerical orbital distributions.

Complex	Orbital	MO composition			
		Ir	Bzq1	Bzq2	Bzq-R
	LUMO+1	3	6	91	0
5a	LUMO	4	91	5	0
	HOMO	31	18	18	33
	HOMO-1	29	16	10	45
	LUMO+1	4	13	83	0
5b	LUMO	4	82	14	0
	HOMO	30	17	17	36
	HOMO-1	28	17	10	45
	LUMO+1	4	15	80	1
5c	LUMO	4	80	16	0
	HOMO	32	23	22	23
	HOMO-1	27	13	6	54
	LUMO+1	4	49	47	0
5d	LUMO	1	1	0	98
	HOMO	32	24	23	21
	HOMO-1	27	14	6	53
	LUMO+1	4	0	96	0
5e	LUMO	1	1	0	98
	HOMO	33	22	22	23
	HOMO-1	28	13	7	52
	LUMO+1	3	97	0	0
5f	LUMO	0	1	1	98
	HOMO	31	20	25	24
	HOMO-1	27	11	10	52
	LUMO+1	4	92	1	3
5g	LUMO	4	0	95	1
	HOMO	31	21	19	29
	HOMO-1	27	16	8	49
	LUMO+1	3	97	0	0
5h	LUMO	4	0	95	1
	HOMO	30	20	17	33
	HOMO-1	25	21	9	45
	LUMO+1	4	78	18	0
5i	LUMO	4	17	78	1
	HOMO	30	21	17	32
	HOMO-1	28	16	9	47
	LUMO+1	4	8	79	9
5j	LUMO	0	37	19	44
	HOMO	27	18	16	39
	HOMO-1	7	27	5	61
	LUMO+1	2	35	27	36
5k	LUMO	3	19	69	9
	HOMO	23	25	14	38
	HOMO-1	11	17	7	65
	LUMO+1	4	80	16	0
5l	LUMO	4	14	77	5
	HOMO	25	24	15	36
	HOMO-1	25	21	13	41

Table 10S. Cartesian coordinates from the optimized structures of S_0 in C_6H_5Cl media for **5a**.

Atom symbol	X	Y	Z
C	-5.13087	-1.75439	-0.73518
C	-3.92862	-2.08424	-0.01784
C	-2.84487	-1.17188	-0.05963
C	-2.97823	0.03526	-0.80396
C	-4.16643	0.34877	-1.50314
C	-5.24777	-0.59542	-1.44419
N	-1.89195	0.86826	-0.80074
C	-4.20955	1.56718	-2.20558
C	-3.10691	2.40174	-2.18295
C	-1.96501	2.02085	-1.46760
C	-3.76375	-3.26913	0.72934
C	-2.56545	-3.49660	1.38667
C	-1.49987	-2.57398	1.32889
C	-1.60768	-1.38743	0.60794
H	-5.10307	1.84429	-2.75437
H	-3.10755	3.34880	-2.70705
C	1.02043	-1.97794	-3.28502
C	2.11622	-2.68103	-2.80870
C	0.26475	-1.12499	-2.45490
C	2.48442	-2.54990	-1.45382
C	3.59532	-3.24058	-0.85469
C	1.70787	-1.69054	-0.63843
C	3.90642	-3.09427	0.46555
C	3.12888	-2.23844	1.31884
N	1.23305	-0.71845	1.46463
C	3.36853	-2.03735	2.69088
C	1.47874	-0.54612	2.76440
C	2.54150	-1.19082	3.40937
C	0.58991	-0.94637	-1.11185
H	4.19396	-2.54676	3.17632
H	0.80393	0.11445	3.29324
H	2.69735	-1.01819	4.46652
Ir	-0.29323	0.15171	0.34947
O	-1.19862	1.16275	2.06902
N	0.95791	1.98947	0.09734
C	-1.11158	2.41090	2.32893
C	-0.26558	3.33764	1.71712
C	0.75269	3.12250	0.74643
H	-0.33903	4.35092	2.08824
C	-2.02529	2.88680	3.44151
H	-1.81169	2.32255	4.35404

H	-3.06495	2.67967	3.17162
H	-1.91620	3.95168	3.64896
C	1.64303	4.32593	0.47768
H	1.17909	5.23486	0.85913
H	1.84350	4.44874	-0.58779
H	2.61035	4.20786	0.97389
C	2.03944	-1.55077	0.73821
C	2.11920	1.88948	-0.73275
C	2.01870	2.00244	-2.12365
C	3.37506	1.64640	-0.16423
C	4.50858	1.53820	-0.96841
C	4.40430	1.66732	-2.35299
C	3.15324	1.89731	-2.92551
H	3.45793	1.54396	0.91191
H	5.47390	1.35098	-0.51058
H	5.28541	1.58278	-2.97888
H	-1.08996	2.65377	-1.42419
H	-6.16400	-0.36543	-1.97696
H	-5.96034	-2.45355	-0.70275
H	-4.57185	-3.99065	0.78411
H	-2.44017	-4.40920	1.96147
H	-0.58584	-2.81168	1.86262
H	0.73357	-2.08625	-4.32672
H	-0.58252	-0.60305	-2.88715
H	2.68587	-3.33089	-3.46425
H	4.19394	-3.89526	-1.48012
H	4.74731	-3.62772	0.89529
H	1.04905	2.17380	-2.57504
H	3.05781	1.99197	-4.00176

Table 11S. Cartesian coordinates from the optimized structures of S_0 in C_6H_5Cl media for 5b.

Atom symbol	X	Y	Z
C	5.38782	1.07344	-1.62332
C	4.34957	1.63274	-0.80004
C	3.18677	0.85887	-0.55961
C	3.08235	-0.43991	-1.13513
C	4.11052	-0.97827	-1.94278
C	5.27709	-0.17088	-2.16998
N	1.93278	-1.1308	-0.86018
C	3.92249	-2.27095	-2.46549
C	2.75946	-2.95857	-2.17018
C	1.78702	-2.35813	-1.36128
C	4.42071	2.91389	-0.21449
C	3.36626	3.36542	0.56273
C	2.21793	2.57713	0.78613
C	2.09508	1.3038	0.23593
H	4.68773	-2.71873	-3.09009
H	2.58452	-3.95718	-2.54935
C	-1.07153	1.70078	-3.26899
C	-1.99293	2.59075	-2.73866
C	-0.27799	0.87256	-2.44931
C	-2.14115	2.67768	-1.33906
C	-3.06036	3.56971	-0.6835
C	-1.331	1.83752	-0.5361
C	-3.16374	3.62627	0.67578
C	-2.34876	2.79142	1.51504
N	-0.6191	1.08147	1.5878
C	-2.38068	2.78852	2.92194
C	-0.66595	1.09799	2.92065
C	-1.53866	1.94016	3.62067
C	-0.38763	0.90818	-1.06053
H	-3.05964	3.45028	3.44868
H	0.01673	0.42807	3.42679
H	-1.53718	1.91694	4.70284
Ir	0.61394	-0.09288	0.39546
O	1.68766	-0.964	2.09645
N	-0.82274	-1.78895	0.59973
C	1.52327	-2.14617	2.55396
C	0.50801	-3.04102	2.2145
C	-0.62401	-2.84196	1.37316
H	0.54008	-3.99626	2.72097
C	2.54729	-2.56753	3.59011
H	2.50976	-1.87838	4.4392

H	3.55083	-2.49403	3.16132
H	2.38626	-3.58361	3.9516
C	-1.65087	-3.96344	1.41443
H	-1.20437	-4.87098	1.81998
H	-2.05627	-4.17679	0.42464
H	-2.49417	-3.69001	2.05506
C	-1.44487	1.91048	0.88013
C	-2.08421	-1.67281	-0.07008
C	-2.20792	-1.97381	-1.43295
C	-3.21558	-1.22453	0.6102
C	-4.44874	-1.09048	-0.03397
C	-4.55867	-1.40753	-1.38905
C	-3.42708	-1.85134	-2.08354
H	-3.13798	-0.97416	1.66226
H	0.87282	-2.87353	-1.10297
H	6.07239	-0.57431	-2.78726
H	6.27803	1.66671	-1.80657
H	5.29563	3.53434	-0.37628
H	3.42239	4.35245	1.01173
H	1.42486	2.98771	1.40214
H	-0.9557	1.63847	-4.34689
H	0.42588	0.19771	-2.9256
H	-2.59443	3.21827	-3.38755
H	-3.68257	4.21234	-1.29833
H	-3.86319	4.30829	1.14702
H	-3.51945	-2.08853	-3.13708
H	-1.3396	-2.30858	-1.98717
H	-5.30177	-0.73769	0.53015
O	-5.71354	-1.31422	-2.11909
C	-6.88941	-0.84216	-1.46656
H	-7.18367	-1.50553	-0.64688
H	-7.6703	-0.838	-2.22496
H	-6.74995	0.17345	-1.08297

Table 12S. Cartesian coordinates from the optimized structures of S_0 in C_6H_5Cl media for 5c.

Atom symbol	X	Y	Z
C	5.29474	1.2289	-1.58222
C	4.24221	1.73885	-0.74506
C	3.09763	0.93103	-0.53166
C	3.02452	-0.35146	-1.1466
C	4.0669	-0.84195	-1.96627
C	5.21457	-0.00086	-2.166
N	1.8906	-1.07593	-0.89602
C	3.90989	-2.12325	-2.52619
C	2.7625	-2.84604	-2.25417
C	1.77424	-2.29183	-1.43175
C	4.28186	3.00278	-0.12036
C	3.2162	3.40529	0.66808
C	2.08602	2.58398	0.86479
C	1.99551	1.3267	0.27464
H	4.6867	-2.53564	-3.16076
H	2.61228	-3.83729	-2.66207
C	-1.17571	1.75304	-3.2287
C	-2.12938	2.59353	-2.67598
C	-0.35662	0.92814	-2.43032
C	-2.28428	2.63489	-1.27484
C	-3.23394	3.47709	-0.59728
C	-1.44869	1.79934	-0.49359
C	-3.34051	3.49267	0.76275
C	-2.4997	2.66228	1.58051
N	-0.71905	1.00379	1.61043
C	-2.53291	2.62025	2.98679
C	-0.76783	0.98289	2.94329
C	-1.66599	1.77969	3.66396
C	-0.47417	0.91756	-1.04219
H	-3.23261	3.24609	3.52987
H	-0.06693	0.3202	3.4338
H	-1.66475	1.72775	4.74509
Ir	0.54671	-0.10432	0.38619
O	1.63762	-1.00751	2.05953
N	-0.85218	-1.8491	0.54824
C	1.49871	-2.19931	2.49291
C	0.49926	-3.10972	2.13478
C	-0.63387	-2.91629	1.30263
H	0.55309	-4.07536	2.61882
C	2.52983	-2.62234	3.5204
H	2.47709	-1.95224	4.38366

H	3.53159	-2.51851	3.09411
H	2.38937	-3.64894	3.85955
C	-1.63867	-4.05725	1.30917
H	-1.17523	-4.96825	1.68616
H	-2.03853	-4.25008	0.31244
H	-2.48675	-3.82193	1.95853
C	-1.56767	1.82789	0.92403
C	-2.1077	-1.71665	-0.10223
C	-2.21967	-1.90478	-1.48702
C	-3.25001	-1.34753	0.62383
C	-4.47494	-1.18864	-0.00798
C	-4.58002	-1.39457	-1.39205
C	-3.43968	-1.75331	-2.12807
H	-3.16957	-1.1824	1.6915
H	0.87202	-2.83667	-1.19076
H	6.02046	-0.36664	-2.79282
H	6.17103	1.84809	-1.74536
H	5.14208	3.64825	-0.26121
H	3.24828	4.37897	1.14731
H	1.28236	2.95648	1.49089
H	-1.05329	1.72801	-4.3073
H	0.37273	0.29357	-2.92309
H	-2.75035	3.21871	-3.30836
H	-3.87687	4.11482	-1.19544
H	-4.06292	4.13777	1.25082
H	-3.51552	-1.9094	-3.19713
H	-1.34224	-2.17407	-2.06022
H	-5.35017	-0.90486	0.56356
C	-5.83828	-1.23757	-2.04821
N	-6.85894	-1.11369	-2.57941

Table 13S. Cartesian coordinates from the optimized structures of S_0 in C_6H_5Cl media for 5d.

Atom symbol	X	Y	Z
C	5.4145	1.04992	-1.80968
C	4.4129	1.61383	-0.94523
C	3.25635	0.84609	-0.66049
C	3.12088	-0.4504	-1.23429
C	4.11229	-0.99255	-2.08385
C	5.27447	-0.1923	-2.35436
N	1.97857	-1.13438	-0.91579
C	3.89369	-2.28161	-2.60359
C	2.7375	-2.96155	-2.26639
C	1.80245	-2.35793	-1.41682
C	4.51378	2.89361	-0.36098
C	3.49361	3.35026	0.45746
C	2.35037	2.56828	0.72576
C	2.20152	1.29716	0.17895
H	4.63021	-2.73251	-3.25961
H	2.53986	-3.95664	-2.6435
C	-1.10299	1.71095	-3.19205
C	-2.02179	2.57999	-2.62464
C	-0.26577	0.89361	-2.40474
C	-2.11881	2.66212	-1.21997
C	-3.02438	3.54028	-0.52798
C	-1.26564	1.83385	-0.45007
C	-3.06993	3.59908	0.83426
C	-2.20716	2.77958	1.63999
N	-0.45652	1.08885	1.64391
C	-2.17607	2.78396	3.04695
C	-0.44305	1.11359	2.97752
C	-1.29259	1.95074	3.71143
C	-0.33045	0.91992	-1.01344
H	-2.83952	3.43965	3.60019
H	0.26845	0.45477	3.45781
H	-1.24165	1.93453	4.79246
Ir	0.72446	-0.0891	0.39861
O	1.87117	-0.97651	2.04666
N	-0.70924	-1.7942	0.68565
C	1.73021	-2.15379	2.51471
C	0.69347	-3.0504	2.22935
C	-0.47663	-2.84868	1.45603
H	0.7535	-4.00703	2.73026
C	2.8047	-2.57793	3.49604
H	2.82177	-1.88042	4.33866

H	3.78294	-2.51863	3.01057
H	2.65382	-3.58894	3.87498
C	-1.50408	-3.96622	1.53681
H	-1.03592	-4.88501	1.88838
H	-1.97175	-4.15534	0.56918
H	-2.30209	-3.71093	2.23968
C	-1.32116	1.9069	0.96994
C	-1.99459	-1.6247	0.1185
C	-2.18771	-1.75861	-1.26599
C	-3.08831	-1.26042	0.92273
C	-4.34124	-1.05018	0.36854
C	-4.50475	-1.20502	-1.00775
C	-3.43617	-1.559	-1.83197
H	-2.9441	-1.134	1.9887
H	-5.18385	-0.76729	0.98384
H	0.8949	-2.86854	-1.12676
H	6.04234	-0.5992	-3.00313
H	6.3004	1.63809	-2.02658
H	5.38507	3.50952	-0.55598
H	3.57264	4.33642	0.90459
H	1.5843	2.98181	1.37282
H	-1.02361	1.65627	-4.27352
H	0.4341	0.23485	-2.90839
H	-2.65822	3.19799	-3.24865
H	-3.68251	4.17114	-1.11675
H	-3.75905	4.27173	1.33306
H	-3.5902	-1.67075	-2.89599
H	-1.34835	-2.0208	-1.89566
N	-5.82262	-0.98986	-1.59895
O	-6.74878	-0.66027	-0.85792
O	-5.95175	-1.14786	-2.81274

Table 14S. Cartesian coordinates from the optimized structures of S_0 in C_6H_5Cl media for 5e.

Atom symbol	X	Y	Z
C	-5.63961	-1.34235	-0.72232
C	-4.47168	-1.76361	0.0038
C	-3.30859	-0.9565	-0.06005
C	-3.33033	0.2374	-0.83614
C	-4.48458	0.63962	-1.54671
C	-5.64937	-0.19731	-1.46267
N	-2.17198	0.96663	-0.85275
C	-4.4143	1.83571	-2.28408
C	-3.23865	2.56436	-2.28375
C	-2.1376	2.10092	-1.55351
C	-4.4146	-2.94011	0.77951
C	-3.24061	-3.26224	1.44098
C	-2.09475	-2.44316	1.36174
C	-2.09676	-1.26814	0.6152
H	-5.27856	2.17849	-2.84247
H	-3.1515	3.49157	-2.83534
C	0.54741	-2.15399	-3.23529
C	1.58657	-2.92003	-2.73084
C	-0.16001	-1.23613	-2.43154
C	1.94459	-2.79003	-1.37265
C	2.9962	-3.54486	-0.74471
C	1.21754	-1.86471	-0.58434
C	3.29665	-3.39712	0.57785
C	2.56762	-2.47478	1.4042
N	0.78327	-0.82149	1.49388
C	2.79924	-2.2682	2.77699
C	1.01861	-0.6471	2.79534
C	2.02198	-1.35523	3.46833
C	0.15935	-1.05519	-1.08736
H	3.58024	-2.82461	3.28351
H	0.38486	0.06833	3.303
H	2.17308	-1.17631	4.52501
Ir	-0.65268	0.14365	0.3354
O	-1.49149	1.27549	2.01457
N	0.75386	1.86471	0.06438
C	-1.2953	2.51294	2.25535
C	-0.36169	3.35098	1.63623
C	0.64337	3.02851	0.68823
H	-0.35014	4.37388	1.98725
C	-2.16988	3.08929	3.35125
H	-1.99976	2.5356	4.27926

H	-3.2221	2.95444	3.08498
H	-1.97854	4.14764	3.52973
C	1.63861	4.14157	0.40182
H	1.23276	5.10203	0.71725
H	1.89223	4.19576	-0.65813
H	2.57078	3.97836	0.95039
C	1.53901	-1.72235	0.79476
C	1.9118	1.62188	-0.7257
C	1.84093	1.61208	-2.12595
C	3.13355	1.33094	-0.11441
C	4.24343	1.05652	-0.90862
C	4.18846	1.05439	-2.29948
C	2.9663	1.33769	-2.8997
H	3.22152	1.31024	0.96237
H	-1.20905	2.65356	-1.52447
H	-6.54097	0.10284	-2.00219
H	-6.53037	-1.96024	-0.67127
H	-5.28556	-3.58254	0.85198
H	-3.19841	-4.16916	2.03638
H	-1.20483	-2.75066	1.90031
H	0.26728	-2.2628	-4.27872
H	-0.96529	-0.66724	-2.88478
H	2.11904	-3.61934	-3.36636
H	3.55733	-4.25002	-1.34949
H	4.09276	-3.97867	1.02947
H	2.88932	1.34136	-3.98018
H	0.89428	1.8223	-2.60684
H	5.0717	0.83473	-2.88145
N	5.52219	0.75114	-0.24627
O	5.56636	0.79314	0.98059
O	6.4871	0.46791	-0.95142

Table 15S. Cartesian coordinates from the optimized structures of S_0 in C_6H_5Cl media for 5f.

Atom symbol	X	Y	Z
C	5.2489	1.41453	-1.2605
C	4.07328	1.98497	-0.66044
C	2.96623	1.13781	-0.40468
C	3.04857	-0.24221	-0.74413
C	4.21431	-0.79206	-1.32389
C	5.31942	0.0903	-1.57726
N	1.94209	-1.00018	-0.46603
C	4.21735	-2.1712	-1.60421
C	3.10038	-2.92498	-1.29878
C	1.98065	-2.30743	-0.7259
C	3.9582	3.34526	-0.30551
C	2.785	3.79951	0.27356
C	1.69643	2.93674	0.52099
C	1.75729	1.58503	0.19345
H	5.09271	-2.6307	-2.05034
H	3.06784	-3.98905	-1.49397
C	-1.07991	1.03961	-3.59849
C	-2.10032	1.93393	-3.31544
C	-0.3037	0.44756	-2.58079
C	-2.3739	2.26773	-1.97272
C	-3.39873	3.19321	-1.56838
C	-1.5836	1.65831	-0.96793
C	-3.6181	3.49673	-0.25632
C	-2.82779	2.89762	0.78362
N	-1.01855	1.3562	1.30796
C	-2.97741	3.15553	2.15889
C	-1.17592	1.62083	2.6061
C	-2.14958	2.51605	3.06614
C	-0.53638	0.73078	-1.23711
H	-3.73496	3.85326	2.499
H	-0.50255	1.10983	3.28201
H	-2.23656	2.69723	4.1297
Ir	0.39472	0.09357	0.44955
O	1.35499	-0.432	2.34794
N	-0.9714	-1.68136	0.82733
C	1.26132	-1.55869	2.93969
C	0.33886	-2.57671	2.67252
C	-0.76465	-2.5774	1.78141
H	0.40993	-3.44559	3.31248
C	2.24909	-1.75958	4.07186
H	2.10913	-0.97369	4.81992

H	3.2672	-1.65791	3.6855
H	2.14489	-2.73158	4.55444
C	-1.76451	-3.70092	1.98552
H	-1.34343	-4.47907	2.62086
H	-2.05894	-4.1434	1.03314
H	-2.66912	-3.32424	2.47192
C	-1.82403	1.9815	0.39668
C	-2.23534	-1.66256	0.18033
C	-2.49418	-2.16655	-1.11029
C	-3.30425	-1.00156	0.80529
C	-4.54084	-0.84772	0.19049
C	-4.75294	-1.331	-1.10097
C	-3.71994	-1.98486	-1.75385
H	-3.13763	-0.59722	1.79588
H	-5.33891	-0.3388	0.71869
H	-5.71063	-1.20599	-1.5905
H	1.09656	-2.87535	-0.479
H	6.21671	-0.32203	-2.02569
H	6.09576	2.0639	-1.45792
H	4.78554	4.02285	-0.48707
H	2.69741	4.84689	0.54577
H	0.80557	3.35431	0.97674
H	-0.86825	0.78704	-4.63288
H	0.48472	-0.24	-2.8673
H	-2.68364	2.37986	-4.11378
H	-4.00531	3.65975	-2.3381
H	-4.39371	4.20119	0.02368
H	-3.85074	-2.38414	-2.75055
N	-1.51103	-2.97744	-1.83543
O	-1.46535	-2.87748	-3.0576
O	-0.80918	-3.75199	-1.18889

Table 16S. Cartesian coordinates from the optimized structures of S_0 in C_6H_5Cl media for 5g.

Atom symbol	X	Y	Z
C	6.02788	-0.22221	-2.82368
C	5.23471	0.72711	-2.08987
C	4.1218	0.25075	-1.35293
C	3.82414	-1.14207	-1.3615
C	4.6097	-2.06453	-2.09009
C	5.73268	-1.55349	-2.82655
N	2.73607	-1.53013	-0.62731
C	4.23813	-3.42076	-2.04151
C	3.13848	-3.7961	-1.29125
C	2.41184	-2.82334	-0.59379
C	5.49969	2.11211	-2.06085
C	4.67413	2.94718	-1.32551
C	3.57065	2.44985	-0.60071
C	3.26558	1.09159	-0.59052
H	4.8141	-4.15944	-2.58821
H	2.82732	-4.83088	-1.22816
C	-0.6265	0.59236	-3.26826
C	-1.37714	1.70878	-2.93425
C	0.31464	0.0341	-2.37874
C	-1.19191	2.31297	-1.6736
C	-1.90768	3.48013	-1.23125
C	-0.23962	1.73605	-0.79819
C	-1.68436	4.04082	-0.00784
C	-0.71544	3.48427	0.89562
N	0.93163	1.72896	1.25591
C	-0.40968	4.00257	2.16782
C	1.20721	2.24112	2.45629
C	0.55227	3.37872	2.94397
C	0.5289	0.57942	-1.11466
H	-0.92491	4.88556	2.53007
H	1.97237	1.7308	3.02675
H	0.81308	3.75568	3.92456
Ir	1.80075	0.05525	0.37732
O	3.20324	-0.28229	2.02901
N	0.37608	-1.2551	1.50934
C	3.10749	-1.19776	2.91391
C	2.00372	-2.02103	3.15205
C	0.7114	-1.98256	2.56286
H	2.11992	-2.73553	3.95565
C	4.33348	-1.35648	3.79145
H	4.54325	-0.4089	4.29635

H	5.20082	-1.58557	3.16563
H	4.21681	-2.13966	4.54096
C	-0.32448	-2.87172	3.23278
H	0.16567	-3.64007	3.83
H	-0.9776	-3.3521	2.50265
H	-0.96211	-2.28659	3.90146
C	-0.01387	2.33257	0.4738
C	-0.99766	-1.17445	1.14469
C	-1.48075	-1.83029	0.00633
C	-1.88927	-0.39108	1.8925
C	-3.22196	-0.27951	1.52462
C	-3.71073	-0.94709	0.38985
C	-2.81523	-1.72276	-0.36092
H	-1.52568	0.13619	2.76691
H	-3.89943	0.32944	2.10942
H	1.55291	-3.0852	0.00821
H	6.3442	-2.25219	-3.38695
H	6.881	0.1427	-3.38669
H	6.34324	2.51262	-2.61276
H	4.87901	4.01323	-1.30594
H	2.96087	3.15395	-0.04477
H	-0.76479	0.13309	-4.24248
H	0.87179	-0.83972	-2.70011
H	-2.09734	2.12188	-3.63215
H	-2.64219	3.91895	-1.89899
H	-2.2352	4.92187	0.30281
H	-0.80439	-2.42544	-0.59356
H	-3.15607	-2.25013	-1.24501
C	-5.12336	-0.81183	0.02228
S	-5.77573	-1.60194	-1.44388
N	-5.99676	-0.13253	0.70164
C	-7.25276	-0.17565	0.12797
C	-7.34755	-0.93387	-1.06186
C	-8.39615	0.4608	0.63165
C	-9.59686	0.32995	-0.05287
C	-9.67598	-0.42639	-1.23385
C	-8.55344	-1.06589	-1.75086
H	-8.32605	1.0426	1.54309
H	-10.4866	0.8179	0.32781
H	-10.6239	-0.5145	-1.75189
H	-8.61806	-1.64783	-2.66219

Table 17S. Cartesian coordinates from the optimized structures of S_0 in C_6H_5Cl media for 5h.

Atom symbol	X	Y	Z
C	-5.72531	1.06077	0.45312
C	-4.54302	1.55796	-0.19747
C	-3.33794	0.82341	-0.06464
C	-3.33329	-0.37587	0.70387
C	-4.50229	-0.85113	1.34208
C	-5.70927	-0.08712	1.18855
N	-2.13585	-1.03478	0.78888
C	-4.40484	-2.04255	2.08366
C	-3.18876	-2.69678	2.15722
C	-2.07606	-2.16559	1.49372
C	-4.51224	2.74193	-0.96314
C	-3.32204	3.14216	-1.54852
C	-2.13447	2.3955	-1.40103
C	-2.10837	1.21619	-0.66103
H	-5.27942	-2.43839	2.58844
H	-3.07791	-3.61734	2.71566
C	0.26367	2.19384	3.35116
C	1.26646	3.04304	2.9091
C	-0.33739	1.24429	2.49971
C	1.69556	2.96516	1.56792
C	2.70859	3.81421	0.99924
C	1.0787	2.00212	0.73229
C	3.06906	3.72444	-0.31339
C	2.44738	2.76881	-1.18814
N	0.81082	0.97742	-1.38204
C	2.73448	2.62648	-2.55836
C	1.09371	0.8683	-2.68111
C	2.05229	1.67849	-3.30138
C	0.05833	1.11051	1.17043
H	3.48044	3.26163	-3.02373
H	0.53422	0.12216	-3.23056
H	2.24441	1.54965	-4.35883
Ir	-0.60118	-0.11059	-0.3084
O	-1.28427	-1.25207	-2.04914
N	0.86257	-1.78398	0.03228
C	-1.06704	-2.49411	-2.25334
C	-0.18402	-3.31624	-1.54969
C	0.7618	-2.97093	-0.54482
H	-0.15597	-4.34965	-1.86798
C	-1.85931	-3.09291	-3.39914
H	-1.63311	-2.5484	-4.32064

H	-2.92878	-2.96788	-3.2064
H	-1.64471	-4.15105	-3.55106
C	1.70656	-4.09464	-0.14905
H	1.28475	-5.05985	-0.42809
H	1.90932	-4.09153	0.92265
H	2.667	-3.98896	-0.6615
C	1.46588	1.91654	-0.63434
C	1.96638	-1.54223	0.90831
C	1.77235	-1.51071	2.2742
C	3.27536	-1.28614	0.37935
C	4.35243	-1.02429	1.28953
C	4.10316	-1.01383	2.68593
C	2.8371	-1.2514	3.1629
H	-1.11623	-2.66112	1.52404
H	-6.61157	-0.44469	1.67239
H	-6.64759	1.62335	0.34926
H	-5.41584	3.32911	-1.08695
H	-3.29996	4.0546	-2.13663
H	-1.23469	2.76185	-1.88317
H	-0.07183	2.26205	4.3817
H	-1.12101	0.61157	2.90378
H	1.71517	3.7676	3.58011
H	3.18765	4.54723	1.64052
H	3.83099	4.37965	-0.72121
C	5.65258	-0.78353	0.76766
C	5.88881	-0.79803	-0.58576
C	4.82626	-1.05101	-1.48459
C	3.55598	-1.28784	-1.01345
H	6.46157	-0.58724	1.46392
H	6.88668	-0.61414	-0.9682
H	2.74994	-1.4751	-1.71069
H	5.01596	-1.05557	-2.55222
H	2.64448	-1.24057	4.22997
H	0.7804	-1.68676	2.66972
H	4.92406	-0.81419	3.36635

Table 18S. Cartesian coordinates from the optimized structures of S_0 in C_6H_5Cl media for 5i.

Atom symbol	X	Y	Z
C	5.62667	1.07315	-1.41368
C	4.56941	1.60935	-0.59913
C	3.38842	0.84337	-0.43418
C	3.28574	-0.42533	-1.07361
C	4.33274	-0.94166	-1.87124
C	5.51718	-0.14242	-2.02191
N	2.11813	-1.10996	-0.86964
C	4.14417	-2.20608	-2.45913
C	2.96221	-2.8883	-2.23476
C	1.97137	-2.31059	-1.43167
C	4.639	2.86027	0.04871
C	3.56575	3.29112	0.81168
C	2.39936	2.51148	0.95956
C	2.27719	1.26782	0.34547
H	4.92366	-2.63694	-3.07801
H	2.78614	-3.86546	-2.66577
C	-0.73301	1.87912	-3.25558
C	-1.66847	2.75302	-2.72319
C	0.0158	1.00308	-2.44354
C	-1.87672	2.77525	-1.32861
C	-2.81263	3.64805	-0.67078
C	-1.11134	1.88756	-0.53329
C	-2.97227	3.64253	0.68399
C	-2.2025	2.75935	1.51626
N	-0.49484	1.02698	1.58123
C	-2.29233	2.69313	2.91902
C	-0.59623	0.98388	2.91041
C	-1.48866	1.80381	3.61197
C	-0.15603	0.97278	-1.06119
H	-2.98558	3.33863	3.44731
H	0.05823	0.28396	3.4133
H	-1.53187	1.73187	4.69113
Ir	0.77136	-0.10895	0.38531
O	1.76385	-1.07851	2.08366
N	-0.70104	-1.7918	0.46209
C	1.58144	-2.28624	2.45873
C	0.577	-3.1544	2.02672
C	-0.53232	-2.89256	1.17464
H	0.59068	-4.14116	2.46973
C	2.56509	-2.77629	3.50339
H	2.49302	-2.14416	4.39359

H	3.58447	-2.67554	3.11996
H	2.39112	-3.81348	3.79112
C	-1.56906	-4.00456	1.12298
H	-1.12336	-4.94846	1.43654
H	-1.98877	-4.12394	0.12344
H	-2.40078	-3.78805	1.79933
C	-1.28289	1.89657	0.87916
C	-1.94649	-1.60385	-0.21253
C	-2.02221	-1.77976	-1.62083
C	-3.07728	-1.22401	0.47874
C	-4.31713	-1.0287	-0.18361
C	-4.39023	-1.22687	-1.59858
C	-3.20815	-1.60506	-2.28895
H	1.04121	-2.82292	-1.22923
H	6.32686	-0.52855	-2.63146
H	6.53059	1.66056	-1.53966
H	5.52757	3.47368	-0.05485
H	3.62082	4.25468	1.30909
H	1.59211	2.90501	1.5681
H	-0.56979	1.86813	-4.32911
H	0.73438	0.34481	-2.92095
H	-2.23464	3.41829	-3.36616
H	-3.40188	4.32594	-1.28007
H	-3.68408	4.31016	1.15714
C	-5.49552	-0.64773	0.51373
C	-5.63231	-1.03688	-2.25885
C	-6.75574	-0.66868	-1.55503
C	-6.68514	-0.47275	-0.15462
H	-3.25203	-1.75106	-3.36338
H	-1.12704	-2.05894	-2.16235
H	-3.02496	-1.07454	1.55197
H	-5.68209	-1.18663	-3.33261
H	-7.69925	-0.52666	-2.07
H	-7.57644	-0.18276	0.3908
H	-5.4432	-0.49722	1.58719

Table 19S. Cartesian coordinates from the optimized structures of S_0 in C_6H_5Cl media for 5j.

Atom symbol	X	Y	Z
C	-6.22089	0.74609	-0.41467
C	-4.98129	1.22677	-0.96309
C	-3.7742	0.60918	-0.54969
C	-3.82401	-0.46046	0.38954
C	-5.04941	-0.91842	0.92668
C	-6.25693	-0.27556	0.48749
N	-2.62092	-1.01141	0.74175
C	-5.0028	-1.9742	1.85536
C	-3.77948	-2.51873	2.20064
C	-2.60907	-2.01405	1.62133
C	-4.89609	2.28506	-1.8914
C	-3.65318	2.68188	-2.35745
C	-2.46474	2.05431	-1.92925
C	-2.49023	1.00077	-1.01911
H	-5.92112	-2.35225	2.29143
H	-3.70626	-3.3339	2.90898
C	-0.80291	2.70396	3.1041
C	0.21241	3.55103	2.6881
C	-1.22186	1.60509	2.3259
C	0.84214	3.31675	1.44805
C	1.88765	4.14626	0.91033
C	0.4063	2.20549	0.68558
C	2.44736	3.89866	-0.30885
C	2.0111	2.79013	-1.11217
N	0.51162	0.87955	-1.2692
C	2.5059	2.48044	-2.39252
C	0.99025	0.61171	-2.48498
C	1.98861	1.39444	-3.07715
C	-0.6238	1.31438	1.10158
H	3.28206	3.09493	-2.83541
H	0.55618	-0.24224	-2.98917
H	2.34259	1.13518	-4.06662
Ir	-0.98784	-0.14636	-0.25666
O	-1.32724	-1.57517	-1.88783
N	0.49139	-1.64925	0.53675
C	-1.05146	-2.8214	-1.84586
C	-0.26913	-3.47363	-0.8894
C	0.51397	-2.91813	0.15968
H	-0.16662	-4.54248	-1.0206
C	-1.63451	-3.63541	-2.98445
H	-1.25379	-3.25184	-3.93584

H	-2.72123	-3.51292	-3.00053
H	-1.39396	-4.6962	-2.90952
C	1.43364	-3.90564	0.85955
H	1.0883	-4.92611	0.69585
H	1.48633	-3.71518	1.93224
H	2.45115	-3.82981	0.46561
C	0.99929	1.95747	-0.5839
C	1.46039	-1.19902	1.48475
C	1.1005	-0.95733	2.78759
C	2.8208	-0.94537	1.06777
C	3.76702	-0.45424	2.0448
C	3.33298	-0.22812	3.38567
C	2.03599	-0.47397	3.74054
H	-1.6404	-2.42645	1.8644
H	-7.20228	-0.62169	0.89084
H	-7.14464	1.2184	-0.73324
H	-5.79954	2.78026	-2.23073
H	-3.58921	3.49875	-3.06986
H	-1.52248	2.41236	-2.32955
H	-1.2934	2.89167	4.05459
H	-2.02632	0.98292	2.70412
H	0.5191	4.39168	3.30113
H	2.2284	4.99308	1.49761
H	3.23047	4.54134	-0.69607
C	5.09102	-0.21537	1.65599
C	5.53139	-0.44309	0.34886
C	4.58958	-0.93395	-0.62569
C	3.26353	-1.16544	-0.24135
H	5.79544	0.15535	2.39453
H	2.56347	-1.52623	-0.98454
H	1.70602	-0.30156	4.75899
H	0.07787	-1.13449	3.09471
H	4.04859	0.14143	4.11213
C	6.88252	-0.20976	-0.05794
C	7.27916	-0.44906	-1.3455
C	6.34869	-0.93731	-2.30953
C	5.04637	-1.17064	-1.95986
H	7.59022	0.1606	0.67664
H	8.3067	-0.26942	-1.64146
H	6.68241	-1.12296	-3.32436
H	4.33789	-1.54265	-2.69258

Table 20S. Cartesian coordinates from the optimized structures of S_0 in C_6H_5Cl media for 5k.

Atom symbol	X	Y	Z
C	6.12929	1.03506	-1.61793
C	5.10923	1.58137	-0.7637
C	3.93065	0.82427	-0.54875
C	3.79273	-0.4452	-1.18012
C	4.80305	-0.97094	-2.01781
C	5.98668	-0.18136	-2.21751
N	2.62853	-1.12015	-0.92874
C	4.58101	-2.23426	-2.59615
C	3.40264	-2.90586	-2.3255
C	2.4492	-2.31928	-1.48438
C	5.2129	2.83411	-0.12397
C	4.17399	3.27506	0.67969
C	3.00929	2.50396	0.87742
C	2.85471	1.25896	0.27341
H	5.33209	-2.67222	-3.24447
H	3.20111	-3.88146	-2.74882
C	-0.29637	1.88921	-3.19704
C	-1.21369	2.75927	-2.62792
C	0.48358	1.01307	-2.41537
C	-1.36826	2.77969	-1.22636
C	-2.27963	3.64995	-0.53187
C	-0.57069	1.89328	-0.46176
C	-2.38393	3.64534	0.82824
C	-1.57771	2.76609	1.62966
N	0.13429	1.03638	1.62675
C	-1.60794	2.70372	3.0351
C	0.08889	0.99675	2.9592
C	-0.774	1.81774	3.69573
C	0.36316	0.97954	-1.02761
H	-2.27915	3.34966	3.59061
H	0.76385	0.29835	3.43636
H	-0.77127	1.74877	4.77595
Ir	1.34321	-0.10781	0.37998
O	2.40402	-1.0844	2.03261
N	-0.13895	-1.77739	0.53041
C	2.22827	-2.28906	2.41975
C	1.19639	-3.14889	2.03799
C	0.05251	-2.87921	1.23618
H	1.22258	-4.13538	2.48102
C	3.25766	-2.78705	3.41534
H	3.25406	-2.13803	4.29609

H	4.25524	-2.7199	2.97162
H	3.07504	-3.81462	3.73087
C	-0.99158	-3.98568	1.22815
H	-0.53309	-4.93462	1.50645
H	-1.46427	-4.09202	0.25104
H	-1.78493	-3.77513	1.95065
C	-0.68388	1.90347	0.95658
C	-1.411	-1.57244	-0.08325
C	-1.53491	-1.70426	-1.50332
C	-2.51085	-1.21888	0.65659
C	-3.78342	-1.00391	0.04527
C	-3.904	-1.1567	-1.38396
C	-2.73493	-1.51246	-2.12527
H	1.52305	-2.8231	-1.24592
H	6.76846	-0.57527	-2.85775
H	7.03167	1.61546	-1.78169
H	6.10061	3.44127	-0.2652
H	4.25534	4.24012	1.17057
H	2.22971	2.90504	1.51643
H	-0.17358	1.88068	-4.27596
H	1.18426	0.35637	-2.9206
H	-1.80578	3.42387	-3.24784
H	-2.89547	4.3254	-1.11708
H	-3.07835	4.31116	1.32897
C	-4.91843	-0.65684	0.7878
C	-5.14506	-0.95205	-1.99392
C	-6.2803	-0.60402	-1.25174
C	-6.16288	-0.45385	0.17892
H	-2.81471	-1.62318	-3.20171
H	-0.65548	-1.96302	-2.07916
H	-2.42207	-1.10185	1.73131
H	-5.23081	-1.0654	-3.07048
H	-4.83278	-0.54359	1.8643
C	-7.55579	-0.39285	-1.86132
C	-8.64874	-0.05629	-1.10928
C	-8.53375	0.09075	0.30383
C	-7.33008	-0.10186	0.92628
H	-7.6415	-0.50508	-2.93727
H	-9.61042	0.10057	-1.58478
H	-9.41015	0.35709	0.8841
H	-7.24331	0.00992	2.00221

Table 21S. Cartesian coordinates from the optimized structures of S_0 in C_6H_5Cl media for 5l.

Atom symbol	X	Y	Z
C	5.82823	0.46734	-1.16893
C	4.70355	1.30314	-0.84667
C	3.49211	0.68446	-0.44627
C	3.42815	-0.73542	-0.36233
C	4.55134	-1.5439	-0.65584
C	5.7592	-0.89097	-1.07806
N	2.23144	-1.26489	0.04428
C	4.41843	-2.93493	-0.49489
C	3.21894	-3.45013	-0.0412
C	2.15131	-2.58395	0.22361
C	4.7404	2.71172	-0.89781
C	3.609	3.43285	-0.55376
C	2.41499	2.79601	-0.15697
C	2.32032	1.40765	-0.0918
H	5.25706	-3.58762	-0.71162
H	3.08544	-4.51241	0.11778
C	-0.20712	0.14174	-3.88126
C	-1.1419	1.16177	-3.96625
C	0.39851	-0.2141	-2.65862
C	-1.49162	1.87614	-2.80186
C	-2.41617	2.97851	-2.78333
C	-0.87467	1.4957	-1.58489
C	-2.68081	3.67735	-1.64188
C	-2.04616	3.33265	-0.39962
N	-0.51214	1.81669	0.72722
C	-2.21476	4.02836	0.81177
C	-0.67817	2.50022	1.86066
C	-1.52166	3.61458	1.93621
C	0.07245	0.43838	-1.47265
H	-2.87671	4.88646	0.85469
H	-0.11933	2.14529	2.7171
H	-1.6216	4.13503	2.88003
Ir	0.76073	0.20294	0.42455
O	1.44357	0.13963	2.5093
N	-0.8373	-1.28113	1.08711
C	1.23936	-0.83208	3.3123
C	0.31221	-1.86718	3.15766
C	-0.72544	-2.00096	2.19377
H	0.29526	-2.5992	3.95401
C	2.09187	-0.80593	4.56587
H	1.90737	0.12482	5.11049

H	3.14939	-0.81038	4.28648
H	1.89199	-1.64908	5.22754
C	-1.76991	-3.05329	2.52966
H	-1.35388	-3.79131	3.21544
H	-2.13507	-3.56318	1.6377
H	-2.63198	-2.59282	3.02123
C	-1.16733	2.2265	-0.39993
C	-2.08069	-1.34055	0.37662
C	-2.21518	-2.11828	-0.79691
C	-3.19117	-0.60879	0.86593
C	-4.44007	-0.63062	0.1412
C	-4.54704	-1.37934	-1.03178
C	-3.47254	-2.13349	-1.50646
H	1.21375	-2.96128	0.60253
H	6.62143	-1.5045	-1.31557
H	6.75207	0.94233	-1.48317
H	5.65048	3.21787	-1.20119
H	3.63836	4.51757	-0.59082
H	1.56534	3.41932	0.09742
H	0.06921	-0.39968	-4.78093
H	1.12664	-1.01803	-2.65757
H	-1.5947	1.4206	-4.91733
H	-2.90015	3.26153	-3.71278
H	-3.36995	4.5147	-1.65606
C	-3.60265	-2.95206	-2.67223
C	-2.56977	-3.73439	-3.10803
C	-1.33322	-3.73119	-2.40466
C	-1.16416	-2.94426	-1.29775
H	-0.51595	-4.35022	-2.75807
H	-0.21553	-2.93574	-0.78625
H	-4.55124	-2.94658	-3.19905
H	-2.68698	-4.35715	-3.98788
C	-5.55662	0.09927	0.65786
C	-5.46584	0.79655	1.82989
C	-3.14439	0.13801	2.08482
C	-4.24035	0.8111	2.5534
H	-6.48648	0.07781	0.09894
H	-6.32309	1.33851	2.21349
H	-2.21998	0.16386	2.64459
H	-4.1763	1.36559	3.48303
H	-5.48932	-1.39523	-1.57025

8. Photophysical measurements

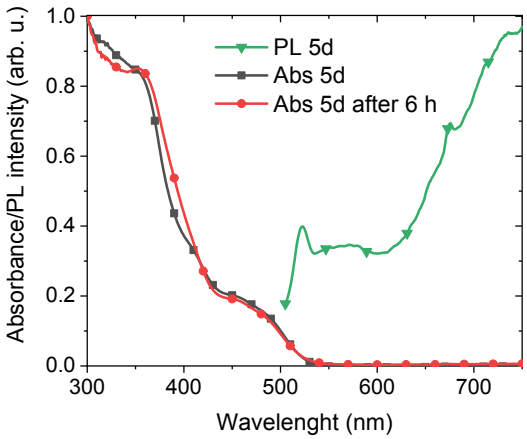

Figure 36S. Normalized absorption and photoluminescence spectra of **5d** in chlorobenzene.

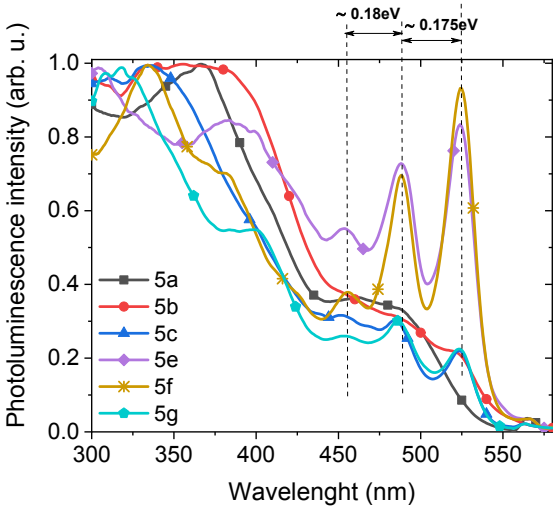

Figure 37S. Normalized photoluminescence excitation spectra (measured at emission band) of the first group (**5a–5g**) of investigated complexes in chlorobenzene.

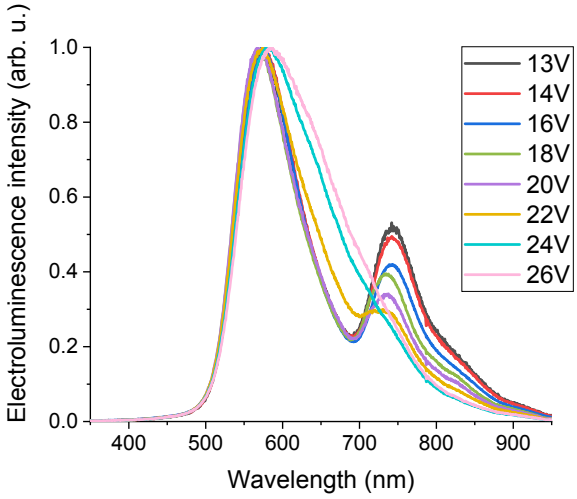

Figure 38S. Normalized EL spectra of PhOLEDs based on PVK/PBD doped with **5l** under incensement of applied voltage.

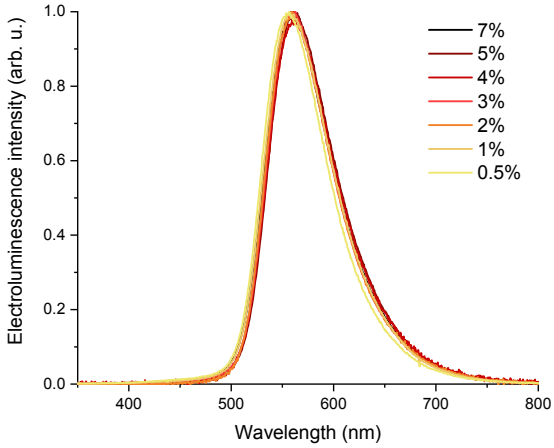

Figure 39S. Normalized EL spectra of PhOLEDs based on PVK/PBD doped with **5h** in different concentrations (from 0.5 to 7 wt%).

FULL PAPER DOI: 10.1002/adsc.201800286

Synthesis of 5-Substituted Benzo[*h*]quinoline Derivatives *via* Reactions Involving C(sp^2)–Br Bond Activation

Bartosz Orwat,[a, b] Myong-joon Oh Oh,[a, b] Maciej Kubicki,[a] and Ireneusz Kownacki[a, b,*]

[a] Faculty of Chemistry, Adam Mickiewicz University in Poznań, St. Umultowska 89b, 61-614 Poznań, Poland
Tel: +48 61 829 1554
Fax: +48 61 829 1555
E-mail: irekk@o365.amu.edu.pl
[b] Center for Advanced Technology, Adam Mickiewicz University in Poznań, Umultowska 89c, 61-614 Poznań, Poland

Received: February 28, 2018; Published online: July 11, 2018

Supporting information for this article is available on the WWW under https://doi.org/10.1002/adsc.201800286

Abstract: In view of literature reports, benzo[*h*]quinoline and its substituted analogues, due to their structural similarity to 2-phenylpyridine derivatives, appear to be very promising *C*,*N*-cyclometalating ligands for iridium-based *Phosphorescent Organic Light Emitting Diode* technology. 5-bromo-benzo[*h*]quinoline aroused our particular interest as a convenient precursor for further transformations, and was successfully functionalized in the course of transition metal-promoted exclusive C–C, C–O and C–N bond formation, yielding a series of 5-substituted benzo[*h*]quinoline derivatives with unique structures and properties. Some of the synthesized compounds seemed to be appropriate starting materials for subsequent transformations, and enabled the preparation of new benzo[*h*]quinoline-based materials, for instance those with fluorine or silsesquioxane groups, which have not been synthesized by the conventional Scraup protocol. In selected transformations, the assistance of microwave irradiation as a non-conventional energy carrier significantly improved efficiency, leading to the formation of desired products with yields of up to 99%.

Keywords: Cross-coupling; Homogeneous catalysis; Ligand design; Microwave chemistry; Nitrogen heterocycles

1 Introduction

Organic chemists have shown moderate interest in benzo[*h*]quinoline (bzqH) since it was first obtained by Scraup in the course of a reaction between 1-naphthylamine and glycerol in the presence of nitrobenzene and sulfuric acid.[1] On the basis of this protocol, some simple alkyl, alkoxy, nitro or halogen-substituted bzqH derivatives have been synthesized with use of starting materials already bearing in their structures the above-mentioned functional groups.[2] A few bioactive bzqH-based derivatives have been obtained also by means of the zinc chloride-mediated Scraup protocol.[3] Unfortunately, this synthetic pathway, involving the formation of a third *N*-aromatic ring, is characterized by low yields of desired products. Moreover, the reactions must be performed in harsh conditions. These two factors have reduced interest in this protocol. In contrast, a few bzqH derivatives have been prepared *via* different types of transformations, including condensation, Diels-Alder reaction, cyclization and more complex processes involving a series of subsequent reactions, occurring in significantly milder conditions.[4] In order to improve the efficiency of nitrogen-containing ring formation, compounds of transition metals, *i.e.* Mn, Fe, Cu, Ru, Rh, Pd, W, Ir[5] or main group elements such as Mg or In,[6] have been proposed as reaction catalysts, resulting in moderate to good yields. Nevertheless, in most cases, these methods require expensive catalysts or specific, non-commercially available substrates. There is only one report in literature concerning *one-pot* synthesis of various azaphenanthrenes *via* palladium-catalyzed Suzuki-Miyaura coupling/aldol condensation cascade reaction, involving the formation of an inner aromatic ring instead of an *N*-cyclic part of the molecule, as takes place in almost all of the aforementioned methods.[7] It is noteworthy that most bzqH derivatives have been obtained while working on methods for the synthesis of new indoles or quinolines. Moreover, it should be emphasized that all methods mentioned in this paragraph are not entirely satisfactory because

they require complex substrates, expensive catalysts, harsh conditions or high specificity of reaction.

Instead of the inefficient method based on the formation of a third aromatic ring, using specific substrates bearing in their structure target functional moieties, an alternative approach leading to functionalized bzqH compounds can be applied *via* direct functionalization of the bzqH core (see Scheme 1). It is possible to obtain the desired compounds through direct catalytic alkylation, arylation, imidation or lithiation,[8] as well as in the course of typical organic stoichiometric transformations, such as nitration or halogenation and subsequent transformation of nitro or halogen groups.[9] The C(sp^2)–H bond at position 10 in the bzqH core is the most reactive part of this molecule, due to its specific location relative to the nitrogen atom in the cavity. There are many examples illustrating the reactivity of this position in processes such as acylation, alkoxylation, arylation, halogenation, and thiolation.[10] Unfortunately, the functionalization of the bzqH molecule in this position has a serious disadvantage, namely blocking the aforementioned specific cavity. The replacement of 10-H with the introduced substituent via C(sp^2)–H bond activation decreases potential applications of the new compounds by hindering the most important fragment of the molecule.

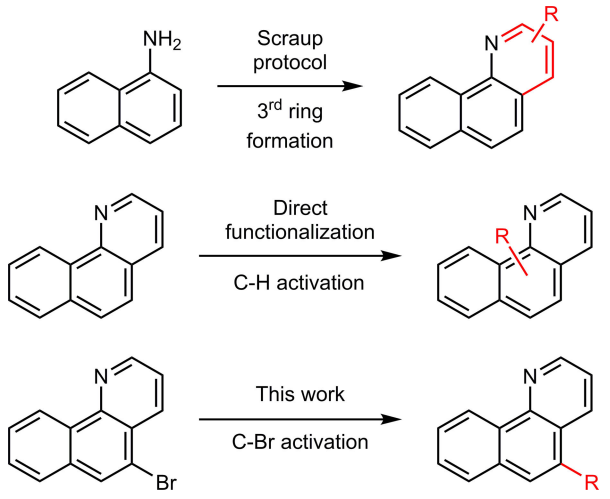

Scheme 1. Comparison of the synthetic protocols for the synthesis of bzqH derivatives.

According to literature, nitration of bzqH in a nitric/sulfuric acid mixture is very inefficient compared to halogenation, which can be performed very selectively and with high yields.[11] However, despite the fact that bromo- and iodo-benzo[*h*]quinolines have been obtained with good regioselectivity and yields,[12] no additional study on the catalytic transformation of these compounds leading to bzqH derivatives has been reported. Taking into account some potential applications of the compounds listed below, it seems pertinent to carry out studies aimed at the development of efficient methods of synthesis, which may lead to new bzqH derivatives with unique properties.

BzqH and its derivatives are considered interesting and useful *C*,*N*-cyclometalating ligands in coordination chemistry, particularly due to their structural similarity to 2-phenylpyridine (ppyH), the heterocyclic compound which is one of the most widely studied and commonly used ligands in the preparation of iridium(III) phosphorescent emitters for organic light emitting diodes (OLEDs).[13] Since 1995, hundreds of publications concerning the relationships between the structure of the ligand, *i.e.* the specific nature of substituents bonded to *C*,*N*-cyclometalating core, for example ppy ligand, and the photophysical properties of the final iridium(III) OLEDS's dopant, such as emitted wavelength, quantum efficiency, excited state lifetime *etc.*, have been published.[14] In this context, bzqH seems to be very intriguing due to its similarity to ppyH (Scheme 2). It contains an ethynylene bridge, which not only stiffens its structure but also extends electron π-conjugation more than in the ppy ligand. However, it does so without changing the pocket size or bite angle, and thus does not disturb its coordination ability. As a matter of fact, there are known organometallic compounds bearing cyclometalated bzq ligand, among which iridium(III) compounds show the most interesting properties.[15] However, the impact of bzq modifications on iridium emitters containing ligands such as these still remains unknown due to the lack of consequently regiofunctionalized bzqH derivatives containing electron-donating, electron-withdrawing, *n*- and *p*-type semiconducting or sterically hindered substituents. A significant part of the known bzqH derivatives are unsuitable for this purpose, due to the presence of substituents at position 2, hindering cyclometalation, or at position 10, making it potentially impossible. After studying the available literature, we chose 5-bromo-benzo[*h*]quinoline (**1**) as the most accessible precursor for further modifications and decided to investigate its ability to undergo structural modification *via* some

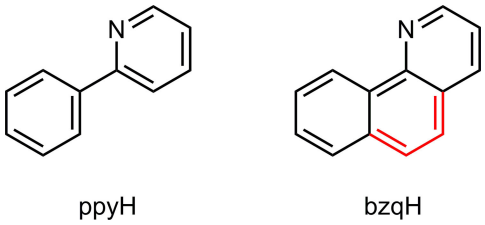

Scheme 2. Chemical structures of 2-phenylpyridine (ppyH) and benzo[*h*]quinoline (bzqH).

well-known organometallic transformations. As a result, we hoped to obtain bzqH derivatives bearing in their structure functional groups with unique properties, which could potentially be interesting and useful for designing iridium-based emitters for application in OLEDs, similarly to ppyH derivatives.

2 Results and Discussion

At first, we focused on equipping the bzqH core with electron-donating substituents. Our area of interest was focused on the substituents characterized by high σ_{para} and low σ_{meta} Hammett parameters since if these groups are properly regiolocalized on the ppyH core, they can tune the wavelength emitted by OLEDs to the blue area.[16] Fluorine is the most commonly used substituent for this purpose, but it has been shown that a methoxy substituent acts similarly and exhibits better stability.[17] Taking into account the aforementioned criteria, as the first example of such substituents, a methoxy moiety was chosen. A few attempts to introduce this group were performed based on procedures described in the literature, such as coupling of aryl bromides with sodium methoxide or methanol in the presence of copper or palladium catalysts, unfortunately, led only to a debrominated product.[18] However, replacement of the sodium cation in the initial methoxide with a lithium cation unexpectedly changed the reaction selectivity. Therefore, the reaction system which included 2 equivalents of lithium methoxide in methanol and 5 mol% of copper(I) iodide as a reaction promotor was found to be very efficient and led to the exclusive formation of the desired methoxylated derivative.[19] The summary of the reaction parameters is shown in Scheme 3. Additionally, it should be emphasized that the assistance of microwaves, as a non-conventional source of heat, allowed full conversion to be reached in a very short reaction time, *ca.* 10 minutes.

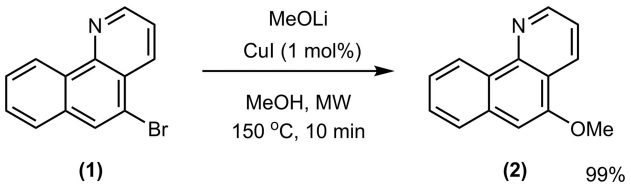

Scheme 3. Copper-catalyzed alkoxylation of **1**.

In the next step, we tried out to introduce a phenoxy group which exhibits Hammett's parameters similar to those of the methoxy moiety but features a much higher steric hindrance. Bearing in mind the more acidic character of a phenolic hydroxyl group, as a consequence of stronger H–O bond polarization and thus lower nucleophilicity of the phenoxy anion in contrast to methoxy anion, the synthetic strategy had to be different than the one previously utilized. The iron-copper catalytic system, which has been described in the literature,[20] applied in the examined reagent system showed moderate efficiency in the conversion of **1** to an appropriate phenoxy-functionalized derivative. Both extension of the reaction time and duplication of the catalyst, as well as phenol loading, resulted in only very slight reaction progress. A short period (*i.e.* 10 minutes) of microwave irradiation showed no significant effect on the conversion of the reagents. However, GCMS analysis showed that extended heating in the microwave pressure reactor (12 h) at an elevated temperature (150 °C) led to total halogen-substituted substrate consumption and its transformation into 5-phenoxybenzo[*h*]quinoline with accompanying small amount of bzqH, as a result of the debromination process. However, the desired product was isolated with only 20% yield. This may be the result of prolonged heating leading to the decomposition of the formed product. In order to avoid the occurrence of undesirable processes, we decided to carry out the phenoxylation reaction at a higher temperature but for a shorter time. Therefore, at this point, we examined the catalytic method described in literature, in which copper(I) halides were successfully used as catalysts in *O*-arylation of phenol in an NMP environment.[21] The model reaction system used for optimization consisted of various loadings of copper (I) chloride, 1.3 eq of phenol and 1.1 eq of cesium carbonate (Scheme 4), as reported. At first, we examined the reaction efficiency under the reported conditions which led to *ca.* 54% conversion of the substrate without the occurrence of debromination (Table 1, attempt 1). Application of the previously described guidelines, along with double or triple catalyst loading, resulted in a significant increase in conversion. Finally, this method after optimization proved to be very efficient. In the course of the reaction, the intended product was selectively obtained without debromination of the initial substrate, and was isolated with 86% yield.

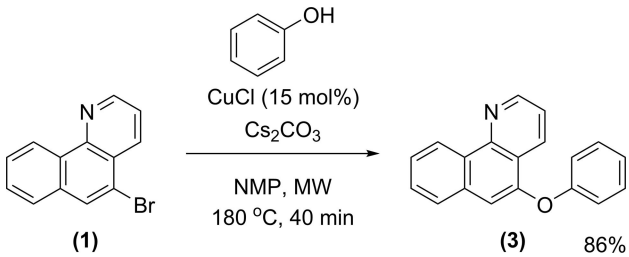

Scheme 4. Copper-mediated aryloxylation of **1**.

Table 1. Optimization for the synthesis of **3**[a]

Attempt	Reaction time [min]	CuCl loading [mol%]	Temperature [°C]	GC conversion [%]
1	960	5	160	54
2	20	10	180	80
3	30	10	180	87
4	40	15	180	98

[a] Conditions: **1** (0.25 mol), phenol (0.325 mol), Cs_2CO_3 (0.275 mol), NMP (1 mL).

In order to complete the series of bzqH derivatives containing an electron-donating substituent, as the last example, an amino group was selected. This type of moiety may endow unique properties to the bzq-cored ligand due to its basic character, unlike methoxy and phenoxy groups. Therefore, to convert **1** to the corresponding amino-functionalized derivative, we tried applying the methods reported in the literature, according to which the series of quinazolines and various other aryl amines were successfully prepared, with the use of aqueous ammonia solution and in the presence of copper(I) oxide, chloride or iodide.[22] It turned out, unexpectedly, that the reaction carried out under the conditions disclosed in the aforementioned publications did not bring positive results. Microwave irradiation of the reaction systems did not show any effect, but only small amounts of 5-chloro-bzqH were observed, which appeared to be a result of the substitution of bromine with chlorine atoms *via* an aromatic Finkelstein-type reaction between **1** and CuCl. Inactivity of **1** in the amination reaction might be caused by its ability to undergo metal coordination, which can have a negative impact on copper catalyst activity. Due to the obstacle encountered in the conversion of **1** to the target derivative through simple amination with ammonia, we were forced to find a solution to this problem in the synthesis process.

In the search for a way to convert bromo-substituted precursor **1** to the corresponding amino derivative, we encountered the concept of ammonia surrogate employment, which we finally decided to examine as most promising.[23] From our point of view, the most convenient method was palladium-mediated Buchwald-Hartwig-type amination of bromoaryls with ketimine as an amino group synthon. For this purpose, benzophenoneimine[24] was prepared and used in our system as the most convenient amino group synthon, which was further coupled with **1** in the presence of a catalytic system created on the basis of $[Pd_2(dba)_3]$/BINAP/NaO*t*Bu, and additionally accelerated with microwaves. Finally, the adapted methodology gave us an almost theoretical yield of imine-substituted bzqH intermediate in a relatively short reaction time (Scheme 5). In the next step, the formed imine was hydrolyzed under typical conditions to the corresponding 5-amino-benzo[*h*]quinoline (**4**), with an overall yield of 90%.

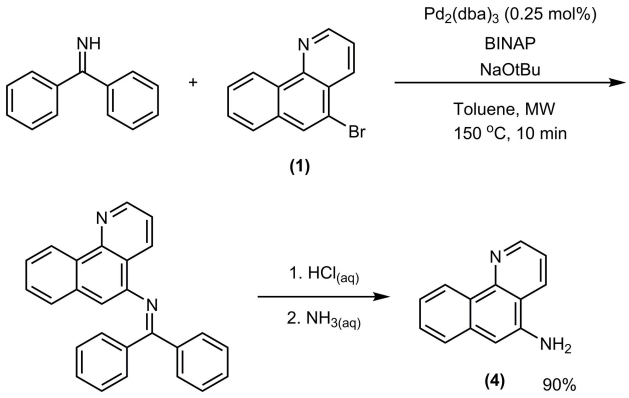

Scheme 5. Two-step synthesis of **4**.

Since the unprotected primary amino group, particularly when bonded to aromatic systems, may undergo some undesirable side-reactions, alkylation was performed in order to protect it. It was essential not to overdose the alkylation reagent and conduct the process in mild conditions to avoid quaternization of both amine and bzqH nitrogen atoms. As a result, 5-dimethylamino-benzo[*h*]quinoline (**5**) was obtained almost quantitatively (Scheme 6).

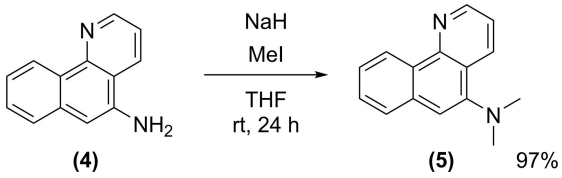

Scheme 6. Alkylation of **4**.

Numerous literature reports concerning iridium (III)-based OLED emitters describe the influence of fluorinated 2-phenylpyridine derivatives as ligands on the shift of emission band to the blue region of the visible light spectrum, with respect to the position in the spectra of non-fluorinated analogues. Among them, the FIrpic complex, the most widely and intensively studied blue phosphorescent emitter containing in its structure two *C*,*N*-cyclometalated 2-(4,6-difluorophenyl)pyridine ligands.[25] Successful applications of a wide range of fluorinated ligands in the synthesis of different blue OLED emitters prompted us to prepare some selected bzqH derivative, bearing weakly electron-withdrawing fluorine atoms. Taking into account the literature on halogenation methodology, the first fluorination test was carried out with

the soft fluorination reagent Selectfluor® both in sulfuric acid and in acetonitrile, similarly to the bromination of bzqH.[26] Unfortunately, GCMS analysis revealed in both post-reaction mixtures the presence of many regioisomers as a consequence of the non-regioselective fluorination process. Facing the inability to control the selectivity of fluorination, we decided to carry out the functional group transformation of one of the previously obtained bzqH derivatives. Retrosynthetic analysis of the desired product permitted the selection of a plausible synthetic pathway with the use of the Balz-Schiemann reaction, involving the conversion of amino-functionalized aromatic derivatives to a diazonium salt with a tetrafluoroborate counterion as a source of fluorine atoms that gives fluoroarenes as a result of its decomposition.[27]

According to the given reference, the previously synthesized **4** was transformed to the corresponding diazonium salt (Scheme 7), which in a further step was converted to 5-fluoro-benzo[h]quinoline (**6**) by thermal decomposition of the latter compound in an ionic liquid containing the same counterion. It is noteworthy that the reaction proceeded smoothly with high regioselectivity and enabled the target product to be obtained with a good yield.

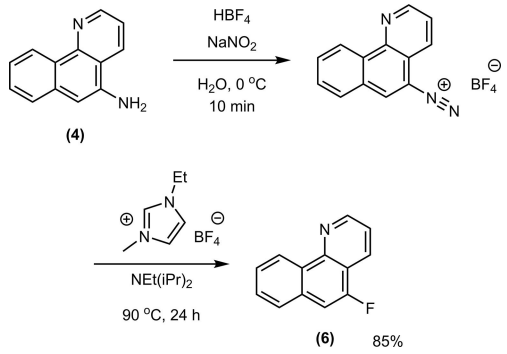

Scheme 7. Synthetic methodology for compound **6** synthesis.

In addition to the synthesis of **6**, an attempt was made to obtain a derivative containing more fluorine atoms. Considering the difficulties associated with the direct fluorination of the bzqH molecule, we decided to use a perfluorinated aryl building block, such as a pentafluorophenyl moiety, the synthetic equivalent of which is pentafluorobenzene. In contrast to other possible coupling methods leading to the C–C bond formation, such as Kumada or Suzuki-Miyaura, in this particular case, the Negishi reaction was chosen as the most convenient protocol. Considering the reactivity of Grignard and organozinc species, the former are more nucleophilic, thus increasing the risk of para-fluorine substitution in the pentafluorophenyl group, which is well-documented in the literature.[28] This side-reaction could cause a decrease in the selectivity of the expected product. On the other hand, the use of boronic acid derivatives, as well as their high reactivity, requires an additional step to isolate them. Therefore, in our case, the formation of an organozinc reagent was more convenient. Our choice is also supported by the fact that the Negishi coupling has been proven to be one of the most commonly used methods for C–C bond formation between complex synthetic intermediates in total synthesis.[29]

The whole procedure for obtaining **7** is presented in Scheme 8. In the first stage of the synthetic pathway, due to the acidic nature of the hydrogen atom located on the aromatic ring bearing five fluorine atoms, deprotonation with ethylmagnesium bromide was performed, resulting in the formation of the corresponding Grignard reagent, which in the next step was converted to pentafluorophenylzinc chloride. Next, the obtained Negishi reagent was subjected to a coupling reaction with **1** in the presence of 2 mol% of palladium(0) complex ([$Pd(PPh_3)_4$]), resulting in 5-pentafluorophenyl-benzo[h]quinoline (**7**) with high yield.

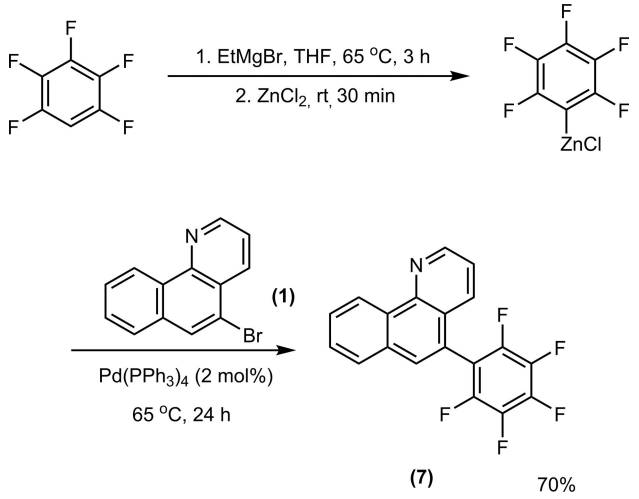

Scheme 8. Negishi reagent formation and coupling thereof resulting in formation of **7**.

Besides the incorporation of substituents characterized by high σ_{para} and low σ_{meta} Hammett parameters to the bzqH core, an attempt was made to equip the skeleton with some well-known *p*-type semiconducting moieties, for instance a triphenylamine motif. Therefore, in the initial stage of the work, *p*-diphenylamino-bromobenzene was transformed to the corresponding Negishi reagent through transmetalation of Grignard intermediate. The subsequent coupling reaction performed with the assistance of 1.5 mol% of palladium homogenous catalyst was found, on the first attempt,

to give a good yield, with the use of a conventional source of heating (Scheme 9). As a consequence, **8** was successfully obtained in a two-step sequence.

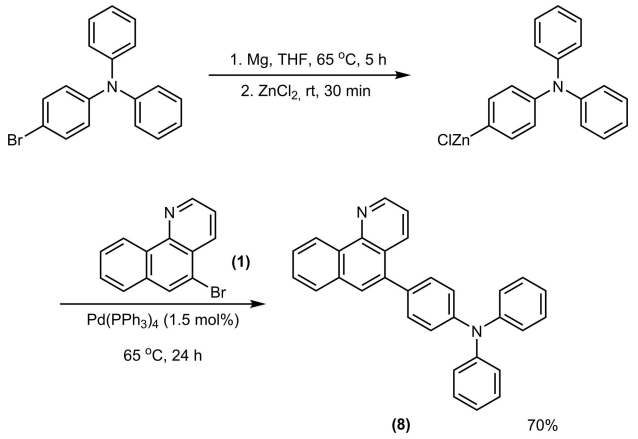

Scheme 9. Negishi reagent formation and coupling thereof resulting in formation of **8**.

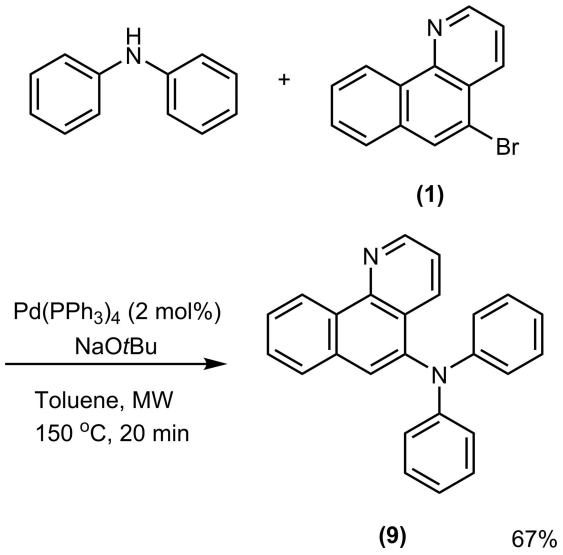

Scheme 10. Buchwald-Hartwig *N*-arylation of **1**.

Bearing in mind the potential application of this type of derivatives as ligands, we decided to enrich the series of compounds with further examples of bzqH equipped with *p*-type semiconducting substituents. Thus, 5-diphenylamino-benzo[*h*]quinoline (**9**) was also synthesized. It has similar properties to the previously described derivative but is characterized by a less π-conjugated system. Its synthesis was carried out *via* palladium-catalyzed C–N, not C–C bond formation as in the case of **8**. The target derivative was prepared by the means of microwave-assisted Buchwald-Hartwig coupling protocol in a one-step method, using a non-polar solvent in the presence of 2 mol% of [$Pd(PPh_3)_4$] as a catalyst and NaOtBu as a base (Scheme 10). Thus, irradiation of the reaction mixture with microwave electromagnetic radiation enabled the final product to be obtained with 67% yield after only 20 minutes of heating.

Another example of moiety reported in literature as a hole-conductive, which we decided to attach to the bzqH core was a carbozolyl substituent. Unfortunately, many attempts at reactions between carbazole and **1** were made, but none of them yielded positive results. Various stoichiometric and catalytic methods making use of the activity of copper and palladium species were examined in this reagent system. However, all failed.[30] All combinations of various palladium pre-catalysts (palladium acetate, [$Pd_2(dba)_3$], [$PdCl_2$(phosphine)$_2$]), phosphines (tri-*tert*-butylphosphine, tricyclohexylphosphine, triphenylphosphine, *rac*-BINAP) with sodium or potassium *tert*-butoxide in toluene were unable to catalyze carbazole *N*-arylation with **1**. We also tried out the method which was successfully applied for the synthesis of **9**, which differs from the considered case only in its use of a slightly different substrate, but it also proved ineffective. Moreover, the desired product formation was not observed after additional microwave irradiation of the reaction mixture over an extended time. At last, this deadlock was broken by changing the synthetic strategy. The target compound **10** was efficiently prepared through the reaction of **4** with 2,2'-dibromobiphenyl leading to 5-membered ring enclosure *via* the Buchwald-Hartwig reaction (Scheme 11).[31] It is worth emphasizing that the catalytic system used in this transformation, developed on the basis of [$Pd_2(dba)_3$]/[$HP(tBu)_3$]BF_4 (10 mol% Pd, 20 mol% of the phosphine), was able to form up two C–N bonds

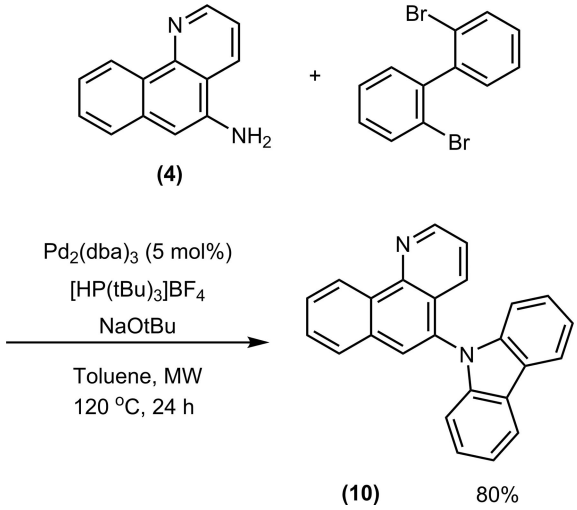

Scheme 11. Successful double Buchwald-Hartwig *N*-arylation leading to formation of **10**.

between the amino group and 2,2'-dibromobiphenyl, but was not efficient enough in C–N bond formation when carbazole and **1** were applied as reagents. However, in order to prevent of side reactions such as the formation of oligomeric byproducts, the reaction temperature was decreased from 150 °C (temperature successfully applied in the syntheses of **4** and **9**) to 120 °C and consequently, the time of microwave irradiation had to be extended to 24 h.

Furthermore, another example of a bzqH derivative bearing a semiconducting moiety, 5-(*N*-phenothiazyl)-benzo[*h*]quinoline (**11**) was exclusively synthesized in the presence of microwave irradiation. On the first attempt, similar reaction conditions as for the synthesis of **9** were applied, with a slightly reduced amount of catalyst added (1.5 mol% Pd). Analysis of the post-reaction mixture revealed total consumption of the substrate and exclusive formation of the desired product **11**. Additional tests allowed us to conclude that the optimal reaction time was 10 minutes, in which full substrate conversion was reached. After a quick workup and easy chromatographic purification, the target compound was isolated with 79% yield (see Scheme 12). Taking into account the photo- and electronic properties, this compound is similar to **9** but bears a sulfur atom bridging two aromatic benzene rings, which increases substituent rigidity. Moreover, the phenothiazine moiety is well-known for its unique photoluminescent and *p*-type semiconducting properties.[32]

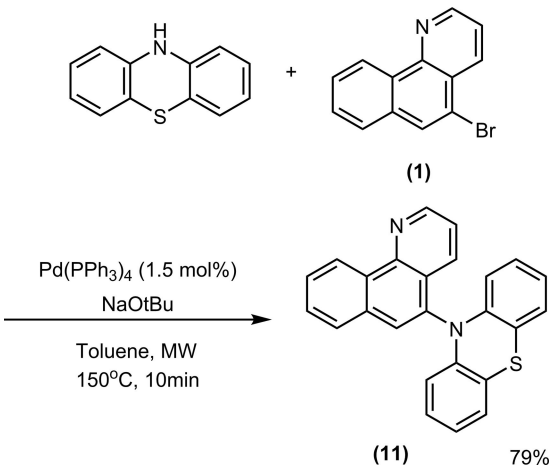

Scheme 12. *N*-arylation of phenothiazine.

Not only electron-donating substituents or semiconducting moieties connected with ligands can influence phosphorescent emitter properties. Literature reports indicate that the bonding of sterically hindered substituents to ligands involved in the structure of phosphorescent emitters has a positive effect on their emission quantum yields due to the prevention of aggregation and, consequently, also the reduction of the triplet-triplet annihilation phenomena, as well as providing better dispersion of emitters in the polymer matrix.[33] There are some reports describing silsesquioxanes as substituents with high steric hindrance of nanometric dimensions, which are important building blocks for optoelectronic materials.[34] Inspired by these reports, we decided to equip the bzqH core with a silsesquioxane moiety. On the basis of literature, we tried to perform Heck coupling between the heptaisobutyl-POSS vinyl group and **1**.[35] Unfortunately, the analysis of the post-reaction mixture did not detect the presence of the expected product. In the face of this failure, we decided that the best solution would be to connect the POSS moiety with bzqH core *via* hydrosilylation, which is a very well documented reaction, commonly used in POSS chemistry.[36] For this purpose, a bzqH derivative containing a hydrosilyl group had to be synthesized. It was created by the Grignard reaction between chlorodimethylsilane and Grignard reagent formed *in situ* (Scheme 13). The order in which the reagents were added was very important, as the attempt to synthesize 5-(benzo[*h*]quinolinato) magnesium bromide and subject it to the nucleophilic substitution with chlorodimethylsilane failed at the stage of the Grignard reagent formation. During the magnesium insertion reaction, a complex black-colored mixture was obtained that did not react further in an expected manner. One way to overcome this problem was the drop-wise addition of **1** solution into the solution containing activated magnesium and chlorodimethylsilane, which forced the immediate conversion of the Grignard reagent into the desired product, isolated with a moderate yield.

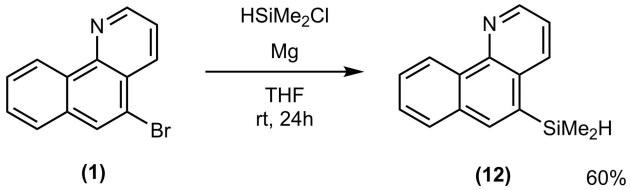

Scheme 13. Synthesis of **12**.

The obtained compound **12** was subsequently used in the hydrosilylation reaction in the presence of a Pt-Karstedt catalyst, resulting in a bzqH derivative containing at position 5 a POSS moiety connected by a $-CH_2CH_2-$ hydrocarbon linker (compound **13**, see Scheme 14). An additional desirable feature of the linker is its flexibility, which hinders the crystallization process and thus favors the formation of amorphous phases. A high glass-transition point is particularly important in the design of the new OLED dopants since the formation of amorphous layers facilitates

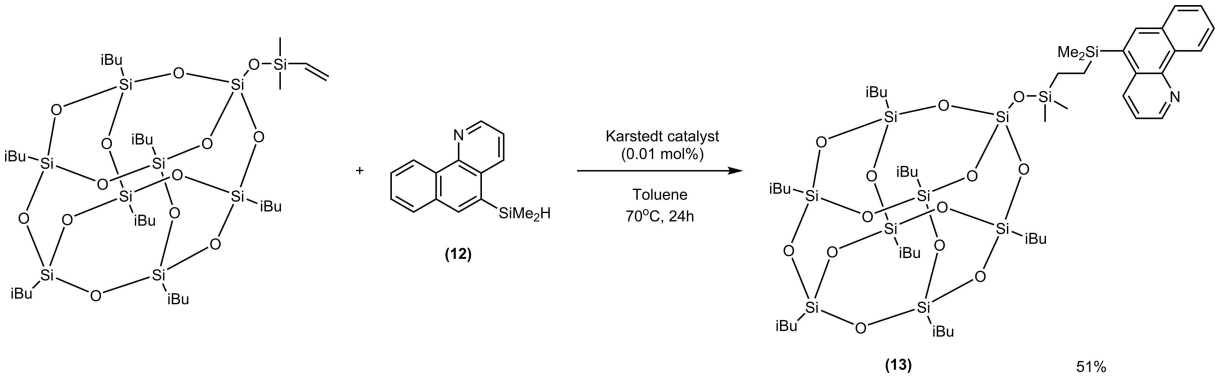

Scheme 14. Hydrosilylation of POSS-OSiMe$_2$CH=CH$_2$ by **12**.

uniformity of the emitters dispersion in the matrix and prevents electrical shortages.[37]

Interestingly, in the CSD (Cambridge Structural Database, version Nov. 2017) there are no examples of organic 5-substituted benzo[*h*]quinolines (without other substituents), and only one example of metal-organic compound ((Benzo[*h*]quinolin-5-yl(methoxy) methylene)-(pentacarbonyl)-chromium(0)).[38] Perspective views of the molecules **1**, **2**, **4**, **6**, **7** and **10** are shown in Figure 1, and some geometrical data is included in *Supporting information*. Molecular structures in the solid state are quite similar for all compounds (Figure 2). The bzqH ring system is approximately planar; in fact, the only differences are, evidently, related to the nature of the substituent at position 5, and these substituents influence mainly the C5–C6–C7 angle (as observed long ago by Domenicano and Murray-Rust for benzene derivatives).[39] Also, dihedral angles between the bzqH ring system and the aromatic substituent in **7** and **10** are very similar (61.73(8)° in **7A**, 67.70(7)° in **7B**, 67.026(19)° in **10**. Only in **4** does the molecule contain a strong hydrogen bond donor (NH$_2$ group) and the N–H···N1 hydrogen bonds connect molecules into infinite chains. In all other structures, only weak interactions determine crystal architectures, but they seem to be quite robust as, for instance, the solvent molecule was not incorporated into the structures in either case. On the other hand, the presence of multiple molecules in 2 of 6 structures ($Z'=3$ in **2**, $Z'=2$ in **7**) indicates some kind of packing conflicts. Table 3 in *Supporting information* lists some details of these interactions. They include halogen C–Br···Br halogen bonding in **1**, C–H···F interactions in **7**, and π···π and C–H···π interactions of differing importance, practically in all cases.

3 Conclusion

A number of methods were proposed to obtain a series of bzqH modified at position 5. A series of substituents with various electron and steric properties were implemented in order to change the electron density on the bzqH core, support *p*-type semiconductivity and reduce aggregation tendency. All synthesized compounds have a coordination pocket, which enables *C*,*N*-cyclometalation of metal atoms, and thus have the potential to be used in OLED technology for the synthesis of *C*,*N*-cyclometalated phosphorescent emitters. Further work on the application of the new compounds is in progress.

Experimental Section

Synthesis of 5-bromo-benzo[*h*]quinoline (1)

The reaction was performed under an air atmosphere. Benzo [*h*]quinoline (24.75 g, 138 mmol) was added portionwise to a reaction flask, containing 220 mL of vigorously stirred concentrated sulfuric acid, at room temperature. After cooling, NBS (24.58 g, 138 mmol) was very slowly added to maintain the temperature inside the flask below 35 °C. After the addition of NBS, the reaction mixture was left for stirring overnight. The post-reaction mixture was slowly poured into 1000 mL of ice-cold water and subsequently very carefully neutralized with saturated ammonia solution to pH = 6. The precipitated product was extracted with chloroform and washed with water 3 times. The organic layer was dried over magnesium sulfate, filtered and concentrated on rotavap to give the crude product as a yellowish oil. The crude product was purified with flash chromatography using 10% diethyl ether: 90% hexanes eluent. The fractions containing over 90% desired product and less than 2% dibrominated benzo [*h*]quinolines (determined by GC) were collected and the solvent was evaporated. Finally, the pure product was obtained as a white crystalline solid after recrystallization from diethyl ether with 56% yield (18.04 g, 69.9 mmol). ^{1}H NMR (400 MHz, $CDCl_3$) δ 9.29–9.24 (m, 1H), 9.01 (dd, J = 4.4, 1.7 Hz, 1H), 8.61 (dd, J = 8.3, 1.7 Hz, 1H), 8.15 (s, 1H), 7.85–7.80 (m, 1H), 7.78–7.68 (m, 2H), 7.62 (dd, J = 8.3, 4.4 Hz, 1H). ^{13}C NMR (101 MHz, $CDCl_3$) δ 149.58, 147.13, 135.78, 133.79, 131.21, 131.14, 129.08, 127.67, 127.17, 125.86, 124.96, 122.68, 119.78. GCMS (EI): 257.1 (100%), 259.1 (93%), 178.2 (58%), 151.1 (44%), 89.1 (30%), 75.1 (30%), 150.0 (28%), 177.2 (28%), 258.3 (19%), 75.9 (14%), 260.2

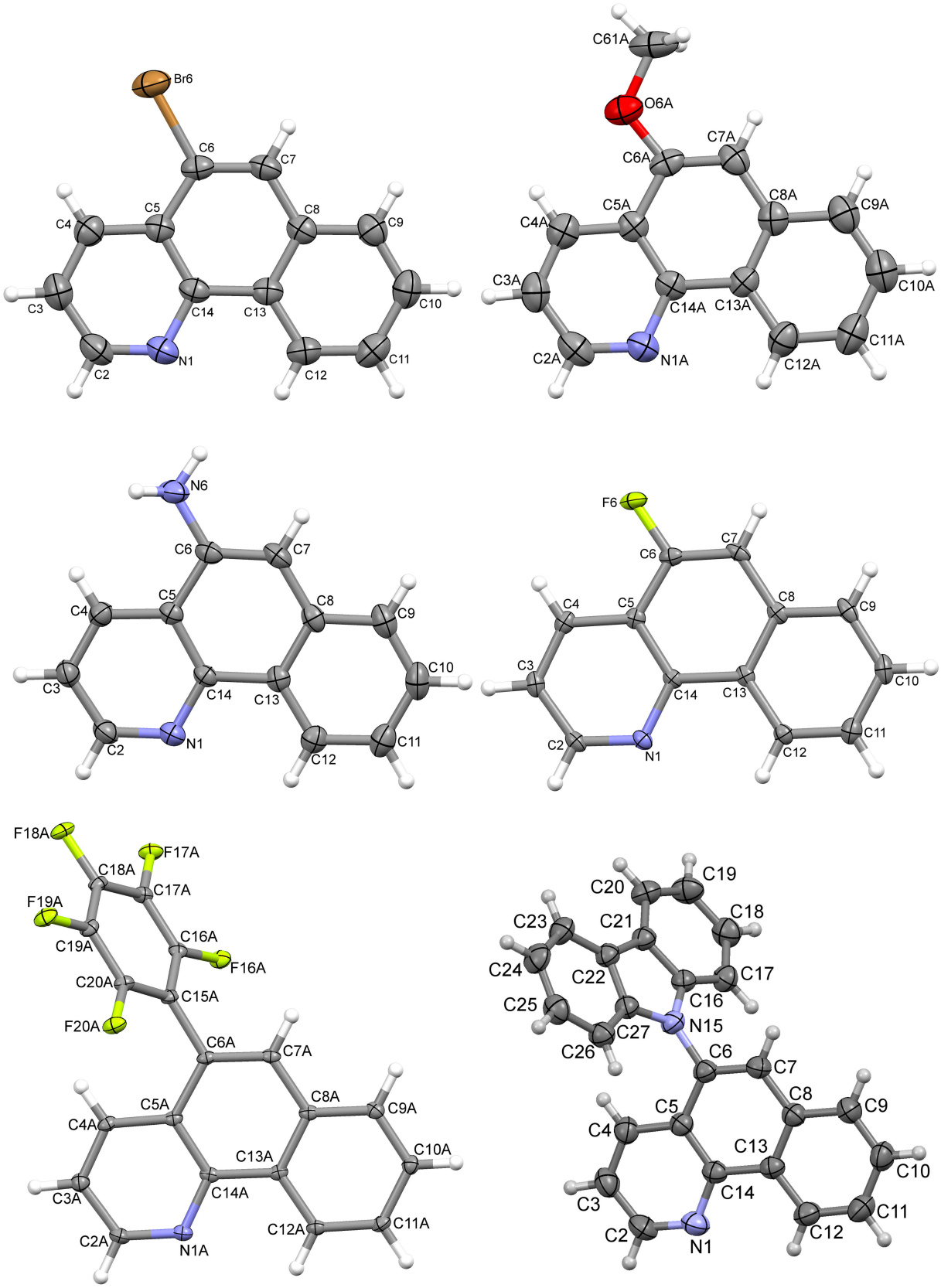

Figure 1. Perspective views of the molecules **1**, **2**, **4**, **6**, **7**, and **10** in crystal structures.

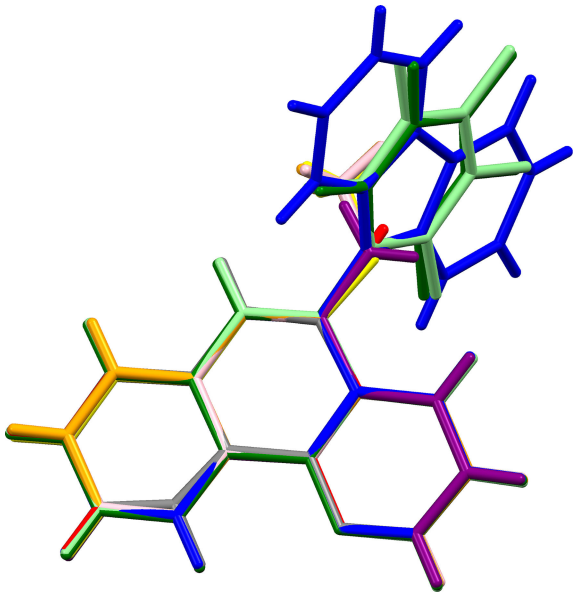

Figure 2. A comparison of geometries of all compounds, whose crystal structures were determined.

(14%), 152.1 (11%), 74.1 (11%). HRMS (ESI) calc. for $C_{13}H_9BrN$: $[M+H]^+$ 257.9918, found 257.9935.

Synthesis of 5-methoxy-benzo[*h*]quinoline (2)

Lithium methoxide (0.294 g, 7.75 mmol), **1** (1.0 g, 3.87 mmol) and copper(I) iodide (37 mg, 0.194 mmol) were charged into a CEM 10 mL reaction vessel. Subsequently, 5 mL of anhydrous MeOH was added and the closed vessel was placed in a CEM microwave reactor. The reaction mixture was heated at150 °C for 10 minutes with P_{max} = 100 W. After cooling, 5 mL of DCM was slowly added and the precipitate was filtered off. All volatiles were evaporated under reduced pressure and the crude product was purified by flash chromatography, using gradient elution, from 100% DCM to 50% AcOEt:50% DCM. The collected fractions were concentrated *in vacuo* to give a white crystalline product, with 99% yield (0.803 g, 3.84 mmol). ^{1}H NMR (300 MHz, $CDCl_3$) δ 9.22–9.12 (m, 1H), 9.01 (dd, J = 4.4, 1.8 Hz, 1H), 8.60 (dd, J = 8.3, 1.8 Hz, 1H), 7.80–7.74 (m, 1H), 7.69–7.55 (m, 2H), 7.52 (dd, J = 8.3, 4.4 Hz, 1H), 7.00 (s, 1H), 4.06 (s, 3H). ^{13}C NMR (75 MHz, $CDCl_3$) δ 152.59, 149.34, 147.27, 134.15, 130.74, 128.64, 127.79, 126.75, 124.79, 124.45, 121.63, 121.49, 102.48, 55.69. GCMS (EI): 209.3 (100%), 166.2 (93%), 140.1 (16%), 210.3 (16%), 194.2 (16%), 139.1 (16%), 167.2 (12%). HRMS (ESI) calc. for $C_{14}H_{12}NO$: $[M+H]^+$ 210.0919, found 210.0929.

Synthesis of 5-phenoxy-benzo[*h*]quinoline (3)

Phenol (0.367 g, 3.9 mmol), **1** (774 mg, 3 mmol), cesium carbonate (1.075 g, 3.3 mmol) and copper(I) chloride (45 mg, 0.45 mmol) were charged into a CEM 80 mL reaction vessel. Subsequently 12 mL of NMP were added and the closed vessel was placed in a CEM microwave reactor. The reaction mixture was heated at180 °C for 40 minutes with P_{max} = 200 W. After cooling, 50 mL of water was added and the precipitate was centrifuged. The precipitate was dissolved in 10 mL of DCM and washed 3 times with 40 mL of 5% NaOH aqueous solution and 7 times with 40 mL of water. The organic layer was dried with anhydrous magnesium sulfate, filtered and concentrated *in vacuo* to give the crude product. The crude product was purified by flash chromatography using gradient elution from 100% hexanes to 50% hexanes: 50% DCM. The combined fractions were concentrated *in vacuo* to obtain a pure product as a white crystalline solid with 86% yield (0.7 g, 2.58 mmol). ^{1}H NMR (300 MHz, $CDCl_3$) δ 9.30–9.21 (m, 1H), 9.06 (dd, J = 4.4, 1.8 Hz, 1H), 8.63 (dd, J = 8.3, 1.8 Hz, 1H), 7.74–7.62 (m, 3H), 7.56 (dd, J = 8.2, 4.4 Hz, 1H), 7.47–7.37 (m, 2H), 7.24–7.10 (m, 4H). ^{13}C NMR (75 MHz, $CDCl_3$) δ 156.96, 150.82, 149.60, 147.65, 133.51, 130.84, 130.15, 128.96, 128.74, 127.22, 125.91, 124.58, 124.11, 122.01, 121.83, 119.51, 111.46. GCMS (EI): 271.2 (100%), 243.2 (33%), 166.0 (28%), 242.2 (26%), 272.3 (21%), 151.0 (15%), 77.1 (12%). HRMS (ESI) calc. for $C_{19}H_{14}NO$: $[M+H]^+$ 272.1075, found 272.1091.

Synthesis of 5-amino-benzo[*h*]quinoline (4)

Compound **1** (1.329 g, 5.15 mmol), sodium *tert*-butoxide (0.675 g, 6.81 mmol), tris(dibenzylideneacetone)-dipalladium (0) (12 mg, 13 μmol) and *rac*-BINAP (24 mg, 39 μmol) were charged into a CEM 80 mL reaction vessel. Subsequently, 13 mL of anhydrous toluene and benzophenone imine (0.968 mL, 1.045 g, 5.77 mmol) were added and the closed vessel was placed in a CEM microwave reactor. The reaction mixture was heated at 150 °C for 10 minutes with P_{max} = 300 W. After cooling, all volatiles were removed under reduced pressure and 20 mL of DCM were added. The solution was washed 3 times with 10 mL of water and concentrated *in vacuo*. The residuals were dissolved in 20 mL of THF and vigorously stirred. Subsequently, muriatic acid (0.823 mL, 0.988 g, 10.3 mmol) was slowly dropped in, which resulted in the instant formation of a beige solid. The solid intermediate hydrochloride was centrifuged and washed twice with 10 mL of THF. After drying in air, the solid was dissolved and vigorously stirred in 10 mL of water, giving a bloody-red, clear solution. During 10 minutes of stirring, a beige solid of benzophenone gradually appeared and was removed by extraction three times with 5 mL of DCM. Next, the aqueous layer was basified to pH = 8 with concentrated aqueous ammonia solution, which resulted in the formation of a beige precipitate. The precipitate was extracted 3 times with 10 mL of DCM. The organic layer was dried over anhydrous sodium sulfate, filtered and concentrated *in vacuo*. The obtained crude product was purified by flash chromatography using gradient elution from 100% DCM to 15% AcOEt: 85% DCM. The collected fractions were concentrated *in vacuo* to give **4** as a yellowish solid in 90% yield (0.895 g, 4.61 mmol). ^{1}H NMR (300 MHz, $CDCl_3$) δ 9.15 (d, J = 8.1 Hz, 1H), 9.01 (dd, J = 4.4, 1.7 Hz, 1H), 8.19 (dd, J = 8.3, 1.7 Hz, 1H), 7.69–7.55 (m, 2H), 7.55–7.47 (m, 2H), 7.00 (s, 1H), 4.10 (s, 2H). ^{13}C NMR (75 MHz, $CDCl_3$) δ 148.77, 147.34, 139.06, 134.69, 129.37, 128.67, 127.49, 125.75, 124.48, 124.03, 121.19, 120.48, 107.93. GCMS (EI): 194.1 (100%), 167.1 (26%), 166.1 (22%), 193.3 (22%), 195.1

(18%), 97.0 (14%), 139.3 (13%), 140.3 (11%), 138.5 (10%). HRMS (ESI) calc. for $C_{13}H_{11}N_2$: $[M+H]^+$ 195.0922, found 195.0928.

Synthesis of 5-(*N,N*-dimethylamino)-benzo[*h*] quinoline (5)

A 60% suspension of NaH in mineral oil (0.424 g, 10.6 mmol) was charged into a Schlenk flask. Next, the solid was washed 3 times with 5 mL of anhydrous toluene, 3 times with 5 mL of anhydrous hexane and dried under reduced pressure. 10 mL of anhydrous THF and **4** (0.686 g, 3.53 mmol) were added to the flask and vigorously stirred. Next, iodomethane (0.471 mL, 1.063 g, 7.42 mmol) was slowly added dropwise and the reaction flask was closed with a bubbler socket and left for stirring for 20 h at room temperature. After reaction completion 1 mL of methanol was very carefully added and all volatiles were removed under reduced pressure. The residual solid was washed 3 times with 10 mL of DCM and the filtrate was concentrated *in vacuo*, giving the product with 97% yield, as a yellowish oil (0.785 g, 3.41 mmol). ^{1}H NMR (300 MHz, $CDCl_3$) δ 9.23–9.15 (m, 1H), 8.99 (dd, $J=4.3$, 1.8 Hz, 1H), 8.58 (dd, $J=8.3$, 1.8 Hz, 1H), 7.82–7.75 (m, 1H), 7.67–7.57 (m, 2H), 7.53 (dd, $J=8.3$, 4.3 Hz, 1H), 7.30 (s, 1H), 2.93 (s, 6H). ^{13}C NMR (75 MHz, $CDCl_3$) δ 148.59, 148.08, 147.78, 134.02, 132.81, 129.04, 128.51, 126.99, 125.47, 124.38, 123.98, 121.20, 113.71, 45.10. GCMS (EI): 222.3 (100%), 221.3 (71%), 179.2 (33%), 206.3 (22%), 178.1 (22%), 151.1 (22%), 180.2 (18%), 205.2 (16%), 223.2 (16%), 207.3 (16%), 166.2 (14%), 194.2 (13%), 152.2 (12%), 103.1 (11%), 220.2 (11%). HRMS (ESI) calc. for $C_{15}H_{15}N_2$: $[M+H]^+$ 223.1235, found 223.1240.

Synthesis of 5-fluoro-benzo[*h*]quinoline (6)

The reaction was performed under an air atmosphere. **4** (0.784 g, 4.04 mmol) was weighted to a reaction vial and tetrafluoroboric (2.64 mL, 3.69 g, 20.18 mmol) acid solution was added, followed by a few mL of water to completely dissolve the substrate to get a bloody-red, clear solution. The mixture was cooled to 0 °C and sodium nitrite aqueous solution (0.306 g, 4.44 mmol) was slowly added, upon vigorous stirring. After 10 minutes, the precipitated red solid was filtered off and washed 4 times with a mixture of 40 mL of diethyl ether and 5 mL of triethyl orthoformate and twice with 20 mL of diethyl ether, and dried in air. The next step was performed under an inert atmosphere. A Schlenk flask was charged with f 1-ethyl-3-methylimidazolium tetrafluoroborate (8.0 g, 40.4 mmol) and the intermediate diazonium salt and left for heating at 90 °C for 24 h. After cooling, *N*-ethyldiisopropylamine (1.378 mL, 1.043 g, 8.07 mmol) was added and the contents were stirred for an additional hour. Next, the product was extracted 3 times with 10 mL of diethyl ether and the combined washes were concentrated *in vacuo*. The crude product was sublimed at 150 °C under pressure 2×10^{-2} Torr to give a pure product as colorless crystals in 85% yield. ^{1}H NMR (300 MHz, $CDCl_3$) δ 9.25–9.16 (m, 1H), 9.03 (dd, $J=4.4$, 1.8 Hz, 1H), 8.44 (dd, $J=8.2$, 1.8 Hz, 1H), 7.86–7.78 (m, 1H), 7.70–7.63 (m, 2H), 7.57 (dd, $J=8.2$, 4.4 Hz, 1H), 7.43 (d, $J=11.0$ Hz, 1H). ^{13}C NMR (75 MHz, $CDCl_3$) δ 155.65 (d, $J=253.1$ Hz), 149.84, 147.37 (d, $J=4.8$ Hz), 132.82 (d, $J=10.1$ Hz), 129.36 (d, $J=5.2$ Hz), 129.14 (d, $J=1.1$ Hz), 129.00, 127.47 (d, $J=5.8$ Hz), 126.36 (d, $J=2.4$ Hz), 124.67 (d, $J=1.4$ Hz), 121.91, 119.34 (d, $J=19.5$ Hz), 108.80 (d, $J=19.0$ Hz). GCMS (EI): 197.2 (100%), 196.1 (30%), 198.3 (14%), 169.2 (10%). HRMS (ESI) calc. for $C_{13}H_9FN$: $[M+H]^+$ 198.0719, found 198.0730.

Synthesis of 5-pentaluofophenyl-benzo[*h*]quinoline (7)

A Schlenk flask was charged with 15 mL of anhydrous THF, 1 M ethylmagnesium bromide THF solution (4.65 mL, 4.65 mmol) and pentafluorobenzene (0.693 mL, 1.052 g, 6.2 mmol). The mixture was heated in an oil bath at 65 °C for 3 h. After cooling, a zinc chloride THF solution (5.04 mL, 5.04 mmol) was added dropwise and the contents were stirred for 30 min. After the completion of transmetalation, **1** (1.0 g, 3.87 mmol) and tetrakis(triphenylphosphine)-palladium(0) (90 mg, 77 µmol) were added. The reaction mixture was heated at 65 °C for 24 h. After the indicated time the mixture was concentrated under reduced pressure and 100 mL of water was added. The formed suspension was extracted 3 times with 20 mL of DCM, the combined washes were dried with anhydrous magnesium sulfate, filtered and concentrated to give the crude product. The crude product was purified by flash chromatography using gradient elution from 100% hexanes to 12% diethyl ether: 88% hexanes. The collected fractions were combined and concentrated *in vacuo* to give the desired product as a white crystalline solid, with 70% yield (0.936 g, 2.71 mmol). ^{1}H NMR (300 MHz, $CDCl_3$) δ 9.37 (d, $J=8.1$ Hz, 1H), 9.06 (dd, $J=4.4$, 1.7 Hz, 1H), 7.95 (d, $J=7.6$ Hz, 1H), 7.88–7.73 (m, 4H), 7.53 (dd, $J=8.3$, 4.4 Hz, 1H). ^{13}C NMR (75 MHz, $CDCl_3$) δ 149.40, 146.83, 133.01, 132.56, 132.19, 131.46–131.26 (m), 128.97, 128.52, 128.36, 124.93, 124.83, 122.31, 121.58–121.45 (m). GCMS (EI): 345.1 (100%), 326.2 (24%), 346.2 (20%), 147.6 (18%), 325.2 (17%), 344.1 (11%) 172.6 (10%). HRMS (ESI) calc. for $C_{19}H_9F_5N$: $[M+H]^+$ 346.0655, found 346.0665.

Synthesis of 5-(4-(*N,N*-diphenylamino)phenylene)-benzo[*h*]quinoline (8)

A Schlenk flask was charged with magnesium turnings (0.182 g, 7.5 mmol) and 20 mL of THF. Magnesium surface was activated by the addition of 1,2-dibromoethane (44 uL, 96 mg, 0.5 mmol) and heating the reaction mixture at 50 °C, until gas evolution ceased (*ca.* 30 min). Next, 4-(*N,N*-diphenylamino)bromobenzene was added and the mixture was heated at 65 °C for 5 h. The mixture was cooled to room temperature and a zinc chloride THF solution (5.75 mL, 5.75 mmol) was added dropwise upon stirring for another 30 min. After the successful formation of the Negishi reagent, **1** (1.291 g, 5 mmol) and tetrakis(triphenylphosphine)palladium(0) (87 mg, 0.075 mmol) were added and the reaction mixture was vigorously stirred at 65 °C for 24 h. After the indicated time, the mixture was concentrated under reduced pressure and 100 mL of water was added. The formed suspension was extracted 3 times with 20 mL of DCM, the combined washes were dried with anhydrous

magnesium sulfate, filtered and concentrated to give the crude product. The crude product was purified by flash chromatography using gradient elution from 100% hexanes to 30% DCM: 70% hexanes. The collected fractions were combined and concentrated *in vacuo* to give the desired product as a white crystalline solid with 70% yield (1.479 g, 3.5 mmol). ^{1}H NMR (300 MHz, $CDCl_3$) δ 9.37–9.28 (m, 1H), 9.03 (dd, J=4.4, 1.7 Hz, 1H), 8.37 (dd, J=8.3, 1.7 Hz, 1H), 7.95–7.88 (m, 1H), 7.80 (s, 1H), 7.73 (tt, J=7.0, 5.1 Hz, 2H), 7.51 (dd, J=8.3, 4.3 Hz, 1H), 7.41 (d, J=8.5 Hz, 2H), 7.36–7.27 (m, 4H), 7.26–7.18 (m, 6H), 7.08 (t, J=7.3 Hz, 2H). ^{13}C NMR (75 MHz, $CDCl_3$) δ 148.71, 147.79, 147.61, 147.03, 137.43, 134.49, 133.38, 133.30, 131.11, 130.93, 129.52, 128.59, 127.92, 127.85, 127.82, 127.03, 125.90, 124.78, 124.58, 123.36, 123.31, 121.66. DEPMS (EI): 422.3 (100%), 423.4 (32%), 488.3 (25%), 421.5 (18%), 489.4 (10%). HRMS (ESI) calc. for $C_{31}H_{23}N_2$: $[M+H]^+$ 423.1861, found 423.1868.

Synthesis of 5-(*N,N*-diphenylamino)-benzo[*h*]quinoline (9)

A CEM 80 mL reaction vessel was charged with **1** (0.5 g, 1.94 mmol), diphenylamine (0.344 g, 2.03 mmol), sodium *tert*-butoxide (0.279 g, 2.91 mmol) and tetrakis(triphenylphosphine)-palladium(0) (45 mg, 39 μmol). Subsequently, 15 mL of anhydrous toluene were added, the vessel was closed and placed in a CEM microwave reactor. The reaction mixture was heated at150 °C for 20 minutes with P_{max}=300 W. After the reaction, all volatiles were removed under reduced pressure and the residuals were washed 3 times with 5 mL of DCM. The washings were combined and concentrated under reduced pressure and the crude product was purified by flash chromatography using gradient elution, starting from 100% hexanes to 100% DCM. Evaporation of the combined fractions gave the desired product as a white crystalline solid (0.448 g, 1.293 mmol) with 67% yield. ^{1}H NMR (300 MHz, $CDCl_3$) δ 9.60 (d, J=7.8 Hz, 1H), 9.28 (dd, J=4.2, 1.5 Hz, 1H), 8.59 (dd, J=8.3, 1.5 Hz, 1H), 8.11–7.95 (m, 3H), 7.94 (s, 1H), 7.69 (dd, J=8.3, 4.4 Hz, 1H), 7.59–7.47 (m, 4H), 7.39 (d, J=8.4 Hz, 4H), 7.29 (t, J=7.3 Hz, 2H). ^{13}C NMR (75 MHz, $CDCl_3$) δ 149.00, 148.31, 148.17, 141.29, 133.89, 133.02, 130.61, 129.41, 128.64, 127.61, 127.59, 127.01, 125.41, 124.61, 122.35, 121.95. GCMS (EI): 346.2 (100%), 269.2 (36%), 347.2 (28%), 345.3 (27%), 243.2 (15%), 268.2 (13%), 173.0 (12%), 77.1 (12%), 242.2 (10%). HRMS (ESI) calc. for $C_{25}H_{19}N_2$: $[M+H]^+$ 347.1548, found 347.1553.

Synthesis of 5-(*N*-carbazolyl)-benzo[*h*]quinoline (10)

A CEM 80 mL reaction vessel was charged with **4** (0.5 g, 2.57 mmol), 2,2'-dibromobiphenyl (0.883 g, 2.83 mmol), sodium *tert*-butoxide (0.742 g, 7.72 mmol), tris(dibenzylideneacetone)dipalladium(0) (0.118 g, 0.129 mmol) and tri-*tert*-butylphosphonium tetrafluoroborate (0.149 g, 0.515 mmol). Subsequently, 20 mL of anhydrous toluene were added, the vessel was capped and placed in a CEM microwave reactor. The reaction mixture was heated at120 °C for 24 h with P_{max}=300 W. After the reaction, all volatiles were removed under reduced pressure and the residuals were washed 3 times with 5 mL of DCM. The washings were combined and concentrated under reduced pressure and the crude product was purified by flash chromatography using gradient elution, starting from 100% hexanes to 60% DCM: 40% hexanes. Evaporation of the combined fractions gave the desired product as a white crystalline solid (0.709 g, 2.059 mmol) with 80% yield. ^{1}H NMR (300 MHz, $CDCl_3$) δ 9.45 (d, J=8.3 Hz, 1H), 9.06 (dd, J=4.3, 1.8 Hz, 1H), 8.28–8.18 (m, 2H), 8.04 (s, 1H), 7.96 (d, J=7.9 Hz, 1H), 7.88 (td, J=8.3, 7.7, 1.5 Hz, 1H), 7.80 (td, J=7.4, 1.4 Hz, 1H), 7.59 (dd, J=8.3, 1.7 Hz, 1H), 7.40–7.29 (m, 5H), 7.10–7.03 (m, 2H). ^{13}C NMR (75 MHz, $CDCl_3$) δ 149.73, 147.77, 142.24, 133.10, 132.18, 131.88, 131.58, 129.03, 128.50, 128.31, 128.25, 126.30, 124.90, 124.63, 123.45, 122.32, 120.62, 120.24, 110.22. GCMS (EI): 344.2 (100%), 171.3 (30%), 172.0 (29%), 342.2 (28%), 345.2 (26%), 343.0 (23%), 170.3 (14%). HRMS (ESI) calc. for $C_{25}H_{17}N_2$: $[M+H]^+$ 345.1392, found 345.1400.

Synthesis of 5-(*N*-phenothiazyl)-benzo[*h*]quinoline (11)

A CEM 10 mL reaction vessel was charged with **1** (0.535 g, 2.0 mmol), phenothiazine (0.418 g, 2.1 mmol), sodium *tert*-butoxide (0.258 g, 2.6 mmol) and tetrakis(triphenylphosphine)-palladium(0) (35 mg, 30 μmol). Subsequently 5 mL of anhydrous toluene was added, the vessel was closed and placed in a CEM microwave reactor. The reaction mixture was heated at 150 °C for 10 minutes with P_{max}=300 W. After the reaction, all volatiles were removed under reduced pressure and the residuals were washed 3 times with 5 mL of DCM. The washings were combined and concentrated under reduced pressure and the crude product was purified by flash chromatography using gradient elution starting from 100% hexanes to 100% DCM. Evaporation of the combined fractions gave a yellow solid which was then washed 2 times with 3 mL of diethyl ether and dried. The desired product was obtained as a white crystalline solid (0.595 g, 1.58 mmol) with 79% yield. ^{1}H NMR (300 MHz, $CDCl_3$) δ 9.40 (d, J=8.1 Hz, 1H), 9.05 (dd, J=4.2, 1.7 Hz, 1H), 8.45 (dd, J=8.3, 1.8 Hz, 1H), 8.05 (s, 1H), 7.98 (d, J=7.8 Hz, 1H), 7.90–7.74 (m, 2H), 7.49 (dd, J=8.3, 4.4 Hz, 1H), 7.06 (dd, J=7.5, 1.7 Hz, 2H), 6.77 (dt, J=23.5, 7.2 Hz, 4H), 6.19 (d, J=8.0 Hz, 2H). ^{13}C NMR (75 MHz, $CDCl_3$) δ 149.75, 148.57, 143.64, 134.54, 133.40, 132.57, 131.86, 131.43, 131.40, 128.89, 128.35, 127.18, 126.90, 124.85, 124.81, 122.93, 122.59, 120.07, 115.91. GCMS (EI): 376.2 (100%), 198.1 (38%), 377.3 (29%), 154.2 (14%), 179.1 (14%), 166.1 (14%), 188.4 (13%), 187.5 (12%), 343.2 (12%), 171.7 (12%), 375.2 (12%), 342.2 (11%), 151.1 (10%), 197.1 (10%). HRMS (ESI) calc. for $C_{25}H_{17}N_2S$: $[M+H]^+$ 377.1112, found 377.1120.

Synthesis of 5-dimethylsilyl-benzo[*h*]quinoline (12)

In a Schlenk flask, a solution of **1** (0.3 g, 1.162 mmol) in 2 mL of anhydrous THF was prepared. A separate Schlenk flask was charged with magnesium turnings (42 mg, 1.743 mmol) and 3 mL of anhydrous THF. The magnesium was activated by addition of 1,2-dibromoethane (15 uL, 33 mg, 0.174 mmol) and heating the reaction mixture at 50 °C until gas evolution ceased (*ca.* 30 min). Next, chlorodimethylsilane (0.329 mL, 0.281 g, 2.91 mmol) was added, followed by the

dropwise addition of a previously prepared solution of **1** in THF. Upon addition of the reagents, a yellow color appeared and then quickly disappeared. The rate of addition was controlled to keep the reaction mixture colorless. After addition of the reagents, the reaction mixture was left at room temperature for 24 h. Then, all volatiles were removed *in vacuo* and the residuals were washed 3 times with 2 mL of DCM. The washings were combined and concentrated under reduced pressure and the crude product was purified by flash chromatography using gradient elution starting from 100% hexanes to 100% diethyl ether. Evaporation of the combined fractions gave the desired product as a yellowish oil (0.166 g, 0.697 mmol) with 60% yield. ^{1}H NMR (300 MHz, $CDCl_3$) δ 9.31 (d, J = 8.0 Hz, 1H), 9.02 (dd, J = 4.4, 1.7 Hz, 1H), 8.45 (dd, J = 8.2, 1.7 Hz, 1H), 8.05 (s, 1H), 7.94–7.86 (m, 1H), 7.80–7.66 (m, 2H), 7.54 (dd, J = 8.2, 4.3 Hz, 1H), 4.91 (hept, J = 3.7 Hz, 1H), 0.55 (d, J = 3.8 Hz, 6H). ^{13}C NMR (75 MHz, $CDCl_3$) δ 148.41, 146.46, 136.32, 135.65, 133.57, 133.01, 132.32, 129.39, 128.42, 128.01, 127.82, 124.52, 121.62, −3.27. GCMS (EI): 236.2 (100%), 237.2 (54%), 222.1 (21%), 206.1 (21%), 238.2 (12%). HRMS (ESI) calc. for $C_{15}H_{16}NSi$: $[M+H]^+$ 238.1052, found 238.1065.

Synthesis of 5-{1-ethylenedimethylsiloxy-3,5,7,9,11,13,15-isobutylpentacyclo-[9.5.1.1^{3,9}.1^{5,15}.1^{7,13}]octasiloxane}-benzo[*h*]quinoline (13)

A Schlenk flask was charged with **12** (53 mg, 0.223 mmol), 1-vinyldimethylsiloxy-3,5,7,9,11,13,15-isobutyl pentacyclo-[9.5.1.1^{3,9}.1^{5,15}.1^{7,13}]octasiloxane (0.225 g, 0.246 mmol) and 2 mL of anhydrous toluene. The mixture was heated to 70 °C in an oil bath and then Karstedt's catalyst (0.5 uL, 0.426 mg, 0.022 μmol) was added, and the reaction mixture was left for 24 h at the same temperature. Then, all volatiles were removed *in vacuo* and the residuals were washed 3 times with 2 mL of DCM. The washings were combined and concentrated under reduced pressure and the crude product was purified by flash chromatography using gradient elution, starting from 100% hexanes to 100% diethyl ether. Evaporation of the combined fractions gave the desired product as a white crystalline solid (0.132 g, 0.114 mmol) with 51% yield. ^{1}H NMR (300 MHz, $CDCl_3$) δ 9.32–9.22 (m, 1H), 8.99 (dd, J = 4.3, 1.7 Hz, 1H), 8.41 (dd, J = 8.2, 1.7 Hz, 1H), 8.00 (s, 1H), 7.93–7.85 (m, 1H), 7.79–7.65 (m, 2H), 7.53 (dd, J = 8.2, 4.3 Hz, 1H), 1.94–1.76 (m, 7H), 0.99–0.89 (m, 43H), 0.65–0.56 (m, 14H), 0.50 (s, 6H), 0.08 (s, 6H). ^{13}C NMR (75 MHz, $CDCl_3$) δ 148.24, 146.79, 136.41, 135.91, 135.08, 133.03, 132.28, 129.61, 128.37, 128.09, 127.69, 124.49, 121.36, 25.85, 25.82, 24.00, 23.96, 22.60, 22.56, 10.13, 7.84, −0.87, −1.87. DEPMS (EI): 236.2 (100%), 238.2 (92%), 294.1 (82%), 253.2 (46%), 237.4 (38%), 220.2 (28%), 295.2 (25%), 368.1 (25%), 488.3 (23%), 239.2 (19%), 179.1 (19%), 178.0 (18%), 206.1 (14%), 219.4 (14%), 235.3 (14%), 222.0 (12%), 254.2 (12%), 296.2 (11%), 267.9 (10%), 234.1 (10%), 151.1 (10%), 489.3 (10%), 221.0 (10%). HRMS (ESI) calc. for $C_{47}H_{88}NO_{13}Si_{10}$: $[M+H]^+$ 1154.3948, found 1154.3963.

Acknowledgements

This work was supported by the National Science Centre of Poland, grant no. UMO-2013/11/B/ST5/01334. The authors declare no competing financial interest.

References

[1] Z. H. Skraup, *Monatsh. Chem.* **1881**, *2*, 139–170.
[2] a) Buu-Hoï, D. Guettier, *C. R. Hebd. Seances Acad. Sci.* **1946**, *222*, 665–666; b) Y. Kitahara, M. Mochii, M. Mori, A. Kubo, *Tetrahedron* **2003**, *59*, 2885–2891; c) W. P. Utermohlen, C. S. Hamilton, *J. Am. Chem. Soc.* **1941**, *63*, 156–159; d) W. E. Parham, D. C. Egberg, S. Salgar, *J. Org. Chem.* **1972**, *37*, 3248–3254.
[3] a) Y. Kitahara, H. Onikura, Y. Shibano, S. Watanabe, Y. Mikami, A. Kubo, *Tetrahedron* **1997**, *53*, 6001–6010; b) Y. Kitahara, M. Mochii, M. Mori, A. Kubo, *Tetrahedron Lett.* **2000**, *41*, 11481–1482.
[4] a) G. Marzaro, L. Dalla Via, A. N. Garcia-Argaez, M. Dalla Via, A. Novel, *Bioorg. Med. Chem. Lett.* **2016**, *26*, 4875–4878; b) G. E. Collis, A. K. Burrell, *Tetrahedron Lett.* **2005**, *46*, 3653–3656; c) K. Kobayashi, K. Yoneda, T. Mizumoto, H. Umakoshi, O. Morikawa, H. Konishi, *Tetrahedron Lett.* **2003**, *44*, 4733–4736; d) M. Alajarin, A. Vidal, M.-M. Ortin, *Tetrahedron* **2005**, *61*, 7613–7621; e) P. Zhang, L. Zhang, Y. Gao, G. Tang, Y. Zhao, *RSC Adv.* **2016**, *6*, 60922–60925; f) J. Tummatorn, C. Thongsornkleeb, S. Ruchirawat, T. Gettongsong, *Org. Biomol. Chem.* **2013**, *11*, 1463–1467.
[5] a) C. J. Evoniuk, G. dos Passos Gomes, M. Ly, F. D. White, I. V. Alabugin, *J. Org. Chem.* **2017**, *82*, 4265–4278; b) Y. Zhang, M. Wang, P. Li, L. Wang, *Org. Lett.* **2012**, *14*, 2206–2209; c) Z. Zheng, G. Deng, Y. Liang, *RSC Adv.* **2016**, *6*, 103478–103481; d) D. K. O'Dell, K. M. Nicholas, *J. Org. Chem.* **2003**, *68*, 6427–6430; e) C.-Z. Luo, P. Gandeepan, Y.-C. Wu, W.-C. Chen, C.-H Cheng, *RSC Adv.* **2015**, *5*, 106012–106018; f) H. Lee, C. S. Yi, *Organometallics* **2016**, *35*, 1973–1977; g) Y. Tsuji, K. T. Huh, Y. Watanabe, *J. Org. Chem.* **1987**, *52*, 1673–1680; h) S. K. Gadakh, S. Dey, A. Sudalai, *Org. Biomol. Chem.* **2016**, *14*, 2969–2977; i) X. Ji, H. Huang, Y. Li, H. Chen, H. Jiang, *Angew. Chem. Int. Ed.* **2012**, *51*, 1–6; j) K. Sangu, K. Fuchibe, T. Akiyama, *Org. Lett.* **2004**, *6*, 353–355; k) H. Aramoto, Y. Obora, Y. Ishii, *J. Org. Chem.* **2009**, *74*, 628–633.
[6] a) K. Anczkiewicz, M. Królikiewicz, Z. Wróbel, K. Wojciechowski, *Tetrahedron* **2014**, *71*, 3924–3931; b) Z. Wróbel *Eur. J. Org. Chem.* **2000**, *2000*, 521–525; c) B. C. Ranu, A. Hajra, U. Jana, *Tetrahedron Lett.* **2000**, *41*, 531–533.
[7] C. Rochais, R. Yougnia, T. Cailly, J. Sopková-De Oliveira Santos, S. Rault, P. Dallemagne, *Tetrahedron* **2011**, *67*, 5806–5810.
[8] a) L. Pokhrel, Y. Kim, T. D. T. Nguyen, A. M. Prior, J. Lu, K.-O. Chang, D. H. Hua, *Bioorg. Med. Chem. Lett.* **2012**, *22*, 3480–3484; b) G. Deng, C.-J. Li, *Org. Lett.* **2009**, *11*, 1171–1174; c) A. Deb, S. Manna, A. Maji, U. Dutta, D. Maiti, *Eur. J. Org. Chem.* **2013**, *2013*, 5251–5256; d) T. Kawakami, K. Murakami, K. Itami, *J. Am.*

Chem. Soc. **2015**, *137*, 2460–2463; e) V. Mamane, F. Louerat, Y. Fort, *Lett. Org. Chem.* **2010**, *7*, 90–93.
[9] M. G. Campbell, S. L. Zheng, T. Ritter, *Inorg. Chem.* **2013**, *52*, 13295–13297
[10] a) A. Hossian, M. K. Manna, K. Mannaab, R. Jana, *Org. Biomol. Chem.* **2017**, *15*, 6592–6603; b) A. R. Dick, K. L. Hull, M. S. Sanford, *J. Am. Chem. Soc.* **2004**, *126*, 2300–2301; c) M. Kim, J. Kwak, S. Chang, *Angew. Chem. Int. Ed.* **2009**, *48*, 8935–8939; d) L. Ilies, M. Kobayashi, A. Matsumoto, N. Yoshikai, E. Nakamura, *Adv. Synth. Catal.* **2012**, *354*, 593–596; e) B. Li, Z.-H. Wu, Y.-F. Gu, C.-L. Sun, B.-Q. Wang, Z.-J. Shi, *Angew. Chem. Int. Ed.* **2011**, *50*, 1109–1113; f) L. Zhu, X. Cao, R. Qiu, T. Iwasaki, V. P. Reddy, X. Xu, S.-F. Yin, N. Kambe, *RSC Adv.* **2015**, *5*, 39358–39365.
[11] a) J. A. Barltrop, K. E. MacPhee, *J. Chem. Soc.* **1952**, 638–642; b) J. Dubarle Offner, G. Schnakenburg, F. Rose-Munch, E. Rose, K. H. Dötz, *Organometallics* **2010**, *29*, 3308–3317.
[12] a) K. K. Sharma, D. I. Patel, R. Jain, *Chem. Commun.* **2015**, *51*, 15129–15132; b) Q. Yu, L. Hu, Y. Wang, S. Zheng, J. Huang, *Angew. Chem. Int. Ed.* **2015**, *54*, 15284–15288.
[13] E. Longhi, L. De Cola in *Iridium(III) in Optoelectronic and Photonics Applications*, *1st ed.*, (Ed.: E. Zysman-Colman), John Wiley & Sons, Chichester, **2017**, 205–262
[14] a) J. Frey, B. F. E. Curchod, R. Scopelliti, I. Tavernelli, U. Rothlisberger, M. K. Nazeeruddina, E. Baranoff, *Dalton Trans.* **2014**, *43*, 5667–5679; b) K. S. Bejoymohandas, A. Kumar, S. Varughese, E. Varathan, V. Subramanian, M. L. P. Reddy, *J. Mater. Chem. C* **2015**, *3*, 7405–7420.
[15] S. Lamansky, P. Djurovich, D. Murphy, F. Abdel-Razzaq, R. Kwong, I. Tsyba, M. Bortz, B. Mui, R. Bau, M. E. Thompson, *Inorg. Chem.* **2001**, *40*, 1704–1711
[16] E. Baranoff, B. F. E. Curchod, F. Monti, F. Steimer, G. Accorsi, I. Tavernelli, U. Rothlisberger, R. Scopelliti, M. Grätzel, M. K. Nazeeruddin, *Inorg. Chem.* **2012**, *51*, 799–811.
[17] a) J. Lee, H. Oh, J. Kim, K.-M. Park, K. S. Yook, J. Y. Lee, Y. Kang, *J. Mater. Chem. C*, **2014**, *2*, 6040–6047; b) V. Sivasubramaniam, F. Brodkorb, S. Hanning, H. P. Loebl, V. van Elsbergen, H. Boerner, U. Scherf, M. Kreyenschmidt, *J. Fluorine Chem.* **2009**, *130*, 640–649; c) R. J. Holmes, S. R. Forrest, T. Sajoto, A. Tamayo, P. I. Djurovich, M. E. Thompson, J. Brooks, Y.-J. Tung, B. W. D′Andrade, M. S. Weaver, R. C. Kwong, J. J. Brown, *Appl. Phys. Lett.* **2005**, *87*, 243507.
[18] a) Y. Furusho, A. Tsunoda, T. Aida, *J. Chem. Soc. Perkin Trans. 1*, **1996**, *0*, 183–190; b) P. Dash, M. Janni, S. Peruncheralathan, *Eur. J. Org. Chem.* **2012**, *2012*, 4914–4917.
[19] J. Huang, Y. Chen, J. Chan, M. L. Ronk, R. D. Larsen, M. M. Faul, *Synlett*, **2011**, *10*, 1419–1422.
[20] Y. Liu, S. Zhang, *Synlett*, **2011**, *2*, 268–272.
[21] P.-F. Larsson, P. Astvik, P.-O. Norrby, *Beilstein J. Org. Chem.* **2012**, *8*, 1909–1915
[22] a) J. Ju, R. Hua, J. Su, *Tetrahedron* **2012**, *68*, 9364–9370; b) H. Xua, C. Wolf, *Chem. Commun.* **2009**, *0*, 3035–3037; c) A. Nobutaka, U. Masatsugu, **2016**, U. S. Patent Application US2016/190487 A1; d) N. Xia, M. Taillefer, *Angew. Chem. Int. Ed.*. **2009**, *48*, 337–339.
[23] a) J. P. Wolfe, J. Ahman, J. P. Sadighi, R. A. Singer, S. L. Buchwald, *Tet. Lett.* **1997**, *38*, 6367–6370; b) G. A. Grasa, M. S. Viciu, J. Huang, S. P. Nolan, *J. Org. Chem.* **2001**, *66*, 7729–7737; c) X. Huang, S. L. Buchwald, *Org. Lett.* **2001**, *3*, 3417–3419; d) D.-Y. Lee, J. F. Hartwig, *Org. Lett.* **2005**, *7*, 1169–1172; e) S. Bhagwanth, A. G. Waterson, G. M. Adjabeng, K. R. Hornberger, *J. Org. Chem.* **2009**, *74*, 4634–4637; f) R. A. Green, J. F. Hartwig, *Org. Lett.* **2014**, *16*, 4388–4391.
[24] P. L. Pickard, T. L. Tolbert, *J. Org. Chem.* **1961**, *26*, 4886–4888.
[25] E. Baranoff, B. F. E. Curchod, *Dalton Trans.* **2015**, *44*, 8318–8329.
[26] a) R. E. Banks, S. N. Mohialdin-Khaffaf, G. S. Lal, I. Sharif, R. G. Syvret, *J. Chem. Soc. Chem. Commun.* **1992**, *0*, 595–596; b) J. Dubarle Offner, G. Schnakenburg, F. Rose-Munch, E. Rose, K. H. Dötz, *Organometallics* **2010**, *29*, 3308–3317.
[27] K. K. Laali, V. J. Gettwert, *J. Fluorine Chem.* **2001**, *107*, 31–34.
[28] a) J. G. Allen, J. Burdon, J. C. Tatlow, *J. Chem. Soc.* **1965**, *0*, 1045–1051; b) H. Amii, K. Uneyama, *Chem. Rev.* **2009**, *109*, 2119–2183.
[29] a) R. Jana, T. P. Pathak M. S. Sigman, *Chem. Rev.* **2011**, *111*, 1417–1492; b) M. M. Heravi, E. Hashemi, N. Nazari, *Mol. Diversity* **2014**, *18*, 441–472; c) W. D. G. Brittain, S. L. Cobb, *Org. Biomol. Chem.* **2018**, *16*, 10–20; d) S. Xu, E. H. Kim, A. Wei, E. Negishi, *Sci. Technol. Adv. Mater.* **2014**, *15*, 044201.
[30] a) R. M. Adhikari, D. C. Neckers, B. K. Shah, *J. Org. Chem.* **2009**, *74*, 3341–3349; b) G. Schansker, S. Z. Tóth, L. Kovács, A. R. Holzwarth, G. Garab, *Biochim. Biophys. Acta*, **2011**, *1807*, 1032–1043; c) J.-Y. Shen, X.-L. Yang, T.-H. Huang, J. T. Lin, T.-H. Ke, L.-Y. Chen, C.-C. Wu, M.-C. P. Yeh, *Adv. Funct. Mater.* **2007**, *17*, 983–995.
[31] K. Nozaki, K. Takahashi, K. Nakano, T. Hiyama, H.-Z. Tang, M. Fujiki, S. Yamaguchi, K. Tamao, *Angew. Chem. Int. Ed.* **2003**, *42*, 2051–2053.
[32] D. B. Shinde, J. K. Salunke, N. R. Candeias, F. Tinti, M. Gazzano, P. P. Wadgaonkar, A. Priimagi, N. Camaioni, P. Vivo, *Sci. Rep.* **2017**, *7*, 46268.
[33] T. Yu, Z. Xu, W. Su, Y. Zhao, H. Zhanga, Y. Baoa, *Dalton Trans.* **2016**, *45*, 13491–13502.
[34] Z. Li, J. Kong, F. K. Wang, C. He, *J. Mater. Chem. C*, **2017**, *5*, 5283–5298.
[35] G. Cheng, N. R. Vautravers, R. E. Morrisa, D. J. Cole-Hamilton, *Org. Biomol. Chem.* **2008**, *6*, 4662–4667.
[36] B. Marciniec, J. Guliński, W. Urbaniak, Z. W. Kornetka in *Comprehensive Handbook on Hydrosilylation*, *1st ed.*, (Ed.: B. Marciniec), Pergamon Press, Oxford, **1992**.
[37] H. Uratani, S. Kubo, K. Shizu, F. Suzuki, T. Fukushima, H. Kaji, *Sci. Rep.* **2016**, *6*, 39128.
[38] J. D. Offner, G. Schnakenburg, F. Rose-Munch, E. Rose, K. H. Dotz, *Organometallics* **2010**, *29*, 3308–3317.
[39] A. Domenicano, P. Murray-Rust, *Tetrahedron Lett.* **1979**, *24*, 2283–2286.

Advanced Synthesis & Catalysis

Supporting Information

Supporting Information

Synthesis of 5-substituted benzo[*h*]quinoline derivatives via reactions involving sp^2-C-Br bond activation

Bartosz Orwat,[a,b] Myong-joon Oh,[a,b] Maciej Kubicki [a] and Ireneusz Kownacki [a,b]*

[a] Faculty of Chemistry, Adam Mickiewicz University in Poznań, St. Umultowska 89b, 61-614 Poznań, Poland
Tel: +48 61 829 1554; Fax: +48 61 829 1555;
[b] Wielkopolska Centre of Advanced Technologies, Umultowska 89c, 61-614 Poznań, Poland;

e-mail: irekk@o365.amu.edu.pl

Table of Contents

1. General information..... S-2
2. X-ray measurements details..... S-4
3. MS spectra..... S-7
4. NMR spectra S-11
5. References..... S-24

1. General information

All syntheses and manipulations were carried out under argon using standard gas-vacuum line unless otherwise specified. Benzo[h]quinoline and chlorodimethylsilane were obtained from ABCR, all other reagents were purchased from Sigma Aldrich and were used without further purification unless otherwise specified/ stated. [noted= rzadziej] . Methanol was dried with sodium, THF with sodium/benzophenone, toluene with sodium/potassium alloy, n-hexane with sodium/potassium alloy and distilled under argon prior to use. NMP was only degassed under reduced pressure and saturated with argon three times. 1-ethyl-3-methylimidazolium tetrafluoroborate was heated at 105 °C for 3 h under vacuum and saturated with argon prior to use. 5-bromo-benzo[h]quinoline preparation was based on the literature-known methodology with minor modifications.[1] 4-(*N,N*-diphenylamino)-bromobenzene[2] and benzophenone imine[3] were prepared according to published procedures.

Flash chromatography purification was performed on a Biotage Isolera One automated system with columns packed with Silicagel 60 Å 230-400 mesh manufactured by Merck. Industrial grade and non-dried solvents were used for automated flash column chromatography. All noted percentage values of eluents composition are referred to volume ratios.

The microwave-assisted reactions were performed using a CEM Discover microwave reactor system.

NMR spectra were measured at room temperature using a Bruker Ultrashield 300 or a Bruker Avance 400 NMR spectrometer. All chemical shifts are reported in δ-scale as parts per million [ppm] (multiplicity, coupling constant *J*, number of protons) relative to the solvent residual peaks as the internal standard. Abbreviations used for signal multiplicity: br = broad, s = singlet, d = doublet, t = triplet, q = quartet, dd = doublet of doublets and m = multiplet.

GC measurements were performed on a Bruker Scion 436 gas chromatograph. GCMS measurements were performed on a Bruker 450 gas chromatograph coupled with a Bruker 320 mass spectroscopy detector. The same mass detector was used to perform DEPMS analysis.

HRMS measurements were performed on a Bruker Impact II UHR Q-TOF instrument in ESI mode.

Diffraction data were collected by the ω-scan technique, at room temperature (**1**, **2**, **4**, **6**) and at 100(1) K (**7**) on Rigaku Xcalibur four-circle diffractometer with Eos CCD detector and graphite-monochromated MoK_α radiation (λ=0.71069 Å), and at room temperature (**10**) on Rigaku SuperNova diffractometer with Atlas CCD detector and mirror-monochromated CuK_α radiation (λ=1.54178 Å). The data were corrected for Lorentz-polarization as well as for absorption effects.[4] Precise unit-cell parameters were determined by a least-squares fit of reflections of the highest intensity (3567 for **1**, 199 for **2**, 2024 for **4**, 1118 for **6**, 14754 for **7**, 3638 for **10**, chosen from the whole experiment. The structures were solved with SHELXT [2] and refined with the full-matrix least-squares procedure on F^2 by SHELXL-2013.[5] All non-hydrogen atoms were refined anisotropically, NH_2 hydrogen atoms in **4** were found in difference Fourier maps and freely isotropically refined, all other hydrogen atoms were placed in idealized positions and refined as 'riding model' with isotropic displacement parameters set at 1.2 times U_{eq} of appropriate carrier atoms. The molecule 6 was found disordered over two positions, mirror-related; the s.o.f.'s converged at 85.0(3)/15.0(3)%; for less-occupied molecule non-hydrogen atoms were refined isotropically. Crystals of **10** were two-component twin, it was taken into account during both data reduction and refinement procedures; BASF factor, showing relative content of both components converged at 51.22(15)/48.78(15)%. Table 1 lists the relevant crystallographic and refinement data.

Crystallographic data for the structural analysis have been deposited with the Cambridge Crystallographic Data Centre, Nos. CCDC-1818627 (**1**), CCDC-1818628 (**2**), CCDC-1818629 (**4**), CCDC-1818630 (**6**), and CCDC-1818631 (**7**), CCDC-1818961 (**10**). Copies of this information may be obtained free of charge from: The Director, CCDC, 12 Union Road, Cambridge, CB2 1EZ, UK. Fax: +44(1223)336-033, e-mail: deposit@ccdc.cam.ac.uk, or www: www.ccdc.cam.ac.uk

2. X-ray measurements details

Table 1. Crystal data, data collection and structure refinement

Compound	**1**	**2**	**4**	**6**	**7**	**10**
Formula	$C_{13}H_8BrN$	$C_{14}H_{11}NO$	$C_{13}H_{10}N_2$	$C_{13}H_8FN$	$C_{19}H_8F_5N$	$C_{25}H_{16}N_2$
Formula weight	258.11	209.24	194.23	197.20	345.26	344.40
Crystal system	monoclinic	monoclinic	monoclinic	monoclinic	orthorhombic	monoclinic
Space group	$P2_1/c$	$P2_1/c$	$P2_1/c$	$P2_1/n$	$P2_12_12_1$	P2/c
a(Å)	5.31759(13)	24.0456(19)	13.1348(8)	6.9034(5)	10.1766(2)	11.4067(5)
b(Å)	13.2431(4)	11.1962(10)	5.2026(3)	9.9212(8)	11.0529(2)	6.7393(3)
c(Å)	14.4070(5)	12.0746(12)	14.7221(9)	13.6384(11)	25.2507(6)	22.7302(10)
α(°)	90	90	90	90		
β(°)	97.736(2)	95.310(8)	105.240(6)	102.697(7)	90	95.728(4)
γ(°)	90	90	90	90		
V(Å^3)	1005.33(5)	3236.8(5)	970.66(10)	911.25(13)	2840.22(10)	1738.62(13)
Z	4	12	4	4	8	4
D_x(g cm^{-3})	1.71	1.288	1.329	1.437	1.615	1.316
F(000)	512	1320	408	408	1392	720
μ(mm^{-1})	4.048	0.082	0.080	0.099	0.141	0.599
Θ range (^{0})	3.24 – 26.56	3.10 – 25.00	2.90 – 25.00	3.66 – 26.56	3.14 – 27.15	3.90 – 76.52
Reflections:						
collected	9705	12444	7750	3090	54952	10813
unique (R_{int})	2003 (0.024)	5701 (0.060)	1706 (0.023)	1748 (0.023)	6007 (0.064)	6244 (0.043)
with I>2σ(I)	1725	2094	1290	1431	5139	5524
R(F) [I>2σ(I)]	0.026	0.061	0.043	0.045	0.044	0.054
wR(F^2) [I>2σ(I)]	0.067	0.062	0.112	0.122	0.097	0.148
R(F) [all data]	0.034	0.181	0.059	0.055	0.055	0.059
wR(F^2) [all data]	0.070	0.080	0.122	0.133	0.103	0.152
Goodness of fit	1.09	0.84	1.05	1.03	1/04	1.07
max/min Δρ (e Å^{-3})	0.31/-0.31	0.19/-0.15	0.12/-0.15	0.28/-0.18	0.29/-0.20	0.16/-0.27

Table 2. Selected geometrical data (Å,º) with s.u.'s in parentheses (if there is more than one line, it refers to the multiple molecules in the asymmetric part of the unit cell). "max_dev" line is the maximum deviation from the least-squares plane calculated for 14 ring-system atoms.

	1	**2**	**4**	**6**	**7**	**10**
N1-C2	1.319(3)	1.333(4) 1.326(4) 1.321(4)	1.324(2)	1.346(5)	1.321(4) 1.325(4)	1.325(3)
N1-C14	1.359(3)	1.350(4) 1.376(4) 1.358(3)	1.3539(17)	1.353(5)	1.356(4) 1.354(4)	1.361(2)
C5-C6	1.431(3)	1.445(4) 1.460(4) 1.446(4)	1.445(2)	1.423(2)	1.459(4) 1.452(4)	1.442(2)
C6-C7	1.345(3)	1.337(4) 1.332(4) 1.337(4)	1.355(2)	1.337(2)	1.355(4) 1.358(5)	1.354(3)
C2-N1-C14	117.6(2)	116.8(3) 117.1(3) 117.2(3)	117.91(13)	117.1(4)	118.0(3) 117.9(3)	117.23(16)
C5-C6-C7	122.50(19)	121.5(3) 121.6(3) 120.5(3)	119.35(14)	123.81(13)	120.2(3) 120.1(3)	120.91(15)
max_dev	0.012(2)	0.023(3) 0.029(3) 0.079(3)	0.0223(11)	0.0444(14)	0.014(3) 0.019(3)	0.0318(17)

Table 3. Weak interaction data (Å, °); Cg denote the centroids of the aromatic rings.

D	H	A	D-H	H···A	D···A	D-H···A
2						
C16B	H16D	Cg1[i]	0.96	2.88	3.512(4)	124
C2A	H2A	Cg2[i]	0.93	2.87	3.704(5)	151
C2C	H2C	Cg3[ii]	0.93	2.84	3.564(4)	135
C9C	H9C	Cg4[iii]	0.93	2.84	3.564(4)	135
4						
N6	H6	N1[iv]	0.92(2)	2.21(2)	3.071(2)	156.5(18)
7						
C2A	H2A	F16B[i]	0.95	2.66	3.249(4)	120
C3A	H3A	F18A[v]	0.95	2.65	3.433(4)	140
C4A	H4A	F17A[v]	0.95	2.68	3.568(4)	155
C9A	H9A	F19A[vi]	0.95	2.69	3.252(4)	119
C10A	H10A	F19A[vi]	0.95	2.63	3.225(4)	121
C3B	H3B	F18B[vii]	0.95	2.56	3.298(4)	135
C4B	H4B	F19B[vii]	0.95	2.67	3.575(4)	160
C7B	H7B	N1A[viii]	0.95	2.69	3.489(4)	143
C9B	H9B	F16B[ix]	0.95	2.58	3.457(4)	153
C10B	H10B	F17B[ix]	0.95	2.59	3.258(4)	128
10						
C18	H18	Cg5[x]	0.93	2.64	3.480(3)	150
C25	H25	Cg6[xi]	0.93	2.76	3.604(3)	151
C3	H3	Cg7[xii]	0.93	2.79	3.559(3)	140
C10	H10	Cg8[xiii]	0.93	2.77	3.565(3)	144
Halogen bonds						
1						
C6-Br6	Br6···Br6[xiv]	C6-Br6···Br6[xiv]				
1.900(2)	3.7944(5)	95.29(7)				

Symmetry codes: [i] 1-x,-1/2+y,1/2-z; [ii] 2-x,-1/2+y,3/2-z; [iii] x,3/2-y,-1/2+z; [iv] x,1/2-y,-1/2+z; [v] -x,-1/2+y,1/2-z; [vi] 1-x,1/2+y,1/2-z; [vii] ½+x,1/2-y,1-z; [viii] ½-x,1-y,1/2+z; [ix] -1/2+x,3/2-y,1-z; [x] 1-x,1-y,1-z; [xi] –x,-y,1-z; [xii]1-x,-y,1-z; [xiii] –x,1-y,1-z; [xiv] 2-x,-y,1-z.

3. MS spectra

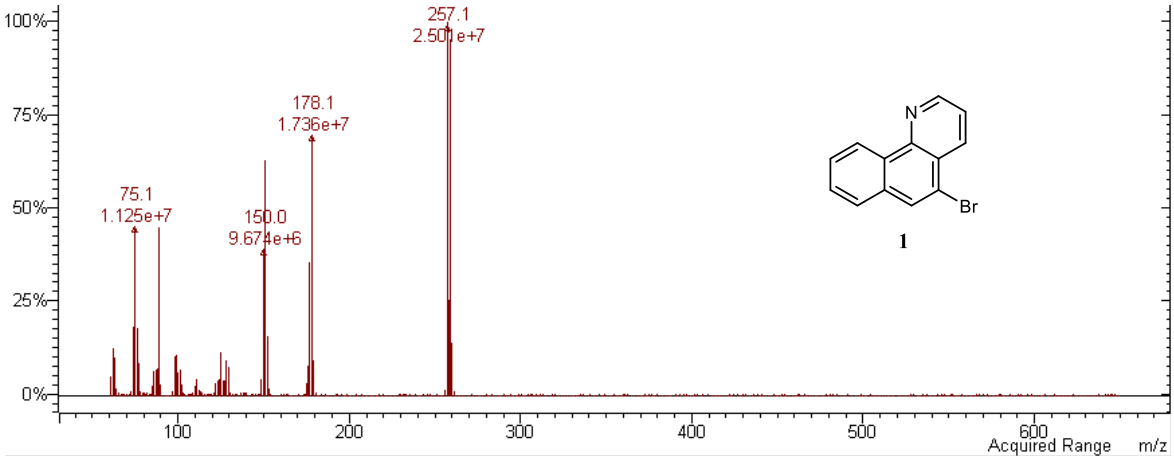
257.1
178.1
1.736e+7
75.1
1.125e+7
150.0
9.674e+6
N
Br
1
100%
75%
50%
25%
0%
100
200
300
400
500
600
Acquired Range
m/z

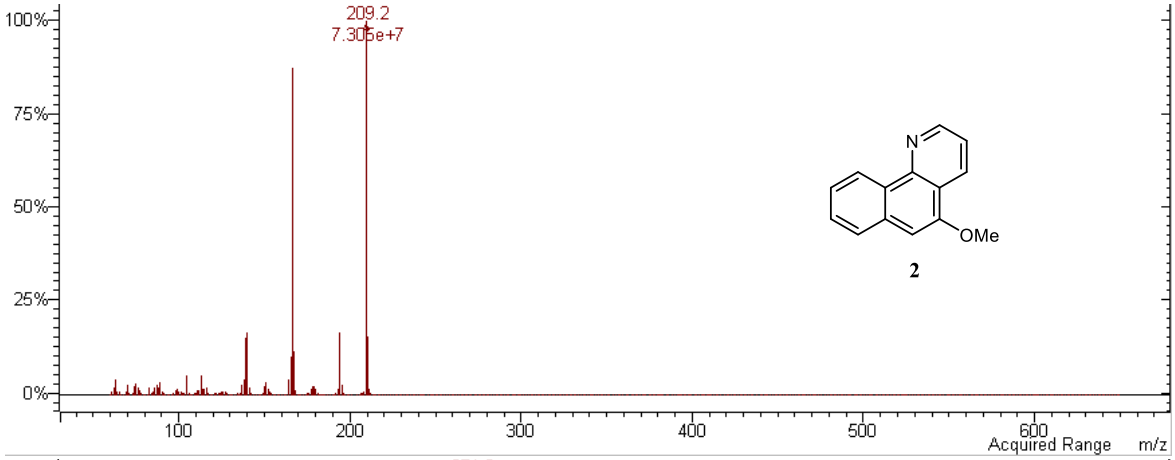
209.2
7.305e+7
N
OMe
2
100%
75%
50%
25%
0%
100
200
300
400
500
600
Acquired Range
m/z

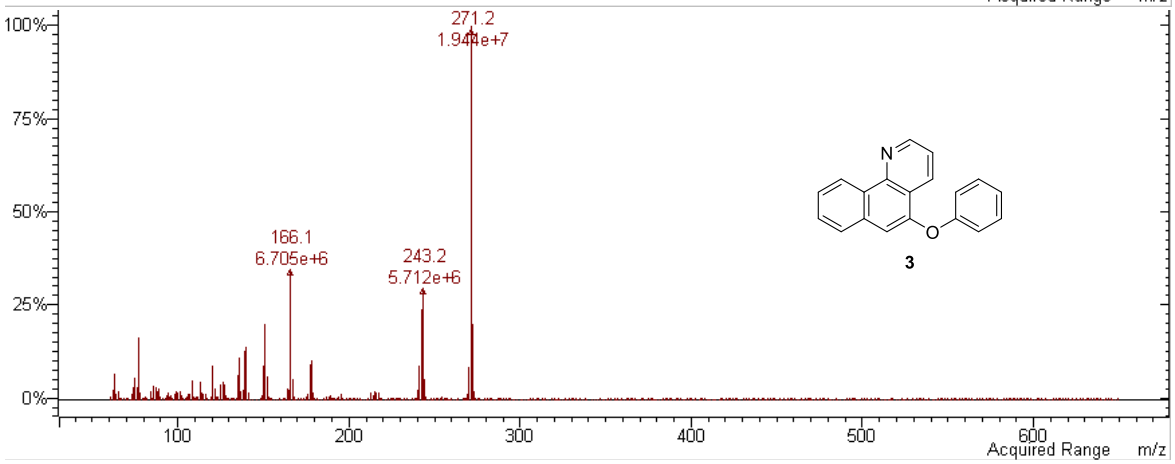
271.2
1.944e+7
166.1
6.705e+6
243.2
5.712e+6
N
O
3
100%
75%
50%
25%
0%
100
200
300
400
500
600
Acquired Range
m/z

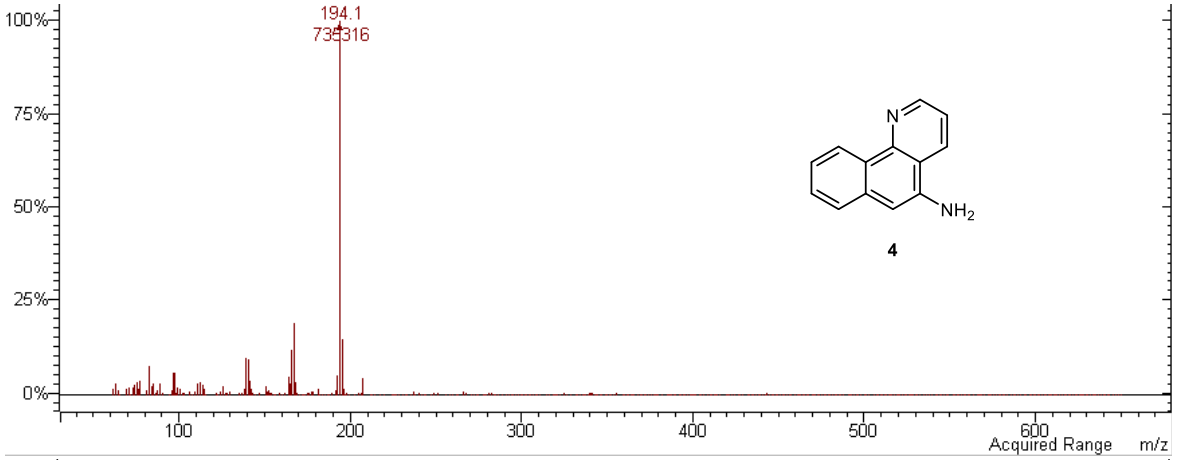
194.1
735316
100%
75%
50%
25%
0%
100
200
300
400
500
600
Acquired Range
m/z
N
NH2

4

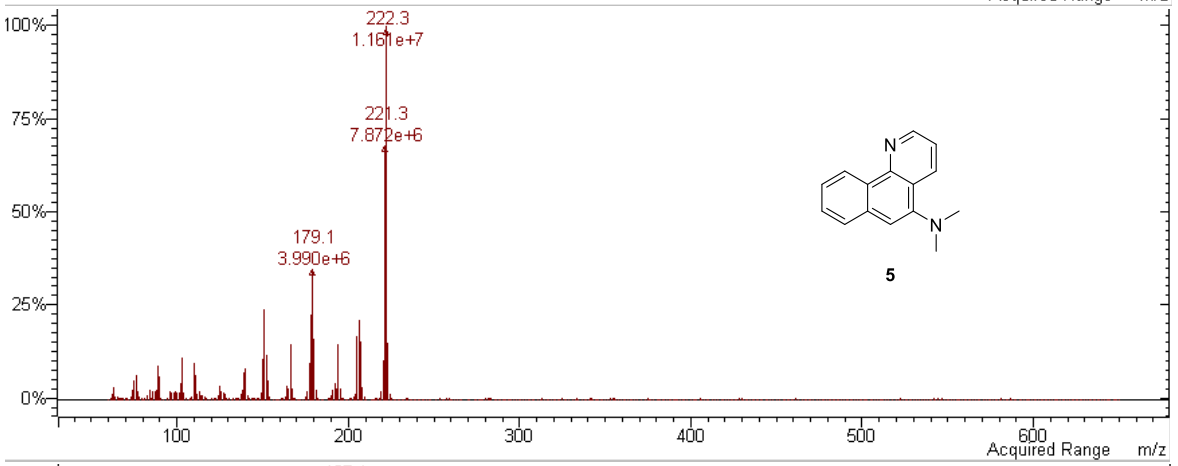
222.3
1.161e+7
221.3
7.872e+6
179.1
3.990e+6
100%
75%
50%
25%
0%
100
200
300
400
500
600
Acquired Range
m/z
N
N

5

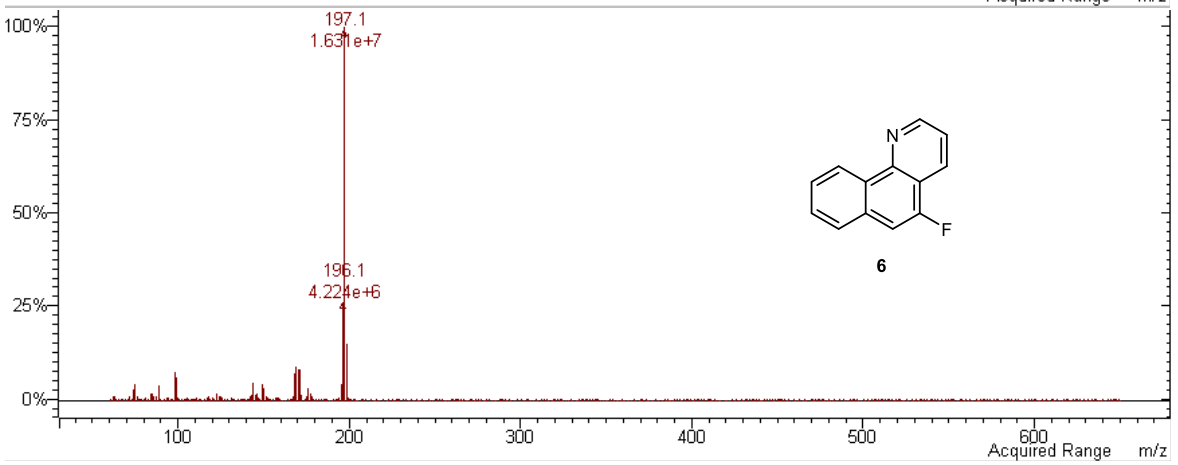
197.1
1.631e+7
196.1
4.224e+6
100%
75%
50%
25%
0%
100
200
300
400
500
600
Acquired Range
m/z
N
F

6

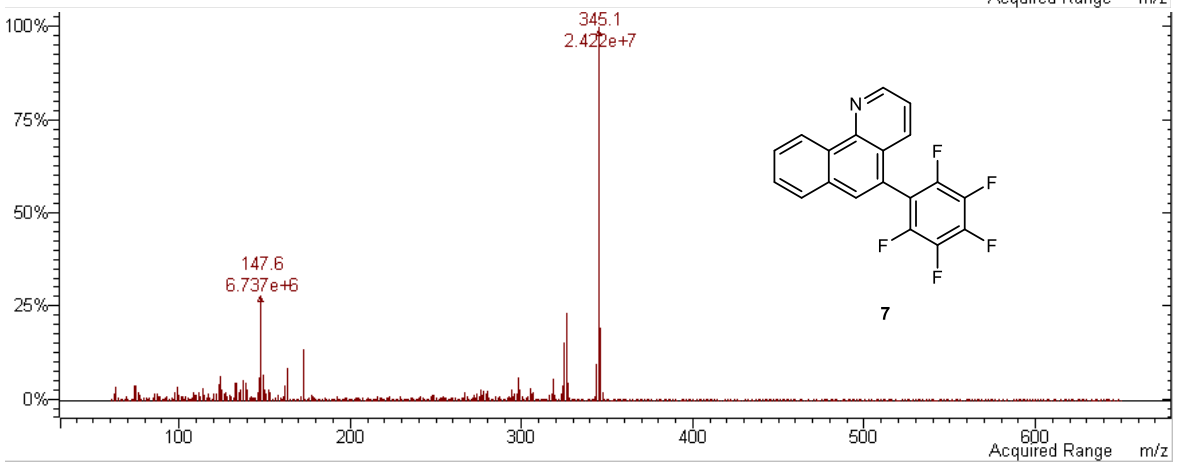
345.1
2.422e+7
147.6
6.737e+6
100%
75%
50%
25%
0%
100
200
300
400
500
600
Acquired Range
m/z
N
F
F
F
F
F

7

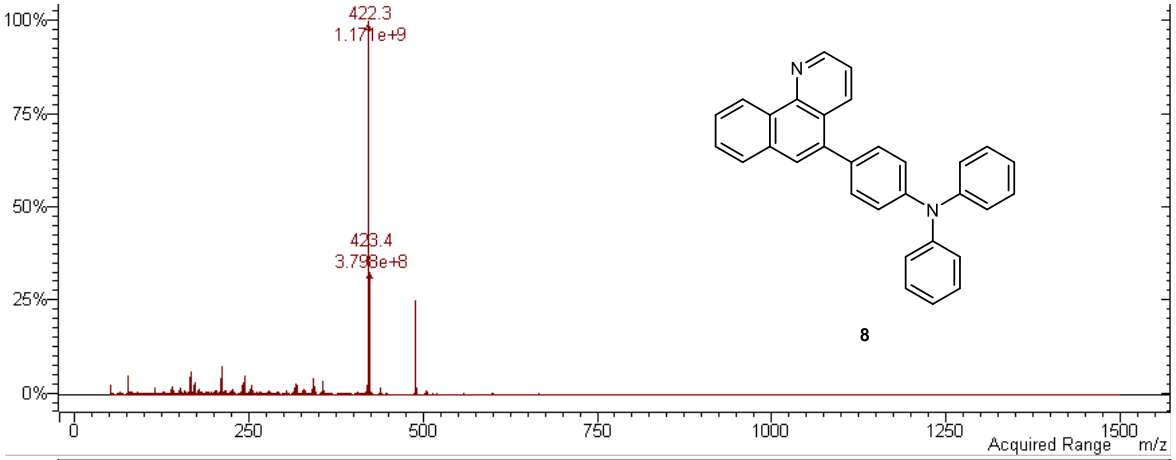
422.3
1.171e+9
423.4
3.798e+8
100%
75%
50%
25%
0%
0
250
500
750
1000
1250
1500
Acquired Range
m/z
N
N

8

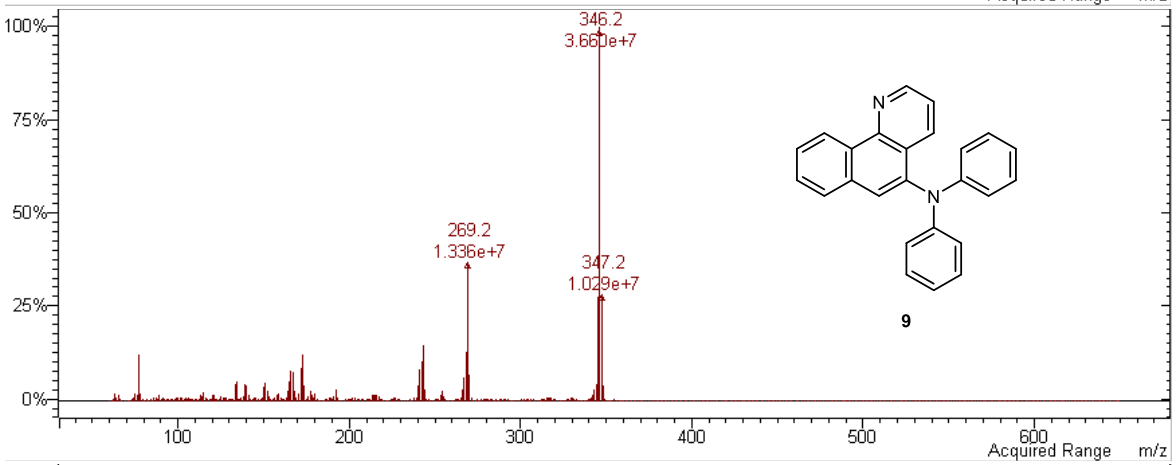
346.2
3.660e+7
269.2
1.336e+7
347.2
1.029e+7
100%
75%
50%
25%
0%
100
200
300
400
500
600
Acquired Range
m/z
N
N

9

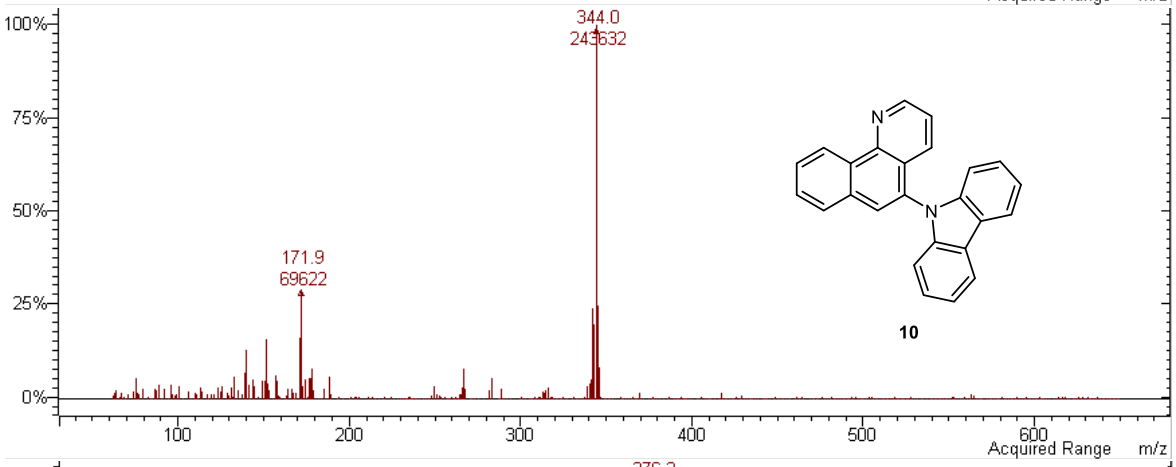
344.0
243632
171.9
69622
100%
75%
50%
25%
0%
100
200
300
400
500
600
Acquired Range
m/z
N
N

10

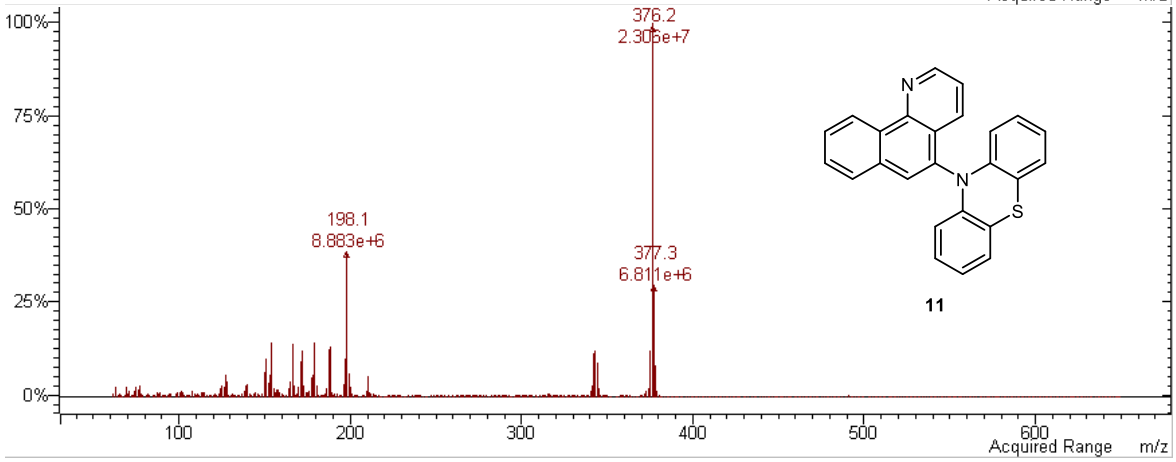
376.2
2.305e+7
198.1
8.883e+6
377.3
6.811e+6
100%
75%
50%
25%
0%
100
200
300
400
500
600
Acquired Range
m/z
N
N
S

11

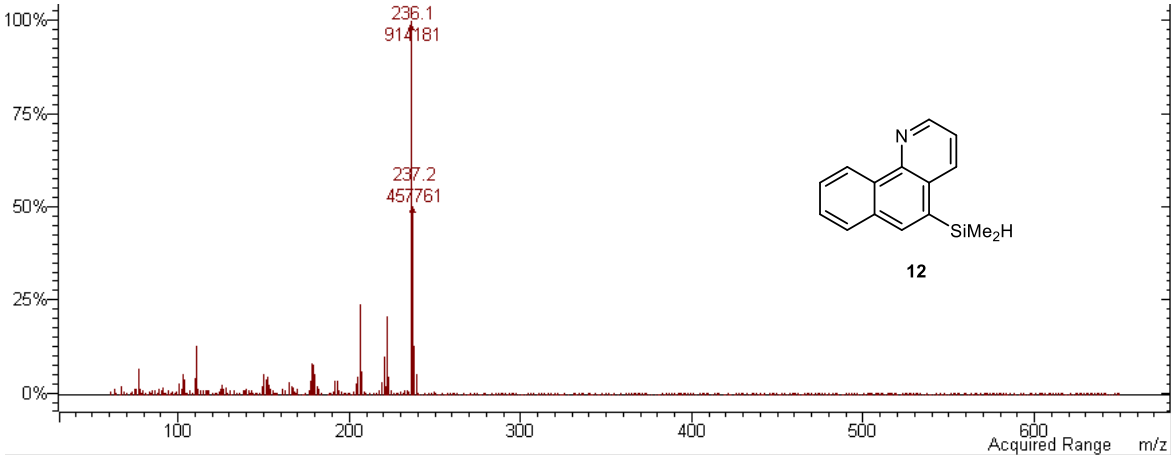
100%
75%
50%
25%
0%
236.1
914181
237.2
457761
100
200
300
400
500
600
Acquired Range
m/z
N
SiMe2H
12

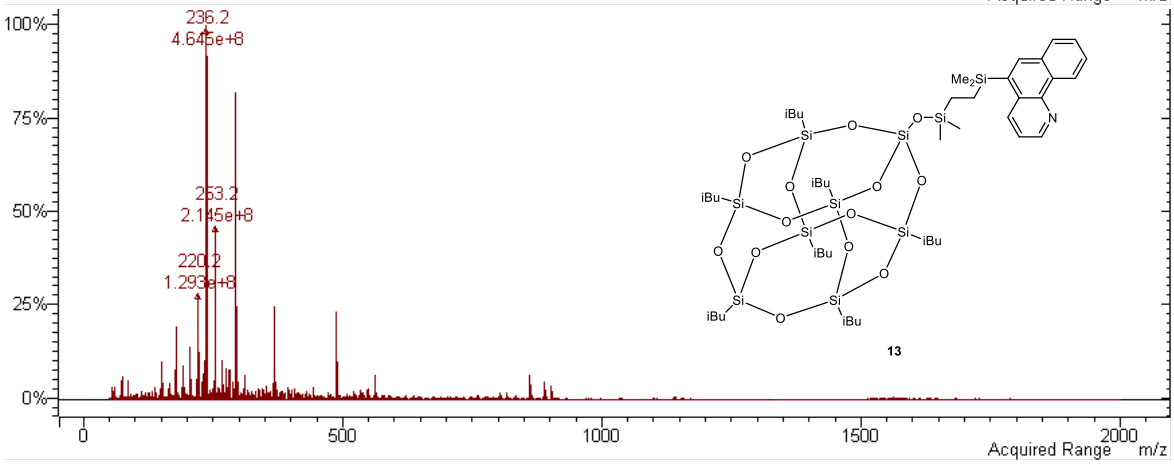
100%
75%
50%
25%
0%
236.2
4.645e+8
263.2
2.145e+8
220.2
1.293e+8
0
500
1000
1500
2000
Acquired Range
m/z
Me2Si
N
iBu
Si
O
13

4. NMR spectra

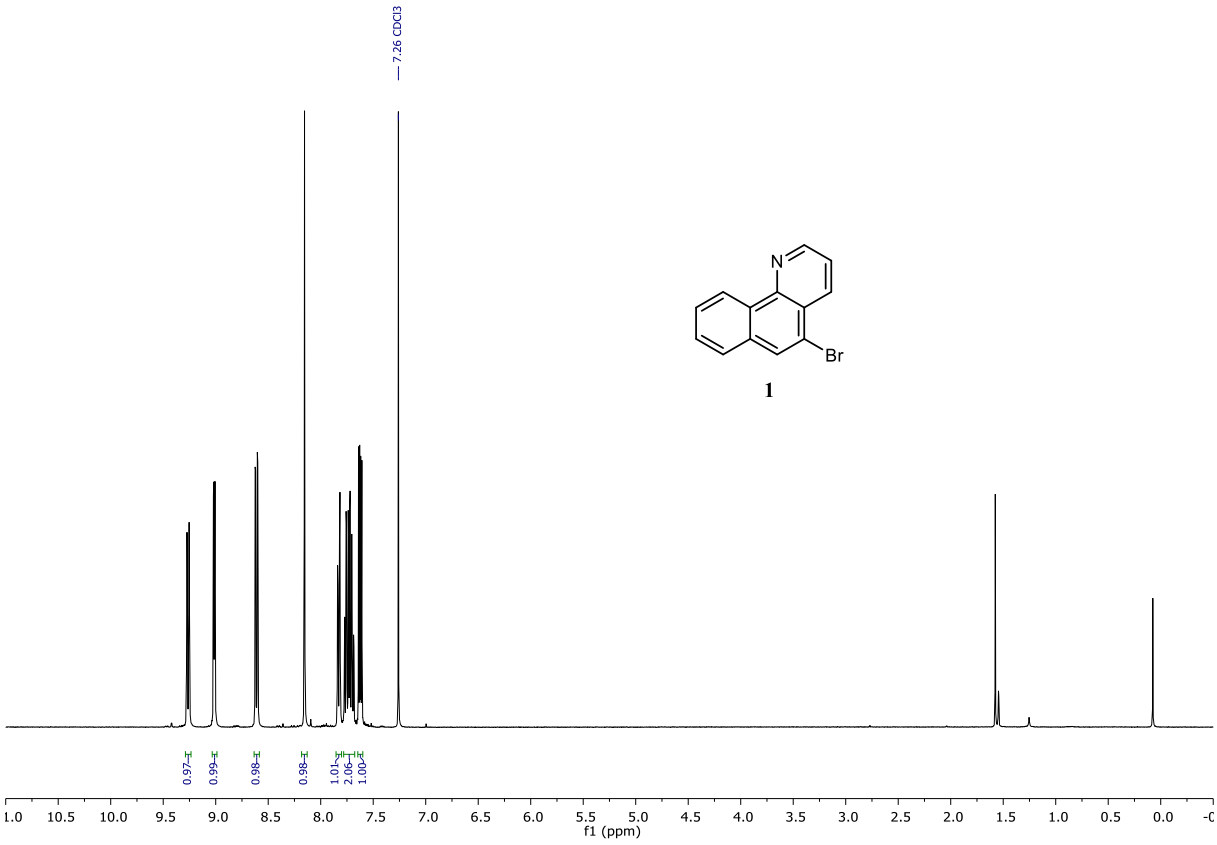

1

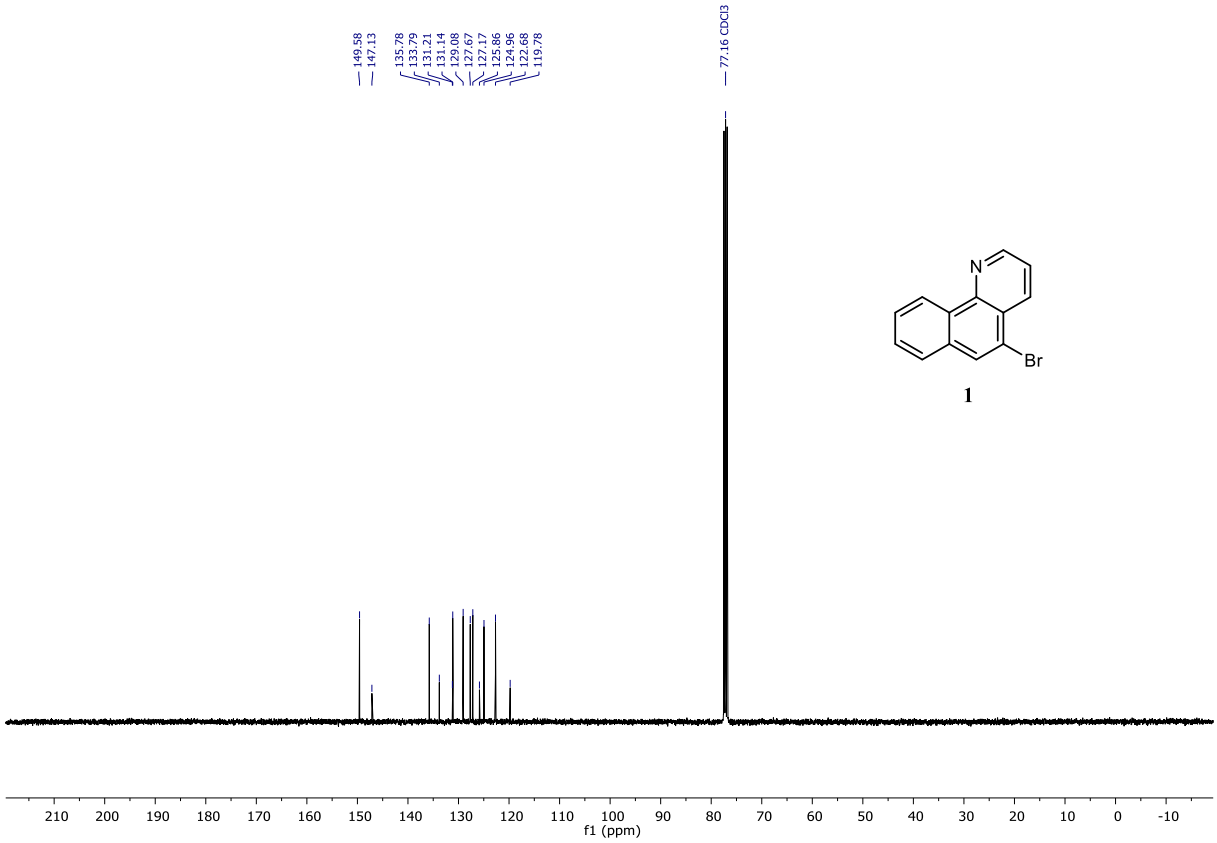

1

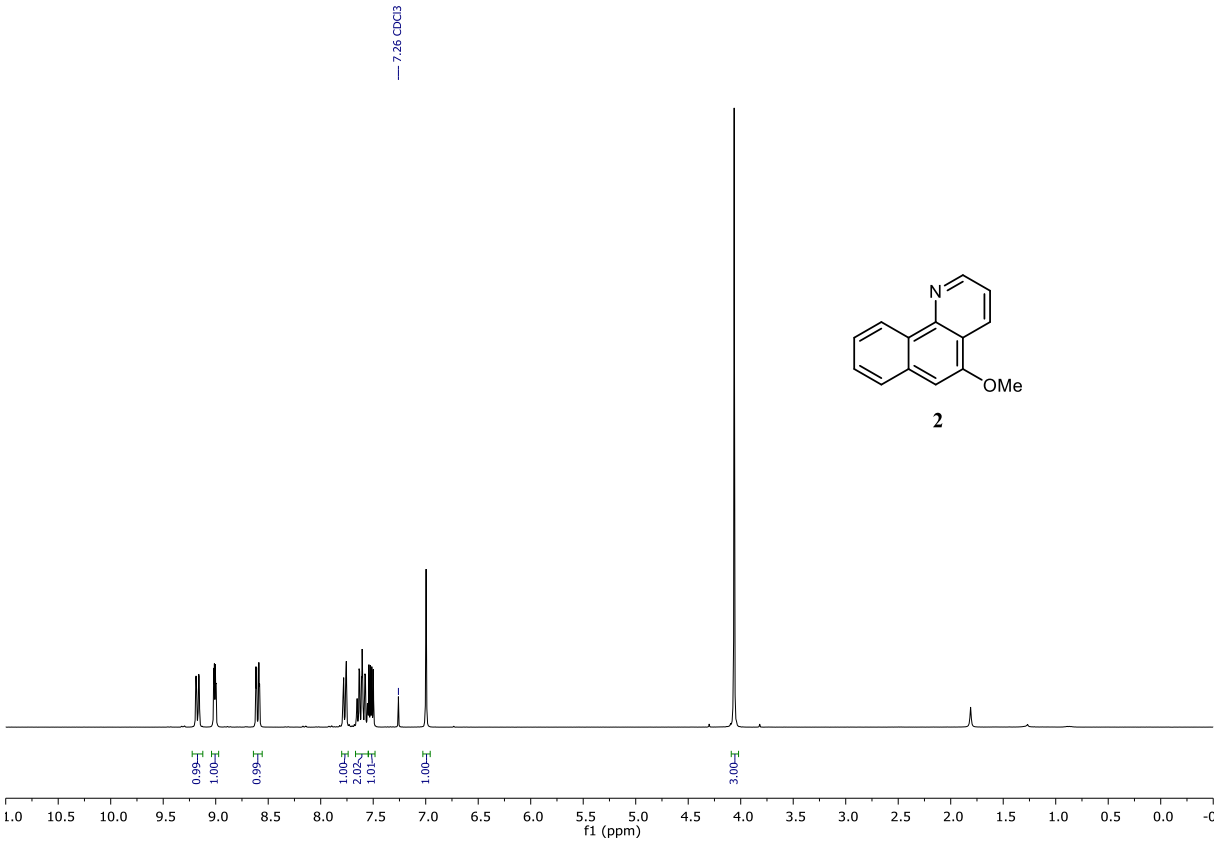
7.26 CDCl3
N
OMe
0.99
1.00
0.99
1.00
2.02
1.01
1.00
3.00
f1 (ppm)

2

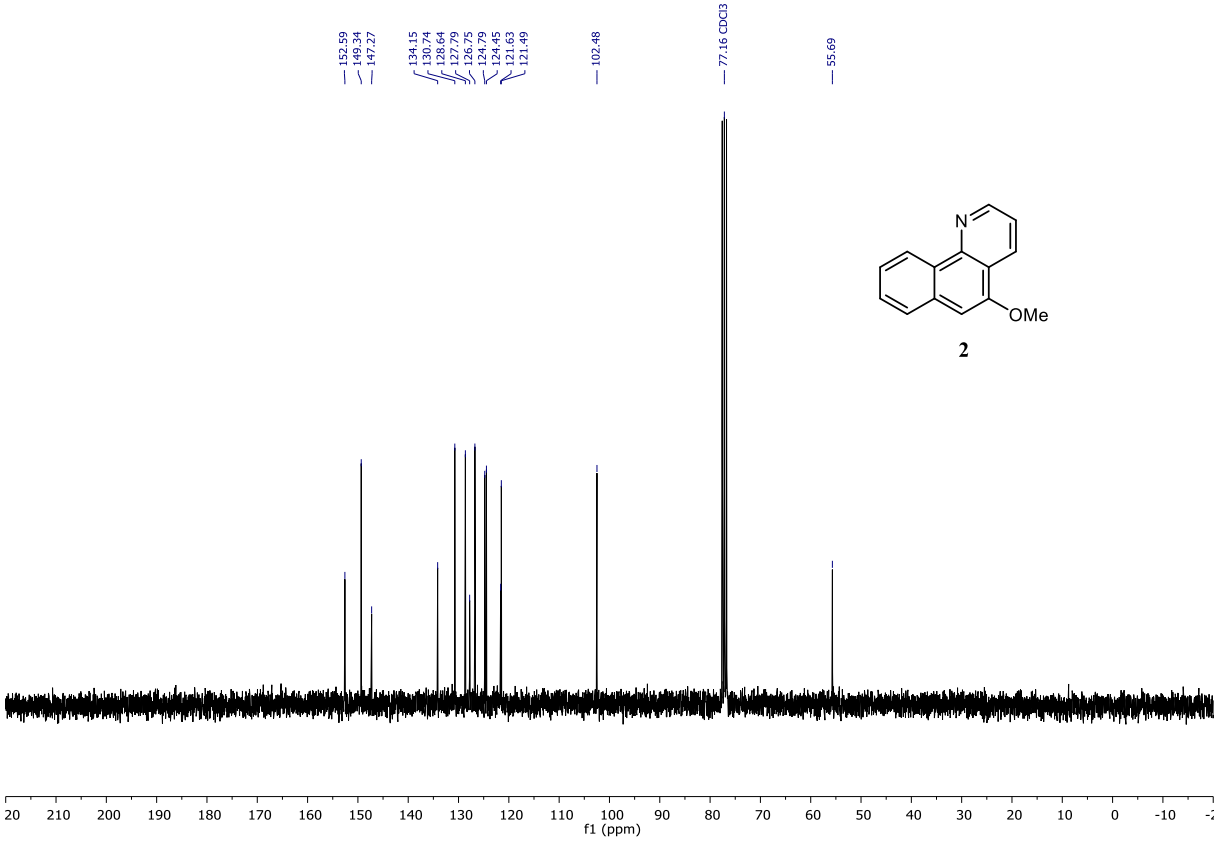
152.59
149.34
147.27
134.15
130.74
128.64
127.79
126.75
124.79
124.45
121.63
121.49
102.48
77.16 CDCl3
55.69
N
OMe
f1 (ppm)

2

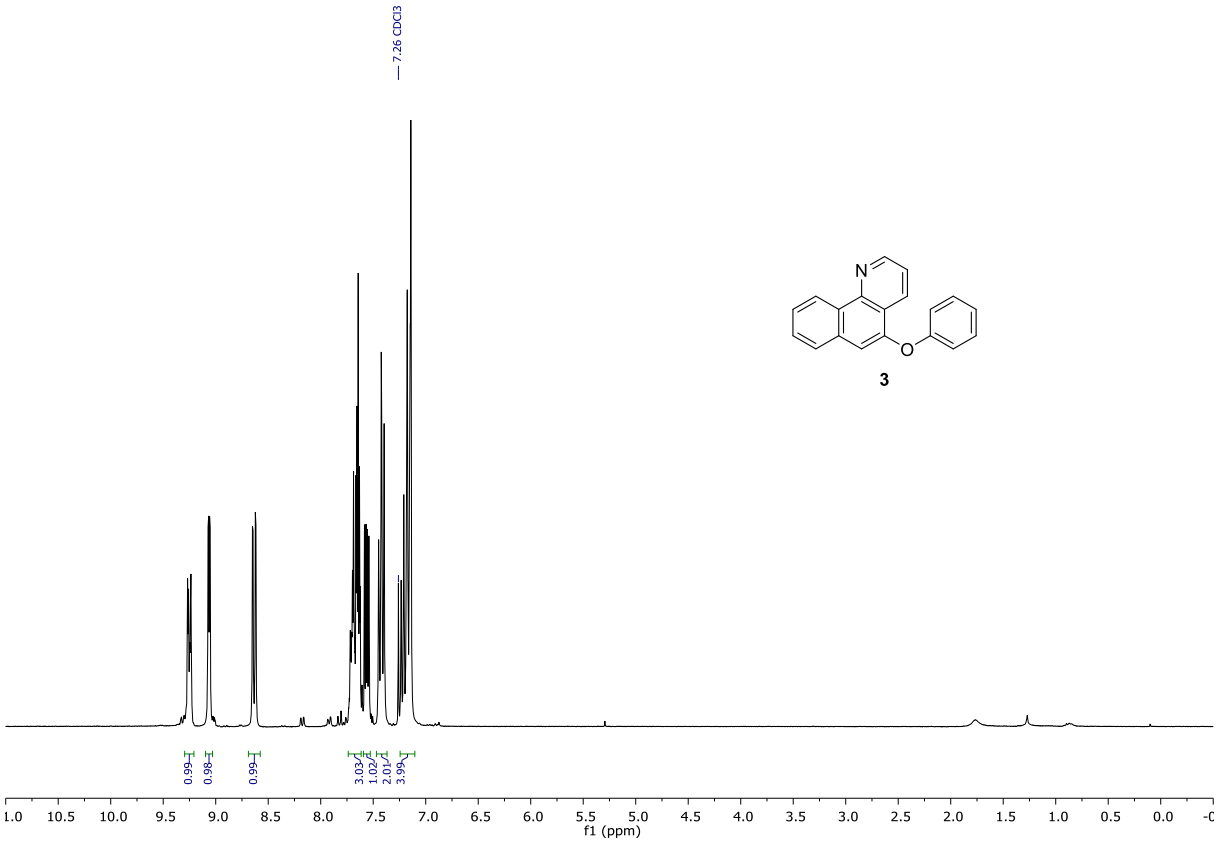
7.26 CDCl3
0.99
0.98
0.99
3.03
1.02
2.01
3.99
f1 (ppm)
3

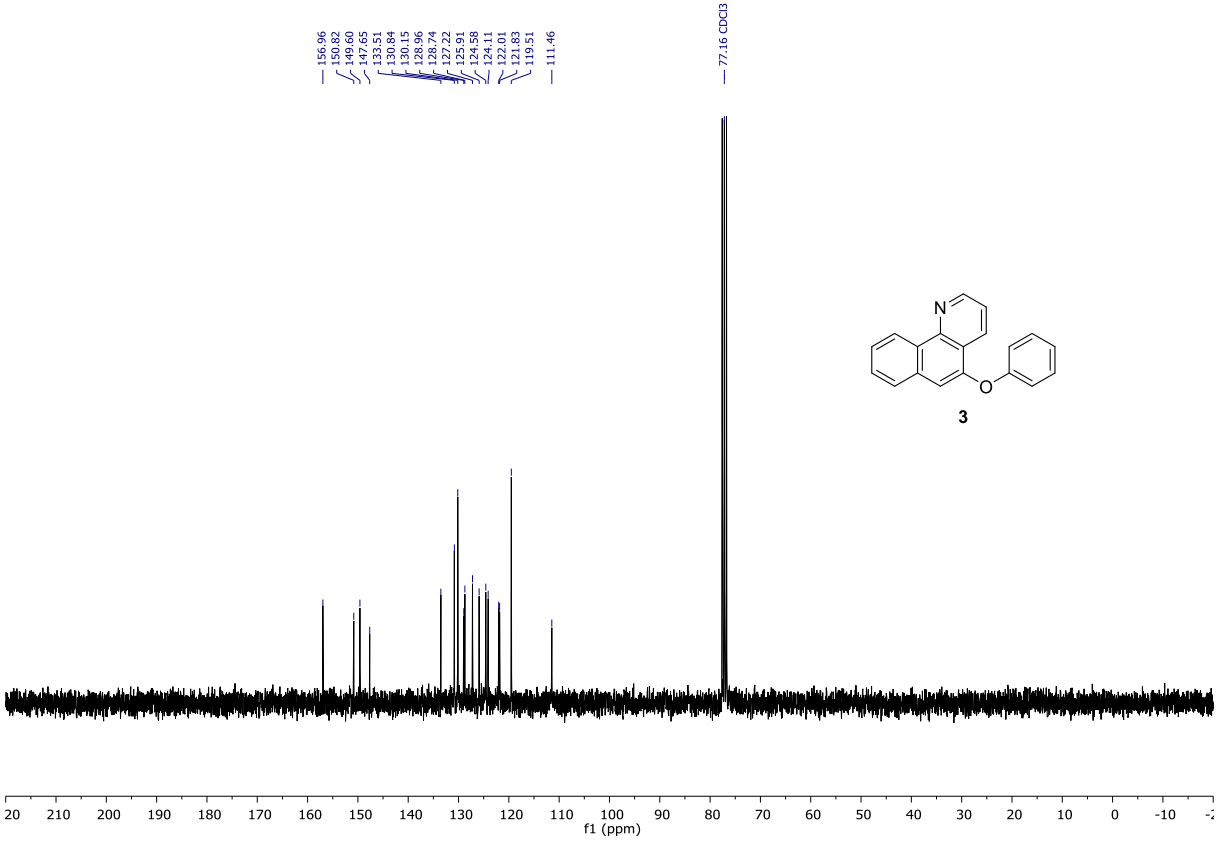
156.96
150.82
149.60
147.65
133.51
130.84
130.15
128.96
128.74
127.22
125.91
124.58
124.11
122.01
121.83
119.51
111.46
77.16 CDCl3
f1 (ppm)
3

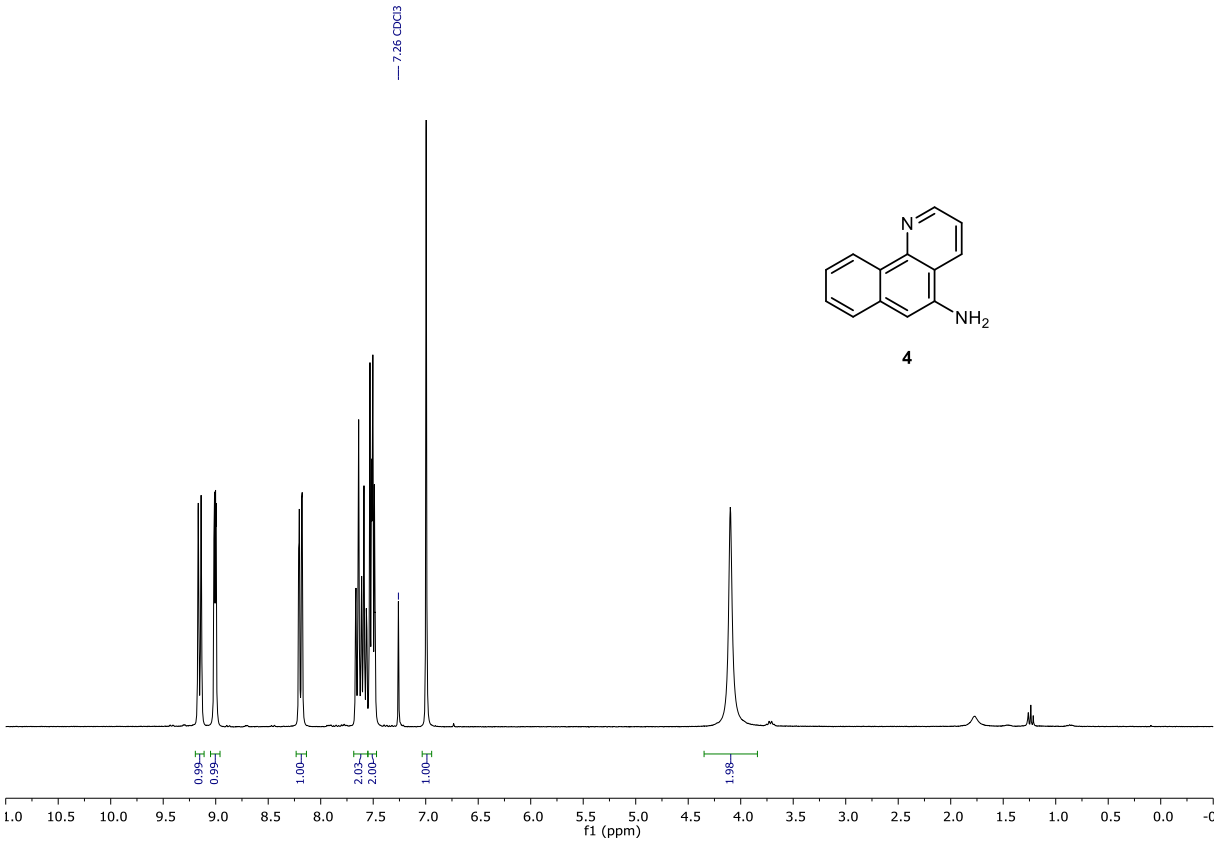
7.26 CDCl3
N
NH2
4
0.99
0.99
1.00
2.03
2.00
1.00
1.98
f1 (ppm)

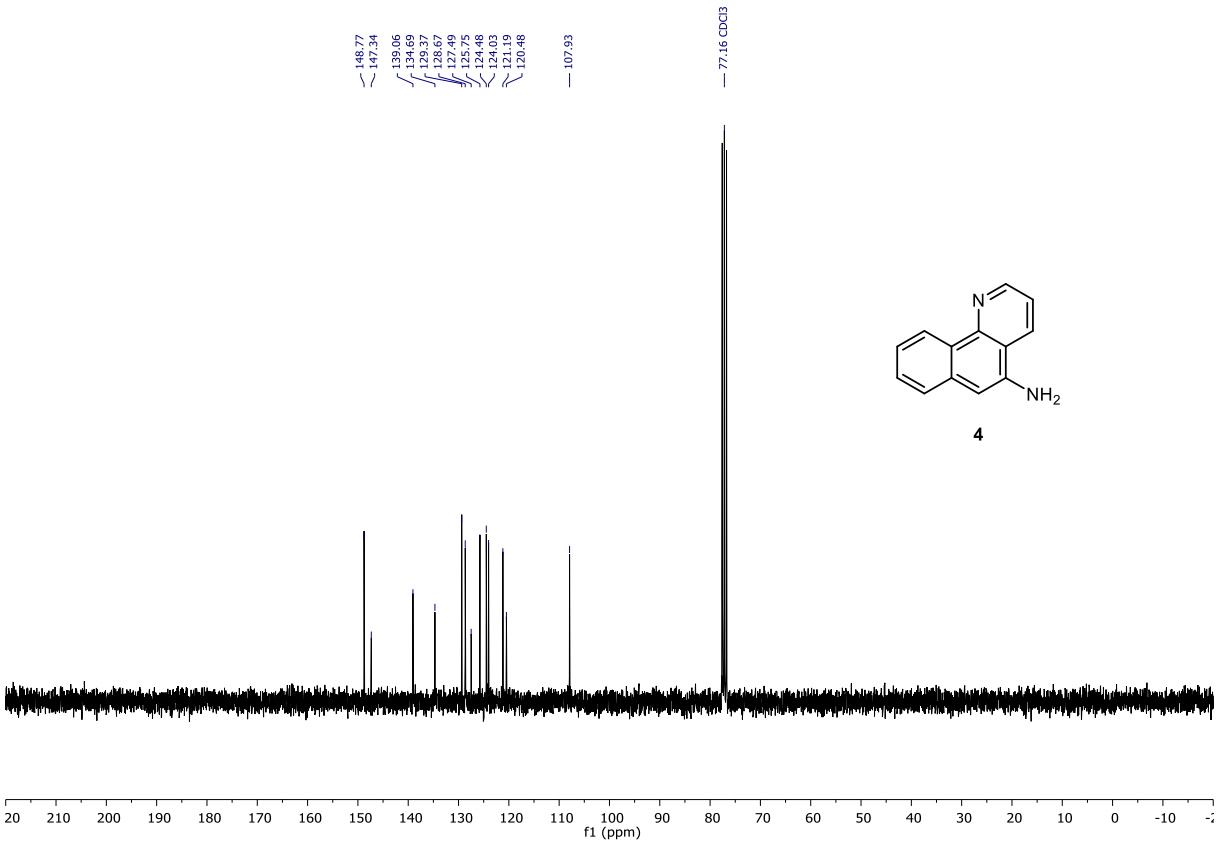
148.77
147.34
139.06
134.69
129.37
128.67
127.49
125.75
124.48
124.03
121.19
120.48
107.93
77.16 CDCl3
N
NH2
4
f1 (ppm)

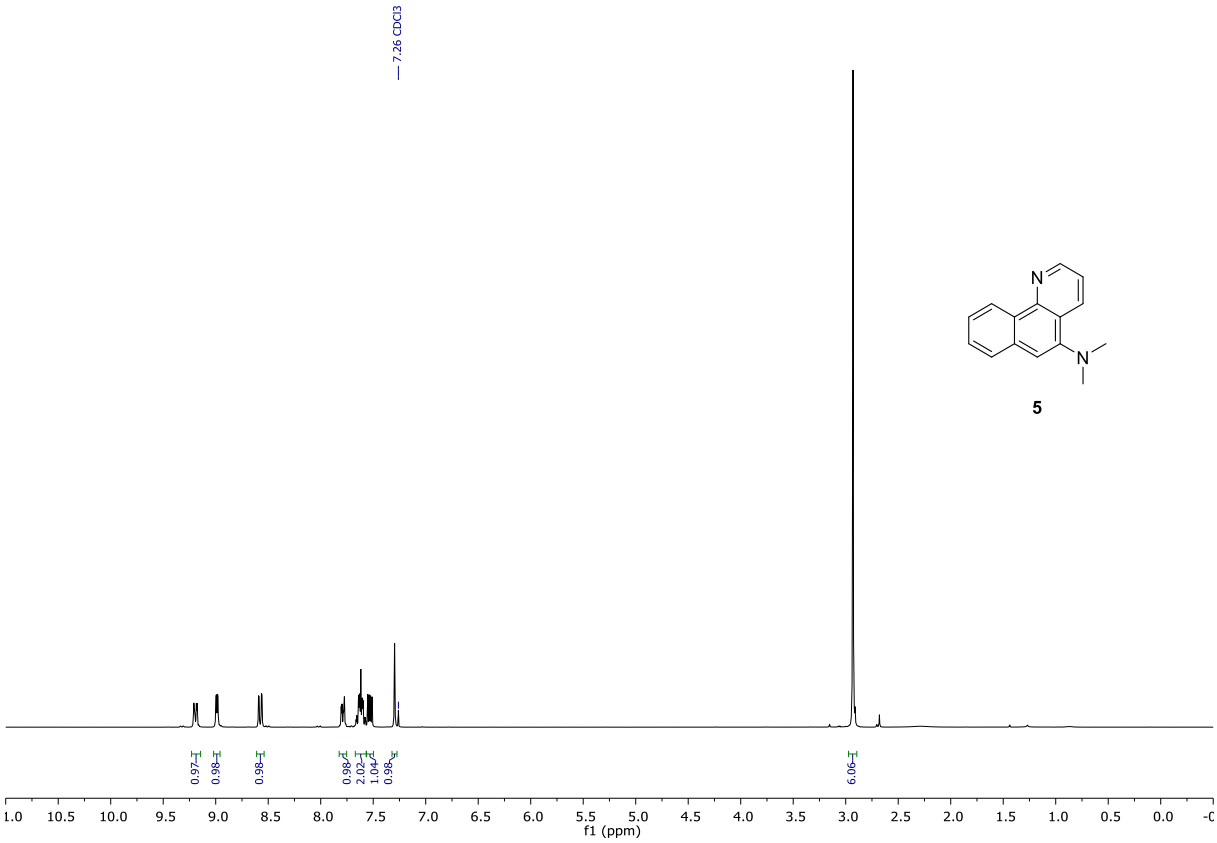
7.26 CDCl3
0.97
0.98
0.98
0.98
2.02
1.04
0.98
6.06
f1 (ppm)
5

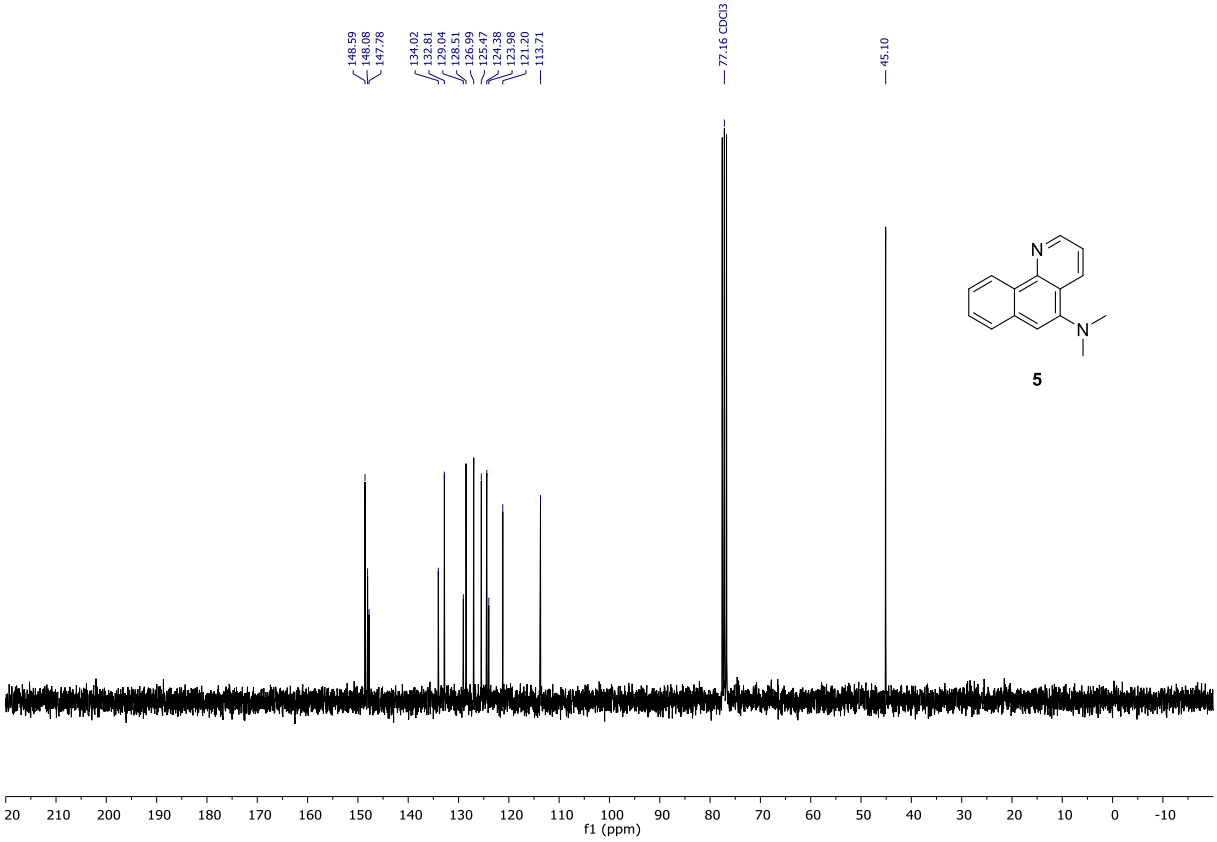
148.59
148.08
147.78
134.02
132.81
129.04
128.51
126.99
125.47
124.38
123.98
121.20
113.71
77.16 CDCl3
45.10
f1 (ppm)
5

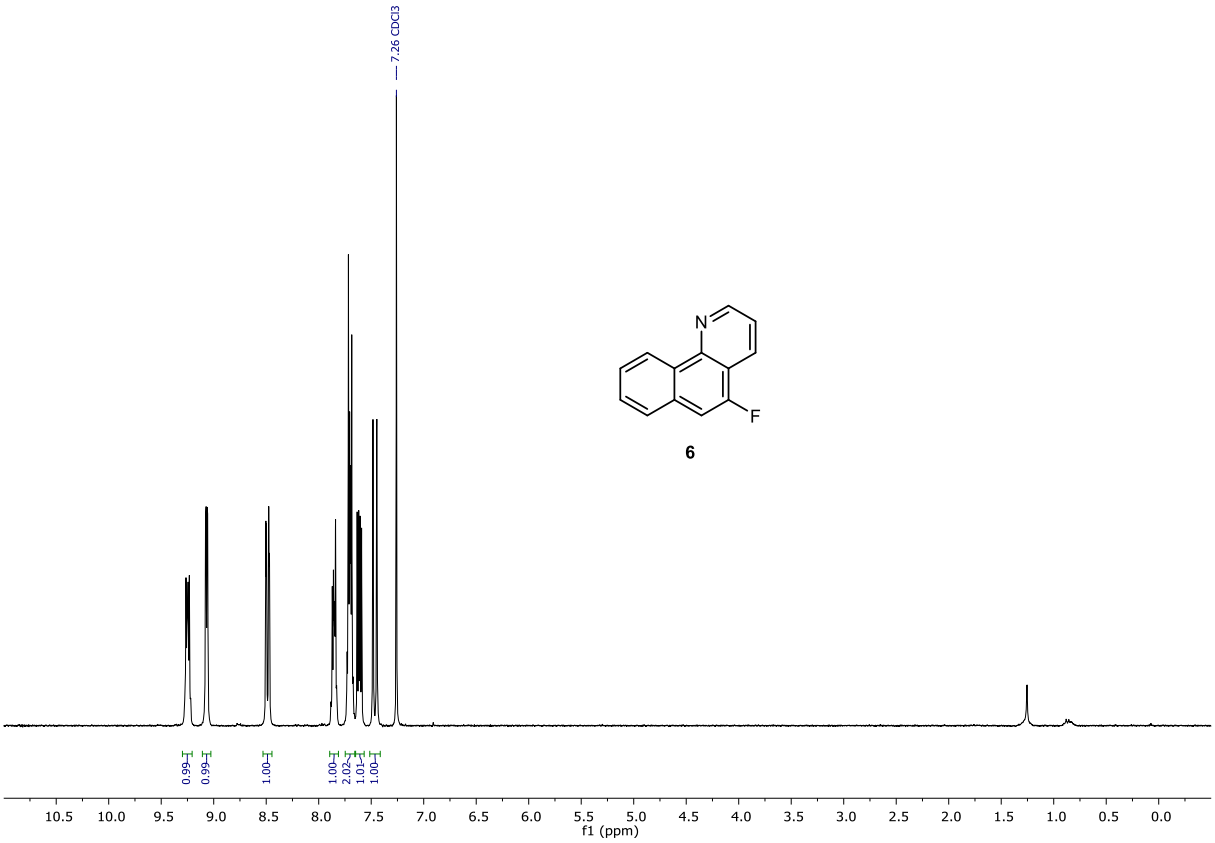
7.26 CDCl3
N
F
6
0.99
0.99
1.00
1.00
2.02
1.01
1.00
10.5 10.0 9.5 9.0 8.5 8.0 7.5 7.0 6.5 6.0 5.5 5.0 4.5 4.0 3.5 3.0 2.5 2.0 1.5 1.0 0.5 0.0
f1 (ppm)

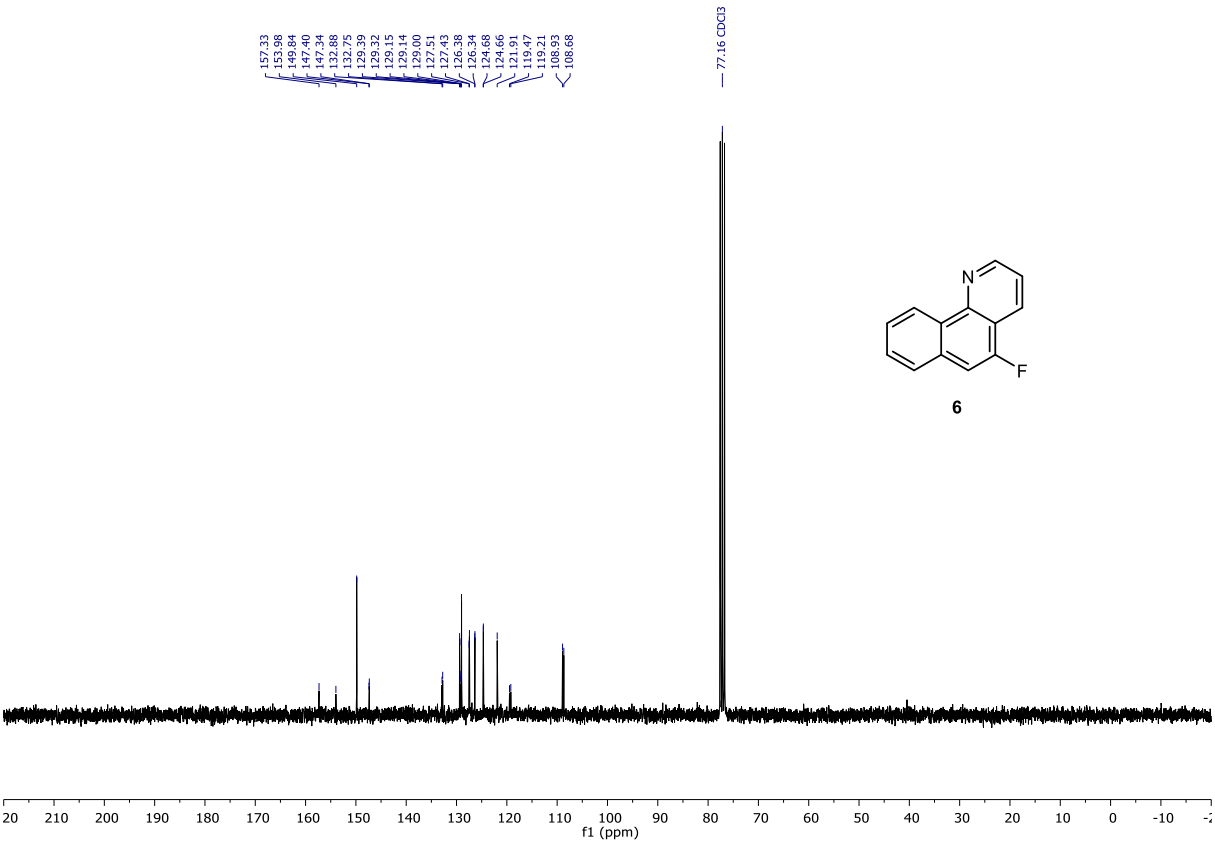
157.33
153.98
149.84
147.40
147.34
132.88
132.75
129.39
129.32
129.15
129.14
129.00
127.51
127.43
126.38
126.34
124.68
124.66
121.91
119.47
119.21
108.53
108.68
77.16 CDCl3
N
F
6
20 210 200 190 180 170 160 150 140 130 120 110 100 90 80 70 60 50 40 30 20 10 0 -10
f1 (ppm)

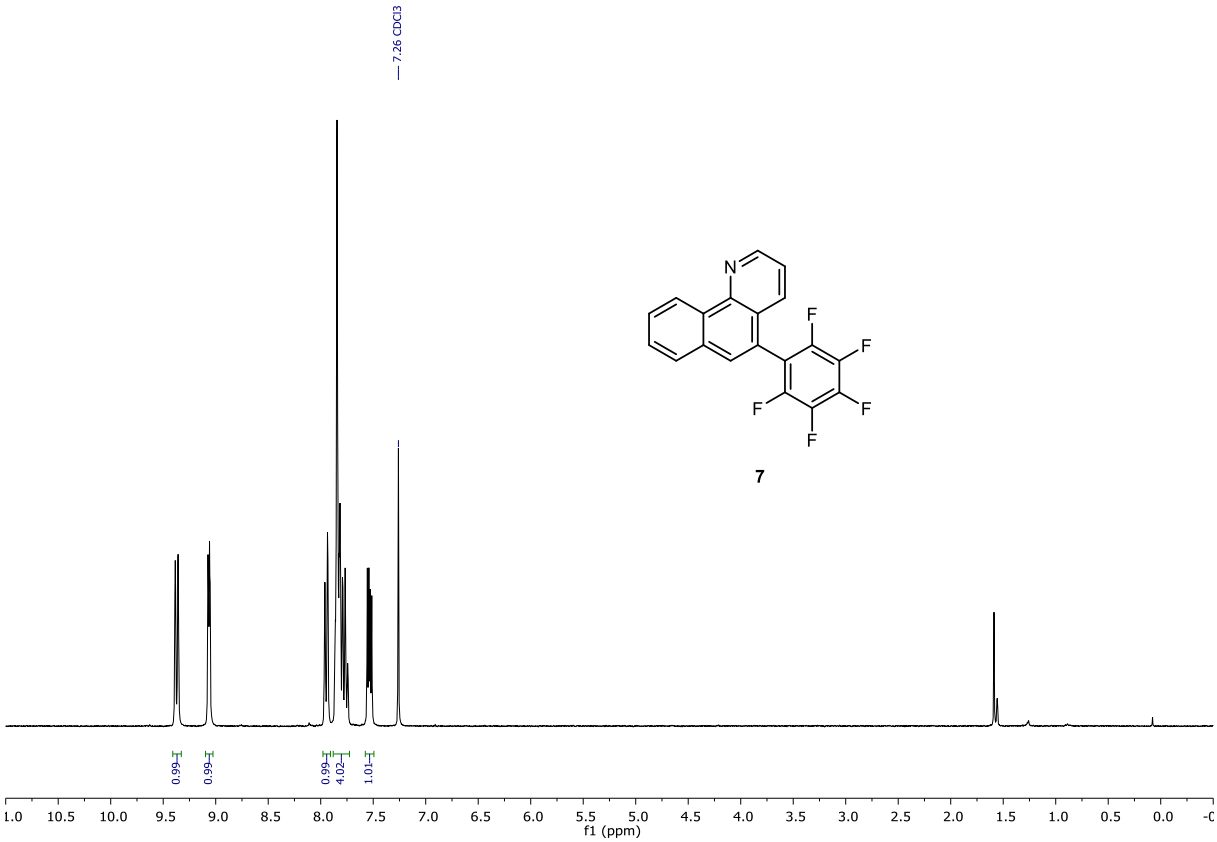
7.26 CDCl3
N
F
F
F
F
F
0.99
0.99
0.99
4.02
1.01
f1 (ppm)

7

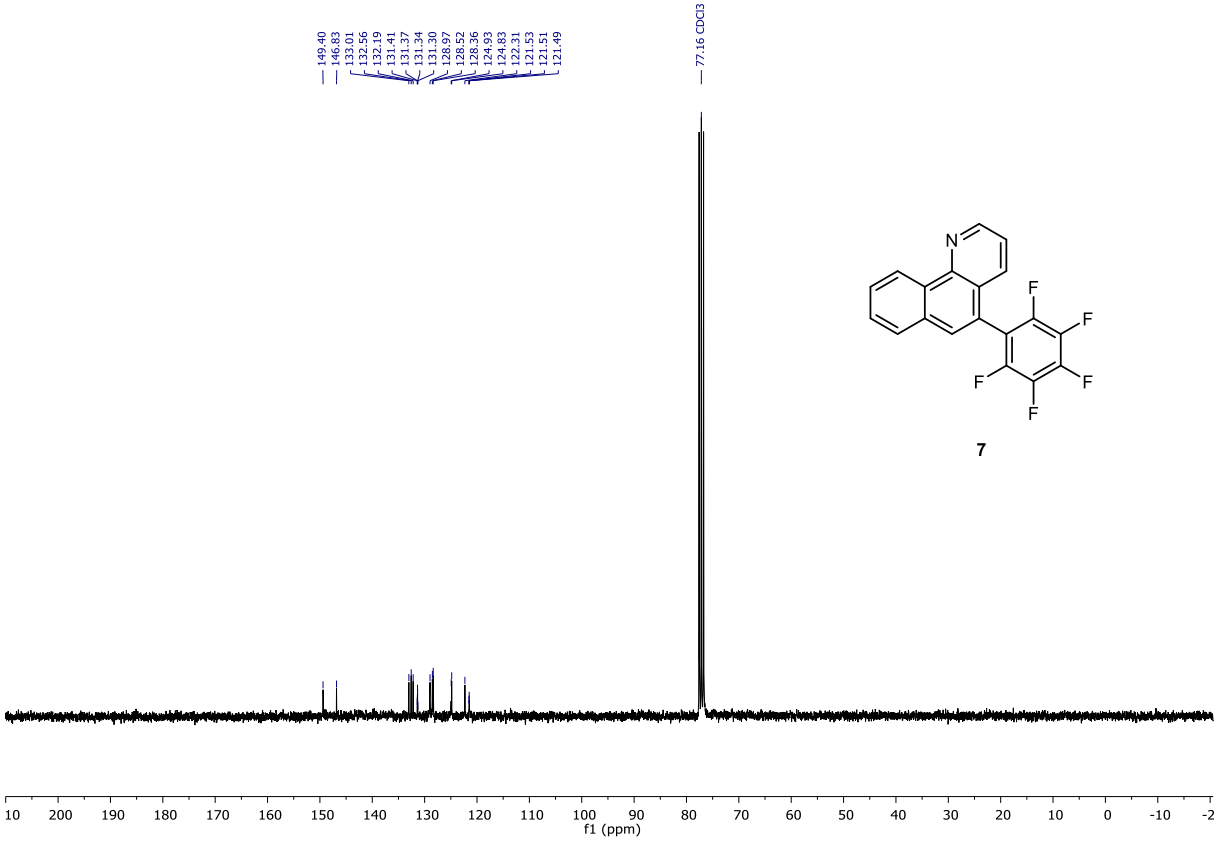
149.40
146.83
133.01
132.56
132.19
131.41
131.37
131.34
131.30
128.97
128.52
128.36
124.93
124.83
122.31
121.53
121.51
121.49
77.16 CDCl3
N
F
F
F
F
F
f1 (ppm)

7

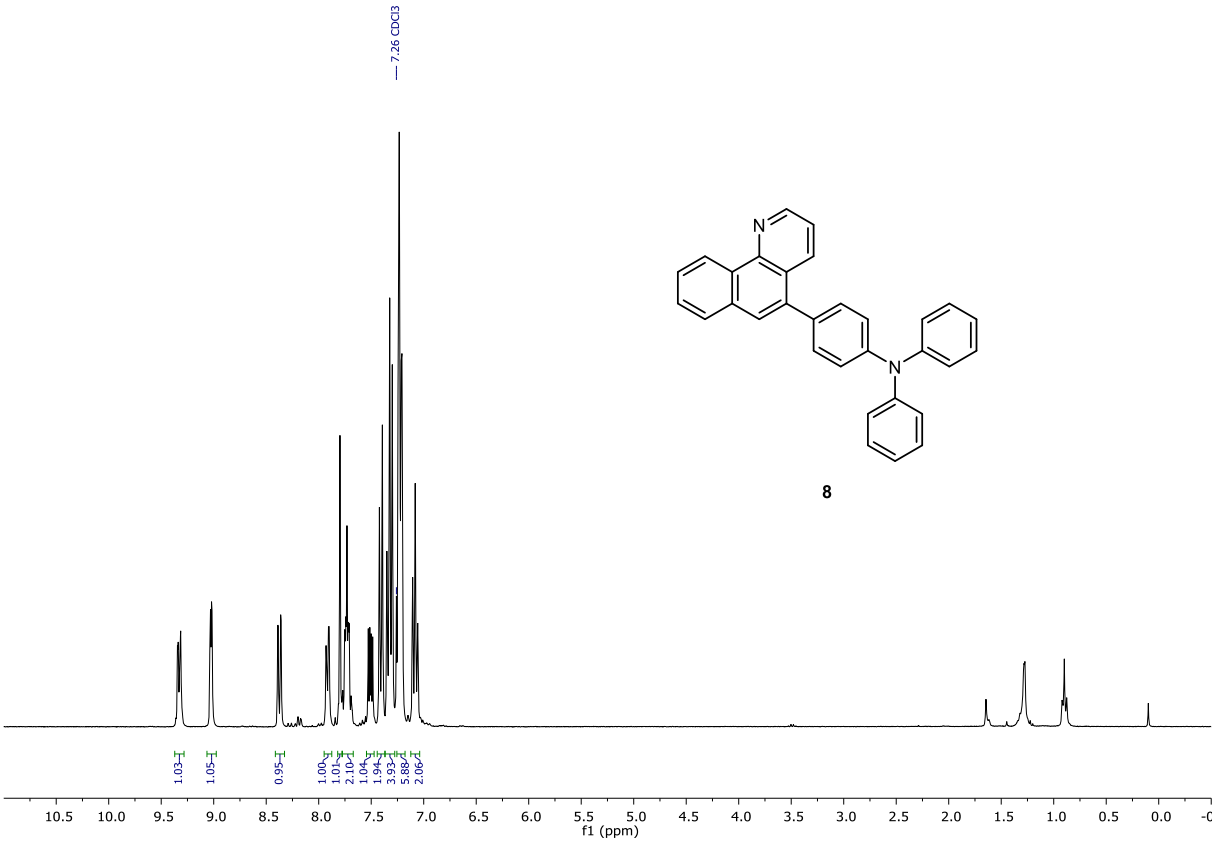
7.26 CDCl3
N
N
8
1.03
1.05
0.95
1.00
1.01
2.10
1.04
1.94
3.93
5.88
2.06
f1 (ppm)

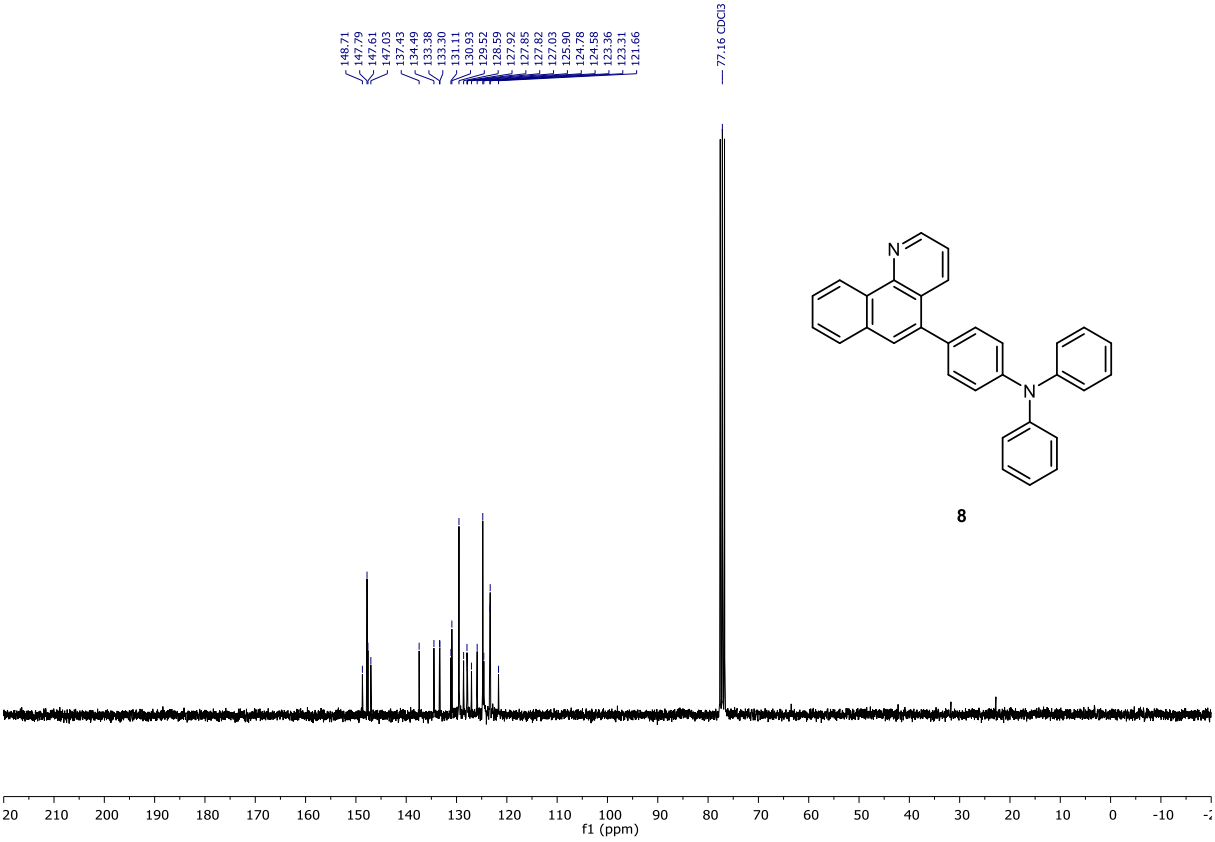
148.71
147.79
147.61
147.03
137.43
134.49
133.38
133.30
131.11
130.93
129.52
128.59
127.92
127.85
127.82
127.03
125.90
124.78
124.58
123.36
123.31
121.66
77.16 CDCl3
N
N
8
f1 (ppm)

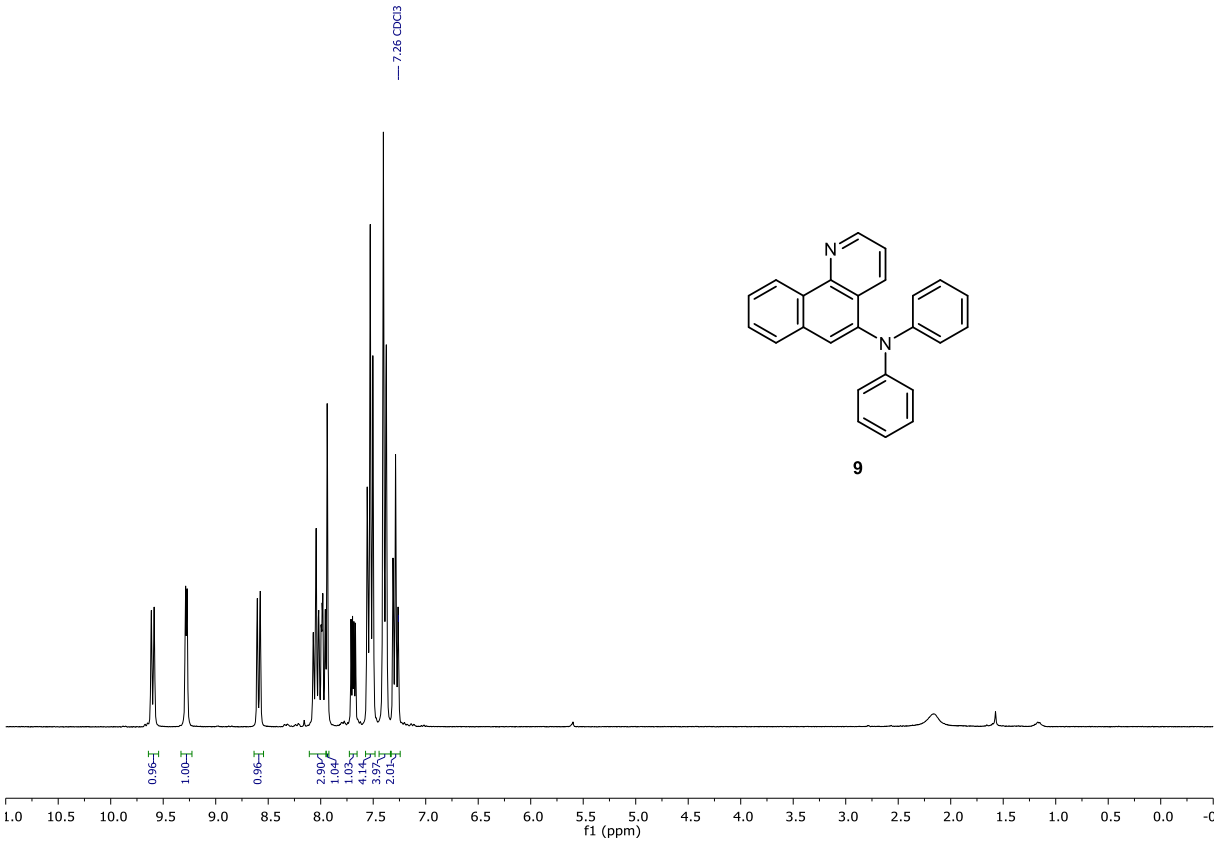
7.26 CDCl3
0.96
1.00
0.96
2.90
1.04
1.03
4.14
3.97
2.01
f1 (ppm)

9

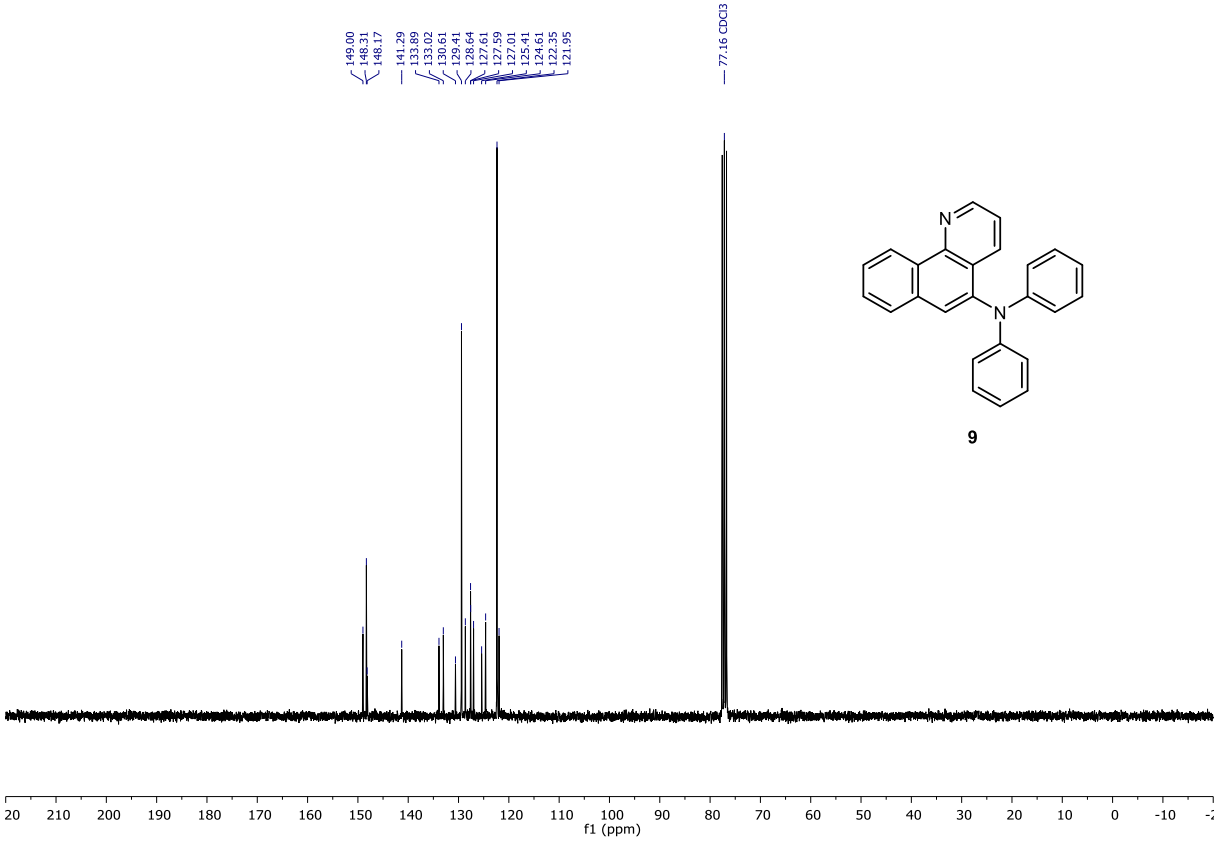
149.00
148.31
148.17
141.29
133.89
133.02
130.61
129.41
128.64
127.61
127.59
127.01
125.41
124.61
122.35
121.95
77.16 CDCl3
f1 (ppm)

9

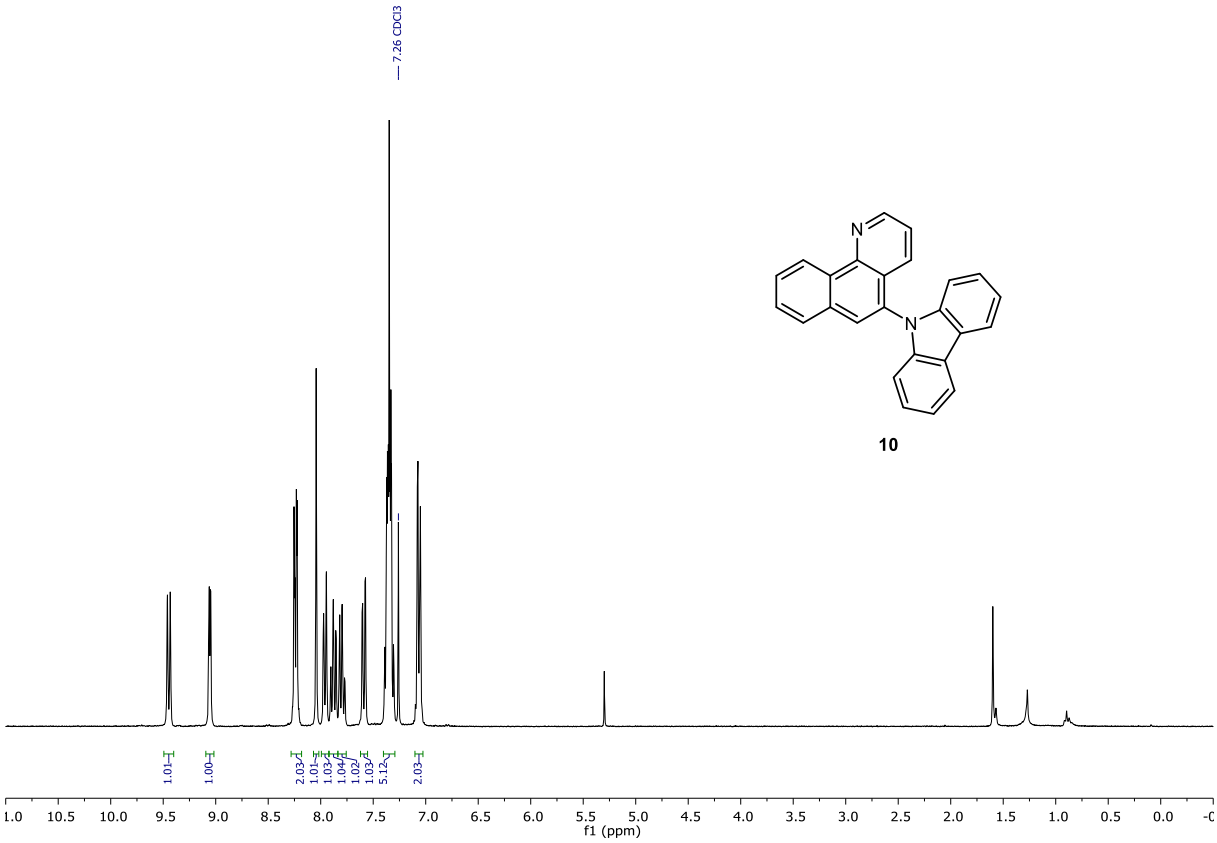
7.26 CDCl3
N
N
10
1.01
1.00
2.03
1.01
1.03
1.04
1.02
1.03
5.12
2.03
f1 (ppm)

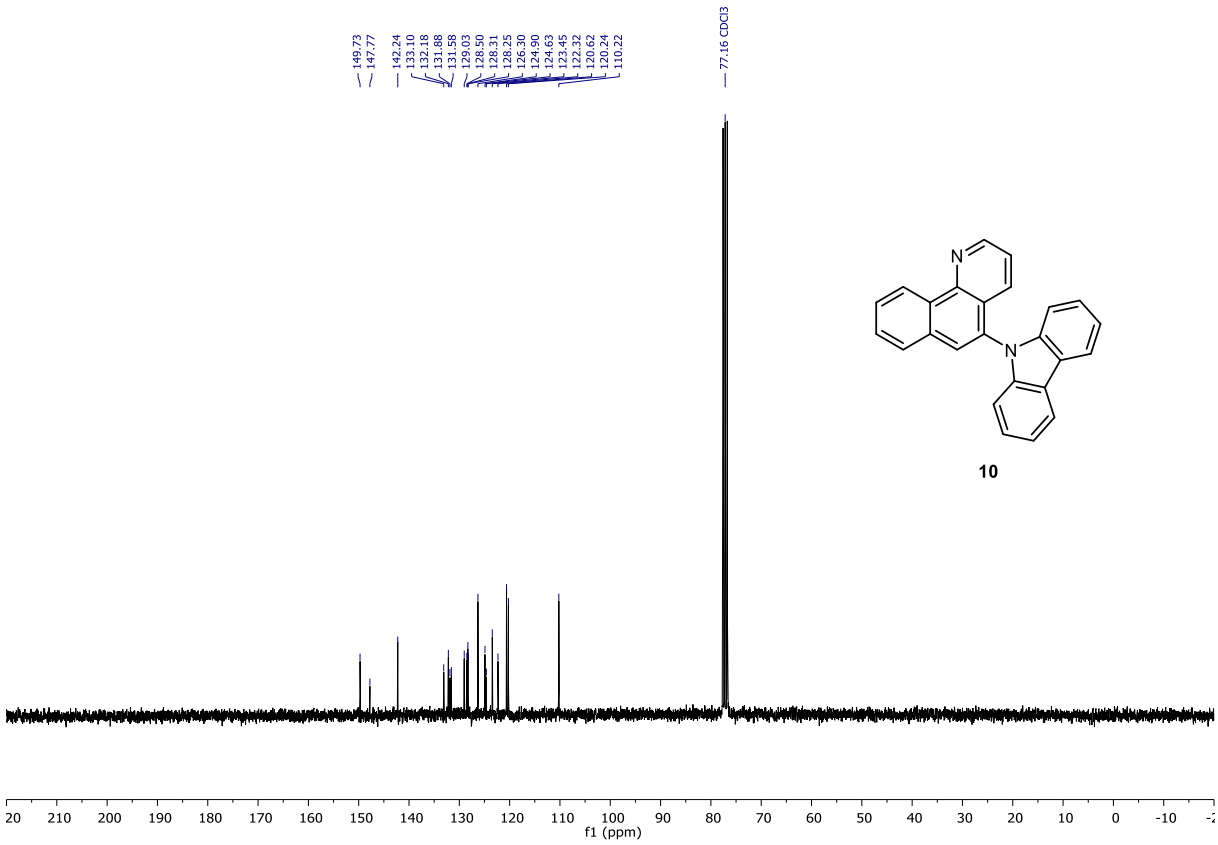
149.73
147.77
142.24
133.10
132.18
131.88
131.58
129.03
128.50
128.31
128.25
126.30
124.90
124.63
123.45
122.32
120.62
120.24
110.22
77.16 CDCl3
N
N
10
f1 (ppm)

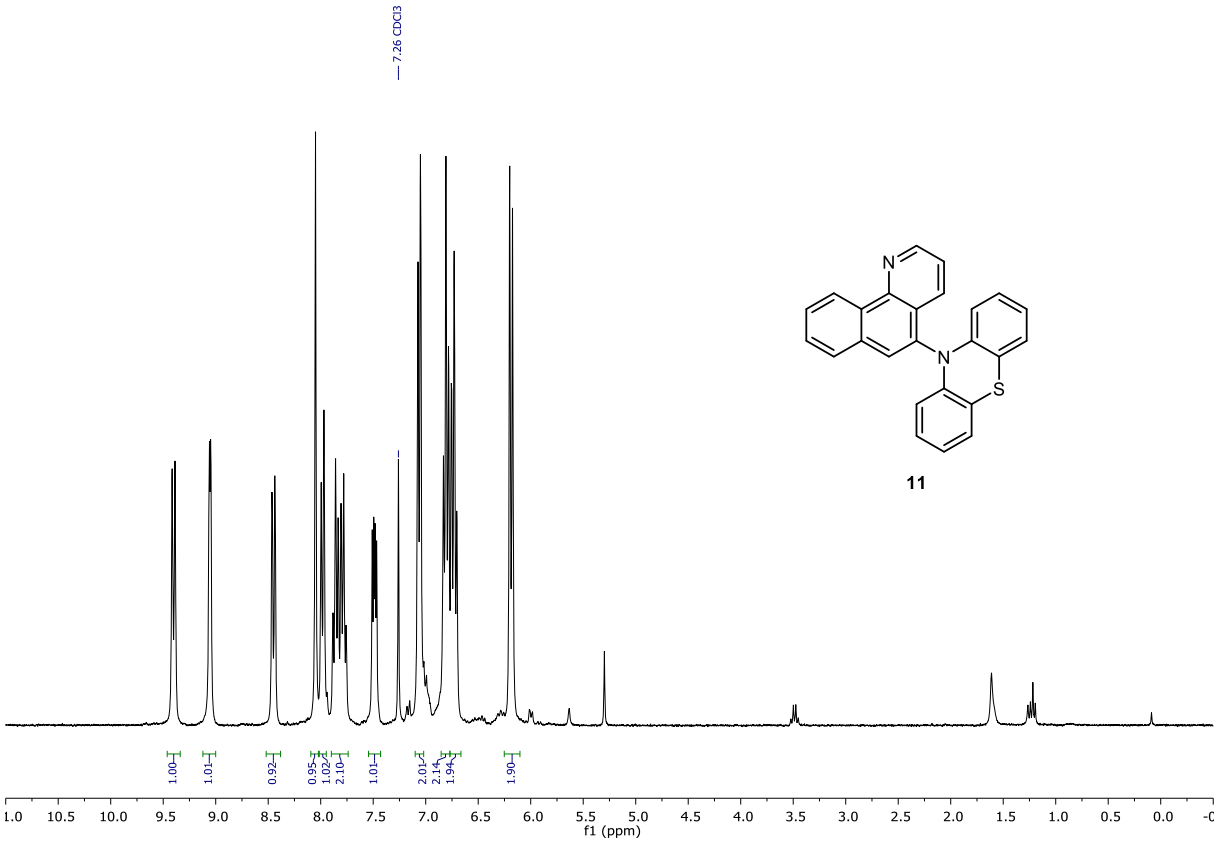
7.26 CDCl3
N
N
S
11
1.00
1.01
0.92
0.95
1.02
2.10
1.01
2.01
2.14
1.94
1.90
f1 (ppm)

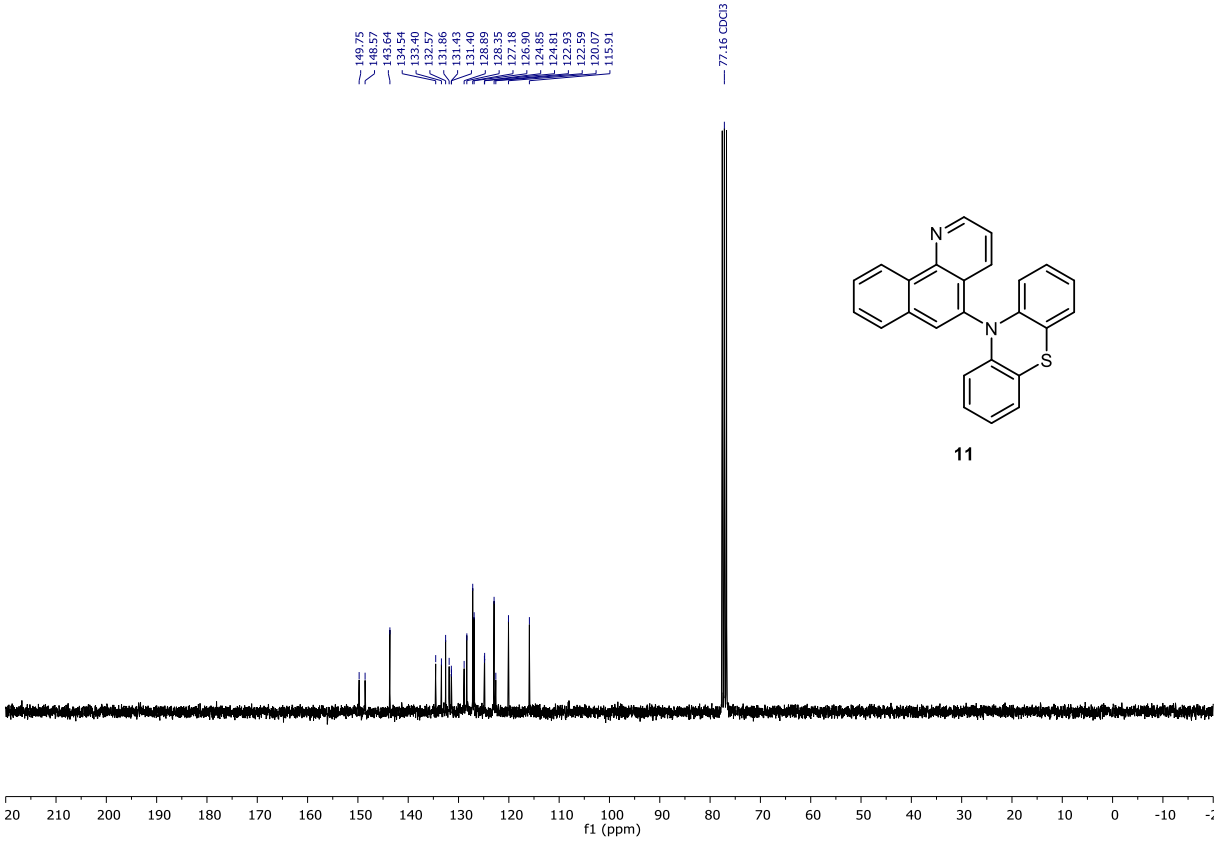
149.75
148.57
143.64
134.54
133.40
132.57
131.86
131.43
131.40
128.89
128.35
127.18
126.90
124.85
124.81
122.93
122.59
120.07
115.91
77.16 CDCl3
N
N
S
11
f1 (ppm)

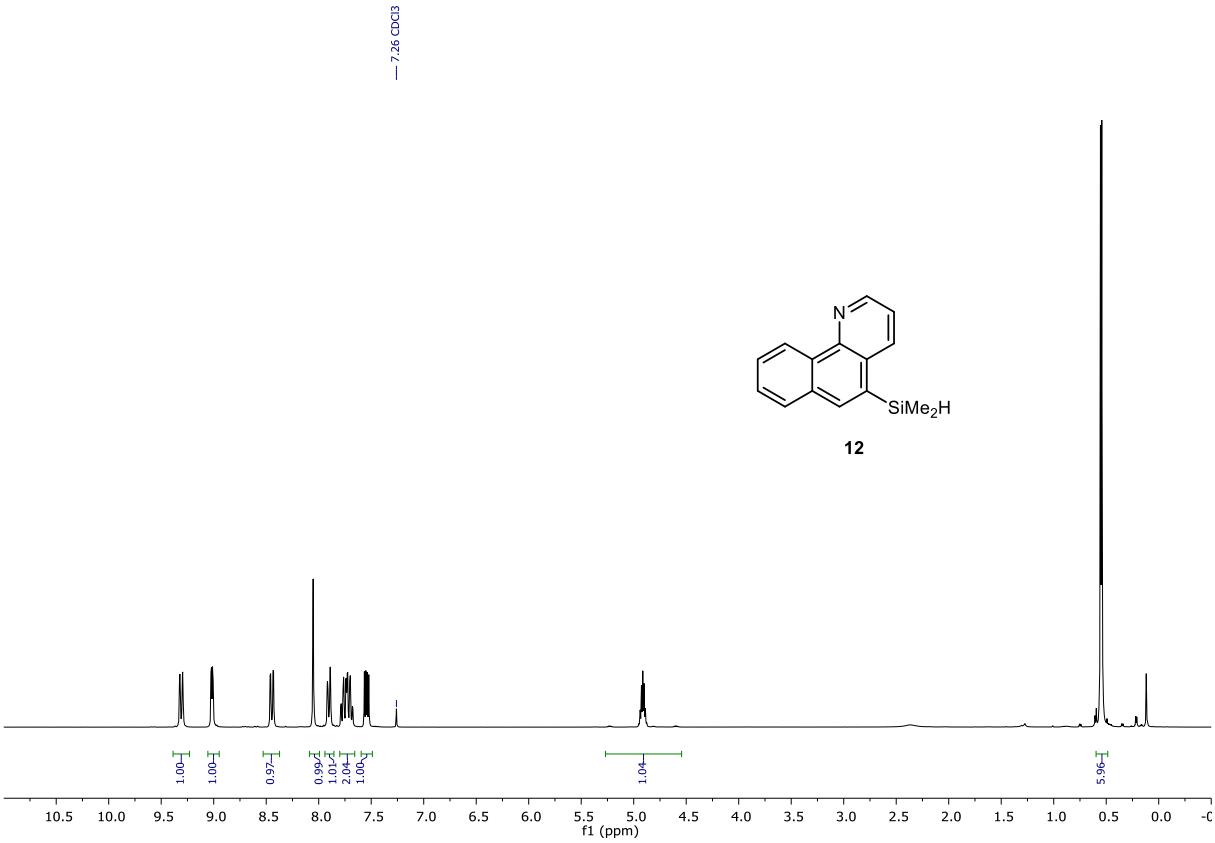
7.26 CDCl3
N
SiMe2H
12
1.00
1.00
0.97
0.99
1.01
2.04
1.00
1.04
5.96
f1 (ppm)

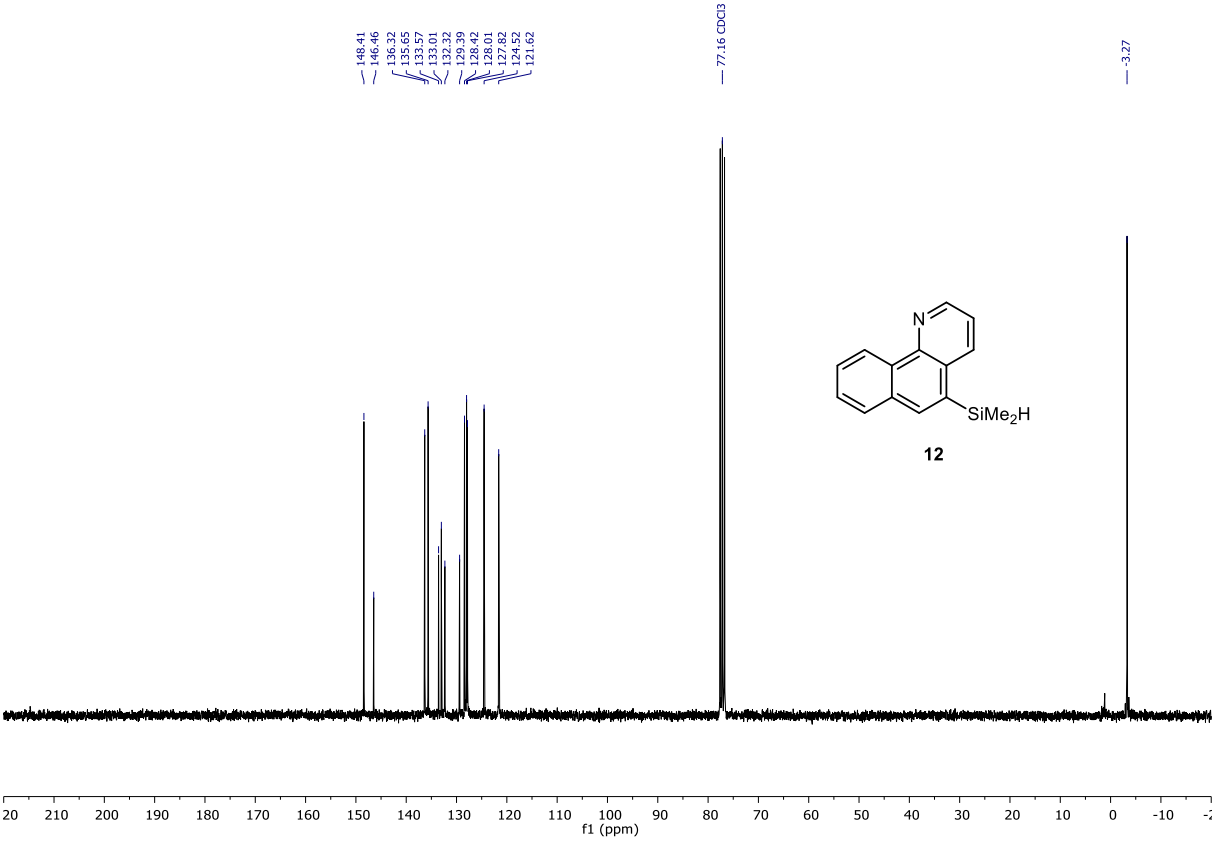
148.41
146.46
136.32
135.65
133.57
133.01
132.32
129.39
128.42
128.01
127.82
124.52
121.62
77.16 CDCl3
-3.27
N
SiMe2H
12
f1 (ppm)

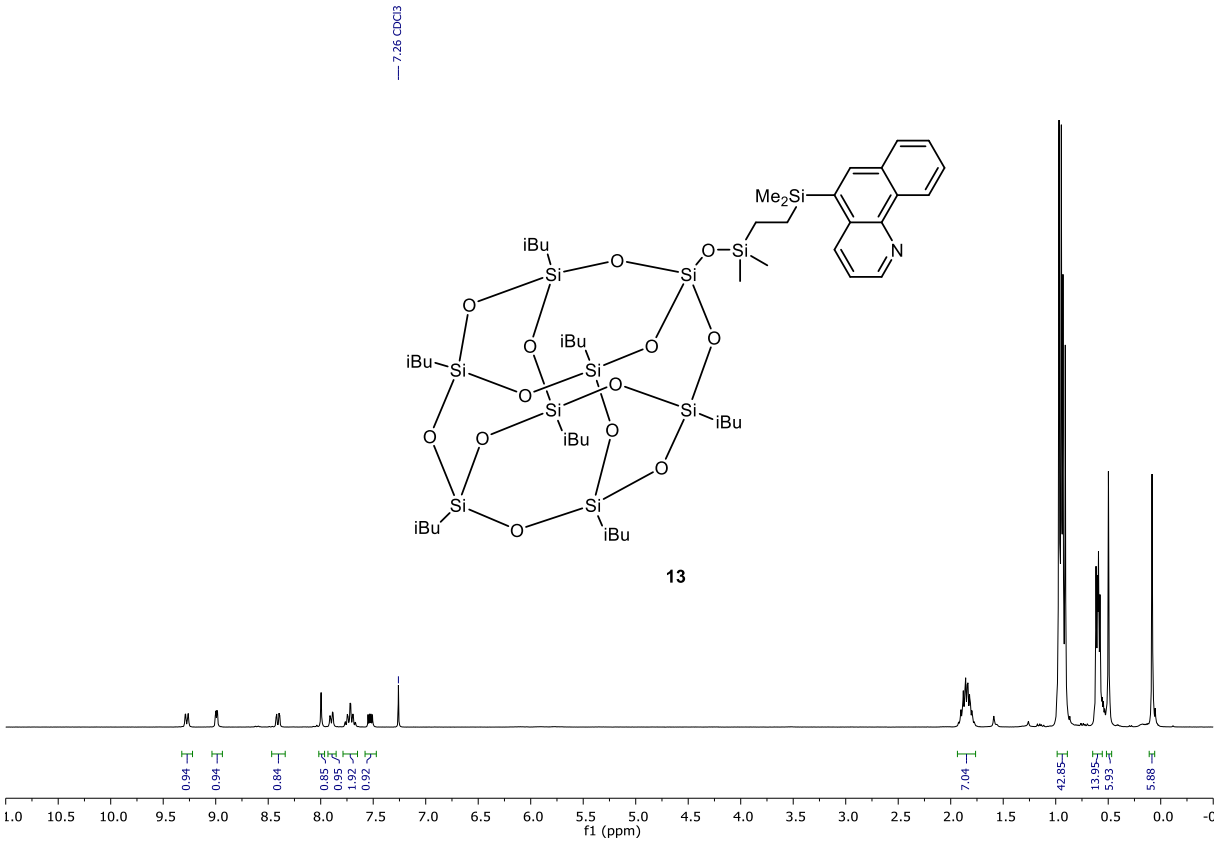
7.26 CDCl3
Me2Si
iBu
Si
O
N
0.94
0.94
0.84
0.85
0.95
1.92
0.92
7.04
42.85
13.95
5.93
5.88
f1 (ppm)

13

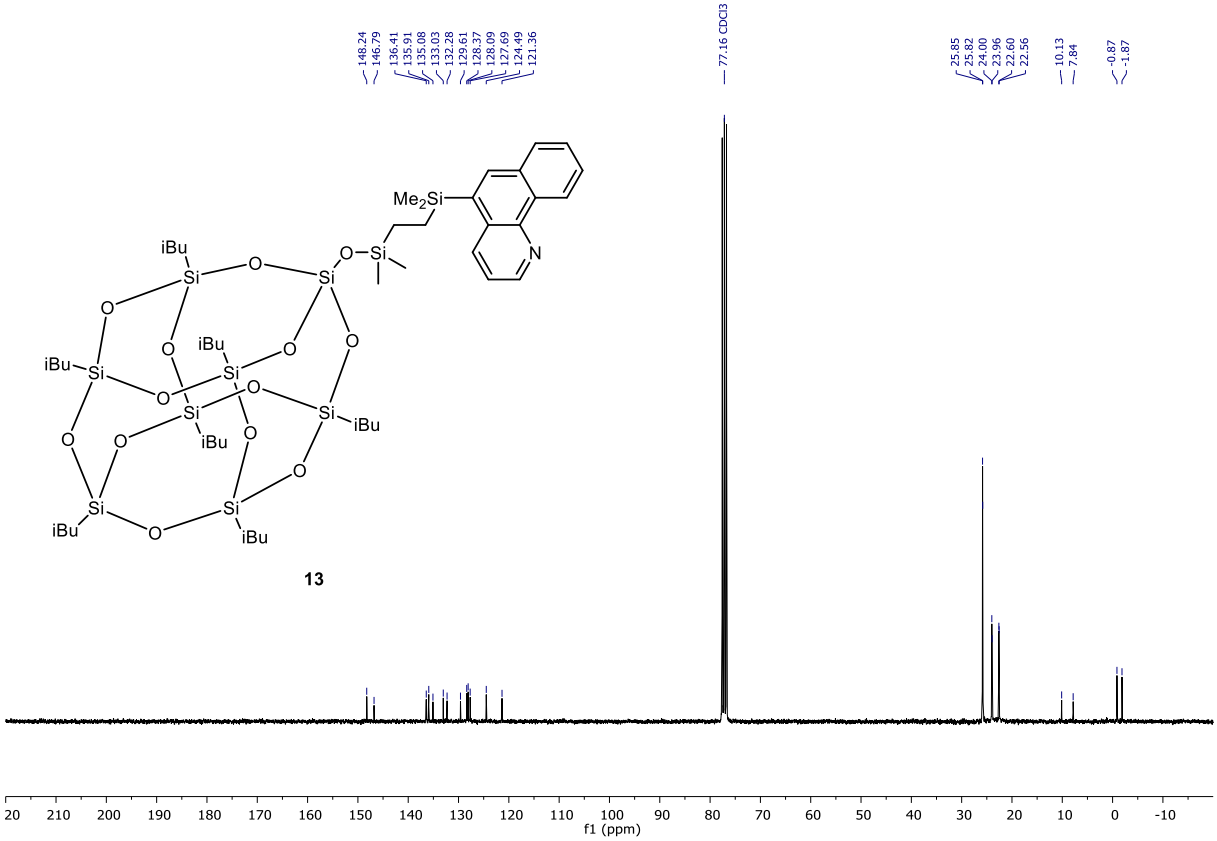
148.24
146.79
136.41
135.91
135.08
133.03
132.28
129.61
128.37
128.09
127.69
124.49
121.36
77.16 CDCl3
25.85
25.82
24.00
23.96
22.60
22.56
10.13
7.84
-0.87
-1.87
Me2Si
iBu
Si
O
N
f1 (ppm)

13

5. References

[1] J. Dubarle Offner, G. Schnakenburg, F. Rose-Munch, E. Rose, K. H. Dötz, *Organometallics* **2010**, *29*, 3308-3317

[2] G. Solladié, J.-F. Saint Clair, M. Philippe, D. Semeria, J. Maignan, *Tetrahedron: Asymmetry* **1996**, *7*, 2359-2364

[3] Y. Zhao, C. Ye, Y. Qiao, W. Xu, Y. Song, D. Zhu, *Tetrahedron*, **2012**, *68*, 1547-1551

[4] CrysAlisPro 1.171.38.34a (Rigaku OD, **2015**)

[5] G. M. Sheldrick, *Acta Crystallogr.*, **2014**, *C71*, 3-8

Inorganic Chemistry

pubs.acs.org/IC Article

Microwave-Accelerated C,N-Cyclometalation as a Route to Chloro-Bridged Iridium(III) Binuclear Precursors of Phosphorescent Materials: Optimization, Synthesis, and Studies of the Iridium(III) Dimer Behavior in Coordinating Solvents

Bartosz Orwat,* Myong Joon Oh, Maciej Zaranek, Maciej Kubicki, Rafał Januszewski, and Ireneusz Kownacki*

Cite This: *Inorg. Chem.* 2020, 59, 9163–9176 Read Online

ACCESS | Metrics & More | Article Recommendations | Supporting Information

ABSTRACT: We present the results of our research on the use of microwaves as an unconventional heat source for the acceleration of iridium(III) chloro-bridged dimer preparation. The results enabled us to revise and improve known guidelines for the very quick and highly efficient synthesis of iridium(III) dimeric complexes in a very simple isolation manner. According to the developed methodology, the already known dimers containing ligands based on the 2-phenylpyridinato motif, as well as new ones stabilized with functionalized benzo[*h*]quinolinato and 2-phenoxypyridinato-based ligands, were efficiently synthesized. The scope of the incorporated ligands included compounds equipped with electron-donating (−Me, −OMe, −OPh, $-NMe_2$), electron-withdrawing (−F, −Br, $-CF_3$, $-C_6F_5$), and hole-transporting ($-NPh_2$, $-C_6H_4NPh_2$) groups. The obtained complexes were characterized by NMR, X-ray diffraction, and electrospray ionization mass spectrometry methods, and their behavior was examined in the presence of coordinating solvents such as dimethyl sulfoxide and acetonitrile. Investigation of the interactions between the above-mentioned solvents and dimers enabled us to confirm the ability of the former to cleave μ-chloride bridges, which enriches the knowledge in the field of organometallic chemistry. This knowledge can be particularly useful for the scientists working in the field of iridium-based materials, helping to avoid misinterpretation of the spectroscopic data.

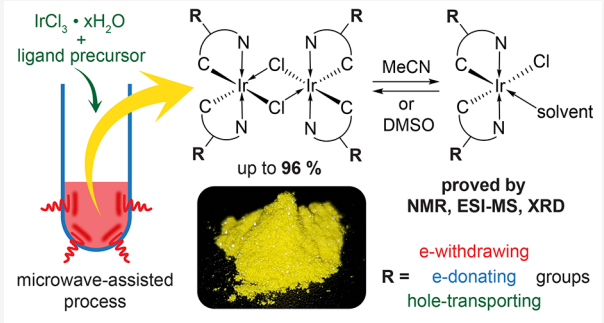

INTRODUCTION

Neutral or cationic C,N-cyclometalated iridium(III) complexes have been studied mainly in the context of their use as biosensors, photocatalysts, and phosphorescent emitters for organic light-emitting diodes (OLEDs).[1−3] Such compounds might be synthesized in different ways, but the most popular way proceeds via chloro-bridged binuclear iridium(III) intermediates. Unfortunately, these intermediates have not received much attention in the literature because they are rarely target molecules for materials chemistry, despite their involvement in the preparation of a vast number of iridium(III) compounds. There are many papers in which the use of iridium(III) dimers as intermediates for highly advanced functional materials of desirable properties has been reported,[4−6] but here we will briefly discuss only the most recent and relevant ones. For instance, various chloro-bridged iridium(III) dimers have recently been applied in the synthesis of methacrylate-functionalized triscyclometalated iridium(III) complexes, to be used in light-mediated atom-transfer-radical polymerization.[7] The iridium(III) complexes played the role of both a monomer and a polymer growth mediator/photocatalyst, which allowed the fabrication of red/green/blue (RGB) pixel arrays and a multicolor OLED prototype made of copolymer brushes, covalently bonded to the indium−tin oxide (ITO) layer by irradiation of the monomer solution. The next example related to this field is a new class of luminescent mechanochromic iridium(III) complexes, also prepared from chloro-bridged iridium(III) dimers as starting materials.[8] Interestingly, the observed red shift of the final iridium coordination compound phosphorescence, being the result of conformational change caused by mechanical stimulation, may be utilized in mechanical and chemical vapor sensors. Apart from the above-mentioned lighting and sensing applications, iridium compounds have been studied as biologically active species. In this context, cationic iridium(III) complexes have

Received: April 11, 2020
Published: June 21, 2020

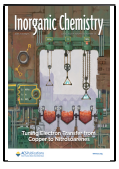

https://dx.doi.org/10.1021/acs.inorgchem.0c01071
Inorg. Chem. 2020, 59, 9163−9176

been examined as biosensors for DNA and RNA detection, as well as conductors for the electrochemical sensing of interferon gamma.[9−11] Another noteworthy example is the decoration of polyhedral oligomeric silsesquioxane with eight iridium(III) cyclometalated moieties in the corner positions.[12] Such organic−inorganic hybrids have been found to be relatively noncytotoxic and to effectively stain the cytoplasm of human cervix epithelioid carcinoma cells, enabling its bioimaging because of the strong photoluminescent properties. As in the previously mentioned examples, synthesis of these interesting compounds also proceeded via chloro-bridged iridium(III) dimers. Finally, there are only a few reports illustrating the use of dimers as such.[13,14] One of them concerns a series of chloro-bridged iridium(III) dimers based on the formyl-substituted 2-phenylpyridinate ligands that have been studied as OLED emitters. It was surprisingly found that, as the content of formyl groups increased, the emission became brighter. This observation has opened up new possibilities for the development of iridium-based phosphorescent dopants because the dimers have been considered to be poorly emissive compounds.[15,16]

Considering the importance of chloro-bridged iridium(III) dimers for the chemistry of iridium-based phosphorescent materials, there are not many papers mainly devoted to their preparation and properties. A significant development in the field began in 1974, when Nonoyama reported the synthesis and characterization of $[Ir(\mu\text{-}Cl)(bzq)_2]_2$.[17] Since then, many reports on the synthesis of C,N-cyclometalated iridium(III) complexes have been published, but as was already mentioned, they very often have not been directly concerned with the intermediate dimers. In some cases, the yields of these precursors were not precisely given or they were not even characterized but used as they were obtained, with the latter being common practice in the research of cyclometalated iridium compounds.[16,18−21] The lack of the above-mentioned experimental information makes evaluation of the synthesis efficiency difficult, especially when the purity of the product remains unknown. In addition, in most of the reported procedures, the synthesis requires prolonged heating (up to 48 h) using conventional heat sources and relatively large amounts of solvent, and sometimes even flash chromatography purification of the product should be made.[22−29] Even then, the products were not always obtained with satisfactory yields. An improvement in the latter aspect is especially in demand because of the high price of iridium, which makes its compounds very costly. The disadvantage of the other methodologies is the need of using an excess of the ligand precursors, which in the case of their sophisticated structures might make them comparatively expensive to the starting iridium material.[30,31] However, there are a few examples of the microwave irradiation protocols, whose application allowed one to shorten the reaction times, raise the reaction temperatures, increase the product yields, and improve the overall reaction economy.[32−35] Unfortunately, the reaction conditions described in these reports are rather mutually inconsistent, and there is still a lack of comprehensive data on the microwave effect on the efficiency of reactions, leading to the chloro-bridged iridium(III) dimers. On the basis of our experience in the acceleration of various chemical transformations by the means of microwave radiation,[36,37] we decided to examine the effect of such an unconventional heat source on the formation of C,N-cyclometalated iridium(III) dimers. We are convinced that the knowledge gained on this subject will be extremely useful for those researchers who want to improve the efficiency of their syntheses and to obtain both known and novel dimers with high yields, as shown here. Recently, we have published results on efficient stoichiometric and catalytic methods for the synthesis of various 5-substituted benzo[*h*]quinolines via C(sp^2)−Br bond activation.[38] The ability of unmodified benzo[*h*]quinoline (**bzqH**) to cyclometalate iridium(III) has already been confirmed per analogiam to 2-phenylpyridine (**ppyH**).[16,34] However, in contrast to countless complexes based on the ppy motif, only several examples of iridium(III) complexes with bzq have been synthesized and characterized as potential electroluminescent phosphors. In our recently published papers on the synthesis and photophysical and emission properties of ionic and neutral iridium complexes with a nonfunctionalized bzq ligand, we have shown that this type of iridium coordination system shows interesting electroluminescent properties, which can be potentially useful in OLED technology.[37,39] Therefore, it would be beneficial for the development of an organometallic phosphor field to extend the scope of complexes equipped with new C,N-cyclometalating ligands, in particular taking into account that our potential ligands include electron-donating and -withdrawing substituents and groups known for their p-type semiconductivity. In addition, our theoretical studies have shown that some of these ligands might be useful in the preparation of emitters for OLEDs.[40] Therefore, we decided to implement 5-functionalized benzo[*h*]quinolines in our research and examine their reactivity in the iridium cyclometalation process. Another innovative part of our work was the obtainment of new dimers containing 6-membered metallacyclic rings based on a 2-phenoxypyridinato motif, a system in which the conjugation of two aromatic rings is prevented. After the successful synthesis of all planned complexes, they were subjected to spectroscopic characterization. We encountered some inconsistences in the interpretation of analytical data reported in the literature, which prompted us to get more deeply into the structural details of compounds synthesized using X-ray diffraction (XRD), NMR, and electrospray ionization mass spectrometry (ESI-MS) techniques. As a result, we explained the behavior of the iridium(III) dimers in specific solvents, which, if not known, may lead to drawing the wrong conclusions in the related research. All of the phenomena clarified here constitute an important contribution to the chemistry of organometallic iridium compounds.

RESULTS AND DISCUSSION

Optimization of the C,N-Cyclometalation Conditions.

As already mentioned above, the lack of a comprehensive comparison of the methods allowing the synthesis of chloro-bridged iridium(III) dimers using conventional and unconventional heat sources prompted us to investigate this issue and to find the optimal conditions for the efficient preparation of such materials. Taking into account that the vast majority of the methods for obtaining dimeric iridium(III) complexes are based on the reactions of iridium(III) chloride hydrate with the appropriate ligand precursors in an alcohol/water environment,[16−35] this system was chosen as a model synthetic protocol for our study. Of the many known examples of such dimers, $[Ir(\mu\text{-}Cl)(ppy)_2]_2$ was selected as the target molecule because of its wide applicability and the availability of the required ligand precursor.[3] In summary, a composition consisting of iridium(III) chloride hydrate, **ppyH**, and a 2-

https://dx.doi.org/10.1021/acs.inorgchem.0c01071
Inorg. Chem. 2020, 59, 9163−9176

methoxyethanol/water (4:1) mixture was chosen as a model reagent system (Scheme 1). We began testing the model reaction by comparing the efficiency of the target dimer formation depending on the mode of thermal treatment of the reaction mixture. Therefore, the reactions were carried out using an oil bath and a microwave reactor. On the basis of our earlier work concerning the synthesis of phosphorescent iridium(III) dopants and the results of the initial tests not described here, the 10 min reaction time was chosen as sufficient to illustrate the effect of the temperature and the influence of microwave radiation on the yield of the product formed.[37] The data illustrating the observed trends are presented in Chart 1. It has been clearly demonstrated that the type of heat source has a significant impact on the reaction outcome. In each reaction conducted at selected temperatures, the yield of the product was higher in the case of the microwave-assisted process. The reason might be that both the iridium precursor and the reaction medium are highly polar, making them susceptible to excitation by microwave absorption. As one can see, the yield was strongly related to the temperature of the reaction. In general, the yield increased with increasing reaction temperature. A significant improvement in the reaction yield was observed when the temperature was elevated up to 150 °C, and when the process was carried out at 170 °C, the yield improvement was much less spectacular. The trend observed is consistent with the literature data stating that 30 min of microwave heating at 190 °C led to an almost quantitative yield of the dimer.[35] However, such harsh conditions can only be applied for thermally and chemically stable ligands because not many moieties and functional groups are able to survive intact in an acidic alcohol/aqueous environment at a temperature close to 200 °C. Indeed, the authors of the cited paper admitted that one of the quinoline-based ligands underwent degradation under the reaction conditions, which prevented formation of the corresponding dimer. Similarly, during some of our initial tests on the formation of iridium(III) dimers stabilized with 5-functionalized benzo[*h*]quinolines at 170 °C, the course of undesirable side reactions was also noted, as evidenced by ^{1}H NMR analyses. For consideration of this issue, it is important to remember that hydrogen chloride (HCl) is evolved as a result of cyclometalation. At first sight, one could think of introducing a HCl scavenger into the reaction system in order to inhibit undesirable processes associated with the presence of a strong acid and to shift the equilibrium toward the desired dimer. On the other hand, it should be remembered that the consumption of HCl would also promote further cyclometalation, leading to the subsequent formation of triscyclometalated iridium(III) species. Therefore, the presence of HCl

Scheme 1. Model Reaction of $[Ir(\mu\text{-}Cl)(ppy)_2]_2$ Synthesis

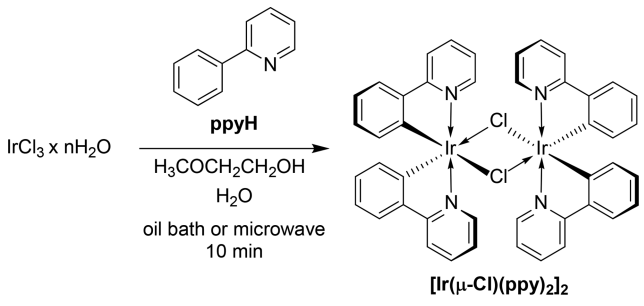

Chart 1. Comparison of the Model Product Yields Obtained in an Oil Bath and a Microwave Reactor

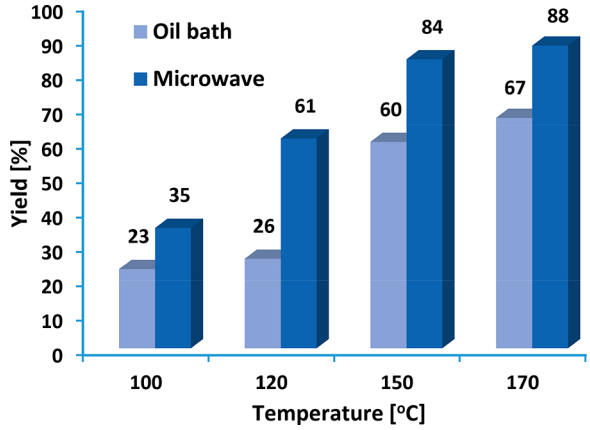

or a Lewis acid in the reaction system is essential for selectivity of the process because it shifts the equilibrium toward dimer formation.[41,42] Considering the above, conducting the process in a sealed microwave-pressurized vial is advantageous because of trapping of the evolving HCl inside. However, HCl consumption may occur under these conditions not only because of the presence of ligand precursors of basic nature but also as a result of the thermal reaction of HCl with alcohol, leading to the corresponding alkyl halide and water.[43] Such a process should be facilitated along with elevation of the reaction temperature. An additional advantage of the proposed microwave-assisted protocol is the very simple product isolation, which only requires filtration and rinsing. Heating of the reaction mixtures at too high temperatures, resulting in the formation of undesired byproducts as a consequence of further cyclometalation or thermal degradation, implies the need for their time-consuming purification, thus cutting out the benefits of a quick and simple microwave-accelerated process. Taking into account all of the aforementioned risks associated with the change in the reaction temperature from 150 to 170 °C, paralleled with a relatively small increase in the yield of the model complex, we decided that running the process at 150 °C is the best compromise between the product yield and simplicity of its isolation.

Our attention was drawn by the fact that in all reported protocols on the preparation of chloro-bridged iridium(III) dimers, the presence of water in the reaction system was required. Interestingly, it has been shown that, even the other solvents, such as acetonitrile (ACN), tetrahydrofuran, and ethylene glycol, were scoped as the reaction medium in the dimer formation with a significant admixture of water.[35] The large number of reports describing the synthesis of iridium(III) dimers in the presence of water and the scarcity of protocols carried out under anhydrous conditions strongly suggest the importance of the role of water in the formation of such complexes. It seems that the presence of water must be even more important for microwave-assisted reactions because this type of radiation is strongly absorbed by polar molecules and stimulates them to collide with each other and with other molecules in the reaction system. Therefore, we decided to carry out the tests under the previously optimized conditions (microwave reactor, T = 150 °C, t = 10 min, and P_{max} = 200 W) with different alcohol/water ratios to evaluate how the water content affects the yield of the product. The results are presented in Chart 2.

https://dx.doi.org/10.1021/acs.inorgchem.0c01071
Inorg. Chem. 2020, 59, 9163−9176

Chart 2. Illustration of the Effect of the Water Content in the Reaction Mixture on the Yield of $[Ir(\mu\text{-}Cl)(ppy)_2]_2$

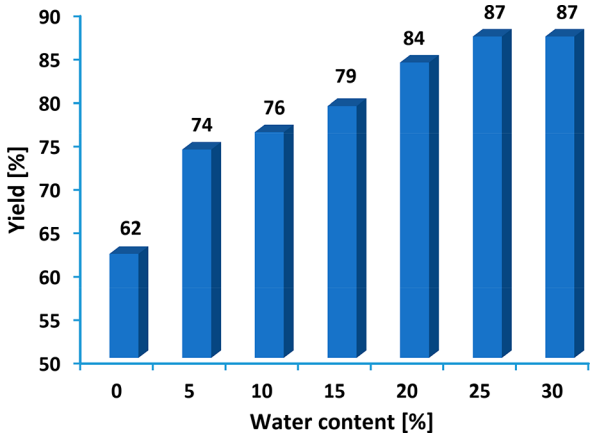

As one can see, the water content in the reaction medium has a significant effect on the yield of the product. The observed trend is clear: the higher the water content, the higher the yield. The effect of the medium composition was also observed by visual evaluation of the postreaction mixture. When no water was added, distinct dark-green particles of unreacted iridium(III) chloride were observed along with the lemon-yellow product. Upon the addition of more water, the color of the obtained solid became more yellow-orange and the dark-green grains were no longer observed, suggesting higher consumption of the starting iridium(III) chloride. We suppose that the progress of the reaction might be controlled by the solubility of iridium(III) salt in the solvent mixture. Because it is an ionic material, the addition of a strongly polar solvent (water) should increase its solubility and hence the availability for cyclometalation. However, the yield reached a *plateau* at 25% water content, showing that its further addition has no beneficial effect. What is more, too high amount of water might raise issues related to the solubility of the ligand, depending on its lipophilic character, which might hamper dimer formation. Another noteworthy observation was the effect on the crystallinity of the product. When no or a low amount of water was present in the reaction mixture, the isolated product was in the form of an amorphous powder. When the reaction was performed in the medium richer in water, the product started to appear as a shiny, crystalline solid. This phenomenon simplified isolation of the product because filtration was much quicker. Considering the above-mentioned aspects, the reaction at 150 °C for 10 min in a 1:3 water/2-methoxyethanol mixture was confirmed to be the optimal conditions for the microwave-accelerated preparation of dimers. We do not recommend increasing the reagents/solvent ratio significantly above the reported one because it resulted in the coformation of insoluble byproducts in our tests.

Synthesis of the Iridium(III) Dimers. The successful optimization of the cyclometalation process encouraged us to apply the developed methodology in the synthesis of the already-known as well as novel chloro-bridged iridium(III) dimers. The scope of the tested ligand precursors consisted of various heterocyclic compounds, including 2-(2,4-difluorophenyl)pyridine (**2,4-diFppyH**), the most intensively studied ligand in the field of iridium-based blue emitters. Fortunately, the F atoms remained intact under the reaction conditions, and the corresponding dimer $[Ir(\mu\text{-}Cl)(2,4\text{-}diFppy)_2]_2$ was obtained with a very high yield of 94%. Of particular interest was **bzqH**, a **ppyH** analogue, which seemed to be a potentially attractive C,N-donating ligand for the iridium dopant system because of its geometric similarity, more rigid structure, and extended electron conjugation system. Indeed, iridium(III) complexes bearing nonfunctionalized bzq

Scheme 2. Scope and Yields of the Synthesized ppy- and bzq-Based Chloro-Bridged Iridium(III) Dimers

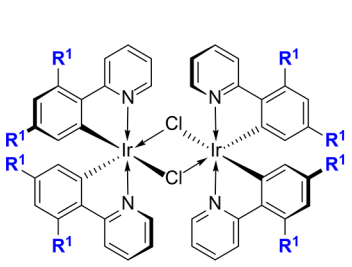

R^1 = ~H
$[Ir(\mu\text{-}Cl)(ppy)_2]_2$ 87 %

R^1 = ~F
$[Ir(\mu\text{-}Cl)(2,4\text{-}diFppy)_2]_2$ 94 %

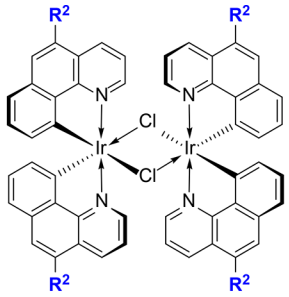

R^2 = ~H
$[Ir(\mu\text{-}Cl)(bzq)_2]_2$ 92 %

R^2 = ~Br
$[Ir(\mu\text{-}Cl)(5\text{-}Brbzq)_2]_2$ 96 %

R^2 = ~OMe
$[Ir(\mu\text{-}Cl)(5\text{-}MeObzq)_2]_2$ 80 %

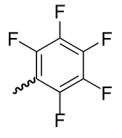

$[Ir(\mu\text{-}Cl)(5\text{-}F_5C_6bzq)_2]_2$ 84 %

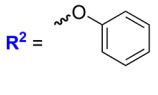

$[Ir(\mu\text{-}Cl)(5\text{-}PhObzq)_2]_2$ 87 %

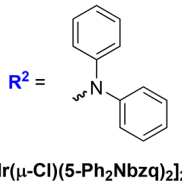

$[Ir(\mu\text{-}Cl)(5\text{-}Ph_2Nbzq)_2]_2$ 82 %

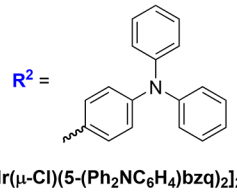

$[Ir(\mu\text{-}Cl)(5\text{-}(Ph_2NC_6H_4)bzq)_2]_2$ 90%

https://dx.doi.org/10.1021/acs.inorgchem.0c01071
Inorg. Chem. 2020, 59, 9163−9176

Scheme 3. Alternative Synthetic Pathway for $[Ir(\mu\text{-}Cl)(5\text{-}Me_2Nbzq)_2]_2$

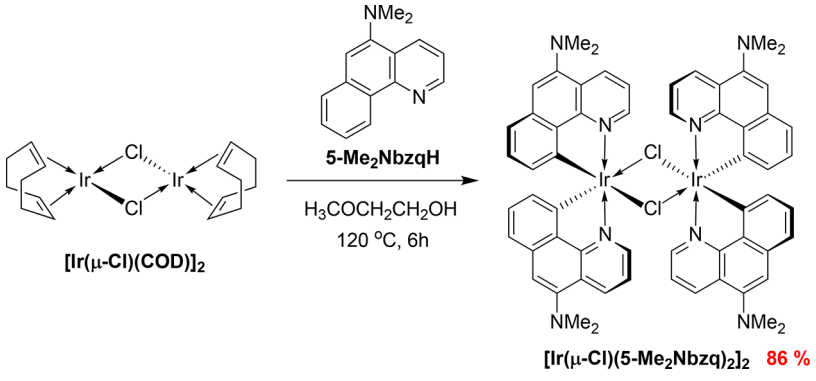

Scheme 4. Formation of Chloro-Bridged Iridium(III) Dimers from 2-Phenoxypyridine Derivatives

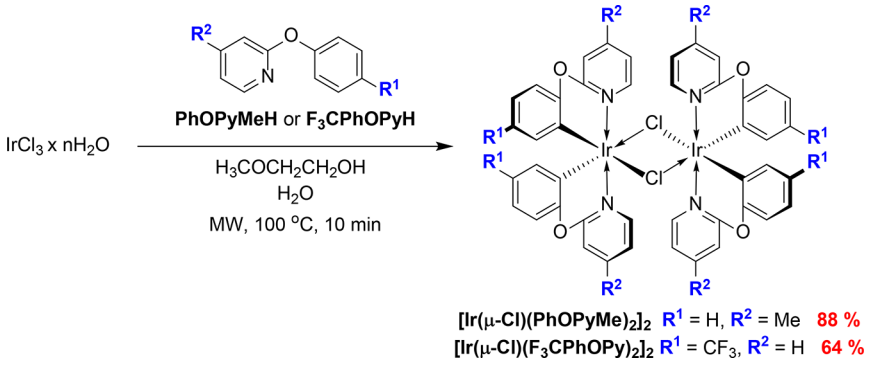

in the coordination sphere have shown interesting electroluminescent properties, which made them potentially useful in OLED technology, as evidenced by us and other groups.[34,37,39,44] The preparation of $[Ir(\mu\text{-}Cl)(bzq)_2]_2$ according to the methodology developed here proved to be very efficient; therefore, we focused on the synthesis of new iridium(III) dimers using bzqH derivatives previously synthesized and characterized in our group.[38] As a result, we obtained a series of new bzq-based chloro-bridged iridium(III) dimers equipped with various functional groups (Scheme 2). The scope of the substituents included electron-donating groups (−OMe and −OPh), electron-withdrawing groups (−Br and $-C_6F_5$), and p-type semiconducting moieties such as $-NPh_2$ and $-C_6H_4NPh_2$. The reactions proceeded very selectively, with no C−Br and C−F bond activation or undesired cyclometalation processes in the case of 5-Ph_2NbzqH. This is the first report on the synthesis of cyclometalated iridium(III) complexes stabilized with functionalized bzq ligands, which might be of great interest considering the applicability and huge popularity of similar iridium(III) dopants with modified ppy ligands. Because the highest occupied molecular orbital (HOMO) of the cyclometalated complex is most often localized on the C,N-cyclometalating ligand, chemical functionalization of the latter is expected to modify the electronic properties of the complex or improve energy transfer due to the antenna effect. In addition, $[Ir(\mu\text{-}Cl)(5\text{-}Brbzq)_2]_2$ constitutes a convenient starting material for further structure modification in the manner of C−Br bond activation. All of the known and new dimers were obtained in high to very high yields, which is advantageous because iridium compounds are expensive and every percentage of yield is of great importance.

In the testing of various 5-substituted benzo[*h*]quinolines toward cyclometalation, we encountered a problem with the reactivity of 5-Me_2NbzqH, in whose case the expected product was obtained with unsatisfactory yield (about 50%) and it was not pure enough. Microwave irradiation was not the cause because the outcome of the reaction carried out in an oil bath was the same. It became evident that the issue was related to the presence of the ligand's functional group, which was definitely characterized by the most basic properties among the tested ones. Considering the chemical nature of the $-NMe_2$ moiety, we suppose that it might be involved in HCl capture, causing both further cyclometalation and transition of the ligand into the salt form. Therefore, the obvious solution was to eliminate the HCl source from the reagent system, iridium(III) chloride in this particular case. Fortunately, Baranoff et al. have reported a procedure for the obtainment of cyclometalated dimers involving the reaction of $[Ir(\mu\text{-}Cl)(COD)]_2$ (COD = 1,5-cyclooctadiene) with a stoichiometric amount of the C,N-donating ligand precursor. As a result, COD ligands are eliminated from the metal coordination sphere without the pH change effect.[45] It is noteworthy that it is a redox process in which iridium(I) in the starting material is oxidized to iridium(III) and the released COD acts as a scavenger of the H evolved in the C,N-cyclometalation process. Implementation of this protocol finally enabled the successful synthesis of $[Ir(\mu\text{-}Cl)(5\text{-}Me_2Nbzq)_2]_2$ (Scheme 3). In this way, we expanded the group of new dimers bearing the bzq ligand equipped with electron-donating substituents (−OMe, −OPh, and $-NMe_2$).

All of the examined ligands, based on the ppy and bzq cores, had one feature in common; namely, they formed 5-membered cyclometalated rings in the dimers' structures. An interesting report describing studies of the photophysical properties of

https://dx.doi.org/10.1021/acs.inorgchem.0c01071
Inorg. Chem. 2020, 59, 9163−9176

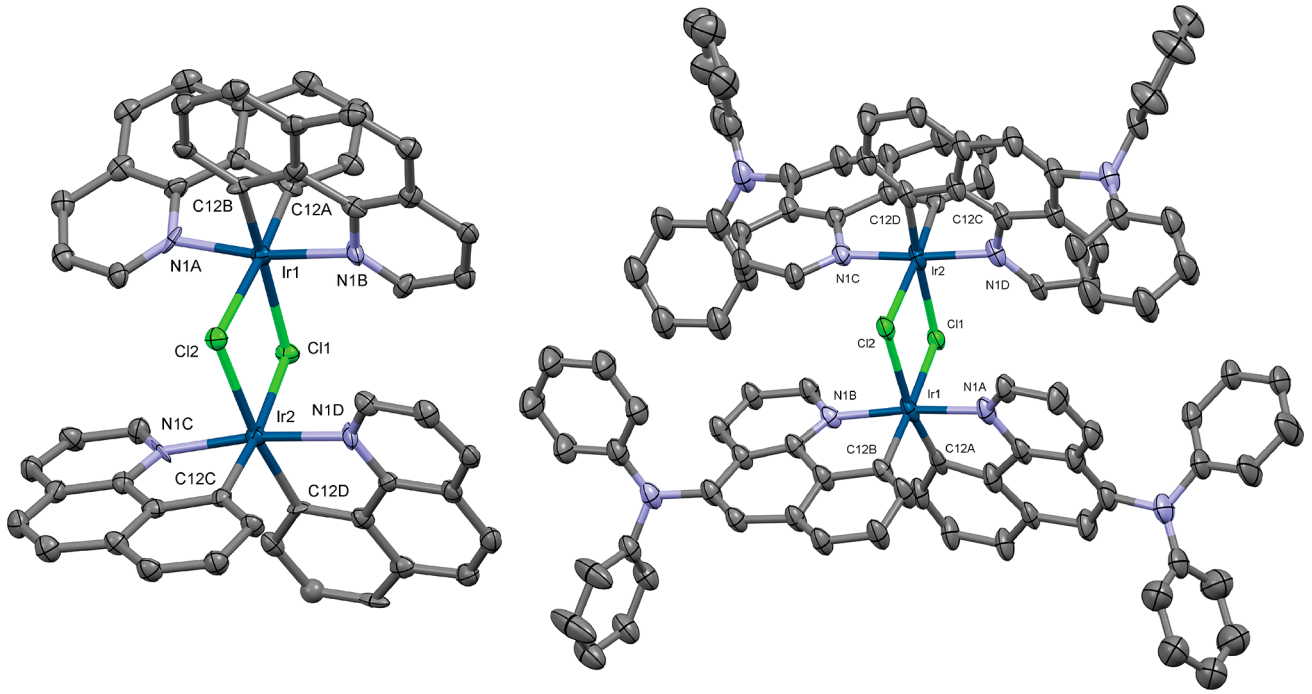

Figure 1. Anisotropic-ellipsoid representations of the dimeric complexes $[Ir(\mu\text{-}Cl)(bzq)_2]_2$ (left) and $[Ir(\mu\text{-}Cl)(5\text{-}(Ph_2N)bzq)_2]_2$ (right). Ellipsoids are drawn at the 30% (left) and 20% (right) probability levels.

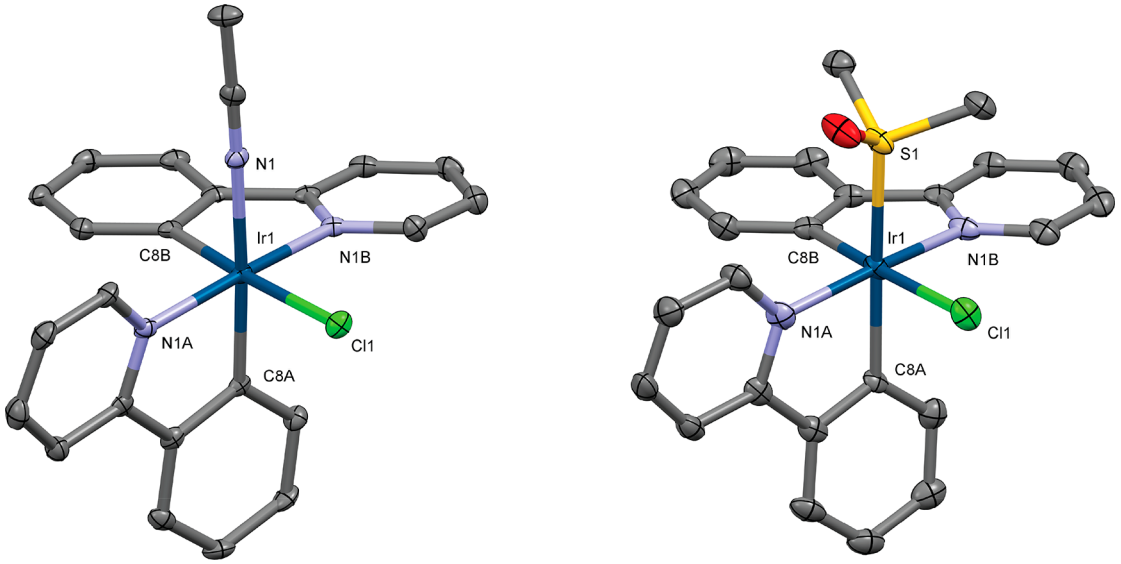

Figure 2. Anisotropic-ellipsoid representations of the monomeric complexes $[Ir(ppy)_2Cl(ACN)]$ (left) and $[Ir(ppy)_2Cl(DMSO)]$ (right). Ellipsoids are drawn at the 50% probability level.

iridium(III) compounds containing 6-membered metallacyclic systems has recently been published.[46] In this paper, 2-benzylpyridine was used as the C,N-cyclometalating ligand precursor. The unique optoelectronic properties of the complexes stabilized with this type of ligand result from the lack of conjugation between two C- and N-donating aromatic systems, caused by the presence of a methylene spacer. These types of C,N-donating ligands are very promising for the development of new iridium-based dopants because their structure allows independent modification of their individual HOMO and lowest unoccupied molecular orbital (LUMO) energy levels by attaching substituents with different electronic properties to the aromatic rings. The introduction of moieties preventing conjugation between the ligand's aromatic moieties might be helpful in more precise and efficient tuning of the emission of the complexes toward blue light.[47−49] This prompted us to synthesize analogous ligand precursors, equipped with an electron-donating substituent on the pyridine moiety or an electron-withdrawing substituent on the phenyl ring, and to examine whether this class of compounds can be used in the microwave-assisted synthesis of chloro-bridged iridium(III) dimers. In order to check it, we synthesized two O-bridged potential ligands, namely, 4-methyl-2-phenoxypyridine (**PhOPyMeH**) and 2-[4-(trifluoromethyl)]phenoxypyridine (**CF_3PhOPyH**),[50,51] and examined them in the respective iridium(III) dimer formation

https://dx.doi.org/10.1021/acs.inorgchem.0c01071
Inorg. Chem. 2020, 59, 9163−9176

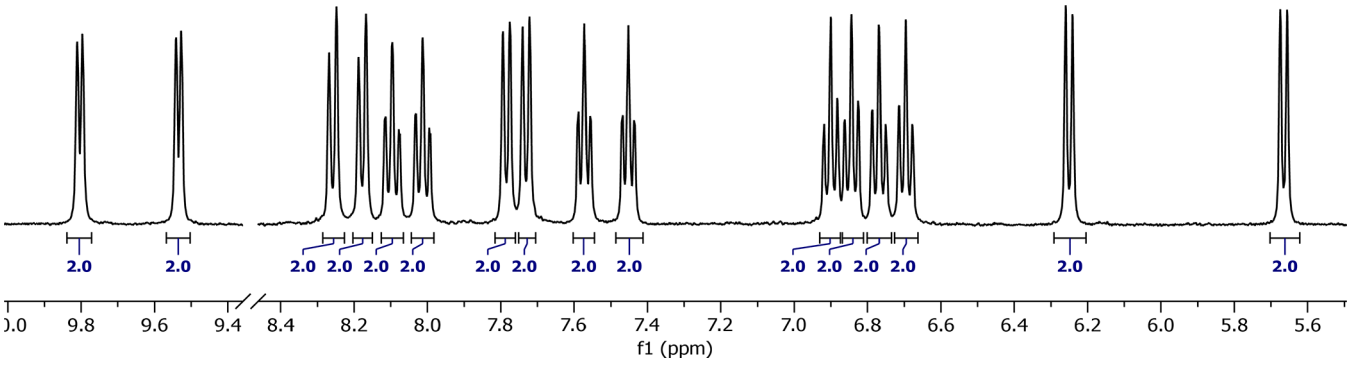

Figure 3. Fragment of the ^{1}H NMR spectrum of $[Ir(\mu\text{-Cl})(ppy)_2]_2$ in DMSO-d_6.

(Scheme 4). Fortunately, the cyclometalation reaction proceeded well under even milder conditions, enabling the successful obtainment of the target iridium(III) dimers.

In summary, it has been demonstrated that the previously optimized reaction conditions allowed the quick and efficient preparation of not only the already-known iridium(III) dimers $[Ir(\mu\text{-Cl})(ppy)_2]_2$, $[Ir(\mu\text{-Cl})(2,4\text{-diFppy})_2]_2$, and $[Ir(\mu\text{-Cl})(bzq)_2]_2$ but also a series of new dimers stabilized with 5-substituted benzo[*h*]quinolinato ligands. Additionally, we obtained new chloro-bridged iridium(III) dimers with the use of ligands based on the 2-phenoxypyridine motif. The functional groups of all of the new compounds make them attractive precursors for application in the field of OLEDs and bioimaging. All of the mentioned dimers were obtained in very short reaction times (10 min) and high to very high yields, which is advantageous for their further applications. After successful preparation of the target compounds, we subjected them to thorough characterization, which is discussed below.

XRD Crystallography. We managed to grow single crystals of a few compounds suitable for XRD structural analysis, which confirmed the proposed structures of the chloro-bridged dimers (Figure 1). Moreover, the crystal structures of the monomeric complexes derived from $[Ir(\mu\text{-Cl})(ppy)_2]_2$ by cleavage with ACN or dimethyl sulfoxide (DMSO) molecules are presented in Figure 2. XRD-suitable crystals of the dimeric complexes were obtained by the slow evaporation of dichloromethane ($[Ir(\mu\text{-Cl})(bzq)_2]_2$) and dichloromethane/2-methoxyethanol/water ($[Ir(\mu\text{-Cl})(5\text{-}Ph_2Nbzq)_2]_2$) solutions. The crystals of the cleaved complexes were obtained by the slow cooling of a hot saturated solution of $[Ir(\mu\text{-Cl})(ppy)_2]_2$ in ACN ($[Ir(ppy)_2Cl(ACN)]$) and diffusion of a saturated $[Ir(\mu\text{-Cl})(ppy)_2]_2$ solution in DMSO into toluene ($[Ir(ppy)_2Cl(DMSO)]$). Crystals of the monomeric forms were obtained for a specific purpose, which is discussed in detail in the next section. Crystallographic details of all of the resolved structures are provided in Table S1. A very similar structure with an identical formula, $[Ir(ppy)_2Cl(ACN)]$, was previously published by Blasberg et al.[52] Even though both dimeric complexes are nonsymmetric, their structures are close to C_i symmetry, with almost planar central Ir_2Cl_2 rings. All Ir^{III} ions are six-coordinated, in quite a regular octahedral fashion (cf. Table S2a). In the Cambridge Structural Database (CSD),[53] there are almost 300 fragments with similar composition (μ-chloro-bridged dimers with aromatic ligands, containing both Ir−N and Ir−C bonds), and in almost all (with five exceptions), the arrangement of N atoms around the Ir center is trans.[54] Taking this into account, together with the Ir−N and Ir−C bond lengths and C−C−C and C−N−C angles, we assigned the inner-coordination-sphere Ir atoms. It should be mentioned that swapping of the C/N atom assignments always gave worse refinement results.

In the monomeric complexes $[Ir(ppy)_2Cl(ACN)]$ and $[Ir(ppy)_2Cl(DMSO)]$, Ir atoms also have the regular octahedral environment, with N atoms from two ppy ligands in trans positions (Table S2b). The fifth and sixth coordination positions are occupied by the solvent molecules and Cl anion. It might be noted that even though for all metals DMSO is coordinated with only a slight preference for a S atom over an O atom (1865 vs 1135 hits in CSD), for iridium complexes, the S atom is almost exclusively used as the coordination center (65 vs 2 in CSD). ppy ligands are slightly twisted along the central C−C bonds (cf. Table S2b). Crystal architectures in all of the structures are determined by close-packing requirements and by weak but numerous C−H···π and $\pi\cdots\pi$ interactions. Many voids filled with diffused electron density were found in the structure of $[Ir(\mu\text{-Cl})(5\text{-}(Ph_2N)bzq)_2]_2$, probably originating from the totally disordered solvent molecules because of the complicated shape of the dimer molecule. Similarly, in the crystal structures of monomeric complexes, the ordered ACN molecule in $[Ir(ppy)_2Cl(ACN)]$ or highly disordered water molecule in $[Ir(ppy)_2Cl(DMSO)]$ filling the voids between the complex molecules were found.

Spectroscopic Analysis and Cleavage of $[Ir(\mu\text{-Cl})(C\text{^}N)_2]_2$. After the successful optimization and synthesis of chloro-bridged iridium(III) dimers, we focused on their spectroscopic characteristics. From the very beginning, our attention was drawn by the appearance of a doubled set of resonances originating from cyclometalated ligands in the ^{1}H NMR spectra of all of the obtained compounds dissolved in DMSO-d_6 (Figures 3 and S1−S10). The recorded spectroscopic images for these types of binuclear compounds seemed unusual at first glance because such compounds bearing N-donating atoms in the trans position, C-donating atoms in the cis position, and two bridging Cl atoms in the cis position should be characterized by chemically equivalent C,N-cyclometalating ligands. In fact, for many reported dimers, only one set of signals originating from the cyclometalating ligands was observed in the ^{1}H NMR spectra.[26,55,56] However, the mentioned spectra were recorded in nonpolar solvents such as CD_2Cl_2 or $CDCl_3$, which prompted us to conclude that the differences in the spectroscopic images might be caused by the polar and coordinative nature of DMSO. In our search for the answer, we referred to the literature, where we found misleading data. In 2011, Li et al. reported the synthesis of $[Ir(ppy)_2(DMSO)_2]PF_6$, for which the given ^{1}H NMR spectroscopic data set accurately reflected those obtained by

https://dx.doi.org/10.1021/acs.inorgchem.0c01071
Inorg. Chem. 2020, 59, 9163−9176

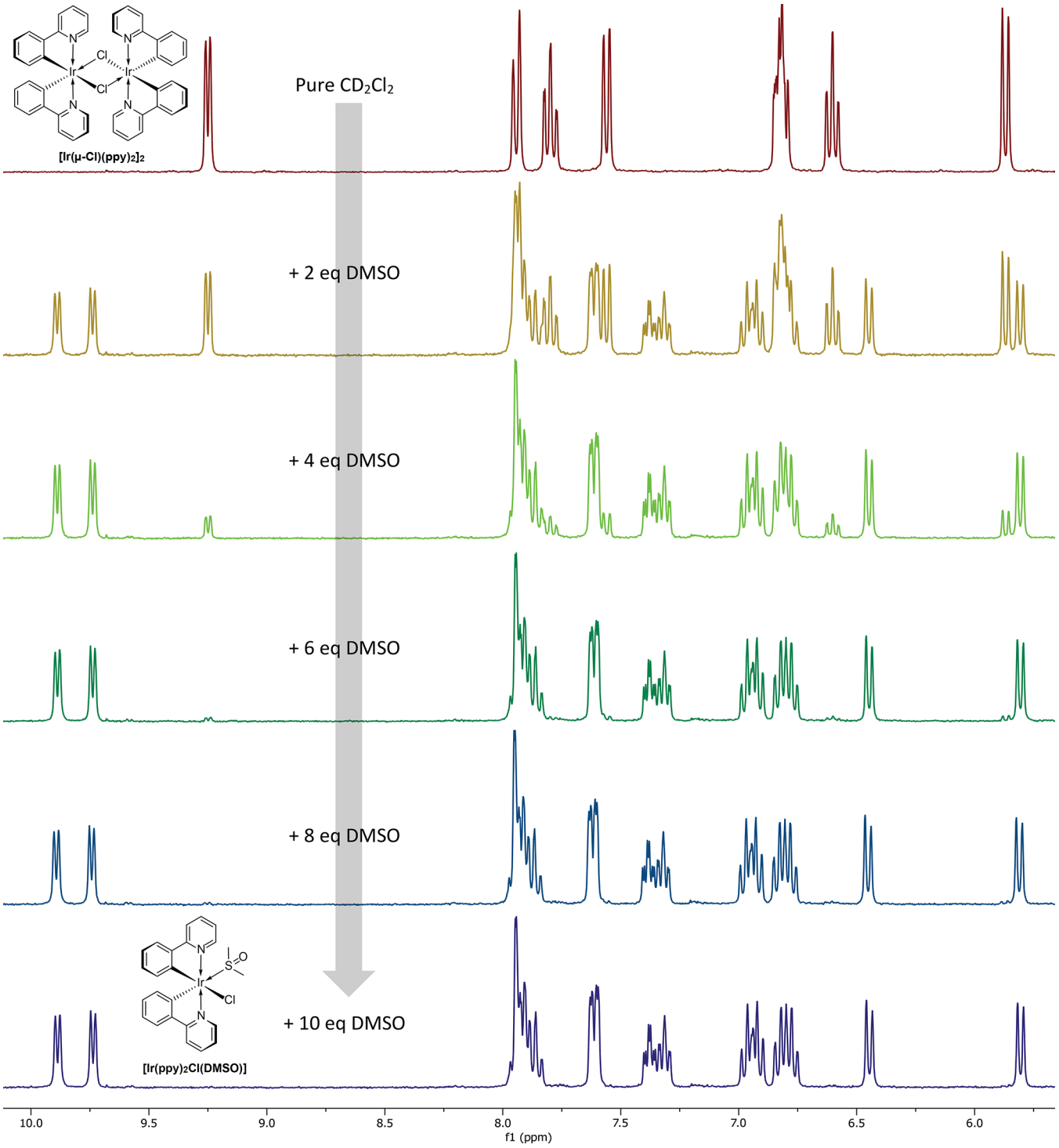

Figure 4. ^{1}H NMR titration of 3 mg of $[Ir(\mu\text{-}Cl)(ppy)_2]_2$ dissolved in 0.7 mL of CD_2Cl_2 (top). Each subsequent spectrum was measured after the addition of about 2 equiv of DMSO, followed by 5 min of shaking at room temperature.

us for $[Ir(\mu\text{-}Cl)(ppy)_2]_2$ in DMSO-d_6.[57] The authors claimed that a DMSO molecule was a sufficiently strong nucleophile to push out the chloride anion from the internal to the external coordination sphere, forming a $[Ir(ppy)_2(DMSO)_2]^+$ cation. However, in our opinion, such a cation with the retained configuration of ppy ligands from the parent dimer should not demonstrate the chemical inequivalence of ligands in the ^{1}H NMR spectrum. On the other hand, Soman et al. reported 1 year later exactly the same ^{1}H NMR data set for $[Ir(\mu\text{-}Cl)(ppy)_2]_2$ in DMSO-d_6 but without the explanation of the mentioned split of signals.[24] In the face of the encountered inconsistency, we decided to study in detail the behavior of chloro-bridged iridium(III) dimers to explain what lies behind the split of the NMR signals. We chose $[Ir(\mu\text{-}Cl)(ppy)_2]_2$ as a model compound and decided to examine its interaction with DMSO as well as ACN. Unlike DMSO, the latter solvent is more convenient for ESI, which enabled us to monitor its interaction with the model dimer also by MS.

Our study started from analysis of the literature on chloro-bridged rhodium(III) and iridium(III) dimers, where we found

https://dx.doi.org/10.1021/acs.inorgchem.0c01071
Inorg. Chem. 2020, 59, 9163−9176

some hints indicating that these compounds might undergo solvation in coordinating solvents [ACN, *N*,*N*-dimethylformamide (DMF), DMSO, and water], to create a monomeric derivatives of the general formula $[Ir(C^N\ ligand)_2Cl(solvent)]$.[15,23] However, it was not fully confirmed at the time of these studies because of re-formation of the original chloro-bridged dimers during the attempts of isolation.[58] Considering the results described in the cited papers, it should be assumed that conversion of the dimer to the solvated monomer is an equilibrium reaction that shifts toward the starting material when the coordinating solvent concentration is lowered, e.g., during isolation. Therefore, it is obvious that isolation of the solvated iridium species should be performed in the presence of a large excess of the coordinating solvent at every step of purification. Considering this condition, crystallization seemed to be the best choice, although it has been suggested that it is unlikely to do that.[58] Therefore, the crystal structures of mononuclear C,N-cyclometalated iridium(III) complexes, obtained as a result of chloro-bridged dimer cleavage by a coordinating solvent, are really scarce.[59] Either way, we also successfully managed to obtain XRD-suitable crystals of $[Ir(ppy)_2Cl(ACN)]$ and $[Ir(ppy)_2Cl(DMSO)]$. Both ACN and DMSO cleaved the chloro-bridged iridium(III) dimer and coordinated to the central atom with the formation of Ir−N and Ir−S bonds. The measured Ir−N bond length was 2.108 Å, while the average Ir−S bond length was 2.346 Å. The solved crystal structures clearly confirmed that the formed species do not have any symmetry elements; thus, their cyclometalated ppy ligands are inequivalent. We suppose that this is the origin of the doubled set of signals from cyclometalated ligands in the NMR spectra measured in DMSO-d_6 but that it is not the only one. The inequivalence of the ppy ligands is enhanced by the difference in the trans effects of the chloride ligand and coordinated solvent, which asymmetrically affects C-donating atoms in the positions trans to them. It is known that nitriles and sulfoxides are the ligands characterized by a stronger trans effect than halides.[60,61] Thus, the coordinated solvent should make the opposing Ir−C bonds weaker than the Ir−C bond in the trans position to the chloride ligand. In the case of $[Ir(ppy)_2Cl(DMSO)]$, it is true, and the Ir−C bond that is opposite to the Ir−S bond is longer by 0.021 Å, on average, than the Ir−C bond that is opposite to the Ir−Cl bond. On the contrary, in $[Ir(ppy)_2Cl(ACN)]$ both Ir−C bond lengths are exactly the same (2.001 Å). This indicates a stronger coordinative nature of DMSO to ACN, a very helpful observation for the explanation of their behavior during NMR analysis, described in the next paragraph. At this point, we can assume that the high-field-shifted set of resonances corresponding to one of the two ppy ligands originates from the ligand in the trans position to the coordinated DMSO molecule. It is clear that the differences in the trans effect are very subtle because the Ir atoms are chelated by ppy ligands, forming 5-membered cyclometalated rings, and, therefore, the distance between elements of the ring cannot be so easily varied. With the aid of XRD analysis, we were able to identify the chemical process occurring during the chloro-bridged iridium(III) dimer dissolution in coordinating solvents, but there was still the question of linking the outcome with the results of NMR spectroscopy.

Following the above conclusions, our next step was ^1H NMR analysis of the crystals to check whether the obtained spectra resemble those obtained after dissolution of iridium(III) dimers in DMSO-d_6. Because the crystallizations were performed in nondeuterated solvents, we expected to observe what happens both with the signals originating from the ppy ligands and with those corresponding to the coordinated solvent molecules. To our surprise, we noticed a significant difference between the NMR spectra of $[Ir(ppy)_2Cl(ACN)]$ and $[Ir(ppy)_2Cl(DMSO)]$ in CD_2Cl_2. In the case of the former, we observed only one set of signals originating from ppy and a singlet in the high-field region (Figure S17). The chemical shift of the singlet corresponded to a free ACN molecule.[62] Moreover, integration showed that the ppy/ACN ratio was 1:1, the same as that in the crystal phase, because there was an extra ACN molecule per $[Ir(ppy)_2Cl(ACN)]$ molecule in the unit cell. Even the addition of a few extra microliters of ACN to the NMR tube did not result in the appearance of signals corresponding to $[Ir(ppy)_2Cl(ACN)]$. Then we decided to measure the ^1H NMR spectrum of $[Ir(\mu\text{-}Cl)(ppy)_2]_2$ in ACN-d_3 because the crystals of $[Ir(ppy)_2Cl(ACN)]$ were obtained after heating of the dimer in pure ACN. However, the spectrum was not interpretable because of the low solubility of the analyte and did not show clear evidence for dimer cleavage (Figure S18). Surprisingly, the product of the cleavage could be crystallized, which proves that it is much more stable in the solid phase than in solution. In this way, we proved that the ability of ACN to cleave $[Ir(\mu\text{-}Cl)(ppy)_2]_2$ is very weak in solution, while the equilibrium between the dimeric and monomeric forms is evidently established, and the stability of $[Ir(ppy)_2Cl(ACN)]$ is enhanced in the crystalline phase. In contrast, many more signals were observed in the ^1H NMR spectrum of $[Ir(ppy)_2Cl(DMSO)]$ crystals dissolved in CD_2Cl_2 (Figure S19). Even more than two sets of resonances originating from ppy were observed along with some minor resonance lines. This indicated that DMSO is a stronger ligand than ACN, resulting in observation of both the chloro-bridged dimer and its cleaved form. The presence of the minor signals could be attributed to the coformed impurities because the crystallization process took about 2 weeks on the bench.[63] Therefore, we decided to perform an NMR titration of $[Ir(\mu\text{-}Cl)(ppy)_2]_2$ in CD_2Cl_2 using DMSO as a titrant to monitor the cleavage process in a more transparent way. Fragments of the spectra recorded at the starting point and after the addition of each DMSO portion are presented in Figure 4. At the beginning, only one set of signals originating from the coordinated ppy was observed, which proved that all of the ligands in the chloro-bridged dimer are chemically equivalent. After the addition of 2 equiv of DMSO per dimer molecule (Ir/DMSO ratio of 1:1), new signals appeared and the intensity of the starting material's signals decreased. All of the resonances were earlier observed in the NMR spectrum of $[Ir(ppy)_2Cl(DMSO)]$ obtained from the crystallization process, which proved that an equilibrium between the same two compounds takes place during the crystallization and titration (Figure S19). The integration of well-separated signals from the low-field region of the spectra allowed one to get rough information about the equilibrium between the cleaved and noncleaved forms. After the addition of a stoichiometric amount of DMSO, the molar ratio of $[Ir(\mu\text{-}Cl)(ppy)_2]_2$/$[Ir(ppy)_2Cl(DMSO)]$ reached 1:3.25. Considering the low concentration of the reactants and the facts that DMSO is a monodentate ligand and that the equilibrium was reached after an arbitrarily assumed 5 min of shaking, we came to the conclusion that the formation of a mononuclear complex is much preferable in this system. What is important is that this

https://dx.doi.org/10.1021/acs.inorgchem.0c01071
Inorg. Chem. 2020, 59, 9163−9176

reaction occurs very smoothly and quickly even in a low concentration of reagents; therefore, there is no need to use such harsh conditions as refluxing in neat DMSO to obtain the desired mononuclear complexes.[59] Further the addition of DMSO equivalents resulted in a shift of the equilibrium toward $[Ir(ppy)_2Cl(DMSO)]$, and total consumption of the starting material was observed after the addition of 10 equiv of DMSO. The equilibrium might be monitored also by observation of the high-field region in the ^1H NMR spectra, where the signals of the cleaving ligand are present. The addition of the first portion of the titrant to the $[Ir(\mu\text{-}Cl)(ppy)_2]_2$ solution resulted in the appearance of a singlet at 2.55 ppm, corresponding to the presence of free DMSO, accompanied by two additional singlets, the first upfield-shifted and second downfield-shifted (Figure S20). The chemical shifts of these resonances in relation to free DMSO were ca. 0.5 ppm, and the number of protons determined on the basis of their integration was the same and exactly corresponded to the number of protons assigned to resonance lines derived from ppy ligands in $[Ir(ppy)_2Cl(DMSO)]$. The break of the chemical equivalence of both protons in the ppy ligands and methyl groups of the coordinated DMSO caused by the lack of symmetry is the evidence of $[Ir(ppy)_2Cl(DMSO)]$ formation. Of course, the coordinated DMSO-d_6 molecules could not be observed in the ^1H NMR spectra measured in DMSO-d_6, but duplication of the resonances assigned to ppy ligands confirms the formation of $[Ir(ppy)_2Cl(DMSO\text{-}d_6)]$ in such an environment. The same behavior was observed for all of the complexes reported herein. The described phenomena might provide an explanation of why, in the given set of spectroscopic data of the substance supposed to be $[Ir(ppy)_2(DMSO)_2]PF_6$, the resonances originating from coordinated DMSO molecules were not observed.[57] It also confirms that the best way to pull out chloride from the inner coordination sphere of iridium(III) is the use of silver(I) salts,[64,65] and the employment of sodium salts might be insufficient. In this way, we confirmed with no doubt that iridium(III) dimers undergo equilibrium cleavage in the presence of coordinating solvents (Scheme 5). Moreover, we have shown that the coordinative nature of DMSO is much stronger than that of ACN, in spite of the difference in the steric hindrance of these solvent molecules. The dimers based on 2-phenoxypyridine also underwent cleavage in the same conditions, but the process was hampered by the low solubility of the species in DMSO, especially in the case of $[Ir(\mu\text{-}Cl)(F_3CPhOPy)_2]_2$. Heating of the sample in DMSO-d_6 led to formation of the cleaved form of the dimer, as confirmed by ^1H NMR analysis, but the desired signals were accompanied by some others originating from coformed species. We suppose that DMSO molecules can substitute the coordinated pyridyls, leading to the formation of a complex mixture of species. Therefore, NMR analysis of $[Ir(\mu\text{-}Cl)(F_3CPhOPy)_2]_2$ in $CDCl_3$ instead of DMSO-d_6 was made.

Scheme 5. Cleavage of $[Ir(\mu\text{-}Cl)(C\wedge N)_2]_2$ with a Coordinating Solvent

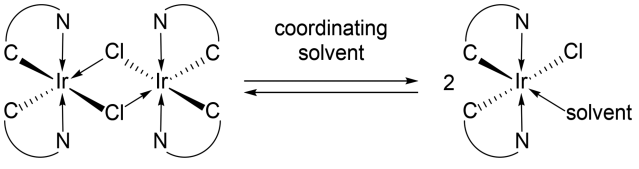

Dimer cleavage might be observed during ESI-MS measurement as well. This is a so-called "soft ionization" technique, which means that a fragmentation is not preferred. Additionally, in this type of analysis, the solution-phase composition is retained in the gas phase. Both features of this technique are very helpful in achieving our goal because they should permit observation of molecular ions of the cleaved form of the studied complexes. In this technique, it is necessary to use polar solvents because the ionization process requires formation of the charged analyte's solution droplets. However, not all polar solvents can be used because volatility is another desired feature. High-boiling solvents such as DMF and DMSO are not compatible with the ESI technique because they contaminate the source and decrease the detector's sensitivity. Because of limitation of the use of high-boiling solvents (such as DMSO) in the ESI-MS technique, measurements were made using ACN, which also proved its ability to cleave the chloro-bridged iridium(III) dimers. In line with our expectations, we observed signals corresponding to both the chloro-bridged dimer and its cleaved form, while the mass peaks corresponding to the cleaved form were dominant in the spectra. The ionization mechanism in positive mode involved abstraction of a chloride anion, not a typical addition of hydrogen, sodium, or potassium cations. During analysis of our compounds, we noticed an important relationship that might have a crucial impact on the interpretation of the results obtained. The appearance of the recorded spectra was strongly affected by the potential applied to the orifice plate that was implemented in the driving software as a declustering potential option (DP, also called cone potential). This parameter has a significant impact on the additional acceleration of the analyte ions in the medium-pressure region of the source, which causes collision-induced dissociation with the background gas.[66] As a result, the MS spectra obtained may not fully reflect the actual molecular structure of the examined substances. For example, adjustment of DP allowed one to control the clusterization/declusterization of polypeptides and the dissociation of ligands from the complex molecules, as in the case of $[H_3Ru_4(CO)_{12}]^-$.[67,68] At the default value of DP, the m/z values corresponding to $[Ir(C\wedge N)_2(ACN)]^+$ and $[Ir(C\wedge N)_2]^+$ in various ratios were observed. This confirmed that the cleaved forms were present in the solution because the cations produced by abstraction of the chloride anion and a weakly bonded ACN molecule were observed. With increasing DP, the abundance of $[Ir(C\wedge N)_2(ACN)]^+$ decreased and almost only $[Ir(C\wedge N)_2]^+$ could be observed. Interestingly, with decreasing DP, the abundance of the ions corresponding to the above-mentioned cations decreased, and the m/z value corresponding to $[Ir(C\wedge N)_2(ACN)_2]^+$ became dominant. When we analyzed the same sample using a mass spectrometer of a different manufacturer without the possibility of adjusting the DP value, the signals corresponding to $[Ir(C\wedge N)_2]^+$ were dominant. This shows that the MS spectra obtained by the ESI-MS technique might be misinterpreted depending on the parameters of the spectrometer used (Figure 5). For example, it is possible to assume that, in the coordinating solvent, the chloro-bridged dimers undergo double coordination of the solvent molecule together with a shift of the chloride anion to an outer coordination sphere, by the observation of $[Ir(C\wedge N)_2(solvent)_2]^+$ as a dominant ion in the spectra. This process might be even more flawed by the involvement of much stronger ligands. Therefore, our recommendation is to

https://dx.doi.org/10.1021/acs.inorgchem.0c01071
Inorg. Chem. 2020, 59, 9163−9176

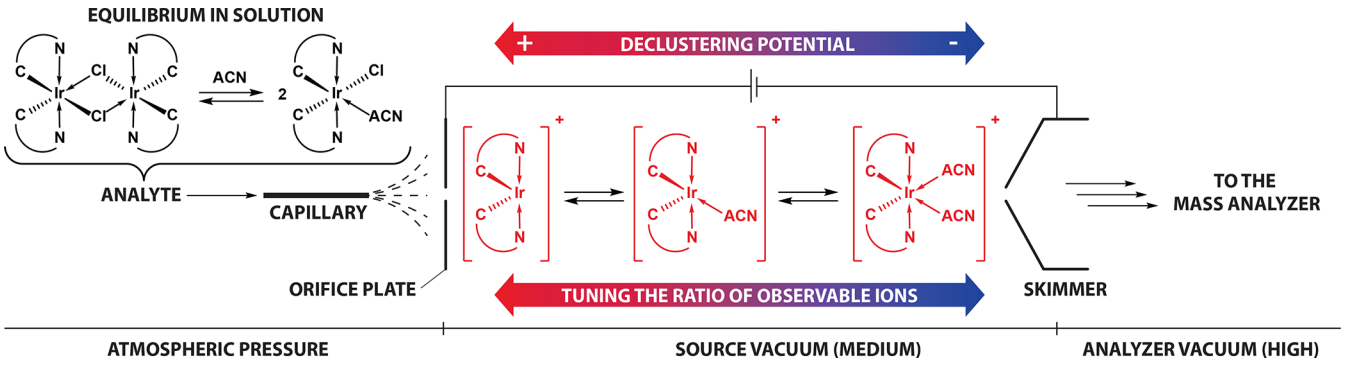

Figure 5. Simplified scheme of the electrospray ion source and relationship between the potential applied to the orifice during the measurement and the observable ions in positive mode.

combine different types of analytical methods in the studies of such processes to avoid misinterpretation of the results.

CONCLUSIONS

In summary, in this work we proved the positive effect of microwave irradiation on the formation of chloro-bridged iridium(III) dimers and the importance of the presence of water in this process. A series of known and novel dimers were obtained in the optimized conditions, and the products were characterized by NMR spectroscopy and MS, which provided strong experimental evidence of the dimers' cleavage with the coordinating solvents. In the first stage of our work, we compared the efficiency of model dimer formation in a microwave reactor and an oil bath, which showed the beneficial effect of the unconventional source of energy at all of the tested temperatures. Moreover, the great impact of the presence of water in the reaction medium was confirmed and assumed to improve both the iridium(III) chloride solubility and absorption of stimulating radiation. All of the tests allowed the establishment of optimal conditions for the obtainment of high-purity dimers with minimization of the occurrence of side reactions, which enabled a very simple isolation process, just filtration and rinsing. According to the developed protocol, a series of known and novel iridium(III) dimers were synthesized very quickly and in high to very high yields. The scope of the tested ligands included compounds based on 2-phenylpiridinato, benzo[*h*]quinolinato, and 2-phenoxypiridinato cores, equipped with electron-donating (−Me, −OMe, and −OPh), electron-withdrawing (−F, −Br, $-CF_3$, and $-C_6F_5$), and p-type semiconducting ($-NPh_2$ and $-C_6H_4NPh_2$) groups. In the case of the ligand bearing a $-NMe_2$ substituent, an alternative synthetic pathway, avoiding HCl involvement, was proposed. All of the new iridium(III) dimers constitute attractive starting materials for the preparation of new OLED emitters or active species for bioimaging. The obtained dimers were characterized by means of ^{1}H NMR spectroscopy and ESI-MS in DMSO and ACN, which revealed the occurrence of a chemical reaction between these solvents and the binuclear iridium complexes. A detailed investigation resulted in a multithreaded explanation of the process, identified as cleavage of the μ-chloride bridges in which DMSO coordination appeared to be much more favorable than ACN coordination. The cleavage was clearly evidenced in solution during NMR titration as well as in the solid phase using XRD structure determination of the model dimer's cleaved forms. Moreover, the crystal structures of the two dimers stabilized with bzq and 5-(Ph_2N)bzq ligands were determined. Finally, ESI-HRMS characterization of the chloro-bridged iridium(III) dimers in ACN not only confirmed formation of the target molecules but also showed how DP adjustment of the spectrometer used varies the spectroscopic image of the analyzed complexes. Our work clearly demonstrated that, depending on the applied potential, a chloride-abstracted cation derived from $[Ir(C\hat{}N)_2Cl(ACN)]$ containing zero-, one-, or two-coordinated solvent molecules becomes dominant in the spectrum. We believe that all of the phenomena explained in this work strongly enrich the knowledge in the field of iridium chemistry, will help in the reconsideration of the results previously reported in the literature, and support interpretation of the experimental data in the upcoming works.

ASSOCIATED CONTENT

Supporting Information

The Supporting Information is available free of charge at https://pubs.acs.org/doi/10.1021/acs.inorgchem.0c01071.

Procedures for the synthesis of ligands, precursors, and complexes, NMR and ESI-HRMS spectra of the new compounds, and X-ray analysis detailed data (PDF)

Accession Codes

CCDC 1895621,1895622, 1897304, and 1897305 contain the supplementary crystallographic data for this paper. These data can be obtained free of charge via www.ccdc.cam.ac.uk/data_request/cif, or by emailing data_request@ccdc.cam.ac.uk, or by contacting The Cambridge Crystallographic Data Centre, 12 Union Road, Cambridge CB2 1EZ, UK; fax: +44 1223 336033.

AUTHOR INFORMATION

Corresponding Authors

Bartosz Orwat − *Faculty of Chemistry and Center for Advanced Technology, Adam Mickiewicz University in Poznań, 61-614 Poznań, Poland*; Email: b.orwat@amu.edu.pl

Ireneusz Kownacki − *Faculty of Chemistry and Center for Advanced Technology, Adam Mickiewicz University in Poznań, 61-614 Poznań, Poland*; orcid.org/0000-0002-5445-760X; Email: irekk@o365.amu.edu.pl

Authors

Myong Joon Oh − *Faculty of Chemistry and Center for Advanced Technology, Adam Mickiewicz University in Poznań, 61-614 Poznań, Poland*

https://dx.doi.org/10.1021/acs.inorgchem.0c01071
Inorg. Chem. 2020, 59, 9163−9176

Maciej Zaranek − *Faculty of Chemistry and Center for Advanced Technology, Adam Mickiewicz University in Poznań, 61-614 Poznań, Poland;* orcid.org/0000-0003-0593-5545
Maciej Kubicki − *Faculty of Chemistry, Adam Mickiewicz University in Poznań, 61-614 Poznań, Poland;* orcid.org/0000-0001-7202-9169
Rafał Januszewski − *Faculty of Chemistry and Center for Advanced Technology, Adam Mickiewicz University in Poznań, 61-614 Poznań, Poland;* orcid.org/0000-0002-5562-6647

Complete contact information is available at: https://pubs.acs.org/10.1021/acs.inorgchem.0c01071

Author Contributions

The manuscript was written through contributions of all authors. All authors have given approval to the final version of the manuscript.

Notes

The authors declare no competing financial interest.

■ ACKNOWLEDGMENTS

The authors acknowledge financial support from the National Science Centre, Poland (Grants 2013/11/B/ST5/01334 and 2018/29/N/ST5/02926).

■ REFERENCES

(1) Zhou, C.; Shi, Y.; Ding, X.; Li, M.; Luo, J.; Lu, Z.; Xiao, D. Development of a Fast and Sensitive Glucose Biosensor Using Iridium Complex-Doped Electrospun Optical Fibrous Membrane. *Anal. Chem.* **2013**, *85*, 1171−1176.
(2) Teegardin, K.; Day, J. I.; Chan, J.; Weaver, J. Advances in Photocatalysis: A Microreview of Visible Light Mediated Ruthenium and Iridium Catalyzed Organic Transformations. *Org. Process Res. Dev.* **2016**, *20*, 1156−1163.
(3) Zysman-Colman, E. *Iridium(III) in optoelectronic and photonics applications*; John Wiley & Sons: Newark, NJ, 2017.
(4) Henwood, A. F.; Zysman-Colman, E. Luminescent Iridium Complexes Used in Light-Emitting Electrochemical Cells (LEECs). *Top. Curr. Chem.* **2016**, *374*, 36.
(5) Kappaun, S.; Slugovc, C.; List, E. J. W. Phosphorescent Organic Light-Emitting Devices: Working Principle and Iridium Based Emitter Materials. *Int. J. Mol. Sci.* **2008**, *9*, 1527−1547.
(6) Ma, D.-L.; Wu, C.; Tang, W.; Gupta, A.-R.; Lee, F.-L.; Li, G.; Leung, C.-H. Recent advances in iridium(III) complex-assisted nanomaterials for biological applications. *J. Mater. Chem. B* **2018**, *6*, 537−544.
(7) Page, Z. A.; Narupai, B.; Pester, C. W.; Bou Zerdan, R.; Sokolov, A.; Laitar, D. S.; Mukhopadhyay, S.; Sprague, S.; McGrath, A. J.; Kramer, J. W.; Trefonas, P.; Hawker, C. J. Novel Strategy for Photopatterning Emissive Polymer Brushes for Organic Light Emitting Diode Applications. *ACS Cent. Sci.* **2017**, *3*, 654−661.
(8) Han, J.; Tang, K.-M.; Cheng, S.-C.; Ng, C.-O.; Chun, Y.-K.; Chan, S.-L.; Yiu, S.-M.; Tse, M.-K.; Roy, V. A. L.; Ko, C.-C. Mechanochemical changes on cyclometalated Ir(III) acyclic carbene complexes − design and tuning of luminescent mechanochromic transition metal complexes. *Inorg. Chem. Front.* **2020**, *7*, 786−794.
(9) Li, C.; Wang, H.; Shen, J.; Tang, B. Cyclometalated Iridium Complex-Based Label-Free Photoelectrochemical Biosensor for DNA Detection by Hybridization Chain Reaction Amplification. *Anal. Chem.* **2015**, *87*, 4283−4291.
(10) Zhao, Y.; Yang, X.; Han, D.; Qi, H.; Gao, Q.; Zhang, C. Cyclometalated Iridium-Complex-Based Label-Free Supersandwich Electrogenerated Chemiluminescence Biosensor for the Detection of Micro-RNA. *ChemElectroChem* **2017**, *4*, 1775−1782.
(11) Miao, X.; Ko, C.-N.; Vellaisamy, K.; LI, Z.; Yang, G.; Leung, C.-H.; Ma, D.-L. A cyclometalated iridium(III) complex used as a conductor for the electrochemical sensing of IFN-γ. *Sci. Rep.* **2017**, *7*, 42740.
(12) Zhu, J.-H.; Tang, B.-Z.; Lo, K. K.-W. Luminescent Molecular Octopuses with a Polyhedral Oligomeric Silsesquioxane (POSS) Core and Iridium(III) Polypyridine Arms: Synthesis, Aggregation Induced Emission, Cellular Uptake, and Bioimaging Studies. *Chem. - Eur. J.* **2019**, *25*, 10633−10641.
(13) Liao, G.; Peng, X.; Li, T.; Ye, Z.; Xiang, X.; Fu, C. The Discovery of an Iridium(III) Dimer Complex as a Potent Antibacterial Agent against Non-Replicating Mycobacterium smegmatis. *Polymers* **2018**, *10*, 297.
(14) Wong, M. Y.; Xie, G.; Tourbillon, C.; Sandroni, M.; Cordes, D. B.; Slawin, A. M. Z.; Samuel, I. D. W.; Zysman-Colman, E. Formylated chloro-bridged iridium(III) dimers as OLED materials: opening up new possibilities. *Dalton Trans.* **2015**, *44*, 8419−8432.
(15) Carlson, G. A.; Djurovich, P. I.; Watts, R. J. Widely varying photophysical properties of ligand-nitrated bis(.mu.-chloro)tetrakis(2-phenylpyridinato)diiridium(III). *Inorg. Chem.* **1993**, *32*, 4483−4484.
(16) Lamansky, S.; Djurovich, P.; Murphy, D.; Abdel-Razzaq, F.; Kwong, R.; Tsyba, I.; Bortz, M.; Mui, B.; Bau, R.; Thompson, M. E. Synthesis and Characterization of Phosphorescent Cyclometalated Iridium Complexes. *Inorg. Chem.* **2001**, *40*, 1704−1711.
(17) Nonoyama, M. Benzo[*h*]quinolin-10-yl-*N* Iridium(III) Complexes. *Bull. Chem. Soc. Jpn.* **1974**, *47*, 767−768.
(18) Tamayo, A. B.; Alleyne, B. D.; Djurovich, P. I.; Lamansky, S.; Tsyba, I.; Ho, N. N.; Bau, R.; Thompson, M. E. Synthesis and Characterization of Facial and Meridional Tris-cyclometalated Iridium(III) Complexes. *J. Am. Chem. Soc.* **2003**, *125*, 7377−7387.
(19) Velusamy, M.; Thomas, K. R. J.; Chen, C.-H.; Lin, J. T.; Wen, Y. S.; Hsieh, W.-T.; Lai, C.-H.; Chou, P.-T. Synthesis, structure and electroluminescent properties of cyclometalated iridium complexes possessing sterically hindered ligands. *Dalton Trans.* **2007**, 3025−3034.
(20) Ionkin, A. S.; Marshall, W. J.; Roe, D. C.; Wang, Y. Synthesis, structural characterization and the first electroluminescent properties of tris- and bis-cycloiridiated complexes of sterically hindered electron-poor 2-(3,5-bis(trifluoromethyl)phenyl)-4-trifluoromethylpyridine. *Dalton Trans.* **2006**, 2468−2478.
(21) Yang, C.-H.; Fang, K.-H.; Su, W.-L.; Wang, S.-P.; Su, S.-K.; Sun, I.-W. Color tuning of iridium complexes for organic light-emitting diodes: The electronegative effect and π-conjugation effect. *J. Organomet. Chem.* **2006**, *691*, 2767−2773.
(22) Hwang, F.-M.; Chen, H.-Y.; Chen, P.-S.; Liu, C.-S.; Chi, Y.; Shu, C.-F.; Wu, F.-I.; Chou, P.-T.; Peng, S.-M.; Lee, G.-H. Iridium(III) Complexes with Orthometalated Quinoxaline Ligands: Subtle Tuning of Emission to the Saturated Red Color. *Inorg. Chem.* **2005**, *44*, 1344−1353.
(23) Sprouse, S.; King, K. A.; Spellane, P. J.; Watts, R. J. Photophysical effects of metal-carbon.sigma. bonds in ortho-metalated complexes of iridium(III) and rhodium(III). *J. Am. Chem. Soc.* **1984**, *106*, 6647−6653.
(24) Soman, S.; Singh Bindra, G.; Paul, A.; Groarke, R.; Manton, J. C.; Connaughton, F. M.; Schulz, M.; Dini, D.; Long, C.; Pryce, M. T.; Vos, J. G. Wavelength dependent photocatalytic H2 generation using iridium−Pt/Pd complexes. *Dalton Trans.* **2012**, *41*, 12678−12680.
(25) Mosca, L.; Khnayzer, R. S.; Lazorski, M. S.; Danilov, E. O.; Castellano, F. N.; Anzenbacher, P., Jr. Sensing of 2,4,6-Trinitrotoluene (TNT) and 2,4-Dinitrotoluene (2,4-DNT) in the Solid State with Photoluminescent Ru^{II} and Ir^{III} Complexes. *Chem. - Eur. J.* **2015**, *21*, 4056−4064.
(26) Kiran, R. V.; Hogan, C. F.; James, B. D.; Wilson, D. V. D. Photophysical and Electrochemical Properties of Phenanthroline-Based Bis-cyclometallated Iridium Complexes in Aqueous and Organic Media. *Eur. J. Inorg. Chem.* **2011**, *2011*, 4816−4825.
(27) Ramlot, D.; Rebarz, M.; Volker, L.; Ovaere, M.; Beljonne, D.; Dehaen, W.; Van Meervelt, L.; Moucheron, C.; Kirsch-De Mesmaeker, A. An Experimental and Theoretical Approach to the Photophysical Properties of Some Rh and Ir Complexes Incorporating

the Dipyrromethene Ligand. *Eur. J. Inorg. Chem.* **2013**, *2013*, 2031−2040.
(28) Laskar, I. R.; Hsu, S.-F.; Chen, T.-M. Investigating photoluminescence and electroluminescence of iridium(III)-based blue-emitting phosphors. *Polyhedron* **2006**, *25*, 1167−1176.
(29) Huang, Y.-T.; Chuang, T.-H.; Shu, Y.-L.; Kuo, Y.-C.; Wu, P.-L.; Yang, C.-H.; Sun, I.-W. Bi-substituted Effect on Phenylisoquinoline Iridium(III) Complexes. *Organometallics* **2005**, *24*, 6230−6238.
(30) Lepeltier, M.; Le Bozec, H.; Guerchais, V.; Lee, T. K.-M.; Lo, K. K.-W. Tris-Cyclometalated Iridium(III) Styryl Complexes and Their Saturated Analogues: Direct Functionalization of $Ir(4\text{-Me-ppy})_3$ and Hydrogen Transfer Process. *Organometallics* **2005**, *24*, 6069−6072.
(31) Chen, H.-Y.; Yang, C.-H.; Chi, Y.; Cheng, Y.-M.; Yeh, Y.-S.; Chou, P.-T.; Hsieh, H.-Y.; Liu, C.-S.; Peng, S.-M.; Lee, G.-H. Room-temperature NIR phosphorescence of new iridium (III) complexes with ligands derived from benzoquinoxaline. *Can. J. Chem.* **2006**, *84*, 309−318.
(32) Monos, T. M.; Sun, A. C.; McAtee, R. C.; Devery, J. J., III; Stephenson, C. R. J. Microwave-Assisted Synthesis of Heteroleptic $Ir(III)^+$ Polypyridyl Complexes. *J. Org. Chem.* **2016**, *81*, 6988−6994.
(33) Alam, P.; Laskar, I. R.; Climent, C.; Casanova, D.; Alemany, P.; Karanam, M.; Choudhury, A. R.; Raymond Butcher, J. Microwave-assisted facile and expeditive syntheses of phosphorescent cyclometallated iridium(III) complexes. *Polyhedron* **2013**, *53*, 286−294.
(34) Scarpelli, F.; Ionescu, A.; Ricciardi, L.; Plastina, P.; Aiello, I.; La Deda, M.; Crispini, A.; Ghedini, M.; Godbert, N. A novel route towards water-soluble luminescent iridium(III) complexes via a hydroxy-bridged dinuclear precursor. *Dalton Trans.* **2016**, *45*, 17264−17273.
(35) Echeverry-Gonzalez, C. A.; Puerto-Galvis, C. E.; Borca, C. H.; Mosquera, M. A.; Luis-Robles, A. F.; Kouznetsov, V. V. Optimization of the synthesis of quinoline-based neutral cyclometalated iridium complexes via microwave irradiation: design of light harvesting and emitting complexes using bulky quinolones. *Org. Chem. Front.* **2019**, *6*, 3374−3382.
(36) Tejchman, W.; Orwat, B.; Korona-Głowniak, I.; Barbasz, A.; Kownacki, I.; Latacz, G.; Handzlik, J.; Żesławska, E.; Malm, A. Highly efficient microwave synthesis of rhodanine and 2-thiohydantoin derivatives and determination of relationships between their chemical structures and antibacterial activity. *RSC Adv.* **2019**, *9*, 39367−39380.
(37) Orwat, B.; Witkowska, E.; Kownacki, I.; Oh, M.-J.; Hoffmann, M.; Kubicki, M.; Grzelak, I.; Marciniec, B.; Glowacki, I.; Luszczynska, B.; Wiosna-Salyga, G.; Ulanski, J.; Ledwon, P.; Lapkowski, M. Microwave-assisted one-pot synthesis of new ionic iridium complexes of $[Ir(bzq)_2(N\wedge N)]^+A^-$ type and their selected electroluminescent properties. *Dalton Trans.* **2017**, *46*, 9210−9226.
(38) Orwat, B.; Oh, M.-J.; Kubicki, M.; Kownacki, I. Synthesis of 5-Substituted Benzo[h]quinoline Derivatives via Reactions Involving $C(sp^2)$−Br Bond Activation. *Adv. Synth. Catal.* **2018**, *360*, 3331−3344.
(39) Witkowska, E.; Orwat, B.; Oh, M.-J.; Wiosna-Salyga, G.; Glowacki, I.; Kownacki, I.; Jankowska, K.; Kubicki, M.; Gierczyk, B.; Dutkiewicz, M.; Grzelak, I.; Hoffmann, M.; Nawrocik, J.; Krajewski, G.; Ulanski, J.; Ledwon, P.; Lapkowski, M. Effect of β-Ketoiminato Ancillary Ligand Modification on Emissive Properties of New Iridium Complexes. *Inorg. Chem.* **2019**, *58*, 15671−15686.
(40) Grzelak, I.; Orwat, B.; Kownacki, I.; Hoffmann, M. Quantum-chemical studies of homoleptic iridium(III) complexes in OLEDs: *fac* versus *mer* isomers. *J. Mol. Model.* **2019**, *25*, 154.
(41) Lepeltier, M.; Dumur, F.; Graff, B.; Xiao, P.; Gigmes, D.; Lalevée, J.; Mayer, C. R. Tris-cyclometalated Iridium(III) Complexes with Three Different Ligands: a New Example with 2-(2,4-Difluorophenyl)pyridine-Based Complex. *Helv. Chim. Acta* **2014**, *97*, 939−956.
(42) Tamura, Y.; Hisamatsu, Y.; Kazama, A.; Yoza, K.; Sato, K.; Kuroda, R.; Aoki, S. Stereospecific Synthesis of Tris-heteroleptic Tris-cyclometalated Iridium(III) Complexes via Different Heteroleptic Halogen-Bridged Iridium(III) Dimers and Their Photophysical Properties. *Inorg. Chem.* **2018**, *57*, 4571−4589.
(43) Gerrard, W.; Madden, R. W.; Tolcher, P. Interaction of alcohols with hydrogen halides. *J. Appl. Chem.* **1955**, *5*, 28−34.
(44) Witkowska, E.; Wiosna-Salyga, G.; Glowacki, I.; Orwat, B.; Oh, M.-J.; Kownacki, I.; Kubicki, M.; Gierczyk, B.; Dutkiewicz, M.; Cieszko, P.; Luszczynska, B.; Ulanski, J.; Grzelak, I.; Hoffmann, M.; Ledwon, P.; Lapkowski, M. Effect of fluorine substitution of the β-ketoiminate ancillary ligand on photophysical properties and electroluminescence ability of new iridium(iii) complexes. *J. Mater. Chem. C* **2018**, *6*, 8688−8708.
(45) Baranoff, E.; Curchod, B. F. E.; Frey, J.; Scopelliti, R.; Kessler, F.; Tavernelli, I.; Rothlisberger, U.; Grätzel, M.; Nazeeruddin, M. K. Acid-Induced Degradation of Phosphorescent Dopants for OLEDs and Its Application to the Synthesis of Tris-heteroleptic Iridium(III) Bis-cyclometalated Complexes. *Inorg. Chem.* **2012**, *51*, 215−224.
(46) Hierlinger, C.; Pal, A. K.; Stella, F.; Lebl, T.; Cordes, D. B.; Slawin, A. M. Z.; Jacquemin, D.; Guerchais, V.; Zysman-Colman, E. Synthesis, Characterization, and Optoelectronic Properties of Iridium Complexes Bearing Nonconjugated Six-Membered Chelating Ligands. *Inorg. Chem.* **2018**, *57*, 2023−2034.
(47) Hierlinger, C.; Cordes, D. B.; Slawin, A. M. Z.; Jacquemin, D.; Guerchais, V.; Zysman-Colman, E. Phosphorescent cationic iridium(III) complexes bearing a nonconjugated six-membered chelating ancillary ligand: a strategy for tuning the emission towards the blue. *Dalton Trans.* **2018**, *47*, 10569−10577.
(48) Song, Y.-H.; Chiu, Y.-C.; Chi, Y.; Cheng, Y.-M.; Lai, C.-H.; Chou, P.-T.; Wong, K.-T.; Tsai, M.-H.; Wu, C.-C. Phosphorescent Iridium(III) Complexes with Nonconjugated Cyclometalated Ligands. *Chem. - Eur. J.* **2008**, *14*, 5423−5434.
(49) Chang, C.-F.; Cheng, Y.-M.; Chi, Y.; Chiu, Y.-C.; Lin, C.-C.; Lee, G.-H.; Chou, P.-T.; Chen, C.-C.; Chang, C.-H.; Wu, C.-C. Highly Efficient Blue-Emitting Iridium(III) Carbene Complexes and Phosphorescent OLEDs. *Angew. Chem., Int. Ed.* **2008**, *47*, 4542−4545.
(50) Li, X.-H.; Ye, A.-H.; Liang, C.; Mo, D.-L. Substituent Effects of 2-Pyridones on Selective O-Arylation with Diaryliodonium Salts: Synthesis of 2-Aryloxypyridines under Transition-Metal-Free Conditions. *Synthesis* **2018**, *50*, 1699−1710.
(51) Takise, R.; Isshiki, R.; Muto, K.; Itami, K.; Yamaguchi, J. Decarbonylative Diaryl Ether Synthesis by Pd and Ni Catalysis. *J. Am. Chem. Soc.* **2017**, *139*, 3340−3343.
(52) Blasberg, F.; Bats, J. W.; Wagner, M.; Lerner, H.-W. (Acetonitrile-κN)chloridobis[2-(pyridin-2-yl)phenyl-κ^2C^1,N]iridium(III). *Acta Crystallogr.* **2011**, *E67*, m1837−m1838.
(53) Groom, C. R.; Bruno, I. J.; Lightfoot, M. P.; Ward, S. C. The Cambridge Structural Database. *Acta Crystallogr., Sect. B: Struct. Sci., Cryst. Eng. Mater.* **2016**, *B72*, 171−179.
(54) Garces, F. O.; Dedeian, K.; Keder, N. L.; Watts, R. J. Structures of ortho-metalated [2-(p-tolyl)pyridine]iridium(III) complexes. *Acta Crystallogr., Sect. C: Cryst. Struct. Commun.* **1993**, *C49*, 1117−1120.
(55) Lowry, M. S.; Hudson, W. R.; Pascal, R. A.; Bernhard, S. Accelerated Luminophore Discovery through Combinatorial Synthesis. *J. Am. Chem. Soc.* **2004**, *126*, 14129−14135.
(56) Garces, F. O.; King, K. A.; Watts, R. J. Synthesis, structure, electrochemistry, and photophysics of methyl-substituted phenylpyridine ortho-metalated iridium(III) complexes. *Inorg. Chem.* **1988**, *27*, 3464−3471.
(57) Li, C.; Yu, M.; Sun, Y.; Wu, Y.; Huang, C.; Li, F. A Nonemissive Iridium(III) Complex That Specifically Lights-Up the Nuclei of Living Cells. *J. Am. Chem. Soc.* **2011**, *133*, 11231−11239.
(58) Schmid, B.; Garces, F. O.; Watts, R. J. Synthesis and characterizations of cyclometalated iridium(III) solvento complexes. *Inorg. Chem.* **1994**, *33*, 9−14.
(59) Santoro, A.; Prokhorov, A. M.; Kozhevnikov, V. N.; Whitwood, A. C.; Donnio, B.; Williams, J. A. G.; Bruce, D. W. Emissive Metallomesogens Based on 2-Phenylpyridine Complexes of Iridium(III). *J. Am. Chem. Soc.* **2011**, *133*, 5248−5251.

https://dx.doi.org/10.1021/acs.inorgchem.0c01071
Inorg. Chem. 2020, 59, 9163−9176

(60) Kukushkin, Y. N. Cis and trans Effects of Dialkyl Sulfoxides in Complex Compounds of Platinum(II). *Chem. zvesti* **1971**, *25*, 380−384.
(61) Patra, S. G.; Datta, D. Ligand field splitting in homoleptic tetrahedral d^{10} transition metal complexes. Spectrochemical series. *Comput. Theor. Chem.* **2018**, *1130*, 77−82.
(62) Fulmer, G. R.; Miller, A. J. M.; Sherden, N. H.; Gottlieb, H. E.; Nudelman, A.; Stoltz, B. M.; Bercaw, J. E.; Goldberg, K. I. NMR Chemical Shifts of Trace Impurities: Common Laboratory Solvents, Organics, and Gases in Deuterated Solvents Relevant to the Organometallic Chemist. *Organometallics* **2010**, *29*, 2176−2179.
(63) Shon, J.-H.; Sittel, S.; Teets, T. S. Synthesis and Characterization of Strong Cyclometalated Iridium Photoreductants for Application in Photocatalytic Aryl Bromide Hydrodebromination. *ACS Catal.* **2019**, *9*, 8646−8658.
(64) Boudreault, P.-L. T.; Esteruelas, M. A.; Mora, E.; Oñate, E.; Tsai, J.-Y. Pyridyl-Directed C−H and C−Br Bond Activations Promoted by Dimer Iridium-Olefin Complexes. *Organometallics* **2018**, *37*, 3770−3779.
(65) Ma, D.-L.; Wong, W.-L.; Chung, W.-H.; Chan, F.-Y.; So, P.-K.; Lai, T.-S.; Zhou, Z.-Y.; Leung, Y.-C.; Wong, K.-Y. A Highly Selective Luminescent Switch-On Probe for Histidine/Histidine-Rich Proteins and Its Application in Protein Staining. *Angew. Chem., Int. Ed.* **2008**, *47*, 3735−3739.
(66) Hunt, S. M.; Sheil, M. M.; Belov, M.; Derrick, P. J. Probing the Effects of Cone Potential in the Electrospray Ion Source: Consequences for the Determination of Molecular Weight Distributions of Synthetic Polymers. *Anal. Chem.* **1998**, *70*, 1812−1822.
(67) Thomson, B. A. Declustering and fragmentation of protein ions from an electrospray ion source. *J. Am. Soc. Mass Spectrom.* **1997**, *8*, 1053−1058.
(68) Henderson, M. A.; Kwok, S.; McIndoe, J. S. Gas-phase reactivity of ruthenium carbonyl cluster anions. *J. Am. Soc. Mass Spectrom.* **2009**, *20*, 658−666.

https://dx.doi.org/10.1021/acs.inorgchem.0c01071
Inorg. Chem. 2020, 59, 9163−9176

Supporting information
for

Microwave-accelerated *C,N*-cyclometalation as a route to chloro-bridged iridium(III) binuclear precursors of phosphorescent materials: optimization, synthesis, and studies of the Ir(III) dimers behavior in coordinating solvents

Bartosz Orwat*[a,b], Myong Joon Oh[a], Maciej Zaranek[a], Maciej Kubicki[a], Rafał Januszewski[a,b], Ireneusz Kownacki*[a,b]

[a] Faculty of Chemistry, Adam Mickiewicz University in Poznań, St. Uniwersytetu Poznańskiego 8, 61-614 Poznań, Poland

[b] Center for Advanced Technology, St. Uniwersytetu Poznańskiego 10, 61-614 Poznań, Poland

Corresponding authors' emails: b.orwat@amu.edu.pl, irekk@o365.amu.edu.pl

Table of contents

Experimental details *S2*

Synthetic procedures and analytical data *S3*

^{1}H and ^{13}C NMR spectra *S10*

ESI-HRMS spectra *S21*

X-ray crystallography *S28*

References *S30*

Experimental details

Dimethyl sulfoxide (DMSO), pentane, 2-methoxyethanol, 2-phenylpyridine, 2-fluoro-4-methylpyridine, 2-fluoropyridine, phenol, 4-trifluoromethylphenol, caesium carbonate, copper(I) chloride, and di-μ-chlorobis(1,5-cyclooctadiene)diiridium(I) were obtained from Sigma-Aldrich; acetonitrile (ACN), *N,N*-dimethylformamide (DMF), and benzo[*h*]quinoline from ABCR GmbH; dichloromethane (DCM), diethyl ether, hexane, 2-propanol, methanol, and sodium hydroxide from Avantor Performance Materials Poland; iridium(III) chloride hydrate from Pressure Chemical Co.; while deuterated solvents were purchased from Deutero GmbH and Sigma-Aldrich. 4-methyl-2-phenoxypyridine,[1] 2-(4-(trifluoromethyl))phenoxypyridine,[2] 2-(2,4-difluorophenyl)pyridine,[3] and 5-functionalized benzo[*h*]quinolines[4] were prepared according to the published procedures.

Reactions accelerated with microwave irradiation were conducted under air atmosphere (unless otherwise indicated) in CEM microwave 10 mL vials with CEM Discover, a pressurized microwave reactor.The reaction progress was monitored by means of a gas chromatograph (Bruker 450-GC) coupled to a mass detector (Bruker MS-320) and thin layer chromatography (TLC). Chemical structures of the obtained compounds were confirmed by nuclear magnetic resonance (NMR) spectroscopy using Bruker Ultrashield 300 MHz and Bruker Ascend 400 MHz Nanobay spectrometers. $CDCl_3$, CD_2Cl_2 and DMSO-d_6 were used for NMR analysis with residual solvent peak as the internal standard (chloroform ^{1}H δ = 7.26 ppm, ^{13}C δ = 77.16 ppm; dichloromethane ^{1}H δ = 5.32 ppm, ^{13}C δ = 54.00 ppm; DMSO ^{1}H δ = 2.50 ppm, ^{13}C δ = 39.52 ppm). High-resolution mass spectroscopy (HRMS) analysis were conducted in electrospray ionization mode (ESI) with time of flight (TOF) mass detector (ABSciex QTOF 5600 and Bruker Impact HD). ESI-HRMS spectra were recorded in positive ionization mode and the analytes were dissolved in HPLC grade ACN. Chromatographic purifications were carried out with preparative flash chromatogram Isolera One from Biotage using self-packed columns with silica gel 60 Å 230-400 mesh (Merck). Celite 545 0.02 – 0.1 mm (Merck) was used as a samplet filler.

Diffraction data were collected by the ω-scan technique, for **[Ir(μ-Cl)(bzq)$_2$]$_2$** at 130(1) K, on Rigaku SuperNova four-circle diffractometer with Atlas CCD detector and mirror-monochromated CuK_α radiation (λ=1.54178 Å), for **[Ir(μ-Cl)(5-Ph$_2$Nbzq)$_2$]$_2$** at room temperature and for **[Ir(ppy)$_2$Cl(ACN)]** and **[Ir(ppy)$_2$Cl(DMSO)]** at 100(1) K on Rigaku Xcalibur four-circle diffractometer with Eos CCD detector and graphite-monochromated MoK_α radiation (λ=0.71069 Å). The data were corrected for Lorentz-polarization as well as for absorption effects.[5] Precise unit-cell parameters were determined by a least-squares fit of reflections of the highest intensity, chosen from the whole experiment. The structures were solved with SHELXT[6] and refined with the full-matrix least-squares procedure on F^2 by SHELXL-2013.[7] All non-hydrogen atoms were refined anisotropically, all hydrogen atoms were placed in idealized positions and refined as 'riding model' with isotropic displacement parameters set at 1.2 (1.5 for methyl groups) times U_{eq} of appropriate carrier atoms. The crystals of dimeric complexes **[Ir(μ-Cl)(bzq)$_2$]$_2$** and **[Ir(μ-Cl)(5-Ph$_2$Nbzq)$_2$]$_2$** were generally of poor quality and numerous attempts to obtain better data were unsuccessful. Therefore, the overall quality indices are rather high, however the structures are appropriate for our goal – to confirm the structures of the products. Some doubts may be related to the positions of nitrogen atoms and possible disorder. In our model we assume that the nitrogen atoms are in trans positions with respect to central Ir ion (as is shown by vast majority of the similar structures found in the CSD[8]). Nevertheless, in the structure of **[Ir(μ-Cl)(5-Ph$_2$Nbzq)$_2$]$_2$** some constraints had to be applied in order to keep the correct geometry of rings; additionally the relatively large voids with diffused electron density have been found; as the attempts to model this density as solvent molecules gave no satisfactory results we decided to use the SQUEEZE procedure.[9]

Crystallographic data for the structural analysis has been deposited with the Cambridge Crystallographic Data Centre, Nos. CCDC 1895621 (**[Ir(μ-Cl)(bzq)$_2$]$_2$**), 1895622 (**[Ir(μ-Cl)(5-Ph$_2$Nbzq)$_2$]$_2$**), 1897304 (**[Ir(ppy)$_2$Cl(ACN)]**) and 1897305 (**[Ir(ppy)$_2$Cl(DMSO)]**). Copies of this information may be obtained free of charge from: The Director, CCDC, 12 Union Road, Cambridge, CB2 1EZ, UK. Fax: +44(1223)336-033, e-mail:deposit@ccdc.cam.ac.uk, or www: www.ccdc.cam.ac.uk.

Synthetic procedures and analytical data

General procedure for the optimization tests

A CEM microwave vial equipped with a magnetic stirrer was charged with 4 mL of water/2-methoxyethanol mixture, 65 mg (0.41 mmol) of 2-phenylpyridine, and 68 mg (0.187 mmol) of iridium(III) chloride hydrate (53 % iridium content). The reaction vessel was closed and placed in a microwave reactor or an oil bath and then heated for indicated time and temperature (max power 200 W in the case of microwave reactor). After that, the reaction mixture was cooled down to the room temperature, 1 mL of water was added and mixed. The supernatant was sucked off with a Hamilton syringe (flat-ended needle, the end of the tip placed close to the bottom of the vessel). Next, 1 mL of methanol was added, the suspension was mixed and the solution was sucked off in the same manner. This procedure was repeated two times more with 1 mL of methanol. If the precipitate was too fine to be filtered in this way, then the solid was centrifuged and washed four times with 1 mL of methanol. The solid residue was dried in an oven at 100 °C for 1 hour. After cooling back to room temperature, 5 mL of dichloromethane was added, and the mixture was stirred for 2 minutes. Then the mixture was filtered through syringe filter and washed twice with 1 mL of fresh solvent. The obtained solution was slowly evaporated in pre-weighted vial, giving a yellow solid.

General procedure for the preparation of 2-phenylpyridine- and benzo[*h*]quinoline-based iridium(III) chloro-bridged dimers

A CEM microwave vial equipped with a magnetic stirrer was charged with 1.0 mL of water, 3.0 mL of 2-methoxyethanol, 0.41 mmol of a ligand, and 68 mg (0.187 mmol) of iridium(III) chloride hydrate (53 % iridium content). The reaction vessel was closed and placed in a microwave reactor and then heated for 10 minutes at 150 °C (max power 200 W). After indicated time, the reaction mixture was cooled down to the room temperature, 1 mL of water was added and mixed. The supernatant was sucked off with a Hamilton syringe (flat-ended needle, the end of the tip placed close to the bottom of the vessel). Next, 1 mL of methanol was added, the suspension was mixed and the solution was sucked off in the same manner. This procedure was repeated two times more with 1 mL of methanol. If the precipitate was too fine to be filtered in this way, then the solid was centrifuged and washed four times with 1 mL of methanol. The solid residue was dried in an oven at 100 °C overnight.

[Ir(μ-Cl)(ppy)$_2$]$_2$

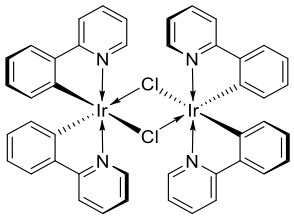

[Ir(-Cl)(ppy)$_2$]$_2$

Yellow solid (87.0 mg, 0.081 mmol). Yield: 87 %.

^{1}H NMR (300 MHz, DMSO-*d*$_6$) δ [ppm]: 9.80 (d, *J* = 5.8 Hz, 2H), 9.53 (d, *J* = 5.8 Hz, 2H), 8.29 – 8.21 (m, 2H), 8.21 – 8.14 (m, 2H), 8.09 (t, *J* = 8.0 Hz, 2H), 8.01 (t, *J* = 7.4 Hz, 2H), 7.78 (d, *J* = 7.6 Hz, 2H), 7.73 (d, *J* = 7.7 Hz, 2H), 7.57 (t, *J* = 6.5 Hz, 2H), 7.45 (t, *J* = 6.2 Hz, 2H), 6.95 – 6.80 (m, 4H), 6.76 (t, *J* = 7.4 Hz, 2H), 6.69 (t, *J* = 7.4 Hz, 2H), 6.25 (d, *J* = 7.7 Hz, 2H), 5.66 (d, *J* = 7.6 Hz, 2H).

ESI-HRMS: calculated for $[C_{22}H_{16}IrN_2]^+$ 501.0938, measured 501.0954.

Elemental analysis calculated (%) for $C_{44}H_{32}Cl_2Ir_2N_4$: C 49.29, H 3.01, N 5.23. Found: C 49.32, H 3.00, N 5.24.

[Ir(μ-Cl)(2,4-DiFppy)$_2$]$_2$

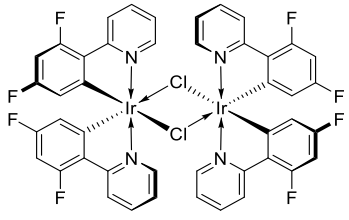

[Ir(-Cl)(2,4-diFppy)$_2$]$_2$

Yellow solid (106.9 mg, 0.088 mmol). Yield: 94 %.

Synthetic procedures and analytical data

^{1}H NMR (400 MHz, DMSO-d_6) δ [ppm]: 9.77 (dd, *J* = 5.9, 0.9 Hz, 2H), 9.55 (dd, *J* = 5.8, 0.9 Hz, 2H), 8.33 – 8.28 (m, 2H), 8.28 – 8.23 (m, 2H), 8.23 – 8.17 (m, 2H), 8.16 – 8.08 (m, 2H), 7.69 – 7.64 (m, 2H), 7.60 – 7.54 (m, 2H), 6.89 – 6.74 (m, 4H), 5.73 (dd, *J* = 8.6, 2.4 Hz, 2H), 5.07 (dd, *J* = 8.8, 2.4 Hz, 2H).

ESI-HRMS: calculated for $[C_{22}H_{12}F_4IrN_2]^+$ 573.0561, measured 573.0575.

Elemental analysis calculated (%) for $C_{44}H_{24}Cl_2F_8Ir_2N_4$: C 43.46, H 1.99, N 4.61. Found: C 43.48, H 2.00, N 4.59.

[Ir(μ-Cl)(bzq)$_2$]$_2$

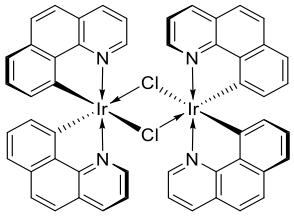

[Ir(-Cl)(bzq)$_2$]$_2$

Yellow solid (100.5 mg, 0.086 mmol). Yield: 92 %.

^{1}H NMR (300 MHz, DMSO-d_6) δ [ppm]: 10.20 (dd, *J* = 5.3, 1.2 Hz, 2H), 9.80 (dd, *J* = 5.2, 1.2 Hz, 2H), 8.73 (dd, *J* = 8.0, 0.9 Hz, 2H), 8.66 (dd, *J* = 8.0, 0.9 Hz, 2H), 8.01 (dd, *J* = 8.1, 5.4 Hz, 2H), 7.94 – 7.85 (m, 10H), 7.42 (d, *J* = 7.7 Hz, 2H), 7.36 (d, *J* = 7.7 Hz, 2H), 7.03 (t, *J* = 7.7 Hz, 2H), 6.94 (t, *J* = 7.6 Hz, 2H), 6.27 (d, *J* = 7.1 Hz, 2H), 5.62 (d, *J* = 7.2 Hz, 2H).

ESI-HRMS: calculated for $[C_{26}H_{16}IrN_2]^+$ 549.0938, measured 549.0935 (error 7.4 ppm).

Elemental analysis calculated (%) for $C_{52}H_{32}Cl_2Ir_2N_4$: C 53.46, H 2.76, N 4.80. Found: C 53.44, H 2.75, N 4.79.

[Ir(μ-Cl)(5-F$_5$C$_6$bzq)$_2$]$_2$

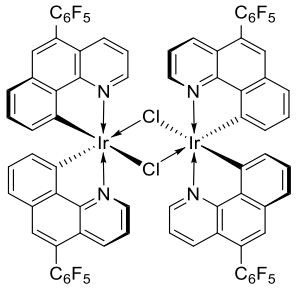

[Ir(-Cl)(5-F$_5$C$_6$bzq)$_2$]$_2$

Orange solid (143.9 mg, 0.078 mmol). Yield: 84 %.

^{1}H NMR (300 MHz, DMSO-d_6) δ [ppm]: 10.31 (d, *J* = 5.3 Hz, 2H), 9.90 (d, *J* = 5.2 Hz, 2H), 8.47 (d, *J* = 8.1 Hz, 2H), 8.40 (d, *J* = 8.0 Hz, 2H), 8.13 (s, 2H), 8.09 (s, 2H), 8.04 (dd, *J* = 8.3, 5.5 Hz, 2H), 7.96 (dd, *J* = 8.3, 5.6 Hz, 2H), 7.54 (d, *J* = 7.9 Hz, 2H), 7.49 (d, *J* = 7.8 Hz, 2H), 7.17 (t, *J* = 7.6 Hz, 2H), 7.07 (t, *J* = 7.6 Hz, 2H), 6.47 (d, *J* = 7.3 Hz, 2H), 5.75 (d, *J* = 7.3 Hz, 2H).

ESI-HRMS: calculated for $[C_{38}H_{14}F_{10}IrN_2]^+$ 881.0623, measured 881.0611.

Elemental analysis calculated (%) for $C_{76}H_{28}Cl_2F_{20}Ir_2N_4$: C 49.82, H 1.54, N 3.06. Found: C 49.84, H 1.55, N 3.08.

Synthetic procedures and analytical data

[Ir(μ-Cl)(5-MeObzq)$_2$]$_2$

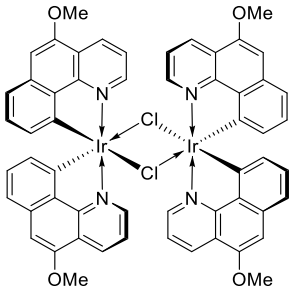

[Ir(m-Cl)(5-MeObzq)$_2$]$_2$

Orange solid (96.4 mg, 0.075 mmol). Yield: 80 %.

^{1}H NMR (300 MHz, DMSO-*d*$_6$) δ [ppm]: 10.19 (dd, *J* = 5.5, 1.2 Hz, 2H), 9.79 (dd, *J* = 5.5, 1.2 Hz, 2H), 8.76 (dd, *J* = 8.2, 1.2 Hz, 2H), 8.71 (dd, *J* = 8.2, 1.2 Hz, 2H), 7.98 (dd, *J* = 8.2, 5.5 Hz, 2H), 7.87 (dd, *J* = 8.2, 5.6 Hz, 2H), 7.31 – 7.19 (m, 8H), 6.93 (t, *J* = 7.6 Hz, 2H), 6.84 (t, *J* = 7.6 Hz, 2H), 6.08 (d, *J* = 6.8 Hz, 2H), 5.45 (d, *J* = 6.7 Hz, 2H), 4.10 (s, 6H), 4.08 (s, 6H).

ESI-HRMS: calculated for $[C_{28}H_{20}IrN_2O_2]^+$ 609.1150, measured 609.1300.

Elemental analysis calculated (%) for $C_{56}H_{40}Cl_2Ir_2N_4O_4$: C 52.21, H 3.13, N 4.35. Found: C 52.25, H 3.15, N 4.33.

[Ir(μ-Cl)(5-Brbzq)$_2$]$_2$

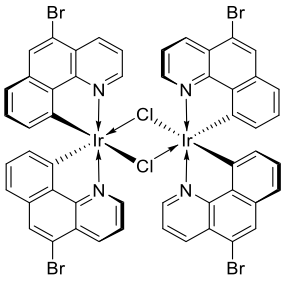

[Ir(-Cl)(5-Brbzq)$_2$]$_2$

Orange solid (133.2 mg, 0.090 mmol). Yield: 96 %.

^{1}H NMR (300 MHz, DMSO-*d*$_6$) δ [ppm]: 10.29 (d, *J* = 5.4 Hz, 2H), 9.87 (d, *J* = 5.3 Hz, 2H), 8.82 – 8.74 (m, 4H), 8.40 (s, 2H), 8.36 (s, 2H), 8.13 (dd, *J* = 8.3, 5.4 Hz, 2H), 8.05 (dd, *J* = 8.2, 5.6 Hz, 2H), 7.47 – 7.42 (m, 2H), 7.42 – 7.36 (m, 2H), 7.06 (t, *J* = 7.5 Hz, 2H), 6.98 (t, *J* = 7.5 Hz, 2H), 6.34 (d, *J* = 7.2 Hz, 2H), 5.64 (d, *J* = 7.1 Hz, 2H).

ESI-HRMS: calculated for $[C_{26}H_{14}Br_2IrN_2]^+$ 706.9120, measured 706.9117.

Elemental analysis calculated (%) for $C_{52}H_{28}Br_4Cl_2Ir_2N_4$: C 42.09, H 1.90, N 3.78. Found: C 42.07, H 1.90, N 3.81.

[Ir(μ-Cl)(5-Ph$_2$Nbzq)$_2$]$_2$

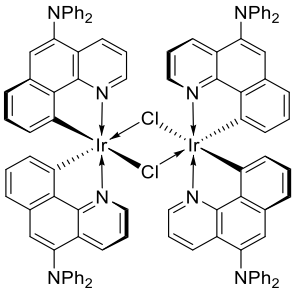

[Ir(-Cl)(5-Ph$_2$Nbzq)$_2$]$_2$

Orange solid (141.0 mg, 0.077 mmol). Yield: 82 %.

Synthetic procedures and analytical data

^{1}H NMR (300 MHz, DMSO-d_6) δ [ppm]: 10.19 (d, *J* = 5.1 Hz, 2H), 9.79 (d, *J* = 5.1 Hz, 2H), 8.45 – 8.34 (m, 4H), 7.88 (dd, *J* = 8.3, 5.5 Hz, 2H), 7.80 (dd, *J* = 8.2, 5.6 Hz, 2H), 7.73 (d, *J* = 4.3 Hz, 4H), 7.40 – 7.23 (m, 20H), 7.12 – 6.91 (m, 28H), 6.32 (d, *J* = 7.1 Hz, 2H), 5.64 (d, *J* = 7.2 Hz, 2H).

ESI-HRMS: calculated for $[C_{50}H_{34}IrN_4]^+$ 883.2411, measured 883.2421.

Elemental analysis calculated (%) for $C_{100}H_{68}Cl_2Ir_2N_8$: C 65.38, H 3.73, N 6.10. Found: C 65.43, H 3.71, N 6.08.

[Ir(μ-Cl)(5-(Ph$_2$NC$_6$H$_4$)bzq)$_2$]$_2$

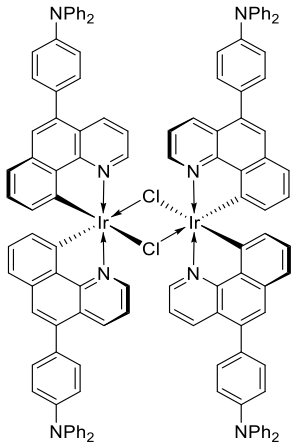

[Ir(-Cl)(5-(Ph$_2$NC$_6$H$_4$)bzq)$_2$]$_2$

This product was additionally washed two times with 1 mL of diethyl ether and two times with 1 mL of hexane. Yellow solid (180.2 mg, 0.084 mmol). Yield: 90 %.

^{1}H NMR (300 MHz, DMSO-d_6) δ [ppm]: 10.27 (dd, *J* = 5.4, 0.8 Hz, 2H), 9.87 (dd, *J* = 5.5, 0.9 Hz, 2H), 8.62 (d, *J* = 8.3 Hz, 2H), 8.54 (d, *J* = 8.2 Hz, 2H), 8.01 (dd, *J* = 8.4, 5.5 Hz, 2H), 7.94 – 7.86 (m, 4H), 7.84 (s, 2H), 7.60 (dd, *J* = 10.8, 8.6 Hz, 8H), 7.46 (d, *J* = 7.8 Hz, 2H), 7.42 – 7.34 (m, 18H), 7.20 – 7.04 (m, 34H), 6.97 (t, *J* = 7.6 Hz, 2H), 6.35 (d, *J* = 7.4 Hz, 2H), 5.69 (d, *J* = 7.2 Hz, 2H).

ESI-HRMS: calculated for $[C_{62}H_{42}IrN_4]^+$ 1035.3038, measured 1035.3043.

Elemental analysis calculated (%) for $C_{124}H_{84}Cl_2Ir_2N_8$: C 69.55, H 3.95, N 5.23. Found: C 69.58, H 3.97, N 5.20.

[Ir(μ-Cl)(5-PhObzq)$_2$]$_2$

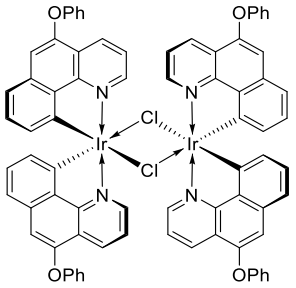

[Ir(-Cl)(5-PhObzq)$_2$]$_2$

Orange solid (125.0 mg, 0.081 mmol). Yield: 87 %.

^{1}H NMR (300 MHz, DMSO-d_6) δ [ppm]: 10.27 (dd, *J* = 5.5, 1.2 Hz, 2H), 9.87 (dd, *J* = 5.5, 1.3 Hz, 2H), 8.84 (dd, *J* = 8.2, 1.3 Hz, 2H), 8.76 (dd, *J* = 8.2, 1.2 Hz, 2H), 8.05 (dd, *J* = 8.2, 5.5 Hz, 2H), 7.94 (dd, *J* = 8.2, 5.6 Hz, 2H), 7.55 – 7.45 (m, 8H), 7.32 – 7.21 (m, 16H), 7.18 (s, 2H), 7.17 (s, 2H), 6.97 (t, *J* = 7.6 Hz, 2H), 6.90 (t, *J* = 7.6 Hz, 2H), 6.24 (dd, *J* = 7.3, 0.6 Hz, 2H), 5.60 (dd, *J* = 7.3, 0.7 Hz, 2H).

ESI-HRMS: calculated for $[C_{38}H_{24}IrN_2O_2]^+$ 733.1464, measured 733.1469.

Elemental analysis calculated (%) for $C_{76}H_{48}Cl_2Ir_2N_4O_4$: C 59.41, H 3.15, N 3.65. Found: C 59.43, H 3.13, N 3.67.

Synthetic procedures and analytical data

[Ir(μ-Cl)(5-Me$_2$Nbzq)$_2$]$_2$

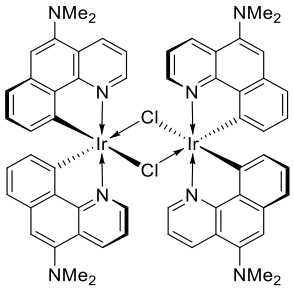

[Ir(-Cl)(5-Me$_2$Nbzq)$_2$]$_2$

A 25 mL Schlenk flask was loaded with 69 mg (0.104 mmol) of **[Ir(μ-Cl)(COD)]$_2$,** 92 mg (0.414 mmol) **5-Me$_2$NbzqH**, and 3 mL of 2-methoxyethanol. Subsequently, the flask was evacuated and backfilled with argon three times. The reaction mixture was stirred at 120 °C in on oil bath for 6 h. After indicated time, the solvent was evaporated under reduced pressure. The residue was taken up in 3 mL of methanol and centrifuged. The precipitate was washed three times with 1 mL of methanol, three times with 1 mL of diethyl ether and two times with 1 ml of hexane. The product was dried under reduced pressure.

Orange solid (119.9 mg, 0.089 mmol). Yield: 86 %.

^{1}H NMR (300 MHz, DMSO-*d$_6$*) δ [ppm]: 10.18 (dd, *J* = 5.5, 0.8 Hz, 2H), 9.78 (dd, *J* = 5.4, 0.8 Hz, 2H), 8.75 (d, *J* = 8.2 Hz, 2H), 8.70 (d, *J* = 8.2 Hz, 2H), 7.97 (dd, *J* = 8.3, 5.5 Hz, 2H), 7.87 (dd, *J* = 8.3, 5.5 Hz, 2H), 7.34 (s, 4H), 7.27 (d, *J* = 7.8 Hz, 2H), 7.23 (d, *J* = 7.7 Hz, 2H), 6.93 (t, *J* = 7.6 Hz, 2H), 6.85 (t, *J* = 7.6 Hz, 2H), 6.12 (d, *J* = 7.2 Hz, 2H), 5.49 (d, *J* = 7.1 Hz, 2H), 2.96 (s, 12H), 2.94 (s, 12H).

ESI-HRMS: calculated for $[C_{30}H_{26}IrN_4]^+$ 635.1782, measured 635.1782.

Elemental analysis calculated (%) for $C_{60}H_{52}Cl_2Ir_2N_8$: C 53.76, H 3.91, N 8.36. Found: C 53.78, H 3.92, N 8.38.

General procedure for the preparation of 2-phenoxypyridine derivatives

A two-neck round-bottom flask equipped with a reflux condenser, magnetic stirrer and inert gas adapter was flushed with argon and filled with 30 mL of anhydrous *N,N*-dimethylformamide. Next, 10 mmol of 2-fluoro-4-methylpyridine (synthesis of **PhOPyMeH**) or 2-fluoropyridine (synthesis of **F$_3$CPhOPyH**), 25 mmol of phenol (synthesis of **PhOPyMeH**) or 4-trifluoromethylphenol (synthesis of **F$_3$CPhOPyH**), caesium carbonate (8.15 g, 25 mmol) and copper(I) chloride (99 mg, 1.0 mmol) were placed into the reaction vessel. Then, it was closed, placed in an oil bath and heated at 140 °C under vigorous stirring. After 20 h, all volatiles were removed under reduced pressure and the residue was extracted twice with 50 mL of hexane / dichloromethane (1:1 v/v). Combined extracts were washed thoroughly with 50 mL of 1 M aqueous NaOH, water, and brine. The resulting solution was dried over anhydrous sodium sulphate, concentrated on a rotary evaporator and dried *in vacuo*, giving pure product.

4-methyl-2-phenoxypyridine **(PhOPyMeH)**

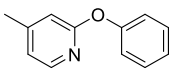

PhOPyMeH

Off-white oil (1.46g, 7.9 mmol). Yield: 79%.

^{1}H NMR (300 MHz, CD_2Cl_2) δ [ppm]: 8.09 (d, 1H, *J*=5.1 Hz), 7.41 (t, 2H, *J*=7.8 Hz), 7.18 (m, 3H), 6.84 (d, 1H, *J*=5.1 Hz), 6.73 (s, 1H), 2.35 (s, 3H).

^{13}C NMR (75 MHz, CD_2Cl_2) δ [ppm]: 164.08, 154.40, 150.99, 147.38, 129.69, 124.54, 121.15, 119.94, 111.80, 21.04.

GCMS (EI, 70 eV), m/z (rel. abundance, %): 184 (100), 185 (85), 156 (60), 65 (24), 157 (17), 51 (11), 186 (10).

Elemental analysis calculated (%) for $C_{12}H_{11}NO$: C 77.81, H 5.99, N 7.56. Found: C 77.85, H 6.00, N 7.58.

Synthetic procedures and analytical data

***2-(4-(trifluoromethyl))phenoxypyridine* (F_3CPhOPyH)**

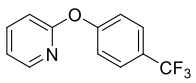

F_3CPhOPyH

White crystalline solid (1.05 g, 4.4 mmol). Yield: 44%.

^{1}H NMR (300 MHz, $CDCl_3$) δ [ppm]: 8.21 (ddd, 1H, *J*=4.9, 1.9, 0.6 Hz), 7.74 (ddd, 1H, *J*=8.3, 7.3, 2.0 Hz), 7.66 (d, 2H, *J*=8.4 Hz), 7.24 (d, 2H, *J*=8.4 Hz), 7.06 (ddd, 1H, *J*=7.2, 5.0, 0.9 Hz), 6.99 (dt, 1H, *J*=8.3, 0.8 Hz).

^{13}C NMR (75 MHz, $CDCl_3$) δ [ppm]: 162.95, 157.09, 147.86, 139.94, 127.15 (q, *J*=3.8 Hz), 126.44, 121.22, 119.45, 112.39.

GCMS (EI, 70 eV), m/z (rel. abundance, %): 238 (100), 239 (97), 211 (50), 78 (37), 51 (23), 115 (20), 240 (12), 220 (10).

Elemental analysis calculated (%) for $C_{12}H_8F_3NO$: C 60.26, H 3.37, N 5.86. Found: C 60.30, H 3.39, N 5.89.

General procedure for the preparation of 2-phenoxypyridine-based *C,N*-cyclometalated iridium(III) chloro-bridged dimers

A CEM microwave vial equipped with a magnetic stirrer was charged with 1.1 mL of water, 3.3 mL of 2-methoxyethanol, 0.44 mmol of a ligand, and 75 mg (0.21 mmol) of iridium(III) chloride hydrate (53 % iridium content). The mixture was degassed under vacuum and the reactor was filled with argon and quickly closed. The reaction vessel was placed in a microwave reactor and then heated for 10 minutes at 100 °C (max power 200 W). After indicated time, the reaction mixture was cooled down to the room temperature and the product was precipitated by addition of water. Fine suspension was centrifuged, a supernatant was discarded, and the precipitate was rinsed with 2 mL of 2-propanol and subsequently 2 mL of pentane. The product was dried in an oven at 70 °C overnight.

[Ir(μ-Cl)(PhOPyMe)$_2$]$_2$

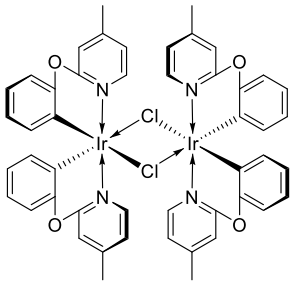

[Ir(-Cl)(PhOPyMe)$_2$]$_2$

Pale yellow dusty solid (108.0 mg, 0.091 mmol). Yield: 88 %.

^{1}H NMR (300 MHz, DMSO-d_6) δ [ppm]: 8.68 (d, *J* = 6.3 Hz, 2H), 8.23 (d, *J* = 6.2 Hz, 2H), 7.33 (s, 2H), 7.28 (s, 2H), 7.10 (d, *J* = 6.1 Hz, 4H), 6.98 – 6.76 (m, 8H), 6.59 – 6.45 (m, 4H), 5.99 (d, *J* = 7.5 Hz, 2H), 5.65 (d, *J* = 7.5 Hz, 2H), 2.44 (s, 12H).

ESI-HRMS: calculated for $[C_{24}H_{20}IrN_2O_2]^+$ 561.1149, measured 561.1160.

Elemental analysis calculated (%) for $C_{48}H_{40}Cl_2Ir_2N_4O_4$: C 48.36, H 3.38, N 4.70. Found: C 48.40, H 3.39, N 4.69.

[Ir(μ-Cl)(F$_3$CPhOPy)$_2$]$_2$

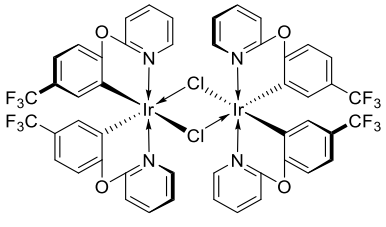

[Ir(-Cl)(F$_3$CPhOPy)$_2$]$_2$

Synthetic procedures and analytical data

Pale yellow dusty solid (92.8 mg, 0.066 mmol). Yield: 64 %.

^{1}H NMR (300 MHz, $CDCl_3$) δ [ppm]: 8.26 – 8.11 (m, 4H), 7.68 – 7.53 (m, 4H), 7.14 (d, *J* = 8.2 Hz, 4H), 7.04 (d, *J* = 8.3 Hz, 4H), 6.97 (d, *J* = 8.3 Hz, 4H), 6.55 – 6.44 (m, 4H), 5.62 (s, 4H).

ESI-HRMS: calculated for $[C_{24}H_{14}F_6IrN_2O_2]^+$ 669.0584, measured 669.0595.

Elemental analysis calculated (%) for $C_{48}H_{28}Cl_2F_{12}Ir_2N_4O_4$: C 40.94, H 2.00, N 3.98. Found: C 40.96, H 2.01, N 4.00.

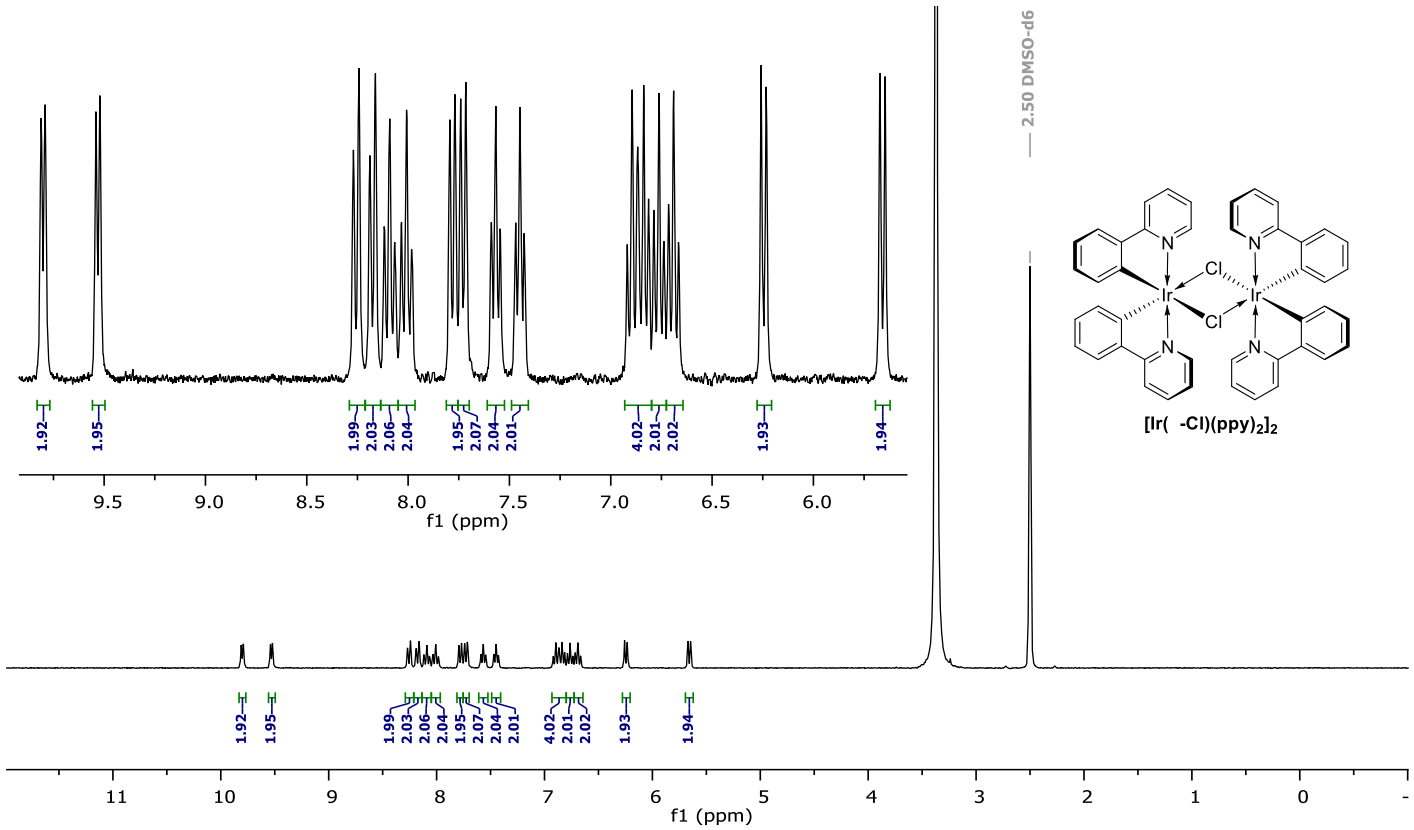

Figure S1. *[1]H NMR (300 MHz, DMSO, 298 K) spectrum of* ***[Ir(μ-Cl)(ppy)$_2$]$_2$***

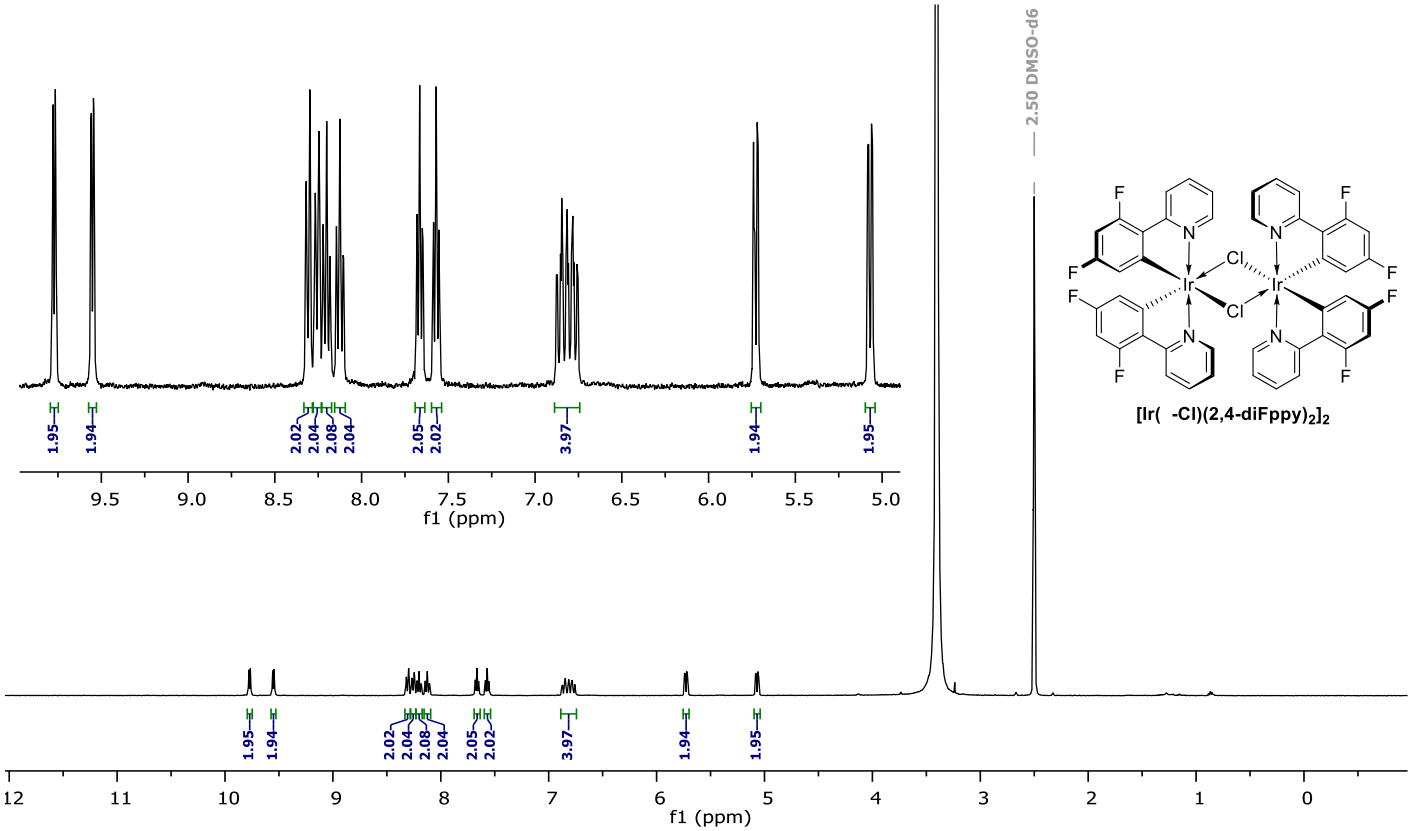

Figure S2. *[1]H NMR (400 MHz, DMSO, 298 K) spectrum of* ***[Ir(μ-Cl)(2,4-diFppy)$_2$]$_2$***

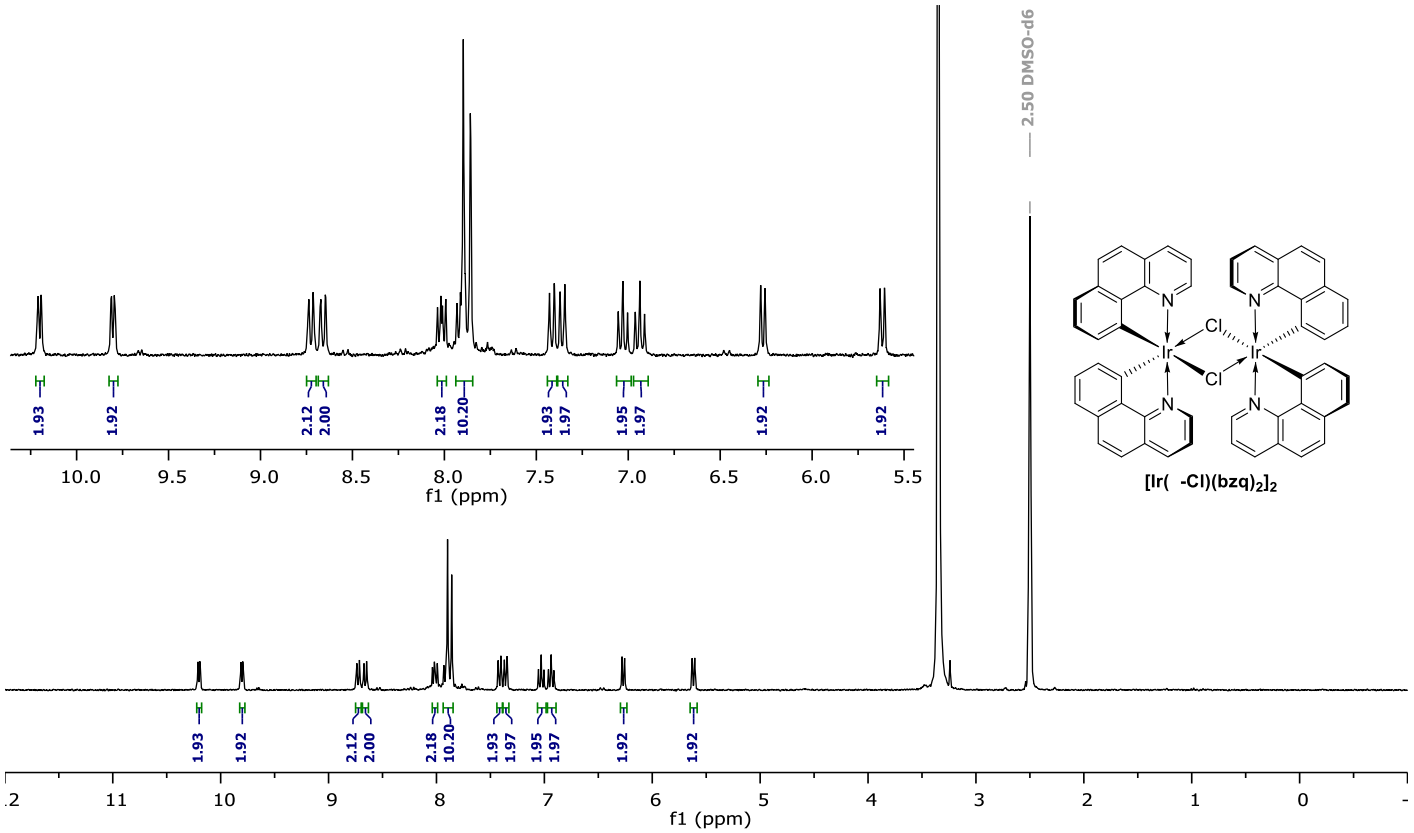

Figure S3. *^{1}H NMR (300 MHz, DMSO, 298 K) spectrum of* ***[Ir(μ-Cl)(bzq)$_2$]$_2$***

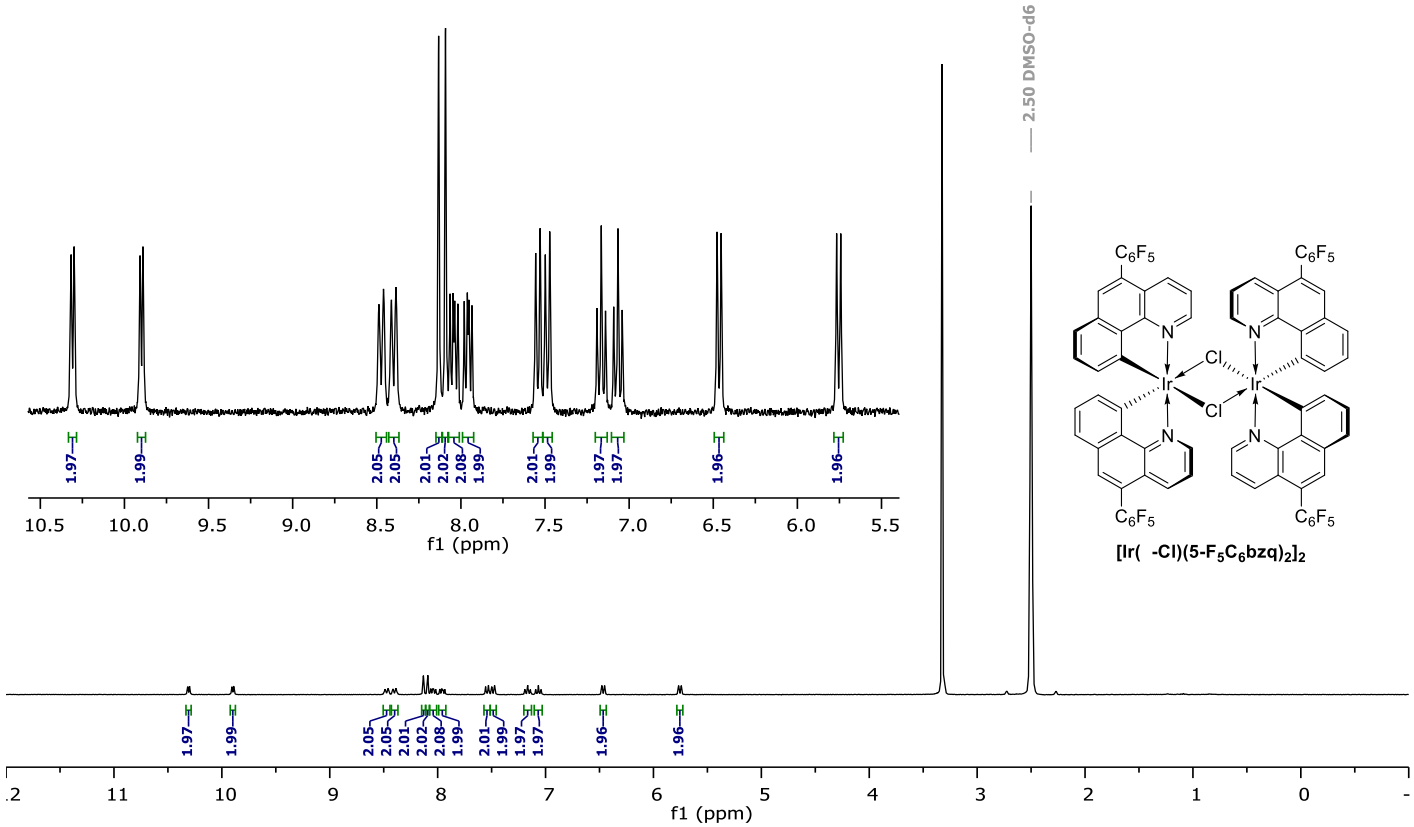

Figure S4. *^{1}H NMR (300 MHz, DMSO, 298 K) spectrum of* ***[Ir(μ-Cl)(5-F$_5$C$_6$bzq)$_2$]$_2$***

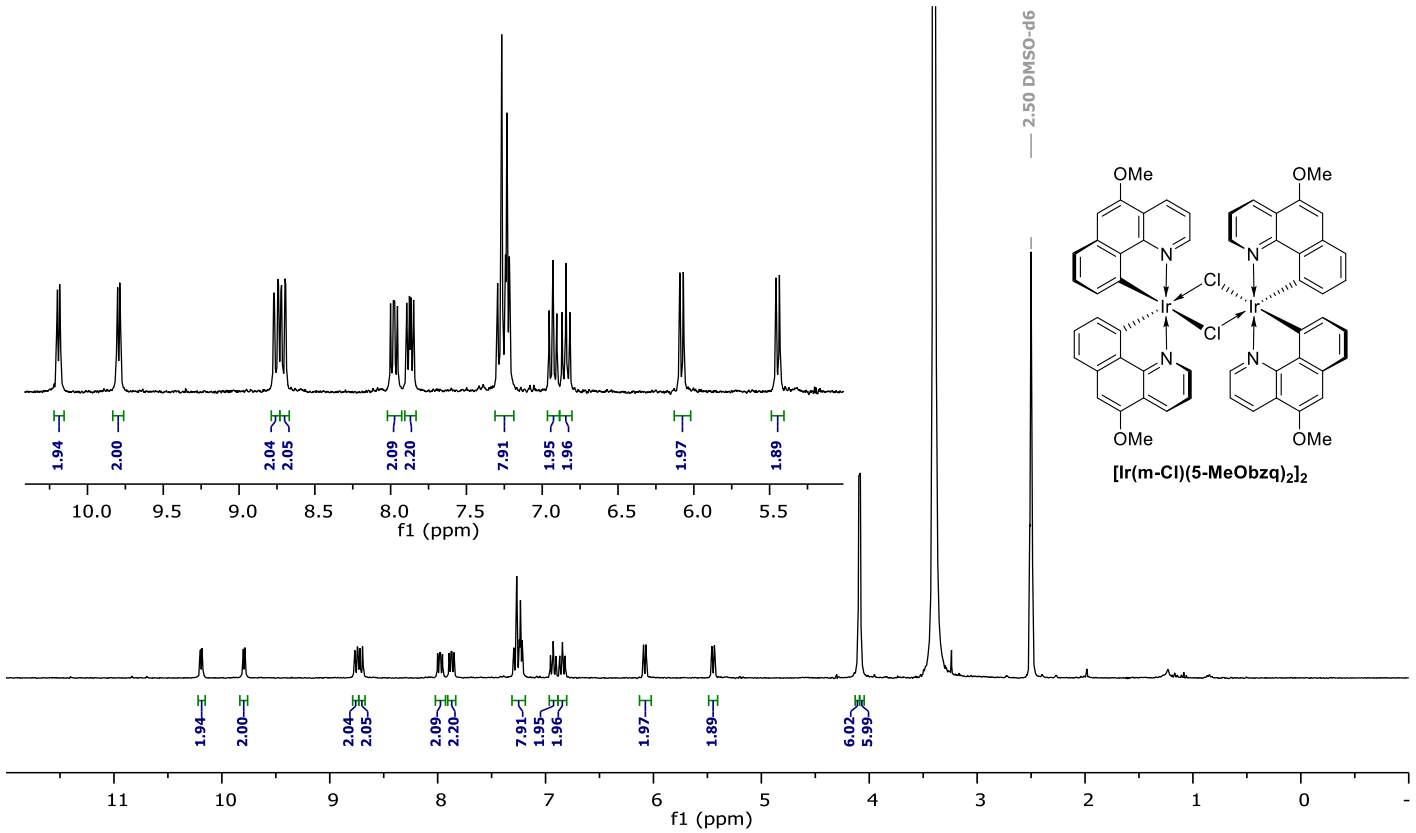

Figure S5. *[1]H NMR (300 MHz, DMSO, 298 K) spectrum of* ***[Ir(μ-Cl)(5-MeObzq)2]2***

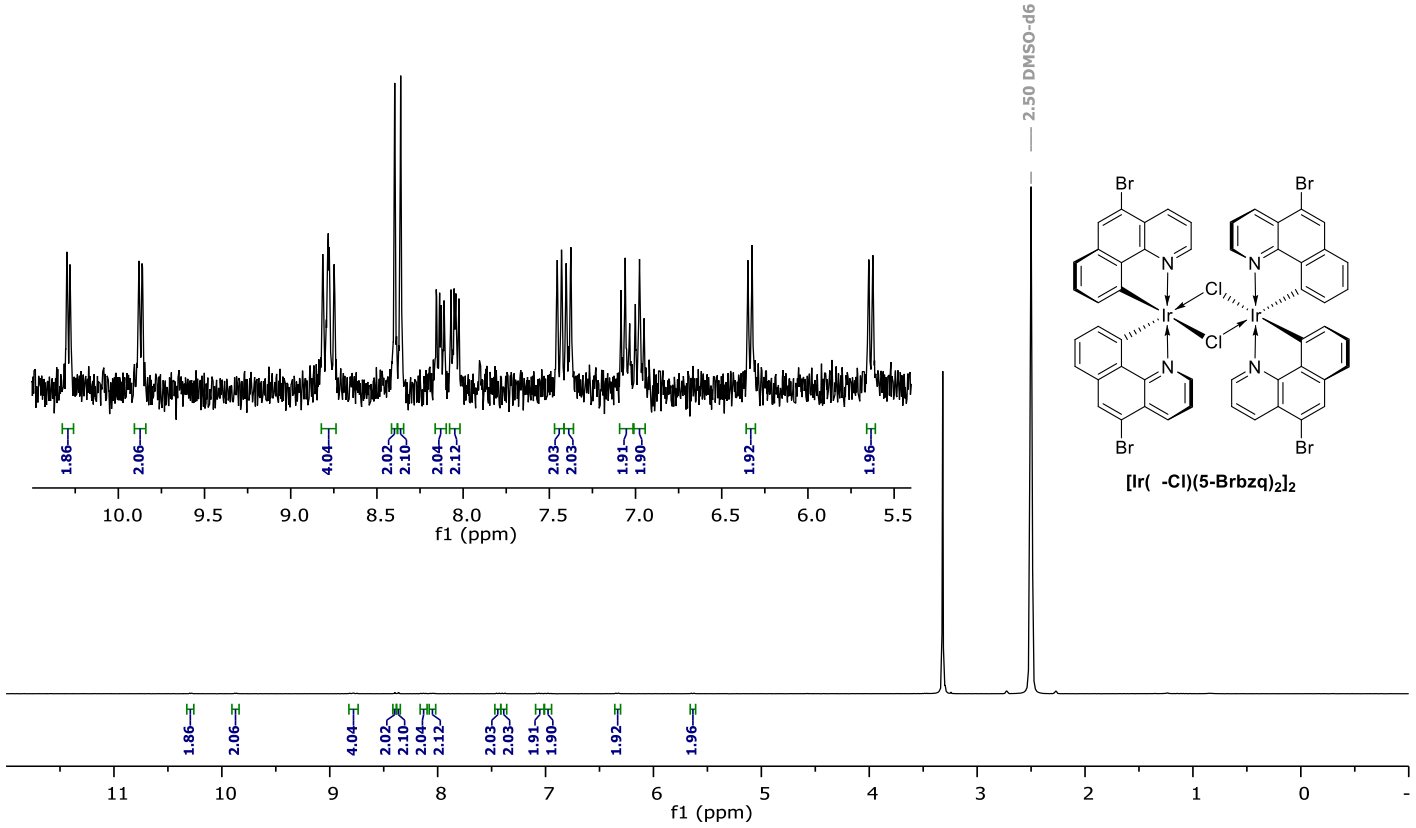

Figure S6. *[1]H NMR (300 MHz, DMSO, 298 K) spectrum of* ***[Ir(μ-Cl)(5-Brbzq)2]2***

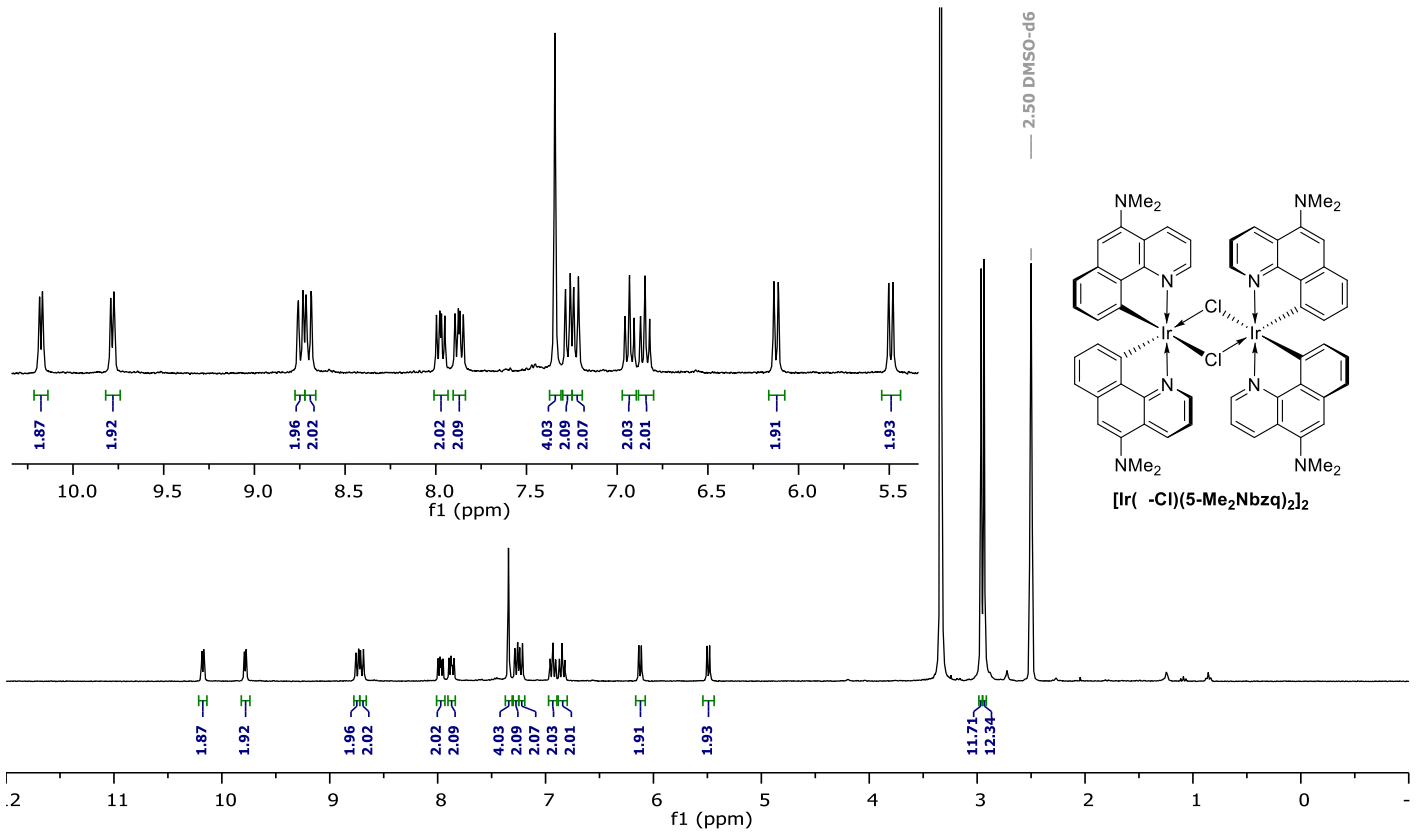

Figure S7. *^{1}H NMR (300 MHz, DMSO, 298 K) spectrum of* ***[Ir(μ-Cl)(5-Me$_2$Nbzq)$_2$]$_2$***

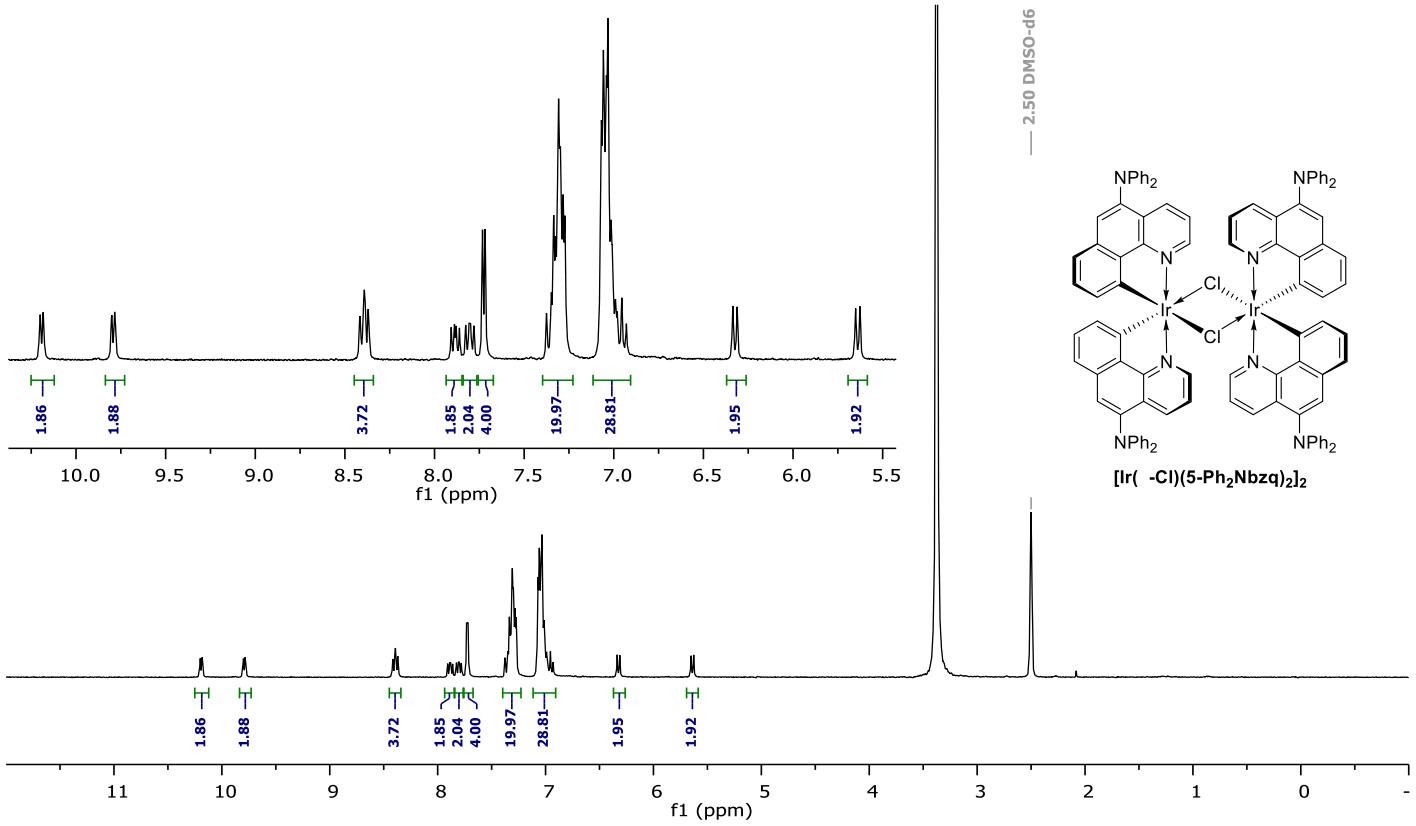

Figure S8. *^{1}H NMR (300 MHz, DMSO, 298 K) spectrum of* ***[Ir(μ-Cl)(5-Ph$_2$Nbzq)$_2$]$_2$***

^{1}H and ^{13}C NMR spectra

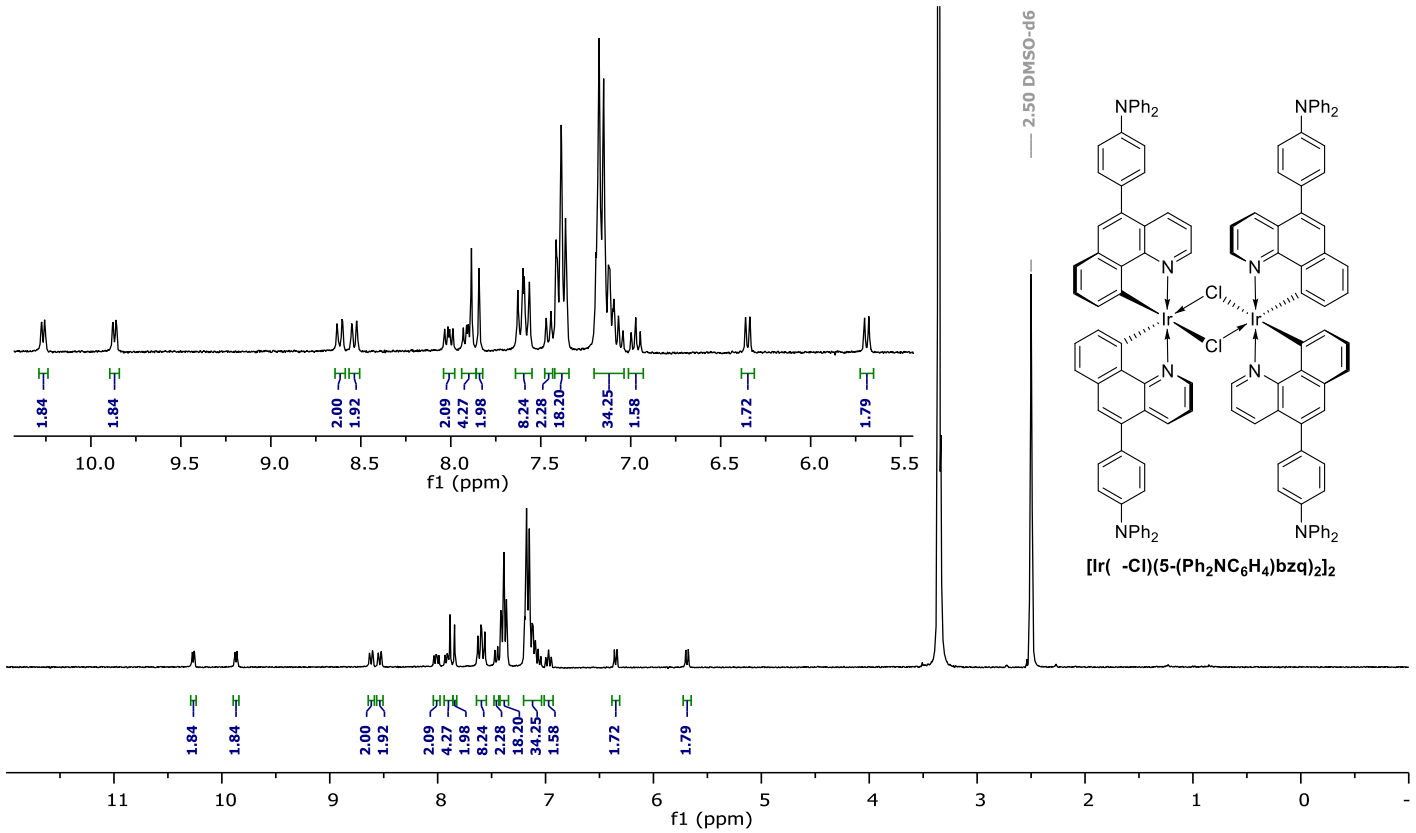

Figure S9. *^{1}H NMR (300 MHz, DMSO, 298 K) spectrum of* ***[Ir(μ-Cl)(5-(Ph$_2$NC$_6$H$_4$)bzq)$_2$]$_2$***

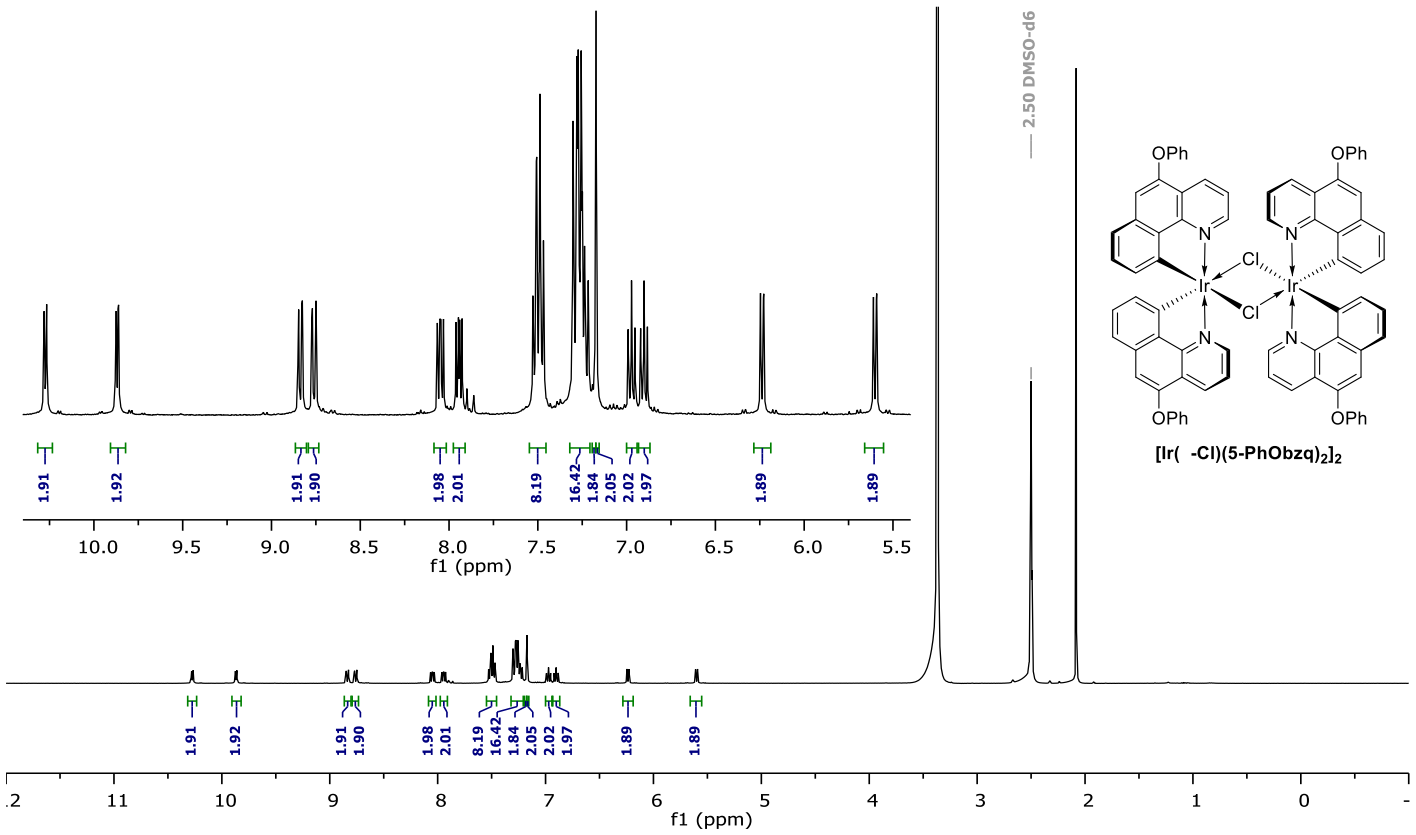

Figure S10. *^{1}H NMR (400 MHz, DMSO, 298 K) spectrum of* ***[Ir(μ-Cl)(5-PhObzq)$_2$]$_2$***

^{1}H and ^{13}C NMR spectra

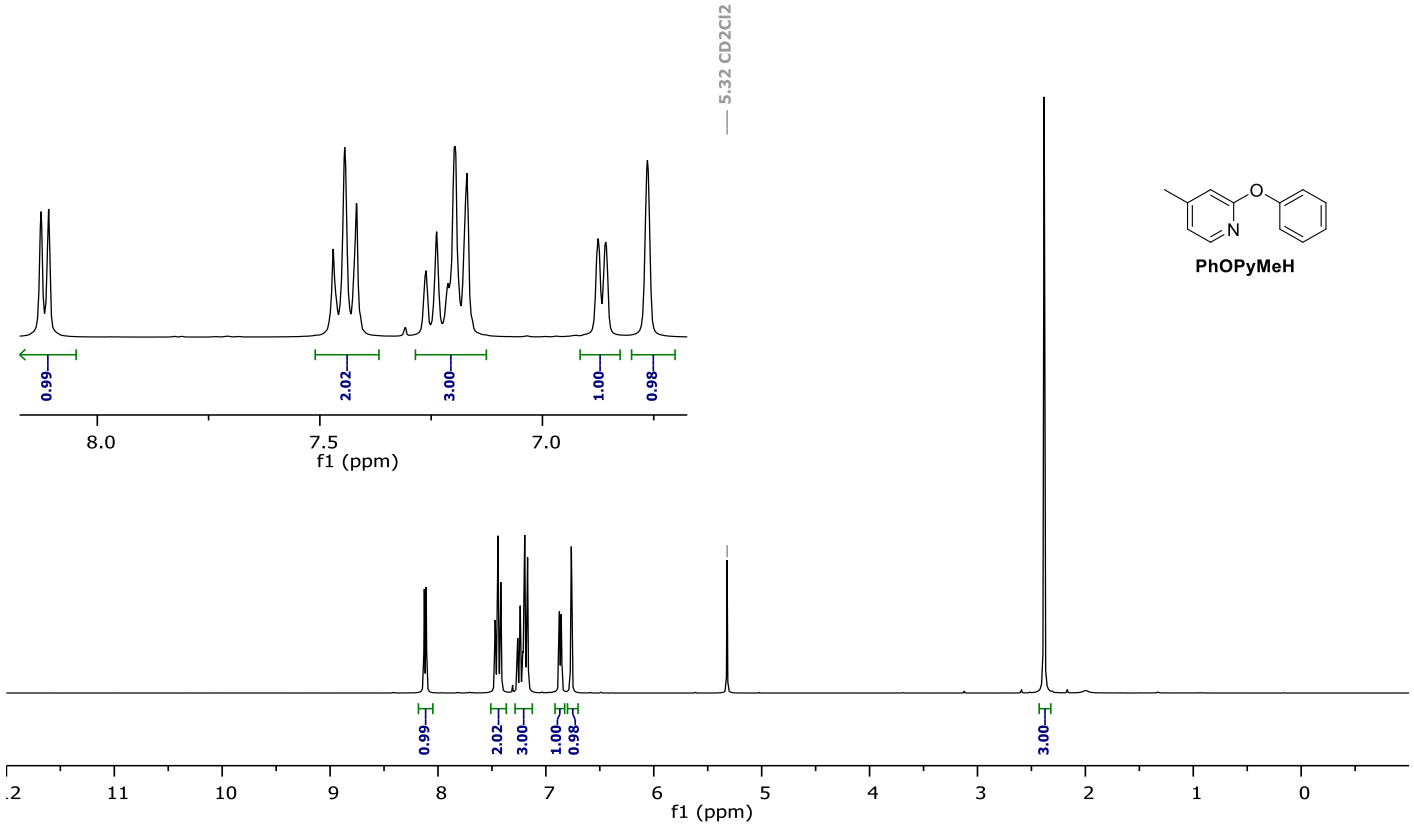

Figure S11. *^{1}H NMR (300 MHz, CD_2Cl_2, 298 K) spectrum of* ***PhOPyMeH***

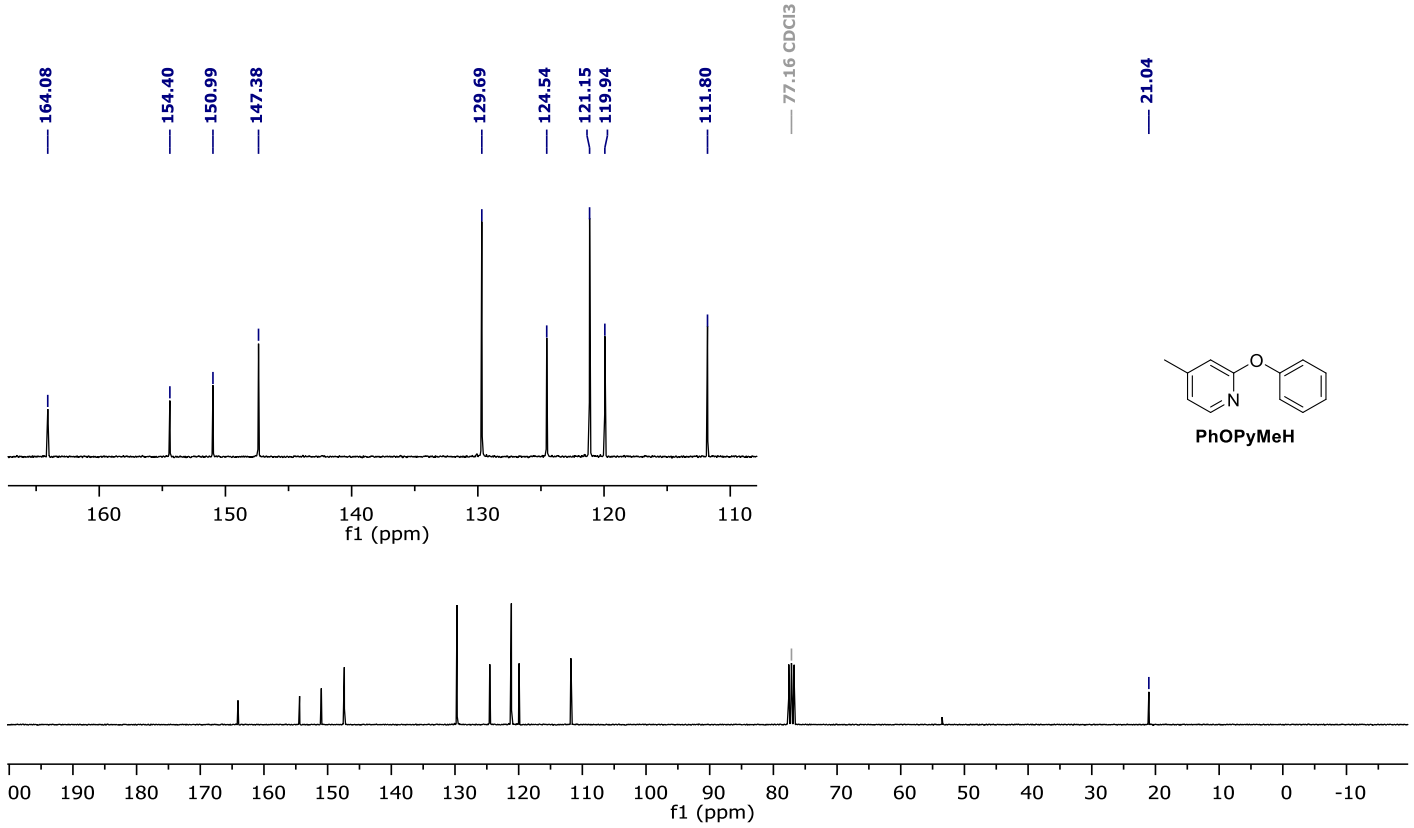

Figure S12. *^{13}C NMR (75 MHz, $CDCl_3$, 298 K) spectrum of* ***PhOPyMeH***

^{1}H and ^{13}C NMR spectra

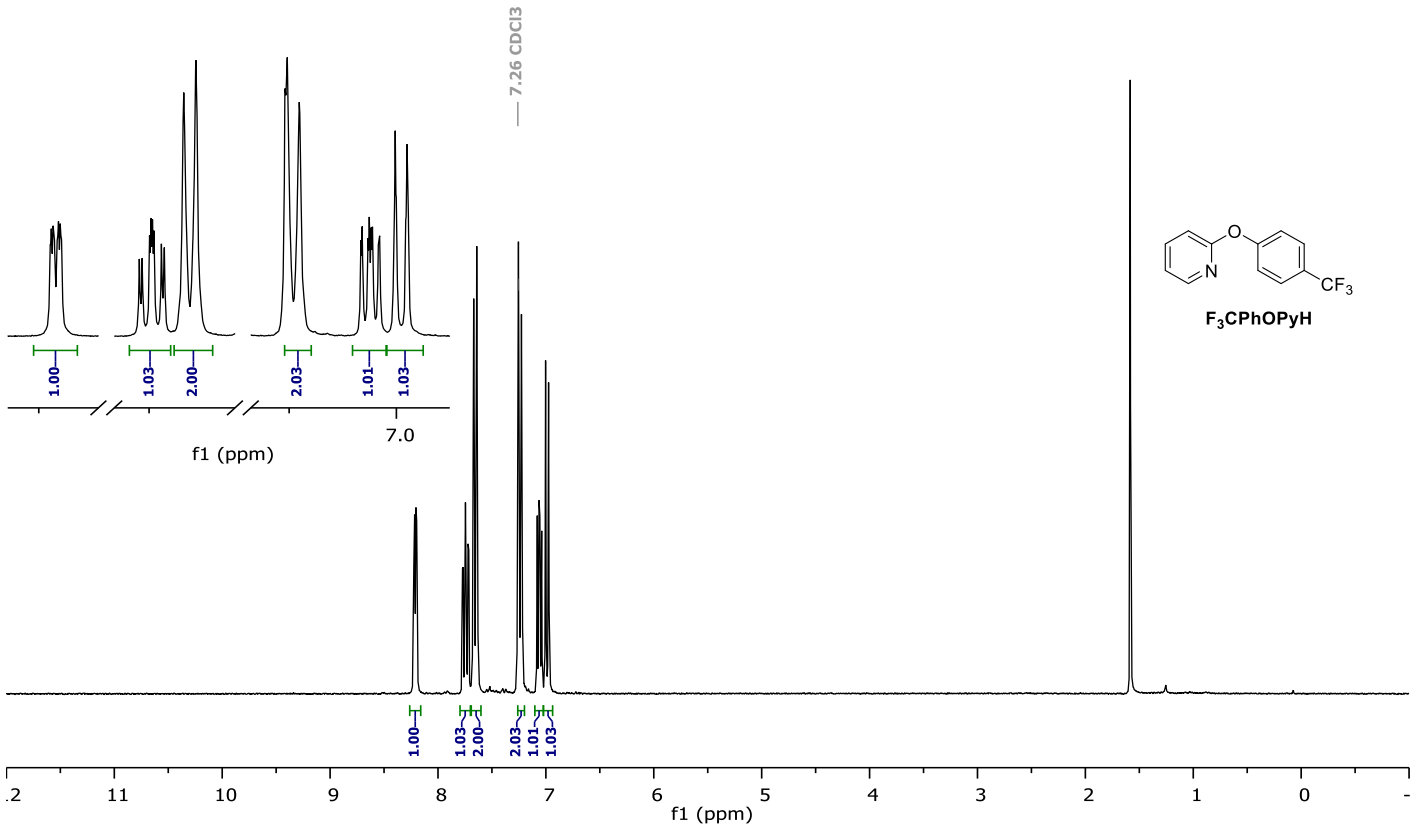

Figure S13. *^{1}H NMR (300 MHz, $CDCl_3$, 298 K) spectrum of* ***F_3CPhOPyH***

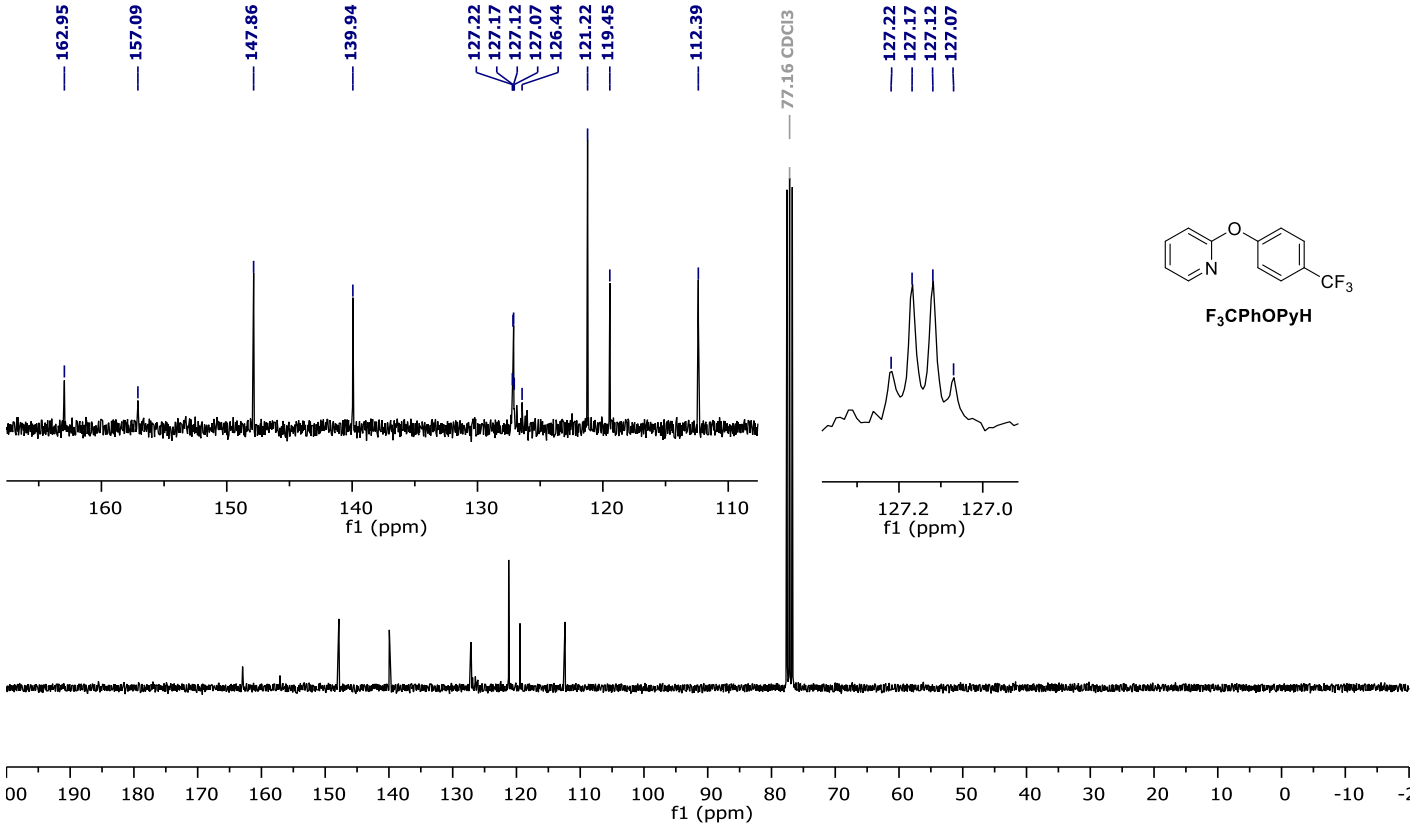

Figure S14. *^{13}C NMR (75 MHz, $CDCl_3$, 298 K) spectrum of* ***F_3CPhOPyH***

^{1}H and ^{13}C NMR spectra

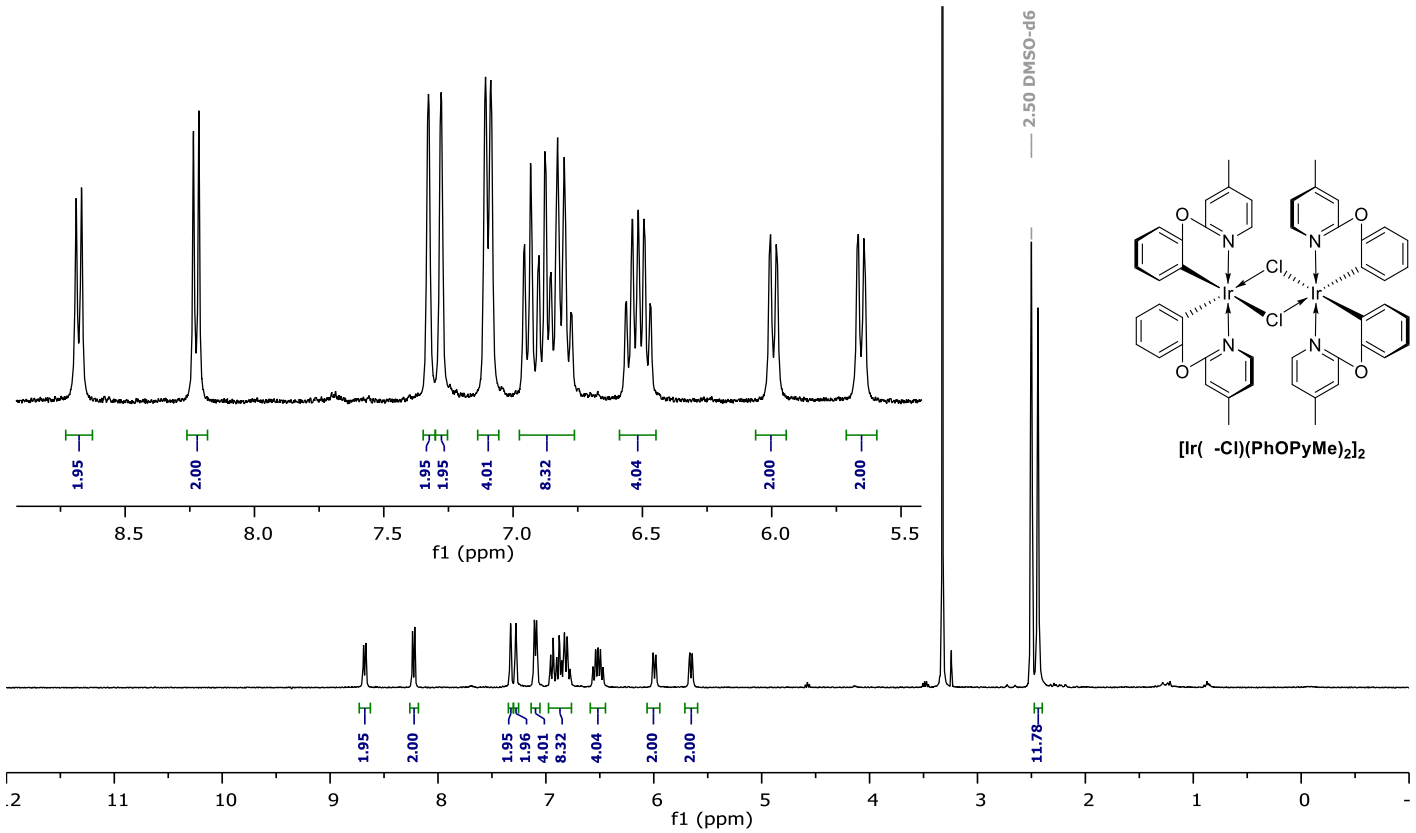

Figure S15. *^{1}H NMR (300 MHz, DMSO, 298 K) spectrum of* ***[Ir(μ-Cl)(PhOPyMe)$_2$]$_2$***

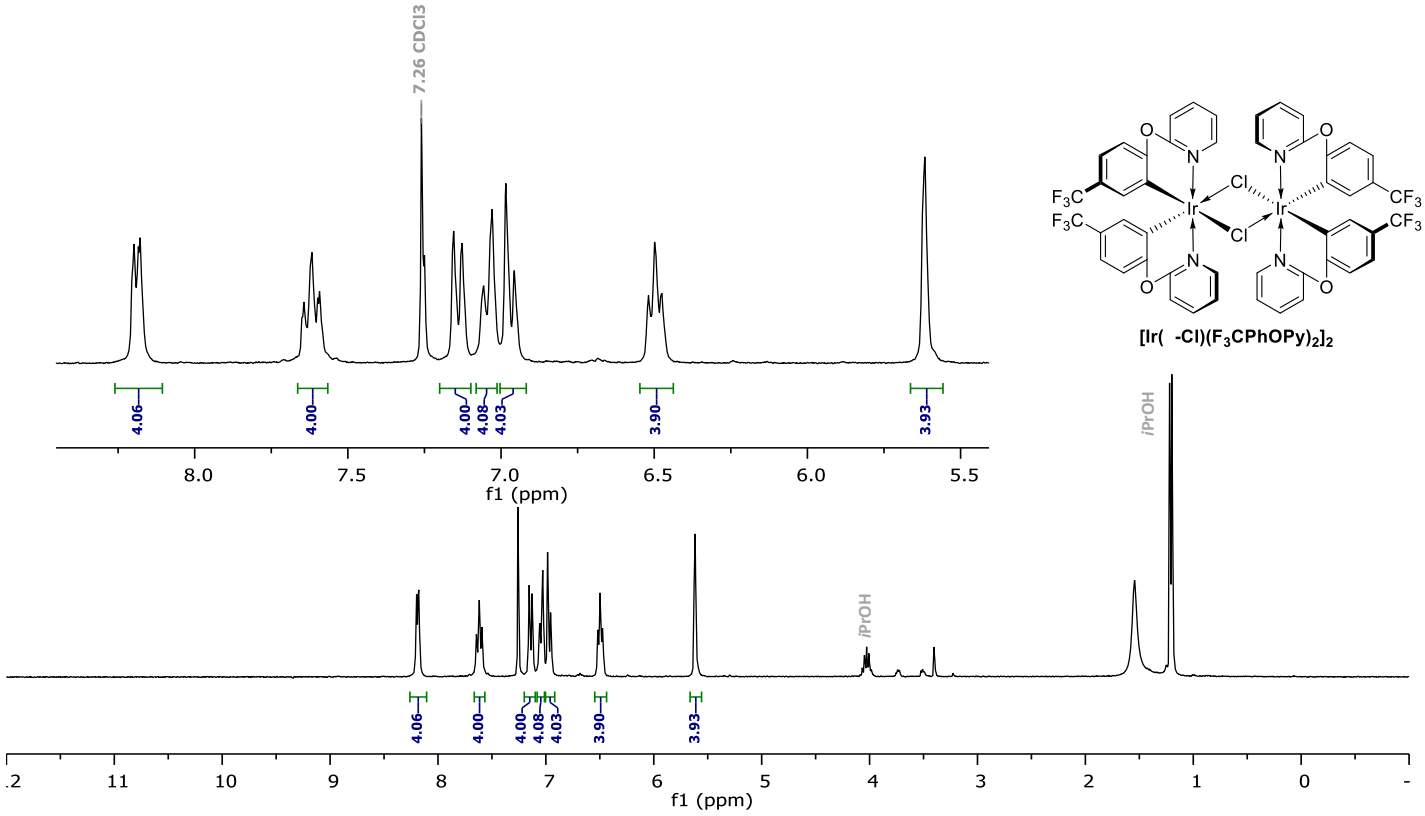

Figure S16. *^{1}H NMR (300 MHz, $CDCl_3$, 298 K) spectrum of* ***[Ir(μ-Cl)(F$_3$CPhOPy)$_2$]$_2$***

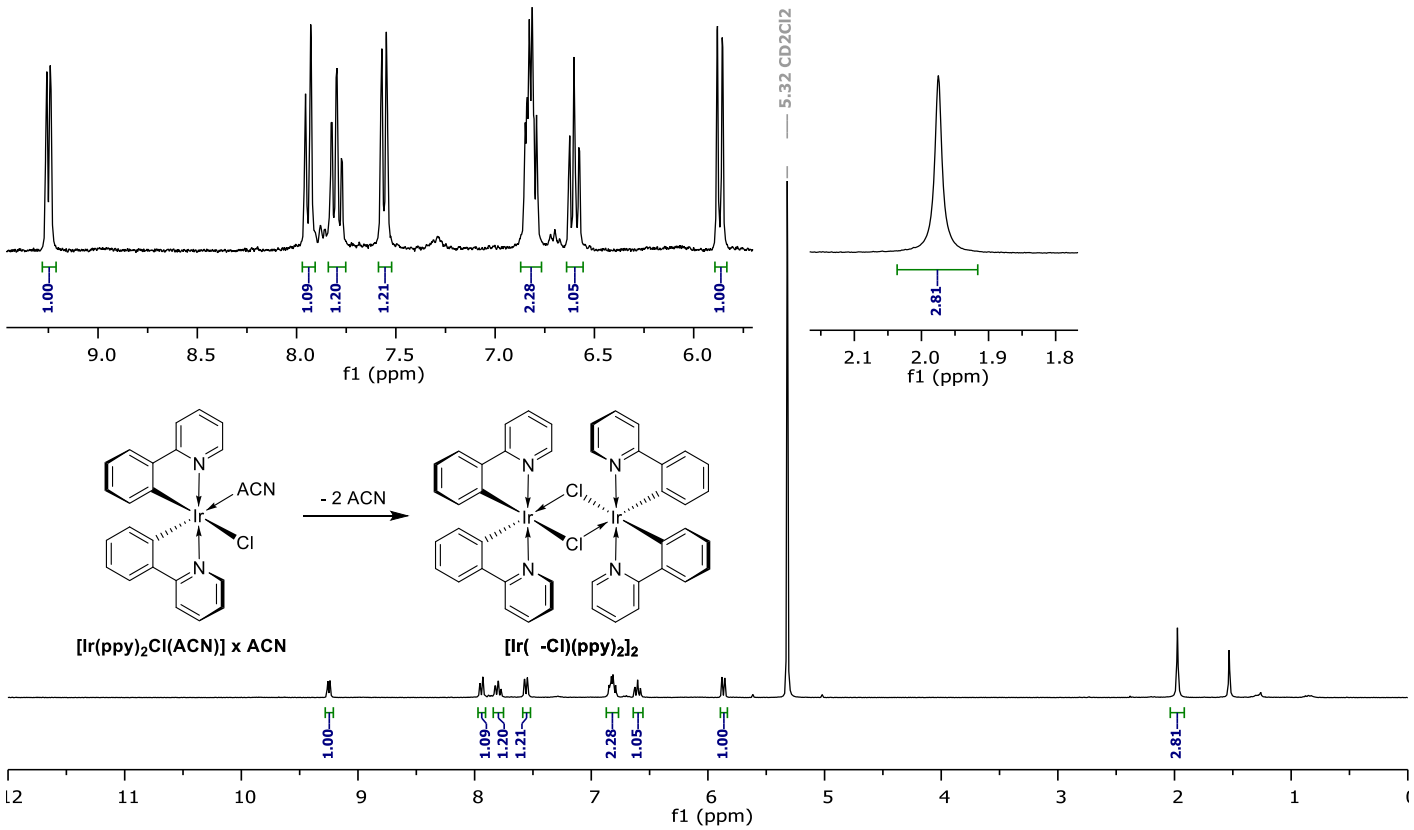

Figure S17. *[1]H NMR (300 MHz, CD_2Cl_2, 298 K) spectrum of* ***[Ir(ppy)$_2$Cl(ACN)]*** *crystals dissolved in CD_2Cl_2*

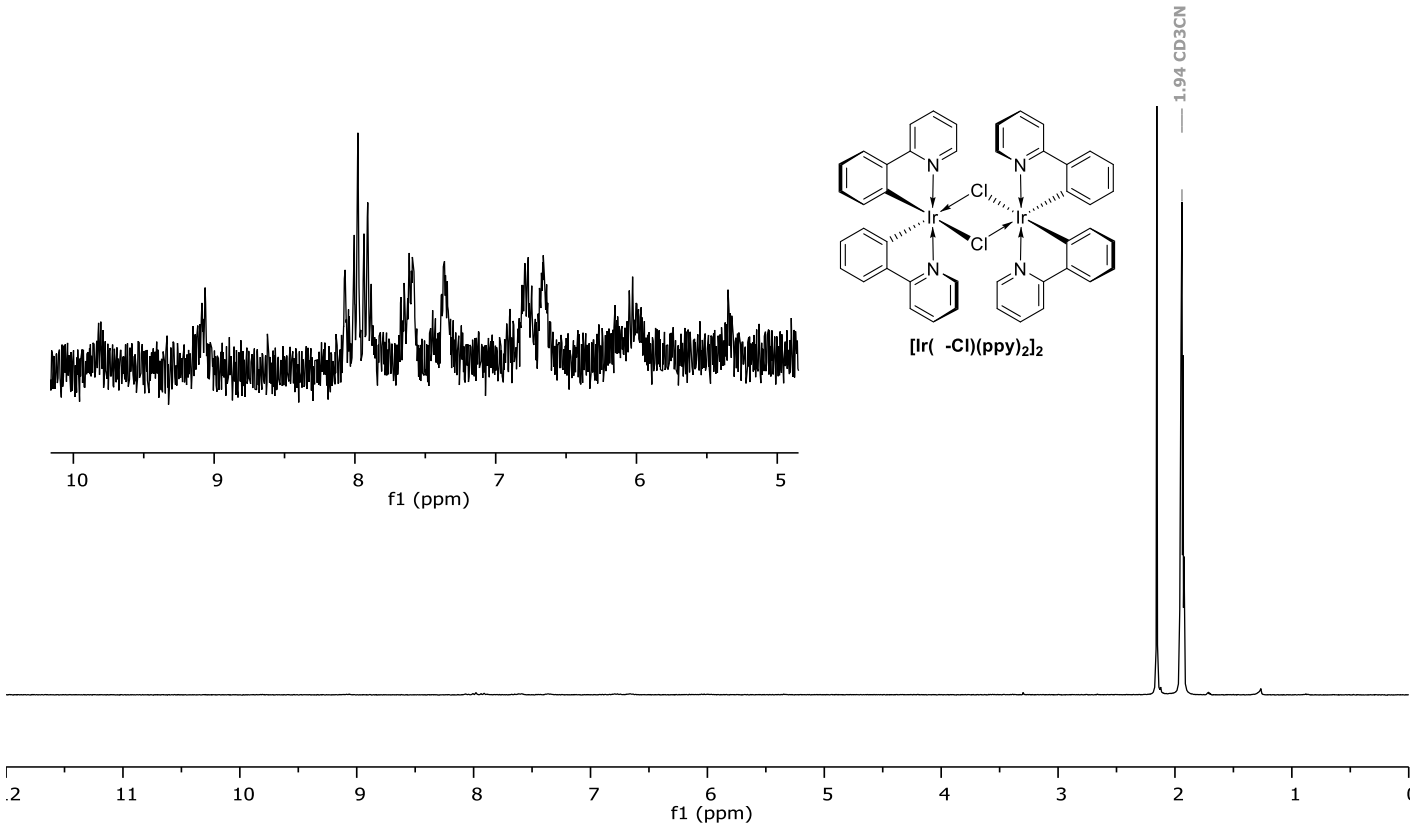

Figure S18. *[1]H NMR (300 MHz, CD_3CN, 298 K) spectrum of* ***[Ir(μ-Cl)(ppy)$_2$]$_2$***

^{1}H and ^{13}C NMR spectra

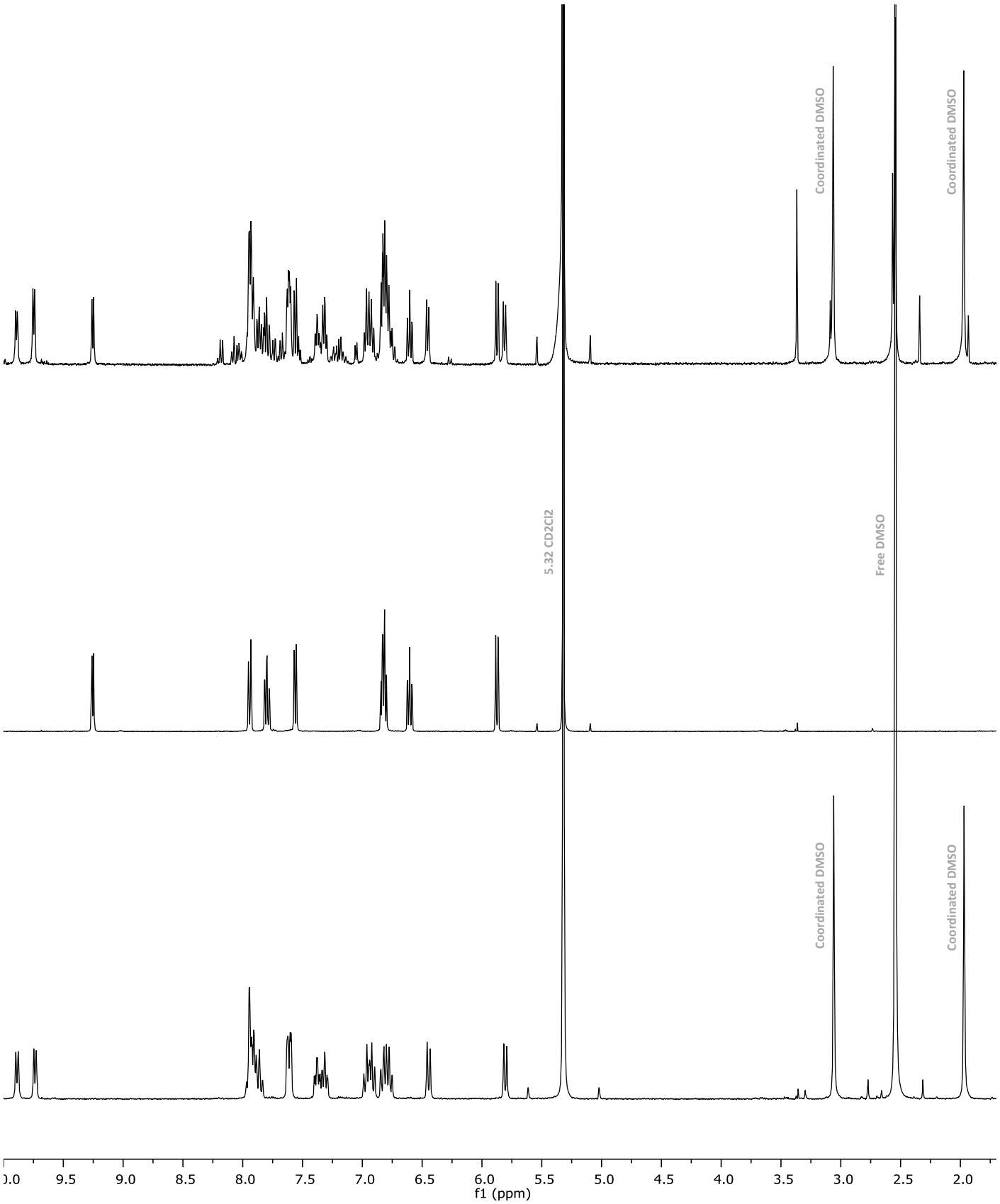

Figure S19. *^{1}H NMR (300 MHz, CD_2Cl_2, 298 K) spectra of* ***[Ir(ppy)$_2$Cl(DMSO)]*** *crystals dissolved in CD_2Cl_2 (top),* ***[Ir(μ-Cl)(ppy)$_2$]$_2$*** *dissolved in CD_2Cl_2 (middle), and* ***[Ir(ppy)$_2$Cl(DMSO)]*** *obtained via titration of* ***[Ir(μ-Cl)(ppy)$_2$]$_2$*** *in CD_2Cl_2 (bottom)*

^{1}H and ^{13}C NMR spectra

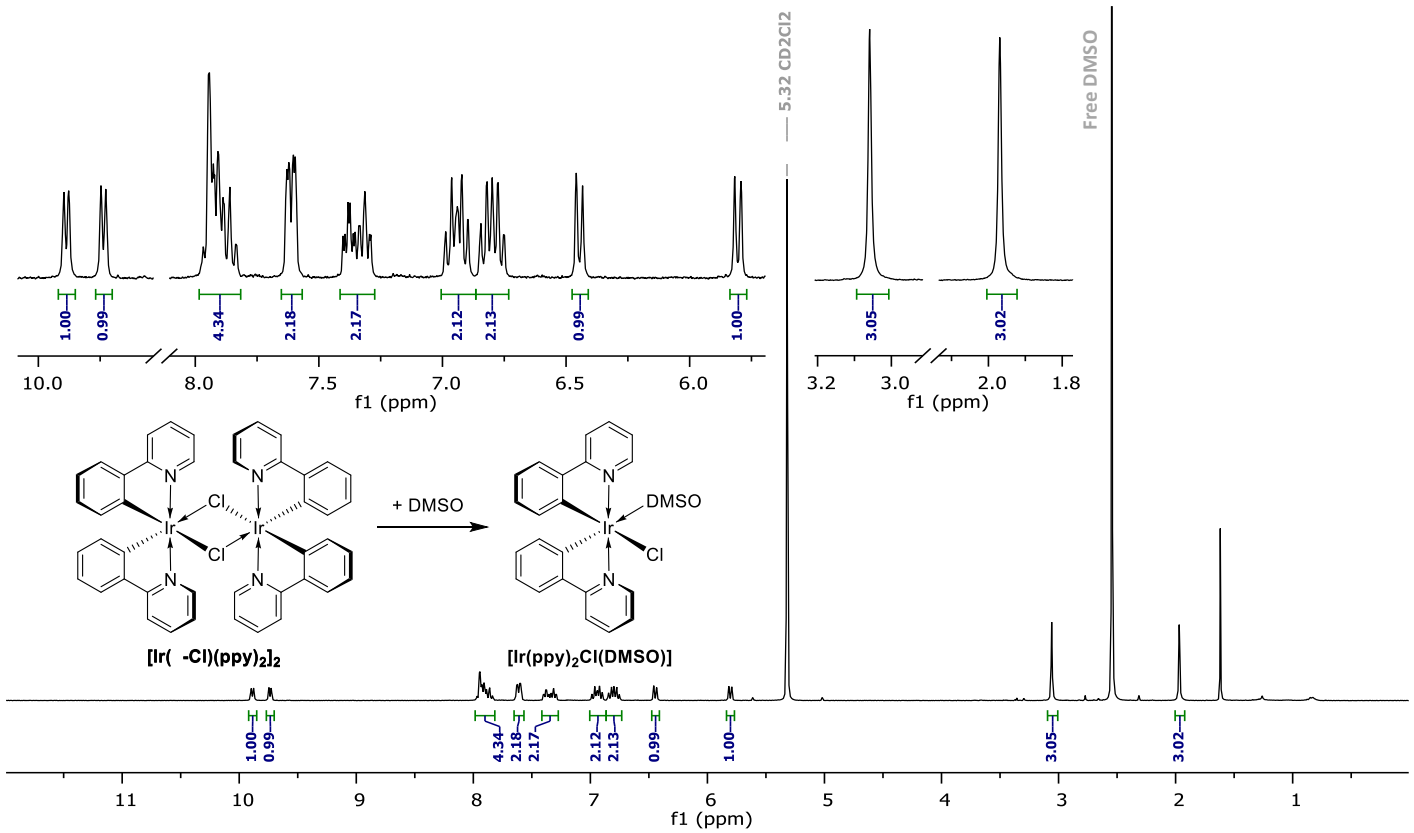

Figure S20. *Final stage of* ***[Ir(μ-Cl)(ppy)$_2$]$_2$*** *titration with DMSO, ^{1}H NMR (300 MHz, CD_2Cl_2, 298 K)*

ESI-HRMS spectra

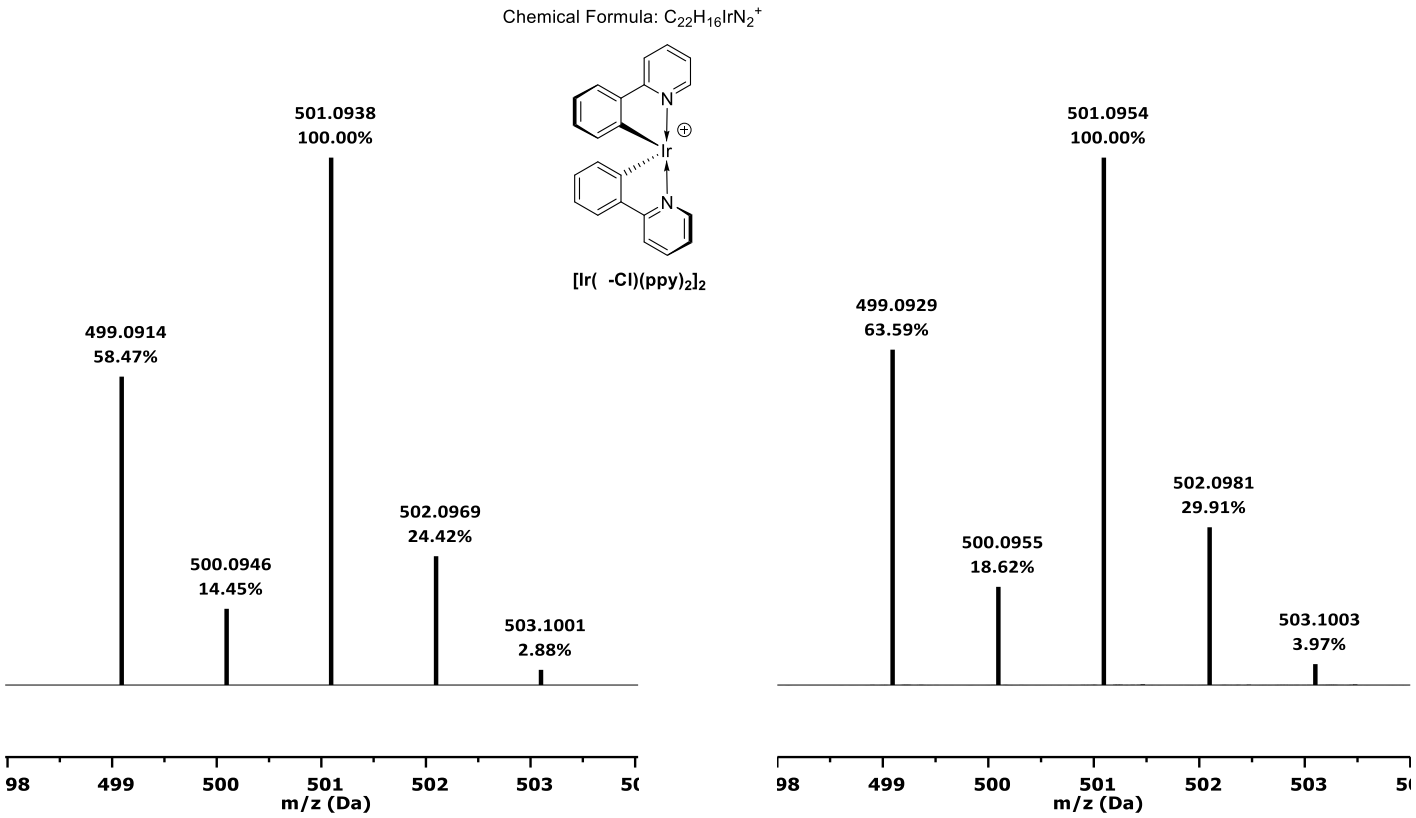

Figure S21. *ESI-HRMS spectrum of* ***[Ir(μ-Cl)(ppy)$_2$]$_2$*** *in acetonitrile, predicted (left) and measured (right)*

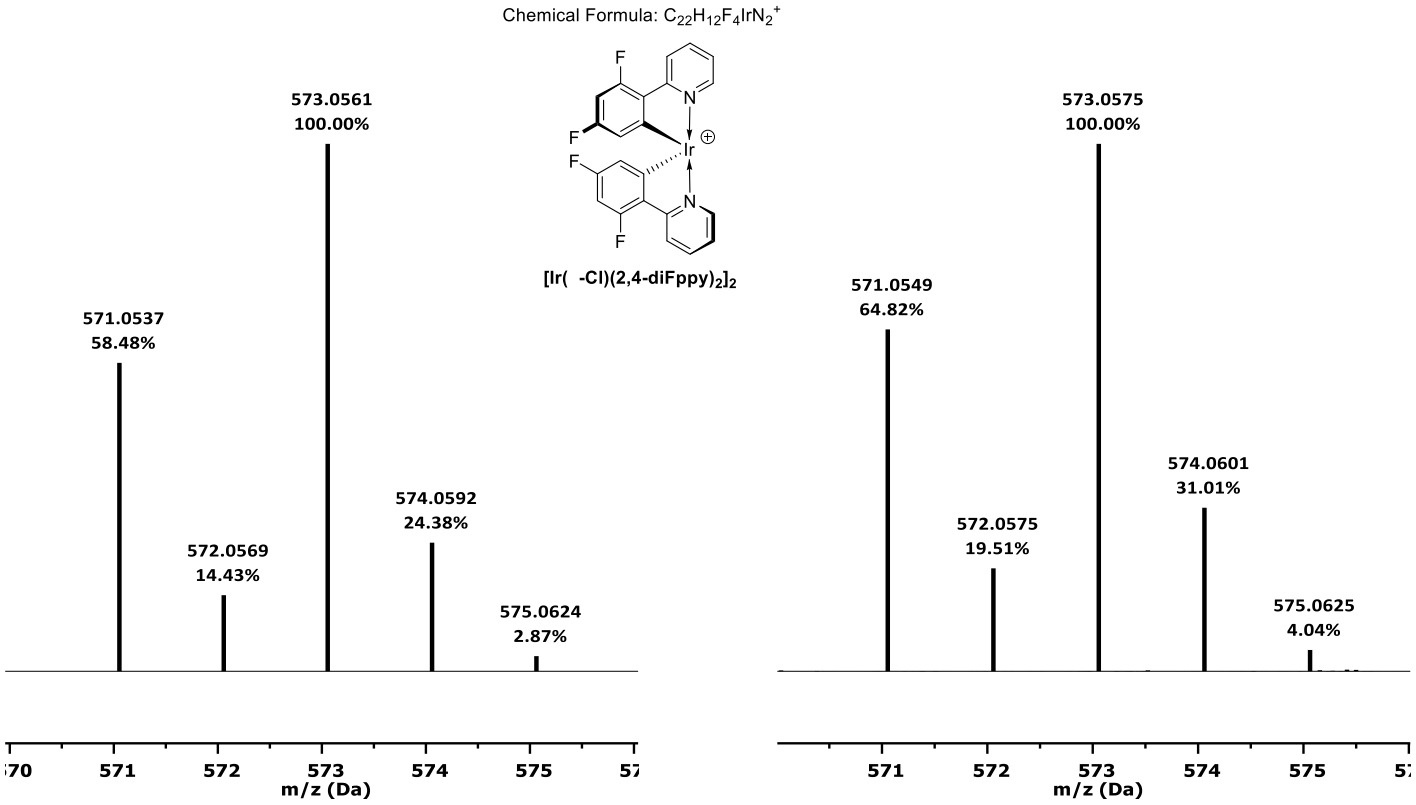

Figure S22. *ESI-HRMS spectrum of* ***[Ir(μ-Cl)(2,4-diFppy)$_2$]$_2$*** *in acetonitrile, predicted (left) and measured (right)*

ESI-HRMS spectra

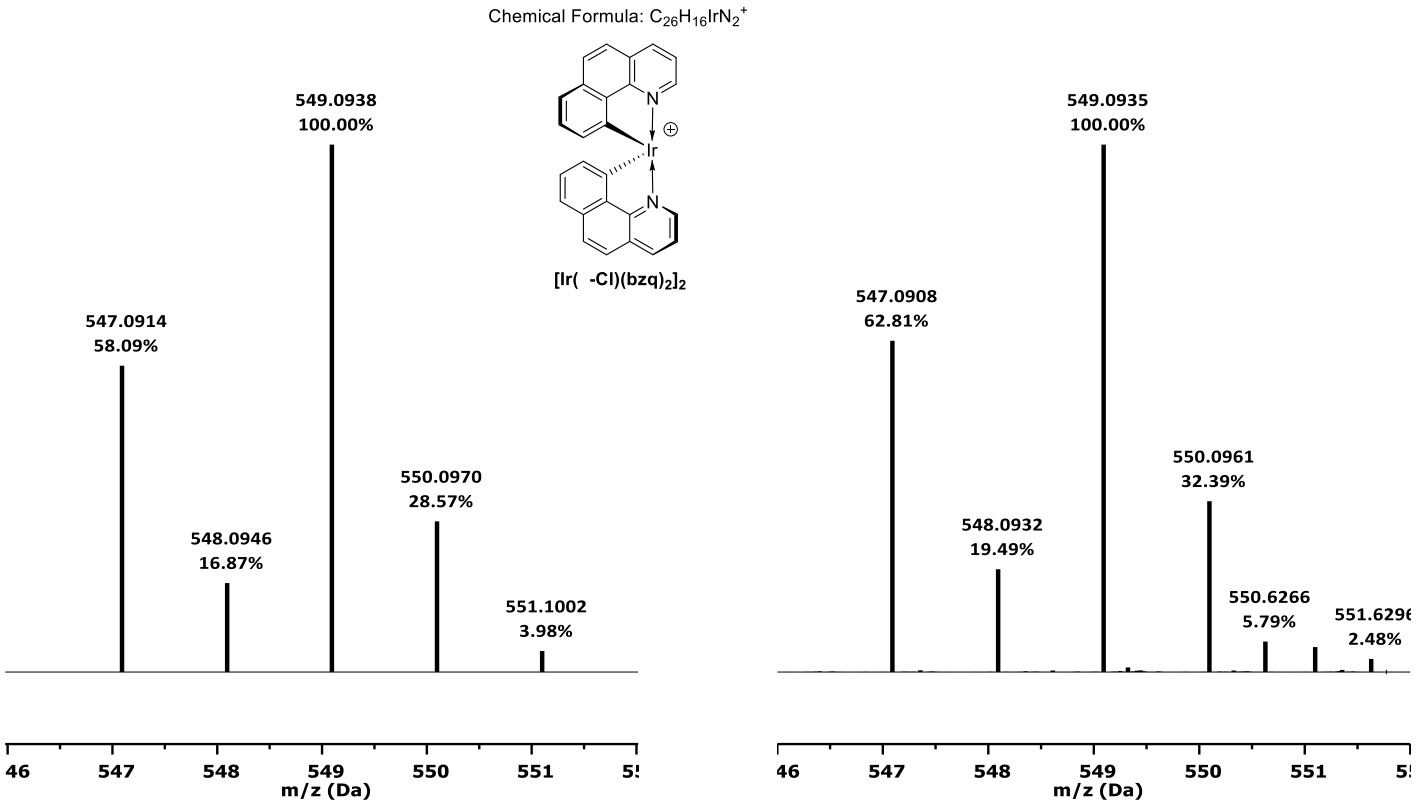

Figure S23. *ESI-HRMS spectrum of* ***[Ir(μ-Cl)(bzq)$_2$]$_2$*** *in acetonitrile, predicted (left) and measured (right)*

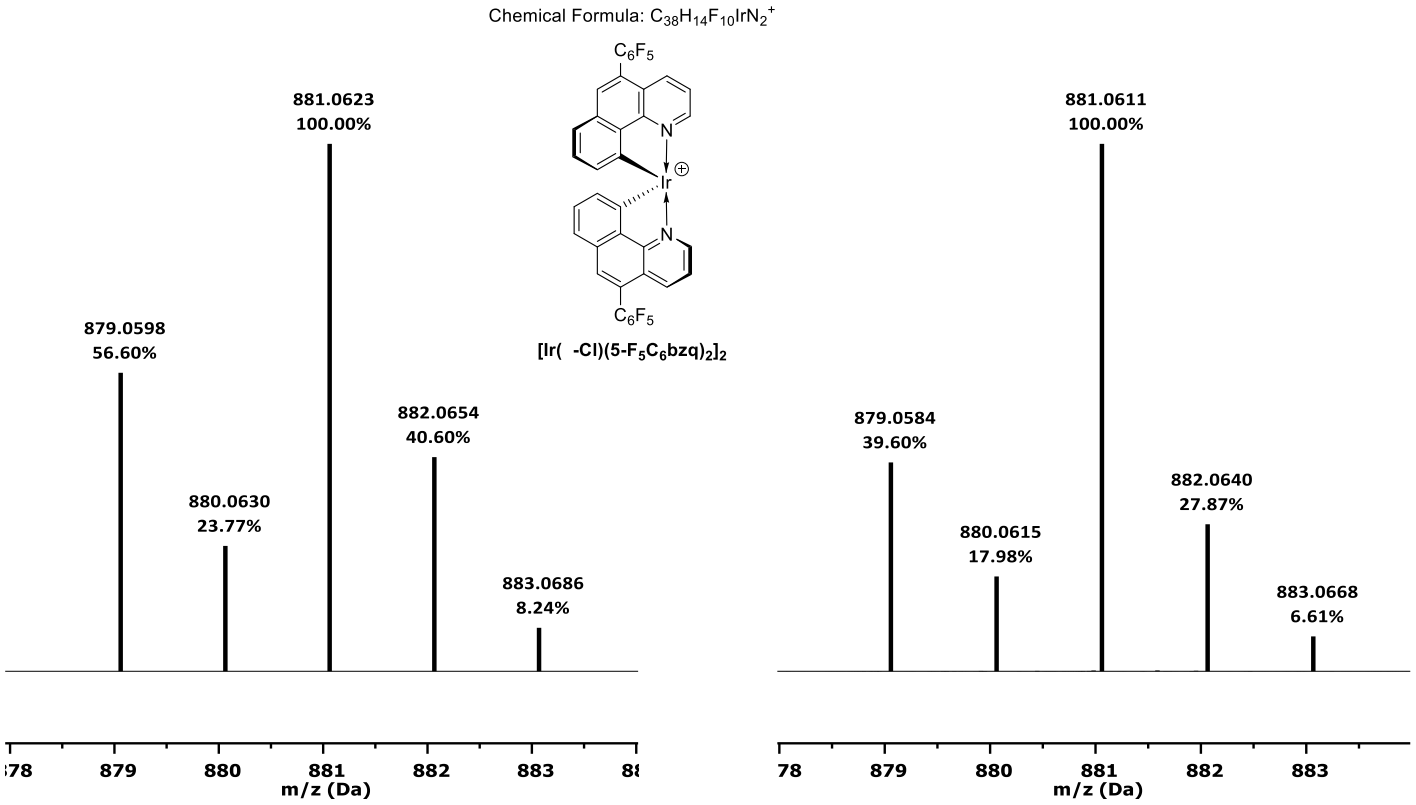

Figure S24. *ESI-HRMS spectrum of* ***[Ir(μ-Cl)(5-F$_5$C$_6$bzq)$_2$]$_2$*** *in acetonitrile, predicted (left) and measured (right)*

ESI-HRMS spectra

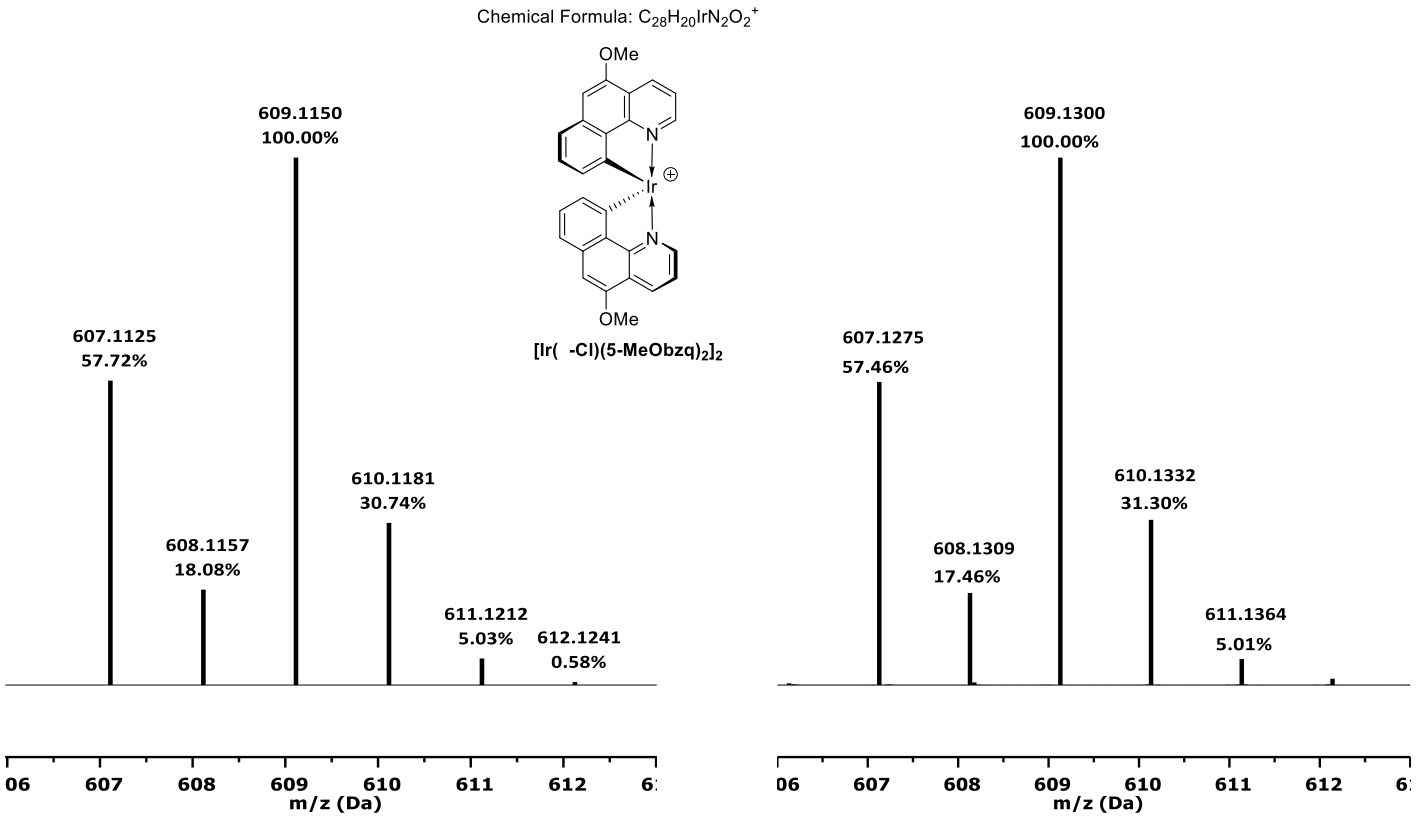

Figure S25. *ESI-HRMS spectrum of* ***[Ir(μ-Cl)(5-MeObzq)$_2$]$_2$*** *in acetonitrile, predicted (left) and measured (right, normalized)*

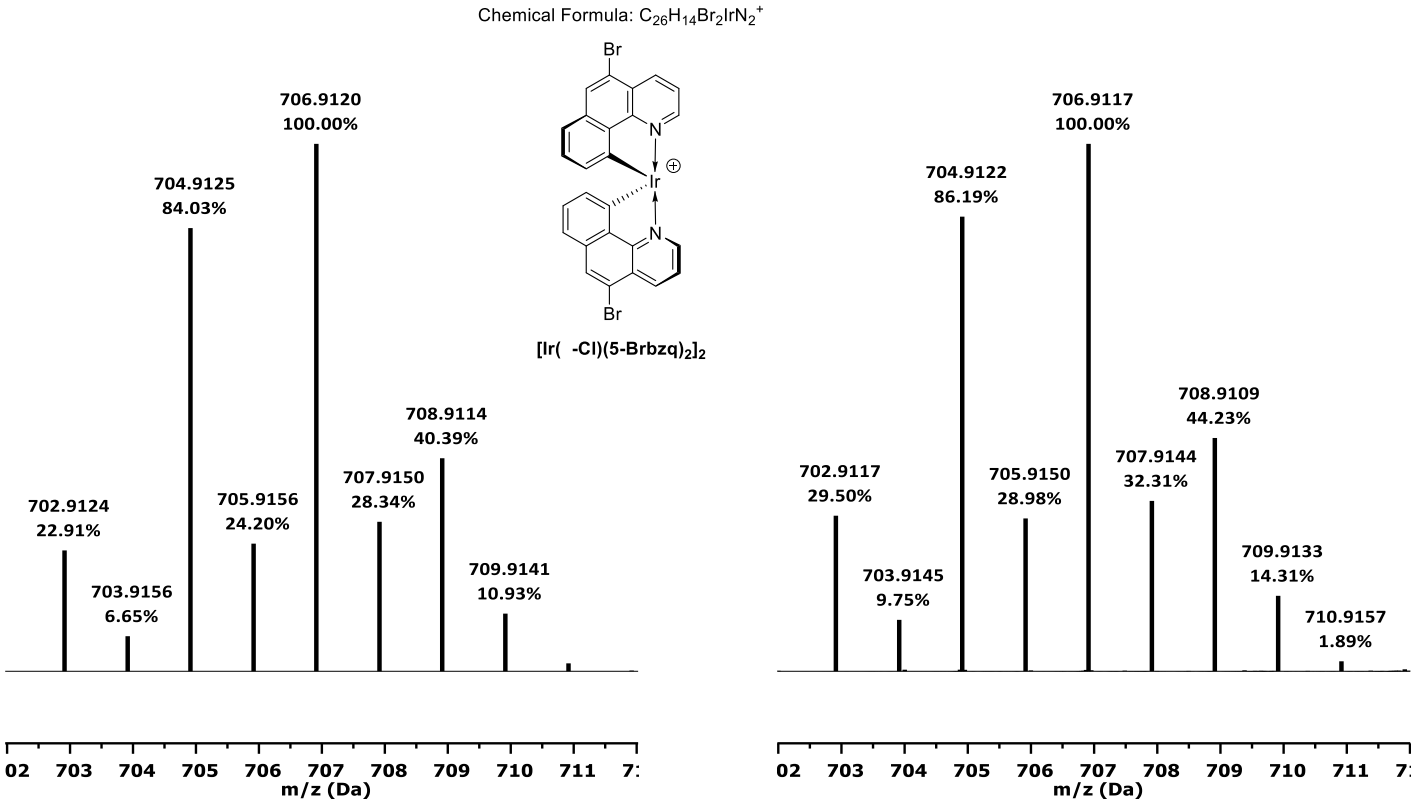

Figure S26. *ESI-HRMS spectrum of* ***[Ir(μ-Cl)(5-Brbzq)$_2$]$_2$*** *in acetonitrile, predicted (left) and measured (right)*

ESI-HRMS spectra

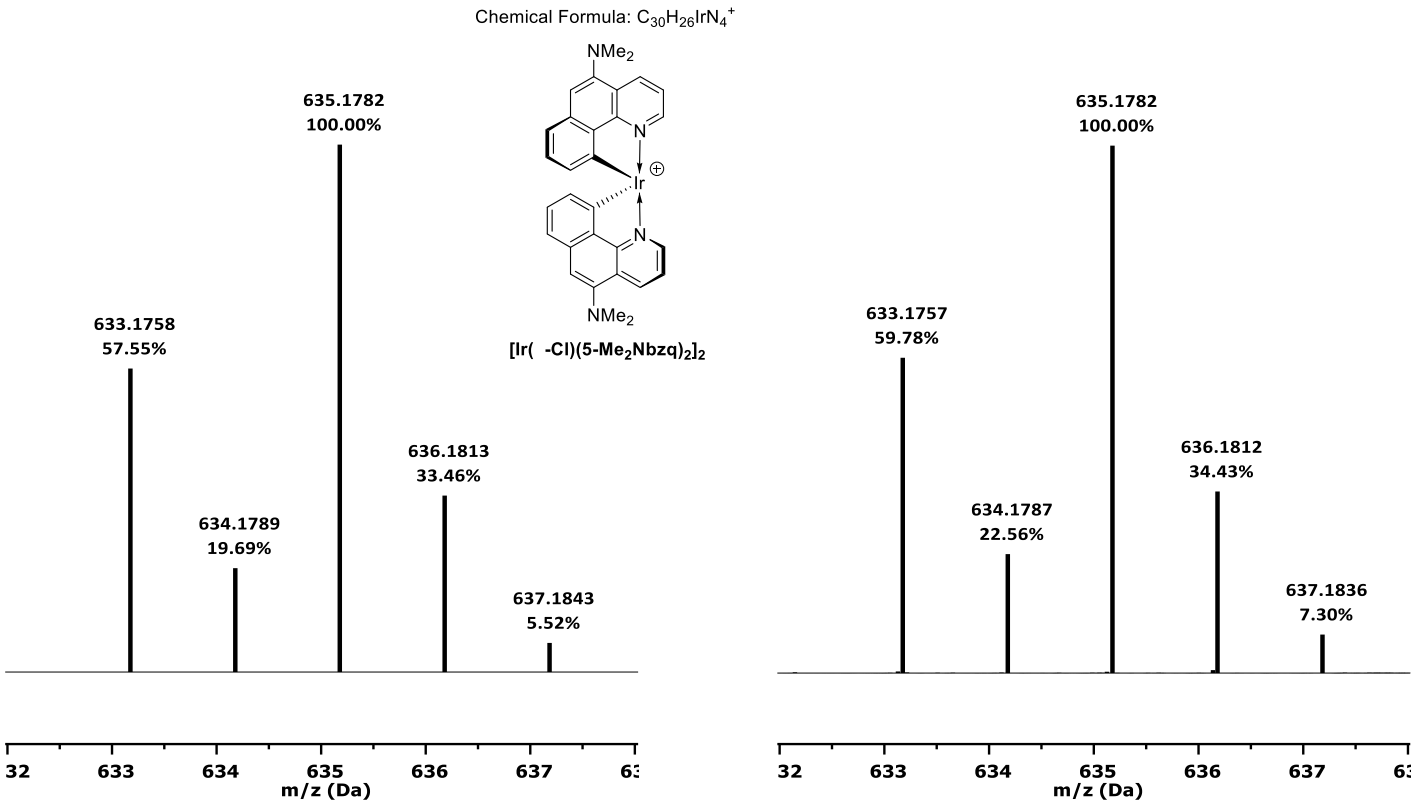

Figure S27. *ESI-HRMS spectrum of* ***[Ir(μ-Cl)(5-Me$_2$Nbzq)$_2$]$_2$*** *in acetonitrile, predicted (left) and measured (right)*

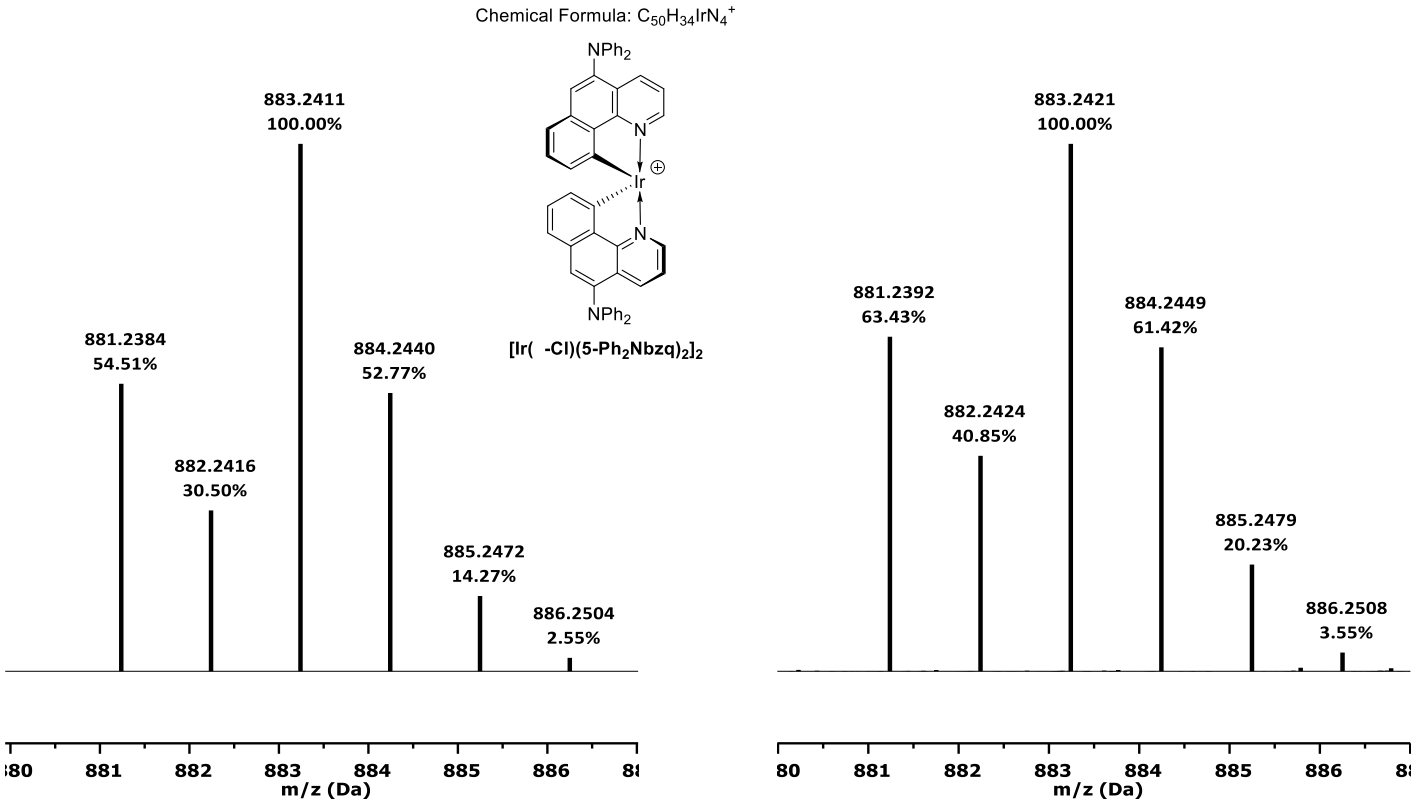

Figure S28. *ESI-HRMS spectrum of* ***[Ir(μ-Cl)(5-Ph$_2$Nbzq)$_2$]$_2$*** *in acetonitrile, predicted (left) and measured (right)*

ESI-HRMS spectra

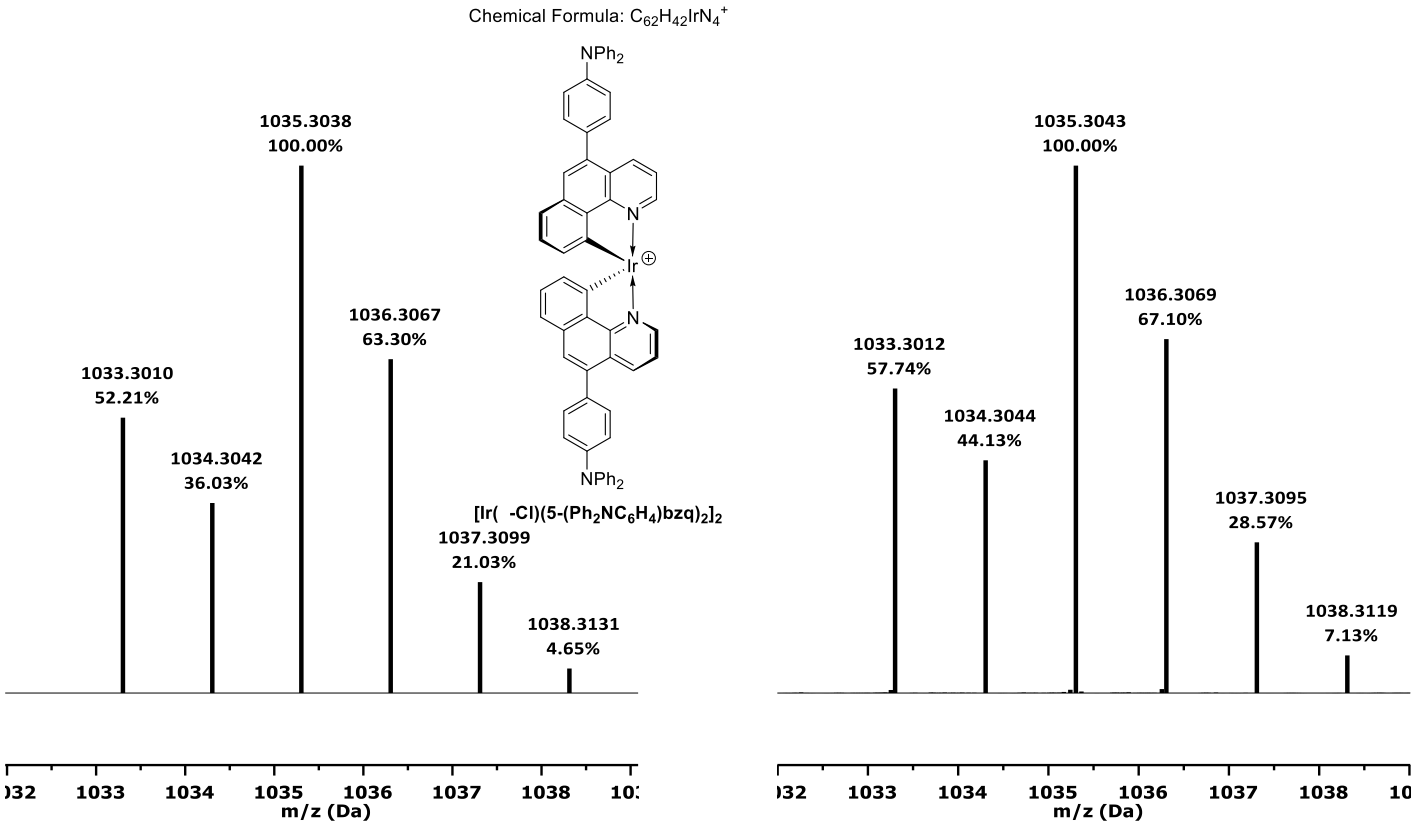

Figure S29. *ESI-HRMS spectrum of* ***[Ir(μ-Cl)(5-(Ph$_2$NC$_6$H$_4$)bzq)$_2$]$_2$*** *in acetonitrile, predicted (left) and measured (right)*

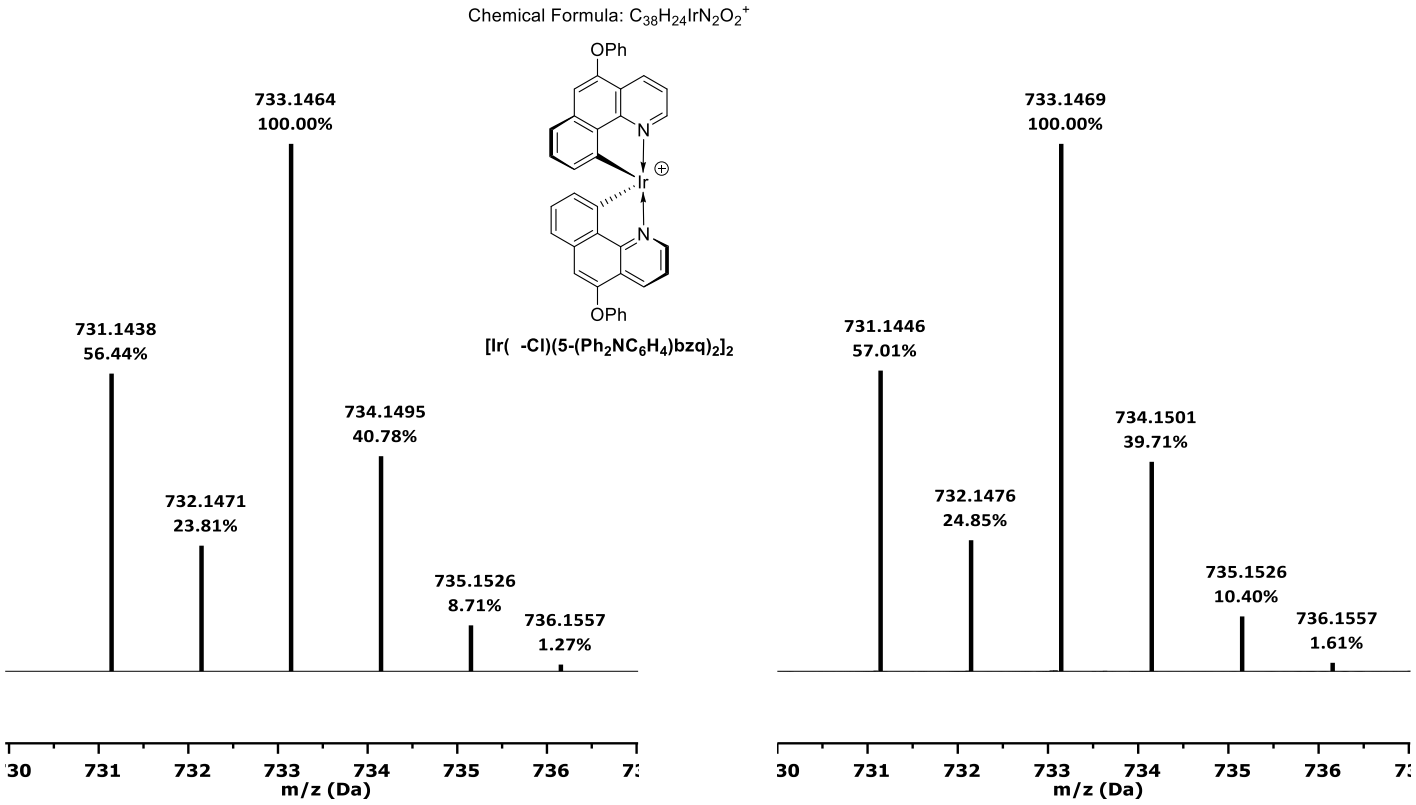

Figure S30. *ESI-HRMS spectrum of* ***[Ir(μ-Cl)(5-PhObzq)$_2$]$_2$*** *in acetonitrile, predicted (left) and measured (right)*

ESI-HRMS spectra

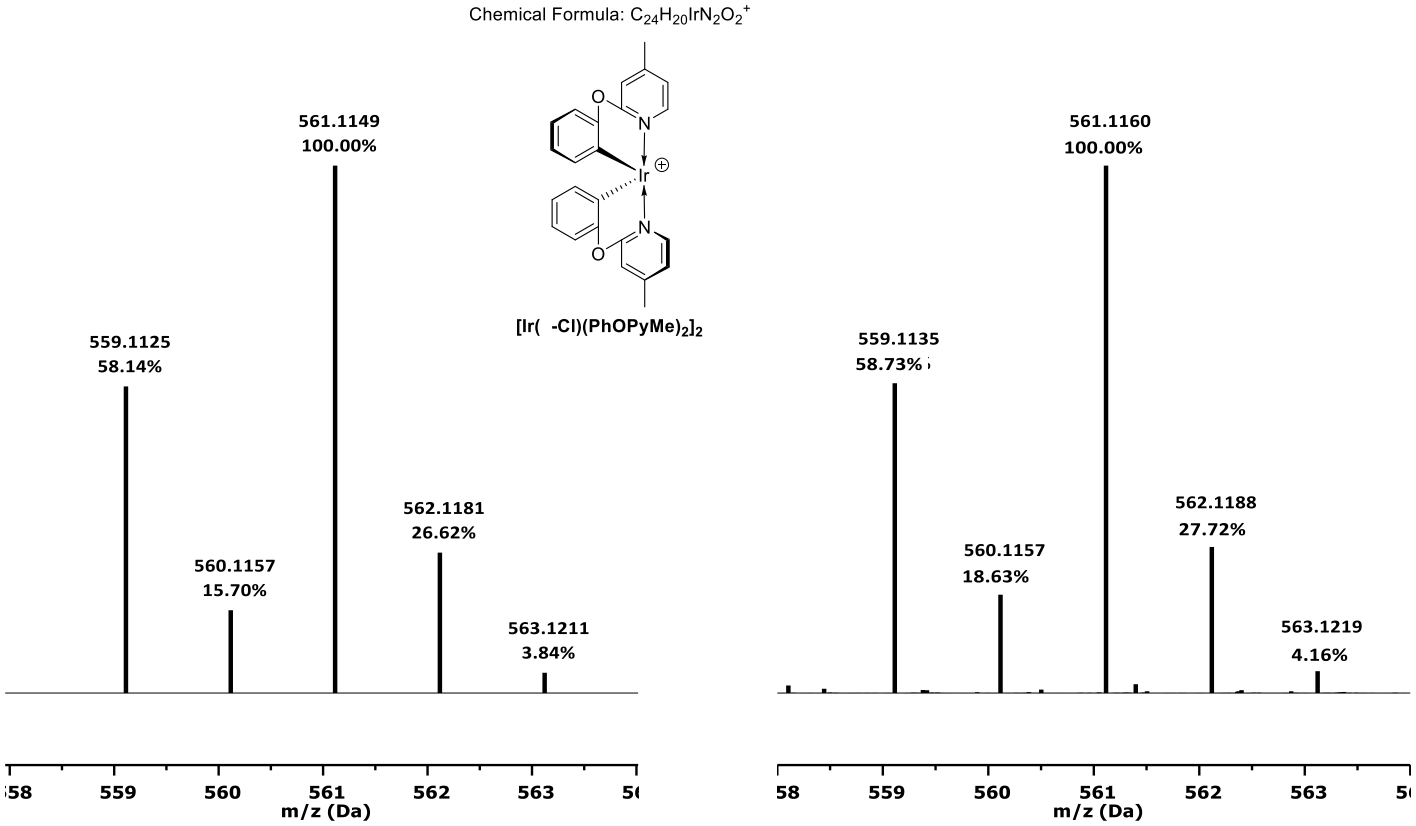

Figure S31. *ESI-HRMS spectrum of* ***[Ir(μ-Cl)(PhOPyMe)$_2$]$_2$*** *in acetonitrile, predicted (left) and measured (right, normalized)*

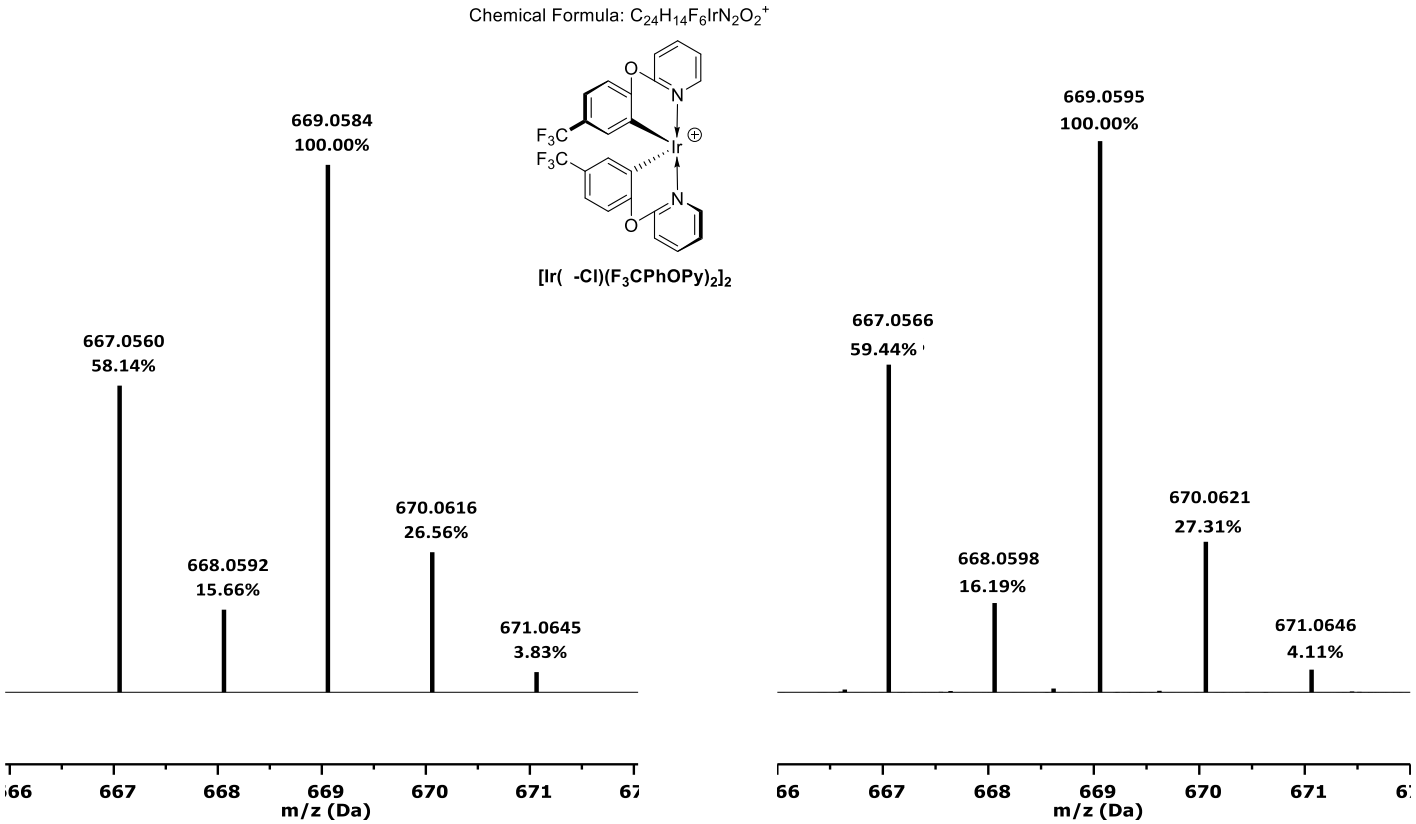

Figure S32. *ESI-HRMS spectrum of* ***[Ir(μ-Cl)(F$_3$CPhOPy)$_2$]$_2$*** *in acetonitrile, predicted (left) and measured (right, normalized)*

ESI-HRMS spectra

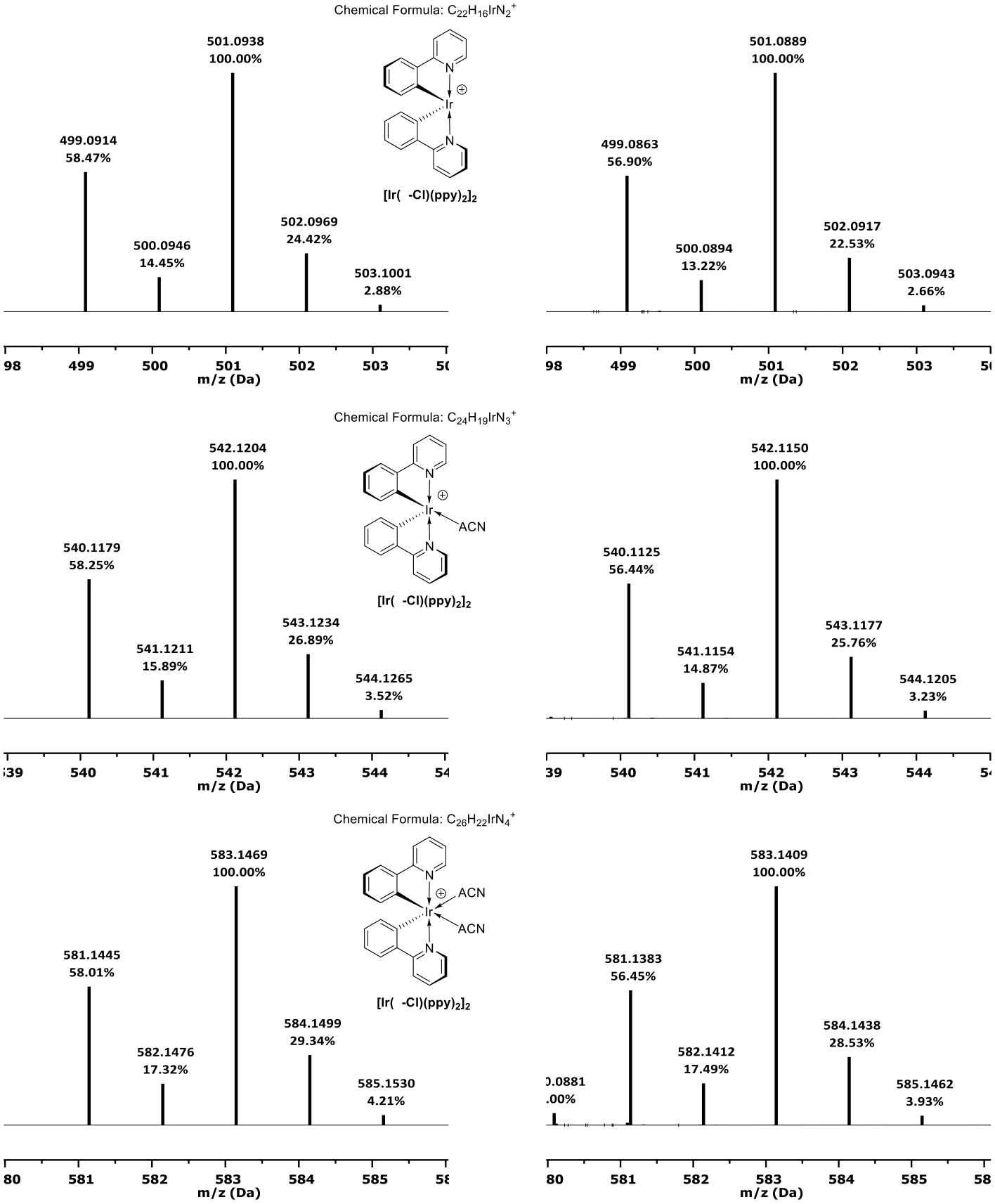

Figure S33. *ESI-HRMS spectrum of* ***[Ir(μ-Cl)(ppy)$_2$]$_2$*** *in acetonitrile at different declustering potential applied (more positive, top; default, middle; more negative, bottom), predicted (left) and measured (right)*

X-ray crystallography

Table S1. *Crystal data, data collection and structure refinement*

Compound	**[Ir(μ-Cl)(bzq)$_2$]$_2$**	**[Ir(μ-Cl)(5-Ph$_2$Nbzq)$_2$]$_2$**	**[Ir(ppy)$_2$Cl(ACN)]**	**[Ir(ppy)$_2$Cl(DMSO)]**
Formula	$C_{52}H_{32}Cl_2Ir_2N_4$	$C_{100}H_{68}Cl_2Ir_2N_8$	$C_{24}H_{19}ClIrN_3 \cdot CH_3CN$	$C_{24}H_{22}ClIrN_2OS \cdot 1/8H_2O$
Formula weight	1168.11	1836.92	618.12	616.40
Crystal system	monoclinic	triclinic	monoclinic	monoclinic
Space group	$P2_1/c$	P-1	I2/a	$P2_1/n$
a(Å)	12.57827(16)	13.6111(13)	17.5287(3)	17.1858(3)
b(Å)	9.54317(14)	17.2172(13)	9.4354(2)	15.2142(3)
c(Å)	33.1530(5)	18.6765(14)	28.8315(4)	17.6902(3)
α(°)	90	76.563(6)	90	90
β(º)	96.3729(14)	83.522(7)	102.475(2)	111.551(2)
γ(°)	90	86.691(7)	90	90
V(Å^3)	3954.98(10)	4227.5(6)	4655.87(15)	4302.06(15)
Z	4	2	8	8
D_x(g cm^{-3})	1.962	1.443	1.764	1.903
F(000)	2240	1824	2400	2394
μ(mm^{-1})	14.429	3.260	5.871	6.448
Reflections:				
collected	17193	31326	24128	35822
unique (R_{int})	7131 (0.034)	14860 (0.211)	5273 (0.024)	9719 (0.026)
with I>2σ(I)	6700	5742	5016	8266
R(F) [I>2σ(I)]	0.0608	0.1384	0.0169	0.0265
wR(F^2) [I>2σ(I)]	0.1525	0.2502	0.0604	0.0746
R(F) [all data]	0.0639	0.2459	0.0187	0.0360
wR(F^2) [all data]	0.1538	0.3072	0.0618	0.0799
Goodness of fit	1.195	1.003	0.979	1.048
max/min Δρ (e·Å^{-3})	2.25/-2.02	4.25/-2.97	1.13/-0.77	1.57/-1.22

Table S2a*. Relevant geometrical features for* ***[Ir(μ-Cl)(bzq)$_2$]$_2$*** *and* ***[Ir(μ-Cl)(5-Ph$_2$Nbzq)$_2$]$_2$*** *(Å,º)*

[Ir(μ-Cl)(bzq)$_2$]$_2$				**[Ir(μ-Cl)(5-Ph$_2$Nbzq)$_2$]$_2$**			
Ir1-N1A	2.124(10)	Ir2-N1C	2.094(10)	Ir1-N1A	2.020(18)	Ir2-N1C	1.953(18)
Ir1-N1B	2.145(10)	Ir2-N1D	2.119(10)	Ir1-N1B	2.050(16)	Ir2-N1D	2.030(18)
Ir1-C12A	2.003(12)	Ir2-C12C	2.000(12)	Ir1-C12A	1.767(18)	Ir2-C12C	2.08(2)
Ir1-C12B	2.007(10)	Ir2-C12D	2.018(19)	Ir1-C12B	2.07(2)	Ir2-C12D	2.02(2)
Ir1-Cl1	2.509(3)	Ir2-Cl1	2.525(3)	Ir1-Cl1	2.472(6)	Ir2-Cl1	2.486(6)
Ir1-Cl2	2.518(3)	Ir1-Cl2	2.496(3)	Ir1-Cl2	2.493(6)	Ir1-Cl2	2.505(6)
N1A-Ir1-N1B	170.2(4)	N1C-Ir2-N1D	171.0(4)	N1A-Ir1-N1B	173.8(8)	N1C-Ir2-N1D	175.5(8)
C12A-Ir1-Cl2	175.7(4)	C12D-Ir2-Cl2	171.7(3)	C12A-Ir1-Cl2	169.7(5)	C12D-Ir2-Cl1	174.3(6)
C12B-Ir1-Cl1	171.8(3)	C12C-Ir2-Cl1	173.7(3)	C12B-Ir1-Cl1	176.1(5)	C12C-Ir2-Cl2	172.3(5)
Max(A)	0.0782(11)	-0.1224(7)		0.0308(19)			
A/B	82.72(14)	C/D	75.53(18)	A/B	82.7(3)	C/D	81.2(4)
				A/A1	72.1(8)	C/C1	60.6(8)
				A/A2	86.4(7)	C/C2	87.4(7)
				A1/A2	74.7(9)	C1/C2	67.7(10)
				B/B1	80.4(8)	D/D1	87.3(8)

				B/B2	77.8(8)	D/D2	77.8(8)
				B1/B2	74.0(9)	D1/D2	69.9(11)

Max(A) is the maximum deviation from the least-squares plane through Ir and Cl atoms, A, B and C, D are the mean least-squares planes of aromatic ring systems coordinated to the same Ir atoms; A1, A2 etc. in ***[Ir(μ-Cl)(5-Ph$_2$Nbzq)$_2$]$_2$*** *denote the mean planes of phenyl rings from appropriate NPh$_2$ groups.*

Table S2b*. Relevant geometrical features for* ***[Ir(ppy)$_2$Cl(ACN)]*** *and* ***[Ir(ppy)$_2$Cl(DMSO)]*** *(Å,[9])*

	[Ir(ppy)$_2$Cl(ACN)]	**[Ir(ppy)$_2$Cl(DMSO)] A**	**[Ir(ppy)$_2$Cl(DMSO)] B**
Ir1-N1A	2.045(2)	2.058(3)	2.061(3)
Ir1-N1B	2.049(2)	2.080(3)	2.083(3)
Ir1-C8A	2.001(3)	2.050(4)	2.042(4)
Ir1-C8B	2.001(1)	2.023(4)	2.025(4)
Ir1-Cl1	2.4950(6)	2.4770(10)	2.4784(9)
Ir1-N1(S1)	2.108(2)	2.3593(10)	2.3335(10)
N1A-Ir1-N1B	173.37(8)	170.19(13)	171.53(12)
C8B-Ir1-Cl1	176.35(8)	177.20(11)	174.13(11)
C8B-Ir1-N1(S1)	176.49(9)	176.07(10)	173.71(10)
A/B	10.33(17)	8.5(2)	7.5(2)
C/D	3.48(12)	2.6(2)	3.0(2)

A, B and C, D are the mean least-squares planes of aromatic ring systems coordinated to the same Ir atoms.

References

[1] X.-H. Li, A.-H. Ye, C. Liang, D.-L. Mo, *Synthesis* **2018**, 50 (08), pp 1699-1710
[2] R. Takise, R. Isshiki, K. Muto, K. Itami, J. Yamaguchi, *J. Am. Chem. Soc.*, **2017**, 139 (9), pp 3340-3343
[3] Y. You, S. Y. Park, *J. Am. Chem. Soc.* **2005**, 127 (36), pp 12438-12439
[4] B. Orwat, M.-J. Oh, M. Kubicki, I. Kownacki, *Adv. Synth. Catal.* **2018**, 360 (17), pp 3331-3344
[5] Rigaku Oxford Diffraction (**2015**) CrysAlis PRO (Version 1.171.38.41)
[6] G. M. Sheldrick, *Acta Cryst.* **2015**, A71, pp 3-8
[7] G. M. Sheldrick, *Acta Cryst.* **2015**, C71, pp 3-8
[8] C. R. Groom, I. J. Bruno, M. P. Lightfoot, S. C. Ward, *Acta Cryst.* **2016**, B72, pp 171-179
[9] A. L. Spek, *Acta Cryst.* **2015**, C71, pp 9-18